As Dry as a (Burnt) Bone –
Histological, Physicochemical, and Osteogenic Reaction-Related Approaches to Identifying the Pre-Burning Condition of Bone

Emese Ilona Végh

D.Phil
Wolfson College
Research Laboratory for Archaeology and the History of Art
University of Oxford
Hilary Term 2022



Thesis presented to the University of Oxford in partial fulfilment of the requirements for the degree of Doctor of Philosophy

Abstract

Burnt human remains are recovered from a variety of contexts as a result of funerary treatment (cremation) in archaeology and fatal fires in a medicolegal context. The timing that this burning takes place compared to the time of death has received a great deal of attention in the literature, with inconclusive results. Cremation after active or passive excarnation, as a funerary rite, was mainly proposed during the prehistory of the British Isles. The postmortem (after death) transformation of the corpse starts during early diagenesis, thus taphonomic changes are thought to have the potential to determine the postmortem interval (PMI) at the time of burning. This thesis aims to provide insight into the taphonomy, early diagenesis and heat-induced changes of bone through an experimental approach with repercussions to both archaeology and forensic science. The thesis is a collection of three interdisciplinary approaches organised into three papers to identify if the corpse was burnt fresh or partially decomposed.

Fleshed pig (*Sus scrofa*) tibiae, used as a proxy for humans, were left exposed in a field in Wytham Woods, Oxfordshire, UK, then collected at 14, 34, 91, 180, 365-day intervals prior to being burnt in an outdoor fire (≤750 °C bone temperature). Fresh (fleshed) tibiae acted as unburnt and burnt controls. In addition to this experimentation, two cremated human bone fragments from Middle/Late Neolithic (ca. 3300–2500 cal BC) Ireland were added to the physicochemical investigations. A variety of techniques were employed across academic disciplines: (1) histological, using microbial bioerosion as a proxy for decomposition by transmitted light microscopy and backscattered electron microscopy (BSEM); (2) physicochemical, investigating the structural changes through Fourier Transform Infrared Spectroscopy (FTIR) and major and trace elemental concentration changes by the wavelength-dispersive electron microprobe (EMP-WDS); and (3) the bone's osteogenic-reaction,

investigating its response to sharp force trauma (SFT) and heat-fracturing compared to its collagen content.

Data analyses were carried out using a variety of methods. Histotaphonomy was assessed quantitatively and systematically by a novel data labelling application developed for this study in Python and Javascript programming languages. The physicochemical results were investigated by unsupervised (PCA) and supervised (LDA) dimensionality reduction techniques and further statistical analyses (linear regression, MANOVA, multivariate comparison of means test). The latter was applied in the morphological investigations as well. All data analyses were done in Jupyter notebook in Python programming language.

Results show that changes in elemental concentration of bone throughout the PMI might indicate whether the bone was burnt fresh or partially decomposed as well as if SFT was inflicted after 6 months of exposure before burning. If SFT is present in the bone, results show that the decrease of perimortem features (irregular edges, splintering, curling or uplifting) and increase of postmortem features (regular shaped, sharp edges) in cutmarks can potentially inform on the timing of SFT infliction in burnt bone. However, microbial bioerosion might not indicate early diagenesis prior to burning. Features resembling microbial bioerosion were present on the fresh burnt bones, indicating that burning is not only able to conceal features but also produce them. The concentration of elements associated with extracellular fluid (K, Na, Cl) change with the PMI and endure burning. K values under 0.07 ± 0.01 wt% in inner and mid-cortical zones of burnt bones suggest that bones were not burnt immediately after death. Using this criterion, results from the Neolithic bone fragments would indicate a PMI of at least weeks to months prior to cremation. Ca, P, Fe, Al, Si, and Sr are not significantly altered with burning, and Fe, Al, Si, Sr are also unaffected by the PMI. In unburnt bone increased crystallinity and carbonate loss are detectable in <1 year, but both are obscured by burning. Structurally, the carbonate to phosphate ratios (C/P) and phosphate high temperature (PHT) are the most

valuable ratios for discriminating between unburnt and burnt bones. Fractures did not depend on the limited collagen loss during the one-year PMI prior to burning. All in all, the amount of potassium in burnt bone is suggested to be the most useful proxy of bone decomposition prior to burning.

Research Laboratory for Archaeology and the History of Art
1 South Parks Road, Oxford, OX1 3TG, United Kingdom

UNIVERSITY OF OXFORD

Statement of Authorship

We hereby give permission to Emese Végh, to use our joint work (cited below) as contribution towards her DPhil (PhD) thesis in Archaeological Science, to be submitted for examination at the University of Oxford.

Végh, E. I., Czermak, A., Márquez-Grant, N., Schulting, R. J. 2021. Assessing the reliability of microbial bioerosion features in burnt bones: A novel approach using feature-labelling in histotaphonomical analysis. Journal of Archaeological Science:Reports 37, 102906.

Végh, E. I., Márquez-Grant, N., and Schulting, R. J. Physicochemical Changes in Bone Bioapatite During the Late Postmortem Interval Pre- and Post-Burning. *Applied Spectroscopy* (in press)

We confirm that to the best of our knowledge, the author contribution statement below is accurate and that as the first author, Emese Végh's contribution towards the work is greater than that of any other co-author.

Author Contribution:

- **Emese Végh**: conceptualisation, research design, data curation, formal analysis, funding acquisition, investigation, methodology, project administration, resources, software, validation, visualisation, writing – original draft, writing – review and editing;
- **Rick Schulting**: conceptualisation, research design, data curation, supervision, provided archaeological samples, validation, writing – review and editing;
- **Nicholas Márquez-Grant**: conceptualisation, supervision, writing – review and editing;
- **Andrea Czermak**: conceptualisation, data curation, formal analysis, methodology.

Signatures:



Professor Rick Schulting (rick.schulting@arch.ox.ac.uk)



Dr Nicholas Márquez-Grant (n.marquezgrant@cranfield.ac.uk)



Dr Andrea Czermak (czermak_andrea@web.de)

Acknowledgements

Firstly, I thank Professor Rick Schulting and Dr Nicholas Márquez-Grant, my supervisors, for their guidance and mentorship throughout this thesis. Special thanks to Rick for his help with the outdoor fire experiments.

I would like to thank my parents, Györgyi Véghné Láczay and Dr Ferenc Végh, for their continued patience, mental, emotional, and financial support in my education. Thanks to them for raising me to value education and knowledge as the main priorities in life and for having a profound belief in my abilities. I also extend my gratitude to my aunt, Professor Ágnes Végh, who has never let me down and provided unwavering support.

I would like to express my deepest gratitude and appreciation to Kevin Lemagnen, who made it possible for me to start and finish my DPhil at the University of Oxford. Kevin lent me money to pay my only partially-funded tuition fees and I could always go to him for help and advice with data science and coding. I am also very grateful to him for helping me develop the data labelling application. Thank you for helping me in every way, this thesis would truly not have been possible without your continued support.

I also extend my gratitude to my co-author Dr Andrea Czermak, who helped me with the methodology for the histology study and for mentoring me. Thank you also to Dr Victoria Smith for her help and assistance on the electron microprobe.

I very much appreciate the secondary standard bone samples provided by Sophie Decrée from the Royal Belgian Institute of Natural Sciences and the Neolithic cremated human bone fragments from Kiltierney provided by the Environment and Heritage Service, Northern Ireland. Also thanks to Professor Nick Barton, for creating the experimental flint blades for the study.

I would like to extend my sincere thanks to Professor Julia Lee-Thorp and Professor Mark Pollard, my D.Phil. assessors, for their feedback and help along the way.

Thank you to the team at Wytham Woods, Oxford, for letting me use the facilities for the taphonomy and burning experiments and to the Anagama team, for assisting me in using their furnace.

I'd like to recognise the assistance received from Professor Robert Hedges, Dr David Chivall, David Pete, Dr Chris Doherty, and Dr Emily Arnold.

I gratefully acknowledge the scholarships, bursaries, and travel grants received from the Meyerstein Foundation, Wolfson College, Sidney Perry Foundation, Stapley Educational Trust, and the University of Oxford.

Especially supportive during finishing my thesis was Dr Kevin Tang, my partner, who reinforced the importance of why I was doing a D.Phil and guiding me towards a career.

I very much appreciate the help of Tansy Branscombe, Katelyn Farrants, and Gary Hung for their assistance with the burning experiments and for keeping me company on the experimental burning days.

Special thanks to Hossein Rafipoor, who gave me support and practical suggestions. I must also thank my friends in Oxford, the Wolfson Secret Santa group (and other Wolfson friends), the Venneit girls, my fellow (current and former) D.Phil students, especially Tansy Branscombe and Dr Lorena Becerra-Valdivia, for their support.

Table of Contents

Abstract 3
List of Figures 14
List of Tables 20
Glossary 23
Symbols 23
Units 23
Abbreviations 24
Chemical Elements, Ion, and Compound Abbreviations 25
Lexicon 26
Chapter I: Introduction 28
I.1 Archaeological Background 30
I.2 Forensic Science Context 36
I.3 Ethnographic Background 38
I.4 Bone 41
I.4.1 Bone Diagenesis 46
I.4.1.1. Microbial Bioerosion 47
I.4.1.2 Mineral Degradation 49
I.4.1.3 Collagen Degradation 50
I.4.2 Heat-Induced Changes 53
I.5 Research Objectives 59
I.6 Thesis Structure and Outline 61
Chapter II: Materials and Methods 63
II.1 Materials 64
II.2 Fourier Transform Infrared Spectroscopy 66
II.2.1. Crystallinity Index or Splitting Factor 68
II.2.2 Other Calculated IR Ratios 69
II.3 Electron Microprobe Analysis 70
II.3.1 Preparation & Analysis 71
II.4 Sampling and Chemical Treatment for Collagen Extraction 73
II.5 Data Analysis & Statistics 74
II.5.1 Linear Regression 75
II.5.2 Coefficient of Variation 75
II.5.3 Dimensionality Reduction 76
II.5.3.3 Multivariate Analysis of Variance 80

II.5.4 Data Labelling Application 81
Chapter III: Paper 1-- Assessing the reliability of microbial bioerosion features in burnt bones: A novel approach using feature-labelling in histotaphonomical analysis 83
Abstract 84
III.1 Introduction 85
III.1.1 Histotaphonomic features in bone 87
III.1.2 Histology of Burnt Bone 93
III.2 Materials and Methods 94
III.2.1 Experiment 94
III.2.2 Analysis 97
III.3. Results 100
III.4. Discussion 107
III.5 Conclusions 114
Chapter IV: Paper 2 -- Physicochemical Changes in Bone Bioapatite During the Late Postmortem Interval Pre- and Post-Burning 116
Abstract 117
IV.1 Introduction 118
IV.1.1 Taphonomic Alterations to the Elemental Concentration and Structure of Bone 119
IV.1.2 Heat Changes to the Physicochemical Structure of Bone 122
IV.2 Materials and Methods 124
IV.2.1 Fourier Transform Infrared Spectroscopy (FTIR) 125
IV.2.2 Electron Microprobe Analysis (EMPA) 127
IV.2.3 Statistical Analysis 128
IV.3 Results 129
IV.3.1 FTIR Results 129
IV.3.2 WDS-EMP Results 134
IV.4 Discussion 142
IV.5 Conclusion 148
Supplementary Material 151
Chapter V: Paper 3 -- Determining the Postmortem Timing of Sharp Force Damage and Fractures in Burnt Bones 158
Abstract 159
V.1 Introduction 160
V.1.1 Fragmentation and Heat-Induced Fracturing 163
V.1.2 Perimortem vs Postmortem Damage 164
V.2 Materials and Methods 166
V.3 Results 173
V.3.1 Heat-induced Fracturing and Collagen Content 173
V.3.2 Perimortem and Postmortem SFT Features 175

V.4 Discussion 180
V.5 Conclusion 184
Chapter VI. Discussion and Conclusion 187
VI. 1 Early Diagenesis 192
VI. 2 Heat-Induced Changes 193
VI. 3 Diagenesis in Burnt Bones 195
VI.4 Limitations 196
VI. 5 Future Research 198
VI.5.1 Diagenetic Resistance 198
VI.5.2 Synthetic (Bio)apatite 200
VI.5.3 Collagen Distribution 201
VI. 6 Conclusion 201
Reference List 204
Appendixes 235
Appendix A: Proof-of-Concept Study 236
A.1 Introduction 236
A.2 Materials and Methods 237
A.2.2 Image Acquisition 241
A.2.3 Qualitative Analyses 243
A.2.4 Analytical Techniques 245
A.3 Results 249
A.4 Discussion and Conclusion 259
Appendix B: Végh, E. I., *et al.,* 2021. Assessing the reliability of microbial bioerosion features in burnt bones: A novel approach using feature-labelling in histotaphonomical analysis. Journal of Archaeological Science:Reports 37, 102906 261
Appendix B: Végh, E. I., *et al.,* 2022. Physicochemical Changes in Bone Bioapatite During the Late Postmortem Interval Pre- and Post-Burning. *Applied Spectroscopy.* https://doi.org/10.1177/00037028221085600 261
Appendix C: Histology Dataset 262
Appendix C.1: Dataset Generated from the Data Labelling Application 262
Appendix D: EMPA Data 370
Appendix D.1: EMPA Dataset 370
Appendix D.2: Removed Data from EMPA 405
Appendix D.3: EMPA Secondary Standards Data 409
Appendix D.4: Graphs of Elemental Concentrations 426
Appendix E: FTIR Data 451
Appendix E.1: IR Spectra 451
Appendix E.2: Frequencies of Interest 460
Appendix E.3: FTIR Measured Ratios 465

Appendix E.4: PCA Plots – FTIR & EMP 468
Appendix E.5: IR Spectroscopy Assignments 472
Appendix F: MANOVA of EMPA and FTIR Dataset 473
Appendix G: Images of Cutmarks 473
Appendix H: Permissions 474

List of Figures

Figure 1 – The structure of the cortical bone and the periosteum (Bartl and Bartl, 2016, 15, Fig. 2.1). 42

Figure 2 -- HAp crystal lattice highlighting the two different positions of phosphate ions (Bone Biology and Mechanics Lab – IUPUI).....43

Figure 3 -- The atomic structure of HAp as a stand-in for bioapatite (Supova, 2014, 548, Fig. 2). 44

Figure 4-- Research Questions of the thesis.....61

Figure 5 -- Schematic of the analytical methods used in the thesis. 64

Figure 6 -- IR spectrum of sample SWFR1_burnt between 800 and 400 cm-1. The crystallinity index or splitting factor (IRSF) was calculated by (A + B)/C), where the A, B and C represent the peak forming the base line. 69

Figure 7-- Example of the calculated carbonate to phosphate (C/P) ratio calculated by A/B on sample SWF5D1Y1_unburnt. The other ratios mentioned were calculated using the same formula. 70

Figure 8 -- Burning of the 14- and 34-day postmortem bones on the pyre. Upper image was taken subsequently after the ignition of the fire, while the lower was taken when the bones have calcined. All outdoor fires were executed in the same manner. The pyres were built on a flat clearing, using bricks to provide support for a wire mesh holding the bones, as well as partial protection from the wind. While offering less control over temperature rather than a furnace, the use of an outdoor fire better reflects real-world conditions due to the more variable temperatures of the fire, and the influence of the wind. Each fire was built and maintained in the same manner, using a mixture of hard and soft woods as fuel.....96

Figure 9 -- Criteria for labelling microbial bioerosion from Brönnimann et al., 2018. 1) Budded MFD; 2) Linear longitudinal MFD; 3) Lamellate MFD; 4) Wedl tunnelling; 5) Wedl 2; 6) Cyanobacterial tunnelling (Brönnimann et al., 2018, 46, Fig. 4). Features that appeared to be similar to linear MFD were not labelled in this study, because they were caused by burning. 99

Figure 10-- Variation of features appearing to be tunnels in the different samples. **A** and **B** are of Volkmann's canals, **C** and **D** are unidentified channels and hence were labelled having the appearance of features consistent with 'cyanobacterial tunnelling', even though there is no clear indication of cyanobacteria being present in a terrestrial context, and the tunnel in **D** appears to be connected to a Haversian canal. The features are indicated by the blue arrows. Note the differences in the width of the tunnels. In the literature, maximum tunnel diameters caused by microorganisms have been reported to be between 0.1 and 2.0 micron (terrestrial), 7-18 microns (freshwater), and 5-19 microns (marine, (Pesquero et al., 2018)). Here, diameters under 20 microns were considered to be 'cyanobacterial tunnelling', while >20 microns were classed as Volkmann's canals. (Transmitted light microscopy, 50x, from left to right: WSF2D2W5_unburnt, WSF2D2W5_burnt, WSF1D1M2_unburnt, WSF1D1M2_burnt).....99

Figure 11 -- The average presence of the taphonomic features at each stage of decomposition before (upper) and after (lower) burning. 102

Figure 12 -- Backscattered electron image of one of the 1-month postmortem unburnt bones (WSF5D1M3_unburnt). Note the brighter (hypermineralised) areas around the black (demineralised) 'tunnels' toward the lower end of the image. These bright areas are in fact not due to bioerosion, but to heavy mineral loading in growing individuals where osteonal bone has not replaced the primary lamellar bone.....105

Figure 13**A** and **B** -- Backscattered electron image of 3-month postmortem unburnt bone (WSF3D3M3_unburnt). Note the accumulation of darker (demineralised) circular areas (appearing to be 'Wedl 2' or enlarged canaliculi, but probably naturally demineralised primary

bone with microcracks) with bright (hypermineralised) areas around. **C**: Transmitted light microscopy image of a thin section from the same sample (WSF3D3M3_unburnt) at 400x magnification.....106
Figure 14 -- Staining of the osteocyte-canalicular network that appears to be Wedl type 2 on one of the fresh burnt control bones (SWF1FR2_burnt_1). The tunnels were labelled 'blind' as 'cyanobacterial tunnelling', but these are Volkmann's canals. Neither of these features should be present on freshly burnt bones. Transmission light microscopy, 100x magnification.....108
Figure 15 -- Staining that appears to be 'Wedl 2'. While it is restricted to some canaliculi on the unburnt 6-months postmortem section (left), it affects all osteons on the same burnt bone (right). 'Wedl type 2' features are probably due to discolouration on the freshly burnt bones. The source of discolouration can be: (1) sooting from combustion gasses infiltrating the osteocyte-canalicular network after most of the organic matter has burnt out; or (2) iron, manganese, or other metal ions infiltrating the osteocyte-canalicular network prior to burning and then reduced to darker species, such as manganese dioxide or magnetite, when the bones were burnt. While the pig tibiae were not buried, those that were exposed for sufficiently long did become partly covered in soil, which may have presented the opportunity for the infiltration of metal ions. (Sample WSF5D6M1_1, transmission light microscopy, 100x magnification).....108
Figure 16 -- Features resembling 'budded MFD' from a 6-months postmortem burnt bone (WSF5D6M3_burnt). Transmitted light microscopy (50x).....109
Figure 17 -- Contrast differences due to burning of a 6-month decayed bone sample (WSF5D6M1_burnt). Note the central mineralised areas. (Electron microprobe, backscatter electron detector image.).....113
Figure 18 -- The FTIR spectra of the means of each PMI group before (upper image) and after (lower image) burning. Labelled are the peak assignments of interest.....130

Figure 19-- Loadings of the principal component analysis when using both the FTIR and EMP dataset.....134
Figure 20 -- Average elemental concentration (wt %) of the experimental bones using the EMPA data. Mean ± 2 standard errors for each measured element as a function of time in unburnt (blue) and burnt (orange) bone. 135
Figure 21 – Average elemental concentration (wt %) of the Neolithic cremated human remains for each zone. Mean ± 2 standard errors for each measured major and trace element in archaeological cremated bone. The backscattered electron microscopy (BSEM) image represents an example of a bone cross section.....136
Figure 22 -- Potassium wt% content in experimental unburnt (upper) and burnt (lower) bone by zone. 139
Figure 23 --Linear discriminant analysis (LDA) on the EMPA dataset. **A**: Separation of unburnt and burnt bone by LDA. Contributions: 'Al2O3': 0.244, 'CaO': -6.882,'Cl': 3.216,'FeO': 0.07,'K2O': 0.607,'MgO':-1.036,'MnO': -0.056, 'Na2O': -0.545,'P2O5': -3.97,'SiO2': -0.902,'SrO': 0.199, 'Total': 13.08. **B:** Clusters created by LDA of the unburnt (left) and burnt (right) PMI groups.....141
Figure 24 -- **A:** An example of a fleshed tibia subjected to sharp force trauma. The skin was carefully cut through and then each incision was produced on the bone itself. **B:** One of the 14-day PMI tibia cut with the same implements. 168
Figure 25--The instruments used for the SFT infliction. **A**: The combat knife (Gerber, USA) used for all knife-related wounds. The knife is comprised of a single edged, non-serrated upper part and a partially serrated part. Both parts had a single edge bevel on the left side. There is a total of 11 serrations of the knife with four patterned double serrations (4.8 mm each). The non-serrated gaps are 5.5 mm long. **B:** The single edged flint blade, which was produced for this

study. The blade's cutting surface is wider than that of the knife, while the width from the point of bevelling is larger.....169
Figure 26-- **A:** The bones soon after the fire was lit. While the two bones in the middle started charring, the other bones are yet to be altered to the same level. **B:** 2.5 h after the start of the outdoor fire, most bones turned white.....171
Figure 27 --The percentage of cutmarks preserved post-burning as a function of time. A cutmark was counted as present if any portion of the kerf was present. F = flint blade, NK = non-serrated knife, SK = partially-serrated knife.....174
Figure 28 -- Fracture severity (number of fragments per bone post-burning) of bones post-burning. 174
Figure 29 -- The percentage of perimortem and postmortem SFT features as a function of time (days) on the kerfs. Hues show the different instruments the trauma was inflicted by – black: flint (F), darker grey: non-serrated grey (NK), lighter grey: partially-serrated knife (SK). **A**: The presence of irregular edges on cutmarks (perimortem feature); **B:** presence of curling or uplifting on the edges of the cutmarks (perimortem feature); **C:** presence of regular shaped edges on cutmarks (postmortem feature); **D:** presence of splintering on cutmarks (perimortem feature); **E:** presence of sharp edges on cutmarks (postmortem feature); **F:** presence of crumbling on cutmarks (postmortem), which did not change significantly with PMI. 177
Figure 30 -- Examples of changes in kerf outline with a particular attention to the kerf edges. All SFT was inflicted by the same instrument, a partially-serrated knife (SK). **A:** Burnt 14-day cutmark (WSF2D2W3_SK2). Note the irregular edges, curling or uplifting at the edges, and splintering; **B:** Burnt 180-day cutmark (WSF5D6M4_SK3). Note the regular shaped and sharp edges, the loss of the irregularity and the still present curling or uplifting at the edges. **C:** Burnt 365-day cutmark (SWF5D1Y1_SK4). It exhibits regular shaped and sharp edges, without irregularity and curling or uplifting.....179

Figure 31-- The observable difference between SFT inflicted by the non-serrated knife and a heat-induced fracture (middle) on a 91-day PMI burnt bone (WSF3D3M3). From left to right: NK4, heat-induced fracture, NK3 (light microscopy image).....183
Figure 32 -- Research questions and answers. 189
Figure 33 – Example of the SFT present on a four-year weathered bone (C1). Weapons used from right to left: non-serrated knife, partially serrated knife, flint blade (five incisions per weapon). 238
Figure 34 – The ceramics kiln used for the control experiment. 239
Figure 35 – The thermocouple is fixed onto the bone kept in place by the bricks. The bricks also served an insulating purpose to keep the heat inside the kiln. 239
Figure 36 – The fully fleshed bone (C5) blazes after an hour in the kiln. 240
Figure 37 -- The striations noted on the pre-burnt cutmarks. It was not possible to observe striations on the kerfs of partially fleshed and fully fleshed bones, because these were hidden by soft tissue. (Notation: C1 and C3: 5-year PMI bones; C2: 5.5 kya bone; C4: fresh defleshed bone; C5: fresh fleshed bone; NK= non-serrated knife; SK= partially-serrated knife; F=flint blade).....250
Figure 38 – Striation features observed on the post-burnt kerfs (notation: C1 and C3: 5-year PMI bones; C2: 5.5 kya bone; C4: fresh defleshed bone; C5: fresh fleshed bone; NK= non-serrated knife; SK= partially-serrated knife; F=flint blade).....250
Figure 39 – Qualitative traits observed on the unburnt control kerfs (Notation: C1 and C3: 5-year PMI bones; C2: 5.5 kya bone; C4: fresh defleshed bone; C5: fresh fleshed bone; NK= non-serrated knife; SK= partially-serrated knife; F=flint blade).....251
Figure 40 – The qualitative features observed on the burnt control cutmarks (Notation: C1 and C3: 5-year PMI bones; C2: 5.5 kya bone; C4: fresh defleshed bone; C5: fresh fleshed bone; NK= non-serrated knife; SK= partially-serrated knife; F=flint blade). 251

Figure 41 – Graph showing the presence or absence of the peri-mortem features observed on the cutmarks proposed by the literature. The left side shows the presence of these features on the cutmarks before burning, and the right side shows the same features post-burning. (Notation: C1 and C3: 5-year PMI bones; C2: 5.5 kya bone; C4: fresh defleshed bone; C5: fresh fleshed bone; NK= non-serrated knife; SK= partially-serrated knife; F=flint blade). 253
Figure 42 - Graph showing the presence or absence of the peri-mortem features observed on the cutmarks proposed by the literature. The left side shows the presence of these features on the cutmarks before burning, and the right side shows the same features post-burning. (Notation: C1 and C3: 5-year PMI bones; C2: 5.5 kya bone; C4: fresh defleshed bone; C5: fresh fleshed bone; NK= non-serrated knife; SK= partially-serrated knife; F=flint blade). 254
Figure 43 – XRD results of the fleshed bone (C5) pre-burnt (black line) and post-burnt (red line). Note the sharper peaks in values post-burning, representing a more crystalline state of hydroxyapatite.....258
Figure 44 – The X-ray diffractrogram of the 5.5 ka archaeological cow bone (C2). Red = post-burnt, black = pre-burnt. Note the additional SiO_2 phase.....259

List of Tables

Table 1-- The reported elemental concentration of bone after Elliott 2002, 430. ±1% variability can happen due to diet, age, and anatomical variation.....46
Table 2 --Microbial bioerosion features, their thought to be causative agents, contexts and environments in the literature.....89
Table 3--Identical histotaphonomic features named differently across the literature. 92
Table 4 -- Histomorphometric and histomorphology changes of burnt bone in the literature. 94

Table 5 -- Correlation Coefficient ('r') and p-value ('p') for each analysed feature on the unburnt and burnt bones. H_0= Presence (in %) of X feature per bone does not change with postmortem time period. ** indicates significant p-values.....103

Table 6 -- Coefficients of variation for each feature on the grouped samples by postmortem period and state of burning.....104

Table 7 -- Analysis of compositional images. 104

Table 8 -- The coefficient of variation (CV) and detection limits (D.L.) of the measured major and trace elements in the secondary standards.....128

Table 9 -- Identified zones of interest and their associated absorption changes on the unburnt and burnt bones. 132

Table 10 – Linear regression and multivariate comparison test (MCT) on the FTIR dataset. Correlation Coefficient ('r') and p-value ('p') for each analysed FTIR parameter on the unburnt and burnt bone in the linear regression section. H_0= X parameter does not increase with postmortem time period. ** indicates significant p-values. The MCT section shows the results of the MANOVA and multivariate comparison testing on the established FTIR ratios as a function of state (unburnt vs. burnt) and time.....133

Table 11 – Linear regression and multivariate comparison test on the EMPA data. Correlation Coefficient ('r') and p-value ('p') are given for each analysed element in unburnt and burnt bone for the linear regression. H_0= X parameter does not increase with postmortem time period. ** indicates significant p-values. HC = around vascular canals; OC = outer cortical; MC = mid-cortical; IC = inner cortical zones. In the multivariate comparison test, p values are derived from both MANOVA and multivariate comparison testing. 138

Table 12 -- Dimensions of the instruments used in this study. NK=non-serrated knife; SK=partially serrated knife, F=flint blade. All instruments were used in a cutting motion. ..170

Table 13 -- The timing of trauma (perimortem vs postmortem) specific features used for the qualitative analysis of the kerfs. 172

Table 14 -- The retained collagen in unburnt bone at different PMIs. 175

Table 15 -- The linear regression results on the perimortem and postmortem SFT features. Significant p-values are bold. 176

Table 16 -- The significant results of the multiple comparison of means when all SFT instruments are considered. 180

Table 17 – Qualitative Features examined on the cutmarks for diagnostic features of timing ('perimortem' vs postmortem trauma) and for instrument classification. 243

Table 18 – Table summarising the presence of absence of the macroscopic heat related fractures on the bones involved in the control study.....255

Table 19 – The investigated FTIR ratios in the pre- and post-burnt bones. 256

Table 20 – Coherence lengths in Å from the XRD data in the pre- and post-burnt bones.....257

Glossary

Symbols

$<$	Less than
$>$	Greater than
$\leq$	Less than or equal to
$\geq$	More than or equal to
A	absorption
H_0	Null hypothesis
p	p-value
r	correlation coefficient, which measures the strength and direction of a linear relationship between two variables on a scatterplot
α	alpha
β	beta
θ	theta (diffraction angle)
λ	lambda (X-radiation wavelength)

Units

%	percent
°C	degree Celsius (or Centigrade)
Å	angstrom (10^{-10} m)
cm	centimetre
cm^{-1}	wavenumber
g	gram
l	litre
m	metre
mg	milligram
ml	millilitre
mm	millimetre
ppm	parts per million
wt %	weight percent
µm	micron (micrometre)

Abbreviations

ANOVA	one-way analysis of variance
API	Type A carbonate to phosphate ratio (FTIR)
APR	Amide to phosphate ratio (FTIR)
ATR	Attenuated total reflection mode used with FTIR
BPI	Type B carbonate to phosphate ratio (FTIR)
BSEM	Backscattered electron microscopy
C/P	carbonate to phosphate molar ratio (FTIR)
Ca/P	calcium to phosphate molar ratio
cal BP	Calibrated years before 1950 (at 95.4% confidence)
CN/P	Cyanamide to phosphate (FTIR)
CO/CO_3	Carbonyl to carbonate ratio (FTIR)
DNA	deoxyribonucleic acid
EDS	Energy-dispersive X-ray spectroscopy
EMP	Electron microprobe
EMPA	Electron microprobe analysis
F	Flint blade
FTIR	Fourier transform infrared spectroscopy
HAp	Hydroxy(l)apatite
HC	Around Haversian canals/vascular canals of bone cross-section
IC	Inner cortical zone of bone cross-section
IR	infrared
IRSF	Infrared splitting factor / crystallinity index
ka	*kilo annum* or thousands of years (ago)
LDA	Linear discriminant analysis
MANOVA	Multivariate comparison of means test
MC	Mid-cortical zone of bone cross-section
MCT	Multivariate comparison of mean test
N/P	Amide I to phosphate ratio (FTIR)
NK	Non-serrated knife
OC	Outer cortical zone of bone cross-section
PCA	Principal component analysis
PHT	phosphate high temperature
PTM	Posttranslational modification
REE	Rare earth elements
SEM	Scanning electron microscopy
SFT	Sharp force trauma/damage
SK	Partially-serrated knife
TeTCP	tetracalcium phosphate
v	vibration
WDS	Wavelength-dispersive X-ray spectroscopy

XRD	X-ray diffraction
ya	Years ago
β-TCP	beta-tricalcium phosphate

Chemical Elements, Ion, and Compound Abbreviations

Al	aluminium
Al_2O_3	aluminium oxide
C	carbon
Ca	calcium
Ca^{2+}	calcium ion
$CaCO_3$	calcium carbonate
CaO	calcium oxide
Cl	chlorine
CN_2^{2-}	cyanamide
CO_2	carbon dioxide
CO_3	carbonate
CO_3^{2-}	carbonate ion
F	fluorine
Fe	iron
FeO	iron oxide
H	hydrogen
K	potassium
K_2O	potassium oxide
Mg	magnesium
MgO	magnesium oxide
Mn	manganese
MnO	manganese(II) oxide
N	nitrogen
Na	sodium
Na_2O	sodium oxide
O	oxygen
O^{2-}	oxygen ion
OH^-	hydroxide
P	phosphorus
P_2O_5	phosphorus pentoxide
PO_4^{3-}	phosphate ion
Si	silicon
SiO_2	silicon dioxide
Sr	strontium

SrO	strontium oxide
KBr	potassium bromide

Lexicon

Adsorption	The adhesion of atoms/ions/molecules to a solid surface, creating a film of the adsorbate.
Bioapatite	Mineral fraction of bone, non-stoichiometric but similar composition and structure to hydroxyapatite (less crystalline than HAp)
Burnt bone	Bone heated in a fire (flame) or in a furnace (only heat)
Calcination	Heated bone to a point when all organic matter and lattice water has left from the bone and when bioapatite had recrystallised. Bone is thought to be fully calcined when it turns white in colour and makes a 'glass-like' or 'fine china' like sound when touched together.
Charred bone	Heated bone (black or grey) to temperatures that allows some organic matter and structural water to disappear but a considerable amount to still be present.
Cremation	The funerary rite of burning the dead
Crystallinity	An indication of crystal size and strain (defect) in apatite. High crystallinity refers to large crystals and low strain and poor crystallinity refers to smaller crystals and larger strain.
Diagenesis (bone)	Physical and chemical changes to bone after death
Diaphysis	The shaft of a long bone
Fossil	The resulting mineral phase from long-term diagenesis
Hydroxy(l)apatite	(HAp) stoichiometric hexagonal crystalline material made out of calcium phosphate
Kerf	A slit or notch made by a sharp force instrument
Putrefaction	The process of decay or rotting of the organic matter in a system.

Stoichiometry	The quantitative relationship between constituents in a chemical substance
Stoichiometry of HAp	Ca/P ratio of 1.67
Substitution	A chemical reaction in which an atom(s), ion(s), or molecule(s) is replaced by another atom(s), ion(s), or molecule(s)
Taphonomy (bone)	The transition of organic remains from the biosphere into the lithosphere as a result of geological, biological, and chemical processes (Lyman, 1994; Haglund and Sorg, 2006)
Thermodynamic stability	A system is in its lowest energy state or in chemical equilibrium with its environment
Warping	Heat-induced shape change in bone

Chapter I: Introduction

Bone is a complex, composite material that goes through continuous modifications during life and after death. Human remains subjected to some form of heat-treatment are frequently recovered from archaeological sites and modern crime scenes. In fact, before the rise of Christianity in Europe, cremation was the dominant funerary practice in many cultures (Kuijt *et al.*, 2014; Schmidt and Symes, 2015). The first evidence of cremation is found in Lake Mungo, Australia, and dates back to circa 30,000 BP (Bowler *et al.*, 1970). Funerary archaeology is an important aspect of archaeology to reconstruct the past, since burial customs represent a crucial source of information, and in some spatiotemporal contexts the only one (Alekshin *et al.*, 1984). Heat affecting human remains, and in particular the skeleton, can take place in accidental fires, funerary rites, in cases of homicide, suicide, forest fires, explosions, or bombings (Schmidt and Symes, 2005; Fairgrieve, 2008; Thompson, 2015). Although it is impossible to completely destroy a skeleton solely by fire (Bass, 1984), bone goes through a drastic series of modifications and is usually left shrunk, warped, discoloured, and fragmented after the fire event (Shipman *et al.*, 1984; Fairgrieve, 2008; Ellingham *et al.*, 2015). The alterations burning cause to bone compromise traditional methods used by osteologists/bioarchaeologists/forensic anthropologists to identify the deceased or learn more about an individual or population's life history. Standard methods, such as biological profile estimation, DNA analysis, and other biomolecular methods are difficult if not impossible to attempt on burnt bones (Ubelaker, 2009). Due to these limitations, it was often the case that archaeological cremated human remains were collected but otherwise neglected, usually laying dormant in museum and University collections, which reflect a huge body of unexplored archaeological material.

The skeleton can be burnt subsequently after death or at various stages of decomposition. There is evidence of burning of human remains years after death in medicolegal cases (Bontrager and Nawrocki, 2008; Garrido-Varas and Intriago-Leiva, 2015) and practices involving burning or cremating the dead once soft tissue had decomposed have been proposed for prehistoric societies across Western and North Western Europe (Wells, 1962, 1978; Chesterman, 1979; Renfrew, 1979; Grévin *et al.*, 1991; Mckinley, 1994, 1999, 2008; McKinley, 2000; Murphy, 2003; Lee, 2006; Dowd, 2008; Smith and Brickley, 2009; Cooney, 2014). A considerable amount of research has attempted to distinguish between bones burnt in a fresh or dried state based on (what was thought to be diagnostic) heat-induced fracture patterns (Baby, 1954; Binford, 1963; Buikstra and Swegle, 1989; Spennemann and Colley, 1989; Etxeberria, 1994; Whyte, 2001; Thompson, 2005; Gonçalves *et al.*, 2011). Considering the amount of academic and medicolegal interest in establishing when bone was burnt compared to the time of death, this thesis uses histology, elemental composition, investigation into structure, and bone's reaction to trauma/damage to elucidate this question. The understanding of how cultures treat their dead is of utmost importance to appreciate the underlying mechanisms in a society, such as the relationship between the living and the dead. Since for a vast portion of the human past cremation was the dominant funerary rite, the pre-cremation treatment of the dead and the time of cremation are invisible for archaeologists. If evidence for the processing of the dead prior to cremation could be identified, it would open a whole new social dimension and understanding of funerary rites in archaeology.

I.1 Archaeological Background

There has been a notable interest in excarnated/defleshed human remains in prehistoric Britain (Carr and Knüsel, 1997; Booth and Madgwick, 2016; Booth and Brück, 2020) as a form of post-processing of the dead. Disarticulated bones might have resulted from: (1) active

excarnation; (2) exhumed bones from old primary burials; or (3) passive excarnation or defleshing through subaerial exposure (Booth and Brück, 2020). It has been argued that excarnation was the most common way to dispose of the dead during the Late Bronze Age and throughout the Iron Age in Southern Britain (Carr and Knüsel, 1997). Radiocarbon dates obtained for unburnt disarticulated human bones from Bronze and early Iron Age sites in Britain have shown that these curated bones were already between a few decades and up to 200 years (in some cases) older than the primary burials they were deposited in (Booth and Brück, 2020). However, in this study the radiocarbon dated remains were not sampled from the same stratigraphic context and thus the offset of the different dates are most probably due to the marine reservoir effect, general uncertainties in radiocarbon dating, and/or calibration processes. Although the authors mention the reservoir effect, it is concluded that the offset is not due to a marine diet because of the obtained $\Delta^{13}C$ values from the accelerator mass spectrometry (AMS). However, AMS produced $\Delta^{13}C$ values should not be used for dietary investigations, as these values should always be measured from the IRMS, because this technique uses the isotope anchor points (standards) as opposed to the AMS [cf.(Szpak *et al.*, 2017)]. In Booth and Brück's (2020) study, no connection between funerary treatment and bone curation was established, which suggests that these were separate practices. Thus, after curation of the bones, cremation as a funerary rite could follow, as the next stage of the post-processing of the dead.

In prehistoric sites from various geographical locations (e.g. Ireland, Scotland, England, France) with cremated bones, archaeologists have suspected that the human remains were not burnt immediately after death. In a Maeshowe type tomb at Quanterness, Mainland Orkney, Scotland, a remarkable amount of bone fragments (>12,000) were discovered with disarticulated well-preserved unburnt fragments next to 'unrecognisable' burnt ones (Chesterman, 1979). It was originally suspected that the human remains were exposed to the

natural environment or buried in sand and after the decomposition of the soft tissues they were cremated, broken into pieces, and brought to the tomb (Chesterman, 1979; Renfrew, 1979). Re-examination of the unburnt remains from this site suggested that these bones were 'ancestral' remains deposited in earlier monuments and then being brought to Quanterness later (Richards, 1988). The excarnation of these unburnt remains was later questioned based on the lack of archaeological signatures of exposure, such as signs of animal gnawing, weathering, and/or disarticulation, and incompleteness in skeletal elements present (Schulting *et al.*, 2010). However, patterns of carnivore modifications and weathering might be ambiguous as their presence is dependent on the amount of time the dead would be exposed and the amount of protection provided during the exposure phase (Booth and Brück, 2020).

At several funerary Neolithic, Bronze Age, and early Iron Age sites in South West England, human remains have been identified to be charred or burnt at 'a dry or close to dry' state (Mckinley 1994, 76) and probably when already fragmented at Hambledon Hill, Dorset (Mckinley, 2008), West Kennet long barrow, Wiltshire (Piggott, 1962; Wells, 1962), Haddenham, Buckinghamshire (Lee, 2006), Potterne, Wiltshire (Mckinley, 2000), and Ham Hill, Somerset (Mckinley, 1999). McKinley (1994; 1999; 2000; 2008) interpreted these bones as being burnt at a dry state based on the varying levels of oxidation (colour change), lack of articulation, and fragmentation. Often the representation of disarticulated human individuals, their modifications, and the way they were deposited suggest prior excarnation of the dead in inhumed remains (Booth and Brück, 2020). Additionally, the insufficient weight of cremated bone deposits and the commingled disarticulated unburnt and cremated bones deposited in waterholes and settlements suggests that potentially cremated remains were pre-processed prior to cremation as well (Booth and Brück, 2020). The rationale behind such treatment of the dead is unknown, but it is thought to be due to 'ritual' or incidental burning (Mckinley, 2000, 2008).

In Neolithic and Bronze Age Irish tombs, such as those of the Boyne Valley and Fourknocks, and caves such as at Kilgreany (Waterman 1978; Dowd, 2008; Cooney, 2014), excavators also suspected that human bodies were either passively or actively excarnated before inhumation and cremation. This means that the bodies were left exposed for an unknown period of time, or the soft tissues were actively removed with implements, before further rituals. At sites such as Tully in Ireland, it has been claimed that the fully fleshed body was burnt (Wells 1978). Neither of these claims were supported by further reasoning, but presumably they were based on the presence or absence of heat-induced fracturing, such as the previously mentioned thumbnail fractures and warping. If the body was actively excarnated through dismemberment and defleshing prior to cremation, signs of sharp force trauma/damage should be present on the burnt bones. A few Bronze Age human remains revealed cutmarks (Booth and Brück, 2020) and excarnation as a funerary right might have continued into the Roman period in Britain (Carr, 2007), as suspected from a defleshed skull displaying cutmarks and perforations (Niblett, 1999). This cranium, with the mandible and teeth removed, was recovered with 14 other disarticulated human bones on the periphery of a 2nd century AD cremation cemetery at Folly lane, St Albans (*ibid*). Due to the presence of cutmarks, active excarnation has also been proposed in the human remains found in the Neolithic and Bronze Age British Isles at Kilgreany cave (Dowd, 2015) and Millin Bay passage tomb in Ireland (Murphy, 2003), and at Adlestrop and West Tump in England (Smith and Brickley, 2009). Active defleshing was suggested to follow passive excarnation (exposure), because it is easier to remove the flesh once the soft tissues have decomposed to some degree (Carr, 2007).

According to Niblett (1999), there are four reasons why it is necessary for the deceased to lie in a mortuary chamber prior to cremation: (1) to house the body until the season comes when the funeral can take place; (2) to allow time and place for the initial rites; (3) to house the body while mourners and family members can pay their respect; and (4) to provide time and place

for the excarnation before the final cremation. The bones were not well preserved enough at Folly Lane to determine how long the bodies 'waited' for cremation. Based on weathering, Niblett (1999) assumes that cremation might have taken place five, ten, or twenty years after the death of the deceased. However, this interpretation is questionable, because heat conceals and causes colour changes and delamination, which are features examined when determining stages of weathering in bones [cf. (Behrensmeyer, 1978)]. Another recurrent argument given for the co-existence of excarnation and cremation in the Early Iron Age Britain is that only <5% of the population is accounted for in excavated cemeteries (Carr and Knüsel, 1997; Carr, 2007), even though those remains were recovered from deposited features that allowed the bones to survive. Passively excarnated, exposed bodies might have been removed by natural agencies (e.g. animal predators), which might be one of the reasons only a small amount of the estimated population is recovered from excavations (Carr, 2007). Furthermore, even the lesser amount of individuals recovered often represent only a few body parts in both inhumation and cremation burials in Iron Age Britain (McKinley, 2000; Carr, 2007). In cremation deposits the presence or absence of the whole skeleton is assessed by the weight of the cremated bone fragments which is often recovered with general pyre debris. If this debris is present, it suggests that the whole of the cremated body was moved from the pyre and specific bone elements were not handpicked for deposition (Fitzpatrick and Powell, 1997).

Examples of suspected passive or active excarnation before cremation outside of the British Isles are present in Late Iron Age cemeteries in Luxembourg and France (Grévin *et al.*, 1991; Lambot *et al.*, 1994). Some of the evidence presented for this come from the modification to material culture, rather than to the bones. For example, in the cemetery of Lamadelaine (Titelberg, Luxembourg) surface exposure of the remains was suspected based on the corrosion and fragmentation of iron fibulae before being burnt (Metzler-Zens *et al.*, 1999). Similar examples are found at Thugny-Trugny, (Ardennes, France) where the existence of a shrine in

the centre of the cemetery enclosure was suggested to have housed the deceased before cremation (Lambot *et al.*, 1994).

Other cutmarks on bones could be caused by intentional trauma and violent actions. While most perimortem trauma seen on skeletons from the Neolithic are blunt force or chopping traumas caused by clubs or stone axes (Schulting, 2012) in the Bronze and Iron Ages sharp force trauma appears as well. A limited number of qualitative features have previously been proposed to have potential for differentiating cutmarks inflicted on wet (i.e. fresh) bone and dry bone (Crowder *et al.*, 2013). These include irregular edges, curling or uplifting at edges, splintering at breaks of cutmarks for wet bone features, and regular shaped cuts, sharp-edged, and discoloured kerfs[1] for dry bone features (Crowder *et al.*, 2013).

Although the previously mentioned studies have only provided visual assessment as a methodology to assess whether the bones were cremated after passive or active excarnation, Grévin *et al.* (1991) did argue to have found supporting evidence of human remains burnt once they had already decomposed at the Bronze Age site of Pincevent, France. The authors proposed that the bones were buried weeks to months prior to cremation based on the postmortem bacterial attack on bone microradiographs (Grévin *et al.*, 1991). Microbial bioerosion was previously proposed to have the potential to differentiate between bones that decomposed with soft tissue and defleshed bones in unburnt bones (e.g. Jans *et al.* 2004; White and Booth 2014). However, to date there is no scientific consensus on the same in burnt bone, thus the use of histotaphonomy is tested in Chapter III in this thesis.

It is likely that excarnation took place in many cultural contexts in inhumed bodies during prehistory and the Roman era. Cremation was present in Central-Southern England, where excarnation was allegedly common. Excarnation was also found in the South of England, the heartland of cremations (Carr and Knüsel, 1997; Carr, 2007). If a signal for decomposition

1 The slit or cutmark produced by a sharp force implement.

could be found that survives burning, it would be possible to estimate the time elapsed between death and cremation in archaeological bone. This would elucidate our understanding of how past cultures handled their dead. In case excarnation was not used for the purposes of curation of the dead, it is possible that past populations gathered human bodies to cremate them together to save resources or to wait for a season adequate for cremation. This has, so far, been impossible to prove in archaeology, as well as why excarnation would take place and why these individuals would be treated in such ways. There have been several theories about the purpose and subjects of excarnation: sacrifice, unnatural or unclean death, death of the outcasts, killing, warfare trophies, massacres, or simply, the ancestors (Carr, 2007). All these theoretical and applied archaeological studies are questionable and show the need to obtain more information about how the dead were treated prior to cremation. Clearly, the way bone is transformed after death, before, during and after cremation (i.e., bone diagenesis) holds the key to characterize the timeline around individuals' cremations, hence it is aimed in this thesis to put it on a more rigorous footing.

I.2 Forensic Science Context

Narrowing down the missing persons list by tracing the biological profiles of skeletons is one of the primary tasks of forensic anthropologists (Dirkmaat *et al.*, 2012). Parameters of a biological profile (sex, age-at-death, stature, ancestry) can be assessed by morphological or osteometric approaches with varying error rates. However, these approaches cannot typically be applied in burnt bone due the severe deformation caused by heat (Randolph-Quinney, 2014b, 2014a). Burning of a body has been used in forensic cases as a way in which the perpetrator attempts to dispose of the body, mask any identification features of the deceased and cover up any evidence of trauma and thus manner and cause of death (Fairgrieve, 2008). Assessment of the circumstances of death are significantly harder if the victim has been subjected to fire

(Symes *et al.*, 2012). Typically, burnt human remains in a clandestine context occur in an outdoor fire, building fire, or car crashes. Cremation burials, when the body or bones are relocated to another site, burnt, and buried, are another criminally-based context as well as setting forest fires to conceal a homicide (Fairgrieve, 2008). Vehicular accidents and aircraft crashes often produce charred bones, demonstrating hot, intense fire for a short duration (Stratton and Beattie, 1999; Fairgrieve, 2008). In a fire scene, the context of the fire is as important as the burnt human remains themselves. Thus, other than recognising burnt human remains, the documentation of the context, accurate recovery, and the application of proper techniques to analyse the remains are all crucial (Fairgrieve, 2008).

If burnt human remains are recovered from a criminally-based context there is a possibility that some type of trauma is available for analysis on the bone. Thus, understanding the difference between heat-induced fracturing and manually induced trauma prior to burning has a profound effect on a forensic investigation (Pope and Smith, 2004; Fairgrieve, 2008; Ubelaker, 2009; Poppa *et al.*, 2011; Végh and Rando, 2017; Alunni *et al.*, 2018). Heat-induced fractures have a characteristic pattern. Indications of perimortem sharp force trauma (SFT) on burnt bone includes sharp margins, kerf walls, blade striae, and sheering of cortical and cancellous bone (Herrmann and Bennett, 1999). Blunt force trauma (BFT) displays diverse fracture patterns and different patterns of fracture propagation than heat-induced fractures (Piekarski, 1970). Gunshot wounds show bevelling, radiating and concentric fractures as opposed to the above-mentioned patterns of heat-induced fractures (Herrmann and Bennett, 1999).

An indication of whether the body was burnt subsequently after death or once it had partially decomposed would potentially allow a burning event to be contextualised. For example, establishing the PMI before the burning of the body would allow investigators to establish the *terminus ante quem,* allowing the reconstruction of the circumstances of the death. There are a

few cases discussed in the forensic anthropological literature where a single individual has been found with differential preservation: parts of the skeleton was burnt while the other part was at various stages of decomposition (Bontrager and Nawrocki, 2008; Garrido-Varas and Intriago-Leiva, 2015). One of these cases involved scattered human remains found in a forest in Chile (Garrido-Varas and Intriago-Leiva, 2015). Parts of the skeleton were burnt and found in a fire pit, while the rest were recovered with considerable amounts of soft tissue. Both the burnt and the unaltered bones presented signs of post-mortem consumption by carnivores. The pattern of burning on the bones did not line up with the normal pattern of thermal destruction of bones (Symes *et al.*, 2008). Based on this evidence, Garrido-Varas and Intriago-Leiva (2015) concluded that the body was burnt post-mortem and the time since death was established as less than 3 years before the discovery of the remains. Although signs of gnawing and patterned thermal destruction together can help conclude when the body was burnt, both burnt and unburnt remains are rarely available for analysis to reach such conclusions in forensic cases and all we are left with is fragmented burnt remains. Contextualising the fire event would be invaluable to confirm or contest witness statement and establishing the intent of the perpetrator. Thus, there is need for better and more accurate methods to determine when the body was burnt compared to the time of death from a single burnt bone fragment.

I.3 Ethnographic Background

Ethnographic and historic information might be of use to clarify funerary behaviours in archaeology. There are ethnographic evidence and historic accounts outlining the variety of practices associated with cremation (Ward and Tayles, 2015). The display of the deceased, and in turn the preceding decomposition of the body prior to cremation has been documented in South East Asia. In historic Thailand a variety of practices are associated with cremation and the preceding treatment of the body depends on the life and death history, as well as the status and wealth of the deceased (Ward and Tayles, 2015). Thus, if the individual had a ‘good’ death

(i.e. due to chronic illness or old age), the body was exposed and displayed to the mourners for a period. If the deceased had a 'bad' death (i.e. violent), the body was burnt immediately after death. In case of a 'good' death and if the family was poorer, the deceased was displayed for only 7 days, while in a wealthy family this period of exposure extended to months to a year (Terwiel, 1975). Extra delays were expected in order to wait for a favourable day for a fire. The cremation was carried out outdoors on a wood pyre and it took approximately three days to completely burn the body. However, it is not clear if the fire was relit during the three-day period (Ward and Tayles, 2015). Next, the family collected the burnt bone fragments. This was done by hand (North Thailand), by raking the bones into a line, collected by hand, and placed in an urn, while the excess was thrown back into the pyre (Central Thailand), or by placing the bones into a pot for cleaning, then draining the water three days later, which culminated in burying the bones or in keeping it in an urn by the family (North East Thailand) (Terwiel, 1975; Ward and Tayles, 2015).

Some of these Thai customs associated with the post-processing of the dead prior to cremation continue into modern times. However, today the timing of cremation does not depend on the manner of death anymore, but solely on the status and wealth of the deceased and their family (Wong, 1998; Falk, 2010; Ward and Tayles, 2015). The wealthy displays their dead for six months before cremating them in a crematorium (Wong, 1998; Falk, 2010). In other areas of SE Asia, such as in Laos, they practice similar funerary rites, but the type of death and wealth of the deceased are not the only determinants for their treatment. The ethnicity and religion of the deceased also play a role (Evans, 1991; Falk, 2010). In historic Laos (around 1660 AD), the high-status dead were buried in a 'well-sealed' coffin for one month and then cremated. The bones were then collected and re-buried (De Marini, 1998). There are no accounts about how deceased of a lower social status were cremated. The rite of excarnation before cremation is

still present in SE Asia, which clearly shows the importance of this funerary treatment (Wong, 1998; Falk, 2010; Ward and Tayles, 2015).

I.4 Bone

At the gross level bone is composed of cortical or compact bone and a trabecular or cancellous bone components classified by its unit of microstructure and microporosity. Cortical bone, which covers the shaft of long bones and forms the outer layer of cancellous bone around joints, is much more dense than trabecular bone and is the primary type of bone used in histological studies (Crowder and Stout, 2011).

At the histological level, the mineralised microscopic anatomy of bone represents the collaborative activity of cellular structures (Crowder and Stout, 2011). Bone is a hierarchically-organised material. First level cortical bone structures include woven bone, primary bone, secondary bone, and plexiform bone. Woven bone is produced initially in all fetal bones, which is later replaced by lamellar bone. This disorganized type of tissue is (rapidly) laid down in adults as an SOS response (repair tissue), such as the callus formed to bridge the gap between fracture healing (Burr and Allen, 2014). Primary bone is laid down in a space where bone has not existed previously or directly onto bone or cartilage without resorption of pre-existing bone (Burr and Allen, 2014). Another quickly laid down bone tissue is the plexiform bone, which is typically seen in rapidly growing animals (e.g. sheep and cows) taking on a 'brick-like' form. Primary and secondary bone tissues contain blood vessels surrounded by concentric rings of bone, but secondary osteons are larger in diameter, have more concentric lamellae and a cement line as their boundary. Primary bone contains less lamellae and typically has smaller vascular channels than secondary bone (Haghighi, 1989). Secondary bone tissues are created by replacing existing bone through remodelling, which entails a series of processes to resorb and replace pre-existing bone, resulting in the Haversian system (Burr and Allen, 2014).

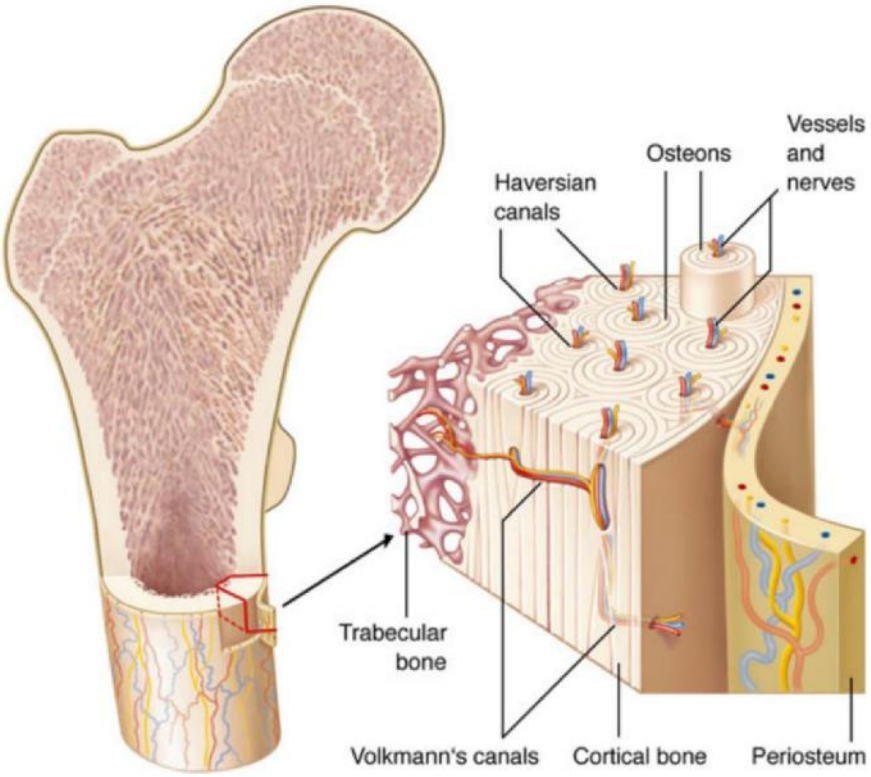


Figure 1. – The structure of the cortical bone and the periosteum (Bartl and Bartl, 2016, 15, Fig. 2.1).

Second level cortical bone structure include the lamellae, osteocyte lacunae, osteocyte canaliculi, and the cement line. Lamellar bone parallel to the periosteal and endosteal surfaces are referred to as circumferential lamellae. The concentric lamellar bone around vascular canals are the Haversian system, and the layers of bone in between them are the interstitial lamellae (Fairgrieve, 2008). Blood vessels, lymph vessels, and nerves run through Haversian canals (Fig. 1). Volkmann's canals also contain blood vessels and run perpendicular to Haversian canals, connecting osteons to each other. The purpose of blood vessels is to provide nutrients to bone and to remove waste from cell remodelling. Around the Haversian canals, layers of lamellae contain lacunae (holes). In living tissue, osteocytes occupy the lacunae, which are the most prominent cell type in bone (Fairgrieve, 2008). These cells have long cellular processes that branch through the canaliculi to contact other osteocytes at gap junctions (Crowder and Stout, 2011). As opposed to cortical bone, cancellous bone lacks true Haversian canals and is made out of an irregular lattice of thin trabeculae (Parker, 2007).

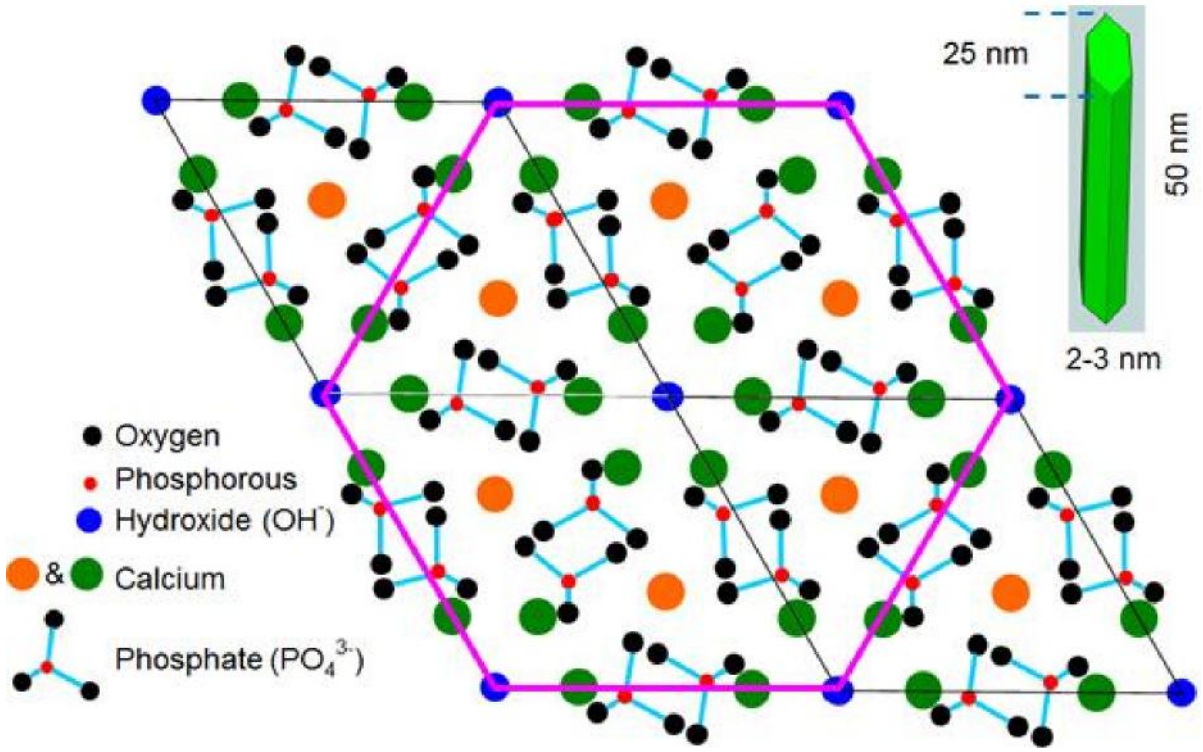


Figure 2 -- HAp crystal lattice highlighting the two different positions of phosphate ions (Bone Biology and Mechanics Lab – IUPUI).

On a molecular and nano level, bone is a composite material consisting of ~55-70 wt% mineral, ~20-35 wt% organic carbon, and ~10-15% water (Rogers and Zioupos, 1999; Elliott, 2002; Caruso *et al.*, 2020). The organic matrix, which is impregnated by the apatite phase, is formed mainly of type I collagen (90 wt%) (Olszta *et al.*, 2007). The rest of the organic is made out of non-collagenous proteins and living cells (Currey, 2002). Hydroxy(l)apatite [HAp, $Ca_{10}(PO_4)_6(OH)_2$] is the basis of all biologically formed apatite, while bioapatite [$(Ca,Mg,Na)_{10-x}[(PO_4)_{6-x}(CO_3)_x](OH)_{2-x}$] is a carbonate-containing variety of HAp, which forms the inorganic component of bone (Elliott, 2002; Rey *et al.*, 2007; Li and Pasteris, 2014). Bioapatite is chemically more complex than HAP; it is non-stoichiometric, its chemical composition is not fixed due to constant ion migration and thus can incorporate a wide variety of elements into its structure (Zapanta Legeros, 1981; Elliott, 2002; Bergslien *et al.*, 2008; Li and Pasteris, 2014). The four essential elements in bioapatite are calcium, phosphorus, oxygen, and channel filling ions (Fig. 2). Ion site vacancies are created by channel sites (discussed

below) and ion exchange is aided by the large surface area to volume ratio of bioapatite crystals (Palmer *et al.*, 2008), as well as the hydrated surface layer containing a variety of mineral ions (Neuman and Weikel, 1955; Rey *et al.*, 2007). They also differ in their Ca/P ratios and their HPO_4^{2-} and CO_3^{2-} contents (Elliott, 2002).

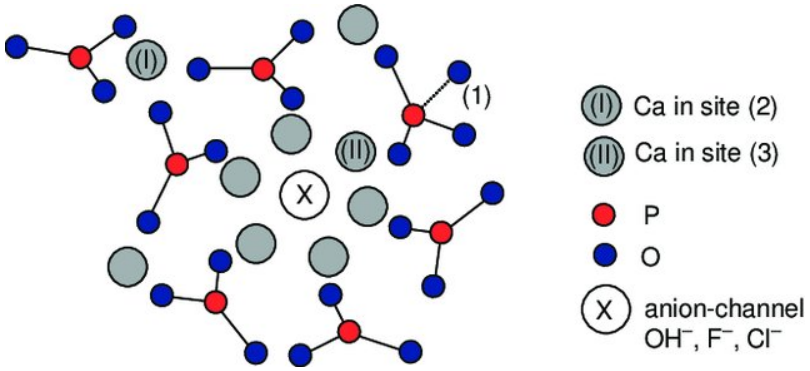


Figure 3 -- The atomic structure of HAp as a stand-in for bioapatite (Supova, 2014, 548, Fig. 2).

Bioapatite crystals are anisotropic (asymmetric) defined by the organisation of ions within the lattice. The arrangement of interstices between phosphate ions creates channels through the bioapatite structure. There are two crystallographically different Ca^{2+} in bioapatite (Fig. 3); four ions called Ca^{2+} (I) are in phosphate interstices, while six Ca^{2+} (II) ions form a calcium channel site along the c-axis found in interstices outside of the phosphate channel sites (Elliott, 2002). Most phosphorus is found in PO_4^{3-}, but a portion can be found in HPO_4^{2-} (*ibid;* Fig. 2). In bioapatite PO_4^{3-} is partially replaced by CO_3^{2-} (Pasteris *et al.*, 2004).

Carbonate is the third most concentrated element in bioapatite after calcium and phosphate (Rey *et al.*, 1989). Two carbonate ions are found in non-equivalent crystallographic locations in bioapatite at 'A' and 'B' sites (LeGeros *et al.* 1969; Rey *et al.* 1989; Danilchenko *et al.* 2005). These are the carbonates that replace hydroxyl groups (LeGeros *et al.*, 1969). B type CO_3^{2-} $[(Ca_{10-x}[(PO_4)_{6-2x}(CO_3)_{2x}](OH)_2]$ occupy the tetrahedral site due to substitution with PO_4 ions (Rey *et al.*, 1989; El Feki *et al.*, 1991; Danilchenko *et al.*, 2005), while A type CO_3^{2-} $[(Ca_{10}(PO_4)_6CO_3)]$ are found in the 'c' axis channel sites as OH^- substitutions (Wopenka and Pasteris, 2005). Thus, bioapatite has a mixture of A and B type carbonates $[(Ca_{10-x}[(PO_4)_{6-}$

$_{2x}(CO_3)_{2x}]$ (CO_3)], but contains a larger amount of the B type (Rey *et al.* 1989; Rey *et al.* 1991; Miller *et al.* 2001). Carbonates can also be adsorbed onto the surface of crystals and hydration layers (Zapanta Legeros, 1981). There is a disagreement in the literature as to whether there are OH^- groups in bone mineral at all. It has been suggested that they are present in bioapatite, but at lower levels than in stoichiometric HAp (Cho *et al.* 2003; Taylor *et al.* 2011); while others suggest that bone has no OH^- groups (Rey *et al.* 1995; Loong *et al.* 2000; Reidsma *et al.* 2016). The disagreement is about whether or not OH^- groups are mostly or completely replaced by CO_3^{2-} in bioapatite (Pasteris *et al.*, 2004; Wopenka and Pasteris, 2005). Carbonates are larger than hydroxyl groups, thus their presence in the structure leads to lattice distortion of the hexagonal crystal structure as well as smaller crystal sizes than HAp (LeGeros, 1991).

Ions and organics stabilise the amorphous precursor phases. These ions and molecules can be expelled from biominerals during crystal maturation (Trueman 2013). A variety of ions reside in bioapatite, such as carbonate, sodium, chloride, magnesium, potassium, and fluoride (Elliott, 2002; Rey *et al.*, 2009). These and other ions are found in bioapatite both within the crystal lattice and on the crystal surfaces (Termine, 1972; Posner, 1985; Pasteris *et al.*, 2004). Water is not only in the hydration layer (adsorbed on the crystallites), but also in the structure of bioapatite, by replacing channel filling ions (Yoder *et al.*, 2012). Ion migration happens by ion exchange, ion incorporation into vacancies and interstitial ions, or through ion substitutions (Neuman and Weikel 1955). To maintain the overall neutral balance in charges, exchange of other ions happen (Wopenka and Pasteris, 2005).

Due to the analytical challenge of analysing the major and trace elements in bioapatite, there are relatively few studies addressing the elemental concentration of the mineral portion of bone (Zapanta Legeros, 1981; Zioupos *et al.*, 1999; Elliott, 2002; Li and Pasteris, 2014; Skinner, 2015; Keenan, 2016; Keenan and Engel, 2017c, 2017a). One of these studies (Elliott, 2002) reported absolute values for human bone (Table 1). However, this table is confusing,

because it only accounts for 59.88% of elements and it is unclear what this amount is a percentage of. Additionally, it is also uncertain if these measurements were taken on fresh or dry bone. Other studies, mostly from the forensic literature, reported specific elements (Byrnes and Bush, 2016) and elemental ratios using XRF and other chemometric tools (Gonzalez-Rodriguez and Fowler, 2013).

Component	Bone (wt%)
Ca	36.6
P	17.1
CO_2	4.8
Na	1
K	0.07
Mg	0.6
Sr	0.05
Cl	0.1
F	0.1
Ca/P molar	1.65

Table 1-- The reported elemental concentration of bone after Elliott 2002, 430. ±1% variability can happen due to diet, age, and anatomical variation.

I.4.1 Bone Diagenesis

Bone diagenesis is the process of chemical, physical, and/or biological alterations to the composition of bone subsequent to death (White and Folkens, 2005). As discussed above, bioapatite is made out of smaller crystals than HAp with a high area/mass ratio. Consequently, bioapatite has higher reactivity and solubility than HAp (LeGeros, 1991), thus it is more susceptible to diagenesis. In the depositional environment bone undergoes a number of histological, structural, elemental, and morphological changes that affect the quality of information retrievable about the individual's life history. The taphonomic variables in the depositional environment can determine whether the bone will be preserved in an archaeological timescale or decay and vanish (Turner-Walker, 2007). Bone diagenesis is a

complex process that is dependent on site-specific variables, such as temperature, soil composition, pH, microbial composition and drainage capabilities of the soils, etc. (Hedges and Millard, 1995; Hedges *et al.*, 1995; Turner-Walker and Jans, 2008). Three distinct diagenetic pathways can be distinguished (Collins *et al.*, 2002): (1) chemical degradation of the organic component (collagen hydrolysis); (2) chemical degradation of the inorganic phase (bioapatite dissolution); and (3) microbial degradation of both the inorganic and organic phases (Child, 1995; Hedges and Millard, 1995; Millard, 2001; Collins *et al.*, 2002; Nielsen-Marsh and Hedges, 2002; Turner-Walker and Jans, 2008; Kontopoulos *et al.*, 2016b; Huisman *et al.*, 2017) . Microbial degradation is thought to occur first, thus this discussion will continue with this pathway.

I.4.1.1. Microbial Bioerosion

Very shortly after death, once the microbiome is no longer under the control of the immune system, microbiological decay of the body starts. Although these bacteria and fungi primarily feed on the soft tissues, they are thought to alter the hard tissues as well through the vasculatures of bones (Bell *et al.*, 1996; Millard, 2001). This type of attack is referred to as microbial bioerosion, which can be traced in unburnt bones. This bioerosion appears as holes, pitted areas, or tunnels, which often have demineralised canals and hypermineralised edges when studied under the backscattered electron microscope (Turner-Walker, 2019).

Morphological changes to bone due to such attack was first described by Wedl (1864) and Roux (1887), and subsequently by Hackett (1981) and Garland (1987). Wedl (1864) described small channels or tunnels penetrating the bone tissue (Wedl tunnelling), of which Roux (1887) identified the causative agent for 'bored channels' as fungi, thought to be the main factor in biological deterioration of bone until Hackett (1981) identified bacterial reorganisation of bone mineral in what was termed microscopic focal destruction (MFD). He described three types of MFD: linear longitudinal, lamellate, and budded (Hackett, 1981).

Garland (1987) discussed several types of diagenetic alterations to bone, such as reduction in birefringence, rounded interlinked tunnels, inclusion, and infiltrations. Hedges and Millard (1995) developed the *Oxford Histological Index* (OHI) to approximate the preservation of bone histology. The OHI is still used in bone histology studies, providing a gross estimate of how much of the bone is affected by bioerosion.

More recent research has so far focused on the presence of MFDs, Wedl tunnelling, Wedl type 2, and cyanobacterial tunnelling and their causative agents on unburnt bones (Bell *et al.*, 1996; Trueman and Martill, 2002; Jans *et al.*, 2004; Nielsen-Marsh *et al.*, 2007; Turner-Walker, 2012; Jans, 2013; White and Booth, 2014; Grine *et al.*, 2015; Kontopoulos *et al.*, 2016b; Kendall *et al.*, 2018; Morales *et al.*, 2018) . Generally, there are still two opposing theories about the origins of these bacteria: endogenous source from the gut (Bell *et al.*, 1996; Trueman and Martill, 2002; Jans *et al.*, 2004; Nielsen-Marsh *et al.*, 2007; Jans, 2013; White and Booth, 2014; Booth, 2016) or exogenous soil bacteria/fungi (Turner-Walker, 2007, 2019; Turner-Walker, 2012; Grine *et al.*, 2015; Kontopoulos *et al.*, 2016b; Kendall *et al.*, 2018; Morales *et al.*, 2018), even though it has (recently) been shown that exogenous bacteria is the cause of microbial bioerosion features on terrestrial remains.[2] Until very recently, it was unknown which organisms cause microbial degradation (though attempts have been made, see Marchiafava *et al.*, 1974; Piepenbrink and Schutkowski, 1987; Child, 1995), whence they originate, when it takes place, how long it continues, and if it could be traced in burnt bones. Recently, metabolomics studies have made a huge difference to our understanding of bone microbial bioerosion (Pesko *et al.*, 2020), such as the association of microbial taxa with specific PMIs (namely Proteobacteria, Firmicutes and Bacteroidetes) (Procopio *et al.*, 2019) and the decrease in the fungal taxonomic richness associated with increasing PMIs (Procopio *et al.*,

[2] Source: G. Turner-Walker's conference presentation at the 9th International Bone Diagenesis Conference, 2021, Évora, Portugal.

2020). Metabolomics have never been used to detect potentially surviving bacteria after burning, which could be a future direction in research. Chapter III investigates microbial bioerosion in unburnt and burnt bones in the late postmortem interval using the microscopic features associated with bioerosion preserved in bone.

I.4.1.2 Mineral Degradation

Once homeostasis is not maintained after death, changes to the crystal structure, mineral dissolution, and absorption of exogenous ions begin. This is mainly caused by the groundwater and soil, and their chemical properties, such as pH and dissolved ions (Hedges and Millard, 1995; Hedges *et al.*, 1995). After the degradation of the organic phase has begun, the mineral fraction is more prone to diagenesis (Hu *et al.*, 2006). Bioapatite is the most stable at pH 7.8 (Berna *et al.*, 2004) and starts dissolving in environments of $<$ pH 6.0 (White and Hannus, 1983). The dissolution is associated with the increased porosity of the mineral after the reduction, or complete removal, of the organic fraction (Lee-Thorp, 2002). Crystallinity, the measure of defects (distortion and/or strain) and crystal sizes, increases during diagenesis. Gradually, bioapatite crystals become larger and more ordered with less distortion (Weiner and Bar-Yosef, 1990; Lee-Thorp and Sponheimer, 2003; Trueman *et al.*, 2004; Thompson *et al.*, 2009). Dental enamel, which is more crystalline than bone bioapatite, is more stable and resistant to diagenesis due to its highly mineralised nature, fewer substitutions, less defects, and larger crystal sizes (LeGeros, 1991; Lee-Thorp and Sponheimer, 2003). When the crystallinity increases (measured by IRSF) and type B CO_3^{2-} increase, HPO_4^{2-} and type A CO_3^{2-} decrease (Miller *et al.*, 2001). Larger crystals are thermodynamically more stable than smaller ones, meaning diagenetic bioapatite becomes less reactive with the environment with time.

Along with these postmortem alterations, elements from the surrounding environment are incorporated or exchanged in bone mineral (Lee-Thorp and Sponheimer, 2003). Ion exchange occurs in bone because bioapatite is very accommodating to chemical substitutions due to

vacancies at ion sites (channel sites) (Palmer *et al.*, 2008). Post-deposition ion migration continues between the bone and the environment. Incorporation of these ions into the bioapatite, especially carbonate, might cause further structural disorder and lattice strain in the crystal structure (Bigi *et al.*, 1995; Yao *et al.*, 2009; Delgado-López *et al.*, 2012; Ghadimi *et al.*, 2013). PO_4^{3-} and OH^- ions undergo substitution by CO_3^2. To maintain the balance of charges, calcium and hydroxyl ions deplete, thus creating vacancies (Zapanta Legeros, 1981; Elliott, 2002; Rey *et al.*, 2007; Li and Pasteris, 2014). CO_3^{2-} ions are one of the constituents of bone measuring at 4-6 wt% (Trueman, 1999); 3-8 wt% (Reidsma *et al.*, 2016), but some percentage of carbonate is also found as HCO_3^-, which increases the solubility and the rate of dissolution in acids compared to HAp (Elliott, 2002). Na, Mg, Sr, U, F, and the REE, as well as other elements depending on the environment, are often incorporated into the crystal structure (Millard and Hedges, 1996; Li and Pasteris, 2014; Keenan and Engel, 2017a; Walden *et al.*, 2018). These substitutions can occur without impairing the crystal lattice stability, which is one of the reasons for crystallinity increase. Chapter IV investigates the compositional and structural alterations of bone mineral during early diagenesis.

I.4.1.3 Collagen Degradation

Although this thesis's emphasis is on bone mineral because burning destroys the organic phase, a discussion on collagen (and protein) degradation is necessary. Bone collagen has been the focus of much biomolecular research in archaeology, because it is easy to extract (by dissolving the mineral) and can be quality checked by its C:N ratio, which makes it the primary choice for aDNA analysis from bone (Law and Hedges, 1989; van Klinken, 1998; Collins *et al.*, 2002; Brock *et al.*, 2013; Sponheimer *et al.*, 2019). Collagen is the most abundant biomolecule in human and animal remains, because of its abundance in bone, resilient structure, and its protection by the physical exclusion of microbial extracellular enzymes

(Collins *et al.*, 1995), even though the exact relationship between collagen and mineral is still debated (Collins *et al.*, 2002; Elston, 2019). When insoluble collagen goes into soluble or biodegradable gelatine, it changes the physical properties of bone (Zioupos *et al.*, 1999; Collins *et al.*, 2002). This transition is accelerated by extreme pH, high temperatures, and presence of organic acids in the collagen structure (Miles *et al.*, 2000). It is retarded by the presence of mineral (Kronick and Cooke, 1996) and tight packing of collagen fibrils (Miles and Ghelashvili, 1999; Collins *et al.*, 2002).

Collagen starts to degrade during life and continues to degrade after death (postmortem). However, age-induced degradation is not the only variable, since collagen yields in archaeological bones also varies widely. Endogenous and exogenous (environmental) variables play a major role (Collins *et al.*, 2002). The two main mechanisms of postmortem protein degradation are biological degradation (see more in section I.1.3.1 and in Chapter III) and the chemical hydrolysis of the peptide bonds. Bioerosion is one of the principal mechanisms in collagen degradation (Marchiafava *et al.*, 1974; Child, 1995; Kendall *et al.*, 2018). Once the bone is partially mineralised, a variety of enzymes chemically start to decompose bone collagen (Child, 1995). It is argued that the chemical deterioration of collagen will be defined by the time and temperature ensemble during the postmortem interval (Collins *et al.*, 1995, 2002). However, other factors play a role as well, such as soil pH, which can exacerbate peptide bond hydrolysis (Collins *et al.*, 1995; Kendall *et al.*, 2018) or local hydrological conditions (Hedges and Millard, 1995).

The estimation of the time of death from proteins have been investigated since the 1960s, mostly led by Knight (Knight and Lauder, 1967; Knight, 1968, 1969). Recent research in diagenesis of the proteins has gained more importance for the accuracy and authentication of endogeneity (Wilson *et al.*, 2012; Schroeter and Cleland, 2016; Simpson *et al.*, 2016). Protein degradation (the breakdown of the protein into peptides, amino acids, and ultimately the

decomposition of amino acids) is a complex process involving the decrease in the range and abundance of proteins present in the bones and an increase in the posttranslational modifications (PTMs) (Hendy, 2021). The extent of diagenesis via the breakdown pathways depends on the protein structure and the surrounding matrix (McMahon *et al.*, 2016), the interaction between the organic and the mineral phases (Demarchi *et al.*, 2016) and the influence of the environment, such as temperature (Smith *et al.*, 2003), presence of water and oxygen (Raff *et al.*, 2008) and pH (High *et al.*, 2015). Different hydrolytic processes can break down peptide bonds either at the internal bond (Bada, 1991), at the C terminus (Kahne and Still, 1988), or at the N terminus (Steinberg and Bada, 1983). Various proteins will break down at different rates, for example, small peptides with hydrophobic amino acids will be hydrolysed at the N terminus via an internal aminolysis reaction (Bada, 1991), while amino acids with larger chains will be more resistant to hydrolysis (van Duin and Collins, 1998). To establish if the peptides are endogenous, the level of amino acid degradation is assessed. This is because certain amino acids degrade over time to form other amino acids, or modifications occurs to their side chains. The rate of degradation has been thought to be somewhat predictable (Hendy, 2021). However, this cannot always be true, because different taphonomic processes can degrade both the organic and the inorganic phases at different rates. For example, amino acid racemization (AAR) dating has been highly criticised (Johnson and Miller, 1997) because it assumes a predictable degradation pattern between the relative degree of L-configuration (living tissue) and D-configuration (after death) of amino acids, as an indication of the postmortem time elapsed (Bravenec *et al.*, 2018). The issue is that taphonomic and diagenetic factors have not routinely been considered, which can affect the rate of racemisation, such as the ambient temperature, pH, presence of water or moisture in the air (Johnson and Miller, 1997). However, AAR dating has been exceedingly successful in highly mineralised tissues, such as dental enamel (Griffin *et al.*, 2009), and different species of shells (Penkman *et al.*,

2008). Since dental enamel is the densest tissue in the human body and HAp is associated with collagen, its protein content survives longer.

PTMs can be due to (1) postmortem degradation; (2) normal biological processes; (3) other factors, such as temperature (Schroeter and Cleland, 2016). Deamidation (removal of an amide group) is the most explored amino acid modification, and mostly of glutamine, which becomes glutamic acid after deamidation (Hendy, 2021). Deamidation can be used to indicate amino acid degradation in bone (Wilson *et al.*, 2012; Cleland *et al.*, 2015), but a lot more work is needed as the contributing factors to this are still mostly unknown. Some studies suggest that the rate of deamidation depends on the temperature, pH, laboratory procedures and the secondary- and tertiary structures of proteins (Simpson *et al.*, 2016; Procopio and Buckley, 2017).

I.4.2 Heat-Induced Changes

I.4.2.1 Fire and Burning

Fire is a chemical reaction (oxidation) that generates heat and light (DeHaan, 2002). The three requirements to make a fire are fuel (i.e. combustible material), heat (i.e. sufficient level of heat to raise fuel temperature to its ignition temperature), and air (i.e. high enough concentration of oxygen to sustain combustion) (Fairgrieve, 2008). The burning of the body tissues progresses in a regular fashion under set circumstances:

(1) the tissues pass through the (clinical) degrees of burn;

(2) blistering and slippage of the skin; *heat rupture* or splitting of soft tissue (DeHaan, 2002);

(3) exposed hypodermis and the underlying subcutaneous fat, due to the dehydration of the epidermis and dermis (fat acts as a source of fuel) (DeHaan *et al.*, 1999); muscle contraction and denaturation of the muscle proteins (Spitz, 1993)

(4) internal organs are exposed and shrunk; the extremities are no longer in a complete state;

(5) torso is broken down;

(6) incineration of the body (Fairgrieve, 2008).

Various tissues will be charred or calcined differently depending on factors, such as the body's position, temperature and exposure to the temperature, type of fuels present, movement of the wind, and the location of the tissue in the body (Fairgrieve, 2008; Symes *et al.*, 2008). Once the muscles are eliminated and the periosteum has flaked off after charring, the direct burning of the bone beings. Bones closest to the surface burn first. Areas covered densely with more soft tissue and points of contact the body has with objects or the ground has a delayed exposure to fire, thus it will be charred later (Fairgrieve, 2008).

I.4.2.2 Heat-Induced Changes to Bone

Bone's response to high temperatures has been widely documented across a number of fields including forensic anthropology, bioarchaeology, biomaterials, and biomedicine (Schiegl *et al.*, 2003; Thompson, 2005; Piga *et al.*, 2009; Beckett *et al.*, 2011). Archaeologists and biological/forensic anthropologists use a variety of macroscopic techniques to characterise the heating temperature and duration of the burning, such as visual inspection, for example of bone colour (Shipman *et al.*, 1984; Devlin and Herrmann, 2008) and heat-induced fracturing (Herrmann and Bennett, 1999; Gonçalves *et al.*, 2011). Long bones exhibit several types of heat-induced fractures, such as longitudinal, transverse, curved transverse (or thumbnail), patina, delamination fractures, and warping (Herrmann and Bennett, 1999; Fairgrieve, 2008).

Visual assessment techniques can give ambiguous results, due to the variable conditions to which a body can be subjected during burning. Generally, four main stages of burning modifications are widely accepted to occur in bones: (1) dehydration, marked by the breakage of the hydroxyl-bonds; (2) pyrolysis, or the loss of the organics; (3) inversion, or the loss of the carbonate elements; and (4) fusion of the HAp crystals (Shipman *et al.*, 1984; Mayne Correia, 1997; Thompson, 2004, 2005; Devlin and Herrmann, 2015; Ellingham *et al.*, 2015). Although temperature ranges have been identified for each stage (Thompson, 2004, 2005; Ellingham *et al.*, 2015), these are dependent on many variables, for example the physical differences among individuals, fat content, oxygen supply, and time spent at peak temperatures (Walker *et al.*, 2008). Since burnt bones are vastly common in both archaeology and forensic science contexts, method development is crucial to maximise the amount and quality of information that can be obtained from them.

The body can be burnt at the time of/soon after death or following a delay of varying duration, from days to weeks to years. There has been a significant number of studies already dealing with establishing whether the burnt bones were skeletonised or not prior to burning based on their fracture pattern. Some aspects of this have been more frequently investigated than others; for example, whether or not warping (i.e. heat-induced shape change) and thumbnail fracturing (curvilinear fracture, which appears as if one's thumbnail was pressed into putty) of the bones, as indicators of fleshed remains, are present. It has been proposed that warping is caused by the contraction of the muscle fibres in fleshed bones, which is absent in burnt dry bones (Baby, 1954; Binford, 1963; Etxeberria, 1994); however, others have noted similar warping on burnt dry bones (Buikstra and Swegle, 1989; Spennemann and Colley, 1989; Whyte, 2001). Thompson (2005) argued that collagen distribution in the bone might be responsible for the presence of warping. More recently Gonçalves *et al.* (2011) concluded that warping and thumbnail fractures do not depend on the presence of soft tissue on the bone, but

rather the amount and/or distribution of collagen-apatite links retained in them. Distinguishing between remains burnt at a fresh or decomposed state is of interest because it has relevance in both archaeological and forensic anthropological contexts. It can enhance our understanding of how different cultures treated their dead in archaeology and can help to establish a timeline in crime scene investigations involving burnt human remains.

I.4.2.3 Colour Changes & Weight

Bone undergoes colour changes during heating, which is associated with loss of bone mass, shrinkage, and fracturing. These changes have been attributed to heat-induced physicochemical alterations (Shipman *et al.*, 1984; Thompson, 2004, 2005; Munro *et al.*, 2007; Devlin and Herrmann, 2008; Ubelaker, 2009). Unheated bone has a creamy colour, which does not alter up to 200°C. Heating at this temperature results in small-scale mass loss, which is due to the loss of surface absorbed water. Between 200 and 500 °C bone darkens to a brownish/blackish colour with further mass loss, which is due to the combustion of the organics, carbonisation, and the loss of lattice-incorporated water (Ellingham *et al.*, 2015). Once the structural carbonates and all the organics are removed the bone turns blueish-grey/grey at around 500-700°C. Above this temperature bone becomes calcined, indicated by its white colour (Thompson, 2004, 2005; Ellingham *et al.*, 2015). However, these temperatures associated with colour change are estimates, since the duration of the fire is not routinely considered, as well as the taphonomic history of the remains, such as previous discolouration (e.g. UV bleaching by the sun), presence of soft tissue, and diagenesis (Shahack-Gross *et al.*, 1997; Symes *et al.*, 2008; Ubelaker, 2009). The different temperature ranges associated with colour changes in different studies is likely due to the varying rates of heating, redox reaction within the flames or if soft tissue present, exposure times, and the size differences of skeletal elements heated.

As previously discussed, bone loses weight through burning from dehydration, the loss of the organics, and potential loss of inorganic minerals. The different losses in weight is probably

due to water retention and thus the temperatures the bone was exposed to. According to modern cremation analogues, an adult individual's full weight after cremation varies between 1000 – 2400 g (mean 1650 g) (McKinley, 2000). However, this weight is rarely attained in archaeological excavations, because the thoroughness with which bone is collected with from the site can significantly alter the weight of the individuals (McKinley, 1997).

I.4.2.4 Histological Changes

There are relatively few studies concerned with the histology of burnt bone. The primary focus has been on estimating fire temperature and duration (Herrmann, 1976, 1977; Nicholson, 1993; Holden *et al.*, 1995; Quatrehomme *et al.*, 1998; Ubelaker, 2009; Absolonova *et al.*, 2013; Imaizumi *et al.*, 2014; Cambra-Moo *et al.*, 2017) or on species identification (Cattaneo *et al.*, 1999). These studies have been conducted using either histomorphometry or histomorphology and the associated changes at certain temperatures can be seen in Chapter III. Table 4. There is disagreement concerning the temperature at which structural changes first occur in bone. Bone's histological structure is nearly identical to that of unburnt bone when burnt under 600°C (Bradtmiller and Buikstra, 1984), 700°C (Herrmann, 1977), 900°C (Squires *et al.*, 2011), and even 1200°C (Cattaneo *et al.*, 1999). Squires *et al.* (2011) state that Haversian and Volkmann's canals cannot be distinguished in bones burnt at 900°C. This observation is important, because Volkmann's canals often resemble cyanobacterial tunnelling. However, it is not clear whether these temperatures were measured on bone or in the fire/heat source, since the former can be much lower than the latter, which might be one source of discrepancy. Other discrepancies can include the method of burning, the type, size, and state of the bone, and presence/absence of soft tissue.

As discussed above, bone shrinks as a result of heating. On a histological level, it is the shrinkage of the relative size of the osteons (by ~16.7%) and not the osteon count that declines (Bradtmiller and Buikstra, 1984; Nelson, 1992). Thus, it is the concentric lamellae that are

primarily affected, and not the circumferential lamellae (Fairgrieve, 2008). In fact, the amount of shrinkage was found to not be affected by the type of structural elements in bone (Hummel and Schutkowski, 1993).

I.4.2.5 Physicochemical Changes

The physicochemical modifications to bioapatite due to heat-treatment are the crystallisation (crystal growth), ion exchange, and the occurrence of additional phases due to the thermal decomposition of the mineral phase. As discussed previously, bioapatite is a very anisotropic material with plenty of lattice strain. When heated, first water evaporates at ~225°C, followed by CO_2 at <500°C, and the disappearance of the organic phase. Structural and secondary carbonates begin to disappear at >500°C with another phase of CO_2 loss (Shipman *et al.*, 1984; Strydonck *et al.*, 2010). However, the loss of CO_2 is not only dependent on the temperature, but on the time of exposure (Van Strydonck *et al.*, 2005). At heating above 600°C, thermal decomposition of the calcium phosphate phase occurs, whilst the crystal size and order of the microstructure increase (Rogers and Daniels, 2002; Beckett *et al.*, 2011). This crystallisation due to heat treatment is predominantly caused by ion loss (Rogers and Daniels, 2002), such as carbonate ions (Wang *et al.*, 2010). It has been proposed that there is differential loss in carbonates, depending on its crystallographic location (Rey *et al.*, 1989). 'A type' CO_3^2 in bioapatite is synthesised at >800 °C, but 'B type' CO_3^2 might be precipitated from solution at only < 100°C (Rey *et al.*, 1989). It has been shown that in dental enamel the amount of B type carbonates decrease due to heat-treatment, while A types first decrease (up to 300°C) and then increase when heated between 300 and 700°C (Shi *et al.*, 2005). Shi *et al.* (2005) have proposed that this increase is due to the released 'B type' carbonates being incorporated at 'A' sites. Simultaneously with this carbonate decrease the hydroxyl groups increase (Stiner *et al.*, 1995).

The onset of crystallisation occurs subsequently after the lattice water is released and the organic phase has completely combusted, due to the shielding effect of collagen on minerals (Etok *et al.*, 2007). Two different temperatures were proposed for identification of the temperature at which the onset of crystallisation occurs: 500°C (Lozano *et al.*, 2003) and 600°C (Rogers and Daniels, 2002; Beckett *et al.*, 2011; Greenwood *et al.*, 2013). Heat-induced crystallisation of bioapatite results in a more HAp like structure than unburnt bioapatite's (Stiner *et al.*, 1995). Therefore, burnt bone is more stable and resistant to postmortem alterations and diagenesis, than unburnt bones (Zazzo *et al.*, 2009; Lebon *et al.*, 2010; Zazzo and Saliège, 2011; Quarta *et al.*, 2013). This means that, once bone is burnt, it is a more reliable substrate for isotopic analysis, radiocarbon dating, and diagenesis studies.

Through thermal decomposition additional crystalline phases are formed in bioapatite. Identified phases include tetra-calcium phosphate (TetCP), calcium oxide (CaO), alpha-tri-calcium oxide (α-TCP), beta-tri-calcium oxide (β-TCP), and magnesium oxide (MgO) (Dorozhkin and Epple, 2002; Mayer, Schlam and Featherstone, 1997; Mkukuma *et al.*, 2004; Beckett, Rogers and Clement, 2011). CaO, TetCP, and α- and β-TCP forms after heating at different temperatures (between ~700°C and 1450°C), as well as the removal of OH^- groups (Liao *et al.*, 1999), the release of CO_2 from the decomposition of CO_3^2 (Haberko *et al.*, 2006), and the formation of calcium oxyapatite. The latter was suggested to be the precursor of the product phases (Brown and Chow, 1976). It is thought that the presence of potassium ions preferentially affect β-TCP formation (Beckett, 2009). MgO substitutions are thought to be lessened by the presence of both Na and K, as they are the preferred substitutions (*ibid*). Variations occur in bioapatite's thermal decomposition depending on its organic content (Mkukuma *et al.*, 2004), and elemental concentration (Mayer *et al.*, 1997).

I.5 Research Objectives

The post-processing of the dead before cremation is a highly debated topic in funerary archaeology, which has so far been impossible to decipher for archaeologists and bone experts by only observing macroscopic differences in heat-induced fracturing. This rite has, however, been documented in historic and modern times in Southeast Asia. The PMI before burning in a forensic context has only been possible to be established in cases where both unburnt and burnt elements of the skeleton were present (Bontrager and Nawrocki, 2008; Garrido-Varas and Intriago-Leiva, 2015). However, typically only burnt bone fragments are recovered, thus better methods are needed for such investigations. Using and developing methods in histology, analytical chemistry, and by studying the bone's osteogenic reaction to trauma and heating, it might be possible to bring light onto prior bone decomposition in burnt bones.

To address this gap in the literature on the invisible treatment of the dead before cremation, this doctoral thesis aims to create a series of research questions with which to elucidate the broad timescale of the postmortem interval of the bone prior to burning. In other words, the main research question of the thesis is whether or not it is possible to identify if bones were fresh or had decomposed prior to burning (Fig. 4). This is accomplished by an actualistic taphonomy experiment, using pig tibiae as a proxy for human bones, and with the use of the following methodological attempts:

(1) histological investigations, using microbial bioerosion as a proxy for decomposition in burnt bones by thin section transmitted light microscopy and backscattered electron microscopy;

(2) structural changes in the decayed unburnt and burnt bones using Fourier Transform Infrared Spectroscopy (FTIR);

(3) major and trace elemental concentration changes in the pre- and post-burning bones using wavelength dispersive electron microprobe (WDS-EMP);

(3) the timing of sharp force trauma (SFT) infliction compared to the time of deposition and burning, by inflicting SFT at different PMIs and subsequently burning the bones;

(4) the presence of thumbnail fractures and warping, as well as the fragmentation severity compared to the retained collagen content of unburnt bone.

The use of macroscopic, histological, elemental, and structural investigations together provides a new mechanism through which the decompositional state and thermal alterations can be examined in bone.

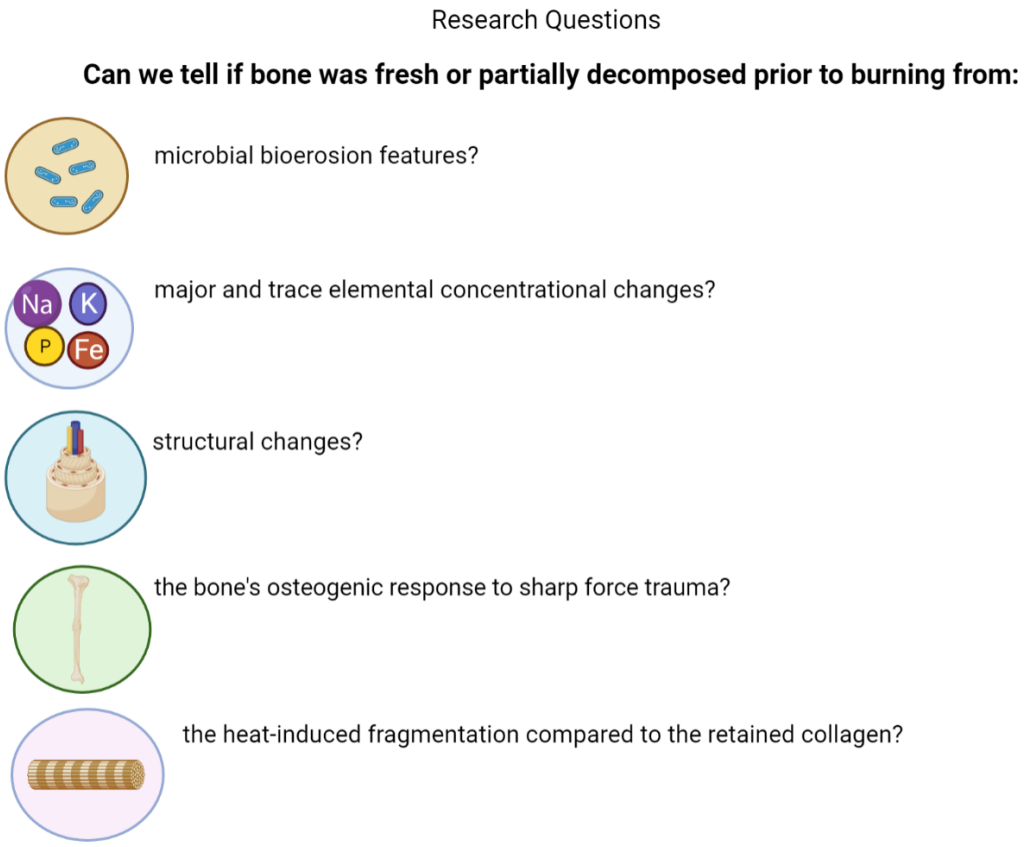


Figure 4-- Research Questions of the thesis.

I.6 Thesis Structure and Outline

The majority of this thesis comprises three scientific papers (Chapters III-V). The first paper (Chapter III) is published in the *Journal of Archaeological Science:Reports*; the second (Chapter IV) is currently in press in the journal *Applied Spectroscopy*; while the third (Chapter V) is in preparation for submission. Prior to the main experiment of the thesis, a small study

was performed (Appendix A) to provide a proof of concept for subsequent research. This small paper uses FTIR and X-ray Diffraction (XRD) in addition to the examination of heat-induced fractures and sharp force trauma features on bones with longer and more differing PMIs.

Chapter I of this thesis comprised of providing a research background in an archaeological, forensic anthropological, and ethnographic context. It then moved onto giving a brief outline of bone, as the material of all the scientific studies in this thesis, on a gross, microscopic, and nano-level. Chapter II describes the materials, main analytical and statistical methodologies used in the three papers in more detail to that found in the scientific papers (Chapter III-V). The methodologies discussed are: (1) Fourier Transform Infrared Spectroscopy (FTIR); (2) Electron microprobe analysis (EMPA); (3) sampling and chemical treatment for collagen extraction; (4) Data and statistical analysis.

Chapter VI summarises the main findings of this thesis and creates a synthesis, as well as discusses possibilities for future research. Additionally, a number of appendixes are attached. As mentioned above, Appendix A encompasses a small proof-of-concept study. Appendix B is the published scientific paper of Chapter III. The histology dataset created by the data labelling application can be viewed in Appendix C and the histology images are included in the electronic file. Appendix D encompasses the major and trace elemental concentrations of the measured bones from the electron microprobe, as well as the removed data, the data from the secondary standards, and the graphs of the chemical concentrations of the grouped bones organised by elements. Appendix E shows the FTIR data, frequencies of interest, and measured ratios, a table on the spectroscopy assignments, and the principal component analysis (PCA) plots. Appendix F encompasses the MANOVA results of the EMPA and FTIR data. Images of cutmarks are uploaded in the electronic file enclosed with the thesis.

Chapter II: Materials and Methods

Although each scientific paper (Chapters III-V) has a section detailing the materials and methodologies used, the main methods are explained in more detail in this Chapter (Fig. 5). Histological methods are not included in this section, as they are explained comprehensively in Chapter III. X-ray diffraction (XRD) was only used and explained in the proof-of-concept study (Appendix A), thus this method is not described here.

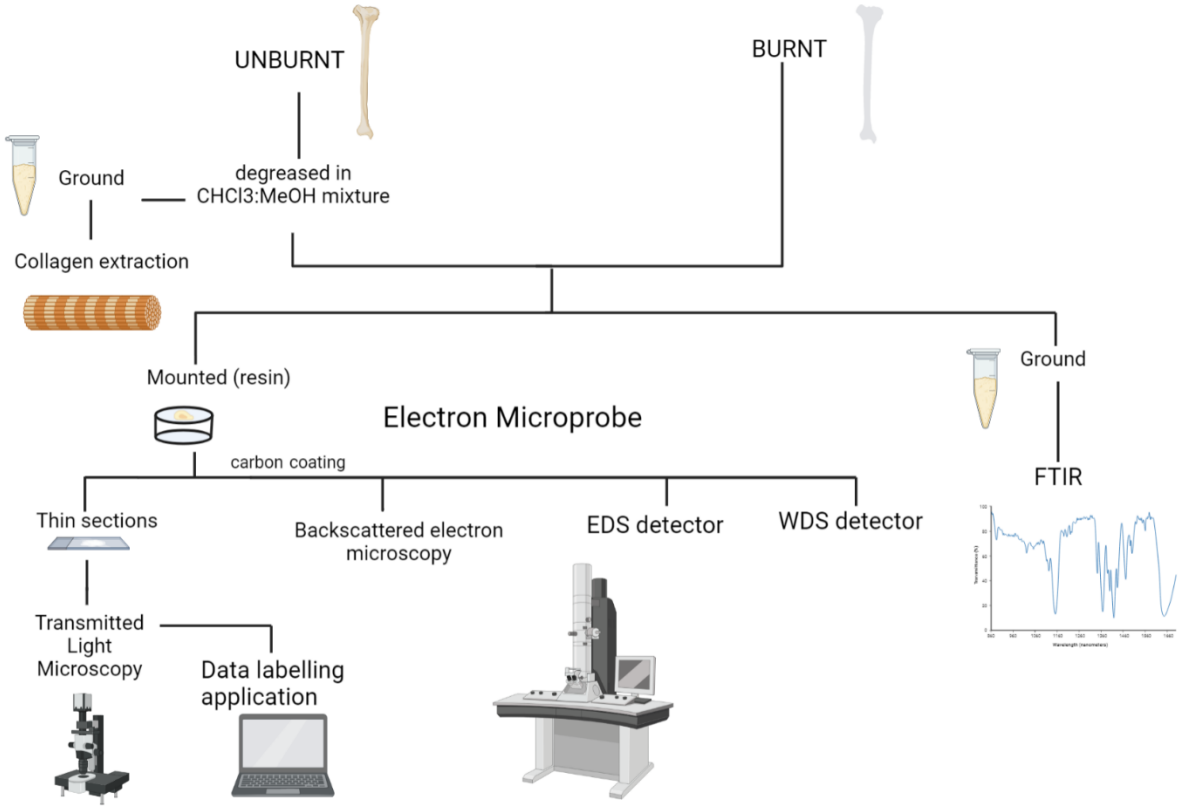


Figure 5 -- Schematic of the analytical methods used in the thesis.

II.1 Materials

For studying the diagenesis and heat-induced changes in human remains, the most direct and realistic approach would be to use human cadavers, as this type of study would be the best way to examine past, present, and future human death investigations and funerary treatments. However, the main limitations for using human remains for this type of research are access to cadavers and limited research facilities, not to mention ethical and legal concerns. There are only a few research facilities around the world where active human remains

donations allow this experimental taphonomy research, mostly in the United States. Furthermore, when human cadavers are donated, they represent a wide range of differences in biological profile, health, manner and circumstances of death, and ante-mortem medication usage (Benbow and Pechal, 2017).

An alternative to human cadavers is animal models. The primary porcine model has been of excellent scientific value (Pringle *et al.*, 2012; Lynch-Aird *et al.*, 2015; Squires *et al.*, 2020), and thus pigs are the choice of material in this thesis. Pigs have also been widely utilised for human cadavers in studies regarding decomposition and burning (Forbes *et al.*, 2005; Lynn and Fairgrieve, 2009; Thompson and Inglis, 2009; Symes *et al.*, 2012). There is an ongoing discussion on how appropriate porcine bone is as human analogues (Matuszewski *et al.*, 2020), but due to the ethical and legal drawbacks of using human cadavers, they are still the most reasonable proxies. Porcine bone macro- and microstructure, mineral concentration and density are similar to humans, as well as the pig gut microbiota (Turner and Wiltshire, 1999; Forbes *et al.*, 2005; Pearce *et al.*, 2007; Wilson *et al.*, 2007; Feng and Jasiuk, 2011; Hollund *et al.*, 2014; White and Booth, 2014; Kontopoulos *et al.*, 2016b). All the pig bones included in this study were tibiae, because of their survival rate in archaeology and their large cortical bone area, which is ideal for histology and spatial elemental concentration investigations (Booth and Madgwick, 2016).

Additionally, two cremated human bone fragments were used for the physicochemical investigations (Chapter IV) to test the results from the experimental study on archaeological human cremated bones. These bone fragments were from burials 1 and 7 at a Middle/Late Neolithic (ca. 3300-2500 cal BC) stone circle in Kiltierney, Co. Fermanagh, Northern Ireland (Daniells *et al.*, 1977). The fragments presented thumbnail fractures, suggestive of high collagen content at the time of burning (Gonçalves *et al.*, 2011). Neolithic Ireland is of interest

in this study, due to the assumptions on the existence of excarnation prior to cremation (see section I.2).

II.2 Fourier Transform Infrared Spectroscopy

Spectroscopic techniques are used to study the absorption and emission of electromagnetic radiation by matter. Infra-red spectroscopy (IR) uses the covalent bonds with electrical dipoles, which have particular frequencies (resonant frequencies) within the infrared region (Atkins *et al.*, 2016). Energy from a beam of infra-red light is absorbed by the vibrating chemical bonds; its resonant energy equals the frequency of the absorbed energy. Thus, IR is applied to identify a particular bond from its absorbed energy, which in turn then establishes the molecular structure of a compound (*ibid)*.

Fourier transform infrared spectroscopy (FTIR) is often used to for the analysis of biomaterials. FTIR detects the vibrational wavelength of chemical functional groups in a material by absorbing infra-red radiation at certain wavenumbers (measured in cm^{-1}). This is because the bonds vibrate at characteristic and known frequencies (De Campos Vidal and Mello, 2011). It allows the coinciding analysis of the organic and mineral phase of bone at any condition of preservation (Howes *et al.*, 2012; Ellingham *et al.*, 2016). Amide I and II bands (C=O and C—N bonds from collagen polypeptides, respectively) represent the organic material in bone. The mineral component is represented by the three vibrational modes of phosphate ($_{v1,v3,v4}PO_4^{3-}$), and carbonate corresponds to two vibrational modes ($_{v2,v3}CO_3^{2-}$). More on the ratios and their wavenumbers can be read in II.2.1 and II.2.2, as well as in Chapter IV.

The produced molecular structures of the sample can be read from the spectrum, which is attainable by transforming the raw data to a spectrum with the Fourier transform algorithm. The more complex the molecules, the more absorption bands, thus the more complex the produced spectra (De Campos Vidal and Mello, 2011). FTIR is an appropriate tool to use in this study, because it has been frequently used to investigate both the diagenetic pathways in

osseous material (Walters *et al.*, 1990; Pleshko *et al.*, 1991; Rey *et al.*, 1991; Koon *et al.*, 2003; Stathopoulou *et al.*, 2008; Trueman *et al.*, 2008), and had partial success at differentiating between heated bone at low, medium, and high temperatures (Thompson *et al.*, 2009; Ellingham *et al.*, 2016). Attenuated Total Reflection (ATR) was chosen instead of KBr discs, as it has been shown to provide more reliable measurements (Thompson *et al.*, 2009; Beasley *et al.*, 2014). It also has the advantage of simpler sample preparation and it is free of possible chemical modification that could potentially occur when in contact with potassium bromide (Stathopoulou *et al.*, 2008).

Powdered pre- and post-burnt samples were used for the FTIR-ATR method with a Cary 600 series FTIR spectrometer 5.3 (Aglient Technologies, Santa Clara, California, USA). A diamond crystal accessory was utilised with an operational range of 30000 to 200 cm^{-1}. Resolution Pro FTIR software (Agilent Technologies, Santa Clara, California, USA) was used for automatic software correction and for generating the backgrounds and the raw data of each sample. After the spectrometer was aligned, a resolution of 4 cm^{-1} was chosen. There were 64 scans taken of each sample and the scan range was set between 4000 and 400 cm^{-1}, which represents mid-IR spectrum analysis. The background was measured after every or every second sample (without the sample) and was calculated automatically by the software. Before the sample was placed on the accessory, the live spectrum was monitored to ensure that there is no noise in the background. The powdered sample was then loaded on the ATR aperture and the arm of the spectroscope was lowered to touch the sample. After each analysis, the file exported to a CSV format. The ATR aperture, the surrounding area, the spatulas, and forceps were cleaned with methanol and the live spectrum was monitored before the new samples were loaded, to avoid possible cross-contamination of samples. Baseline corrections were made at around 450, 800, 900, and 1200 cm^{-1} by observing the nearest minima by eye. Statistical error

was estimated by measuring the same sample a number of times and calculating the mean of the set.

II.2.1. Crystallinity Index or Splitting Factor

Crystallinity index or splitting factor (IRSF) has been intensively researched and applied to both burnt and diagenetically altered bone (Stiner *et al.*, 1995; Koon *et al.*, 2003; Munro *et al.*, 2007; Olsen *et al.*, 2008; Gonçalves, 2012). In this thesis this was assessed as a quantitative measure of the structural order of crystals of the inorganic (phosphate) portion of bone (Fredericks *et al.*, 2012). High IRSF indicates larger and well-ordered crystals, while low IRSF suggests poorly organised crystalline apatite content (Nagy *et al.*, 2008). It is calculated from the two absorption peaks at 605 and 565 cm^{-1} (Fig. 6), which peaks are the splitting of the $_{v3}PO_4$ domain (Olsen *et al.*, 2008; Thompson *et al.*, 2009; Ellingham *et al.*, 2016). The intensity of the maximums at around 605cm^{-1} and 565 cm^{-1} might also be indicators of fluoridation (Nagy *et al.*, 2008, 56). Each sample's height and location were recorded. The heights of these peaks were calculated and then divided by the minimum height in between them (Stiner *et al.*, 1995; Thompson and Inglis, 2009) as it is described in Nagy *et al.* (2008).

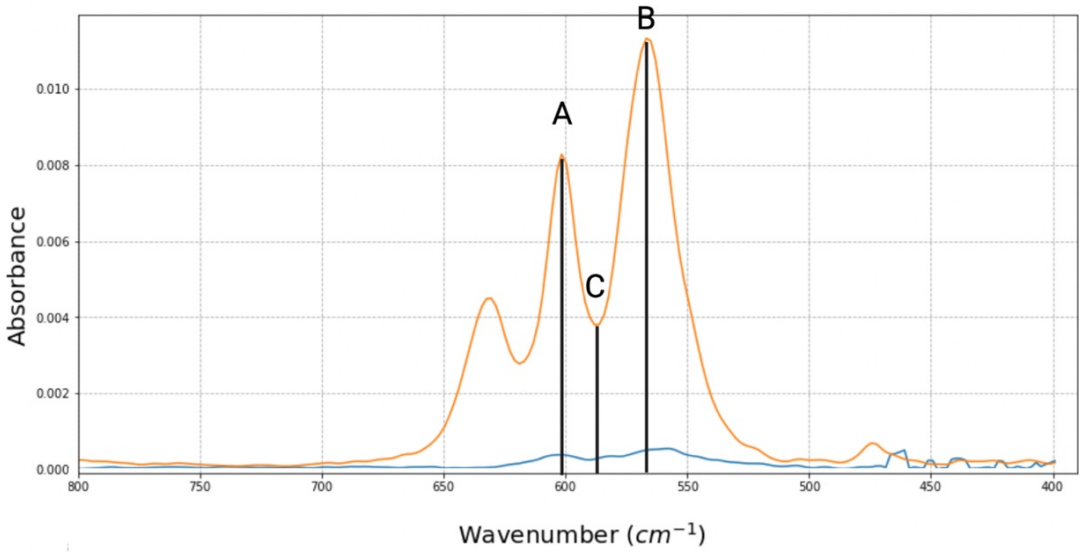


Figure 6 -- IR spectrum of sample SWFR1_burnt between 800 and 400 cm-1. The crystallinity index or splitting factor (IRSF) was calculated by (A + B)/C), where the A, B and C represent the peak forming the base line.

II.2.2 Other Calculated IR Ratios

Other calculated ratios include the (1) carbonate (CO_3) to phosphate (P) ratio (C/P = A_{1415}/A_{1035}, Fig. 7), which informs on the total carbonate content of the sample; (2) the carbonyl (CO) to carbonate (CO_3) ratio (C/C= A_{1650}/A_{1415}), which provides the ratio of organics to the mineral phase; (3) the type B carbonate to phosphate ratio (BPI = A_{1415}/A_{603}); (4) the type A carbonate to phosphate ratio (API = A_{1540}/A_{603}); (5) the type B to type A carbonates (C/C = A_{1450}/A_{1415}); (6) cyanamide to phosphate (CN/P = A_{2010}/A_{1035}); (7) the phosphate high temperature (PHT = A_{625}/A_{610}); and the (8) Amide I to phosphate ratio (N/P = A_{1660}/A_{1035}), which informs on the organic to mineral ratio (Thompson *et al.*, 2009).

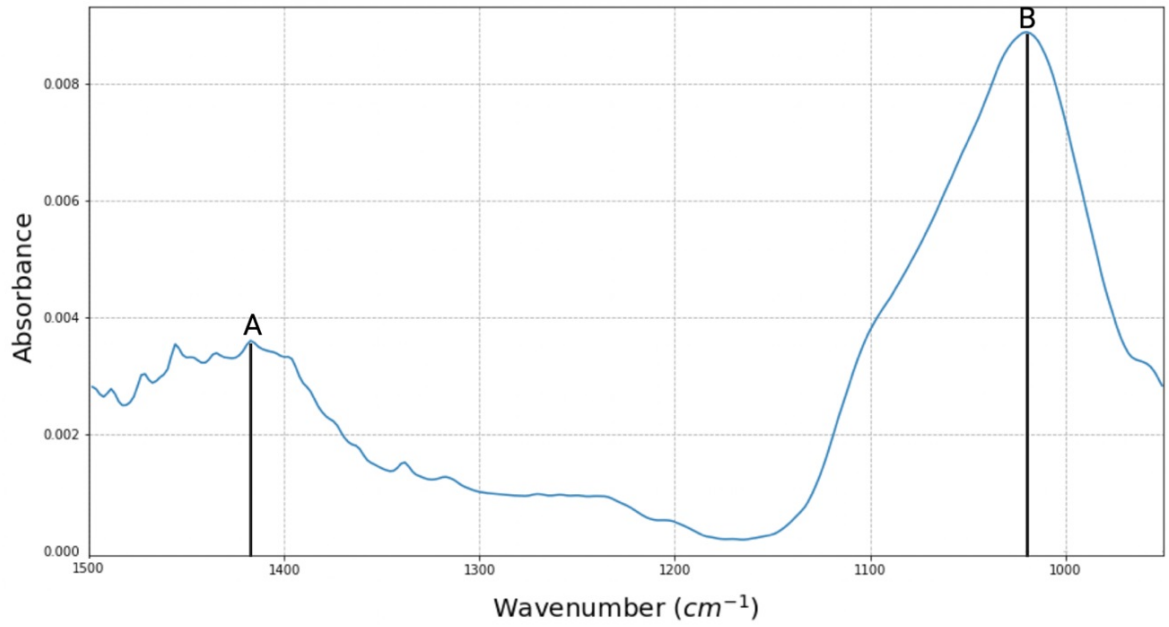


Figure 7-- Example of the calculated carbonate to phosphate (C/P) ratio calculated by A/B on sample SWF5D1Y1_unburnt. The other ratios mentioned were calculated using the same formula.

Although two organic-to-mineral ratios were assessed, amide I (N/P ratio) holds the most significance, since it shows the decomposition in the intermolecular collagen cross-links. The ($_{v}$(C=O)) vibration approximately at 1660 cm^{-1} shows the preservation of amide I; the ($_{v}$(C—N)) vibration at around 1550 cm^{-1} is the amide II, and amide III is represented by the weak peaks at around 1250 cm^{-1} (Thompson *et al.*, 2009; Ellingham *et al.*, 2016). Thus, the most significant amide I peak (at 1660 cm^{-1}) is used in combination with the $_{v1v3}PO_4$ peak around 1035 cm^{-1} (Fredericks *et al.*, 2012) as the primary indication for collagen content in the IR spectra.

II.3 Electron Microprobe Analysis

Electron Microprobe Analysis (EMPA) was used in this thesis to measure the major and trace elemental concentration of unburnt and burnt pig bones at different PMIs, as well as the Neolithic cremated human bone fragments. The postmortem elemental concentration of bone depends on the substitutions from the environment (see section I.1.1).

EMPA is a standard-based microanalytical technique, which produces fully quantitative chemical results of solid material at as low as 1-micron scale. It is widely used for material characterisation (Lambert *et al.*, 1983; Woodman *et al.*, 1984; Pyle *et al.*, 2002; Rinaldi and Llovet, 2015; Llovet *et al.*, 2021). EMPA uses two types of spectrometers: energy-dispersive (EDS) for solid state detectors and wavelength-dispersive (WDS) for crystal diffractors with gas detectors (Llovet *et al.*, 2021). Both mounted spectrometers work by collecting characteristic X-rays from a polished surface of a specimen that is bombarded with electrons. EDS sorts X-rays by energy and produces the entirety of the energy spectrum. EDS was used in this study to qualitatively determine and WDS to quantitatively measure the elemental composition of unburnt and burnt bone. To quantitatively assess a micron-scale spot in a material, an electron beam is focused upon a point on the sample in order to compare the standards of known composition and the characteristic generated X-ray intensity of the element in the sample while correcting for the variations in the matrix effects between the standard and the sample (Llovet *et al.*, 2021). The ratio of the generated X-ray intensity from the sample and the known intensity of the standard is the *k-ratio* (Castaing, 1951). However, the emitted X-rays have a different intensity from the generated intensity, due to the effects of electron backscattering, the inter-elemental absorption, and fluorescence of X-rays in the matrix of a sample (Walshaw, 2018). These matrix effects might increase or decrease the X-ray production and change the X-ray emission intensity compared to the reference standard (Llovet *et al.*, 2021). These issues are resolved by a series of calculations known as matrix corrections (e.g. ZAF, Phi Ro Z, XPP) to reach a sensitivity as high as 1-100 ppm level and a commonly accepted 1-2% accuracy range (Walshaw, 2018; Llovet *et al.*, 2021).

II.3.1 Preparation & Analysis

The unburnt bone samples were defatted in a 2:1 chloroform:methanol mixture for 8 to 20 weeks. Defatting was estimated to be completed once the liquid mixture had no visible solid

particles and discolouration. A total of 56 unburnt and burnt bone fragments were embedded into epoxy cold mounting resin and a catalyst or hardener (Spectrographic Ltd., Leeds, UK) and placed under vacuum in a desiccator to ensure diffusion of the resin into bone pores and to prevent bubble formation. Mounted blocks were then ground with carbon papers of progressively finer grit size (800, 1200, 2500) using a grinding and lapping machine (Buehler, Lake Bluff, IL, USA), making sure that the front facing surface of the block are ground flat.

The protocol used are the standard preparation protocol for the EMP at the Research Laboratory for Archaeology and the History of Art (RLAHA), University of Oxford. The blocks were then polished on a Buehler wheel using 3 μm diamond paste (DP-Paste M, Struers A/S) and a satin woven acetate polishing cloth (DP-Dac, Struers A/S) for 30 minutes following another 5-minute cycle using another polishing cloth with 1 μm monocrystalline diamond suspension (MetaDi, Buehler). Water was added every 5 minutes to the process during both polishing phases. Faultless polishing is critical for precise and accurate analysis on the electron microprobe, so the emission of X-rays is emitted from the same level of polished surface of the sample. The mounts were cleaned in an ultra-sonic water bath after each phase, then finished with another round of ultra-sonic bath in petroleum ether (40°-60°C, analytical reagent grade, Fisher Scientific) for 7 minutes. Samples were then carbon-coated using a carbon evaporation coater (HHV Auto 360), the carbon acting as a conductive layer to prevent charging. Carbon-coating was completed at the Department of Earth Science, University of Oxford, while the rest of the described preparation were done at the RLAHA, University of Oxford.

A JEOL JXA-8200 electron microprobe was used for this study at RLAHA. The EDS detector was used only to determine what elements are present in the bones, but the main focus was on quantitative (WDS) EMPA by spot analysis. Spot analysis was performed in the outer cortical, mid-cortical, inner cortical zones and around Haversian canals. This type of spatial analysis is essential, since the outer layer of the bone might have a different distribution of

elements than the mid- or inner cortical bone adjacent to the medullary cavity. An accelerating voltage of 15 kV, 10 nA beam current and 10-micron beam were used to analyse the polished samples. Peak count times were 30 s for P, Al, Na, Si, K and Ca; 40 s for Cl; and 60 s for Mg, Sr, Fe and Mn. Background counts were collected for half the peak count time either side of the peak (Pyle *et al.*, 2002). Homogeneous, well-characterised standards are the basis of WDS-EMPA; thus the microprobe was calibrated using a range of mineral standards, and the accuracy of the calibration and data was verified by analysing apatite standards (Durango, Bamble and Wilberforce) and previously analysed secondary bone standards (Appendix D) at the start of every run. Reference materials were within ±1 standard deviation of the preferred values (Jochum *et al.*, 2006). Analytical errors of the EMPA and detection limits for the measured elements are provided in chapter IV, Table 4. and more information on the use of the technique in chapter IV.

II.4 Sampling and Chemical Treatment for Collagen Extraction

The following description of sampling and chemical treatment for collagen extraction was only performed on the unburnt bones, since burning destroys the organic component. Thus, bone in this section always refers to the unburnt samples. The bone samples used for this part of the study were also defatted in a 2:1 chloroform:methanol mixture for 8 to 20 weeks. The described works below were in line of the Oxford Radiocarbon Accelerator Unit (ORAU) procedure for chemical pretreatment and collagen extraction for radiocarbon dating (Brock *et al.*, 2010).

The bone samples were manually cleaned by aluminium oxide powder air abrasion to remove visually assessable contaminants. Then, the fragments were cut and finely crushed with a pestle and mortar or with a tungsten carbide spherical burr drill bit. Approximately ~500 mg of bone powder was weighed in an electronic balance. Preceding the treatment, each sample

was placed into a pre-baked (500 °C) glass tube with its unique identification number (bone sample number). The pre-baking took place to remove organic contaminants. The collagen extraction protocol at ORAU is a modified Longin-method, consisting of (1) acid-base-acid (ABA) protocol; (2) gelatinisation; (3) EZEE-filtration; and if a large amount of contamination suspected (4) ultra-filtration (Brock *et al.*, 2010). However, since the experimental bones used in this study were modern, ultrafiltration was not needed. Thus, the powdered samples were rinsed with 0.5 mol/L hydrochloric acid three times with 1-2 h interval between them. After each wash the samples were centrifuged. The last HCl rinse was left in the fridge for 24 h. Then the decalcified solution was rinsed with Milli-Q ™ ultrapure distilled, deionised water and centrifuged for 3 washes. A 0.1 mol/L sodium hydroxide soak for 30 mins followed to remove humic substances and non-collagenous residues. Samples were again rinsed with Milli-Q ™ three times. Gelatinisation was done by a hot acid solution (pH 3, 70°C) for 20 h and filtered using pre-cleaned EZEE-filters™. The filtered gelatine was then collected and transferred into a new pre-baked glass tube. The samples were then frozen at -18 °C and lyophilised in a VaCo 5 freeze-dryer (Zirbus, Germany) for ~20 h. The resulting collagen was weighed on an electronic balance and the resulting yield gave an indication of the percentage of collagen preserved in the bones.

II.5 Data Analysis & Statistics

All data analysis was performed using Python programming language in Jupyter notebook environment, except the data labelling application for histology (section II.5.4), which also used a number of other languages. Descriptive statistics and linear regression (as implemented in *spicy* and *stats* libraries) were used in each scientific paper to measure the strength of the relationship between the measured changes and the postmortem interval (PMI) in both the unburnt and burnt bones. Dimensionality reduction techniques (as implemented in

scikit-learn library) were used in Chapter IV, while MANOVA and multivariate comparison tests were performed in Chapters IV and V.

II.5.1 Linear Regression

Regression helps to decipher whether, or not, and how features influence the other or how variables are connected. Linearity in algebra means there is a linear relationship between two or more variables. In a 2D space this would result in a straight line. Thus, linear regression predicts a dependent variable value (y) by being given independent variables (x), assuming that there is a linear relationship between x and y. The equation for a straight line is:

$$Y = mx + b$$

where m is the slope of the line and b is the intercept. The optimum intercept and the slope together give the most likely line (or least mean error) that can describe the relation between the variables (Olive, 2017).

Linear regression was chosen as we assume time (or PMI) has a linear relation with the other parameters and it is present in all experiments. In the analyses time is always an independent variable, and the studied features are dependent variables or covariates. After data management in *pandas*, *spicy.stats* library in Python was used to produce the graphs and the results of the linear regressions. The linear regressions' null hypothesis was always that parameter X does not change with PMI/time and the statistical significance was assessed by associated p-values to the regression coefficients ($\alpha = 0.05$).

II.5.2 Coefficient of Variation

The coefficient of variation (CV) was used to evaluate the scattering of parameters in each group with different PMI and state (unburnt or burnt) and/or features (depending on the dataset and article). CV is a measure of relative variability between groups controlling for differing means and is expressed by:

$$CV = \frac{SD}{\bar{x}}$$

where SD is the standard deviation and $\bar{x}$ is the mean. Multiplying the coefficient by 100 is an option to report results as a percentage, but in this thesis, results are presented as proportions. The higher the CV, the greater the level of dispersion around the mean. Consequently, the lower the CV, the more centred the data around the mean.

II.5.3 Dimensionality Reduction

Reducing the number of input variables can help with better visualisation of the data and improve performance in statistical analyses. This was especially important in large datasets with many variables like the EMPA and FTIR datasets in Chapter IV, which had thousands of datapoints rendering any meaningful analysis difficult to perform. The aim at dimensionality reduction techniques is to reduce the number of features in a dataset without losing useful information. It would also be very difficult to visualise data in higher dimensions, so reducing the space to 2D allows for better pattern recognition. The two dimensionality reduction techniques used in this thesis were Principal Component Analysis (PCA) and Linear Discriminant Analysis (LDA).

II.5.3.1 Principal Component Analysis

Principal Component Analysis (PCA) is a dimensionality reduction technique that extracts a new set of variables (principal components) from an existing high dimensional set of variables (Pearson, 1901). Each principal component (PC) is a normalised linear combination of the input variables that can explain variance in the data. The first PC (Z^1) is expressed as:

$$Z^1 = \Phi^{11}X^1 + \Phi^{21}X^2 + \Phi^{31}X^3 + \ldots + \Phi p^1 Xp$$

where Φp^1 is the loading vector for PC1 and $X^1..X^p$ are normalised predictors. The loadings are restricted to a sum of square equals to 1 to avoid arbitrary scaling of variance and

hence define a direction. The line described by the first PC produced in the *p* dimensional space has the minimum total distance to all of the observations. The total distance from a line to the data point is measured using the average squared Euclidean distance. To perform PCA the data is shifted and normalised such that the mean of X^p equals to 0 and standard deviation of each variable equals to 1.

PCA finds the "best" line according to different criteria. It maximises the variance of values and in the meantime gives minimum error orthogonal to the line. The relation between these two criteria can be described by the Pythagoras theorem (Hotelling, 1933; Gulmine and Akcelrud, 2006). In short, the higher the variance, the lower the error is because their sum is equal to the total variance in the data which is constant. The covariance matrix is a square matrix representing the covariance of the variables with *each other*. This square symmetric matrix can then be diagonalised by a new orthogonal system determined by its eigenvectors and eigenvalues. The eigenvalues will be located in a diagonal matrix and the eigen vectors in columns of an orthogonal matrix, i.e. the correlation between columns is 0. The variance of a projection is expressed by the sum of the eigenvalues. PC1 is given by the first eigenvector of the covariance matrix.

PCA was performed with the Python language *scikit-learn* implementation in the following way. First, the data were loaded into a *DataFrame* data structure where features were separated into columns. Then, the features were demeaned and normalised with a standard scaler (using *sklearn StandardScaler*), meaning that the values were replaced by the distance from the sample mean in standard deviation units. Then, from *sklearn.decomposition* PCA was imported to fit the transformation to the scaled data. The resulting projections were visualized in 2D graphs defined by the first and second principal components (PC1 and PC2, respectively) plotted using *matplotlib.pyplot*. The point in this new coordinate show the loadings associated to each data point. The scatter plot of PCA makes it possible to visualise and observe groups

of samples as well as outliers and investigate inherent patterns in the data. The loading plots help to visualise which attribute is corresponding to the groupings and outliers. In this study, PCA is used to identify grouping methods that show maximum variation between PMI groups and state (unburnt/burnt) as well as extracting key indicators from the EMPA and FTIR datasets in Chapter IV.

PCA was performed on the FTIR ratio values (N=11), rather than on the whole spectra. This was done because PCA is not able to determine which wavenumbers count as a peak, which is of importance in the spectra. Thus, a convoluted band can have the highest value, but it does not mean that it would be a peak of interest in the study. Peak identification was done first by visualising the band to confirm that it is an actual peak, and then the value and wavenumber were recorded for the ratio calculations. This would not have been possible if the whole spectra would have been given to the algorithm. PCA simply takes the average of the largest value at each wavenumber, which is an issue in spectral data, because there can be shifts in the wavenumbers, even if it is the same peak belonging to the same mode. Peak shifts in the spectra are common and are caused by substitutions in the bioapatite, which PCA would not be able to identify as the same functional group.

II.5.3.2 Linear Discriminant Analysis

Linear Discriminant Analysis (LDA) is a supervised classification algorithm and a dimensionality reduction technique that works by projecting a labelled dataset into a new space that separates the data points by their assigned class using the best fit. The model seeks to find the linear combination of predictors by maximising the between-group variance relative to the within-group variance (Kuhn and Johnson, 2013). Matrix factorisation is at the core of LDA, exactly like in PCA, so data standardisation is needed. LDA assumes a common positive definite covariance matrix for all the groups. The main difference between PCA and LDA (for the purposes of this study) is that while PCA is an unsupervised classification technique, LDA

is a supervised approach, where an algorithm relies on labelled input data to estimate a function that can predict output values (Ngailo, 2020).

LDA models estimate the mean and covariance from the input data for each class and makes predictions by estimating the probability that new input datapoints belong to *a priori* classes. The class with the highest probability will be determined as the predicted class for any new data point. This is based on the Bayes Theorem of probability estimation (Bayes, 1764) of the output class given the input variables by assessing the probability of each class and the probability of the data point belonging to that class:

$$P(Y = k|X = x) = \frac{\pi_k * f_k(x)}{\sum_l \pi_l * f_l(x)}$$

where π_k is the prior probability of each class, k is the index of output class, and x is the input data, $f_l(x)$ is the estimated probability of x fitting into class l. Adding the assumption that each class has a Gaussian distribution and making simplifications to the above equation can be expressed as:

$$D_k(x) = x * (\frac{\mu_k}{\sigma^2}) - (\frac{\mu_k^2}{2\sigma^2}) + ln(PI_k)$$

where D is the discriminant function and $D_k(x)$ is then the function for class determined by x, μ_k is the mean value of all x belonging to class k. This leaves μ_k, σ^2, and π_k to be estimated from the input data (Kuhn and Johnson, 2013).

LDA was a better statistical model for the purposes of this study than PCA since it considers data labels as well as the features. *A priori* categories in this study were state (unburnt vs burnt), PMI (0, 14, 34, 91, 180, and 365 days), zone (outer-, mid-, inner-cortical, and around vascular canals) in the EMPA dataset and state and PMI in the FTIR dataset. Each sample's confidence score determined the parameter based on which they were placed into one of these categories. After data management and normalisation (by *StandardScaler*), *sklearn* Python

library was used with its LDA function and plotting of the results were done using *numpy, matplotlib* and its *pyplot* package.

II.5.3.3 Multivariate Analysis of Variance

Multivariate analysis of variance (MANOVA) is an extension of the analysis of variance (ANOVA) to multiple dimensions. One-way ANOVA investigates the effects of independent variables on dependent variables by assessing only one dependent variable at a time. MANOVA also performs the same function but by assessing multiple dependent variables simultaneously (Stevens, 2002). This means that while ANOVA cannot identify patterns in multiple dependent variables, MANOVA can.

Pairwise posthoc test or multivariate comparison test (MCT) is performed when particular experimental conditions have statistically significant mean difference or a specific aspect between the group means are present (Lee and Lee, 2018). When the null hypothesis is rejected by MANOVA, it is still not known how one group differs from others, thus MCT with the pairwise Tukey method was performed in Chapter IV. The Tukey method assumes that every comparison is independent and it was chosen because it tests every possible pairing within the groups being tested (Lee and Lee, 2018).

MANOVA was used in Chapter IV to examine for statistical differences in one dependent variable (PMI) by multiple independent grouping variables (EMPA and FTIR datasets) using *Statsmodels* Python library. This was coupled with MCT to identify which specific groups significantly differed from one another. MCT was also applied from the *Statsmodels* Python library.

II.5.4 Data Labelling Application

The data/feature labelling application was built to statistically assess the areas of bones affected by microbial bioerosion and heat-induced microscopic changes in Chapter III. It was built using Python programming language and the Flask framework on the backend and Javascript, HTML, CSS with bootstrap and jQuery on the frontend. The backend in Python uses Flask as a server for a web application. Functions were built to manage images, cut them into samples, pick images to be displayed in the UI and update data accordingly. A UI with an image viewer as well as several buttons for labelling and a settings menu for configuration was also built. Using the settings menu, the user can choose the folder where images and the output file for the data should reside. The Python application will then automatically read all images and generate samples using *scikit-image*, a Python library for image processing. Once a grid of $n * m$ was built, the samples corresponded to squares from the original images. The user of the application is then presented with samples drawn at random and prompted to input a label. After confirming the label(s), the data is passed from the UI to the Python application. The Python application saves the result in a CSV file for further analysis. The CSV contains information about what image the sample originates from, what block in that image, and what labels were added. The user is then presented with a new sample. The application keeps showing unlabelled samples until all samples have been labelled. A 'skip' button was added, which made it possible to skip unlabelled images (squares from an image), but the image was later recycled into the unlabelled images and the user was prompted to add label(s) on it at a later point. Since all data are saved in a file, a user can do labelling in as many batches as they want and return to it later.

The use of this data labelling application allowed for the quantitative assessment of the percentage of areas affected by microbial bioerosion and/or heat-induced histological changes

(Chapter III). The random selection of the images excluded bias in labelling, hence the samples were examined ‘blind’ by the observer.

Chapter III: Paper 1-- Assessing the reliability of microbial bioerosion features in burnt bones: A novel approach using feature-labelling in histotaphonomical analysis

---

Published as below:

Végh, E. I., Czermak, A., Márquez-Grant, N., Schulting, R. J. 2021. Assessing the reliability of microbial bioerosion features in burnt bones: A novel approach using feature-labelling in histotaphonomical analysis. Journal of Archaeological Science:Reports 37, 102906. https://doi.org/10.1016/j.jasrep.2021.102906

Abstract

Objectives: Recent histotaphonomic studies have focused on the presence of features thought to be caused either by bacteria (microscopic focal destruction/MFD and cyanobacterial tunnelling) or fungal (Wedl tunnelling types 1 and 2) attack on unburnt bone. Identifying these characteristics on burnt bones could indicate the state of decomposition before burning, with important repercussions for both archaeological and forensic contexts.

Materials and Methods: Fleshed pig (Sus scrofa, N=25) tibiae were left exposed on a field, then collected at 14-, 34-, 91-, 180-, 365-day intervals before being burnt in an outdoor fire (≤750 °C). Fresh (fleshed) legs (N=10) acted as unburnt and burnt controls. Thin sections were examined using transmitted light microscopy and backscattered scanning electron microscopy. Diagenetic traits were quantitatively and systematically assessed by a novel data labelling application developed for this study.

Results: Features meeting the published characteristics of microbial bioerosion ('Wedl tunnelling', 'lamellate' and 'budded MFD') were significantly correlated with time since deposition on the unburnt bones. The presence of features resembling 'Wedl 2 tunnelling' on fresh burnt bones indicates that they are an artefact. Only budded MFD increased significantly over time in the burnt groups. Features meeting the published characteristics of Wedl 2 tunnelling were present on the fresh burnt bones.

Discussion: The presence of many features seemingly indistinguishable from those caused by bioerosion on the freshly burnt control bones suggests that burning is not only able to conceal features thought to be the result of bioerosion but can produce them as well. Thus, such features are not a reliable indication of bioerosion. Budded MFD may be a viable indicator but more research is required.

Keywords

Microbial bioerosion, burning, bone, cremation, taphonomy

III.1 Introduction

Understanding early postmortem changes to the body is of interest in many fields, including archaeology, physical anthropology, forensic science, palaeobiology, and palaeontology. Deciphering early bone diagenesis and shedding light on the processes that lead to fossilisation present a challenge, one that is further exacerbated when bone is subjected to cremation. Identifying bioerosion on burnt bones would open the possibility of establishing whether a body had gone through a decomposition phase with soft tissue still present prior to burning. This research aims to investigate whether bioerosion features can be used as an indication of decomposition on burnt bones, which has implications to understanding funerary practices in the archaeological record as well as understanding the sequence of events leading to deposition in forensic investigations.

Burning of the body can occur either when the body is fully fleshed (e.g. homicide, suicide, accidental fires, cremation) or once it has decomposed to different degrees (e.g. burning to conceal evidence of murder, cremation, accidental fires, freeing up space in a cemetery) in both archaeological and forensic contexts. Early studies mainly focused on establishing whether bone was at either of the two extremes – fleshed or dry – of the spectrum when burnt (Baby, 1954; Binford, 1963; Buikstra and Swegle, 1989; Etxeberria, 1994; Spennemann and Colley, 1989; Whyte, 2001). The methods employed were primarily macroscopic, recording the presence of warping and of thumbnail fractures (Buikstra and Swegle, 1989; Spennemann and Colley, 1989; Whyte, 2001). However, this has been shown to be related primarily to collagen content (Gonçalves *et al.,* 2011). Currently, it remains challenging to identify the body's state of decomposition before burning.

A reliable method of establishing the body's stage of decomposition at the point of burning would help determine whether this occurred immediately or sometime after death. In

archaeology, the interaction between anthropogenic and natural processes is vital to understand human behaviour connected to past funerary rites. For example, it has been suggested that at some Neolithic and Bronze Age sites in Ireland, including the passage tombs of the Boyne Valley and Fourknocks, as well as Kilgreany cave (Waterman *et al.*, 1978; Dowd, 2008; Cooney, 2014), human remains were either passively or actively excarnated before inhumation and cremation. At other Irish sites, such as Tully, the excavators claimed that the bodies were burnt with full soft tissue coverage (Wells, 1978). These claims were based on supposedly diagnostic fracture patterns, which, as noted above, may be problematic.

There are a few cases discussed in the forensic anthropological literature in which a single individual has been found partially burnt (Bontrager and Nawrocki 2008; Garrido-Varas and Intriago-Leiva 2015). The postmortem intervals were established using both the signs of carnivore gnawing and patterned thermal destruction. However, usually only fragmented calcined remains are encountered. Thus, there is a need for better and more accurate methods of determining the stage of decomposition from a single burnt skeletal fragment.

Bone is a complex, composite material, which undergoes diagenetic alterations post-deposition. Three distinct diagenetic pathways can be distinguished (Collin *et al.,* 2002): (1) chemical degradation of the organic component (collagen hydrolysis); (2) chemical degradation of the inorganic phase (bioapatite dissolution); and (3) microbial degradation of both phases (Child, 1995; Hedges and Millard, 1995; Millard, 2001; Collins *et al.,* 2002; Nielsen-Marsh and Hedges, 2002; Huisman *et al.,* 2017; Turner-Walker and Jans, 2008; Kontopoulos *et al.,* 2016). Pathway 3 presumably happens either (1) rapidly after death as it is thought to be linked to putrefaction processes involving soft tissues (Collins *et al.*, 2002; Jans, 2005; Fernández-Jalvo *et al.*, 2010; Huisman *et al.*, 2017) or (2) by soil bacteria post-deposition (Turner-Walker, 2012; Kendall *et al.*, 2018; Turner-Walker, 2019). This study

focuses on this pathway's (i.e., microbial degradation) supposedly diagnostic features in an effort to shed light on the early postmortem history of the remains.

Histotaphonomy, the taphonomy of bone at the microstructural level, has been often employed by researchers to investigate the biological deterioration of bone (White and Booth, 2014; Kontopoulos *et al.*, 2016a). Many studies use features of bacterial attack on unburnt bones to inform on the initial postmortem period of the body (Child, 1995; Jans *et al.*, 2004; Nielsen-Marsh *et al.*, 2007; Hollund *et al.*, 2012, 2014; White and Booth, 2014). Whether the origin of the bioerosive bacteria is endogenous or exogenous, most studies focus on archaeological bone (Jans *et al.*, 2002; Turner-Walker and Jans, 2008; Brönnimann *et al.*, 2018), and some on recent bone (Yoshino *et al.*, 1991; White and Booth, 2014; Kontopoulos *et al.*, 2016a; Lemmers *et al.*, 2020). Furthermore, to our knowledge there have only been two studies on histotaphonomic features on burnt bones (Grévin *et al.,* 1991; Lemmers *et al.*, 2020). Grévin *et al.* (1991) reported that human bones from a Late Bronze Age site at Pincevent, France, had been buried for weeks to months prior to cremation based on microradiographs showing 'typical' postmortem bacterial attack. Recently, Lemmers *et al.* (2020) proposed that bioerosion features survive in burnt bones and can be readily distinguished from alterations in the microstructure caused by burning.

All scholarship agrees that there is a need for more experimental histological studies. This paper aims to assess whether bioerosion features are useful indicators of decomposition in burnt bones.

III.1.1 Histotaphonomic features in bone

The specific causative agents of microstructural changes are poorly known, but mainly they are attributed to bacteria, fungi, or marine based organisms (Bell, 2012a). Microbiological decay of the body commences soon after death. Bacteria and fungi alter hard tissues by entering through bone's vasculature (Bell *et al.,* 1996; Millard, 2001). The bacterial flora in the gut

initially affect the bone from the endosteal surface, while exogenous bacteria from the environment (e.g. soil) attack the bone from the periosteal surface (Hackett, 1981; Jans, 2008; Daniel and Chin 2010; Boaks *et al.,* 2014; White and Booth, 2014; Kontopoulos *et al.*, 2016).

Morphological changes to bone resulting from bioerosion was first described by Wedl (1864) and Roux (1887), and subsequently by Hackett (1981) and Garland (1987). These changes include (1) small channels (Wedl, 1864) caused by fungi (Roux, 1887), (2) microscopic focal destruction (MFD), which can be linear longitudinal, lamellate, or budded (Hackett, 1981), and (3) other types of diagenetic changes, such as reduction in birefringence, inclusions, and infiltrations (Garland, 1987). Hedges, Millard, and Pike (1995) developed the *Oxford Histological Index* (OHI) to approximate the preservation of bone histology. The OHI is still used in bone histology studies, providing an ordinal scale assessment of the degree to which bone is affected by bioerosion. We build on this here by including a quantitative assessment of the percentage of the bone affected.

More recent research has focused mainly on the presence of MFD, Wedl tunnelling, Wedl type 2, and cyanobacterial tunnelling on unburnt bone (see Table 2).

Feature	Appearance	Causative agent	Context and Environment
Microscopic Focal Destruction (MFD)	Linear, Budded, or Lamellate structures around Haversian canals	Endogenous bacteria (Bell *et al.*, 1996; Trueman and Martill, 2002; Jans *et al.*, 2004; Nielsen-Marsh *et al.*, 2007; Jans, 2013; White and Booth, 2014)	Terrestrial
		Soil bacteria (Turner-Walker, 2007; Grine *et al.*, 2015; Kontopoulos *et al.*, 2016a; Kendall *et al.*, 2018; Morales *et al.*, 2018)	
Wedl tunnelling	Dendritic structures	Fungi (Hackett, 1981; Bell *et al.*, 1991; Trueman and Martill, 2002)	Marine (Garland, 1987; Millard, 1993)
			Terrestrial: surface exposed and/or buried de-fleshed bones (Trueman and Martill,

			2002; Jans, 2008; Brönnimann *et al.*, 2018)
			Oxygenated, wet environments in neutral to acidic soils (Huisman *et al.*, 2009, 2017)
Wedl type 2/Enlarged canaliculi/enlarged osteocyte lacunae/Non-Wedl MFD	Enlarged canaliculi, resembling a spider-like structure	Fungi (Trueman and Martill, 2002; Kontopoulos *et al.*, 2016a; Kontopoulos, 2019)	Terrestrial
		Bacteria (White and Booth, 2014; Booth, 2016)	
Cyanobacterial tunnelling	Tunnelling from periosteal surface of bone	Bacteria (Bell *et al.*, 1991; Jans, 2008; Bell, 2012; Turner-Walker, 2012, 2014)	Marine- or fresh water (Bell *et al.*, 1991; Jans, 2008; Bell, 2012; Turner-Walker, 2012, 2014b)

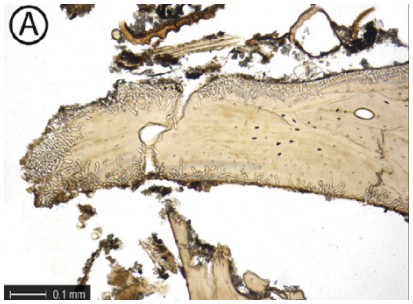
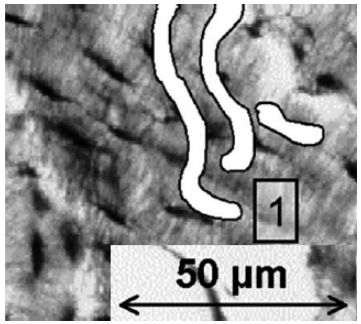
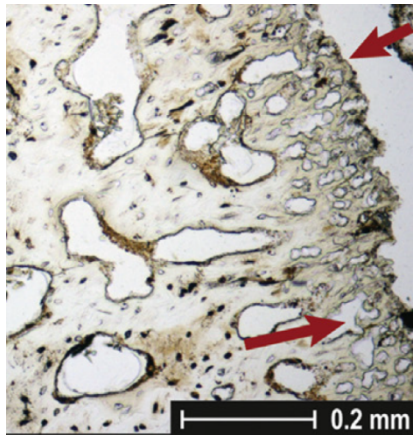
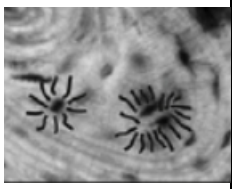
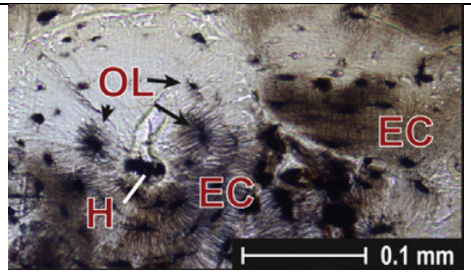
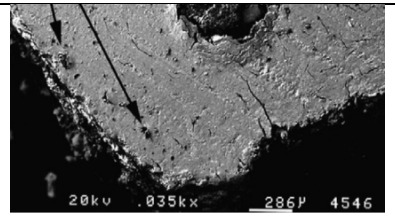
Table 2 --Microbial bioerosion features, their thought to be causative agents, contexts and environments in the literature.

Diagenetic features on bones are usually studied under either transmitted light microscopy (Jans *et al.,* 2002; Jans *et al.,* 2004; Jans 2005; Tjelldén *et al.,* 2018) or electron microscopy (Bell *et al.,* 1991; Bell, 2012b; Turner-Walker, 2014), with a few studies employing both methods (Huisman *et al.,* 2017; Turner-Walker 2019). General changes in bone microstructure due to bacterial attack manifest in demineralised (darker) and adjacent hypermineralised (brighter) areas on the backscattered scanning electron microscope (BSEM), which recently has been proposed to be a more effective means of identifying bioerosion features (Turner-Walker, 2019).

Complicating discussion of histotaphonomical features is the fact that morphologically identical or similar features have been given different terms in the literature (see Table 3). For example, the same dendritic features often called Wedl tunnels (Brönnimann *et al.*, 2018), are also called as non-Wedl MFD (Fernández-Jalvo *et al.*, 2010), Wedl type 2 (Trueman and Martill, 2002; Brönnimann *et al.*, 2018), lichen penetration (Fernández-Jalvo *et al.,* 2010), and early stage of non-Wedl MFD (White and Booth, 2014). This distinction is crucial, since for

example Wedl tunnelling are thought to be caused by fungi from the burial environment (Fernández-Jalvo *et al.,* 2010; Brönnimann *et al.,* 2018), while non-Wedl MFD have been attributed to bacterial activity, most often from the gut (Bell *et al.*, 1996; Trueman and Martill, 2002; Jans *et al.*, 2004; Nielsen-Marsh *et al.*, 2007; Jans, 2013; White and Booth, 2014). The present study uses the terminology outlined by Brönnimann *et al.* (2018) because of its clear illustrations and descriptions.

1

Feature	Different naming of the features across the literature			
	 Cyanobacterial tunnelling, (Huisman *et al.,* 2017, 20, Fig 4.A)	 Wedl tunnelling (Jans *et al.,* 2004, 89, Fig 1)	 Cyanobacterial tunnelling (Brönnimann *et al.,* 2018, 50, Fig 4G)	 Wedl tunnelling -- no scale provided, x170 (Hackett, 1981, 251, Fig 2)
	 Wedl type 2 (Brönnimann *et al.,* 2018, 50, Fig 4E)		 Lichen penetration (Fernández-Jalvo *et al.,* 2010, 74, Fig 7.4)	

		Expanded osteocytic lacunae and canaliculi due to environmental infiltration (Tjelldén *et al.* 2018, 412, Fig. 6)		

Table 3--Identical histotaphonomic features named differently across the literature.

III.1.2 Histology of Burnt Bone

The primary focus of burnt bone histology studies has been on estimating fire temperature and duration (Herrmann, 1976, 1977; Nicholson, 1993; Holden *et al.,* 1995a,b; Quatrehomme *et al.*, 1998; Ubelaker, 2009; Absolonova *et al.,* 2013; Imaizumi *et al.,* 2014; Cambra-Moo *et al.,* 2017) or on species identification (Cattaneo *et al.*, 1999) using histomorphometry or histomorphology (Table 4). There is a considerable disagreement between different authors on when, and if, identifiable histological changes take place. The histological structure of bone has been variously reported to be nearly identical to that of unburnt bone when burnt under 600°C (Bradtmiller and Buikstra, 1984), 700°C (Herrmann, 1977), 900°C (Squires *et al.,* 2011), or 1200°C (Cattaneo *et al.*, 1999). However, it is unknown whether these were bone or air temperatures, which might be a source of discrepancy. Other complicating factors include the method of burning (e.g., furnace or natural fire), the type, size, and state of the bone, and the presence/absence of soft tissues.

Investigating histomorphological changes due to burning are essential to the current study, because these can influence the appearance of microbial bioerosion and hence their recognition to identify the postmortem stage at which the bones were burnt.

<table>
<tr><th>Temperature (°C)</th><th>Histomorphometric Changes</th><th>Histomorphology Changes</th></tr>
<tr><td>500</td><td>Increase in size and number of cracks due to differential shrinkage of bone tissues (Imaizumi et al., 2014)</td><td>Cracking, minute fissures, separation of the osteons from interstitial lamellae (Imaizumi et al., 2014)</td></tr>
<tr><td><600</td><td colspan="2">No change, identical to unburnt bones (Absolonova et al., 2013)
No cracking with minimal carbon deposits (Hanson and Cain, 2007)
Microfeatures identifiable, but less well preserved (Carroll and Squires, 2020)</td></tr>
<tr><td rowspan="2">600</td><td>Increase in osteon size diameter (Bradtmiller and Buikstra, 1984)</td><td rowspan="2">Individual lamellae often indistinguishable (Nelson, 1992)
Histological structures disappear with extensive carbon deposits (Hanson and Cain, 2007)</td></tr>
<tr><td>Haversian canals increased in size while the osteon’s diameter decreased (Nelson, 1992)</td></tr>
<tr><td><700</td><td colspan="2">No change, identical to unburnt bones (Herrmann, 1976, 1977)
Cracks present outwards of vascular canals (Hanson and Cain 2007)</td></tr>
</table>

700-800	Structural changes occur (Herrmann, 1976, 1977; Hummel and Schutkowski, 1987; Absolonova *et al.*, 2013)	
800	No changes below, shrinkage above (Van Vark, 1970)	No major changes below (Van Vark, 1970)
	No significant shrinkage (Cattaneo *et al.,* 1999)	Lamellar structure of bone is lost (Holden *et al.*, 1995b)
900	Microstructural changes occur (Squires *et al.*, 2011)	Haversian and Volkmann's canals cannot be distinguished, no microstructure preserved (Squires *et al.*, 2011) Granular surface appears (Fernández Castillo *et al.*, 2013) 700-900 °C: Degeneration of microscopic structures (<60% of area, Carroll and Squires, 2020)
1000	Shrinkage occurs (Cattaneo *et al.,* 1999)	Haversian canals survive, while Volkmann's canals, circumferential lamellae, resorption cavities are hard to differentiate (Absolonova *et al.*, 2013) Few misshapen Haversian canals survive, but 86.3% of sample area show complete fusion of hydroxyapatite (Caroll and Squires, 2020)
1200	Microstructural changes start to occur (Cattaneo *et al.,* 1999)	
1400		Haversian Canals and osteocyte lacunae indistinguishable (Holden *et al.*, 1995b)
1600	All structural features are completely destroyed (Holden *et al.*, 1995b; Fairgrieve, 2008)	

Table 4 -- Histomorphometric and histomorphology changes of burnt bone in the literature.

III.2 Materials and Methods

III.2.1 Experiment

Fleshed *Sus scrofa domesticus* (pig) tibiae were sourced from a local butcher, euthanised at 18 months. All limbs were kept in a freezer at –18°C until collection. Pigs, in addition to being easily sourced, have been widely utilised as a substitute for human bodies in decomposition, fire, and histology studies (Forbes *et al.*, 2005; Lynn and Fairgrieve, 2009; Thompson and Inglis, 2009; Bonney *et al.*, 2011; Symes *et al.*, 2012; White and Booth, 2014;

Kontopoulos *et al.*, 2016a). There is an ongoing discussion on how appropriate pigs are as human analogues (Matuszewski *et al.*, 2020), but they are considered to be reasonable proxies in many respects, including bone macro- and microstructure, remodelling, mineral concentration and density, as well as gut microbiota (Turner and Wiltshire, 1999; Forbes *et al.,* 2005; Pearce *et al.*, 2007; Wilson *et al.*, 2007; Feng and Jasiuk, 2011; Hollund *et al.,* 2014; White and Booth, 2014; Kontopoulos *et al.,* 2016). Long bones were chosen for the study because of their common use in histological studies, their large cortical bone area, and their survival rate (Booth and Madgwick, 2016).

The pig tibiae (N=25) were left to decay for 14, 34, 91, 180, and 365 days prior to burning on an outdoor fire. Fresh fleshed bones (N=10) served as unburnt and burnt control samples. The first round of fleshed tibiae were sub-aerially deposited on an open grassland area at Wytham Woods, Oxfordshire, England, in June 2018 and between February and June 2019. The exposed tibiae were protected from scavengers with a cage covered by layers of iron mesh. Scavenging produced tooth marks on nearly all bones, but only a few bones were completely removed from the cage (one of the 180-day and four of the 365-day postmortem bones).

Wytham Woods is located in a temperate climate with moderate to high rainfall averaging 717 mm, with monthly mean temperatures ranging from 1.6 °C in January to 20.3 °C in July with a long-term annual mean of 10.0 °C (Taylor *et al.*, 2011). At collection bones were partially covered by the soil, which may have instigated exogenous bioerosion. Soil pH range from 3 to 7 (Taylor *et al.,* 2011).



Figure 8 -- Burning of the 14- and 34-day postmortem bones on the pyre. Upper image was taken subsequently after the ignition of the fire, while the lower was taken when the bones have calcined. All outdoor fires were executed in the same manner. The pyres were built on a flat clearing, using bricks to provide support for a wire mesh holding the bones, as well as partial protection from the wind. While offering less control over temperature rather than a furnace, the use of an outdoor fire better

reflects real-world conditions due to the more variable temperatures of the fire, and the influence of the wind. Each fire was built and maintained in the same manner, using a mixture of hard and soft woods as fuel.

Pyres were built and maintained in the same manner, each fire lasting 2.5-3 hours, until the bones calcined (Fig. 8). Bone temperatures were monitored by a thermocouple, averaging 553 °C, with a recorded maximum of 751 °C. Maximum fire temperatures reached 995 °C. The bones were left to cool and subsequently collected for transport.

III.2.2 Analysis

Unburnt samples were defatted in a 2:1 chloroform:methanol mixture for between 8 and 20 weeks, in order to remove fat infilling the pores of bone tissues. Samples were taken before and after burning from the minimum diameter of the tibiae diaphyses. Samples were embedded undecalcified in transparent epoxy cold mounting resin and a catalyst (Spectrographic Ltd., Leeds, UK), in order to impregnate the bones within a solid medium to facilitate sectioning for microscopical analysis (Garland, 1987). The resin blocks (N=56) were then placed into a desiccator with vacuum pump to inhibit bubble formation. Two transverse thin sections (~50-70 μm) were cut from each sample using a Buehler saw fitted with a diamond blade (Buehler, Lake Bluff, IL, USA) and subsequently fixed onto glass slides using Eukitt mounting medium (Merck, Darmstadt, Germany) and covered with microscope glass slides.

The slides were examined under a Leica DM 2500 P transmission light microscopy (Leica, Wetzlar, Germany) using normal and polarised light at 50x, 100x, and 400x magnification. Each sample was composed of three to five images, which were taken across the bone with a USB camera (Brunel Microscopes Ltd., Chippenham, UK) per thin section at 50x magnification to represent bone from the periosteal to the endosteal surfaces, through the mid-cortical region for quantitative analysis. Higher magnification images were taken to observe and document more closely the features of interest.

Diagenetic traits on the optical microscopy images (N=270) were quantitatively assessed by calculating the percentage of areas affected by diagenetic and/or heat-induced features. This was done by a human observer clicking on the features present on each block (N=27,000) of randomly selected images in a data labelling application built for this study in Python (Flask web framework) and Javascript (jQuery library) programming languages. Each image (at 50x magnification) was divided into 100 equal blocks. The random selection of images across all samples by the application excluded bias in labelling, hence the samples were examined 'blind'. Results were automatically saved into a database recording whether a feature was present or absent within a block. The cumulative score of the 100 blocks estimates the proportion of the initial image that contains a given feature. Features (Fig 9) were labelled according to descriptions in Brönnimann *et al.* (2018, 46, Fig. 1), which are in turn based on figures in Jans (2004, 89, Fig. 1) and Hackett (1981, 250, Fig. 1). Features were initially labelled according to their closest comparanda in the literature, with no presuppositions being made regarding the veracity of the labels. This usage is indicated by single quotation marks. Some features were more variable in appearance than those discussed in the literature. For example, the label 'cyanobacterial tunnelling' was applied when the tunnels looked the most like the image in Brönnimann *et al.* (2018) taking into account tunnel diameters (Fig. 9) after re-examination of all images by the same researcher (EIV).

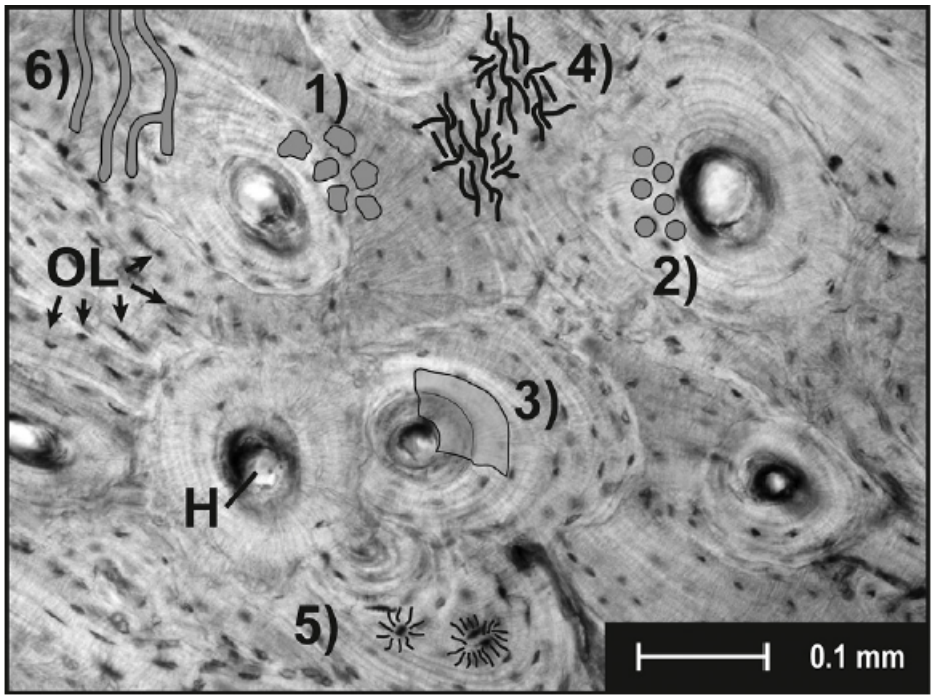


Figure 9 -- Criteria for labelling microbial bioerosion from Brönnimann *et al.*, 2018. 1) Budded MFD; 2) Linear longitudinal MFD; 3) Lamellate MFD; 4) Wedl tunnelling; 5) Wedl 2; 6) Cyanobacterial tunnelling (Brönnimann *et al.*, 2018, 46, Fig. 4). Features that appeared to be similar to linear MFD were not labelled in this study, because they were caused by burning.

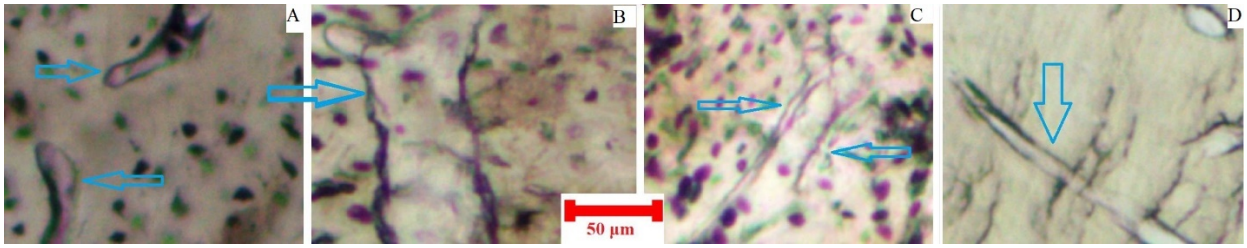


*Figure 10-- Variation of features appearing to be tunnels in the different samples. **A** and **B** are of Volkmann's canals, **C** and **D** are unidentified channels and hence were labelled having the appearance of features consistent with 'cyanobacterial tunnelling', even though there is no clear indication of cyanobacteria being present in a terrestrial context, and the tunnel in **D** appears to be connected to a Haversian canal. The features are indicated by the blue arrows. Note the differences in the width of the tunnels. In the literature, maximum tunnel diameters caused by microorganisms have been reported to be between 0.1 and 2.0 micron (terrestrial), 7-18 microns (freshwater), and 5-19 microns (marine, (Pesquero et al., 2018)). Here, diameters under 20 microns were considered to be 'cyanobacterial tunnelling', while >20 microns were classed as Volkmann's canals. (Transmitted light microscopy, 50x, from left to right: WSF2D2W5_unburnt, WSF2D2W5_burnt, WSF1D1M2_unburnt, WSF1D1M2_burnt).*

The prevalence of features on unburnt and burnt bones was then statistically analysed using Jupyter notebook in Python programming language (*pandas*, *matplotlib*, *seaborn*, *SciPy*, and *numpy* libraries). Linear regression was used to measure the strength of the relationship between the presence (in percentage) of each taphonomic feature and the length of the

postmortem period before and after burning, with statistical significance assessed by associated p-values ($\alpha = 0.05$). The null hypothesis was that the presence (in %) of a given feature per bone does not increase with the postmortem interval. The coefficient of variation (CV) was used to assess the dispersion of the features in different decompositional stages and burning status.

Validation of whether or not features were due to bioerosion was then undertaken using a BSEM detector in the electron microprobe. The contrast on the images resulting from demineralised and hypermineralised areas can be used to identify bioerosion (Turner-Walker, 2019). The resin blocks were ground with carborundum paper of progressively finer grit size (800, 1200, 2500). The blocks were then polished on a Buehler wheel and a satin woven acetate polishing cloth (DP-Dac, Struers A/S) using 3 μm and 1 μm monocrystalline diamond paste and suspension (DP-Paste M, Struers A/S and MetaDi, Buehler, respectively) for 30 and 5 minutes, respectively. The mounts were cleaned in an ultra-sonic bath in petroleum ether (40°-60°C). Samples were carbon-coated using a carbon evaporation coater (HHV Auto 360), the carbon acting as a conductive layer to prevent charging.

III.3. Results

The percentage of given features present for each decompositional stage before and after burning is shown in Fig. 11. The most common taphonomic features affecting the largest percentage of the bone areas were hairline cracks and those similar to what has been described in the literature as 'Wedl type 2'. The latter feature was absent from the unburnt fresh/control group but was present on the freshly burnt controls. 'Wedl 2' was also present after only 2 weeks of deposition on both the unburnt (26.32%) and burnt (26.43%) groups. After 1 year, this feature was present on over half of the areas investigated (53.5%).

The unburnt control group presented a very small number of 'Wedl tunnelling' (0.75%), 'Wedl 2' (0.75%), 'lamellate' (0.25%) and 'budded MFD' (0.50%) and tunnels resembling

‘cyanobacterial tunnelling’ (3.5%). These are attributed to human labelling errors, and quantify labelling error, which is negligible for almost all categories, due to the impossibility of bioerosion being present on the control bones. As cyanobacterial tunnelling cannot be present on these bones, they are almost certainly mislabelled Volkmann’s canals. Hairline cracks are abundant on this group (22.5%). This group should not show any sign of microbial bioerosion, since the pigs were dismembered shortly after death and were not exposed to soil. Conversely, the burnt fresh/control group exhibited significantly higher percentages of features consistence with ‘Wedl tunnelling’ (4.25%), ‘Wedl 2’ (11.68%) and tunnels resembling ‘cyanobacterial tunnelling’ (7.56%) as identified in the literature.

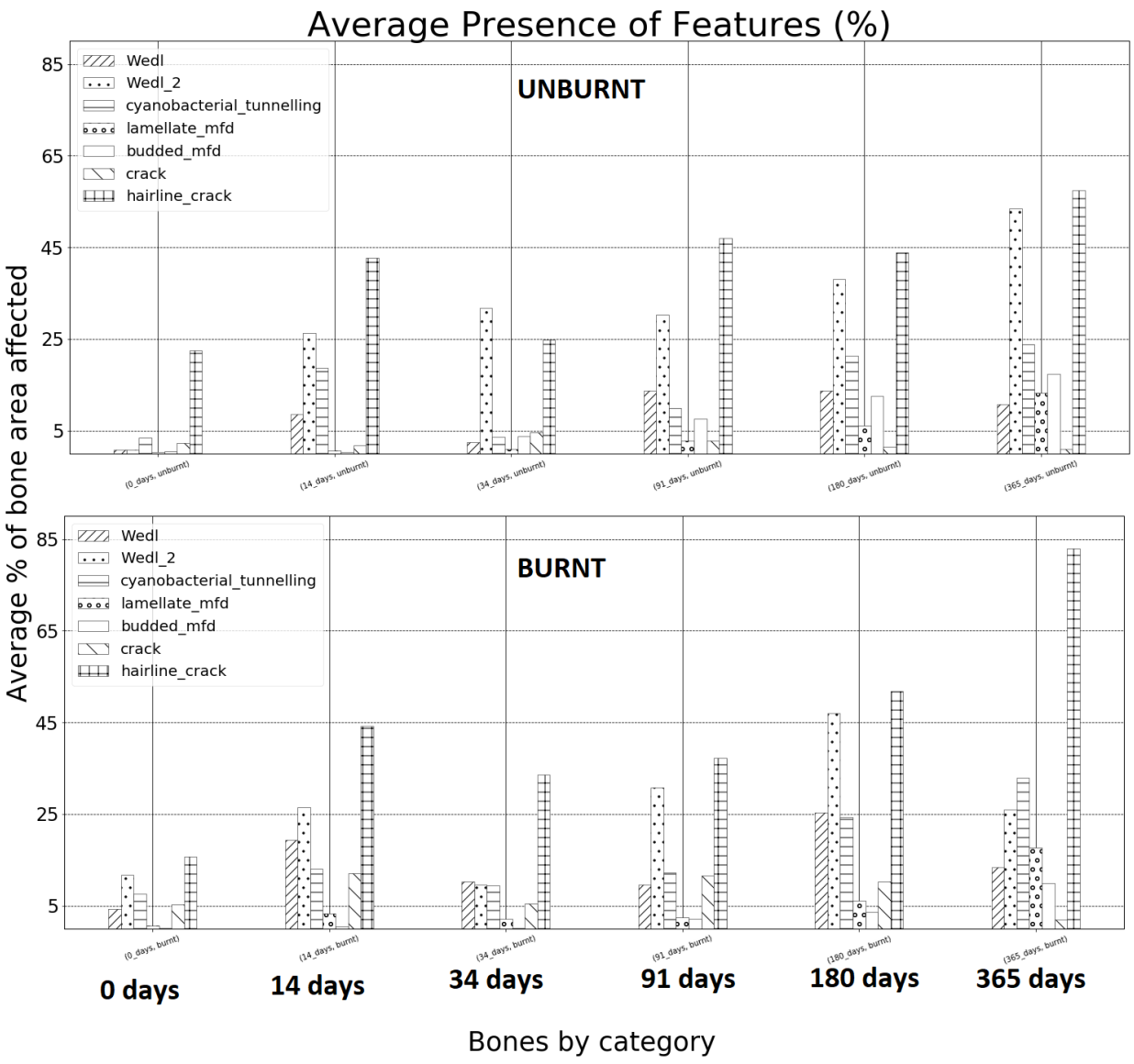


Figure 11 -- The average presence of the taphonomic features at each stage of decomposition before (upper) and after (lower) burning.

Diagenetic features increase for most bone categories after burning in all decompositional stages. There was a moderate positive linear correlation between time passed since deposition and percentage of the presence of 'Wedl tunnelling' ($r=0.442$, $p<0.0001$), 'lamellate MFD' ($r=0.493$, $p<0.001$), 'budded MFD' ($r=0.531$, $p<0.001$) on the unburnt bones, while hairline cracks ($r=0.278$, $p<0.017$), showed a weaker correlation with time, though it remained significant (Table 5). Weak but significant correlations were observed for 'Wedl 2' ($r=0.254$, $p<0.012$) and 'budded MFD' ($r=0.296$, $p<0.006$) in burnt bones.

Feature	r[3] unburnt	p unburnt	r burnt	p burnt
Wedl tunnelling	0.442	0.00009**	-0.016	0.886
Wedl 2	0.170	0.151	0.254	0.012**
Cyanobacterial tunnelling	-0.204	0.084	0.114	0.312
Lamellate mfd	0.493	0.00001**	0.091	0.412
Budded mfd	0.531	0.000001**	0.296	0.006**
Crack	0.064	0.591	0.184	0.095
Hairline crack	0.278	0.017**	0.159	0.150

*Table 5-- Correlation Coefficient ('r') and p-value ('p') for each analysed feature on the unburnt and burnt bones. H_0= Presence (in %) of X feature per bone does not change with postmortem time period. ** indicates significant p-values.*

The coefficient of variation (CV) shows that hairline cracks had the lowest variability between samples of the same decompositional stage (Table 6), while 'lamellate' and 'budded MFD' showed the greatest variability. In general, features were less variable pre-burning than post-burning. The 91 days unburnt, 180 and 365 days postmortem unburnt and burnt bones had the lowest CV scores across all features. The 14-day burnt bones with features recalling 'budded MFD' (2.73) showed the highest variability.

Coefficient of Variation (CV)								
Bones		**Wedl**	**Wedl_2**	**Cyanobacterial tunnelling**	**Lamellate MFD**	**Budded MFD**	**Cracks**	**Hairline cracks**
0 days	unburnt	1.27	0.66	0.82	2.00	1.15	0.75	0.50
	burnt	1.37	1.71	1.00	1.83	2.73	0.89	1.18
14 days	unburnt	0.72	0.52	0.56	1.36	2.07	1.82	0.30
	burnt	1.15	0.94	0.63	1.00	4.00	0.68	0.61
34 days	unburnt	1.24	0.64	0.73	1.10	1.33	0.94	0.60
	burnt	0.80	1.05	0.71	1.73	2.07	0.74	0.57
91 days	unburnt	0.49	0.70	0.60	0.95	0.98	1.20	0.24
	burnt	1.22	0.94	1.16	1.37	2.21	1.10	0.78
180 days	unburnt	0.43	0.64	0.40	0.55	0.67	1.40	0.31
	burnt	0.93	0.35	0.45	0.87	0.60	0.79	0.45
365 days	unburnt	0.80	0.51	0.36	0.25	0.50	2.00	0.27
	burnt	0.60	0.78	0.50	0.11	0.26	1.00	0.02

[3] [Comment since publishing]: 'r' was noted here as the correlation coefficient, when in reality r^2 was used. Thus, the values represent the r^2 values.

Table 6-- Coefficients of variation for each feature on the grouped samples by postmortem period and state of burning.

The BSEM images (Table 7) present bioerosion-like hypermineralised 'tunnels', which are due to heavy mineral loading in growing individuals (Fig. 12), and thus not the result of bioerosion. A small number of images indicate initial stages of bacterial attack on some of the exposed unburnt bones, for instance one of the 3-months exposed unburnt bones (Fig. 13). Bioerosion was not present on any of the burnt samples. Generally, contrast varied across the burnt bones, while there was no significant difference across the unburnt bones.

Decompositional stage	**State**	**Contrast difference present? (trabecular, mid-cortical, periosteal)**	**Tunnels/cracks with hypermineralised rims?**
Fresh	unburnt	No	No
Fresh	burnt	Yes	No
2 weeks	unburnt	No	No
2 weeks	burnt	Yes	Not generally, except 1
1 month	unburnt	No	Yes
1 month	burnt	No	No
3 months	unburnt	No	Yes, around tunnels/cracks and Wedl 2/MFD
3 months	burnt	Yes	No
6 months	unburnt	No	No
6 months	burnt	Yes	No
12 months	unburnt	No	No
12 months	burnt	Yes	No, but grey colour around tunnels

Table 7-- Analysis of compositional images.

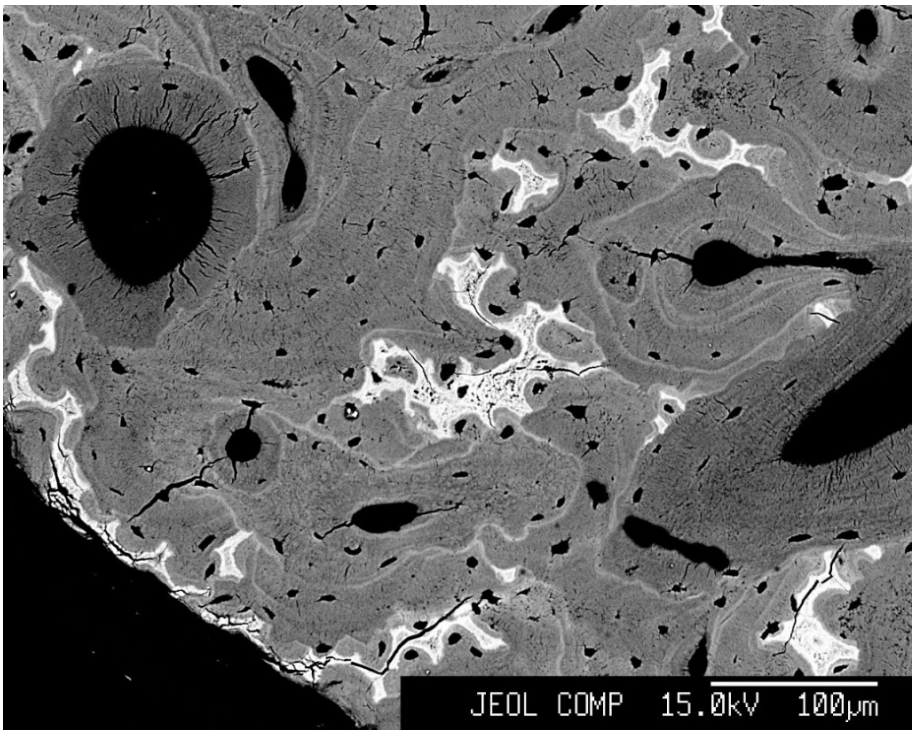


Figure 12 -- Backscattered electron image of one of the 1-month postmortem unburnt bones (WSF5D1M3_unburnt). Note the brighter (hypermineralised) areas around the black (demineralised) 'tunnels' toward the lower end of the image. These bright areas are in fact not due to bioerosion, but to heavy mineral loading in growing individuals where osteonal bone has not replaced the primary lamellar bone.

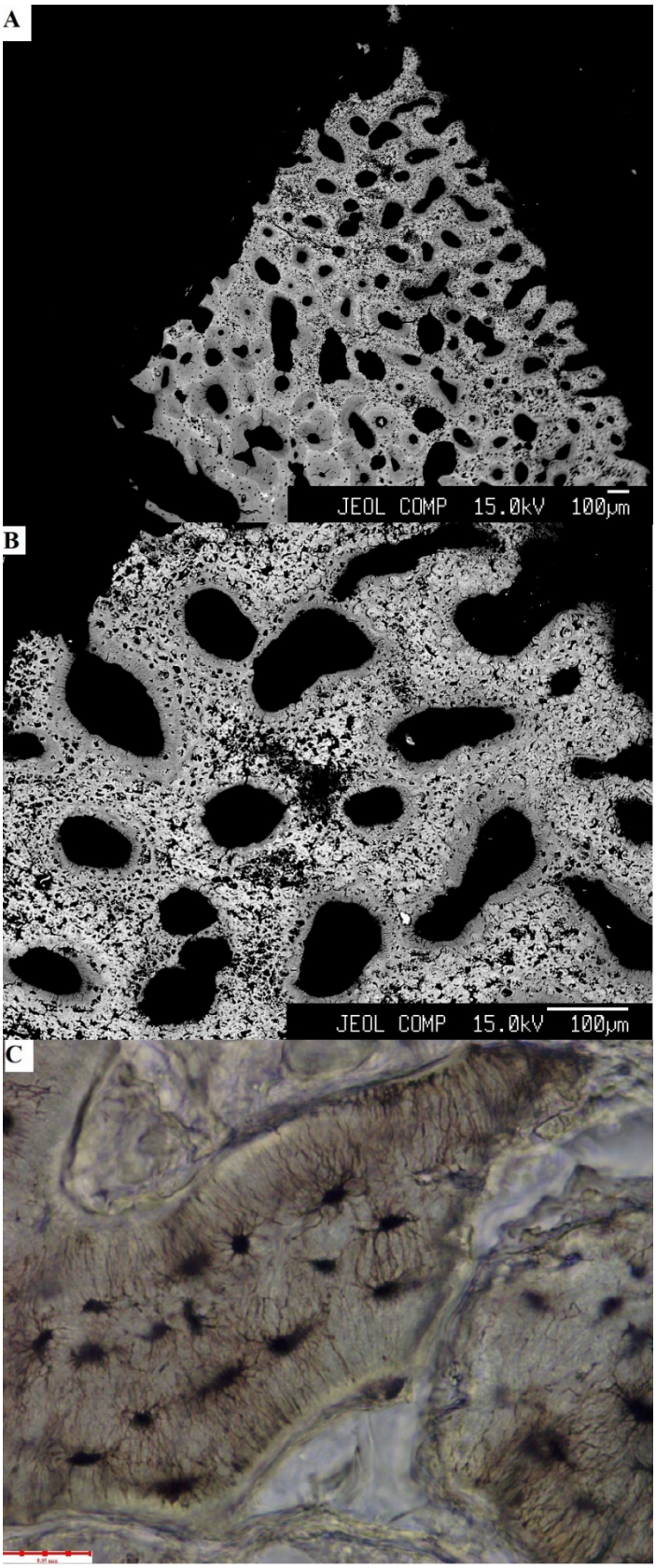


*Figure 13**A** and **B** -- Backscattered electron image of 3-month postmortem unburnt bone (WSF3D3M3_unburnt). Note the accumulation of darker (demineralised) circular areas (appearing to be 'Wedl 2' or enlarged canaliculi, but probably naturally demineralised primary bone with microcracks) with bright (hypermineralised) areas around. **C**: Transmitted light microscopy image of a thin section from the same sample (WSF3D3M3_unburnt) at 400x magnification.*

III.4. Discussion

Three features associated in the literature with microbial bioerosion are present on the burnt fresh/control group but absent on the fresh unburnt group. The clear implication is that, despite their apparent similarity, these are not bioerosional features but are instead artefacts induced by burning. The feature labelled as 'Wedl type 2' appears on 11.68% of the areas affected on the burnt fresh/control bones (Fig. 14). The frequency of 'Wedl 2' shows a statistically significant relationship with postmortem time interval only in the burnt samples. This feature has been alternatively interpreted as an indication of bioerosion caused by fungi (Trueman and Martill, 2002), but the aetiology of enlarged lacunae and canaliculi is uncertain and has also been associated with staining, mineral infiltration, and burning (Hanson and Cain, 2007; White and Booth, 2014). Supporting this, it was found here that these are in fact carbonised osteocyte cells trapped in the canaliculi due to burning (Fig 15). This observation challenges the interpretation of the cremated remains reported by Grévin *et al.* (1991), where researchers noted these enlarged canaliculi (referred to here as 'Wedl 2') to be the sign of a delay of weeks to months before cremation. The high variance (CV=1.71) of 'Wedl 2' presence on the freshly burnt samples further suggests that the feature was produced by fire.

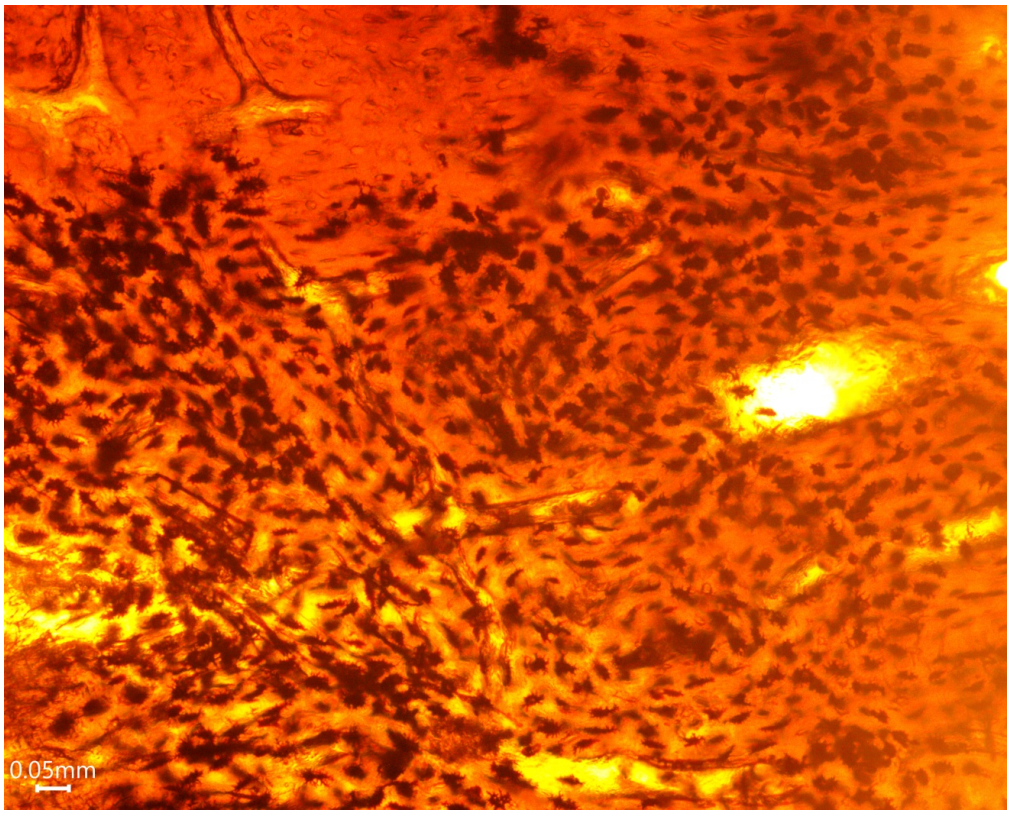


Figure 14 -- Staining of the osteocyte-canalicular network that appears to be Wedl type 2 on one of the fresh burnt control bones (SWF1FR2_burnt_1). The tunnels were labelled 'blind' as 'cyanobacterial tunnelling', but these are Volkmann's canals. Neither of these features should be present on freshly burnt bones. Transmission light microscopy, 100x magnification.

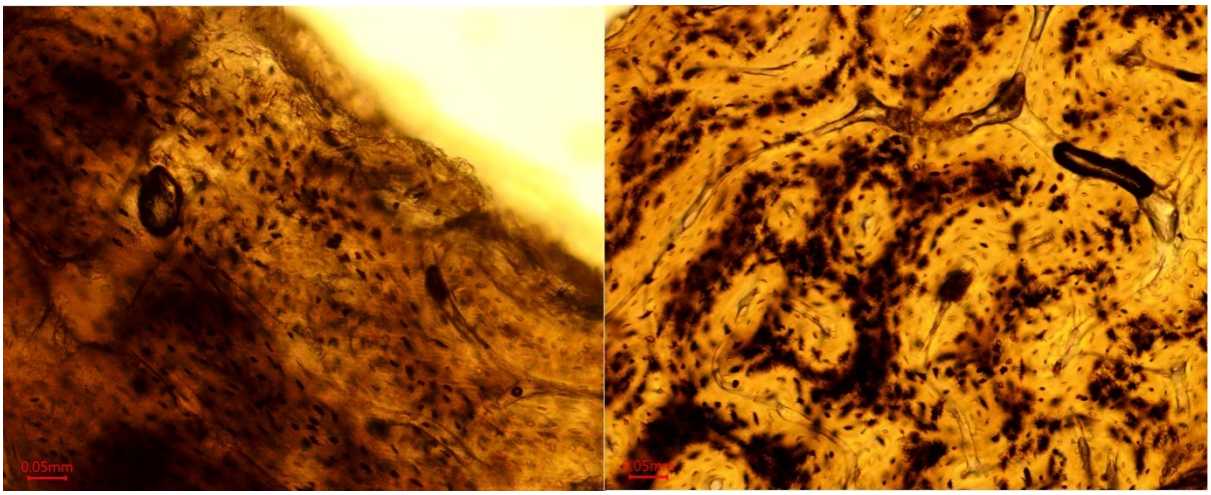


Figure 15 -- Staining that appears to be 'Wedl 2'. While it is restricted to some canaliculi on the unburnt 6-months postmortem section (left), it affects all osteons on the same burnt bone (right). 'Wedl type 2' features are probably due to discolouration on the freshly burnt bones. The source of discolouration can be: (1) sooting from combustion gasses infiltrating the osteocyte-canalicular network after most of the organic matter has burnt out; or (2) iron, manganese, or other metal ions infiltrating the osteocyte-canalicular network prior to burning and then reduced to darker species, such as manganese dioxide or magnetite, when the bones were burnt. While the pig tibiae were not buried, those that were exposed for sufficiently long did become partly covered in soil, which may

have presented the opportunity for the infiltration of metal ions. (Sample WSF5D6M1_1, transmission light microscopy, 100x magnification).

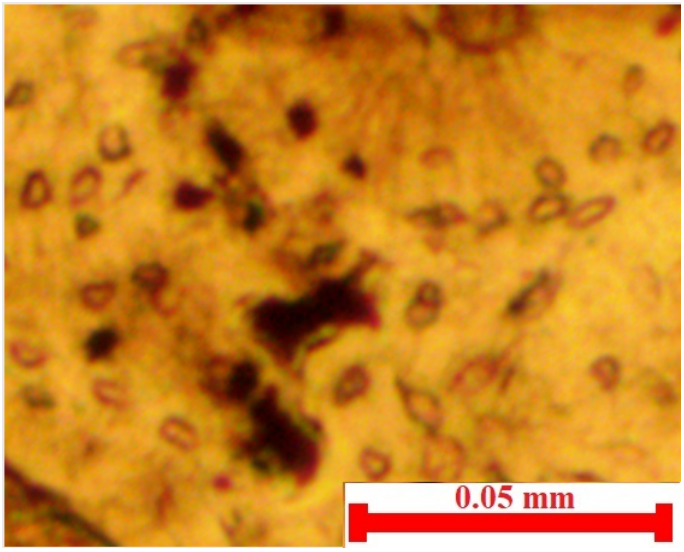


Figure 16 -- Features resembling 'budded MFD' from a 6-months postmortem burnt bone (WSF5D6M3_burnt). Transmitted light microscopy (50x).

The frequency of features labelled as 'Wedl tunnelling', and 'lamellate MFD' increase significantly with decay time on unburnt bones, and although they were present, they showed no correlation with time since deposition in the burnt groups. Wedl tunnelling is thought to be attributed to surface exposed and/or buried de-fleshed bones from terrestrial environments (Trueman and Martill, 2002; Jans, 2008; Brönnimann *et al.,* 2018) and should only happen in oxygenated wet environments in neutral to acidic soils (Huisman *et al.,* 2009, 2017). Most bones were covered by soft tissue to different degrees. Less soft tissue coverage means bone desiccation begins earlier, which might limit the intensity of bioerosion (Jans *et al.*, 2004; Nielsen-Marsh *et al.,* 2007). Although the 1-month postmortem unburnt bones were much less affected by 'Wedl tunnelling', the other groups with soft tissues were more affected by this feature. Therefore, no difference was found in bones with remnants of soft tissues and de-fleshed (by scavenging) bones in the mean bone areas affected by 'Wedl tunnelling'. Sub-aerial exposure, the water-logged soil, and the pH (3-7; (Farmer, 1995) suggest Wedl tunnelling should be present (Huisman *et al.*, 2009, 2017), but the fact that it was more frequent in the

burnt than in the unburnt bones suggests that similar features are not due to fungal activity and can be produced by burning.

Although the literature suggests that MFD might indicate an endogenous source of bacteria, here it can be ruled out. 'Budded MFD' was the only feature to consistently show a statistically significant correlation with time since deposition for both the unburnt and burnt groups. Post-burning this relationship becomes less robust, suggesting that these features are more likely to be lost or at least become less visible through burning. In addition, this was the least reliably present on all bones, followed by 'lamellate MFD'. 'Budded MFD' (Fig. 16) appeared on the unburnt bones after just 34 days, but it was rarely observed on the same burnt group (0.19%), increasing slightly in the 3-month postmortem group (2.14%). Its presence reaches 10% after a year of decomposition post-burning, suggesting that 'budded MFD' can also be produced by burning.

If bone colonization by microorganism occurs and manifests as budded MFD, it must happen before burning, because this destroys the organic component on which bacteria feed (Grévin *et al.,* 1991). The seasonality of functional activity of microbial communities associated with putrefaction has been investigated (Pechal *et al.*, 2013). It was noted that the carbon consumption of bacterial communities in bone was the highest in Spring, when the 1- and 3-month postmortem bones were placed in the cage. The appearance of budded MFD after just 1-month postmortem would conventionally be attributed to endogenous bacteria that spread through the bone's vasculature causing bioerosion; however, since the pigs were dismembered shortly after death and frozen until they were deposited in the cages, endogenous bacteria as a source can be excluded. Although time is thought to be the least important factor in bioerosion (Piepenbrink, 1986; Piepenbrink and Schutkowski, 1987; Bell *et al.*, 1996), it is likely that soil bacteria attacks bone over a longer timescale when bones are buried, especially given that organics (i.e., collagen) can survive for millennia. It has been shown that microbial

extracellular enzyme activity for carbon cycling enzymes significantly increases in soil closer to the surface (Upton *et al.*, 2020). Thus, the pig legs in this experiment, lying on and partially submerged in the soil, were arguably exposed to more soil microorganisms than if they would have been buried. Although the types of soil bacteria are environment-specific such that the bioerosion features might manifest differently at various locations, a large-scale study carried out by Brönnimann *et al.* (2018) did not find any relationship between sediment type and intensity of microbial bioerosion.

Previous studies found that the first microscopic changes due to burning appear at varying temperatures ranging from 600-1200°C. It is unknown where these temperatures were measured (bone or air in furnace). In this study maximum mean bone temperatures reached ≤750°C, while fire temperatures were as high as 995°C. If burnt and unburnt bone microstructure is indeed indistinguishable at these temperatures, it is possible that these subtle microscopic changes (e.g. 'Wedl 2' and 'MFD') caused by burning are mistaken for bioerosion features. In general, the presence/absence of features on unburnt bones was less variable than on burnt bones, meaning not all the bones are affected the same way by fire. Variations might be due to the movement of the wind, flame height, soft tissue coverage, and this variation might not be present when bones are burnt in a furnace. Thus, it is argued here that experiments conducted on an outdoor fire give a better indication of real-life conditions in both forensic and archaeological cases than bones burnt in a furnace.

Squires *et al.* (2011) noted that bones cremated at temperatures between 600-900°C should have very few, if any, Volkmann's canals surviving. Conversely, it is argued here that Volkmann's canals do survive 'intense cremation', as they were observed on all burnt bones. They were recorded on 3.5% of fresh, unburnt samples, giving an indication of their expected frequency. The fact that the bones were deposited in a terrestrial context – and hence not

exposed to cyanobacteria – further suggests that these features are mostly Volkmann's canals, which can assume a variety of forms depending on the angles at which the bone is sectioned, and so may be responsible for this discrepancy.

Hairline cracks are most probably due to the contraction and expansion of bone attributable to weather changes, explaining the feature's positive correlation with longer decay times in the unburnt groups, which disappeared post-burning. Cracks are considered to be indications of collagen degradation (Huisman *et al.*, 2017), but no statistically significant increase was observed with time of deposition. Neither feature appears to be a useful indicator for degradation in the bones, not least because the preparation of thin sections and/or burning can cause them. The black enlarged lacunae and canaliculi may be present because of carbon incorporation into the uneven surfaces of bone.

Demineralised and hypermineralised foci were sometimes present on the BSEM images of the unburnt bones. However, these foci did not resemble tunnels on BSEM images published by Fernández-Jalvo *et al.* (2010) and Turner-Walker (2019). Bright, heavily mineralised areas on the unburnt bones (e.g. Fig. 12) may instead relate to the structure of bone in young individuals, in which osteonal bone has not yet replaced the primary lamellar bone, producing a mixture of darker, less dense (younger) and heavier mineralised (older) areas (Boskey and Coleman, 2010), which can be mistaken for tunnelling. Hypermineralised areas with a less diffused degradation pattern than has been previously documented (Turner-Walker and Syversen, 2002; Turner-Walker and Peacock, 2008) suggest early bacterial bioerosion in some of the 3-months postmortem unburnt bones. All bioerosion-like features were obliterated through the burning process (Fig. 17). Therefore, BSEM is not a useful technique for identification of bioerosion features on burnt bones.

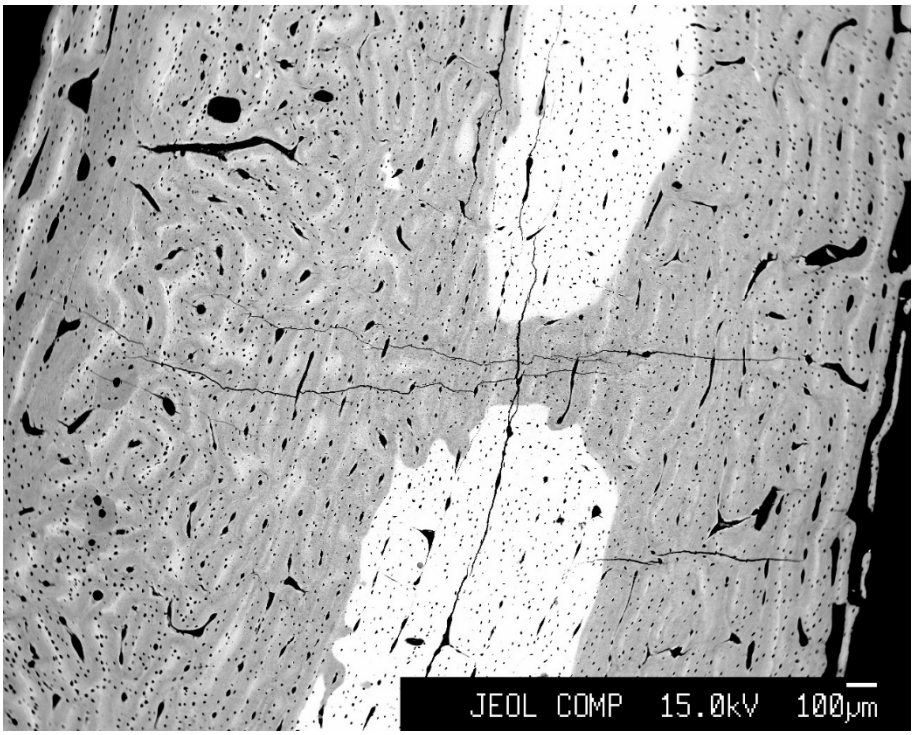


Figure 17 -- Contrast differences due to burning of a 6-month decayed bone sample (WSF5D6M1_burnt). Note the central mineralised areas. (Electron microprobe, backscatter electron detector image.)

This study was conducted simultaneously with another recent study by Lemmers *et al.* (2020), with similar overall aims and methods. Although they suggest that bioerosion lesions have the potential to act as a proxy for the pre-burnt condition of the body, the opposite is suggested here. The cause of this discrepancy might be that in the current study fresh, fleshed tibiae were burnt as controls, while the freshest bones in Lemmers *et al.*'s (2020) study were >3 years postmortem and may have been embalmed with a decomposition accelerator compound.[4] In our study features indistinguishable from bioerosional features as described in the literature appeared on the fresh burnt controls, suggesting that they were produced by burning.

Limitations of the present study include the use of pigs as a proxy for humans and their young age (18 months), which might make them more susceptible to bioerosion due to the

[4] [Comment since publishing] The bones used in Lemmers et al.'s (2020) study used human remains recovered from cemeteries, which is the reason that they might have been embalmed.

higher amount of organic matter in the bones. The data from the 1-year postmortem group are based on two samples, because the rest were removed by scavengers during the exposure phase. It was not possible to get access to a microtome, so thin sections were cut with a Buehler saw, producing a less consistent thickness across samples. All labelling was executed by one researcher (EIV) and due to the sheer number of blocks (N=27,000) some may have been incorrectly labelled. Balanced against this is the consistency in approach to identification that this permitted. Finally, the bones were not exposed to endogenous bioerosion, which should be the focus of future studies.

III.5 Conclusions

This study aimed to establish the utility of diagenetic features as a proxy for the body's state of decomposition prior to incineration. Ours is the first histotaphonomic study to apply a data labelling application, built for this purpose, to statistically assess bioerosion. We highlight the inconsistency in the literature concerning the naming of diagenetic features and their considered aetiologies. Although most recent literature is concerned with what the source of bacteria is (i.e. endogenous or exogenous), verification of which of these features are in fact caused by microbial bioerosion is more urgent. Our results showed that Wedl tunnelling, Wedl 2, and lamellate MFD are not reliable indicators of decomposition because similar features appear on freshly burnt bones, and thus can be caused by other factors, such as burning. Budded MFD was the only feature that showed a statistically significant increase in bone areas affected on both the unburnt and burnt groups. However, burning considerably reduced the visibility of this feature. Features labelled here as similar to 'cyanobacterial tunnelling' were in fact probably Volkmann's canals, which survived cremation on all bones. Hairline cracks did not appear to be informative on decay. Although BSEM is a useful tool in bioerosion studies in unburnt bones, it cannot be used on burnt bones. In summary, it can be argued that microbial bioerosion features are not accurate proxies for the body's pre-burning condition and caution

should be practised when identifying these in bones in both forensic and archaeological contexts.

Acknowledgements

The study was supported by the Meyerstein Foundation, School of Archaeology, University of Oxford. We would like to thank Prof. Robert Hedges for his insights into the study and Dr Victoria Smith for her help on the electron microprobe. We would also like to thank Mr Kevin Lemagnen for his help and support while developing the data labelling application. We thank the anonymous reviewers for their careful reading, valuable comments, and improvements made to the paper.

Funding

This work was supported by the Meyerstein Foundation, School of Archaeology, University of Oxford.

Chapter IV: Paper 2 -- Physicochemical Changes in Bone Bioapatite During the Late Postmortem Interval Pre- and Post-Burning

---

Végh, E. I., Márquez-Grant, N., and Schulting, R. J. 2022. Physicochemical Changes in Bone Bioapatite During the Late Postmortem Interval Pre- and Post-Burning. *Applied Spectroscopy* https://doi.org/10.1177/00037028221085600

Abstract

Postmortem chemical transformation of bone bioapatite can take place during early diagenesis resulting in a more thermodynamically stable mineral phase. This paper examines the impact of a 1-year postmortem interval on unburnt and burnt bone's structural and chemical alterations. This question is of importance for the reconstruction of funerary practices involving cremation in the archaeological record, as well as forensic anthropological investigations. Fleshed pig (*Sus scrofa*) tibiae were left exposed in a field, then collected at 14, 34, 91, 180, 365-day intervals prior to being burnt in an outdoor fire (≤750 °C bone temperature). Fresh (fleshed) tibiae acted as unburnt and burnt controls. Also included in the study were two cremated human bone fragments from Middle/Late Neolithic (ca. 3300–2500 cal BC) Ireland. Samples were analysed for major and trace elements by wavelength dispersive electron microprobe analyser (EMP-WDS) and molecular structures by Fourier Transform Infrared Spectroscopy (FTIR). Linear regression, PCA, LDA, and MANOVA were performed for statistical analysis. Results indicate that the concentrations of elements associated with extracellular fluid (K, Na, Cl) change with the postmortem interval (PMI) and survive burning. K values under 0.07 ± 0.01 wt% in inner and mid-cortical zones of burnt bones suggest that bones were not burnt immediately after death. Using this criterion, results from the archaeological samples would indicate a PMI of at least weeks to months prior to cremation. Ca, P, Fe, Al, Si, and Sr are not significantly altered with burning, and Fe, Al, Si, Sr are also unaffected by the PMI. In unburnt bones increased crystallinity and carbonate loss are detectable in <1 year, but both are obscured by burning. Structurally, the carbonate to phosphate ratio (C/P), phosphate high temperature (PHT), and cyanamide to phosphate (CN/P) are the most useful ratios for discriminating between unburnt and burnt bones.

Keywords

cremation, electron microprobe, FTIR, taphonomy, potassium

IV.1 Introduction

Thermally altered human bones occur in both forensic and archaeological contexts. Burnt bones can result from accidental fires or arson, or mask the victim's identity as well as the cause and manner of death in a homicide case (Bontrager and Nawrocki, 2008; Symes *et al.*, 2008; Garrido-Varas and Intriago-Leiva, 2015). Since antiquity, cremation has been a common funerary practice in many cultures, though there are often questions regarding the state of the corpse at the time of burning (Stiner *et al.*, 1995; Bennett, 1999; Théry-Parisot, 2002; Schiegl *et al.*, 2003; Dibble *et al.*, 2009; Clark and Ligouis, 2010; Gonçalves *et al.*, 2011; Snoeck *et al.*, 2014; Yravedra *et al.*, 2017). In several tombs and burials of Neolithic, Bronze, and Iron Age Ireland (Waterman *et al.*, 1978; Wells, 1978; Dowd, 2008; Cooney, 2014), Scotland (Chesterman, 1979; Renfrew, 1979), England (Piggott, 1962; Wells, 1962; Mckinley, 1994, 1999, 2008; Carr and Knüsel, 1997; Niblett, 1999; McKinley, 2000; Carr, 2007; Booth and Brück, 2020), and France (Grévin *et al.*, 1991; Lambot *et al.*, 1994), for example, human remains may have been excarnated before cremation, while in other cases bodies seem to have been burned soon after death (Wells, 1978; Dowd, 2008; Cooney, 2014). Some of this interpretation is based on heat-induced fracture patterns including thumbnail fractures and warping, associated with the burning of fresh bones in early studies (Baby, 1954; Binford, 1963; Buikstra and Swegle, 1989; Spennemann and Colley, 1989; Etxeberria, 1994; Whyte, 2001). However, more recent research has shown that these fractures do not depend on the presence of soft tissues, but rather on collagen content and distribution (Thompson, 2005; Gonçalves *et al.*, 2011). Recent attempts to identify bone decomposition prior to burning through histotaphonomical analysis (Lemmers *et al.*, 2020) may be unreliable (Végh *et al.*, 2021). Identifying when burning took place after death presents a challenge, one addressed here through a study of the physicochemical changes of bones pre- and post-burning up to 1-year post-deposition.

If changes in elemental concentrations to bone are detectable after a short period of deposition/postmortem interval (PMI; in the current study 2 weeks to 1 year) and they survive burning, it can be hypothesised that it is possible to inform on the pre-burning condition, i.e., on whether bodies were fresh or partly decomposed when burnt. Although effects of diagenesis on the elemental concentration had been investigated (Kohn and Moses, 2013; Keenan and Engel, 2017a; Walden *et al.*, 2018), no studies have examined these changes after exposure to heat. Therefore, this study aims to assess the potential of compositional and structural changes in unburnt and burnt bone to help distinguish between fresh and variably taphonomically-altered bones within a defined post-mortem interval. The results of this experiment are compared to the chemical composition of archaeological (Neolithic) cremated bones. Our hypothesis based on previous studies (e.g. Keenan and Engel, 2017a; Walden *et al.*, 2018) is that these changes can occur weeks following deposition by the loss of endogenous elements in vivo and from the uptake of exogenous elements from the environment. We further hypothesise that these changes will be observed in the burnt bones since inorganic mass loss is negligible in bones burnt at up to 900°C (Reidsma *et al.*, 2016).

IV.1.1 Taphonomic Alterations to the Elemental Concentration and Structure of Bone

Bone is a composite material consisting of ~55-70 wt% mineral, ~20-35 wt% organic carbon, and ~10-15% water (Rogers and Zioupos, 1999; Elliott, 2002; Caruso *et al.*, 2020). Hydroxylapatite [HAp, $Ca_{10}(PO_4)_6(OH)_2$] is the basis of all biologically formed apatite, while bioapatite [$(Ca,Mg,Na)_{10-x}[(PO_4)_{6-x}(CO_3)_x](OH)_{2-x}$] is a carbonate-containing variety of HAp, which forms the inorganic component of bone (Elliott, 2002; Rey *et al.*, 2007; Li and Pasteris, 2014). Bioapatite is chemically more complex than HAp; it is non-stoichiometric, and can incorporate a wide variety of elements into its structure (Zapanta Legeros, 1981; Elliott, 2002; Bergslien *et al.*, 2008; Li and Pasteris, 2014).

The chemical profile of bone (Suppl. 1) results from the combination of the pre-mortem (e.g., diet, inhalation) and postmortem (e.g., degradation, soil) incorporation and release of elements. However, it is modified by taphonomic (post-mortem) factors, which can be natural (e.g., weathering, mineral replacement, microbial attack) or anthropogenically-induced (e.g., inhumation, sub-aerial exposure, disarticulation and defleshing, burning, etc.) (Fernández-Jalvo and Andrews, 2016; Márquez-Grant *et al.*, 2017). Early decomposition includes the hydrolysis of collagen, and the first biological, chemical, and structural changes to bioapatite (Child, 1995; Sponheimer and Lee-Thorp, 1999; Harbeck and Grupe, 2009; Keenan, 2016). Bioerosion causes increased surface areas which either encourages mineral dissolution or enhances the movement of ions and substitutions, eventually leading to a more thermodynamically stable mineral phase (Keenan *et al.*, 2015). Organic loss has been associated with increased ion transport (Child, 1995; Keenan *et al.*, 2015) due to the open pore spaces between the mineral phase, facilitating the movement of fluids, microorganisms, and dissolved ions (Keenan, 2016), unless pore spaces are blocked by ingress of trace elements from the environment (Kohn, 2008). Fossils, the resulting mineral phase from late diagenesis, have a wide variety of substitutions, but most commonly have F- and Ca-enriched apatite phases (Sponheimer and Lee-Thorp, 1999; Berna *et al.*, 2004; Keenan, 2016), or CO_3^{2-} loss (Wright and Schwarcz, 1996). An experiment in which modern bones were exposed for up to 30 years on soil surfaces in Kenya showed that crystal sizes increase in number and size with time (Trueman *et al.*, 2004).

Bone composition is susceptible to changes as soon as bone is exposed to the environment, which has been documented in unburnt modern (Benmansour, 2012; Keenan and Engel, 2017a; Walden *et al.*, 2018), archaeological (Marín Arroyo *et al.*, 2008; Gallello *et al.*, 2013; López-Costas *et al.*, 2016), and fossil bone (Keenan *et al.*, 2015), but regarded as negligible (Schutkowski *et al.*, 1999). Bioapatite can accommodate various substitutions at

every site of the crystal lattice, which makes it one of the most diverse minerals (Keenan and Engel, 2017a, 2017c). Cations (metals) substitute for Ca(1) and Ca(2) (Zazzo *et al.*, 2020), while anions for phosphates, carbonates, and hydroxyls. Trace elemental uptake due to ion exchange can occur after one week, while after a year a more thermodynamically stable mineralogical phase shift to F- and Fe-enriched apatite phases can be seen (Keenan and Engel, 2017a). Non-uniform, non-linear increases (Mn, Fe, Ca, F) and decreases (Cl, Na) were also seen in bone buried >1 year. However, the calcium to phosphate ratio (Ca/P) remains constant during putrefaction (Ezzo, 1994; Ellingham *et al.*, 2018), while a decrease of carbonate to phosphate (C/P) has been identified after burial for 1 year. The latter is due to either carbonate loss (A and B), increased phosphate content, or the loss of organic material in bone (Keenan and Engel, 2017a).

Much of the work on trace element uptake into bone has revolved around rare earth elements (REE) and uranium (Williams, 1988; Trueman and Tuross, 2002; Trueman, 2013), which are taken up by bioapatite over 10^3 – 10^6 years post-mortem (Trueman and Tuross, 2002). In modern bone, Ca, P (from bioapatite), Fe, Na, K (associated with bodily fluids), F, Mg, Al, Si, Cl, and Mn (associated with trace elements from soil) are usually studied. Fe, Al, and Mn are often abundant in weathered soils but are less likely to enter into solution (Pate and Hutton, 1988). If this does occur, Al and Mn do not only affect the outermost layers of bone, but are measurable as contaminants in the mid-cortical region in archaeological bone (Lambert *et al.*, 1991). Fe is stored in vivo in blood, bodily organs (Muñoz *et al.*, 2009; Walden *et al.*, 2018), with a minuscule amount being surface-bound in bone (Ezzo, 1994; Muñoz *et al.*, 2009). The decrease of Na and K has been linked to the dehydration of bone during decomposition (Walden *et al.*, 2018). Mg is surface-bound in bioapatite, and although it has been shown not to be much affected by diagenesis, very small amounts can be incorporated into the bioapatite lattice (Walden *et al.*, 2018). In buried bone cations diffuse inward toward the pores from the

outer cortex (Trueman, 2013). Adsorption will cease once equilibrium is reached with the surrounding pore waters (Millard and Hedges, 1996), also evidenced by the slowing and halting of trace element leaching during fossilisation (de Winter *et al.*, 2019). The rate of approaching equilibrium with pore waters is dependent on the element concentration, mobility in the environment, and the adsorption coefficient (i.e. a constant relating to the speed a molecule will bind to the surface of bioapatite at defined conditions) (Millard and Hedges, 1996; Trueman, 2013).

IV.1.2 Heat Changes to the Physicochemical Structure of Bone

Generally, heat-induced changes in bone go through the following stages: (1) dehydration of the bone with the breakage of hydroxyl bonds and water removal; (2) organic component (lipids and proteins) decomposition around 400-500°C; (3) inversion, marked by carbonate loss (CO_3^{2-} disappears completely at ~ 700°C); and (4) fusion of the crystals (>700°C) when the crystallites grow in size and OH^- and PO_4^{2-} rearranges within the pores which are now vacant of organics and water (Thompson, 2005; Marques *et al.*, 2018).

Many studies have investigated the elemental compositional changes of burnt bone in archaeological and experimental contexts (Shipman *et al.*, 1984; Williams, 1988; Grupe and Hummel, 1991; Subira and Malgosa, 1993; Stiner *et al.*, 1995; Cattaneo *et al.*, 1999; Bergslien *et al.*, 2008; Schultz *et al.*, 2008; Gallello *et al.*, 2013), and for biomaterials research (e.g. Raspanti *et al.*, 1994; Guizzardi *et al.*, 1995; Holden *et al.*, 1995; Holden *et al.*, 1995; Rogers and Daniels, 2002; Hiller *et al.*, 2003). During the burning process, bone is susceptible to chemical substitutions (Strydonck *et al.*, 2010). Although in theory, most inorganic elements in bone should not change at temperatures possible to reach in an outdoor fire, the inorganic mass loss has been shown to fluctuate around 2.8 wt% independent from temperature during heating up to 900°C (Reidsma *et al.*, 2016). Various heat-induced elemental changes have been documented (Suppl. 2.).

The main structural changes observed include the reordering of phosphate, the decrease/loss of carbonate, and increased crystallinity (Holden *et al.*, 1995; Stiner *et al.*, 1995; Person *et al.*, 1996; Munro *et al.*, 2007; Lebon *et al.*, 2010; Reidsma *et al.*, 2016), which start to occur at 600/700°C (Munro *et al.*, 2007; Thompson *et al.*, 2013; Reidsma *et al.*, 2016). Extensions to the α-lattice and changes to the c-lattice parameters are accompanied by the release of lattice carbonate and possibly water, which results in an increase in crystal size and crystallinity (Wang *et al.*, 2010). At temperatures around 730°C, a new phase of beta-tricalcium-phosphate (β-TCP) appears in bioapatite, which remains stable at high temperatures (Hidouri *et al.*, 2019). The appearance of β-TCP signals the thermal decomposition of the apatite phase, which happens due to non-stoichiometric substitutions/P ratio (i.e. <1.67) (Raynaud *et al.*, 2002; Hidouri *et al.*, 2019). Another secondary phase by-product is CaO, which appears at >700°C (Mckinnon *et al.*, 2020) is due to the thermal decomposition of $CaCO_3$ (Karunadasa *et al.*, 2019).

As regards diagenetic processes, most research has investigated chemical changes to bone post-burning and after deposition (Subira and Malgosa, 1993; Gallello *et al.*, 2013), which was thought to be similar in cremated bone as in unburnt bone in earlier research (Williams, 1988; Subira and Malgosa, 1993). However, these studies were observational with no controls, (Williams, 1988) and only referring to calcium (Subira and Malgosa, 1993). Bioapatite is less reactive post-deposition in an archaeological timescale (Lee-Thorp, 2002; Trueman *et al.*, 2004) and especially after burning because the crystals transform into a more stable thermodynamic phase (Snoeck *et al.*, 2014); thus the inorganic structure seems to remain stable post-burning. The amount of organic material in bone prior to burning appears to affect thermal decomposition as traced through OH^-, carbonate (type A and B), β-TCP, tetracalcium phosphate (TetCP), loss of CO_2 and water content,(Mkukuma *et al.*, 2004) and presence of cyanamide (Snoeck *et al.*, 2014).

IV.2 Materials and Methods

The material and experimental protocol employed here follows that of a parallel study (Végh *et al.*, 2021), which examined the histotaphonomic features in unburnt and burnt bones to inform on the PMI. Fleshed pig (*Sus scrofa domesticus)* tibiae (N=22) were allowed to decay exposed within a cage for 14 (N=5), 34 (N=5), 91 (N=5), 180 (N=5), and 365 (N=2) days prior to burning on an outdoor fire in Wytham Woods, Oxfordshire, UK. Fresh pig tibiae (N=10) served as controls throughout the study, without being exposed. Over time the exposed bones became partially submerged in soil and vegetation; however, experimental studies have found no significant differences in elemental concentrations in buried and surface-exposed bones (Walden *et al.*, 2018).

Wytham Woods is located in a temperate climate with annual precipitation averaging 717 mm and mean winter and summer temperatures of 1.6°C and 20.3°C, respectively. Soil pH ranges widely from 3 to 7 (Taylor *et al.*, 2011). Bones were burnt on an outdoor fire, which was executed in the same manner with each event lasting from 2.5-3 hours until the bones were deemed to be fully calcined based on their appearance. A thermocouple was used to directly monitor bone temperature, with a mean of 553°C and a recorded maximum of 751°C (Végh *et al.*, 2021).

Bone samples were taken from diaphyses before and after burning to maintain consistency with other studies of elemental concentration (Grupe, 1988; Schutkowski *et al.*, 1999; Walden *et al.*, 2018). The unburnt samples were defatted in a 2:1 chloroform: methanol mixture. The composition and atomic-level structure of the bones were analysed from: (1) polished resin blocks using wavelength-dispersive X-ray spectroscopy (WDS) on an electron microprobe (EMP); and (2) powders using Fourier Transform Infrared Spectroscopy (FTIR) in attenuated total reflection (ATR) mode. EMP-WDS allows spatially resolved analysis of a

single bone. This approach is essential, since the outer layer of the bone may have a different distribution of elements than the mid- or inner cortical bone adjacent to the medullary cavity (cf. (Gallello *et al.*, 2013)). FTIR has been used previously to determine bone composition (organic and inorganic) and bone structure, such as the infrared splitting factor (IRSF), which provides insights into bone crystallinity (e.g. Snoeck *et al.*, 2014; Keenan and Engel, 2017a).

Additionally, two cremated human bone fragments from burials 1 and 7 at a Middle/Late Neolithic (ca. 3300–2500 cal BC) stone circle in Kiltierney, Co. Fermanagh, Northern Ireland (Daniells *et al.*, 1977) were included. The fragments presented thumbnail fractures, suggestive of high bone collagen content at the time of burning (Gonçalves *et al.*, 2011). They were analysed with EMP, to compare their bone chemistry to the experimental results.

IV.2.1 Fourier Transform Infrared Spectroscopy (FTIR)

FTIR was used to retrieve structural and molecular information from the unburnt and burnt bones. This has been frequently used to investigate both the diagenetic pathways in osseous material (Walters *et al.*, 1990; Pleshko *et al.*, 1991; Rey *et al.*, 1991; Koon *et al.*, 2003; Stathopoulou *et al.*, 2008; Trueman *et al.*, 2008), to differentiate between heated bone at low, medium, and high temperatures (Thompson *et al.*, 2009; Ellingham *et al.*, 2016), and to characterise modern and archaeological burnt bone (Snoeck *et al.*, 2014, 2016). ATR was chosen instead of KBr discs, as it has been shown to provide more reliable measurements and fewer chemical modifications (Stathopoulou *et al.*, 2008; Thompson *et al.*, 2009, 2011; Beasley *et al.*, 2014; Ubelaker, 2015).

The powdered pre- and post-burnt samples were measured with a Cary 600 series FTIR spectrometer 5.3 (Agilent Technologies, Santa Clara, California, USA). A diamond crystal accessory was utilised with an operational range of 30000 to 200 cm^{-1}. Resolution Pro FTIR software (Agilent Technologies, Santa Clara, California, USA) was used for automatic

software correction and for generating the backgrounds and the raw data for each sample. After the spectrometer was aligned, a resolution of 4 cm^{-1} was chosen. Sixty-four scans were taken of each sample with scan range set between 4000 and 400 cm^{-1}, which represents mid-IR spectrum analysis. The background was measured after at least every second sample. Before the sample was placed on the accessory, the live spectrum was monitored to ensure no background noise. Baseline corrections were made at around 450, 800, 900, and 1200 cm^{-1}. T The calculated ratios included those from the literature: the crystallinity index/splitting factor (IRSF) (Stiner *et al.*, 1995; Munro *et al.*, 2007; Thompson and Inglis, 2009; Gonçalves *et al.*, 2011), amide to phosphate (APR) (Fredericks *et al.*, 2012), carbonate (type B) to phosphate (C/P), amount of type B carbonate (BPI) (Thompson *et al.*, 2009), type A carbonate to phosphate (API) (Thompson *et al.*, 2009; Grunenwald *et al.*, 2014), type B to type A carbonates (C/C), cyanamide to phosphate (CN/P) (Snoeck *et al.*, 2014), carbonyl to carbonate (CO/CO_3), amide I to phosphate (N/P) ratios and the phosphate high temperature (PHT) (Thompson *et al.*, 2013) (Suppl. 3). Additionally, the presence of β-TCP was noted when present as a peak at 1123 cm^{-1} and as a shoulder at 547 cm^{-1} (Piga *et al.*, 2016). Presence of β-TCP implies that burnt bone reached >700℃. If this β-TCP peak is present at 1123 cm^{-1}, IRSF loses its usefulness in estimating crystallinity. It was also suggested that the presence of this peak might be associated with Mg substitution for Ca in the bone (Piga *et al.*, 2016). Type A carbonates (~1540 cm^{-1}) were not evaluated in unburnt bone, because its peak overlaps with amide II (Grunenwald *et al.*, 2014). However, it was included in the burnt bone spectra evaluations, because organics were removed by heating. The peak heights were evaluated by observing the maximum height from the data at around the associated absorbance using Jupyter notebook in Python programming language. If a slight frequency shift was present (±5 cm^{-1}), the maximum height between this interval was recorded for the ratio calculations and the extent of shift noted.

IV.2.2 Electron Microprobe Analysis (EMPA)

A total of 58 unburnt and burnt bone fragments were embedded undecalcified into epoxy cold mounting resin and a catalyst (Spectrographic Ltd., Leeds, UK) and placed under vacuum in a desiccator to ensure diffusion of the resin into bone pores. Mounted blocks were then ground with carbon papers of progressively finer grit size (800, 1200, 2500) using a grinding and lapping machine (Buehler, Lake Bluff, IL, USA). The blocks were then polished on a Buehler wheel using 3 mm diamond paste (DP-Paste M, Struers A/S) and a satin woven acetate polishing cloth (DP-Dac, Struers A/S) for 30 minutes following another 5-minute cycle using another polishing cloth with 1 mm monocrystalline diamond suspension (MetaDi, Buehler). The mounts were cleaned in an ultra-sonic water bath after each phase, then finished with another round of ultra-sonic bath in petroleum ether (40°-60°C, analytical reagent grade, Fisher Scientific). Samples were carbon-coated using a carbon evaporation coater (HHV Auto 360), the carbon acting as a conductive layer to prevent charging.

Major and trace element compositions were determined using a wavelength-dispersive JEOL JXA-8200 electron microprobe at the Research Laboratory for Archaeology and the History of Art (RLAHA), University of Oxford, UK. An accelerating voltage of 15 kV, 10 nA beam current and 10-micron beam were used to analyse the polished samples. Peak count times were 30 s for P, Al, Na, Si, K and Ca; 40 s for Cl; and 60 s for Mg, Sr, Fe and Mn. Background counts were collected for half the peak count time either side of the peak (Pyle *et al.*, 2002). The microprobe was calibrated using a range of mineral standards, with accuracy verified by analysing apatite secondary standards (Durango, Bamble and Wilberforce)[5] (Carlson *et al.*, 1999) and previously analysed secondary bone standards provided by the Directorate Earth and History of Life, Royal Belgian Institute of Natural Sciences, at the start of every run. Reference

[5] [Comment since publishing]: The used secondary standards are homogenous apatite trace-element reference materials.

materials were within ±1 standard deviation of the preferred values (Jochum *et al.*, 2006). Analytical errors of the electron microprobe analysis (EMPA) and detection limits for the measured elements are provided in Table 8. K and Mg were in much higher concentration in the samples than in the secondary standards, meaning that their error rates presented a lower value. Thus, the standard deviation percentage (SD%) was measured for these elements which were 37.87 SD% for K and 3.83 SD% for Mg. A total of 617 measurements were taken from the outer cortical layer (OC), mid-cortical region (MC), inner cortical layer (IC), and around vascular canals (HC) on the transverse bone sections. This excludes 82 points that were removed from the dataset, because the sum of elements was less than expected in bone (total elements measured <50%) due to errors in locating and focusing the electron beam.

Element	Secondary Standards	Confidence Interval (CV)	Detection limit
P	Bamble, Durango, Bone	0.79	0.07
Na	Bamble, Durango, Bone	6.90	0.02
Cl	Bamble, Durango, Bone	3.49	0.01
K	Bone	17.22 (SD%: 37.87)	0.01
Fe	Bamble, Durango, Bone	33.99	0.01
Al	Wilberforce	1.71	0.03
Si	Bamble, Durango, Wilberforce	16.81	0.04
Sr	Bamble, Durango, Wilberforce, Bone	57.62	0.03
Mn	Bamble, Durango, Wilberforce, Bone	65.20	0.01
Mg	Bamble, Wilberforce, Bone	2.82 (SD%: 3.83%)	0.02
Ca	Bamble, Durango, Bone	0.51	0.01

Table 8- The coefficient of variation (CV) and detection limits (D.L.) of the measured major and trace elements in the secondary standards.

IV.2.3 Statistical Analysis

The absorption peaks, ratios from the FTIR and the elemental concentration EMPA data were analysed using Python programming language. Descriptive statistics and linear regression were used to measure the strength of the relationship between the measured changes

and the PMI in both the unburnt and burnt bones, with statistical significance assessed by associated p-values ($\alpha = 0.05$). The null hypothesis was that parameter X does not increase with PMI. The coefficient of variation (CV) was used to evaluate the scattering of parameters in each group with different PMI and burning status.

Principal Component Analysis (PCA) and Linear Discriminant Analysis (LDA) were used to identify the main elements of interest and FTIR ratios were used to differentiate between PMI groups and burning states. LDA was a better statistical model for the purposes of this study. *A priori* categories in this study were state (unburnt vs burnt), PMI (0-365 days), and zone (outer-, mid-, inner-cortical, and around vascular canals). Each sample's confidence score determined the parameter based on which they were placed into one of these categories. Multivariate analysis of variance (MANOVA) was used to examine for statistical differences on one dependent variable (PMI) by independent grouping variables (EMPA and FTIR datasets) in *Statsmodel*s Python library. This was coupled with pairwise posthoc multivariate comparison testing (MCT) to identify which specific groups significantly differed from one another.

Datapoints below detection points (Suppl. 6) were entered as 0.00 in the EMPA data. Both FTIR and EMPA dataframes were scaled for the analyses using Sklearn Python library. All data analyses were performed in Jupyter Notebook in Python programming language.

IV.3 Results

IV.3.1 FTIR Results

The spectra of unburnt and burnt bone were investigated in different regions and their associated changes were noted as a function of length of PMI and burning (Fig. 18; Table 9). A change in the intensity of peaks from 0 to 365 days PMI groups were found at several frequencies.

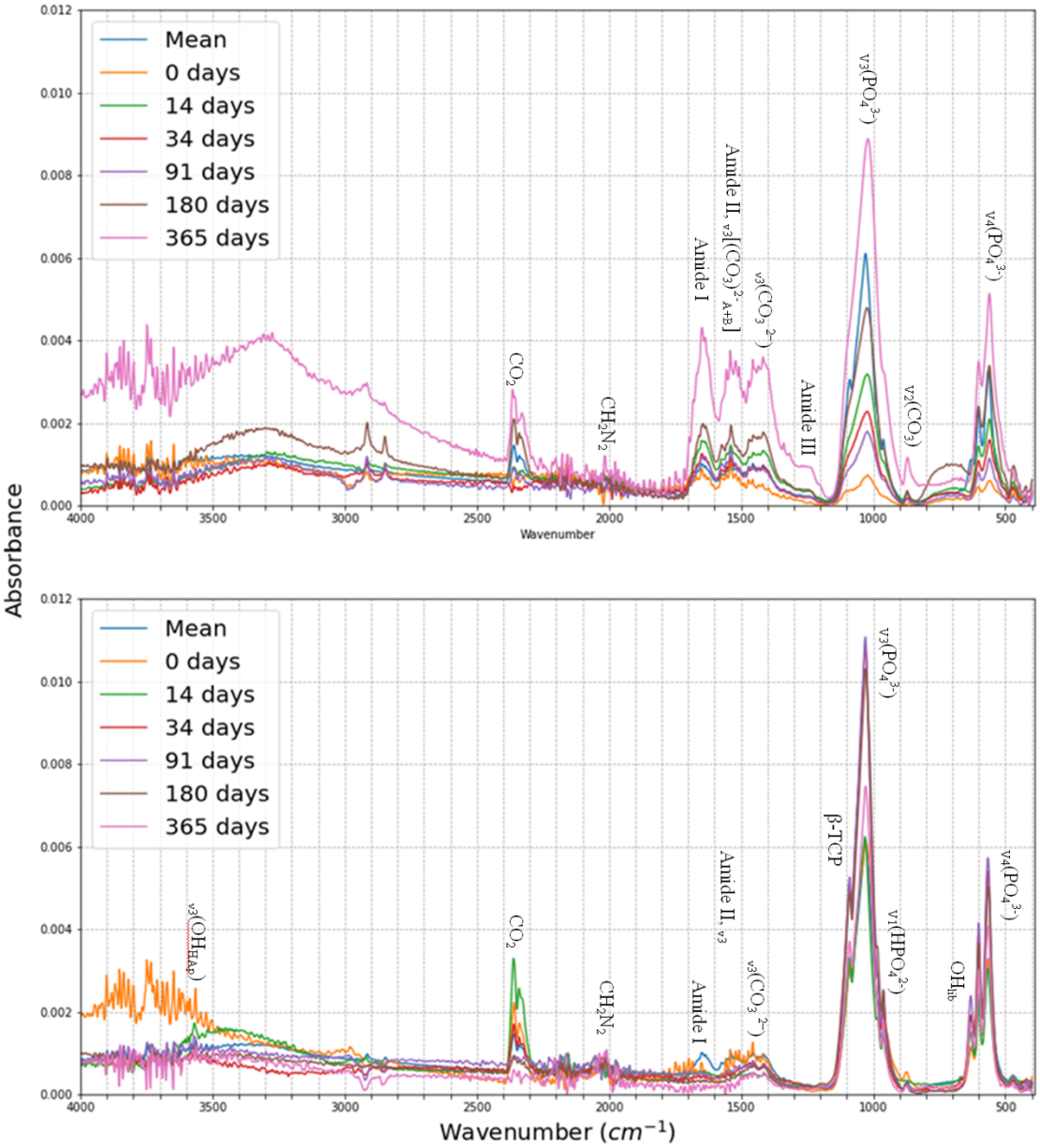


Figure 18 -- The FTIR spectra of the means of each PMI group before (upper image) and after (lower image) burning. Labelled are the peak assignments of interest.

Wavenumber (cm-1)	**Functional Group**	**Mode**	**Bone Samples**	
			Unburnt	**Burnt**
3570	Apatitic hydroxyl groups ($_{vs}OH^-$)	OH stretching (Goodman, 2001; Marques *et al.*, 2018)	N/A	Intensity decreases with longer PMI
3600-2700	Organic fraction and water(Holcomb and Younger, 1980)	C-H and O-H stretching (Praprotnik and Janežič, 2005)	Convoluted bands, no peaks	N/A

2400-2300	(atmospheric) CO_2	C≡O stretching (Gerakines *et al.*, 1995)	Doublet of bands (traces of CO_2 from atmosphere)	Doublet of bands (traces of CO_2 from atmosphere)
2010	Cyanamide (CH_2N_2)(Dowker and Elliott, 1979; Snoeck *et al.*, 2014)	C-N stretching	Weak peak present, highest in 365-day group	Weak peak present, highest in 365-day group
1660	Amide I(Marques *et al.*, 2018) (C=O) and water	C-O stretching and H-O-H bending	Decreases with longer PMI	Very weak bands: highest 0-day group, lowest 365-day
1550	Amide II(Marques *et al.*, 2018) (N-H)	N-H bending	Decreases with longer PMI	Very weak bands: highest 0-day group, lowest 365-day
1250	Amide III(Marques *et al.*, 2018) (N-H)	N-H bending	Shoulder on all groups, except a very weak peak in the 0-day group	N/A
1600-1300	Stretching modes of carbonate ions (LeGeros *et al.*, 1969; Holcomb and Younger, 1980)	C-O stretching	Three broad bands with additional peaks; highest: 365-day, lowest: 0-day, mixed in between	Weak bands, highest; 0-day, lowest: 14-day
1415	B type carbonates $_{v3}(CO_3^{2-})_B$ (LeGeros *et al.*, 1969; LeGeros and LeGeros, 1983)	C-O stretching	Highest of the carbonate peaks, highest in 365-day, lowest in 0-day	Weak peaks: highest in 0-day, lowest in 365-day
1540	A type carbonates $_{v3}(CO_3^{2-})_A$ (LeGeros *et al.*, 1969)	C-O stretching	Overlaps with Amide II	Weak peaks: 0-day highest, 365-day lowest
1123	Extra peak, due to appearance of β-TCP (Piga *et al.*, 2016)	P-O stretching [anti-symmetric (v3)]	No extra peak. Shoulder on the 0 and 91-day groups.	Extra peak around 1080-1090 cm-1 on all groups except 34-day group
960-1200	$_{v1, v3}$ (PO_4^{3-}) (Marques *et al.*, 2018)	P-O stretching [symmetric (v1) and anti-symmetrics (v3)]	No peaks, shoulders. Most intense: 365-day, least intense: 0-day	Present. Highest intensity: 0, 91, 180-day; weakest: 14-day
872-879	Carbonates (three sub-bands): type A, type B, 'labile' $_{v2}(CO_3)$ (Holcomb and Younger, 1980; Rey *et al.*, 1989; Thompson and Inglis, 2009)	out-of-plane bending C-O	Present, but as a convolution of the three sub-bands. Highest: 365-day, weakest: 0-day. All the rest are clustered around the same absorbance value.	Present, but as a convolution of the three sub-bands. Decreases with longer PMI. Most intense: 0-day > 14-day. Other groups: clustered around the same lower value
640 - 620	Apatitic hydroxyl groups (Mamede *et al.*, 2018; Marques *et al.*, 2018)	(OH) librational	N/A	Present. Intensity of peak: 91 > 34 > 180 > 365 >14 > 0-day
600-500	$_{v4}(PO_4^{3-})$ (LeGeros *et al.*, 1969; LeGeros and LeGeros, 1983)	P-O bending	2 peaks ($_{v3}$ splitting). Most intense: 365-day, least intense: 0-day	3 peaks ($_{v3}$ splitting and OH_{lib} band). $_{v3}$ intensity: 91 > 34 > 180 > 365 > 0 > 14-day
547	Shoulder, due to appearance of β-TCP (Piga *et al.*, 2016)	P-O bending (LeGeros *et al.*, 1969; LeGeros and LeGeros, 1983)	Present on all. 365-day: strong, 180-day: moderate, 91-, 34-, and 14-day: weak, 0-day: very weak	N/A

Table 9 - Identified zones of interest and their associated absorption changes on the unburnt and burnt bones.

The majority of the mean IRSF values for the unburnt bones ranged between 2.88 and 3.30, with the exception of the 365-day bone (5.04) (Suppl. 4). There was an increase in all mean IRSF values post-burning (37.77-57.27%) across all groups, except for the 365-day PMI sample, which decreased by 5.35%. In unburnt bone, the 365-day group's high IRSF value was significantly different than all other PMI group (Table 3). CV values showed very low variation across samples within the same PMI groups. IRSF gives an indication of highest reached temperature and cremation efficiency, due to increased crystallinity values. The sequence of crystallinity of the PMI groups is: 91 > 0 > 180 & 365 > 34 > 14 days. This sequence does not follow the PMI order and it is likely due to the variation in burning conditions (e.g. temperature, duration, position in the pyre), which are the dominant factors affecting crystallinity.

The results of the linear regression (Table 10) show that there was a strong positive linear correlation between IRSF and time since deposition in unburnt bone ($r=0.856$, $p<0.029$). This increase in structural ordering suggests the early post-mortem recrystallisation of bioapatite is already measurable in the first 1 year of PMI. BPI was negatively correlated with PMIs in unburnt bone ($r=-0.876$, $p<0.022$) (Table 3). Although there was no linear change in any of the proposed parameters for PMI estimation in the burnt bone, MANOVA and MCT revealed that IRSF, C/C, and CO/CO_3 ratios were significantly different in various PMI groups in burnt bone, as well as IRSF, BPI, C/C, and PHT in unburnt bone (Table 10).

FTIR Parameters	Linear Regression				Multivariate comparison of means test		
	Unburnt		**Burnt**		**PMI** (PR>F)		**State** (PR>F)
	r^2	**p**	**r^2**	**p**	**unburnt**	**burnt**	
IRSF	0.856	**0.029**	0.2	0.704	**0.000002**	**0.014**	**0.001**
C/P	-0.531	0.278	-0.557	0.251	0.505	0.561	**0.001**
BPI	-0.876	**0.022**	-0.619	0.19	**0.006**	0.638	**0.001**
API	N/A	N/A	-0.631	0.179	N/A	0.667	N/A
CO3/P	0.269	0.606	-0.049	0.926	N/A	N/A	N/A
C/C	0.08	0.879	0.096	0.855	**0.034**	**0.003**	**0.024**

CN/P	-0.701	0.12	-0.039	0.941	0.535	0.316	**0.003**
CO/CO3	-0.655	0.158	-0.519	0.29	0.16	**0.003**	**0.005**
PHT	0.679	0.138	-0.159	0.763	**0.032**	0.055	**0.001**
N/P	-0.46	0.357	-0.508	0.303	N/A	N/A	N/A
APR	-0.542	0.267	-0.492	0.321	N/A	N/A	N/A

*Table 10 – Linear regression and multivariate comparison test (MCT) on the FTIR dataset. Correlation Coefficient ('r') and p-value ('p') for each analysed FTIR parameter on the unburnt and burnt bone in the linear regression section. H_0= X parameter does not increase with postmortem time period. ** indicates significant p-values. The MCT section shows the results of the MANOVA and multivariate comparison testing on the established FTIR ratios as a function of state (unburnt vs. burnt) and time.*

Unburnt bone at 0 and 91-day PMI displayed an extra shoulder at 1123 cm^{-1}, which is assigned for either β-TCP or Mg substitution (Piga *et al.*, 2016). All burnt bone had an extra peak at 1100-1080 cm^{-1}, except the 34-day post-mortem group. No burnt bone displayed a shoulder at 547 cm^{-1}, but it was a common feature in the unburnt bone, intensity ranging from strong (365-day) to very weak (0-day), which translation band also suggest Mg-OH substitutions (Kloprogge *et al.*, 2004). Mg shows a non-uniform, non-linear increase in the unburnt bone through the PMI in the EMPA data.

PCA indicated that the ratios explained 81.67% of the variance in the dataset with the first (PC1) and second (PC2) principal components accounting for 66.67% and 15.00%, respectively. Loadings show that all ratios contributed to PC1, with IRSF (0.74), BPI (0.35), and CO/CO_3 (0.33) being the largest (Fig. 19), while the main contributors to discrimination by LDA were C/P for burnt bone and PHT and CN/P for unburnt bone (Suppl. 5). Both PCA and LDA differentiated between unburnt and burnt bone, but not between PMI groups.

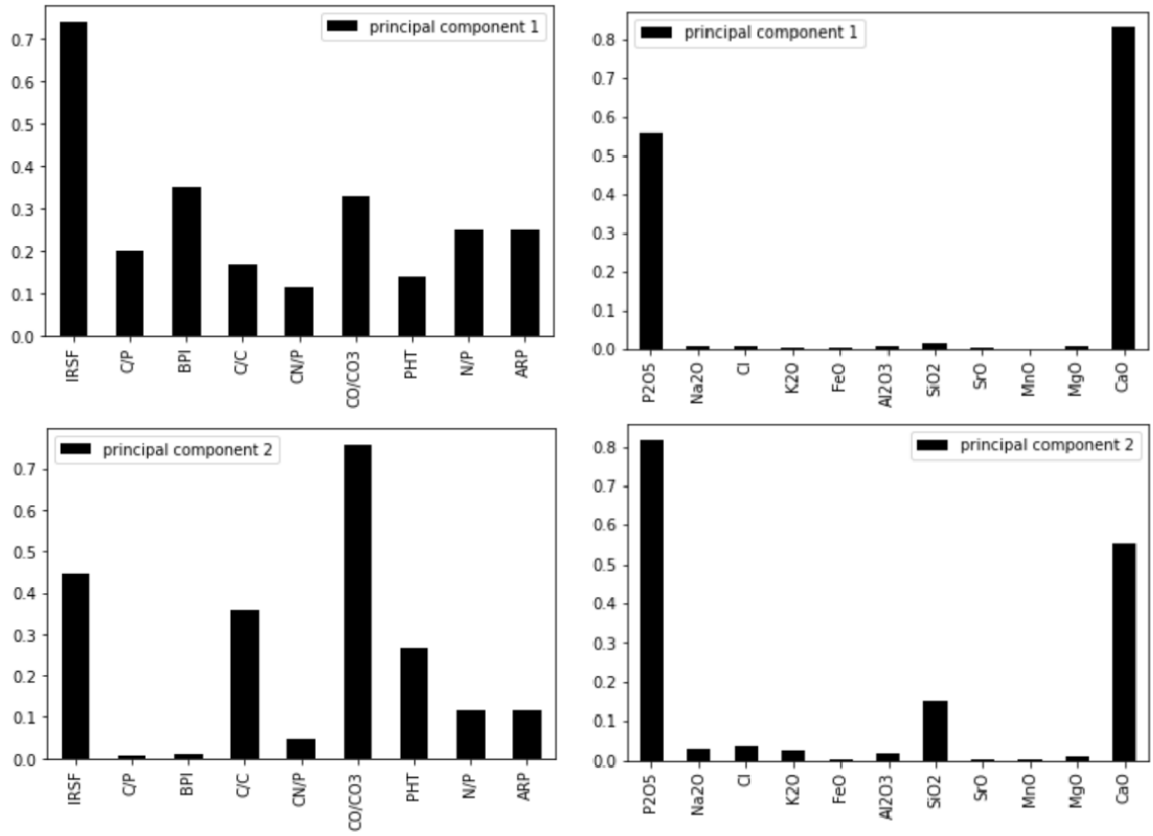


Figure 19-- Loadings of the principal component analysis when using both the FTIR and EMP dataset.

IV.3.2 WDS-EMP Results

WDS-EMP data were analysed spatially for major and trace elemental concentration (Suppl. 6) of unburnt and burnt bone at different PMIs. Variations in elemental concentrations as a function of time in the experimental bone are visualised in Fig. 20. The most highly variable zones in unburnt bone across all elements were the OC (0.60) and HC (0.50), while IC (0.49) and MC (0.46) were the lowest. The mid-cortical and the inner cortical zones showed the lowest variability across all samples.

In the archaeological cremated bone (KILT) P and Ca remained relatively stable in all zones, while K, Fe, Al, Si, Sr, Mn, and Mg display very high values in the outer cortical layers, suggesting diffusion of elements from the soil (Fig. 21). The highest CV scores were recorded for Sr, especially in the outer cortical layers.

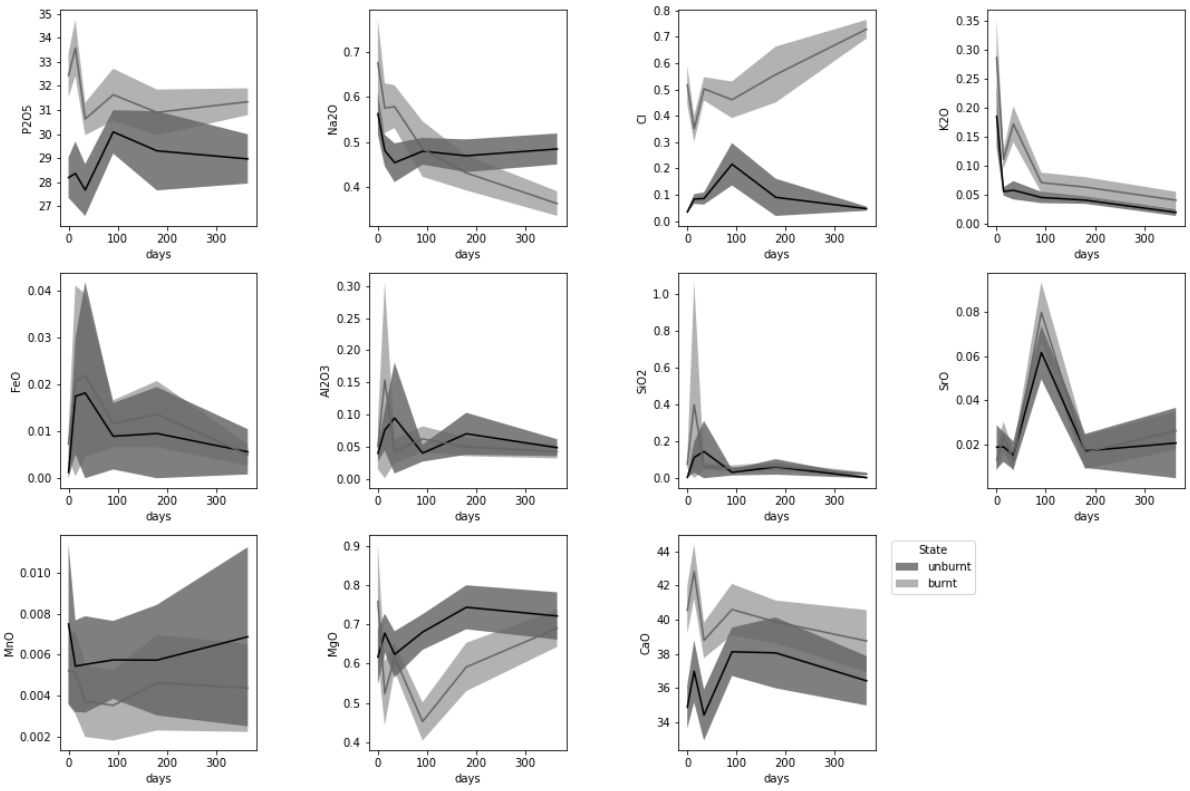


Figure 20 -- Average elemental concentration (wt %) of the experimental bones using the EMPA data. Mean ± 2 standard errors for each measured element as a function of time in unburnt (blue) and burnt (orange) bone.

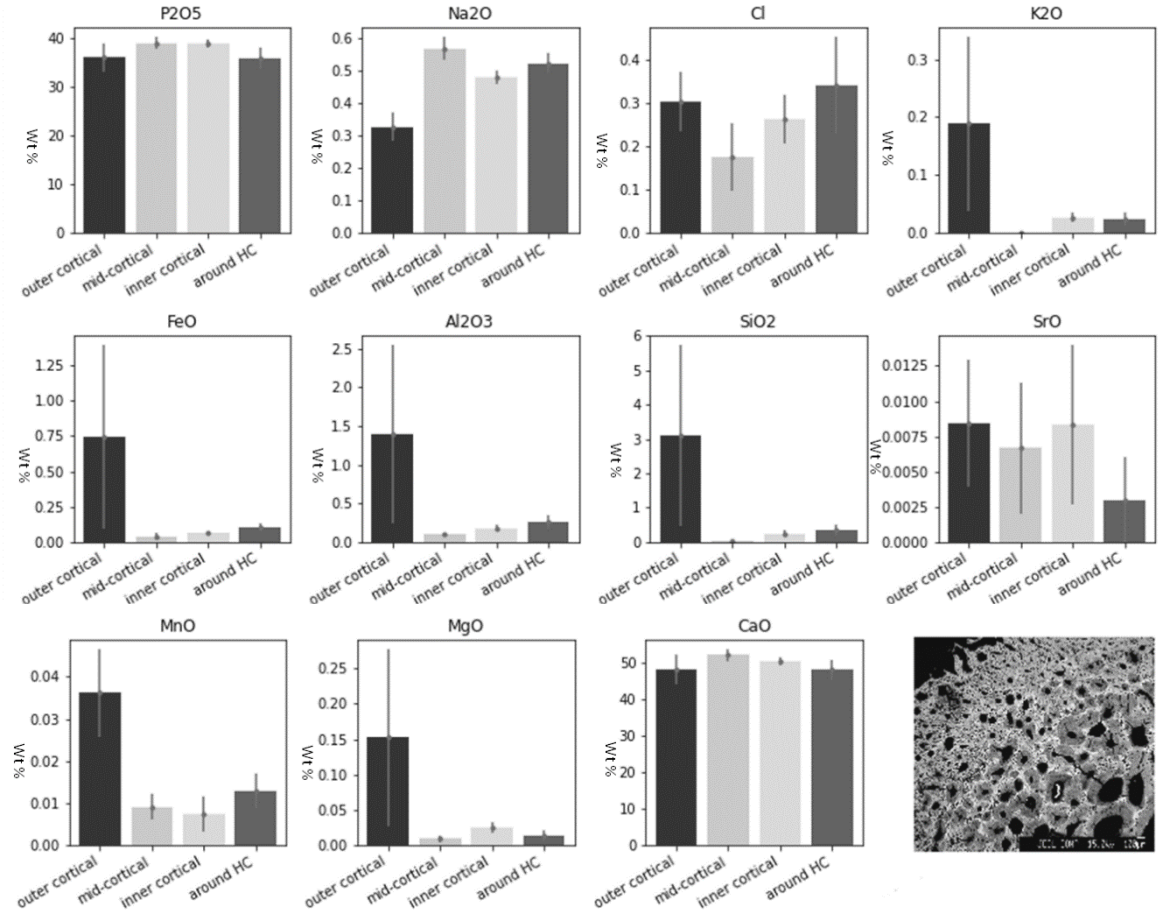


Figure 21 – Average elemental concentration (wt %) of the Neolithic cremated human remains for each zone. Mean ± 2 standard errors for each measured major and trace element in archaeological cremated bone. The backscattered electron microscopy (BSEM) image represents an example of a bone cross section.

Linear regression analysis (Table 11) shows that in unburnt bone only K, Mn, and Mg in unburnt bone and Na, Cl, and K in burnt bone changed in a linear fashion with time. K was the only element that decreased both in the unburnt and burnt bone sections overall, and separately in the IC and HC zones (Fig. 22). There were no significant trends in the Ca/P ratios and all zones presented similar values (between 1.23 and 1.29) while the archaeological samples were insignificantly higher (1.35).

Element	**Location**	Linear Regression				Multivariate Comparison Test (MCT)		
		Unburnt		**Burnt**		**PMI**		
		r^2	**p**	**r^2**	**p**	**Unburnt**	**Burnt**	**State**
P2O5	OC	0.602	0.206	0.204	0.699			
	MC	0.246	0.638	-0.276	0.597			
	IC	0.217	0.68	-0.572	0.236	0.419	**0.000	**0.001

	HC	0.063	0.905	-0.428	0.397			
	All	**0.277**	**0.19**	**-0.284**	**0.179**			
Na2O	OC	-0.172	0.745	-0.676	0.141	0.061	**0.000	**0.001
	MC	-0.436	0.388	-0.873	**0.023			
	IC	0.561	0.247	-0.889	**0.018			
	HC	0.236	0.652	-0.872	**0.023			
	All	**-0.051**	**0.813**	**-0.744**	****0.000**			
Cl	OC	-0.397	0.436	0.830	**0.041	**0.000	**0.000	**0.001
	MC	-0.099	0.852	0.702	0.120			
	IC	-0.142	0.789	0.843	**0.035			
	HC	-0.009	0.986	0.801	0.055			
	All	**-0.162**	**0.449**	**0.690**	****0.000**			
K2O	OC	-0.655	0.158	-0.54	0.269	**6.05E-26	**9.15E-23	**0.001
	MC	-0.603	0.205	-0.666	0.149			
	IC	-0.834	**0.039	-0.810	**0.050			
	HC	-0.551	0.257	-0.804	0.054			
	All	**-0.552**	****0.005**	**-0.578**	****0.003**			
FeO	OC	-0.413	0.416	-0.397	0.436	0.767	0.302	0.839
	MC	0.614	0.195	-0.097	0.855			
	IC	-0.153	0.773	0.011	0.983			
	HC	-0.493	0.321	-0.395	0.438			
	All	**-0.160**	**0.454**	**-0.251**	**0.238**			
Al2O3	OC	-0.304	0.558	-0.027	0.96	0.633	0.209	0.900
	MC	-0.497	0.316	0.502	0.311			
	IC	-0.441	0.382	0.690	0.129			
	HC	0.715	0.111	-0.423	0.403			
	All	**-0.127**	**0.555**	**-0.171**	**0.424**			
SiO2	OC	-0.498	0.315	-0.780	0.067	0.283	0.493	0.497
	MC	-0.584	0.223	-0.519	0.291			
	IC	-0.391	0.443	-0.507	0.304			
	HC	-0.045	0.932	-0.370	0.470			
	All	**-0.242**	**0.255**	**-0.206**	**0.335**			
SrO	OC	0.178	0.736	0.025	0.963	**0.000	**3.03E-32	0.470
	MC	-0.255	0.625	0.215	0.682			
	IC	0.086	0.872	-0.052	0.922			
	HC	0.128	0.809	0.023	0.966			
	All	**0.027**	**0.899**	**0.054**	**0.804**			
MnO	OC	0.637	0.173	-0.473	0.344	0.952	0.692	**0.031
	MC	-0.873	**0.023	0.123	0.817			
	IC	-0.567	0.241	0.137	0.795			
	HC	0.523	0.287	-0.085	0.872			
	All	**0.127**	**0.553**	**-0.062**	**0.772**			
MgO	OC	0.709	0.115	0.182	0.731	**0.048	**0.000	**0.003
	MC	0.402	0.429	0.621	0.189			

	IC	0.780	0.068	-0.418	0.409			
	HC	0.480	0.335	0.379	0.458			
	All	**0.456**	****0.025**	**0.138**	**0.52**			
CaO	OC	0.753	0.084	0.642	0.169	0.089	**0.001	**0.001
	MC	0.137	0.795	-0.555	0.253			
	IC	0.078	0.884	-0.668	0.147			
	HC	0.071	0.894	-0.637	0.174			
	All	**0.286**	**0.176**	**-0.354**	**0.090**			

*Table 11 – Linear regression and multivariate comparison test on the EMPA data. Correlation Coefficient ('r^2') and p-value ('p') are given for each analysed element in unburnt and burnt bone for the linear regression. H_0= X parameter does not increase with postmortem time period. ** indicates significant p-values. HC = around vascular canals; OC = outer cortical; MC = mid-cortical; IC = inner cortical zones. In the multivariate comparison test, p values are derived from both MANOVA and multivariate comparison testing.*

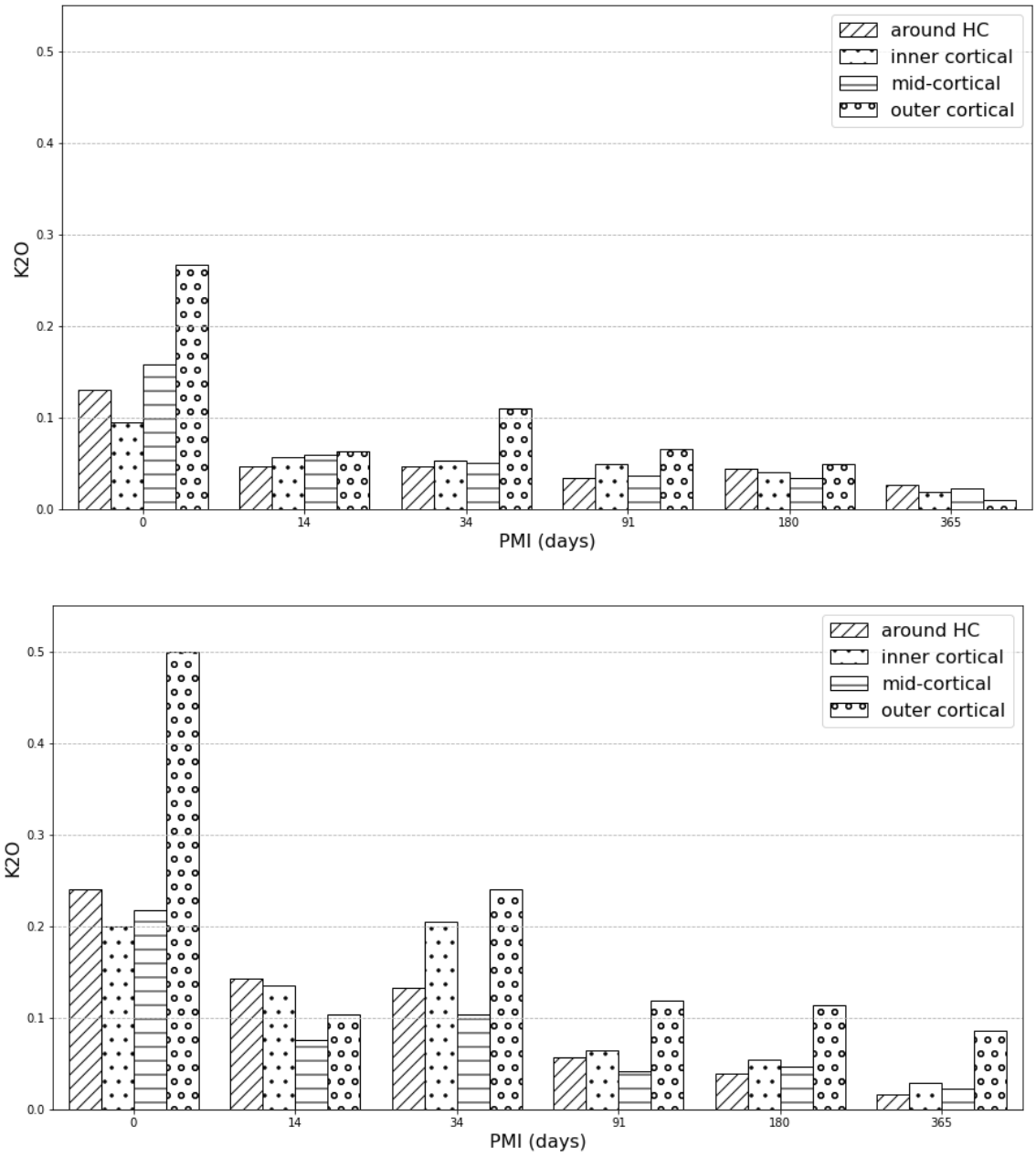


Figure 22 -- Potassium wt% content in experimental unburnt (upper) and burnt (lower) bone by zone.

PCA showed that the first principal component (PC1) explained 93.49% of the variance and the second principal component (PC2) explained 4.19%, with the key discriminators being Ca and P (Fig. 19). LDA was used to reduce the features (elements), classify samples, and subsequently visualising the classification according to the defined categories (state, PMI, zone). When the data were transformed into a two-feature (unburnt vs burnt) linear

discriminant dataset, the two states were clearly differentiated (Fig. 23A). LDA did not clearly differentiate between the PMI groups, with slightly more separation of PMIs in unburnt bone (Fig. 23B). MANOVA and MCT showed that P, Na, Cl, K, Mn, Mg, and Ca were significantly associated with burning, while Fe, Si, Sr, and Al were not (Table 11). An overall significant difference was observed between PMI groups in Cl, K, Sr, and Mg levels in unburnt bone, and in P, Na, Cl, K, Sr, Mg, and Ca values in burnt bone (Table 11). The fresh group differed significantly in K values from all other PMI groups in both unburnt and burnt bone by MANOVA and MCT.

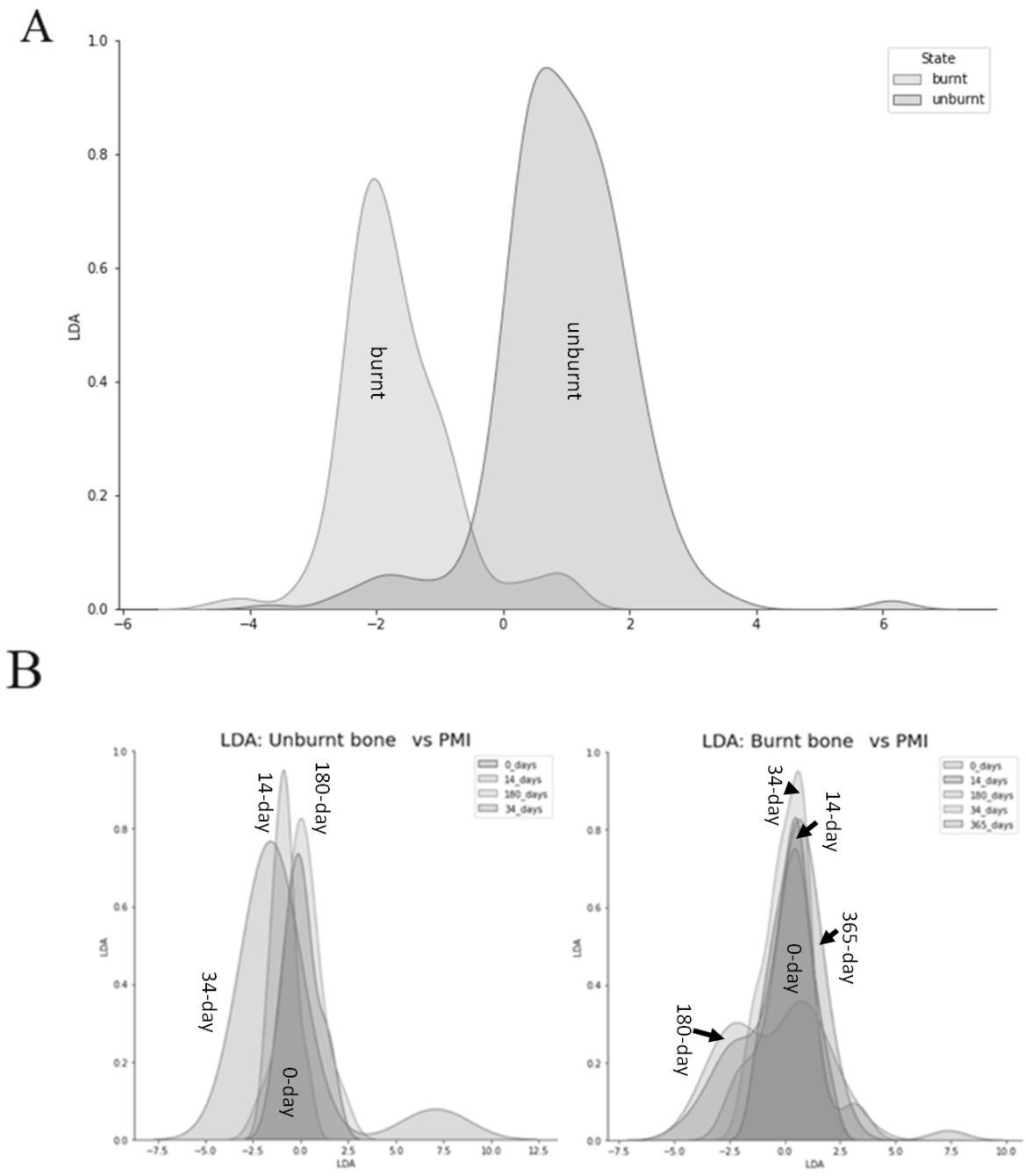


*Figure 23 --Linear discriminant analysis (LDA) on the EMPA dataset. **A**: Separation of unburnt and burnt bone by LDA. Contributions: 'Al2O3': 0.244, 'CaO': -6.882,'Cl': 3.216,'FeO': 0.07,'K2O': 0.607,'MgO':-1.036,'MnO': -0.056, 'Na2O': -0.545,'P2O5': -3.97,'SiO2': -0.902,'SrO': 0.199, 'Total': 13.08. **B:** Clusters created by LDA of the unburnt (left) and burnt (right) PMI groups.*

IV.4 Discussion

This study on the early diagenesis and burning of bioapatite has shown that both structural and chemical changes are observable after only 1-year PMI. Potassium elemental concentration decreased with PMI and survived burning, making it the best discriminator between bone burnt fresh and partially decomposed. This decrease compared to experimental bone suggests that endogenous K had decayed prior to cremation in the Neolithic bone, thus the bodies might have been left to decompose prior to further funerary treatment. While decrease in carbonates and increase in crystallinity were documented in only 1 year of surface exposure, these were masked by burning. Ca, P, Fe, Al, Si, and Sr did not significantly change with heat-treatment and Fe, Al, Si, and Sr were not associated with time since deposition either.

Crystallinity increases in a linear fashion with PMI in unburnt bone and burnt bone shows higher crystallinity compared to unburnt bone. This is in agreement with the literature (e.g., (Thompson *et al.*, 2013; Snoeck *et al.*, 2014)), except the 365-day burnt group where results show a slight decrease, which may be the result of the bone's already higher crystallinity or small-scale temperature variation across individual bones. The lack of linear increase in burnt bone crystallinity with time suggests that burning overrides the increase in IRSF due to early diagenesis in the first 6 months of the PMI. As crystallinity increased, carbonate content decreased in a linear fashion in the unburnt bone, in line with other studies (Miller *et al.*, 2001; Keenan and Engel, 2017b). Keenan and Engel (2017b) documented significant carbonate loss at 3 years PMI, with insignificant decrease after 1 year but increase compared to that value in 2 years, while here A and B carbonates to phosphate ratios showed a significant linear decrease throughout only a year PMI. However, B type carbonates only significantly changed prior to 3 months PMI compared to the 365-day group. Burning, again, obscured the effects of early diagenesis of carbonate loss.

β-TCP signals the thermal decomposition of the apatite phase and should be detectable in bones burnt at >700°C (Raynaud *et al.*, 2002; Piga *et al.*, 2009; Hidouri *et al.*, 2019), which was reached in this study for a short duration. There is an extra peak at ~1100-1080 cm^{-1} on all burnt bone spectra, which might be due to a shift in the spectra and might still represent β-TCP. However, the lack of a shoulder at 547 cm^{-1} suggests otherwise. Surprisingly, all unburnt bone displayed a shoulder at 547 cm^{-1}. These shoulders cannot be due to β-TCP in unburnt bone, but are probably due Mg substitutions for Ca (Piga *et al.*, 2016). However, there were no outstanding elevated levels of Mg in the unburnt bone (unburnt mean Mg levels ranged between 0.01 and 0.82 wt%). Mg values in all zones are slightly higher in the 180- and 365-day groups than those with shorter PMIs, suggesting a non-uniform, non-linear increase. However, Mg-values were highly variable in burnt bone. With a melting point of 650°C, this might be due to the burning efficiency of the different fire events. Therefore, β-TCP as a thermal decomposition product might not have occurred, but Mg ions might have increased despite its reduced competitiveness in substituting due to the crystal lattices' more accommodating nature for sodium and potassium (Beckett, 2009). Another possibility is that β-TCP did appear as a thermal decomposition product, but post-cooling it was not possible to detect, as it is not thermally stable (Greenwood *et al.*, 2013).

As the bones were burnt in an outdoor fire, burning efficiency was variable. Burning efficiency could be estimated for the different PMI groups from the N/P ratios and IRSF. The sequence from highly efficient to less efficient from N/P was 91- and 180-day > 365-day > 34-day > 0-day > 14-day, while from IRSF data it was 91-day > 0-day > 180- and 365-day > 34-day > 14-day. The differing placement of the 0-day group in the two sequences might be due to the placement of the different fat-content of the individual fresh legs, since fat acts as a fuel during burning, increasing temperature when more fat is present and resulting in higher crystallinity. MANOVA results confirmed that all FTIR ratios designed to assess cremation

efficiency (Thompson, 2005; Thompson *et al.*, 2009, 2013) differ significantly in unburnt and burnt bone. In both cases, the 91-day group was the most efficiently cremated and the 14-day group the least. This might explain why only the 14-day and the 0-day groups showed significantly different values in P in burnt bone. Ca and P, the two major elements in bone, were otherwise insignificant in both the unburnt and burnt groups. Sr was significantly different in the most efficiently burnt group (91-day) than in all others, but this difference was present in its unburnt state as well; thus, it was not due to burning.

Other than Mn, the increase in all other element's atomic percentage is higher in burnt 0-day (fresh) bone than in unburnt fresh bone. However, it appears this is due to the decrease in organic content and thus does not essentially indicate a real increase in the mineral phase. Ca, P, Fe, Al, Si, and Sr changes through the PMI stages in the same fashion in unburnt and burnt bone, meaning they are not highly affected by burning at ≤750°C and their amount in burnt bone is representative of their pre-burnt levels. The results for Sr are in agreement with those of Snoeck *et al.* (Snoeck *et al.*, 2014), who did not find changes in Sr isotopic signals following experimental cremation. Fe showed an initial increase at 14-day PMI and a sharp decrease thereafter, which is due to soft tissue putrefaction and aligns with the literature (Walden *et al.*, 2018).

Only three elements (K, Na, Cl) were found to be affected by time since deposition in the first year PMI. Potassium and sodium are associated with moisture in bone and their decrease signifies dehydration (Walden *et al.*, 2018). Here, potassium was the most useful element in differentiating between fresh (0-day) and all other PMI groups in unburnt bone. In addition, K showed an overall linear decrease in both unburnt and burnt bone area for all zones combined. The unburnt group's potassium values suggest rapid depletion of K in 2 weeks (from mean 0.16 wt% to mean 0.06 wt%), after which depletion slowed down. Environmental factors might have altered the rate of depletion in the OC and IC zones. After 34 days, bone had a

higher K-value in the OC zones, which coincides with the time at which the specimens started to be noticeably partially submerged into the soil. The burnt experimental bone always had higher K-levels than unburnt, but followed the same pattern of depletion. Although KOH has a relatively low melting point (360 °C), it was found in apatitic aorta deposits burnt at 720 °C (Danilchenko *et al.*, 2018), suggesting that it is bound to the crystal. K was previously found to be localised in the removed organic bone material (Bushinsky *et al.*, 2000) and was suggested to be present mainly in a labile state, meaning it is localised on the mineral crystal surface with low migration activity (Danilchenko *et al.*, 2018). However, the latter study's limitations included a more limited detection limit of EDS and the inability to evaluate the contributions to the labile fraction corresponding to surface-localised water-soluble compounds related to the organic matrix. Since organic material was removed by burning in the present study's bones, meaning that the oxidation of carbon was complete (assessed by the white colour of calcined bones without black ash/carbon left behind), but K was still detectable by EMPA, it is possible that K integrates into the crystal lattice. The 0-day burnt bioapatite samples always had K-values ≥0.20 wt%, while after 14 days this decreased to <0.14 wt% in all areas. The OC zones also showed depletion but at a slower rate than other areas. After 3 months, all K concentrations at IC, MC, and HC zones were ≤0.06 wt% and <12 wt% at OC areas. Thus, K-levels of <0.07 ± 0.001 wt% in the inner and mid-cortical zones, and around vascular canals of burnt bone suggest that the corpse was not burnt immediately after death, but after around 3 months. The outer cortical zones might show higher K concentrations due to uptake of potassium from the soil. It has to be noted that these bones were surface exposed and that dehydration would be expected to be slower had they been buried. In the Neolithic human bone fragments, endogenous K was below detection limit in the mid-cortical bone sections. Exogenous K (mean 0.08 wt%) from the soil might have diffused into the OC layers and to a lesser degree from the IC end and through the HC zones. Since bioapatite is less

susceptible to changes post-burning, due to increased crystallinity (Lee-Thorp, 2002; Trueman *et al.*, 2004; Snoeck *et al.*, 2014; Gallo *et al.*, 2021), this might mean that potassium essentially depleted in the Neolithic samples prior to cremation. Therefore, these bodies might have been left to decompose prior to cremation, to a degree that endogenous potassium was no longer present. Based on the experimental results of this study, in which K-values were never below the detection point at any zone, the postmortem interval prior to cremation in the archaeological bone can be suggested to have been >1 year.

Sodium is also associated with extracellular fluid in the body (Walden *et al.*, 2018). The 0-day burnt group showed higher values than the unburnt group, which is in agreement with Ellingham *et al.* (Ellingham *et al.*, 2018) In the experimental burnt samples there was a slight decrease between the 0-day (0.54 wt%) and 14-day (0.46 wt%) groups, after which it remained stable (0.45 – 0.48 wt%). Previously, Na was shown to have a tendency of mass transfer, leaving the crystals at 720 °C and increasing at 760 °C, which was suggested to be due to the reversible exchange of CO_3^{2-} (Danilchenko *et al.*, 2018). Here, Na showed a linear decrease with time in heated bones. The decrease of Na in the EMPA data is confirmed and supported by the decrease of CO_3 ions in the FTIR data (Yoo *et al.*, 2021). The initial value was 54% lower than in modern human bone reported by Elliott (Elliott, 2002). This discrepancy might be due to inter-species differences in calcium-substituting ions, such as Na, but studies on them are sparse (Beckett *et al.*, 2011). The Na value of 0.47 wt % for the Neolithic bone is consistent with that of unburnt archaeological bone reported in the literature (Lambert *et al.*, 1985). The burnt bone demonstrated that MC, IC, and HC zones had similar Na-values, while OC zone was depleted. Normally, Na leaches out of the layers of bone closest to the environment over time (Parker *et al.*, 1974; Lambert *et al.*, 1985), but these bones were broken. Nevertheless, it seems to explain why the experimental burnt bone had higher Na values in the OC zones 1-year post-mortem than the archaeological samples.

Cl values in burnt bone behaved almost inversely proportional to unburnt bone over time. Cl-enriched phases might appear in early diagenetic bone through the incorporation of Cl^- facilitated by the protonation of hydroxyl ions (Keenan, 2016), and/or by burning above 600°C (Maiti and Freund, 1981), up to <800 °C in defleshed bone and <900°C in fleshed bone (Ellingham *et al.*, 2018). OH sites in bone can be substituted with Cl (Yoo *et al.*, 2021). An OH-Cl peak was observed in the FTIR spectra of the burnt bones in all PMI groups, suggesting that Cl substitution for OH started in these bones. Our results are supported by the agreement between the EMPA and the FTIR results and previous studies' results showing Cl incorporation when HAp is heated above 600°C (Maiti and Freund, 1981).

PCA and LDA formed clearly separate clusters of unburnt and burnt groups, but were unable to distinguish between PMI groups. C/P, PHT and CN/P were the main discriminating ratios between the state of bone. Thus, FTIR is a useful technique in differentiating between unburnt and burnt bone, but it cannot detect early diagenesis up to 1-year postmortem in burnt bone. The main discriminating chemical elements between unburnt and burnt bone were Ca and Cl by LDA, and Ca and P by PCA.

Ca/P molar ratios remained fundamentally constant not only during soft tissue putrefaction (Ezzo, 1994), but also at 1 year PMI. The fact that this ratio did not present significant alterations with burning makes it a characteristic signature of bone, further supported by the similar Ca/P ratios of the archaeological and experimental burnt bone. Ratios were much lower than for stoichiometric HAp, due to the lattice housing carbonates and other elements (Elliott, 2002), Both Ca and P remained stable during the entire PMI. For Ca, this is in agreement with Reidsma *et al.* (Reidsma *et al.*, 2016), but in contrast to findings by Subirà and Malgosa (Subira and Malgosa, 1993) and McKinnon *et al.* (Mckinnon *et al.*, 2020). Although a decrease in C/P ratio had been documented after 1 year of burial (Keenan and Engel, 2017b), here C/P ratios (from the FTIR dataset) did not change significantly with PMI,

suggesting a stable ratio of carbonate to phosphate during the studied PMI in the same unburnt or burnt groups. The discrepancy with Keenan and Engel's (2017b) results might be due to the fact that their experimental alligator bones had evidence of microbial bioerosion, while this was not present in this study's bones (Végh *et al.*, 2021). Nevertheless, time since deposition does not seem to be the driving cause of C/P variation.

The outer cortical layer's highest variation in elements in unburnt bone demonstrates that exogenous elements diffuse into the bone in less than 1 year and endogenous elements are lost. However, zones around the vascular canals show the most varied elemental chemistry once bone is burnt. The high variability in concentration around osteons aligns with a microsampling study of unburnt bone by Scharlotta *et al.* (Scharlotta *et al.*, 2013) which found the presence of diagenetically unaltered zones further from the osteons. K, Si, Al, and Fe were barely detectable in the mid-cortical section in the archaeological bone; while the levels of these elements were high in the OC layers. However, in the experimental bone, the MC section did exhibit changes in elemental concentration with time. In other words, the mid-cortical section is more resistant to diagenesis than other areas of the bone, but it is also taphonomically altered, evidenced in <1-year postmortem.

IV.5 Conclusion

Fire drastically changes the morphological and chemical profile of bone making it notoriously difficult to derive information about circumstances surrounding death and deposition or burial of an individual. This includes how cultures treated their dead prior to and during cremation, and how cause and manner of death are identified after burning in forensic cases. Our investigation indicates that crystallinity increases in unburnt bone are detectable during the first year postmortem. B-type carbonate content decreased rapidly in the first 3 months PMI in unburnt bone, after which it slowed down. Both changes are masked by burning. The thermal decomposition of the apatite phase did not occur post-burning from the lack of β-

TCP signals in the IR spectra. The presence of these signals in unburnt bone suggests Mg substitutions, supported by the non-uniform, non-linear increase of Mg values with time from the EMPA data.

Major (Ca, P) and some trace elements (Fe, Al, Si, Sr) were not significantly associated with thermal treatment, while Fe, Al, Si, and Sr were not associated with the PMI. K, Na, Mg, and Cl were the only elements associated with time since deposition in the experimental bone. Potassium showed a potential to estimate the late postmortem interval/early diagenesis in both unburnt and burnt bone in the first year postmortem. Potassium rapidly depleted in bone after 2 weeks and continued to decrease over 1-year PMI. It is proposed here that if the K-values are under 0.07 ±0.01 wt% in the inner and mid-cortical zones of burnt bone then they were not burnt subsequently after death, but after at least 3 months decomposition in a surface exposed environment, or after a few months/years if buried, since burial slows down dehydration. Since K was present in calcined bones, it is proposed here that it might not exclusively be present in the organic phase of bones. In the Neolithic human cremated bones endogenous potassium is below detection limits. Therefore, if the bioapatite crystal structure truly become thermodynamically stable after burning at high temperatures as previous studies indicate (Lee-Thorp, 2002; Trueman *et al.*, 2004; Snoeck *et al.*, 2014), then it suggests that cremation of these corpses were delayed by at least some weeks following death.

Sodium, which is also associated with the extracellular fluid, rapidly decreased in 2 weeks in both unburnt and burnt bone, after which it remained stable in the former, but continued to decrease at a higher rate in the latter. The decrease of Na in the burnt bones was also confirmed by the decrease of CO_3 ions. The increase of Cl in the burnt bones with time was confirmed by the EMPA data and the start of the Cl substitutions for OH by the OH-Cl peaks in the FTIR data.

PCA and LDA were moderately successful at differentiating between unburnt and burnt bone, but not between PMIs of up to 1 year. C/P, PHT, and CN/P from the FTIR and Ca, Cl, and P from the EMPA were the best discriminators for unburnt vs burnt state of bone. This study demonstrates that Ca/P molar ratios do not change significantly due to PMI or burning in the experimental and only insignificantly change in the archaeological bone. However, C/P ratios might be dependent on the presence of microbial bioerosion rather than the time since deposition. Elemental chemistry analysis demonstrated that the mid-cortical zone is the least affected by contamination in both a modern and archaeological timescale.

This study has relevance for the assessment of postmortem interval, deposition environment, and time of burning in analysis of archaeological cremated bones and of burnt human remains in forensic cases.

Supporting Information

Please find supplementary material provided with this file.

Acknowledgments

We would like to thank Dr Victoria Smith for her help and assistance on the electron microprobe and Sophie Decree from the Directorate Earth and History of Life, Royal Belgian Institute of Natural Sciences for providing the secondary bone standards for the EMPA analysis of this study. We would also like to thank the team at Wytham Woods, Oxfordshire, UK for allowing us to conduct the taphonomy experiment and outdoor burning at their site. The Kiltierney samples were provided by the Environment and Heritage Service, Northern Ireland. We would also like to thank the anonymous reviewers for the valuable comments and improvements made to the paper.

Funding

The authors disclosed receipt of the following financial support for the research of this article: This work was supported by the Meyerstein Foundation, School of Archaeology, University of Oxford.

Supplementary Material

Component	Bone (wt%)
Ca	36.6
P	17.1
CO_2	4.8
Na	1
K	0.07
Mg	0.6
Sr	0.05
Cl	0.1
F	0.1
Ca/P molar	1.65

Suppl. 1 - The reported elemental concentration of bone ±1% variability due to diet, age, and anatomical variation (after Elliott 2002, 430).

Heat-Induced Elemental Changes in Bioapatite			
Element(s)	**Noted Differences**	**Notes**	**Citations**
Sr, Mg, Zn, Cu, Ba, V, Mn, Pb	Lower in archaeological calcined bones than in unburnt bones.	Potential contamination from the soil in unburnt bones.	(Gallello *et al.*, 2013)
Sr	Stable	Calcined bones do not exhibit uptake or loss of Sr, making them a reliable substrate for strontium isotope analysis.	(Snoeck *et al.*, 2016)
Ca	Increase	Not statistically significant	(Subira and Malgosa, 1993)
	Stable	Together with P	(Reidsma *et al.*, 2016)
	Decrease	Different between temperature groups, but not between archaeological and modern bones.	(Mckinnon *et al.*, 2020)
Mg, F	Decrease	At >500°C and only in specific surface zones	(Hidouri *et al.*, 2019)
Fe	Increase	Uptake in archaeological charred enamel suggested to be caused by pores and fissures from burning.	(de Winter *et al.*, 2019)

Suppl. 2. -- Documented differences in elemental concentration due to burning in bone in the literature.

Wavenumber (cm^{-1})	Notation	Assignment	Information retrieved
(565 + 603)/595	IRSF	Crystallinity Index or Splitting Factor, splitting between the $_{v3}PO_4$ domain	Reveals the structural order of the crystals of the inorganic portion of bones (Stiner *et al.*, 1995; Koon *et al.*, 2003; Munro *et al.*, 2007; Nagy *et al.*, 2008; Olsen *et al.*, 2008; Thompson and Inglis, 2009; Gonçalves *et al.*, 2011)
1660/1035	APR	Amide to phosphate ratio	Collagen to phosphate ratio(Fredericks *et al.*, 2012)
1415/1035	C/P	Carbonate (CO_3) to phosphate (P) ratio	B type carbonate content of the sample (Thompson *et al.*, 2009)
1415/603	BPI	Type B carbonate to phosphate ratio	Amount of type B carbonate
1540/603	API	Type A carbonate to Phosphate	Amount of type A carbonate (only calculated from burnt bone due to overlap with amide II)(Grunenwald *et al.*, 2014)
1450/1415	C/C	type B to type A carbonate	Amount of type B carbonate compared to type A carbonate
2010/1035	CN/P	Cyanamide (CN_2^{2-}) to phosphate	Cyanamide presence(Snoeck *et al.*, 2014)
1650/1415	CO/CO3	Carbonyl to Carbonate ratio	Organic to mineral ratio
625/610	PHT	Phosphate high temperature	Bones burnt >700^{0}C(Thompson *et al.*, 2013)
1660/1035	N/P	Amide I to Phosphate	Organic to mineral ratio

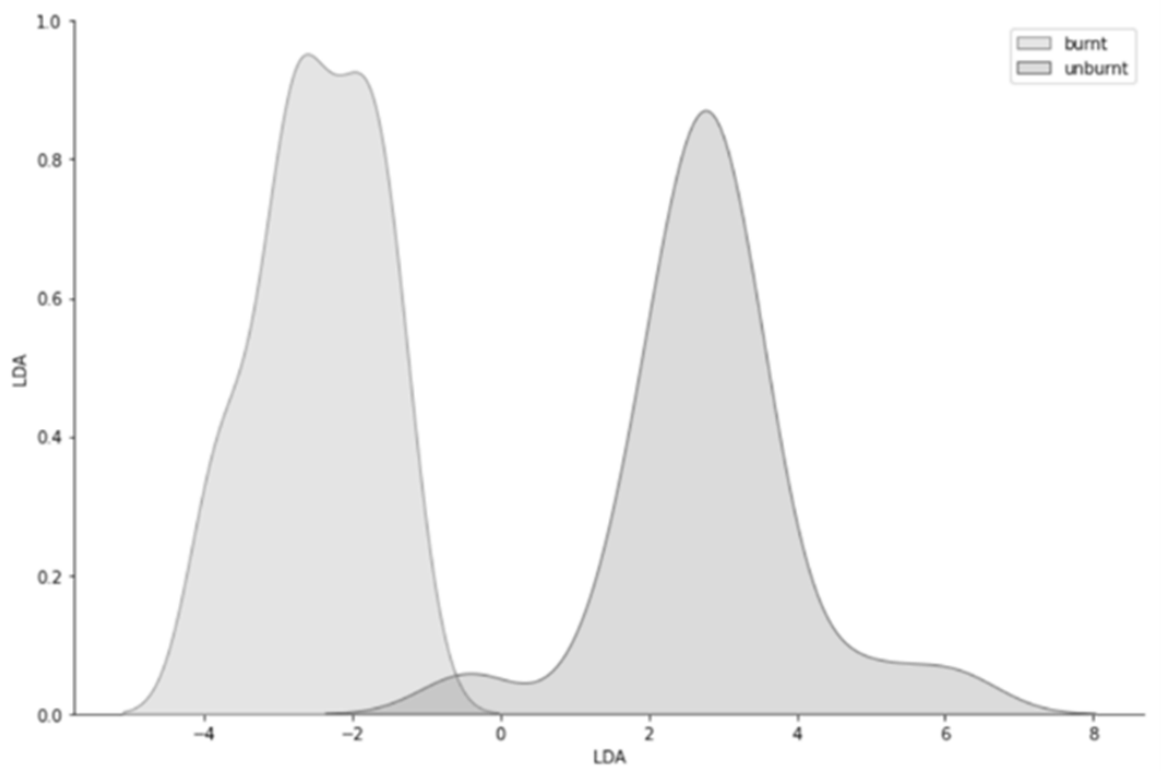
Suppl. 3. - Measured IR ratios and their assignments from the literature.

Descriptive Statistics of the IRSF Measurements

PMI (days)	Sample	Unburnt	Burnt	Mean Unburnt	Mean Burnt	Mean % increase	Std Unburnt	Std burnt	CV unburnt	CV burnt
0	WSFresh	3.16	5.16	3.08	5.03	52.42	0.44	0.19	0.13	0.04
	SWF2FR3	2.99	5.04							
	SWF2FR4	N/A	4.93							
	WS4_FR	N/A	5.24							
	WS5_FR	N/A	4.76							
14	WSF2D2W1	2.49	3.58	2.88	4.10	42.36	0.23	0.75	0.08	0.18
	WSF2D2W2	2.91	5.08							
	WSF2D2W3	3.06	3.2							
	WSF2D2W4	3.01	4.56							
	WSF2D2W5	2.95	4.07							
34	WSF3D1M1	3.18	4.71	3.23	4.45	37.77	0.21	0.27	0.06	0.06

	WSF3D1M2	3.53	4.29							
	WSF3D1M3	2.98	4.68							
	WSF3D1M4	3.31	4.06							
	WSF3D1M5	3.14	4.49							
91	WSF3D3M1	3.48	5.04	3.31	5.19	57.27	0.12	0.37	0.03	0.07
	WSF3D3M2	3.28	5.57							
	WSF3D3M3	3.22	5.41							
	WSF3D3M4	3.25	4.75							
180	WSF5D6M1	2.96	5.26	3.07	4.77	0.55	0.07	0.34	0.03	0.07
	WSF5D6M2	3.03	4.36							
	WSF5D6M3	3.16	4.55							
	WSF5D6M4	3.12	4.83							
	WSF5D6M5	3.1	4.85							
365	SWF5D1Y1	5.04	4.77	5.04	4.77	-5.35	0.00	0.00	0.00	0.00

Suppl. 4 - The mean IRSF values for the unburnt and burnt groups at different PMIs.



Suppl. 5 -- Linear Discriminant Analysis (LDA) on the FTIR dataset to discriminate between states (unburnt vs burnt) bone. Contributions: 'ARP': -3.806, 'BPI': 3.204, 'C/C': -3.97, 'C/P': -21.982, 'CN/P': 14.449, 'CO/CO3': -1.345, 'IRSF': 4.651, 'N/P': -3.806, 'PHT': 19.552.

PMI	State	Zone	N	**P2O5**		**Na2O**		**Cl**		**K2O**		**FeO**		**Al2O3**		**SiO2**		**SrO**		**MnO**		**MgO**		**CaO**	
				mean	CV	mean	CV	mean	CV	mean	CV	mean	CV	mean	CV	mean	CV	mean	CV	mean	CV	mean	CV	mean	CV
0 days	U	HC	3	27.87	0.07	0.51	0.18	0.03	0.00	0.13	0.00	0.00	0.00	0.03	1.00	0.00	0.00	0.02	1.00	0.01	1.00	0.56	0.16	33.81	0.09
		IC	2	27.24	0.02	0.46	0.02	0.04	0.00	0.10	0.10	0.00	0.00	0.05	0.20	0.00	0.00	0.00	0.00	0.01	1.00	0.54	0.20	34.03	0.04
		MC	5	29.34	0.05	0.57	0.11	0.03	0.33	0.16	0.50	0.00	0.00	0.05	0.40	0.01	3.00	0.02	1.00	B.D.	0.00	0.68	0.16	37.31	0.05
		OC	6	27.69	0.06	0.62	0.16	0.04	0.25	0.27	0.44	B.D.	0.00	0.04	0.75	0.00	0.00	0.02	1.00	B.D.	0.00	0.62	0.31	33.67	0.06
		Total	16	**28.03**	0.05	**0.54**	0.11	**0.03**	0.33	**0.16**	0.31	**0.00**	0.00	**0.04**	0.50	**0.00**	0.00	**0.02**	1.00	**0.01**	1.00	**0.60**	0.20	**34.70**	0.06
	B	HC	14	32.44	0.12	0.86	0.65	0.35	0.46	0.24	0.75	B.D.	0.00	0.10	3.20	0.08	0.88	0.01	2.00	B.D.	0.00	0.75	0.71	41.34	0.12
		IC	22	32.79	0.16	0.57	0.40	0.56	0.80	0.20	0.55	B.D.	0.00	0.04	2.25	0.06	0.83	0.01	2.00	B.D.	0.00	0.85	1.20	42.07	0.17
		MC	18	32.15	0.06	0.58	0.41	0.51	0.33	0.22	0.50	B.D.	0.00	0.02	1.50	0.09	1.33	0.02	1.00	B.D.	0.00	0.59	0.17	40.40	0.05
		OC	18	32.28	0.11	0.77	0.66	0.60	0.47	0.50	0.90	B.D.	0.00	0.05	0.80	0.07	1.00	B.D.	0.00	B.D.	0.00	0.82	0.13	38.20	0.18
		Total	72	**32.42**	0.11	**0.69**	0.55	**0.51**	0.51	**0.29**	0.72	**N/A**	0.00	**0.05**	2.40	**0.08**	1.00	**0.01**	2.00	**N/A**	0.00	**0.75**	0.59	**40.50**	0.13
14 days	U	HC	12	29.49	0.12	0.46	0.13	0.08	0.75	0.05	0.40	B.D.	0.00	0.05	1.20	0.02	1.50	0.02	1.50	B.D.	0.00	0.72	0.18	38.31	0.11
		IC	16	28.18	0.08	0.47	0.34	0.09	0.67	0.06	0.33	0.02	3.00	0.10	1.40	0.08	1.63	0.01	3.00	B.D.	0.00	0.63	0.29	36.94	0.11
		MC	18	30.95	0.10	0.56	0.13	0.05	0.40	0.06	0.50	B.D.	0.00	0.03	1.33	0.02	1.50	0.03	0.67	B.D.	0.00	0.78	0.12	40.35	0.12
		OC	7	20.16	0.32	0.33	0.33	0.14	0.93	0.06	0.50	0.08	0.75	0.16	1.25	0.59	1.14	B.D.	0.00	B.D.	0.00	0.45	0.47	26.11	0.31
		Total	53	**27.19**	0.14	**0.46**	0.22	**0.09**	0.78	**0.06**	0.50	**0.05**	0.60	**0.09**	1.22	**0.18**	1.17	**0.02**	1.00	**N/A**	0.00	**0.65**	0.23	**35.43**	0.15
	B	HC	15	31.78	0.19	0.62	0.53	0.33	0.48	0.14	0.64	0.06	3.00	0.58	2.28	1.67	3.60	0.02	1.50	B.D.	0.00	0.61	0.85	40.83	0.17
		IC	17	35.60	0.13	0.56	0.30	0.33	0.82	0.13	0.54	0.01	2.00	0.04	0.50	0.06	1.17	0.03	1.00	B.D.	0.00	0.53	0.53	45.66	0.15
		MC	21	34.41	0.13	0.57	0.42	0.30	0.57	0.08	0.50	B.D.	0.00	0.03	1.00	0.02	1.50	0.02	1.00	B.D.	0.00	0.43	0.74	44.37	0.13
		OC	17	32.15	0.11	0.55	0.31	0.46	0.43	0.10	0.50	0.02	1.50	0.03	1.00	0.09	1.00	0.02	1.50	B.D.	0.00	0.56	0.36	39.77	0.14
		Total	70	**33.49**	0.14	**0.58**	0.40	**0.35**	0.57	**0.11**	0.55	**0.03**	2.00	**0.17**	2.06	**0.46**	3.37	**0.02**	1.50	**N/A**	0.00	**0.53**	0.62	**42.66**	0.15
34 days	U	HC	10	28.75	0.08	0.49	0.27	0.08	0.38	0.05	0.60	B.D.	0.00	0.04	0.75	0.05	1.00	0.02	1.00	B.D.	0.00	0.71	0.15	36.61	0.10

		IC	11	26.76	0.12	0.43	0.42	0.08	0.38	0.05	0.60	B.D.	0.00	0.07	0.57	0.14	1.14	0.01	2.00	B.D.	0.00	0.52	0.46	32.67	0.12
		MC	12	28.53	0.09	0.47	0.15	0.07	0.43	0.05	0.40	B.D.	0.00	0.05	1.00	0.02	2.00	0.01	2.00	B.D.	0.00	0.69	0.16	35.43	0.11
		OC	5	25.41	0.23	0.41	0.37	0.17	1.00	0.11	1.00	0.11	1.73	0.38	1.89	0.65	2.17	0.02	1.50	0.01	0.00	0.53	0.32	31.48	0.24
		Total	38	**27.36**	0.13	**0.45**	0.29	**0.10**	0.60	**0.07**	0.71	**0.11**	0.45	**0.13**	1.62	**0.22**	1.86	**0.02**	1.00	**0.01**	1.00	**0.61**	0.26	**34.05**	0.14
	B	HC	13	30.65	0.12	0.58	0.22	0.47	0.40	0.13	0.77	B.D.	0.00	0.07	1.86	0.06	1.00	0.01	2.00	B.D.	0.00	0.62	0.29	39.13	0.14
		IC	16	30.95	0.11	0.62	0.42	0.51	0.20	0.20	0.75	B.D.	0.00	0.03	1.33	0.06	0.83	0.02	1.00	B.D.	0.00	0.59	0.27	38.99	0.12
		MC	17	31.18	0.04	0.53	0.26	0.45	0.38	0.10	0.30	B.D.	0.00	0.04	1.50	0.05	1.00	0.01	2.00	B.D.	0.00	0.59	0.20	39.91	0.04
		OC	17	29.74	0.07	0.59	0.32	0.58	0.36	0.24	0.54	0.06	0.00	0.04	1.25	0.09	1.00	0.01	2.00	B.D.	0.00	0.67	0.15	37.20	0.11
		Total	63	**30.63**	0.08	**0.58**	0.31	**0.50**	0.34	**0.17**	0.59	**0.06**	0.67	**0.04**	1.75	**0.06**	1.00	**0.01**	2.00	**N/A**	0.00	**0.62**	0.23	**38.81**	0.10
91 days	U	HC	11	31.17	0.06	0.48	0.23	0.22	1.36	0.03	0.67	B.D.	0.00	0.03	1.33	0.02	1.50	0.06	0.83	B.D.	0.00	0.77	0.09	38.97	0.11
		IC	10	30.65	0.09	0.46	0.17	0.25	1.16	0.05	0.60	B.D.	0.00	0.03	1.33	B.D.	0.00	0.07	0.57	B.D.	0.00	0.57	0.21	39.56	0.10
		MC	15	30.49	0.11	0.54	0.17	0.16	1.38	0.04	0.50	B.D.	0.00	0.03	1.00	0.03	1.67	0.06	0.50	B.D.	0.00	0.76	0.08	39.12	0.14
		OC	11	27.93	0.12	0.41	0.20	0.27	1.26	0.07	0.71	0.03	1.67	0.07	1.00	0.07	1.29	0.06	0.83	B.D.	0.00	0.57	0.37	34.60	0.11
		Total	47	**30.06**	0.09	**0.47**	0.19	**0.22**	1.27	**0.05**	0.60	**0.03**	0.67	**0.04**	1.00	**0.04**	1.25	**0.06**	0.67	**N/A**	0.00	**0.67**	0.18	**38.06**	0.12
	B	HC	16	29.89	0.20	0.57	0.61	0.44	0.64	0.06	0.33	0.02	1.50	0.12	1.17	0.07	1.14	0.07	0.71	B.D.	0.00	0.46	0.41	38.10	0.20
		IC	17	31.89	0.07	0.58	0.48	0.49	0.51	0.06	0.33	B.D.	0.00	0.05	0.80	0.06	1.00	0.08	0.63	B.D.	0.00	0.45	0.40	40.53	0.09
		MC	17	34.22	0.13	0.48	0.23	0.34	0.85	0.04	0.50	B.D.	0.00	0.03	0.67	0.04	1.25	0.08	0.75	B.D.	0.00	0.42	0.60	44.29	0.15
		OC	18	30.51	0.11	0.32	0.38	0.56	0.54	0.12	1.00	0.01	2.00	0.06	0.83	0.04	2.00	0.08	0.75	B.D.	0.00	0.47	0.40	39.37	0.12
		Total	68	**31.63**	0.13	**0.49**	0.45	**0.46**	0.61	**0.07**	0.71	**0.01**	2.00	**0.06**	1.00	**0.05**	1.40	**0.08**	0.75	**N/A**	0.00	**0.45**	0.44	**40.57**	0.14
180 days	U	HC	8	27.44	0.33	0.42	0.36	0.22	2.14	0.04	0.50	B.D.	0.00	0.08	1.13	0.02	1.50	0.02	1.50	B.D.	0.00	0.70	0.34	34.39	0.30
		IC	6	30.77	0.12	0.49	0.10	0.05	0.60	0.04	0.50	B.D.	0.00	0.05	0.60	0.06	1.00	B.D.	0.00	B.D.	0.00	0.67	0.16	39.14	0.13
		MC	14	29.98	0.09	0.53	0.11	0.06	0.50	0.03	0.33	B.D.	0.00	0.04	0.75	0.03	1.00	B.D.	0.00	B.D.	0.00	0.81	0.11	39.87	0.10
		OC	10	28.94	0.16	0.41	0.29	0.05	0.40	0.05	0.60	0.03	2.00	0.12	1.42	0.14	1.71	0.03	0.67	0.01	1.00	0.73	0.30	37.79	0.15

		Total	38	**29.28**	0.17	**0.46**	0.20	**0.10**	1.40	**0.04**	0.50	**0.03**	0.67	**0.07**	1.14	**0.06**	1.50	**0.03**	0.67	**0.01**	1.00	**0.73**	0.22	**37.80**	0.16
	B	HC	8	31.09	0.13	0.38	0.32	0.33	1.03	0.04	0.25	0.01	3.00	0.06	1.17	0.08	0.88	0.02	1.00	B.D.	0.00	0.67	0.24	39.43	0.16
		IC	11	28.86	0.12	0.38	0.26	0.73	0.59	0.05	0.40	0.03	1.00	0.04	0.75	0.09	1.00	0.02	1.50	B.D.	0.00	0.57	0.33	37.42	0.11
		MC	12	31.22	0.06	0.48	0.13	0.49	0.53	0.05	0.20	B.D.	0.00	0.03	1.33	0.02	2.00	0.01	3.00	B.D.	0.00	0.58	0.31	41.40	0.04
		OC	10	32.61	0.04	0.47	0.38	0.64	0.31	0.11	0.82	B.D.	0.00	0.07	0.57	0.07	1.00	0.01	2.00	B.D.	0.00	0.57	0.46	41.07	0.05
		Total	41	**30.94**	0.09	**0.43**	0.26	**0.54**	0.57	**0.06**	0.67	**0.02**	1.00	**0.05**	1.00	**0.07**	1.00	**0.02**	1.00	**N/A**	0.00	**0.60**	0.33	**39.83**	0.09
365 days	U	HC	3	29.45	0.05	0.53	0.21	0.03	0.33	0.03	0.67	0.00	0.00	0.07	0.43	0.02	1.50	0.03	1.00	0.02	0.50	0.76	0.01	37.22	0.05
		IC	7	27.89	0.08	0.48	0.13	0.06	0.17	0.02	0.50	B.D.	0.00	0.04	0.50	0.00	0.00	0.02	2.00	B.D.	0.00	0.69	0.16	34.53	0.09
		MC	4	30.25	0.05	0.49	0.10	0.04	0.25	0.02	0.50	B.D.	0.00	0.03	0.67	0.00	0.00	0.01	3.00	B.D.	0.00	0.75	0.17	38.12	0.05
		OC	2	29.41	0.08	0.43	0.12	0.04	0.00	0.01	0.00	0.02	1.00	0.07	0.14	0.00	0.00	0.03	1.33	0.01	1.00	0.70	0.43	38.43	0.03
		Total	16	**29.25**	0.06	**0.48**	0.15	**0.04**	0.25	**0.02**	0.50	**0.01**	1.00	**0.05**	0.40	**0.00**	0.00	**0.02**	1.50	**0.01**	1.00	**0.73**	0.18	**37.07**	0.05
	B	HC	11	30.65	0.08	0.30	0.27	0.76	0.22	0.02	0.50	B.D.	0.00	0.05	1.00	0.03	1.00	0.02	1.50	B.D.	0.00	0.76	0.18	38.30	0.07
		IC	11	30.64	0.05	0.35	0.17	0.80	0.09	0.03	0.67	B.D.	0.00	0.05	0.80	0.02	1.50	0.02	1.50	B.D.	0.00	0.51	0.18	37.87	0.05
		MC	12	32.08	0.03	0.45	0.20	0.64	0.17	0.02	1.00	B.D.	0.00	0.04	0.75	0.02	1.50	0.04	0.75	B.D.	0.00	0.70	0.16	38.03	0.32
		OC	14	31.81	0.07	0.35	0.23	0.73	0.12	0.09	0.78	B.D.	0.00	0.03	0.67	0.03	1.00	0.02	1.50	B.D.	0.00	0.77	0.22	40.41	0.07
		Total	48	**31.30**	0.06	**0.36**	0.22	**0.73**	0.15	**0.04**	0.75	**N/A**	0.00	**0.04**	1.00	**0.02**	1.50	**0.03**	1.00	**N/A**	0.00	**0.68**	0.19	**38.65**	0.12
Neol.	B	HC	10	35.92	0.19	0.52	0.19	0.34	1.03	0.02	2.00	0.10	0.90	0.26	1.12	0.35	1.37	0.00	1.38	0.01	1.00	0.01	2.00	48.11	0.18
		IC	12	38.98	0.08	0.48	0.15	0.26	0.77	0.03	1.00	0.06	0.00	0.18	0.78	0.24	1.50	0.01	1.49	B.D.	0.00	0.03	1.00	50.54	0.07
		MC	12	39.13	0.12	0.57	0.23	0.17	1.59	B.D.	N/A	0.04	2.00	0.10	0.70	0.04	1.50	0.01	1.30	B.D.	0.00	B.D.	0.00	52.13	0.11
		OC	13	36.15	0.29	0.33	0.48	0.30	0.83	0.19	2.84	0.74	0.00	1.39	2.97	3.09	3.08	0.01	3.08	0.04	1.00	0.15	3.00	48.22	0.29
		Total	47	**37.54**	0.17	**0.47**	0.23	**0.27**	1.00	**0.08**	1.88	**0.24**	0.00	**0.48**	2.42	**0.93**	2.80	0.01	1.81	**0.02**	1.00	**0.06**	2.17	**49.75**	0.16

Suppl. 8. - Mean major and trace elements chemistry , coefficient of variation (CV) of the unburnt (U) and burnt (B) bone samples with different PMIs. N= analysis per specimen.

Chapter V: Paper 3 -- Determining the Postmortem Timing of Sharp Force Damage and Fractures in Burnt Bones

---

Abstract

Major complications in the analysis of burnt human remains include distinguishing whether bone was fresh or dry at the time of burning and whether trauma/damage was inflicted 'perimortem' or postmortem. Burning of the body is common in both medicolegal and archaeological contexts. Some prehistoric societies are suggested to have passively or actively defleshed human remains prior to cremation, mostly classified based on the lack of warping and thumbnail fractures, which are dependent on the amount and distribution of bone collagen at the time of burning. The distinction between perimortem and postmortem sharp force trauma (SFT) features have rarely been investigated on burnt bones. This study investigates whether perimortem and postmortem SFT features are distinguishable on burnt bone, the rate of cutmark survival, and the presence of heat-induced fractures compared the bone's pre-burnt collagen content.

Pig (*Sus scrofa domesticus*) tibiae (N=25) were left to decay in a field for 14, 34, 91, 180, and 365 days in Wytham Woods, Oxfordshire, UK. Prior to burning, bones were inflicted with SFT by a non-serrated and partially-serrated combat knife and a flint blade (N=15 per bone). Cutmarks made on fresh, fleshed bones were used as a control as well as an untraumatized bone which was included at each fire event. Cutmark survival, perimortem vs postmortem features, and heat-induced fractures were recorded in burnt bones and collagen was extracted from unburnt bones. Statistical analysis included linear regression and MANOVA.

Fractures did not depend on the limited collagen loss during the one-year PMI prior to burning. Major changes in the SFT features appeared after 6 months of exposure in burnt bones. The decrease of perimortem features (irregular edges, splintering, curling or uplifting) and

increase of postmortem features (regular shaped, sharp edges) can potentially inform on the timing of SFT infliction in burnt bones.

Keywords

Sharp-force trauma, burning, taphonomy, perimortem, human remains

V.1 Introduction

Differentiation between perimortem injury and postmortem damage on skeletal remains presents a major challenge in archaeological and medicolegal contexts. Perimortem injury refers to trauma inflicted around the time of death in forensic anthropology, and thus it is trauma that was inflicted on fresh or 'wet' bone (Byers, 2007; Wheatley, 2008). An added complication for the differentiation of perimortem and postmortem trauma/damage occurs when dealing with burnt skeletal remains. Although the skeleton cannot be destroyed solely by fire (Bass, 1984), the alterations fire or heat cause to bone compromise methods used by osteologists to identify age and sex, pathology, and possible pre-existing trauma (Schmidt and Symes, 2005; Thompson, 2015). Bone goes through a series of chemical and morphological changes until it becomes fully calcined, including differential soft tissue loss, colour changes, fracturing, histological changes, and structural reordering of the bioapatite crystals (Shipman *et al.*, 1984; Fairgrieve, 2008; Thompson, 2015). The two most important factors determining the nature and severity of these changes are the temperature and duration of heat, but other variables play a role as well, such as the location (i.e. outdoors vs indoors), abundance of oxygen, clothing, accelerants, etc. (DeHaan, 2012).

In a medicolegal context a variety of events can lead to the recovery of burnt human remains/human remains from fatal fires, such as homicide, suicide, accidental fires, explosions, wildfires, and transportation accidents (Fairgrieve, 2008; Ubelaker, 2009). Fire can be employed on a corpse in an attempt to hide forensic evidence, such as the victim's identity and

evidence of struggle (Fairgrieve, 2008). Two real-life cases of this have been reported in the forensic anthropological literature (Bontrager and Nawrocki, 2008; Garrido-Varas and Intriago-Leiva, 2015), where the postmortem interval (PMI) and time of burning were established based on animal gnawing, patterned thermal destruction, and heat-induced fractures. Since human bones are compromised by heat-induced changes, identification of the remains becomes exceptionally complex and, in many cases, impossible; thus, studies on burnt bone are of extreme importance in forensic science (Fairgrieve 2008; Symes *et al.* 2008).

Due to the difficulty of analysing such material, assessment of burnt human remains were rare in the earlier archaeological scholarship with some exceptions (Gejvall, 1947; Merbs, 1967; McKinley, 2000, 2004). At many prehistoric funerary sites in England, Ireland, Scotland, France, and Luxembourg (Lambot *et al.*, 1994), archaeologists have proposed that human cadavers were burnt dry or after the soft tissue had already decomposed. The state of skeletal remains may have been attained in various ways: from active removal of the flesh using tools; from the exhumation of interred burials after some period of time; or from passive excarnation through subaerial exposure (Booth and Brück, 2020). Although excarnation might have been the dominant funerary rite for much of the Late Bronze Age and Iron Age in Southern Britain (Carr and Knüsel, 1997), this type of treatment before cremation has so far been invisible for archaeologists. Until recently (Végh *et al.*, 2022), there were no publications to our knowledge on estimating the postmortem interval of sub-aerial exposure (i.e., passive excarnation) prior to burning from a single burnt bone fragment; but indirect evidence from bone deposits have been found suggesting the existence of excarnation as a separate funerary rite from cremation. These include:

(1) differing radiocarbon dates from unburnt bones in the same deposits (Booth and Brück, 2020);

(2) disarticulated unburnt and burnt bones within the same context on a pyre (Chesterman, 1979; Renfrew, 1979);

(3) bacterial attack on burnt bone (Grévin, Baud, and Susini, 1991; though see Végh *et al.* 2021);

(4) discolouration (oxidation) and fragmentation associated with dry bone at various sites (Wells 1962; Piggott 1962; Lee 2006; Mckinley 1999; 2000; 2008);

(5) insufficient weight of cremation deposits (Booth and Brück, 2020);

(6) absence of heat-induced fractures characteristic of burnt fresh bone (Wells, 1978; Cooney, 2014);

(7) cutmarks on skulls and bones in a cremation cemetery (Niblett, 1999; Kilpatrick, 2021);

(8) signs of weathering on cremated bone (Chesterman, 1979);

(9) the lack of representation of all major body parts in deposits (McKinley, 2000; Carr, 2007); and

(10) the corrosion and fragmentation of iron fibulae before cremation (Metzler-Zens *et al.*, 1999).

Additionally, historic and ethnographic accounts confirm the existence of this ritual in a form of display of the dead prior to cremation in South East Asia (Terwiel, 1975; Evans, 1991; Wong, 1998; Falk, 2010; Ward and Tayles, 2015).

Many of these archaeological examples are questionable; for example those interpreting sigs of weathering as due to excarnation (point 8 above) [cf. (Behrensmeyer, 1978)]. The present study uses points 4, 6, and 7 to establish and validate the use of fragmentation, heat-induced fracturing, and signs of active excarnation (cutmarks) on burnt bone through an experimental approach. If perimortem and postmortem sharp-force trauma (SFT) induced prior to burning are distinguishable in bones with ≤ 1-year PMI post-burning, it might be possible to confirm or refute the idea of active excarnation (soft tissues removed with an instrument) in

prehistoric cremated bones together with information on type of cutmark, location and number of marks on the skeleton. This study investigates (1) what the percentage of preserved cutmarks after burning; (2) whether it is possible to tell if SFT was inflicted subsequently after death or after a certain amount of time within a year on burnt bones; and (3) if retained collagen content affects heat-induced fracture characteristics and warping, and the appearance of SFT on burnt bone.

V.1.1 Fragmentation and Heat-Induced Fracturing

Characteristics of heat-induced fracturing include longitudinal, transverse, curved transverse (thumbnail), patina, delamination and warping (Baby 1954; Shipman *et al.* 1984; Mayne 1990; Pope and Smith 2004; Pope 2007; Symes *et al.* 2008). These are possible to record because post-burning breakage or fracturing/fragmentation can be distinguished from heat-induced fractures by the colouration and charring of the fractured surface (Buikstra and Swegle, 1989; Symes *et al.*, 2008; Dirkmaat *et al.*, 2012). Thumbnail fractures and warping were proposed to be associated with fresh bones burnt with soft tissue (Baby, 1954; Binford, 1963; Buikstra and Swegle, 1989; Spennemann and Colley, 1989; Etxeberria, 1994; Whyte, 2001), but these features were subsequently shown to be problematic, as they may relate to the amount and/or distribution of collagen within the bone cortex (Thompson, 2005; Gonçalves *et al.*, 2011). Gonçalves *et al.* (2011) concluded that warping is present on 'dry' bones if enough collagen is retained in the bones to enable bending. This is due to collagen decay in dry bones, which reduces bone elasticity making the bone weaker to mechanical forces (Zioupos *et al.*, 1999). Similar conclusions have been drawn regarding thumbnail fractures (Gonçalves *et al.* 2011). However, the latter study did not include measurements of collagen content in the bones before experimental burning, which is especially important in the present study because the bone's collagen content can also influence the characteristics of trauma or damage at the time of burning. Bone contains ~20-35 wt% organic material, of which the most abundant

biomolecule is type I collagen (Rogers and Zioupos, 1999; Collins *et al.*, 2002; Elliott, 2002; Caruso *et al.*, 2020). Collagen degradation begins even during life but is much more pronounced after death. Since this research investigates a multi-stage funerary rite in which the body is first excarnated and then processed prior to burning, and collagen content affects both the heat-induced fractures and the appearance of trauma/damage, the extent of postmortem collagen loss is investigated in this study.

V.1.2 Perimortem vs Postmortem Damage

Differentiation between wet ("perimortem") versus dry (postmortem) bone sharp force trauma/damage features (both referred to as SFT below) has so far not been attempted on burnt bones. However, observational studies and reports on archaeological cremated bone with possible pre-burning inflicted SFT exist (Cressey *et al.*, 2003; Kilpatrick, 2021). For instance, on a burnt skull fragment, cutmarks inflicted pre-burning were recognised from a Bronze Age cemetery in Scotland (Cressey *et al.*, 2003), but it was not possible to determine if the marks were inflicted pre- or post-mortem (*ibid*). Another skull fragment with a linear defect from Dunragit, Galloway, Scotland, was also interpreted as a cutmark, due to its different appearance (sharp edges) as opposed to the other weathered damages (rounded edges) (Kilpatrick, 2021). It has been assumed that this SFT was inflicted around the time of death and prior to burning (*ibid*). Most scholarship agrees that pre-existing trauma may be distinguished from heat-induced fractures (Pope and Smith, 2004; Ubelaker, 2009; Poppa *et al.*, 2011; Végh and Rando, 2017; Waltenberger and Schutkowski, 2017; Alunni *et al.*, 2018). Pre-existing SFT exhibits different characteristics, such as presence of tool marks (e.g. striations), thicker bevelling, and kerf/fracture discolouration, due to the exposed internal bone structure (Ubelaker and Adams, 1995; Mayne Correia, 1997; Herrmann and Bennett, 1999; Pope, 2007; Symes *et al.*, 2008; Dirkmaat *et al.*, 2012; Galloway *et al.*, 2014). SFT is distinguishable from heat-induced fracturing using the presence of fracture lines, striations on kerf walls, and from the chipping

of bone (Berryman and Symes, 1998; Bass, 2005; Byers, 2007). However, heat-induced fragmentation can obscure SFT on bones, which can result in overlooked trauma (Emanovsky *et al.*, 2002), while step and transverse heat fractures were found to be often indistinguishable from SFT (Mata Tutor *et al.* 2021)

Establishing the timing of the injury (antermortem, perimortem, postmortem) is crucial in forensic investigation as it can assist with reconstruction of manner and cause of death (Sauer, 1998, 2003; Kemp, 2016). While antemortem trauma is more easily identified using evidence of regeneration (callus), distinguishing 'perimortem' from postmortem trauma/damage is more difficult (Pope, 2007; Galloway *et al.*, 2014; Symes *et al.*, 2014). The perimortem stage can extend months or even years after death depending on the microenvironment (Sauer, 1998; White, 2000; Symes *et al.*, 2002; Moraitis and Spiliopoulou, 2006; Galloway *et al.*, 2014). Bone elasticity can measurably deteriorate only 5 hours after death (Fitzgerald, 1977) and the moisture content in bone can decline rapidly in the first two months postmortem (Wieberg and Wescott, 2008), but fresh bone fracture characteristics may persist for several months to years postmortem (Maples, 1986; Ubelaker and Adams, 1995; Wheatley, 2008). Furthermore, taphonomic agents might produce postmortem damage on bones that may be confused with perimortem trauma (Sauer, 1998). Perimortem and postmortem trauma are usually distinguished using staining/colour differences of the fracture surfaces, the fracture pattern morphology, the angle of fracture margins, and other taphonomic modifications (e.g. carnivore gnawing, weathering, vegetation) (Symes *et al.* 2002; Haglund and Sorg 2006; Sorg 2019). Some research has focused on percussion fractures on animal bones (Bonnichsen, 1979; Johnson, 1985), which is when a bone is hit with an instrument (most often hammerstone) to extract marrow cavity from long bones. Johnson (1985) showed that when percussion is performed on fresh bones, a loading point is identifiable, as opposed to dry bones. However,

when bones are fleshed, soft tissue dissipates most of the impact that would otherwise produce the fracture (Galloway *et al.*, 2014).

There is significantly less research on the timing of sharp force trauma (SFT) infliction as opposed to blunt force trauma (Crowder *et al.*, 2013; Galloway *et al.*, 2014). A number of qualitative features have previously been proposed to have potential for differentiating cutmarks inflicted on wet and dry bone (Crowder *et al.*, 2013). SFT on fresh bones tends to exhibits irregular edges, curling or uplifting at edges, splintering at breaks of cutmarks, and splintered bone connected to existing bone structures (Mayne, 1990; Sauer, 1998; Symes *et al.*, 2008; Ubelaker, 2009; Crowder *et al.*, 2013). Dry bone features include regular shaped cuts, sharp-edged, discoloured kerfs, and complete separation from existing bone structures into numerous pieces (Mayne, 1990; Symes *et al.*, 2008; Crowder *et al.*, 2013; Symes *et al.*, 2014; Wedel, 2014; Devlin and Herrmann, 2015). The present study uses these features to distinguish between "perimortem" and postmortem SFT in burnt bones.

V.2 Materials and Methods

Fleshed *Sus Scrofa domesticus* (pig) tibiae (N=25) were left to decay for 14, 34, 91, 180, and 365 days within a cage in a field in Wytham Woods, Oxfordshire, UK (Végh *et al.*, 2021). Fleshed, fresh tibiae served as a control for the PMI groups. After each postmortem interval (PMI), four[6] tibiae were collected and manually inflicted with sharp force trauma (SFT) by three different instruments. One of the bones from each PMI stage was left without trauma to serve as a control for heat-induced fractures. The 0-day control tibiae were subjected to the same trauma following collection from a local butcher and immediately before burning (Fig.

[6] Although five tibiae were deposited per PMI, some of the bones were removed from the cage by animals. One bone was removed from the 34-day group and four from the 365-day group.

24). The instruments were chosen based on their analogues and commonality in both modern and archaeological times: a non-serrated knife (NK), a partially serrated knife (SK), and a flint blade (F; Fig. 25, Table 12). This way, changes could be monitored on several type of cutmarks with different morphology. Five cutmarks were produced per instrument on each bone, totalling 15 SFT per bone. Kerfs were produced by a constant force by cutting the bone twenty times with all instruments. All cut-marks were produced manually by one right-handed person in order to limit the variability of the cut-mark features as much as possible.

In addition to the experimentally burnt pig bones, a 5.5k ya old unburnt cow bone from Ireland was included in the study. It was experimentally burnt in a kiln at mean 515°C temperature for 2 h 45 mins (App. A). This bone was included as a no- to low-collagen (<0.5% collagen measured from %N) control for the heat-induced fracturing investigations.



*Figure 24 -- **A:** An example of a fleshed tibia subjected to sharp force trauma. The skin was carefully cut through and then each incision was produced on the bone itself. **B:** One of the 14-day PMI tibia cut with the same implements.*

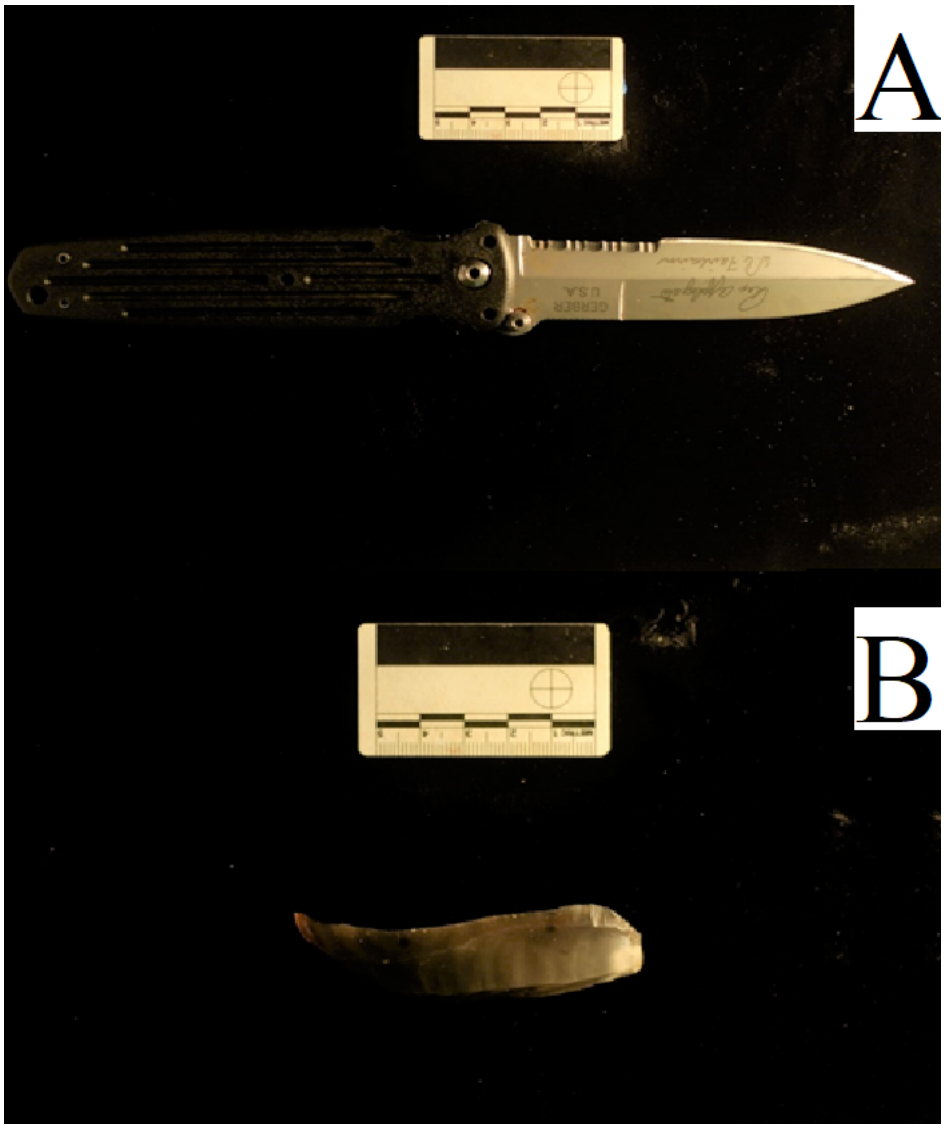


*Figure 25--The instruments used for the SFT infliction. **A**: The combat knife (Gerber, USA) used for all knife-related wounds. The knife is comprised of a single edged, non-serrated upper part and a partially serrated part. Both parts had a single edge bevel on the left side. There is a total of 11 serrations of the knife with four patterned double serrations (4.8 mm each). The non-serrated gaps are 5.5 mm long. **B:** The single edged flint blade, which was produced for this study. The blade's cutting surface is wider than that of the knife, while the width from the point of bevelling is larger.*

Instrument	Cutting Edge Length (mm)	Blade width (from root of bevelling; mm)	Blade width (most upper point; mm)
NK	70	1.09	0.66
SK	35	1.95	0.66
F	78.95	1.69	0.98

Table 12 -- Dimensions of the instruments used in this study. NK=non-serrated knife; SK=partially serrated knife, F=flint blade. All instruments were used in a cutting motion.

Following the SFT, the bones were burnt in an outdoor fire as described in Végh *et al.* (2021). An outdoor fire was preferred over a furnace due to its more realistic burning process in terms of the loss of SFT due to fragmentation [cf. (Pope and Smith 2004)]. Bone temperatures were monitored continuously throughout the burning events, with an average of 553 °C and a recorded maximum of 751 °C, for 2.5 – 3.5 hours per fire event, until the bones became calcined (Fig. 26). The bones were left to cool to ambient temperature before collection, since hot bones are extremely fragile [cf. (Alunni *et al.*, 2018)]. After collection, the bones were photographed with a Nikon D2Xs camera fitted with a 60mm Nikon macro lens. The images used for the visualisation of the trauma were taken with light microscopy (Wild Photomacroscope, Wild Heerbrugg, Heerbrugg, Switzerland) fitted with a LMscope, VTC4x2 (LCMOS, Brunel Microscopes Ltd., Chippenham, UK) USB camera together with ToupView 3.7 (ToupTek Photonics, Zhejiang, China) software. The lowest magnification used was 6.3x after calibration in order to visualise larger areas of the cut-marks, and for details 16x magnification was used. Images of the cutmarks were stitched together using Image Composite Editor 2.0.3 (Microsoft, Redmond, Washington, USA). For qualitative analysis, only the light microscopy images were used, as they produced more detailed images of the cutmarks than the macroscopic images.

The presence of cutmarks were recorded for each bone to quantify the likelihood of cutmarks survival post-burning with repercussions on the proportion of such marks likely to be recovered after cremation in an archaeological and forensic context. The kerf features were qualitatively analysed by the first author (EV) based on established features of fresh/green bone and dry bone trauma features (Table 13). Features assessed were irregular edges (IRR), curling or uplifting (CUR), splintering (SPL), and flaking (FLA) for perimortem and regular shaped

kerf (RES), sharp edges (SHA), discolouration (DIS), and crumbling (CRL) for postmortem features.



*Figure 26-- **A:** The bones soon after the fire was lit. While the two bones in the middle started charring, the other bones are yet to be altered to the same level. **B:** 2.5 h after the start of the outdoor fire, most bones turned white.*

Perimortem vs Postmortem SFT Features			
'Perimortem'/Green Bone Features		**Postmortem/Dry Bone Features**	
Feature	**Appearance**	**Feature**	**Appearance**
Irregular edges (IRR)	The edges of the cutmark are not straight or follow the shape of the instrument.	Regular shaped kerf (RES)	The edges of the cutmark appear regular, following the shape of the instrument.
Curling or uplifting (CUR)	Elevation at the edge/shoulder of the kerfs.	Sharp edges (SHA)	Kerf edges and walls appear sharp without splinters.
Splintering (SPL)	Splintered pieces on kerf walls and/or edges that tend to be attached to one another (wall projections).	Discolouration (DIS)	The kerf is a different colour to the surrounding bone.
Flaking (FLA)	Layer of bone come or fall away from the surface (edge or wall of the kerf) in flakes.	Crumbling (CRL)	Uneven edged lumps at the start or end of the kerfs or on kerf floors.

Table 13 -- The timing of trauma (perimortem vs postmortem) specific features used for the qualitative analysis of the kerfs.

The presence and severity of heat-induced fractures were recorded on the burnt bones by counting the total number and the type of fractures. Those classed as heat-induced fractures of interest to this study were thumbnail (curved transverse) and warping fractures. Other heat-induced fractures expected in long bones were present in all bones (e.g., longitudinal and transverse).

Since a bone's response to trauma depends on its viscoelastic properties, and thus its moisture and collagen content; it has been shown that the amount of collagen in the bone prior to burning can affect heat-induced fracture patterns (Thompson, 2005; Gonçalves *et al.*, 2011). Thus, the retained collagen in the unburnt bone was measured for each PMI group in order to determine its impact on kerf features, fracturing severity, and the presence of thumbnail fracture and warping. Samples for collagen extraction were taken from the smallest diameter of the diaphysis of each tibia. Duplicate samples were taken from two randomly chosen bones to assess differences in collagen distribution in a single bone. The unburnt samples were defatted in a 2:1 chloroform:methanol mixture for up to 20 weeks. Surface contamination of

the dried bones was removed by AlO_2 shotblaster. Then, the bones were finely crushed and ground and ~500 mg of the resulting bone powder was weighed in an electronic balance. Bone powder was decalcified with a modified Longin method (Longin, 1971), by 0.5 mol/L HCl, with fresh acid replaced three times and left overnight. The decalcified solution was then rinsed with Milli-Q® ultrapure distilled water, followed by 0.1 mol/L NaOH soak for 30 mins to eliminate humic substances and non-collagenous residues. Samples were then rinsed with Milli-Q®, washed with 0.5 mol/L HCl to remove atmospheric CO_2, and rinsed again. Gelatinisation was done by a hot acid solution (pH 3, 70 °C) for 20 h. The gelatinised solution was EZEE filtered, frozen at -18°C for 4 h, and freeze dried. Collagen yields were precision weighed on an electronic balance. The 5.5k year-old cow rib bone's collagen content was estimated by %N measurement.

The data from the cutmark features, heat-induced fractures, and collagen measurements were statistically analysed using descriptive statistics, linear regression, MANOVA, and multivariate comparison testing in Jupyter notebook in Python programming language.

V.3 Results

V.3.1 Heat-induced Fracturing and Collagen Content

The percentage of original cutmarks preserved per instrument is presented in Fig. 27. Cutmark survival was not associated with PMI ($r=-0.358$, $p<0.485$), and the 180- and 365-day bones had the most cutmarks preserved as opposed to the fresher samples. Fracturing severity, the number of fragments post-burning, did not show a linear decrease with time since deposition or with collagen content (Fig. 28). The presence of introduced SFT did not affect fracture severity or type of heat-induced fracturing. Thumbnail fractures and warping were present in most samples. Thumbnail fractures were absent only in two bones: a 14-day (WSF2D2W5) and a 91-day (WSF3D3M4) sample. Warping was absent only in a 14-day

(WSF2D2W4) and in two 180-day (WSF5D6M1 and WSF5D6M2) samples. The archaeological cow rib bone with <0.5% collagen presented no heat-induced fractures.

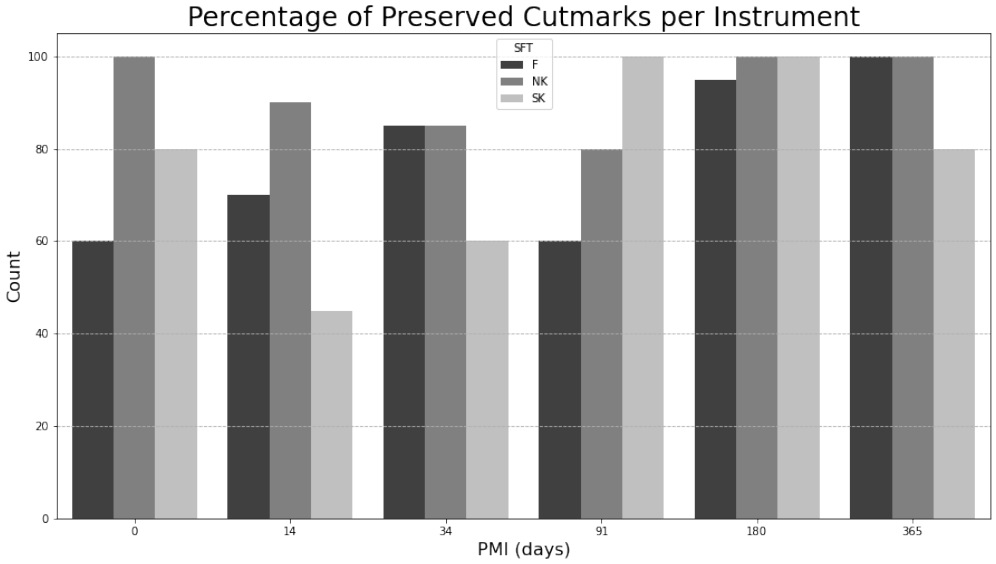


Figure 27 --The percentage of cutmarks preserved post-burning as a function of time. A cutmark was counted as present if any portion of the kerf was present. F = flint blade, NK = non-serrated knife, SK = partially-serrated knife.

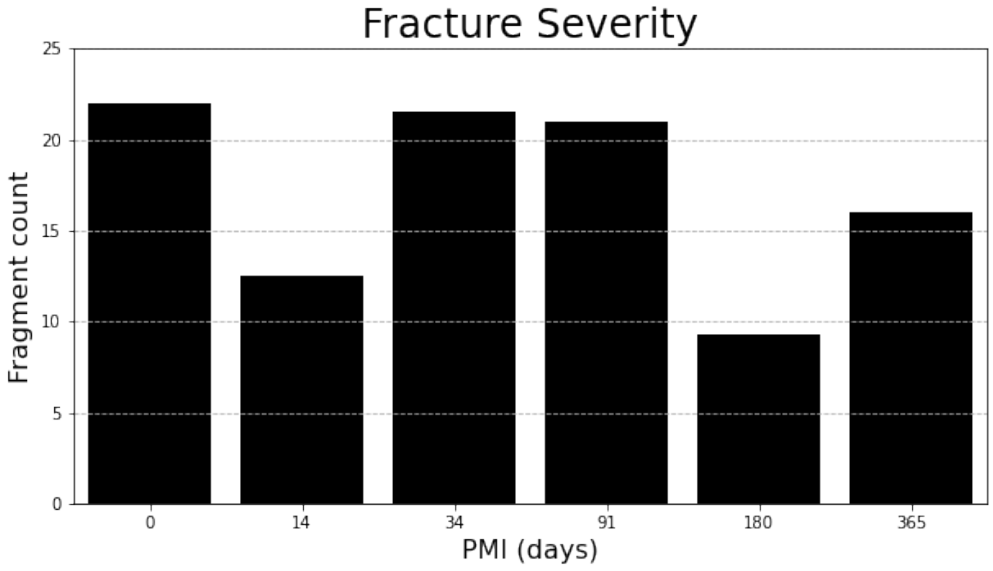


Figure 28 -- Fracture severity (number of fragments per bone post-burning) of bones post-burning.

Collagen content in fresh bone is between ~20-35 wt % (Rogers and Zioupos, 1999), while here retained collagen in samples prior to burning ranged from 10.25% (365-day sample) to 23.80% (14-day sample; Table 14). The 14-day samples presented the highest mean values

(20.70%) and the 91-day ones the lowest (14.98%), but no linear decrease was observed in collagen content through time ($r=-0.508$, $p<0.382$). However, duplicate measurements from the same bones suggest that the amount of collagen can vary greatly by location in the same bone (e.g., WSF3D3M2 had a 7.34% difference, Table 14).

PMI (days)	Sample	Starting Weight (mg)	Collagen yield (mg)	Collagen %	Mean (%)	ST (%)	Coeff. Var.
14	WSF2D2W1	562	98.19	17.47	20.70	2.77	0.13
	WSF2D2W2	515	119.67	23.24			
	WSF2D2W3	513	104.31	20.33			
	WSF2D2W4	554	103.44	18.67			
	WSF2D2W5	588	139.93	23.80			
34	WSF3D1M1	537	103.92	19.35	17.39	3.99	0.23
	WSF3D1M2	518	87.89	16.97			
	WSF3D1M3	230	48.56	21.11			
	WSF3D1M4	526	56.61	10.76			
	WSF3D1M5	484	90.82	18.76			
91	WSF3D3M1	506	81.77	16.16	14.98	2.88	0.19
	WSF3D3M2.1	471	52.34	11.11			
	WSF3D3M2.2	597	110.17	18.45			
	WSF3D3M3	574	75.05	13.07			
	WSF3D3M4	528	84.92	16.08			
180	WSF5D6M1	585	128.74	22.01	16.55	3.38	0.20
	WSF5D6M2	591	103.53	17.52			
	WSF5D6M3	532	72.49	13.63			
	WSF5D6M4	593	85.76	14.46			
	WSF5D6M5	527	79.84	15.15			
365	SWF5D1Y1.1	208	21.31	10.25	16.08	8.25	0.51
	SWF5D1Y1.2	515	112.84	21.91			

Table 14 -- The retained collagen in unburnt bone at different PMIs.

V.3.2 Perimortem and Postmortem SFT Features

There was a linear decrease in the appearance of three perimortem features (irregular edges, curving or uplifting, and splintering) and an increase in two postmortem SFT features (regular shaped edges, sharp edges) with time (Table 15; Fig. 29). Kerfs inflicted by NK were the only features that were not significantly impacted by time in the appearance of curling or uplifting

of the edges. Regular shaped edges and sharp edges were observed in a linearly increasing fashion with time (Fig. 30) regardless of the instrument. However, these two features were sometimes present at earlier PMIs on the flint-inflicted cutmarks (Fig 29C-E). Flaking, discolouration, and crumbling were not associated with time in the first year of PMI in burnt bones. Flaking was always present, regardless of PMI or instrument.

Timing	Feature	NK		SK		F		All SFT	
		r^2	p	r^2	p	r^2	p	r^2	p
Perimortem	IRR	-0.874	**0.023**	-0.906	**0.013**	-0.839	**0.037**	-0.798	**7.19E-05**
	CUR	-0.728	0.101	-0.882	**0.020**	-0.858	**0.029**	-0.729	**0.001**
	SPL	-0.833	**0.040**	-0.870	**0.024**	-0.639	0.172	-0.731	**0.001**
	FLA	0.221	0.674	0.000	1.000	-0.527	0.282	-0.173	0.493
Postmortem	RES	0.876	**0.022**	0.927	**0.008**	0.896	**0.016**	0.818	**3.41E-05**
	SHA	0.960	**0.002**	0.926	**0.008**	0.964	**0.002**	0.905	**2.54E-07**
	DIS	-0.330	0.523	-0.400	0.432	-0.351	0.495	-0.306	0.218
	CRL	0.502	0.310	0.616	0.193	0.219	0.677	0.352	0.152

Table 15 -- The linear regression results on the perimortem and postmortem SFT features. Significant p-values are bold.

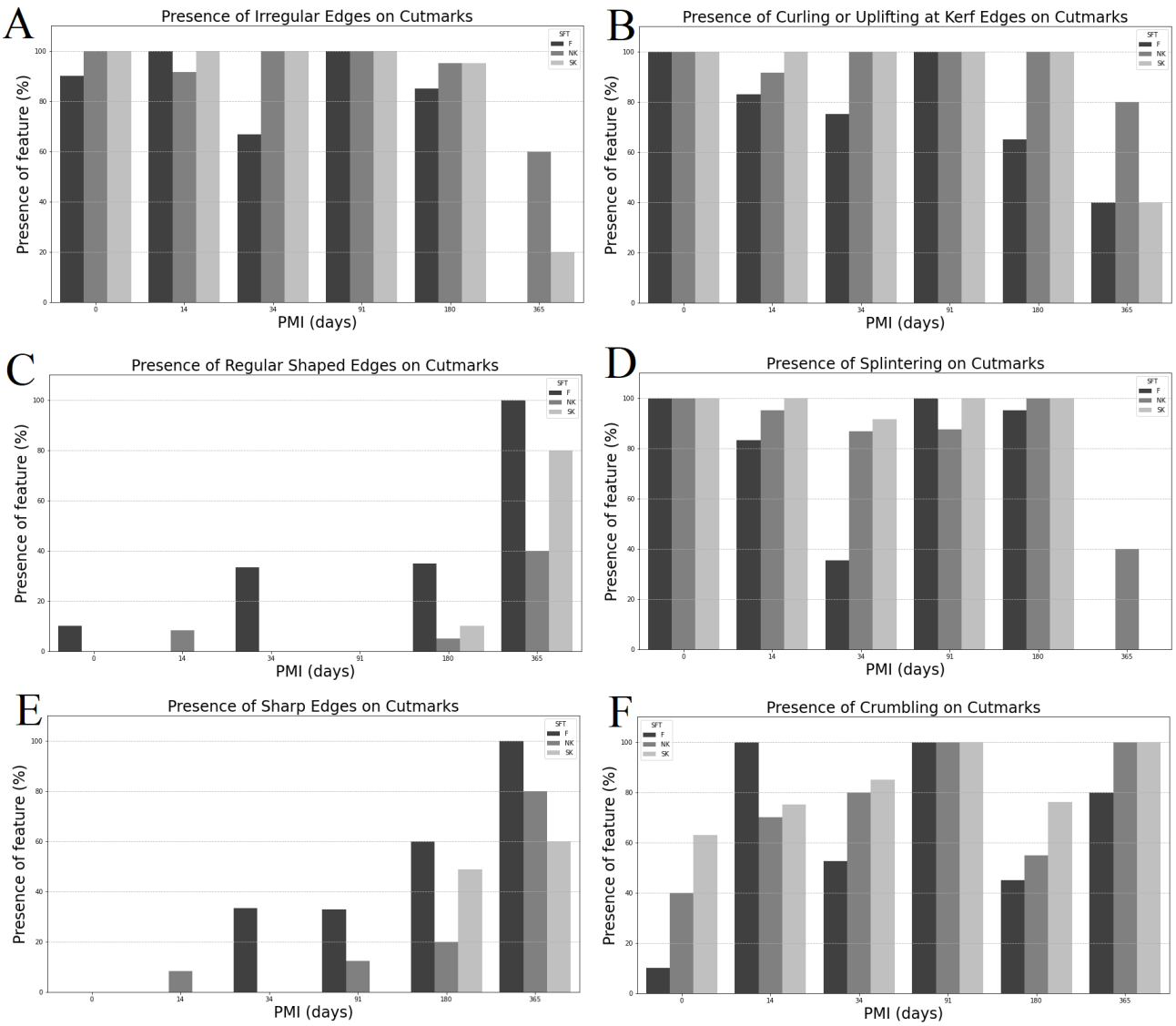


*Figure 29 -- The percentage of perimortem and postmortem SFT features as a function of time (days) on the kerfs. Hues show the different instruments the trauma was inflicted by – black: flint (F), darker grey: non-serrated grey (NK), lighter grey: partially-serrated knife (SK). **A**: The presence of irregular edges on cutmarks (perimortem feature); **B:** presence of curling or uplifting on the edges of the cutmarks (perimortem feature); **C:** presence of regular shaped edges on cutmarks (postmortem feature); **D:** presence of splintering on cutmarks (perimortem feature); **E:** presence of sharp edges on cutmarks (postmortem feature); **F:** presence of crumbling on cutmarks (postmortem), which did not change significantly with PMI.*

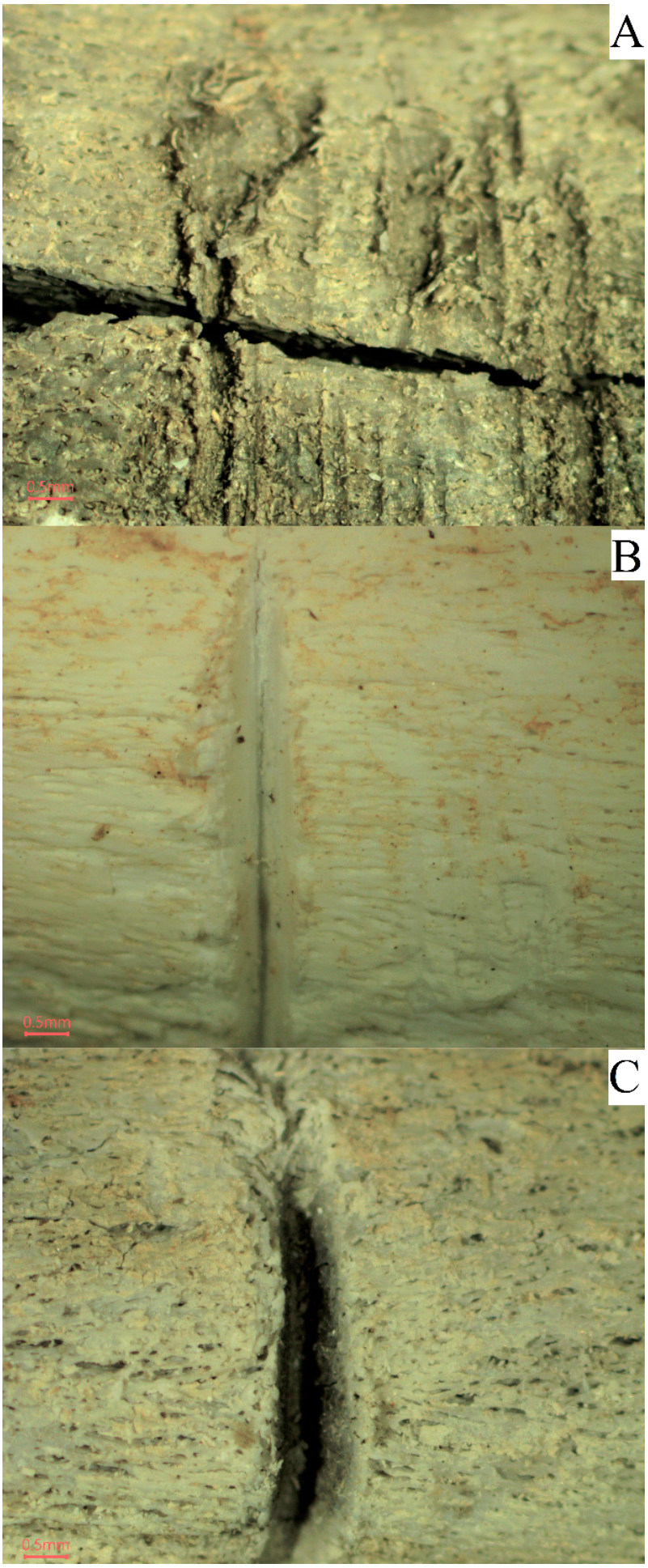

A
0.5mm
B
0.5mm
C
0.5mm

Figure 30 -- Examples of changes in kerf outline with a particular attention to the kerf edges. All SFT was inflicted by the same instrument, a partially-serrated knife (SK). ***A:*** *Burnt 14-day cutmark (WSF2D2W3_SK2). Note the irregular edges, curling or uplifting at the edges, and splintering;* ***B:*** *Burnt 180-day cutmark (WSF5D6M4_SK3). Note the regular shaped and sharp edges, the loss of the irregularity and the still present curling or uplifting at the edges.* ***C:*** *Burnt 365-day cutmark (SWF5D1Y1_SK4). It exhibits regular shaped and sharp edges, without irregularity and curling or uplifting.*

The multiple comparison of means results show the differences that were observed between PMI groups (Table 16). When the instrument type was not selected for and all SFT was considered, the 365-day group was significantly different from all other PMI groups across a number of features (IRR, SPL, RES). SHA appeared after 6 months postmortem on all types of cutmarks and were also observed on the 1-year PMI group.

SFT inflicted by NK showed significant differences only in SPL, where the 365-day group was different from the 0-, 14-, and 180-day groups. SK trauma had a significant difference between the 365-day PMI groups and all other groups across a number of features: IRR, CUR, SPL, RES, SHA. Kerfs inflicted by the flint showed no significant difference between any PMI groups for any feature.

Multiple Comparison of Means: Features with significant differences between PMI groups (all instruments)				
Features	**group1**	**group2**	**meandiff**	**p-adj**
Irregular edges	0-day	365-day	-2.83	0.001
	14-day	365-day	-2.85	0.001
	180-day	365-day	-2.63	0.001
	34-day	365-day	-2.52	0.001
	365-day	91-day	2.97	0.001
Curling/Uplifting	0-day	365-day	-2.09	0.0348
	365-day	91-day	2.09	0.0348
Splintering	0-day	365-day	-3.09	0.001
	14-day	365-day	-2.84	0.001

	180-day	34-day	-0.97	0.0312
	180-day	365-day	-3.03	0.001
	34-day	365-day	-2.07	0.001
	365-day	91-day	2.95	0.001
Flaking	N/A	N/A	N/A	N/A
Regular shaped edges	0-day	365-day	2.64	0.001
	14-day	365-day	2.66	0.001
	180-day	365-day	2.13	0.003
	34-day	365-day	2.34	0.0014
	365-day	91-day	-2.76	0.001
Sharp edges	0-day	180-day	1.28	0.0278
	0-day	365-day	2.39	0.0015
	14-day	180-day	1.2	0.0078
	14-day	365-day	2.31	0.001
	34-day	365-day	2.06	0.0046
	365-day	91-day	-1.94	0.0156
Discolouration	N/A	N/A	N/A	N/A
Crumbling	0-day	91-day	1.79	0.0169

Table 16 -- The significant results of the multiple comparison of means when all SFT instruments are considered.

V.4 Discussion

The results of this study demonstrate that the number of fragments, warping, and thumbnail fractures do not depend on the slight decrease in collagen content of the bone during the first-year postmortem. Although collagen content did not linearly decrease with time, some bones suffered considerable collagen loss within only one-year postmortem [the greatest amount of lost (~50-33%) was observed in one of the 365-day samples]. The decrease of perimortem features (irregular edges, splintering, curling or uplifting) and increase of postmortem features

(regular shaped, sharp edges) can potentially inform on the timing of SFT infliction in burnt bones as postmortem features start to appear after 6 months PMI and are observable in burnt bones.

Recently it has been shown that in human remains burnt 10 years postmortem, only 13% of the inflicted SFT and chopping trauma could be identified post-burning (Mata Tutor *et al.*, 2021). Here, this loss was not due to heat damage obscuring the kerfs. When the pre-existing SFTs were present they were always distinguishable from heat-induced fractures, in agreement with the literature (Pope and Smith, 2004; Ubelaker, 2009; Poppa *et al.*, 2011; Végh and Rando, 2017; Waltenberger and Schutkowski, 2017; Alunni *et al.*, 2018). It was also not due to the fracturing severity, or how many bone fragments the bones broke into post-burning. Rather, it was due to the location of these fractures. The fresher the bone was, the more likely it was for the longitudinal and transverse heat-induced fractures to slice the kerfs perpendicularly, resulting in the loss of small burnt bone fragments.

Gonçalves *et al.* (2011) proposed that warping and thumbnail fractures might be due to the collagen content and/or distribution in the bone cortex. Supporting this, the experimentally burnt Neolithic cow rib bones (<0.5% collagen) showed no thumbnail fractures or warping, and in fact it showed no heat-induced fractures. However, in the experimental pig bones no connection was found between the presence of thumbnail fractures and warping and collagen content in the ≤ 1-year PMI bones, which might be due to the limited length of the PMI. In fact, one of the only bones that did not present thumbnail fracture (14-day PMI; WSF2D2W5) showed the highest collagen content (23.80%) of all bones. Duplicate collagen measurements taken from the same part of bone resulted in variable collagen preservation, which suggests that collagen distribution can vary not only in the same bone, but also in the same bone area. This aligns with previous research on variable intra-skeletal N content in archaeological bone (Jacob *et al.*, 2018). Thus, collagen presence and distribution might determine whether these

fractures are present, but if distribution in the same bone can be highly varied, it might not add to our understanding of when the bone was burnt. Although the cool-temperate climate and the length of PMI did not allow for significant collagen loss in these bones, excarnation and further post-mortem processing before cremation is unlikely to occur after many years (<1-2 years) which would be a sufficient PMI for significant collagen loss. It is simply suggested here that more research is needed in bone collagen distribution. Nevertheless, the overwhelming presence of thumbnail fractures and warping in the bones would make all of these bones classified as bones burnt in a fresh state (Baby 1954; Binford 1963; Buikstra and Swegle 1989; Spennemann and Colley 1989; Etxeberria 1994; Whyte 2001), even when burnt after 6 to 12 months exposure to the elements.

The features used to distinguish 'perimortem' vs postmortem cuts (Mayne, 1990; Sauer, 1998; Symes *et al.*, 2008; Ubelaker, 2009; Crowder *et al.*, 2013) survived burning and were observable on burnt cutmarks. It was always possible to distinguish SFT from heat-induced fractures due to their shape and the sharper and more jagged edges of the heat-induced fractures (Fig. 31). The presence of the two postmortem (regular shaped edges and sharp edges) features in burnt bones have the potential to be used to discriminate between SFT inflicted >6 months postmortem before burning. If regular shaped kerfs and sharp edges are present on cutmarks on burnt bones, it is likely that the SFT was inflicted over 6 months after death prior to the fire event. The strongest case for this was presented by the SK-inflicted kerfs, in which all cutmarks started to present regular shaped and sharp edges only after 6 months postmortem, while the other kerfs produced by NK and F were only less likely to show these two postmortem features in the bones with shorter PMIs. In most cases, the 365-day group's kerfs did not display irregular edges and splintering, meaning these features are mostly lost somewhere between 6 months to 1-year postmortem in surface-exposed remains. The perimortem (irregular edges and splintering) and postmortem (regular shaped edges and sharp edges) features might not be

associated with retained collagen in the ≤ 1-year exposed bones, since there was neither significant difference between collagen contents of the PMI groups, nor significant decrease with time either. It is proposed here that moisture, other than collagen, might cause the difference in the bone's viscoelastic response to trauma. Rapid moisture loss was previously documented after 2 months, after which the decrease was steadier (Wieberg and Wescott, 2008). However, here no significant differences in moisture quantity were observed until 6 months PMI, even if the bones were surface exposed. Unburied and surface exposed bones should lose moisture faster than buried ones.



Figure 31-- The observable difference between SFT inflicted by the non-serrated knife and a heat-induced fracture (middle) on a 91-day PMI burnt bone (WSF3D3M3). From left to right: NK4, heat-induced fracture, NK3 (light microscopy image).

There was a linear decrease with PMI in the appearance of curling and uplifting of the kerf edges in cutmarks inflicted by SK and F, but this feature seems to be associated with both the PMI and the type of instrument, since this decrease was not present in cutmarks caused by NK. This is probably because the lack of serrations on the blade edge did not separate bone fibres

in both directions. Although discolouration at cutmark edges was suggested as an indication of trauma inflicted in unburnt dry bones (Mayne, 1990; Crowder *et al.*, 2013; Galloway *et al.*, 2014), burning completely obscured this colour change. Since crumbling at the bottom of the kerfs was not associated with either PMI or type of instrument (Fig. 29F), it cannot determine the timing of trauma infliction. Flaking was always present in and around the kerfs, thus it is not a reliable indication of 'perimortem' trauma in burnt bones in the first one year of PMI. It is possible that bones might not need to be dry for this feature to disappear post-burning.

Limitation of this study include using disarticulated bones rather than the whole skeleton, and the lack of comparison between buried and surface-exposed samples prior to burning. The length of PMI in this study was not sufficient to result in significant collagen loss in a cool-temperature and moist climate. Other than sharp force trauma, blunt force and chopping trauma should be included in future studies. Therefore, further research is needed in collagen distribution in the same and different areas of the same bone at different stages of early diagenesis, as well as in different environments and climates (e.g., at the tropics, deserts, etc.). Additionally, future research should ideally be carried out in whole human cadavers, both buried and surface-exposed.

V.5 Conclusion

This study attempted to differentiate between freshly burnt and early diagenetic burnt bones up to 1-year postmortem interval by assessing (1) SFT features inflicted by three different sharp force instruments; (2) heat-induced fractures relating to fresh bone (thumbnail fractures and warping); (3) fracture severity; and (4) retained collagen content. To the knowledge of the authors this is the first study to inflict SFT at different PMIs but subsequently before burning as well as attempting to compare heat-induced fracture types to the bone's measured collagen content.

Fracturing severity of the bones did not depend on PMI, but cutmarks inflicted on the longer PMI bones (180- and 365-day) were more likely to be preserved, due to the location of the heat-induced fractures. Thumbnail fractures and warping were present on almost all of the bones and did not depend on retained collagen content. These fractures might be more closely associated with other (non-collagenous) moisture in the bone or the highly variable collagen distribution in the same bone.

The timing specific SFT features (perimortem vs postmortem) survived burning in this study, which made it possible to inform on the postmortem interval before burning. It is proposed here that the loss of some of these perimortem features (irregular edges, splintering, and curling or uplifting) with the appearance of some postmortem features (regular shaped and sharp edges) on cutmarks might be good indications of delay between the time of death and the burning event. The loss of these features is steady and continuous, but 6 months of surface exposure of the remains might produce significant and noticeable reductions in the investigated perimortem SFT features. The appearance of regular shaped kerfs and sharp edges might be the best indication of the body being surface exposed for 6 months after death and before burning, especially when the SFT was caused by (partially-) serrated instruments. One year of surface exposure was not long enough for flaking to disappear, regardless of the type of weapon. Colour differences at trauma surfaces were obscured by burning-induced colour changes and crumbling was not related to PMI or the type of instrument in burnt bones. The results of this study contribute to the understanding of the effects of heat-induced changes and to the recognition of osteogenic reaction for applications both in osteoarchaeology and forensic anthropology.

Acknowledgements

We would like to thank the team at Whytam Woods, Oxford, for allowing us to use the woods for the exposure phase and the outdoor burnings. We would also like to thank Professor Nick Barton for providing the flint blades for the trauma infliction.

Funding

This study was funded by the Meyerstein Foundation, School of Archaeology, University of Oxford.

Chapter VI. Discussion and Conclusion

This doctoral thesis aimed to build a series of methodologies to investigate if skeletal remains were burnt fresh (subsequently after death with flesh present) or decomposed. In other words, it aimed to elucidate the time elapsed between death or deposition and the fire event. This was explored through an actualistic taphonomy experiment using pig tibiae, as a proxy for humans, with postmortem intervals (PMIs) prior to burning ranging from 0-365 days after which they were subsequently burnt in an outdoor fire. Investigations of the bones through histology, FTIR, EMPA, SFT-analysis, heat-induced fracturing, and collagen preservation have enabled the elucidation of the timescale of PMI prior to burning. For the electron microprobe analysis, mid- to late-Neolithic cremated human remains were included, besides the experimental pig bones (see Chapter IV). The three scientific papers presented three attempts to answer the overarching research question of whether the bone was burnt fresh or partially decomposed (Fig. 32). It is suggested here that decreased trace elemental values of endogenous potassium in the burnt bones provide the strongest evidence of bone decomposition prior to burning. Additionally, if damage from a sharp force instrument was present, the features' appearances changed 6 months after death/deposition due to the osteogenic reaction of the decomposed bone, which is observable post-burning.

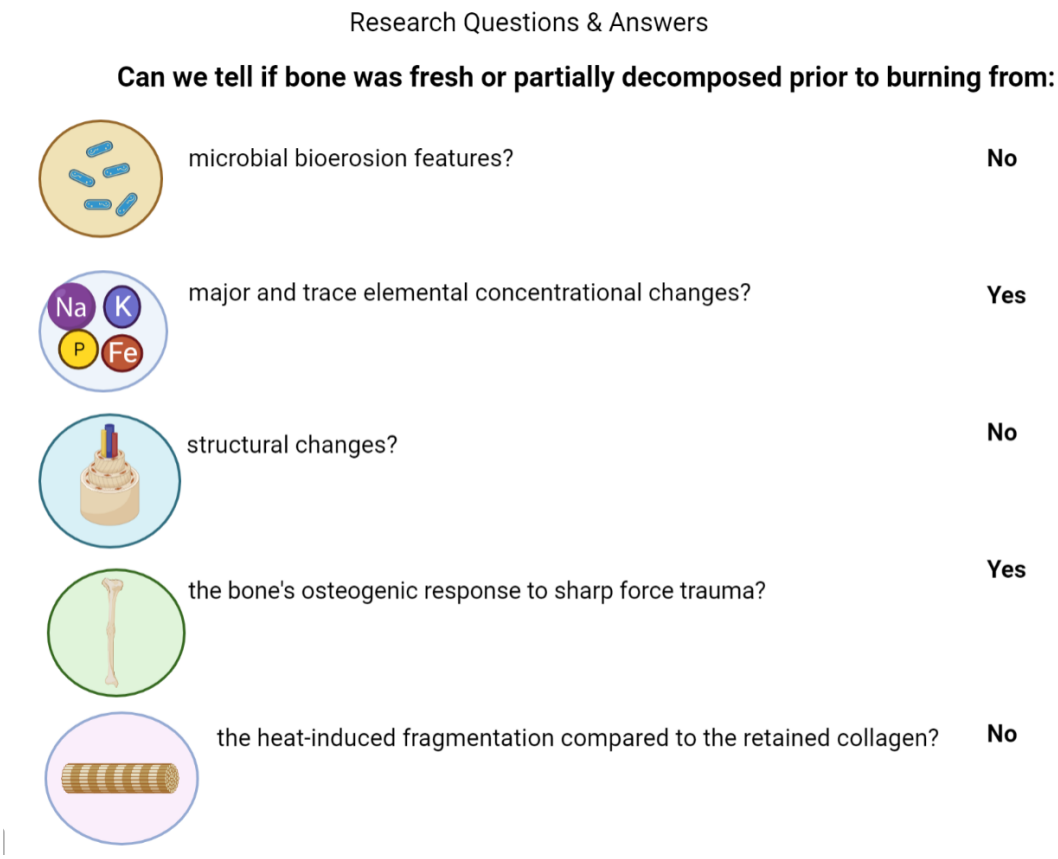


Figure 32 -- Research questions and answers.

The histological investigations of taphonomic features in Chapter III aimed to identify bioerosion on burnt bones. If microbial bioerosion would be possible to identify in burnt bones, it would open the possibility to establish whether the bone was burnt fresh (with soft tissue present) or had gone through partial decomposition prior to burning. This study did not manage to associate microbial bioerosion features with time since deposition (or PMI) in burnt bones and found that burning cannot only conceal such features, but produce them as well. The strongest evidence for this was presented by the presence of 'Wedl 2' on the fresh/control burnt bones. Wedl 2 has been interpreted as an indication of bioerosion caused by fungi (Trueman and Martill, 2002) and early bacterial attack (White and Booth, 2014). However, the results of this study (Chapter III) found that the features resembling 'Wedl 2' in the fresh burnt bones are in fact carbonised osteocyte cells trapped in the canaliculi (Chapter III, Fig. 15; see discussion in section III.3). The significance of this study is that since microbial bioerosion features can

be produced by burning, they are unreliable indicators of bioeroded bones both in an unburnt and burnt state viewed under the transmission light microscope. Although BSEM is a better tool than transmission light microscopy for identifying microbial bioerosion in unburnt bones (Turner-Walker, 2019), all bioerosion-like features were obliterated on the BSEM images by the burning process. These findings challenge the observations and interpretations of burnt human bone histology of previous studies (Grévin *et al.*, 1991; Lemmers *et al.*, 2020).

The second attempt used the structural and elemental concentration of the bone's inorganic phase to elucidate the survival of early diagenetic physicochemical changes in burnt bones (see Chapter IV). Although fire drastically changed the structure of the bones, the trace elements and their decrease/increase were measurable even in the burnt bones. Three elements (K, Na, Cl) significantly (and linearly) changed with time in the burnt bones and since K and Na are associated with the extracellular fluid, their decrease signifies dehydration (see discussion in section IV.4). However, data presented within this thesis suggest that this change survives burning, and thus, bone decomposition is traceable in the burnt remains. Potassium content in the mid-cortical regions of burnt bones is significantly different after 3 months of surface exposure from fresh bones and it steadily decreases thereafter. The underlying objective of the thesis, whether it is possible to tell if bones were burnt fresh or partially decomposed, was accomplished by the elemental concentration investigations through EMPA and by the investigations into the perimortem and postmortem features in cutmarks. This finding of the endured decrease of potassium in modern burnt bone has major repercussions in forensic science.

The results of the EMPA demonstrated that Ca and P are the major compositional components of bone mineral, but other elements such as Na, K, Al, Sr, Mn, and Mg are also consistently present in fresh modern unburnt and burnt bone in all investigated zones. Cl, Fe, and Si diffuse into the bone post-deposition, either from the extracellular fluid (Cl), from the

soil (Si), or from both sources (Fe). The EMPA results from the archaeological cremated bones clearly demonstrate which of the studied elements diffuse into the bone from the soil. K, Fe, Al, Si, Mn, and Mg had the highest concentration in the outer cortical regions, while they were completely depleted or showed a much lower concentration in the mid-cortical zones. Sr showed similar concentrations in other parts of the bone cross-section as it did in the outer cortical zones. But Sr is just as diagenetic as the other mentioned elements, while Sr is also normally present in higher (trace) amounts than the other elements in bone.

Magnesium within bone plays a role in the restriction of crystallite morphology and stability (Barinov *et al.*, 2006). Magnesium can easily replace calcium and affect the HAp lattice stability (Barinov *et al.*, 2006) and even partial substitution of Ca for Mg reduces the thermal stability of bioapatite (Fadeev *et al.*, 2003). The sudden decrease of Mg until 91-day postmortem, followed by the gradual increase in the burnt experimental bone suggests that surface bound Mg was lost first and then structural Mg to some extent partially replaced Ca. This is also evidenced by the moderate decrease of Ca after 3 months postmortem in the burnt bones, suggesting the change in the structural Mg and Ca. The decrease in Mg in the first 3 months does not seem to affect the amount of Ca, which is the reason for the interpretation of the loss of surface bound Mg during this period.

Sodium was suggested to not play a major role in the mechanism of substitution of carbonate because it is only present as an impurity second phase (Gibson *et al.*, 2002). However, Na has compatibility with Ca in terms of their effective ionic radii as opposed to Mg substitution for Ca due to their ionic radii's very different sizes. When a much smaller ion (e.g. magnesium) substitutes a larger ion (e.g. calcium), it destabilises the apatite lattice, which results in the formation of tricalcium phosphate crystallisation (Barinov *et al.*, 2006). In unburnt bone the loss of Na is a sign of dehydration, but in this study Na-levels stayed stable

in unburnt bone throughout the 1-year PMI. Na significantly decreases in the burnt bones with time, which suggests that heating accelerates the process of Na loss.

The third attempt (Chapter V) was also successful in answering the overarching research question of the thesis. Chapter V focused on the bone's osteogenic reaction to sharp force trauma/damage and its survival post-burning, as well as on heat-induced fractures and fracturing severity of bones decomposed to different degrees. Bone shows a different osteogenic reaction to SFT even after only 6 months of deposition post-burning, based on the investigated perimortem (irregular edges, curling or uplifting, and splintering) and postmortem (regular shaped edges and sharp edges) SFT features. However, no linear decrease in collagen content through time was observed, thus the changes in kerf appearance (perimortem vs postmortem) might not be due to the collagen content of the bone (see discussion in section V.4). In fact, all perimortem and postmortem SFT features endured burning, except discolouration.

VI. 1 Early Diagenesis

In the unburnt bones, statistically significant linear changes with time were found in the FTIR dataset. IRSF (measure of crystallinity) increased while B-type carbonates decreased during the 1-year postmortem interval. This shows that diagenesis begins and is already measurable within the first year PMI (of surface exposure). From the elemental compositional investigations, K, Mn, and Mg changed in a linear fashion with time in the unburnt samples during the one-year PMI.

Chapter III showed that the collagen preserved can vary even during the one-year interval after death and in some PMI groups a significant loss of collagen was recorded. Moreover, multiple measurements from the same bone showed that collagen content varied largely even within the same area of the bone. Since thumbnail fractures and warping were almost always recorded, even if collagen content was much lower than expected, they might

not depend on the amount of collagen retained in the bone, but *only* the distribution of it. There was no linear decrease in the absolute measurements of collagen in the bones, but there was a general non-linear decrease. Cracks in the bone microstructure are considered to be an indication of collagen degradation (Huisman *et al.*, 2017), but in the experimental bones no statistically significant increase was observed with increasing PMI from the histology results. The lowest amount of collagen measured was from one of the 365-day samples (SWF5D1Y1.1) with 10.25%. This bone still showed birefringence under the polarised transmitted light microscope. The collagen loss and dehydration of the samples were not severe enough in one-year postmortem surface exposure to produce cracks (from dehydration), affect the heat-induced fracturing types, or the fragmentation severity.

As evidenced, early diagenesis is measurable from the inorganic and partly the organic fractions already during one year of bone surface exposure. In the Neolithic cremated remains exogenous elements diffused into the cortical bone through the outer cortical layer and to a lesser extent through the vascular canals.

VI. 2 Heat-Induced Changes

The morphological, histological, structural, and chemical analyses of the experimentally burnt bones have achieved the aim of demonstrating a general response of bone heat treatment of variably fresh bones burnt in an outdoor pyre. The general response identified by this thesis comprised of heat-induced fracturing, colour change, organic loss, histomorphological changes, crystallisation, elemental concentration changes, and unlikely, but potential thermal decomposition of the HAp phase.

Bone temperatures of this study reached a maximum mean of 750°C and histological changes were observed on the bone microstructure. Previous histological studies showed that the first histological changes due to heat appear at varying temperatures between 600 and

1200°C (Herrmann, 1977; Bradtmiller and Buikstra, 1984; Cattaneo *et al.*, 1999; Squires *et al.*, 2011). Although it is unclear if these temperatures were bone or air temperatures, the results of this study fit into the above-mentioned temperature range. Volkmann's canals were always observable on the experimental bones as opposed to the findings of Squires *et al.* (2011). Cracking and minute fissures were a very common feature on the bones, which were noted to appear at 500°C (Imaizumi *et al.*, 2014). However, these might have been caused by the laboratory handling and preparation of the thin sections, since these features were also very common on the unburnt bones. Individual lamellae were identifiable with extensive carbon deposits, which were previously reported not to be present together (Hanson and Cain, 2007). It is not possible to predict the heating temperature of the bones only from the histological changes of the experimental bones due to the variable temperature ranges and the associated histomorphological changes reported in the literature.

The organic loss and crystallisation were assessed by FTIR in the burnt bones. Recrystallisation was also confirmed by X-ray Diffraction (XRD) on a few bones of the proof-of-concept study (Appendix A) by observing greater resolution of diffraction peaks and decreased broadening in the burnt bones compared to the unburnt ones. Sharper peaks indicate increase in crystallite size and a more perfect lattice with less strain. On the IR spectra, OH^- group peaks appeared on the burnt bone peaks, while carbonate groups decreased after burning, which is one of the reasons for the higher crystallinity. The removal of carbonates and the appearance of hydroxyl groups mean that there is less lattice distortion of the crystal lattice (LeGeros, 1991).

The only change that can occur to the contents of the unit cell during heating is ion exchange with the atmosphere. The amount of Ca, Na, Mg, and P ions should be fixed within the apatite phase until thermal decomposition of the HAp phase occurs (Beckett, 2009). It is possible that the thermal decomposition of the HAp phase started after burning, assessed by

the appearance of β-TCP peak on the FTIR spectra, but it is unlikely. Thus, the changes in elemental concentrations of these elements, namely the non-linear, non-uniform increase of Mg and the linear decrease of Na, in the burnt samples represent changes caused during the exposure phase prior to burning.

Structurally, the main discriminant contributors between unburnt and burnt bones are the carbonate to phosphate ratio (C/P), the phosphate high temperature (PHT), and the cyanamide to phosphate (CN/P) ratios. Ca, Mg, Mn, Na, P, Cl, Fe, K, and Sr were the discriminating elements identified by the algorithm when the elemental composition data was analysed through a two-feature (unburnt vs burnt) linear discriminant dataset. Therefore, these parameters should be the focus of interest in burnt bone elemental chemistry research.

VI. 3 Diagenesis in Burnt Bones

This thesis aimed to identify early diagenetic signals in bones *before* burning. However, the post-burning diagenetic alterations to cremated bone have to be considered as well. Crystallinity increase renders the bone mineral more stable and less reactive with the environment. Crystallinity is a more important factor over porosity for post-burial alterations (Snoeck *et al.*, 2015). Thus, burnt bone is far less susceptible to postmortem alterations than unburnt bone. It has been demonstrated that isotopic composition of calcined bone is not affected by post-burning burial conditions (Snoeck *et al.*, 2014, 2016). However, when acetic acid was used to remove diagenetic elements, modern calcined bones were slightly more reactive than archaeological cremated bones (*ibid)*. Therefore, there might be a change in elemental composition of burnt bones after they had been buried, but it is probably negligible. This slight change would mostly happen on the outer cortical zones of bones, while the mid-cortical section should be unaltered, as demonstrated by the compositional measurements from the burnt Neolithic bones from Kiltierney (Chapter IV, Fig. 21). Although it is yet unknown

whether the contaminants in these bones, such as K, Fe, Al, Si, Sr, Mn, and Mg, diffused into the bone post-burning and post-burial or during exposure *before* burning, it is evident that this only affected the outer cortical areas of the bone cross-sections.

Since in a medicolegal context, there is no need to consider the effects of hundreds to thousands of years of a burial setting, potassium can be directly used in modern burnt bones for PMI estimation prior to burning. Na, Cl, and Mg also show potential for the same purpose in burnt bones.

VI.4 Limitations

One of the most obvious limitations of this study is the use of pigs, as proxy for humans, when interpreting or applying results to human remains. There is an ongoing discussion on how appropriate animal (especially pig) models are as human analogues (Matuszewski *et al.*, 2020). However, pig bones were chosen as a proxy for humans in the experiments, because they have been widely utilised as a substitute for human bodies in decomposition, fire, and histology studies (Forbes *et al.*, 2005; Lynn and Fairgrieve, 2009; Thompson and Inglis, 2009; Bonney *et al.*, 2011; Symes *et al.*, 2012; White and Booth, 2014; Kontopoulos *et al.*, 2016a), and they are easy to obtain. Additionally, porcine bone macro- and microstructure are representative of humans; the process of healing and remodelling, the bone's morphology, the lamellar structure, the mineral concentration and mineral density of bone, body weight, distribution of subcutaneous fat, and their gut microbiota have close similarity to human body and bone (Turner and Wiltshire, 1999; Forbes *et al.*, 2005; Pearce *et al.*, 2007; Wilson *et al.*, 2007; Feng and Jasiuk, 2011; Hollund *et al.*, 2014; White and Booth, 2014; Kontopoulos *et al.*, 2016b).

Another limitation in connection with the material of this study is that the pig tibiae used were from pigs that were butchered at 18 months. At such young age there is a higher amount

of organic matter in the bones than older individuals, thus in histological studies theoretically there would be a higher chance of bioerosion. However, this was not an issue here since there was no conclusive evidence for microbial bioerosion in any of the bones. Additionally, the bones were only sub-aerially deposited and there is a lack of comparison with buried remains in this study. However, it is likely that exposure of the deceased would happen above ground and not buried, as evidenced by the ethnographic studies discussed in section I.4.

The first exposure experiment was interrupted and abandoned, due to the material of the study being removed by scavengers. To overcome this, the second experiment used cages reinforced with further 'chicken mesh', stapled down with metal pegs, tied to a fence and locked the 'door' of the cages. Yet, they were broken into again by scavengers and three of the 365-day PMI group's bones were stolen. Thus, this group's results are only based on two samples each for the unburnt and burnt bone groups. Furthermore, during the main (second) experiment, the 14-day postmortem group was placed into the cage for exposure at an especially warm period when smaller scavengers, that could easily get access to the cage without removing the bones (i.e., mice), were more active. This resulted in a fast and complete defleshing of these bones in only two-weeks, which might have influenced the rate of histological, structural, and elemental decomposition.

For the histological study, a diamond blade-fitted Buehler saw was used, due to the lack of access to a microtome. Although this type of saw is often used in histological studies, it produces less consistent thickness of the thin-sections than a microtome would. Finally, the most promising results to answer the overarching question of this thesis were provided by the potassium concentration using EMPA. However, this study has not yet fully demonstrated the diagenetic resistance of potassium in a larger sample of archaeological cremated bones. The only analysis on archaeological cremated bones were performed from one site, which limits the method's application to further material without further confirmation of the methods. Due

to the ongoing COVID-19 pandemic and the associated laboratory closures, it was not possible to get access to an XRD. Thus, the only the proof-of-study (Appendix A) used this technique. It would have been extremely beneficial for the main study to determine the structure of the substituted bioapatite before and after burning.

VI. 5 Future Research

Although this investigation has provided a methodological foundation with which to study the timing of cremation compared to the time of death, the continued refinement of the techniques and the search for other proxies for decomposition in the bone will yield more reliable and meaningful results.

VI.5.1 Diagenetic Resistance

The work presented in Chapter IV demonstrated that trace elemental analysis in unburnt and burnt bones has the potential to inform on the pre-burning condition of the dead. Potassium concentrations significantly decreased with time in both the unburnt and the burnt bones. As mentioned in the limitations, potassium trace elemental concentrations were only measured in archaeological cremated bones from one site. Thus, it was hypothesised here that the Neolithic cremated human remains from Kiltierney, Ireland, were exposed/curated/excarnated before cremation. However, the results of the present study are not altogether sufficient to confirm this hypothesis (in archaeological bone) and apply it to a wide range of archaeological sites with cremation burials. In other words, it has not yet been demonstrated whether potassium (and other elements that showed significant change, such as Na or Cl) is diagenetically resistant in cremated bones on an archaeological timescale. If potassium is diagenetically resistant, the way that C, O, and Sr isotopes are in calcined bone (Snoeck *et al.*, 2015), it would be possible to estimate the time elapsed between death and cremation and to elucidate our understanding of how past cultures treated their dead. In case excarnation was not used for the purposes of

curation of the dead, it is possible that past populations gathered human bodies to cremate them together to save resources or to wait for a season adequate for cremation (i.e. dry season).

Thus, testing the post-burial diagenetic resistance of K, Na, and Cl should be the next step in future research in this area. This should be done by (1) experimental contamination experiments and pre-treatments (using acetic acid or hydrochloric acid as 'cleaning agents' to remove the diagenetic compounds); (2) measurements of elemental concentrations and comparison in μ-XRF, EMPA, and LA-ICP-MS; and finally (3) establish the diagenetic resistance and accuracy of using K, Na, and/or Cl as a signal for prior decomposition in burnt bones studying archaeological cremations from different cultures and geographical areas. Research in this area will likely produce positive results, because it is likely that endogenous potassium had depleted prior to cremation in the studied Kiltierney bones (Chapter IV). Here, K-values were only under detection limit in the mid-cortical section and were high in the outer cortical zones and around vascular canals. This seems logical, since exogenous potassium is expected to diffuse into the bone from the soil. After acetic acid treatment, K-values should be under detection limit in all zones in these bones if human remains were truly excarnated for ≥1 year prior to cremation.

A further potential confirmation of the usage of K-levels as a proxy for decomposition prior to burning could be to compare historically cremated bones (e.g. Roman), where there is written evidence of when the bodies were cremated and how they were handled prior to cremation, with Neolithic and Bronze Age cremated bones from sites where a lapse between death and cremation is suspected from Ireland, Scotland, England, Luxemburg, and France. If the K-values of Roman cremated bones in the mid-cortical areas are detectable with the EMPA but endogenous K had depleted from the cremated prehistoric bones, it would prove that potassium values are in fact an excellent indicator of decomposition prior to cremation for use in archaeology. If a pattern would exist of different amounts of endogenous potassium

preserved in the mid-cortical zones of cremated bones, it would also be possible to compare different culture's funerary traditions. For example, if some cultures only burnt their dead seasonally (e.g., only in Winter or Summer), after a few human remains gathered, or preserved the dead for further rituals for months or years prior to cremation. Other gains from this type of research would result in elucidating how the dead were stored while 'waiting' for cremation (i.e., exposed indoors, outdoors, or buried). This could be studied with an actualistic taphonomy experiment, similar to the one of this study, but in which bones are both buried and sub-aerially exposed to compare the effect of structural changes and elemental concentrations of being buried. It would also be beneficial if cremated archaeological bone composition would be compared with the burial soil composition.

One of the risks of this study would be if new methodologies would fail to produce archaeologically relevant results (i.e., if none of the elements are diagenetically resistant). Still, these would be useful results, since they would inform the community on what methods to focus on in the future. However, if the development of a new methodology is successful, it would open up a whole new field of funerary archaeology, looking at rites and treatments of the dead prior to cremation.

VI.5.2 Synthetic (Bio)apatite

To further understand the time elapsed between death and burning, it is necessary to understand the impact of different temperatures on the trace elements of interest and what state these elements are present in the mineral phase (e.g. labile state or incorporated into the crystal). After determination of the structure and elemental composition of unburnt and burnt archaeological bones (with EMP/μ-XRF/ICP-MS and XRD), HAp could be synthetised with 'real' bioapatite substitutions [i.e. diagenetic elements; e.g. from extracellular fluid (K, Na, Cl) and from soil (Sr, Mn, F, Fe)] and study their thermal behaviour and configuration. The effects of heating and the survival rate of the elements of interests/substitutions would be studied and

compared in the synthetic apatite and archaeological bones. The results would then be analysed and modelled with predicted targets reached on both the synthetic and archaeological bioapatites to help determine signals of decomposition that survives burning. The newly established methods could then be applied onto archaeological cremation cemeteries all around the world. The results of such a study would not only highly enhance our understanding of burnt bone, but could confirm past funerary practices in terms of time elapsed between death and cremation, place of storage/display of the deceased prior to cremation, and it could establish spatiotemporal maps with the dispersion of excarnation before cremation as a rite.

VI.5.3 Collagen Distribution

Due to the unexpected results of the measured collagen contents (i.e. large inter- and intra-bone variation during a short PMI), further studies about the decay of the organic phase is encouraged here. The varied range of collagen measurements, even in the same bone and in the same bone area, varied largely. Further studies should investigate the effects of surface exposure on collagen content and the distribution of collagen in the bones. This should be studied by taking samples from several of the same parts of the same bone from different individuals and by using different methods for measurement (i.e., only EZEE filtration, EZEE- and ultrafiltration, FTIR amide to phosphate ratios). Environmental factors could be experimentally researched this way. For example, by only taking samples from the part of the bone that was exposed to UV-rays versus the part of the bone that was partially submerged into the soil or covered by vegetation.

VI. 6 Conclusion

The present research aimed to address when the body was burnt compared to the time of death by looking at the state of the bone (i.e., fresh or partially decomposed) at the time of burning. This highly debated question in archaeology and forensic anthropology has previously only been investigated macroscopically (heat-induced fractures) and histologically (microbial

bioerosion). Here, heat-induced fractures, thought to be associated with burning of fresh bones, were revealed to not be an indication of the presence of flesh or the amount of collagen retained in the bone. The histotaphonomical investigations demonstrated that microbial bioerosion features are unreliable in both unburnt and burnt bones, because identical features can be caused by burning, evidenced by their presence in uncontaminated burnt fresh (fleshed) bone. Structural changes investigated by IR spectroscopy were not useful in differentiating between differentially decomposed bones after burning due to the dramatic heat-induced changes in bone crystal structure. However, trace elemental analysis in unburnt and burnt bone was found to have the potential to inform on the pre-burning condition of the dead. In this experimental study (Chapter V), potassium concentration significantly decreased with time in the unburnt, surface-exposed bones during the one-year postmortem interval. These values survived burning in the calcined remains and it was suggested that a potassium concentration of <0.07 ±0.01 wt% indicate that the bone was burnt at least 3 months after death. This finding has major repercussions to medicolegal cases in which burnt human remains are recovered. Based on these results, it is possible that the investigated cremated human bone fragments from the Neolithic site of Kiltierney, Ireland, might not have been burnt immediately after death and in case of surface-exposure, this period between death and cremation might have been over a year, which was the maximum time interval investigated in the experimental study.

It has also been shown that bone behaves differently to sharp force trauma infliction after only 6 months of deposition post-burning, based on the investigated perimortem (irregular edges, curling or uplifting, and splintering) and postmortem (regular shaped edges and sharp edges) SFT features. However, no linear decrease in collagen content through time was observed, thus the changes in kerf appearance (perimortem vs postmortem) might not be due to the collagen content of the bone.

As this study demonstrated, the right chemical taphonomy methods can elucidate on the time elapsed between death and the burning of the body, which opens a range of potential further research in funerary archaeology, such as studying the pre-burning condition and the treatment of the dead in archaeological populations where cremation was the dominant, or the only, funerary rite. The results are already applicable and have a high potential in contributing to the reconstruction of timelines at a crime scene. These results open the possibility to elucidate on the current understanding of past funerary rites, practices, and social dimensions in spatiotemporal areas where cremation was practiced. Results from this thesis suggest that the application of trace elemental analysis (especially potassium concentrations) on burnt archaeological human remains from a number of prehistoric cultures would elucidate when bodies were burnt compared to their time of death.

Reference List

Absolonova, K., Veleminsky, P., Dobisikova, M., Beran, M. and Zocova, J. (2013) 'Histological Estimation of Age at Death from the Compact Bone of Burned and Unburned Human Ribs', *Journal of Forensic Sciences*, 58(s1). doi:10.1111/j.1556-4029.2012.02303.x.

Alekshin, V.A., Bartel, B., Dolitsky, A.B., Gilman, A., Kohl, P.L., Liversage, D. and Masset, C. (1984) 'Burial Customs as an Archaeological Source [and Comments]', *Current anthropology*, 24(2), pp. 137–149. doi:10.1086/202960.

Alunni-Perret, V., Muller-Bolla, M., Laugier, J.P., Lupi-Pegurier, L., Bertrand, M.F., Staccini, P., Bolla, M. and Quatrehomme, G. (2005) 'Scanning electron microscopy analysis of experimental bone hacking trauma', *Journal of Forensic Sciences*, 50(4), pp. 796–801.

Alunni, V., Nogueira, L. and Quatrehomme, G. (2018) 'Macroscopic and stereomicroscopic comparison of hacking trauma of bones before and after carbonization', *International journal of legal medicine*, 132(2), pp. 643–648. doi:10.1007/s00414-017-1649-8.

Atkins, P.W., Jones, L. and Laverman, L. (2016) *Chemical principles : the quest for insight*. Seventh ed. London.

Baby, R.S. (1954) 'Hopewell Cremation Practices', *Papers in Archaeology. Ohio Historical Society*, pp. 1–7.

Bada, J.L. (1991) 'Amino Acid Cosmogeochemistry', *Philosophical transactions. Biological sciences*, 333(1268), pp. 349–358. doi:10.1098/rstb.1991.0084.

Barinov, S.., Rau, J.., Fadeeva, I.., Cesaro, S.N., Ferro, D., Trionfetti, G., Komlev, V.. and Bibikov, V.Y. (2006) 'Carbonate loss from two magnesium-substituted carbonated apatites prepared by different synthesis techniques', *Materials research bulletin*, 41(3), pp. 485–494. doi:10.1016/j.materresbull.2005.09.017.

Bartelink, E.J., Wiersema, J.M. and Demaree, R.S. (2001) 'Quantitative Analysis of Sharp-Force Trauma: An Application of Scanning Electron Microscopy in Forensic Anthropology', *Journal of Forensic Sciences*, 46(6), p. 15148J. doi:10.1520/JFS15148J.

Bartl, R. and Bartl, C. (2016) *Bone disorders : biology, diagnosis, prevention, therapy*. Switzerland: Springer.

Bass, W.M. (1984) 'Is it possible to consume a body completely in a fire?', in Rathbun, T.A. and Buikstra, J.E. (eds) *Human Identification: Case Studies in Forensic Anthropology*. Springfield, MA, pp. 159–167.

Bass, W.M. (2005) *Human Osteology: A Laboratory and Field Manual*. 5th edn. Missouri Archaeological Society.

Bayes, T. (1764) 'An Essay Toward Solving a Problem in the Doctrine of Chances', *Philosophical Transactions of the Royal Society of London*, 53, pp. 370–418.

Beasley, M.M., Bartelink, E.J., Taylor, L. and Miller, R.M. (2014) 'Comparison of transmission FTIR, ATR, and DRIFT spectra: Implications for assessment of bone bioapatite diagenesis', *Journal of Archaeological Science*, 46(1), pp. 16–22. doi:10.1016/j.jas.2014.03.008.

Beckett, S. (2009) *Inter-species variation in bone mineral*. PhD thesis, Cranfield University.

Beckett, S., Rogers, K.D. and Clement, J.G. (2011) 'Inter-species variation in bone mineral behavior upon heating', *Journal of Forensic Sciences*, 56(3), pp. 571–579. doi:10.1111/j.1556-4029.2010.01690.x.

Behrensmeyer, A.K. (1978) 'Taphonomic and ecologic information from bone weathering', *Paleobiology*, 4(2), pp. 150–162. doi:10.1017/S0094837300005820.

Bell, L. S. (2012) 'Histotaphonomy', in Crowder, C. and Stout, S. (eds) *Bone Histology: An Anthropological Perspective*. Boca Raton, FL: Taylor & Francis, pp. 241–251.

Bell, Lynne S. (2012) 'Identifying Postmortem Microstructural Change to Skeletal and Dental Tissues using Backscattered Electron Imaging', in Bell, L.S. (ed.) *Forensic Microscopy for Skeletal Tissues*. Humana Press, pp. 173–190.

Bell, L.S., Skinner, M.F. and Jones, S.J. (1996) 'The speed of post mortem change to the human skeleton and its taphonomic significance', *Forensic Science International*, 82(2), pp. 129–140. doi:10.1016/0379-0738(96)01984-6.

Bell, L S, Boyde, A., Jones, S.J. and Bell, Lynne S (1991) 'Diagenetic Alteration to Teeth In Situ Illustrated by Backscattered Electron Imaging', 13, pp. 173–183.

Bello, S.M. and Soligo, C. (2008) 'A new method for the quantitative analysis of cutmark micromorphology', *Journal of Archaeological Science*, 35(6), pp. 1542–1552. doi:10.1016/j.jas.2007.10.018.

Benbow, E.M. and Pechal, J.L. (2017) 'Approaches and considerations for forensic microbiology decomposition research', in Carter, D.O., Tomberlin, J.K., Benbow, E.M., and Metcalf, J.L. (eds) *Forensic Microbiology*. New York: John Wiley & Sons, Inc, pp. 56–70.

Benmansour, N.Z.R.Z.M. (2012) 'Determination of 210 Pb in human skeletal remains from Morocco : implications for time since death assessment', pp. 315–319. doi:10.1007/s10967-011-1416-0.

Bennett, J.L. (1999) 'Thermal alteration of buried bone', *Journal of Archaeological Science*, 26(1), pp. 1–8. doi:10.1006/jasc.1998.0283.

Bergslien, E.T., Bush, M. and Bush, P.J. (2008) 'Identification of cremains using X-ray diffraction spectroscopy and a comparison to trace element analysis', *Forensic Science International*, 175(2–3), pp. 218–226. doi:10.1016/j.forsciint.2007.07.004.

Berna, F., Matthews, A. and Weiner, S. (2004) 'Solubilities of bone mineral from archaeological sites: the recrystallization window', *Journal of Archaeological Science*, 31(7), pp. 867–882. doi:10.1016/j.jas.2003.12.003.

Berryman, H. and Symes, S.A. (1998) 'Recognizing Gunshot and Blunt Cranial Trauma through Fracture Interpretation', in Reichs, K. (ed.) *Forensic Osteology: Advances in the Identification of Human Remains*. 2nd edn. Springfield, IL, pp. 333–353.

Bigi, A., Foresti, E., Gandolfi, M., Gazzano, M. and Roveri, N. (1995) 'Inhibiting effect of zinc on hydroxylapatite crystallization', *Journal of Inorganic Biochemistry*, 58(1), pp. 49–58. doi:10.1016/0162-0134(94)00036-A.

Binford, L.R. (1963) 'An analysis of cremations from three Michigan sites', *Wisconsin Archaeologist*, 44, pp. 98–110.

Boaks, A., Siwek, D. and Mortazavi, F. (2014) 'The temporal degradation of bone collagen:

A histochemical approach', *Forensic Science International*, 240, pp. 104–110. doi:10.1016/j.forsciint.2014.04.008.

Bonney, H., Colston, B.. and Goodman, A.. (2011) 'Regional variation in the mechanical properties of cortical bone from the porcine femur', *Medical Engineering and Physics*, 33(4), pp. 513–520. doi:10.1016/j.medengphy.2010.12.002.

Bonnichsen, R. (1979) *Pleistocene Bone Technology in the Beringian Refugium*. Ottawa: National Museums of Canada: Mercury Series.

Bontrager, A.B. and Nawrocki, S.P. (2008) 'A Taphonomic Analysis of Human Cremains from the Fox Hollow Farm Serial Homicide Site', in Schmidt, C.W. and Symes, S.A. (eds) *The Analysis of Burned Human Remains*. Elsevier Ltd/Academic, pp. 211–226. doi:10.1016/B978-0-12-800451-7.00013-9.

Booth, T.J. (2016) 'An Investigation Into the Relationship Between Funerary Treatment and Bacterial Bioerosion in European Archaeological Human Bone', *Archaeometry*, 58(3), pp. 484–499. doi:10.1111/arcm.12190.

Booth, T.J. and Brück, J. (2020) 'Death is not the end: radiocarbon and histo-taphonomic evidence for the curation and excarnation of human remains in Bronze Age Britain', *Antiquity*, 94(377), pp. 1186–1203. doi:10.13184/aqy.2020.132.

Booth, T.J. and Madgwick, R. (2016) 'New evidence for diverse secondary burial practices in Iron Age Britain: A histological case study', *Journal of Archaeological Science*, 67, pp. 14–24. doi:10.1016/j.jas.2016.01.010.

Boskey, A.L. and Coleman, R. (2010) 'Critical reviews in oral biology & medicine: Aging and bone', *Journal of Dental Research*, 89(12), pp. 1333–1348. doi:10.1177/0022034510377791.

Bowler, J.M., Rhys, J., Allen, H. and Thorne, A.G. (1970) 'Pleistocene human remains from Australia: A living site and human cremation from Lake Mungo, western New South Wales', *World Archaeology*, 2(1), pp. 39–60.

Bradtmiller, B. and Buikstra, J.E. (1984) 'Effects of burning on human bone microstructure: a preliminary study', *Journal of Forensic Sciences*, 29(2), pp. 535–40.

Bravenec, A.D., Ward, K.D. and Ward, T.J. (2018) 'Amino acid racemization and its relation to geochronology and archaeometry', *Journal of separation science*, 41(6), pp. 1489–1506. doi:10.1002/jssc.201701506.

Brock, F., Geoghegan, V., Thomas, B., Jurkschat, K. and Higham, T. (2013) 'Analysis of bone "collagen" extraction products for radiocarbon dating', *Radiocarbon*, 55, pp. 445–463. doi:10.2458/azu_js_rc.55.16304.

Brock, F., Higham, T., Ditchfield, P. and Ramsey, C.B. (2010) 'Current Pretreatment Methods for AMS Radiocarbon Dating at the Oxford Radiocarbon Accelerator Unit (Orau)', *Radiocarbon*, 52(1), pp. 103–112. doi:10.1017/S0033822200045069.

Brönnimann, D., Portmann, C., Pichler, S.L., Booth, T.J., Röder, B., Vach, W., Schibler, J. and Rentzel, P. (2018) 'Contextualising the dead – Combining geoarchaeology and osteo-anthropology in a new multi-focus approach in bone histotaphonomy', *Journal of Archaeological Science*, 98, pp. 45–58. doi:10.1016/j.jas.2018.08.005.

Brown, W.E. and Chow, L.C. (1976) 'Chemical Properties of Bone Mineral', *Annual review*

of materials science, 6(1), pp. 213–236. doi:10.1146/annurev.ms.06.080176.001241.

Buikstra, J.E. and Swegle, M. (1989) 'Bone modification due to burning: experimental evidence', in Bonnichsen, R. and Sorg, M. (eds) *Bone modification*. College Station, TX: The Centre for the Study of the First Americans, pp. 247–58.

Burr, D.B. and Allen, M.R. (2014) *Basic and Applied Bone Biology*. London: Waltham, MA.

Bushinsky, D.A., Gavrilov, K.L., Chabala, J.M. and Levi-Setti, R. (2000) 'Contribution of Organic Material to the Ion Composition of Bone', *Journal of bone and mineral research*, 15(10), pp. 2026–2032. doi:10.1359/jbmr.2000.15.10.2026.

Byers, S. (2007) *Introduction to Forensic Anthropology*. 3rd edn. Boston, MA: Pearson Education INC.

Byrnes, J.F. and Bush, P.J. (2016) 'Practical Considerations in Trace Element Analysis of Bone by Portable X-ray Fluorescence', *Journal of forensic sciences*, 61(4), pp. 1041–1045. doi:10.1111/1556-4029.13103.

Cambra-Moo, O., Barroso Bermejo, R., García Gil, O., Bueno Ramírez, P., Rascón Pérez, J., González Martín, A., de Balbín Behrmann, R., Booth, T.J., Jans, M.M.E., Kars, H., Nielsen-Marsh, C.M., Smith, C.I., Nord, A.G., Arthur, P., Earl, N., *et al.* (2017) 'The Effect of Soft Tissue on Temperature Estimation from Burnt Bone Using Fourier Transform Infrared Spectroscopy', *Journal of Forensic Sciences*, 35(1), pp. 1–8. doi:10.1038/s41598-018-34376-w.

De Campos Vidal, B. and Mello, M.L.S. (2011) 'Collagen type I amide I band infrared spectroscopy', *Micron*, 42(3), pp. 283–289. doi:10.1016/j.micron.2010.09.010.

Carlson, W.D., Donelick, R.A. and Ketcham, R.A. (1999) 'Variability of apatite fission-track annealing kinetics: I. Experimental results', *American Mineralogist*, 84, pp. 1213–1223.

Carr, G. (2007) 'Excarnation to cremation: continuity or change?', in Haselgrove, C. and Moore, T. (eds) *The Later Iron Age in Britain and Beyond*. Oxford: Oxbow, pp. 446–455.

Carr, G. and Knüsel, C. (1997) 'The ritual framework of excarnation by exposure as the mortuary practice of the early and middle Iron Ages of central southern Britain', in Gwilt, A. and Haselgrove, C. (eds) *Reconstructing Iron Age societies: new approaches to the British Iron Age*. Oxford: Oxbow Books, pp. 167–173.

Carroll, E.L. and Squires, K.E. (2020) 'Burning by numbers: A pilot study using quantitative petrography in the analysis of heatвЂђinduced alteration in burned bone', *International journal of osteoarchaeology*, 30(5), pp. 691–699. doi:10.1002/oa.2902.

Caruso, V., Marinoni, N., Diella, V., Berna, F., Cantaluppi, M., Mancini, L., Trombino, L., Cattaneo, C., Pastero, L. and Pavese, A. (2020) 'Bone diagenesis in archaeological and contemporary human remains: an investigation of bone 3D microstructure and minero-chemical assessment', *Archaeological and Anthropological Sciences*, 12(8), p. 162. doi:10.1007/s12520-020-01090-6.

Castaing, R. (1951) *Application of electron probes to local chemical and crystallographic analysis*. University of Paris [English translation by Duwez, P and Wittry DB, California Institute of Technology, 1955].

Cattaneo, C., DiMartino, S., Scali, S., Craig, O.E., Grandi, M. and Sokol, R.J. (1999) 'Determining the human origin of fragments of burnt bone: A comparative study of

histological, immunological and DNA techniques', *Forensic Science International*, 102(2–3), pp. 181–191. doi:10.1016/S0379-0738(99)00059-6.

Chesterman, J.T. (1979) 'Investigation of the human bones from Quanterness', in Renfrew, C. (ed.) *Investigations in Orkney*. London: The Society of Antiquaries of London, pp. 97–111.

Child, A.. (1995) 'Towards and Understanding of the Microbial Decomposition of Archaeological Bone in the Burial Environment', *Journal of Archaeological Science*, 22(2), pp. 165–174. doi:10.1006/jasc.1995.0018.

Clark, J.L. and Ligouis, B. (2010) 'Burned bone in the Howieson's Poort and post-Howieson's Poort Middle Stone Age deposits at Sibudu (South Africa): behavioral and taphonomic implications', *Journal of archaeological science*, 37(10), pp. 2650–2661. doi:10.1016/j.jas.2010.06.001.

Cleland, T.P., Schroeter, E.R. and Schweitzer, M.H. (2015) 'Biologically and diagenetically derived peptide modifications in moa collagens', *Proceedings of the Royal Society. B, Biological sciences*, 282(1808), pp. 1–6. doi:10.1098/rspb.2015.0015.

Collins, M.J., Nielsen–Marsh, C.M., Hiller, J., Smith, C.I., Roberts, J.P., Prigodich, R. V., Wess, T.J., Csapò, J., Millard, A.R. and Turner–Walker, G. (2002) 'The survival of organic matter in bone: a review', *Archaeometry*, 44(3), pp. 383–394. doi:10.1111/1475-4754.t01-1-00071.

Collins, M.J., Riley, M.S., Child, A.M. and Turner-Walker, G. (1995) 'A Basic Mathematical Simulation of the Chemical Degradation of Ancient Collagen', *Journal of Archaeological Science*, 22, pp. 175–183.

Cooney, G. (2014) 'The Role of Cremation in Mortuary Practice in the Irish Neolithic', in Kuijit, I. (ed.) *Transformation by Fire: The Archaeology of Cremation in Cultural Context. Amerind Studies in Archaeology*. University of Arizona Press, pp. 189–206.

Cressey, M., Sheridan, A., Church, M., Gabra-, T., Mckinley, J., Northover, P. and Warren, G. (2003) 'The excavation of a Bronze Age cemetery at Seafield', 133, pp. 47–84.

Crowder, C., Rainwater, C.W. and Fridie, J.S. (2013) 'Microscopic analysis of sharp force trauma in bone and cartilage: A validation study', *Journal of Forensic Sciences*, 58(5), pp. 1119–1126. doi:10.1111/1556-4029.12180.

Crowder, C. and Stout, S.D. (2011) 'Bone histology : an anthropological perspective'. Boca Raton: CRC Press (Taylor & Francis eBooks).

Currey, J.D. (2002) *Bones: structure and mechanics*. Princeton. Princeton.

Daniel, J.C. and Chin, K. (2010) 'The role of bacterial mediated precipiration in the permineralization of bone', *PALAIOS*. SEPM (Society for Sedimentary Geology), pp. 507–516. doi:10.2110/palo.2009.p09-120r.

Daniells, M.J., Williams, B.B. and Larmour, R.A. (1977) 'Excavations at Kiltierney Deerpark, County Fermanagh', *Ulster journal of archaeology*, 40, pp. 32–41.

Danilchenko, S.N., Kalinkevich, A.N., Moskalenko, R.A., Kuznetsov, V.N., Kochenko, A. V, Husak, E. V, Starikov, V. V, Fuyan, L.I.., Meng, J. and Jinjun, L.. (2018) 'Structural and crystal-chemical characteristics of the apatite deposits from human aortic walls', *Interventional medicine and applied science*, 10(2), pp. 110–119.

doi:10.1556/1646.10.2018.24.

Danilchenko, S.N., Pokrovskiy, V.A., Bogatyrov, V.M., Sukhodub, L.F. and Sulkio-Cleff, B. (2005) 'Carbonate location in bone tissue mineral by X-ray diffraction and temperature-programmed desorption mass spectrometry', *Crystal research and technology (1979)*, 40(7), pp. 692–697. doi:10.1002/crat.200410410.

DeHaan, J.D. (2002) *Kirk's fire Investigation*. fifth edit. Upper Saddle River: NJ: Prentice Hall.

DeHaan, J.D. (2012) 'Sustained Combustion of Bodies: Some Observations', *Journal of forensic sciences*, 57(6), pp. 1578–1584. doi:10.1111/j.1556-4029.2012.02190.x.

DeHaan, J.D., Campbell, S.J. and Nurbakhsh, S. (1999) 'Combustion of animal fat and its implications for the consumption of the fire', *Sci Justice*, 39(1), pp. 27–38.

Delgado-López, J.M., Iafisco, M., Rodríguez, I., Tampieri, A., Prat, M. and Gómez-Morales, J. (2012) 'Crystallization of bioinspired citrate-functionalized nanoapatite with tailored carbonate content', *Acta biomaterialia*, 8(9), pp. 3491–3499. doi:10.1016/j.actbio.2012.04.046.

Demarchi, B., Hall, S., Roncal-Herrero, T., Freeman, C.L., Woolley, J., Crisp, M.K., Wilson, J., Fotakis, A., Fischer, R., Kessler, B., Rakownikow Jersie-Christensen, R., Olsen, J. V., Haile, J., Thomas, J., Marean, C.W.M., *et al.* (2016) 'Protein sequences bound to mineral surfaces persist into deep time.', *eLife*, 5, p. e17092. doi:10.7554/eLife.17092.

Devlin, J.B. and Herrmann, N.P. (2008) 'Bone colour as an interpretive tool of the depositional history of archaeological cremains', in Schmidt, C.W. and Symes, S.A. (eds) *The Analysis of Burned Human Remains*. Elsevier Ltd., pp. 109–128.

Devlin, J.B. and Herrmann, N.P. (2015) 'Bone Color as an Interpretive Tool of the Depositional History of Archaeological Cremains', in Schmidt, C. and Symes, S.A. (eds) *The Analysis of Burned Human Remains*. 2nd edn, pp. 109–128.

Dibble, H., Berna, F., Goldberg, P., McPherron, S., Mentzer, S., Niven, L., Richter, D., Sandgathe, D., Théry-Parisot, I. and Turq, A. (2009) 'A Preliminary Report on Pech de l'Azé IV, Layer 8 (Middle Paleolithic, France)', *Paleoanthropology*, 7(3), pp. 182–219. doi:10.4207/pa.2008.art30.

Dirkmaat, G.C., Olson, G.O., Klales, A.R. and Getz, S. (2012) 'The role of forensic anthropology in the recovery and interpretation of the fatal-fire victim', in Dirkmaat, D.C. (ed.) *A Companion to Forensic Anthropology*. John Wiley & Sons, Inc., pp. 113–135.

Dorozhkin, S. V and Epple, M. (2002) 'Biological and Medical Significance of Calcium Phosphates', *Angewandte Chemie (International ed.)*, 41(17), pp. 3130–3146. doi:10.1002/1521-3773(20020902)41:17<3130::AID-ANIE3130>3.0.CO;2-1.

Dorset, D.L. (1998) 'X-ray Diffraction: A Practical Approach', *Microscopy and Microanalysis*, 4(5), pp. 513–515.

Dowd, M.A. (2008) 'The use of caves for funerary and ritual practices in Neolithic Ireland', *Antiquity*, 82, pp. 305–317.

Dowd, M.A. (2015) *The Archaeology of Caves in Ireland*. Oxbow Books. Available at: http://ebookcentral.proquest.com/lib/oxford/detail.action?docID=2167185.

Dowker, S.E.P. and Elliott, J.C. (1979) 'Infrared adsorption bands from NCO- and NCN2- in heated carbonate-containing apatites prepared in the presence of NH4 + ions', *Calcified Tissue International*, 29, pp. 177–178.

van Duin, A.C.. and Collins, M.J. (1998) 'The effects of conformational constraints on aspartic acid racemization', *Organic geochemistry*, 29(5), pp. 1227–1232. doi:10.1016/S0146-6380(98)00098-9.

Ellingham, S.T.D., Thompson, T.J.U. and Islam, M. (2016) 'The Effect of Soft Tissue on Temperature Estimation from Burnt Bone Using Fourier Transform Infrared Spectroscopy', *Journal of Forensic Sciences*, 61(1), pp. 151–159.

Ellingham, S.T.D., Thompson, T.J.U. and Islam, M. (2018) 'Scanning Electron Microscopy–Energy-Dispersive X-Ray (SEM/EDX): A Rapid Diagnostic Tool to Aid the Identification of Burnt Bone and Contested Cremains', *Journal of Forensic Sciences*, 63(2), pp. 504–510. doi:10.1111/1556-4029.13541.

Ellingham, S.T.D., Thompson, T.J.U., Islam, M. and Taylor, G. (2015) 'Estimating temperature exposure of burnt bone - A methodological review', *Science and Justice*, 55(3), pp. 181–188. doi:10.1016/j.scijus.2014.12.002.

Elliott, J.C. (2002) 'Calcium phosphate biominerals', in Kohn, M.J., Rakovan, J., and Hughes, J.M. (eds) *Phosphates: Geochemical, Geobiological and Material Importance, Reviews in Mineralogy and Geochemistry, vol. 48, Mineralogical Society of America*. Washington, DC, pp. 427–454.

Elston, P. (2019) *Relationship between Collagen and Mineral in Bone Adapted for Different Biological Function*. dissertation. UCL (University College London).

Emanovsky, P., Hefner, J.T. and Dirkmaat, D.C. (2002) 'Can Sharp Force Trauma To Bone Be Recognized After Fire Modification? An Experiment Using Odocoileus virginianus (White-Tailed Deer) Ribs', in *54th Annual Meeting of the American Academy of Forensic Sciences*. Atlanta, GA, pp. 1–4.

Etok, S., Valsami-Jones, E., Wess, T., Hiller, J., Maxwell, C., Rogers, K., Manning, D., White, M., Lopez-Capel, E., Collins, M., Buckley, M., Penkman, K. and Woodgate, S. (2007) 'Structural and chemical changes of thermally treated bone apatite', *Journal of Materials Science*. Boston: Springer US, pp. 9807–9816. doi:10.1007/s10853-007-1993-z.

Etxeberria, F. (1994) 'Aspectos macroscópicos del hueso sometido al fuego: revisión de las cremaciones descritas en el País Vasco desde la arqueologia', *Munibe*, 46, pp. 111–116.

Evans, G. (1991) 'Reform or Revolution in Heaven? Funerals among Upland Tai', *The Australian journal of anthropology*, 2(1), pp. 81–97. doi:10.1111/j.1835-9310.1991.tb00128.x.

Ezzo, J.A. (1994) 'Putting the chemistry back into archaeological bone chemistry analysis -- modeling potential palaeodietary indicators', *J. Anth. Arch.*, 13, pp. 1–34.

Fadeev, I. V., Shvorneva, L.I., Barinov, S.M. and Orlovskii, V.P. (2003) 'Synthesis and Structure of Magnesium-Substituted Hydroxyapatite', *Inorganic Materials*, 9, pp. 1102–1105.

Fairgrieve, S.I. (2008) *Forensic Cremation Recovery and Analysis*. Boca Raton, FL: CRC Press.

Falk, M.L. (2010) 'Recovery and Buddhist practices in the aftermath of the Tsunami in Southern Thailand', *Religion (London. 1971)*, 40(2), pp. 96–103. doi:10.1016/j.religion.2009.12.002.

Farmer, A. (1995) 'Soil chemistry change in a lowland english deciduous Woodland 1974–1991', *Water, Air, and Soil Pollution*, 85(2), pp. 677–682. doi:10.1007/BF00476907.

El Feki, H., Rey, C. and Vignoles, M. (1991) 'Carbonate ions in apatites: Infrared investigations in the v4 CO3 domain', *Calcified Tissue International*, 49(4), pp. 269–274. doi:10.1007/BF02556216.

Feng, L. and Jasiuk, I. (2011) 'Multi-scale characterization of swine femoral cortical bone', *Journal of Biomechanics*, 44(2), pp. 313–320. doi:10.1016/j.jbiomech.2010.10.011.

Fernández-Jalvo, Y. and Andrews, P. (2016) *Atlas of taphonomic identifications : 1001+ images of fossil and recent mammal bone modification*. Dordrecht (Vertebrate paleobiology and paleoanthropology).

Fernández-Jalvo, Y., Andrews, P., Pesquero, D., Smith, C., Marín-monfort, D., Sánchez, B., Geigl, E. and Alonso, A. (2010) 'Early bone diagenesis in temperate environments Part I : Surface features and histology', *Palaeogeography, Palaeoclimatology, Palaeoecology*, 288(1–4), pp. 62–81. doi:10.1016/j.palaeo.2009.12.016.

Fernández Castillo, R., Ubelaker, D.H., Acosta, J.A.L., de la Rosa, R.J.E. and Garcia, I.G. (2013) 'Effect of Temperature on Bone Tissue: Histological Changes', *Journal of Forensic Sciences*, 58(3), pp. 578–582. doi:10.1111/1556-4029.12093.

Fitzgerald, E.R. (1977) 'Postmortem transition in the dynamic mechanical properties of bone', *Medical physics (Lancaster)*, 4(1), pp. 49–53. doi:10.1118/1.594383.

Fitzpatrick, A.P. and Powell, A.B. (1997) *Archaeological excavations on the route of the A27 Westhampnett bypass, West Sussex, 1992*. Salisbury: Trust for Wessex Archaeology (Wessex Archaeology report ; nos. 12, 21).

Forbes, S.L., Stuart, B.H. and Dent, B.B. (2005) 'The effect of the method of burial on adipocere formation', *Forensic Science International*, 154(1), pp. 44–52. doi:10.1016/j.forsciint.2004.09.109.

Fredericks, J.D., Bennett, P., Williams, A. and Rogers, K.D. (2012) 'FTIR spectroscopy: A new diagnostic tool to aid DNA analysis from heated bone', *Forensic Science International: Genetics*, 6(3), pp. 375–380. doi:10.1016/j.fsigen.2011.07.014.

Gallello, G., Kuligowski, J., Pastor, A., Diez, A. and Bernabeu, J. (2013) 'Biological mineral content in Iberian skeletal cremains for control of diagenetic factors employing multivariate statistics', *Journal of archaeological science*, 40(5), pp. 2477–2484. doi:10.1016/j.jas.2013.01.022.

Gallo, G., Fyhrie, M., Paine, C., Ushakov, S. V, Izuho, M., Gunchinsuren, B., Zwyns, N. and Navrotsky, A. (2021) 'Characterization of structural changes in modern and archaeological burnt bone: Implications for differential preservation bias', *PloS one*, 16(7), pp. e0254529–e0254529. doi:10.1371/journal.pone.0254529.

Galloway, A., Zephro, L. and Wedel, V.L. (2014) 'Diagnostic Criteria for the Determination of Timing and Fracture Mechanism', in Wedel, V.L. (ed.) *Broken Bones: Anthropological Analysis of Blunt Force Trauma*. Springfield, IL: Charles C Thomas, pp. 47–59.

Garland, A.N. (1987) ‘A histological study of archaeological bone decomposition’, in Boddington, A., Garlands, A.N., and Janaway, R.C. (eds) *Death, Decay, and Reconstruction: Approaches to Archaeology and Forensic Science*. Manchester: Manchester University Press, pp. 109–126.

Garrido-Varas, C. and Intriago-Leiva, M. (2015) ‘The interpretation and reconstruction of the post-mortem events in a case of scattered burned remains in Chile’, in Thompson, T. (ed.) *The Archaeology of Cremation: burned human remains in funerary studies*. Havertown: Oxbow Books, pp. 227–242.

Gejvall, N.G. (1947) *Bestamning av brända ben franforntida graver, Fornvannen*. Stockholm: H.I.

Gerakines, P.A., Schutte, W.A., Greenberg, J.M. and Dishoeck, E.F. (1995) ‘The infrared band strengths of H2O, CO and CO2 in laboratory simulations of astrophysical ice mixtures’, *Astronomy and Astrophysics*, 296, pp. 810–818.

Ghadimi, E., Eimar, H., Marelli, B., Nazhat, S.N., Asgharian, M., Vali, H. and Tamimi, F. (2013) ‘Trace elements can influence the physical properties of tooth enamel’, *SpringerPlus*, 2(1), pp. 1–12. doi:10.1186/2193-1801-2-499.

Gibson, I., Rehman, I., Best, S. and Bonfield*, W. (2002) ‘Characterization of the transformation from calcium-deficient apatite to β-tricalcium phosphate’, *Journal of Materials Science: Materials in Medicine*, 11(12), pp. 799–804. doi:10.1023/A:1008905613182.

Goldstein, J.I., Newbury, D.E., Echlin, P., Joy, D.C., Lyman, C.E., Lifshin, E., Sawyer, L. and Michael, J.R. (2003) *Scanning Electron Microscopy and X-Ray Microanalysis*. New York: Kluwer Academic.

Gonçalves, D. (2012) ‘The micro-analysis of human burned bones: some remarks’, *Cuadernos do GEEvH*, 1(September), pp. 32–40. Available at: https://estudogeral.sib.uc.pt/handle/10316/21101.

Gonçalves, D., Thompson, T.J.U. and Cunha, E. (2011) ‘Implications of heat-induced changes in bone on the interpretation of funerary behaviour and practice’, *Journal of Archaeological Science*, 38(6), pp. 1308–1313. doi:10.1016/j.jas.2011.01.006.

Gonzalez-Rodriguez, J. and Fowler, G. (2013) ‘A study on the discrimination of human skeletons using X-ray fluorescence and chemometric tools in chemical anthropology’, *Forensic science international*, 231(1), pp. 407.e1-407.e6. doi:10.1016/j.forsciint.2013.04.035.

Goodman, D. (2001) ‘Encyclopedia of Analytical Chemistry: Applications, Theory, and Instrumentation’, *CHOICE: Current Reviews for Academic Libraries*, 39(2), p. 287.

Greenwood, C., Rogers, K., Beckett, S. and Clement, J. (2013) ‘Initial observations of dynamically heated bone’, *Crystal Research and Technology*, 48(12), pp. 1073–1082. doi:10.1002/crat.201300254.

Grévin, G., Baud, C. and Susini, A. (1991) ‘Etude anthropologique et paléopathologique d ’ un adulte inhumé puis incinéré provenant du site de Pincevent (Seine-et-Marne)’, pp. 77–87.

Griffin, R.., Chamberlain, A.., Hotz, G., Penkman, K.E.. and Collins, M.. (2009) ‘Age estimation of archaeological remains using amino acid racemization in dental enamel: A comparison of morphological, biochemical, and known ages-at-death’, *American Journal of*

Physical Anthropologynthropology, 140(2), pp. 244–252. doi:10.1002/ajpa.21058.

Grine, F.E., Bromage, T.G., Daegling, D.J., Burr, D.B. and Brain, C.K. (2015) 'Microbial osteolysis in an Early Pleistocene hominin (Paranthropus robustus) from Swartkrans , South Africa', *Journal of Human Evolution*, 85, pp. 126–135. doi:10.1016/j.jhevol.2015.05.004.

Grunenwald, A., Keyser, C., Sautereau, A.., Crubézy, E., Ludes, B. and Drouet, C. (2014) 'Revisiting carbonate quantification in apatite (bio)minerals: a validated FTIR methodology', *Journal of Archaeological Science*, 49, pp. 134–141. doi:10.1016/j.jas.2014.05.004.

Grupe, G. (1988) 'Impact of the Choice of Bone Samples on Trace Element Data in Excavated Human Skeletons', *Journal of Archaeological Science*, 15(2), pp. 123–129.

Grupe, G. and Hummel, S. (1991) 'Trace element studies on experimentally cremated bone. I. Alteration of the chemical composition at high temperatures', *Journal of Archaeological Science*, 18(2), pp. 177–186. doi:10.1016/0305-4403(91)90046-R.

Guizzardi, S., Raspanti, M., Martini, D., Scandroglio, R., Govoni, P. and Ruggeri, A. (1995) 'Low-temperature heat-deproteinated compact bone to heal large bone defects', *Biomaterials*, 16(12), pp. 931–936. doi:10.1016/0142-9612(95)93118-W.

Gulmine, J. V. and Akcelrud, L. (2006) 'Correlation between structure and accelerated artificial ageing of XLPE', *European Polymer Journal*, 42, pp. 553–562.

Haberko, K., Bućko, M.M., Brzezińska-Miecznik, J., Haberko, M., Mozgawa, W., Panz, T., Pyda, A. and Zarębski, J. (2006) 'Natural hydroxyapatite—its behaviour during heat treatment', *Journal of the European Ceramic Society*, 26(4), pp. 537–542. doi:10.1016/j.jeurceramsoc.2005.07.033.

Hackett, C.J. (1981) 'Microscopial Focal Destruction (Tunnels) in Exhumed Human Bones', *Medicine, Science and the Law*, 21(4), pp. 243–265. doi:10.3868/s050-004-015-0003-8.

Haghighi, P. (1989) 'Structure, function and adaptation of compact bone', *Skeletal Radiology*, pp. 506–506. doi:10.1007/BF00351748.

Haglund, W.D. and Sorg, M.H. (2006) *Forensic taphonomy : the postmortem fate of human remains*. Boca Raton.

Hanson, M. and Cain, C.R. (2007) 'Examining histology to identify burned bone', *Journal of Archaeological Science*, 34(11), pp. 1902–1913. doi:10.1016/j.jas.2007.01.009.

Harbeck, M. and Grupe, G. (2009) 'Experimental chemical degradation compared to natural diagenetic alteration of collagen: Implications for collagen quality indicators for stable isotope analysis', *Archaeological and Anthropological Sciences*, 1(1), pp. 43–57. doi:10.1007/s12520-009-0004-5.

Hedges, R.E.., Millard, A.R. and Pike, A.W.. (1995) 'Measurements and Relationships of Diagenetic Alteration of Bone from Three Archaeological Sites', *Journal of Archaeological Science*, 22(2), pp. 201–209. doi:10.1006/jasc.1995.0022.

Hedges, R.E.M. and Millard, A.R. (1995) 'Bones and Groundwater: Towards the Modelling of Diagenetic Processes', *Journal of Archaeological Science*, 22(2), pp. 155–164. doi:10.1006/jasc.1995.0017.

Hendy, J. (2021) 'Ancient protein analysis in archaeology', *Science Advances*, 7(3), pp. 1–12. doi:10.1126/sciadv.abb9314.

Herrmann, B. (1976) ‘Neuere Ergebnisse zur Beurteilung menschilcher Brandknochen’, *Z. Rechtsmedizin*, 17, pp. 191–200.

Herrmann, B. (1977) ‘On histological investigations of cremated human remains’, *Journal of Human Evolution*, 6(2), pp. 101–103. doi:10.1016/S0047-2484(77)80112-7.

Herrmann, N.P. and Bennett, J.L. (1999) ‘The Differentiation of Traumatic and Heat-Related Fractures in Burned Bone’, *Journal of Forensic Sciences*, 44(3), p. 14495J. doi:10.1520/JFS14495J.

Hidouri, M., Dorozhkin, S. and Albeladi, N. (2019) ‘Thermal Behavior, Sintering and Mechanical Characterization of Multiple Ion-Substituted Hydroxyapatite Bioceramics’, *Journal of Inorganic and Organometallic Polymers and Materials*, 29(1), pp. 87–100. doi:10.1007/s10904-018-0969-6.

High, K., Milner, N., Panter, I. and Penkman, K.E.. (2015) ‘Apatite for destruction: investigating bone degradation due to high acidity at Star Carr’, *Journal of Archaeological Science*, 59, pp. 159–168. doi:10.1016/j.jas.2015.04.001.

Hiller, J.C., Thompson, T.J.U., Evison, M.P., Chamberlain, A.T. and Wess, T.J. (2003) ‘Bone mineral change during experimental heating: An X-ray scattering investigation’, *Biomaterials*, 24(28), pp. 5091–5097. doi:10.1016/S0142-9612(03)00427-7.

Holcomb, D.W. and Younger, R.A. (1980) ‘Thermal decomposition of human tooth enamel’, *Calcified Tissue International*, 31(1), pp. 198–201.

Holden, J.L., Clement, J.G. and Phakey, P.P. (1995) ‘Age and temperature related changes to the ultrastructure and composition of human bone mineral’, *Journal of Bone and Mineral Research*, 10(9), pp. 1400–1409. doi:10.1002/jbmr.5650100918.

Holden, J.L., Phakey, P.P. and Clement, J.G. (1995) ‘Scanning electron microscope observations of heat-treated human bone’, *Forensic Science International*, 74(1), pp. 29–45. doi:10.1016/0379-0738(95)01735-2.

Hollund, H.I., Ariese, F., Fernandes, R., Jans, M.M.E. and Kars, H. (2012) ‘Testing an alternative high-throughput tool for investigating bone diagenesis: FTIR in Attenuated Total Reflection (ATR) mode’, *Archaeometry*, 55(3), pp. 507–532. doi:10.1111/j.1475-4754.2012.00695.x.

Hollund, H.I., Jans, M.M.E. and Kars, H. (2014) ‘How are teeth better than bone ? An investigation of dental tissue diagenesis and state of preservation at a histological scale (with photo catalogue)’, *Internet Archaeology*, 36.

Hotelling, H. (1933) ‘Analysis of a complex of statistical attributes into principal components’, *Journal of Educational Psychology*, 24, pp. 417–441.

Howes, J.M., Stuart, B.H., Thomas, P.S., Raja, S. and O’Brien, C. (2012) ‘An Investigation of Model Forensic Bone in Soil Environments Studied Using Infrared Spectroscopy’, *Journal of Forensic Sciences*, 57(5), pp. 1161–1167. doi:10.1111/j.1556-4029.2012.02236.x.

Hu, Y., Ambrose, S.H. and Wang, C. (2006) ‘Stable isotopic analysis of human bones from Jiahu site, Henan, China: implications for the transition to agriculture’, *Journal of Archaeological Science*, 33(9), pp. 1319–1330. doi:10.1016/j.jas.2006.01.007.

Huisman, D.J., Raemaekers, D.C.M. and Jongsmans, A.G. (2009) ‘Investigating Early Neolithic land use in Swifterbant (NL) using micromorphological techniques’, *Catena*, 78(3),

pp. 185–197.

Huisman, H., Ismail-Meyer, K., Sageidet, B.M. and Joosten, I. (2017) 'Micromorphological indicators for degradation processes in archaeological bone from temperate European wetland sites', *Journal of Archaeological Science*, 85(C), pp. 13–29. doi:10.1016/j.jas.2017.06.016.

Hummel, S. and Schutkowski, H. (1993) 'Bedeutungen für die Leichenbranddiagnose. Mit 4 Abbildungen und 1 Tabelle im Text', *Zeitschrift für Morphologie und Anthropologie*. Stuttgart: E. Schweizerbart'sche Verlagsbuchhandlung, pp. 1–9.

Imaizumi, K., Taniguchi, K. and Ogawa, Y. (2014) 'DNA survival and physical and histological properties of heat-induced alterations in burnt bones', *International Journal of Legal Medicine*. Berlin/Heidelberg: Springer Berlin Heidelberg, pp. 439–446. doi:10.1007/s00414-014-0988-y.

Jacob, E., Querci, D., Caparros, M., Barroso Ruiz, C., Higham, T. and Devièse, T. (2018) 'Nitrogen content variation in archaeological bone and its implications for stable isotope analysis and radiocarbon dating', *Journal of Archaeological Science*, 93, pp. 68–73. doi:10.1016/j.jas.2018.02.019.

Jans, M. (2008) 'Microbial bioerosion of bone - a review', in Wisshak, M. and Tapanila, L. (eds) *Current Developments in Bioerosion*. Berlin, Heidelberg: Springer, pp. 397–493.

Jans, M.M.E. (2005) *Histological Characterisation of Diagenetic Alteration of Archaeological Bone*. PhD thesis, Vrije Universiteit Amsterdam.

Jans, M.M.E. (2013) 'Microscopic destruction of bone', in Pokines, J.T. and Symes, S.A. (eds) *Manual of Forensic Taphonomy*. CRC Press, Taylor & Francis group, pp. 19–35.

Jans, M.M.E., Kars, H., Nielsen-Marsh, C.M., Smith, C.I., Nord, A.G., Arthur, P. and Earl, N. (2002) 'In Situ Preservation of Archaeological Bone: a Histological Study Within a Multidisciplinary Approach', *Archaeometry*, 44, pp. 343–352.

Jans, M.M.E., Nielsen-Marsh, C.M., Smith, C.I., Collins, M.J. and Kars, H. (2004) 'Characterisation of microbial attack on archaeological bone', *Journal of Archaeological Science*, 31(1), pp. 87–95. doi:10.1016/j.jas.2003.07.007.

Jochum, K.P., Stoll, B., Herwig, K., Willbold, M., Hofmann, A.W., Amini, M., Aarburg, S., Abouchami, W., Hellebrand, E., Mocek, B., Raczek, I., Stracke, A., Alard, O., Bouman, C., Becker, S., *et al.* (2006) 'MPI-DING reference glasses for in situ microanalysis: New reference values for element concentrations and isotope ratios', *Geochemistry, Geophysics, Geosystems*, 7(2), p. Q02008. doi:10.1029/2005GC001060.

Johnson, B.J. and Miller, G.H. (1997) 'Archaeological Applications of Amino Acid Racemization', *Archaeometry*, 39(2), pp. 265–287. doi:10.1111/j.1475-4754.1997.tb00806.x.

Johnson, E. (1985) 'Current Developments in Bone Technology', *Advances in Archaeological Method and Theory*, 8, pp. 157–235.

Kahne, D. and Still, W.C. (1988) 'Hydrolysis of a Peptide Bond in Neutral Water', *Journal of the American Chemical Society*, 110(22), pp. 7529–7534.

Karunadasa, K.S.., Manoratne, C.., Pitawala, H.M.T.G.. and Rajapakse, R.M.. (2019) 'Thermal decomposition of calcium carbonate (calcite polymorph) as examined by in-situ high-temperature X-ray powder diffraction', *The Journal of Physics and Chemistry of Solids*, 134, pp. 21–28. doi:10.1016/j.jpcs.2019.05.023.

Keenan, S.W. (2016) 'From bone to fossil: A review of the diagenesis of bioapatite', *American Mineralogist*, 101(9), pp. 1943–1951. doi:10.2138/am-2016-5737.

Keenan, S.W. and Engel, A.S. (2017a) 'Early diagenesis and recrystallization of bone', *Geochimica et Cosmochimica Acta*, 196, pp. 209–223. doi:10.1016/j.gca.2016.09.033.

Keenan, S.W. and Engel, A.S. (2017b) 'Reconstructing diagenetic conditions of bone at the Gray Fossil Site, Tennessee, USA', *Palaeogeography, Palaeoclimatology, Palaeoecology*, 471, pp. 48–57. doi:10.1016/j.palaeo.2017.01.037.

Keenan, S.W., Engel, A.S., Roy, A. and Lisa Bovenkamp-Langlois, G. (2015) 'Evaluating the consequences of diagenesis and fossilization on bioapatite lattice structure and composition', *Chemical geology*, 413, pp. 18–27. doi:10.1016/j.chemgeo.2015.08.005.

Kemp, W.L. (2016) 'Postmortem Change and its Effect on Evaluation of Fractures', *Academic Forensic Pathology*, 6(1), pp. 28–44. doi:10.23907/2016.004.

Kendall, C., Marie, A., Eriksen, H., Collins, M.J., Turner-Walker, G. and Kontopoulos, I. (2018) 'Diagenesis of archaeological bone and tooth', *Palaeogeography, Palaeoclimatology, Palaeoecology*, 491, pp. 21–37. doi:10.1016/j.palaeo.2017.11.041.

Kilpatrick, M.C. (2021) 'Dunragit the Prehistoric Heart of Galloway Appendix 8: Human Cremated Bone', in Bailie, W. (ed.) *Dunragit -- The Prehistoric Heart of Galloway*. Glasgow: GUARD Archaeology, p. Appendix 8, 1-15.

van Klinken, G.. (1998) 'Bone Collagen Quality Indicators for Palaeodietary and Radiocarbon Measurements', *Journal of Archaeological Science*, 26(6), pp. 687–695. doi:10.1006/jasc.1998.0385.

Kloprogge, J.T., Hickey, L. and Frost, R.L. (2004) 'FT-Raman and FT-IR spectroscopic study of synthetic Mg/Zn/Al-hydrotalcites', *Journal of Raman Spectroscopy*, 35(11), pp. 967–974. doi:10.1002/jrs.1244.

Knight, B. (1968) 'Estimation of the Time Since Death: A Survey of Practical Methods', *Journal - Forensic Science Society*, 8(2), pp. 91–96. doi:10.1016/S0015-7368(68)70452-7.

Knight, B. (1969) 'Methods of Dating Skeletal Remains', *Medicine, science, and the law*, 9(4), pp. 247–252. doi:10.1177/002580246900900408.

Knight, B. and Lauder, I. (1967) 'Proceedings of the British Association in Forensic Medicine', *Medicine, science, and the law*, 7(4), pp. 205–208. doi:10.1177/002580246700700408.

Kohn, M.J. (2008) 'Models of diffusion-limited uptake of trace elements in fossils and rates of fossilization', *Geochimica et cosmochimica acta*, 72(15), pp. 3758–3770. doi:10.1016/j.gca.2008.05.045.

Kohn, M.J. and Moses, R.J. (2013) 'Trace element diffusivities in bone rule out simple diffusive uptake during fossilization but explain in vivo uptake and release', *Proceedings of the National Academy of Sciences*, 110(2), p. 419. doi:10.1073/pnas.1209513110.

Kontopoulos, I. (2019) 'Bone diagenesis in a Mycenaean secondary burial (Kastrouli, Greece)', *Archaeological and Anthropological Sciences*, 11(10), pp. 5213–5230.

Kontopoulos, I., Nystrom, P. and White, L. (2016a) 'Experimental taphonomy : post-mortem microstructural modifications in sus scrofa domesticus bone', *Forensic Science International*,

266(April 2019), pp. 320–328. doi:10.1016/j.forsciint.2016.06.024.

Kontopoulos, I., Nystrom, P. and White, L. (2016b) 'Experimental taphonomy: post-mortem microstructural modifications in Sus scrofa domesticus bone', *Forensic Science International*, 266, pp. 320–328. doi:10.1016/j.forsciint.2016.06.024.

Koon, H.E.C., Nicholson, R.A. and Collins, M.J. (2003) 'A practical approach to the identification of low temperature heated bone using TEM', *Journal of Archaeological Science*, 30(11), pp. 1393–1399. doi:10.1016/S0305-4403(03)00034-7.

Kronick, P.L. and Cooke, P. (1996) 'Thermal stabilization of collagen fibres by calcification', *Connective Tissue Research*, 33, pp. 275–282.

Kuhn, M. and Johnson, K. (2013) *Applied predictive modeling*. New York: Springer.

Kuijt, I., Quinn, C.P. and Cooney, G. (2014) *Transformation by Fire: The Archaeology of Cremation in Cultural Context*. Tuczon, AZ: Ebook Central.

Lambert, J.B., Simpson, S.V., Buikstra, J.E. and Hanson, D. (1983) 'Electron microprobe analysis of elemental distribution in excavated human femurs', *American Journal of Physical Anthropology*, 62(4), pp. 409–423. doi:10.1002/ajpa.1330620406.

Lambert, J.B., Vlasak, S., Simpson, Szpunar, C.B. and Buikstra, J.E. (1985) 'Bone diagenesis and dietary analysis', *Journal of human evolution*, 14(5), pp. 477–482. doi:10.1016/S0047-2484(85)80026-9.

Lambert, J.B., Xue, L. and Buikstra, J.E. (1991) 'Inorganic analysis of excavated human bone after surface removal', *Journal of archaeological science*, 18(3), pp. 363–383. doi:10.1016/0305-4403(91)90072-W.

Lambot, B., Friboulet, M. and Méniel, P. (1994) 'Le site protohistorique d'Acy Romance (Ardennes) II. Les nécropoles dans leur contexte régional 1986-1988-1989', *Reims: Mémoire de la Société Archéologique Champenoise*, 8, pp. 241–42.

Langford, J. I.; Wilson, A.J.C. (1978) 'Scherrer after Sixty Years: A Survey and Some New Results in the Determination of Crystallite Size', *Journal of Applied Crystallography*, 11, pp. 102–113.

Law, I.A. and Hedges, R.E.M. (1989) 'A Semi-Automated Bone Pretreatment System and the Pretreatment of Older and Contaminated Samples', *Radiocarbon*, 31(3), pp. 247–253. doi:10.1017/S0033822200011759.

Lebon, M., Reiche, I., Bahain, J.-J., Chadefaux, C., Moigne, A.-M., Fröhlich, F., Sémah, F., Schwarcz, H.. and Falguères, C. (2010) 'New parameters for the characterization of diagenetic alterations and heat-induced changes of fossil bone mineral using Fourier transform infrared spectrometry', *Journal of Archaeological Science*, 37(9), pp. 2265–2276. doi:10.1016/j.jas.2010.03.024.

Lee-Thorp, J. (2002) 'Two decades of progress towards understanding fossilization processes and isotopic signals in calcified tissue minerals', *Archaeometry*, 44(3), pp. 435–446. doi:10.1111/1475-4754.t01-1-00076.

Lee-Thorp, J. and Sponheimer, M. (2003) 'Three case studies used to reassess the reliability of fossil bone and enamel isotope signals for paleodietary studies', *Journal of Anthropological Archaeology*, 22(3), pp. 208–216. doi:10.1016/S0278-4165(03)00035-7.

Lee, F. (2006) ‘Human skeletal remains’, in Evans, C. and Hodder, I. (eds) *A woodland archaeology. Neolithic Sites at Haddenham. The Haddenham project: volume 1*. Cambridge: MacDonals Institute for Archaeological Research, pp. 140–153.

Lee, S. and Lee, D.K. (2018) ‘What is the proper way to apply the multiple comparison test?’, *Korean journal of anesthesiology*, 71(5), pp. 353–360. doi:10.4097/kja.d.18.00242.

LeGeros, R.Z. (1991) *Calcium Phosphates in Oral Biology and Medicine*. vol 15. Basel: Karger.

LeGeros, R.Z. and LeGeros, J.P. (1983) ‘Carbonate analyses of synthetic, mineral and biological apatites’, *Journal of Dental Research*, 82, p. 259.

LeGeros, R.Z., Trautz, O.R., Klein, E. and LeGeros, J.P. (1969) ‘Two types of carbonate substitution in the apatite structure’, *Experientia*, 25(1), pp. 5–7. doi:10.1007/BF01903856.

Lemmers, S.A.M., Gonçalves, D., Cunha, E., Vassalo, A.R. and Appleby, J. (2020) ‘Burned Fleshed or Dry ? The Potential of Bioerosion to Determine the Pre-Burning Condition of Human Remains’, *Journal of Archaeological Method and Theory*, 27, pp. 972–991.

Li, Z. and Pasteris, J.D. (2014) ‘Chemistry of bone mineral, based on the hypermineralized rostrum of the beaked whale Mesoplodon densirostris.’, *American Mineralogist*, 99(4), p. 645. doi:10.2138/am.2014.4571.

Liao, C.-J., Lin, F.-H., Chen, K.-S. and Sun, J.-S. (1999) ‘Thermal decomposition and reconstitution of hydroxyapatite in air atmosphere’, *Biomaterials*, 20(19), pp. 1807–1813. doi:10.1016/S0142-9612(99)00076-9.

Llovet, X., Moy, A., Pinard, P.T. and Fournelle, J.H. (2021) ‘Electron probe microanalysis: A review of recent developments and applications in materials science and engineering’, *Progress in materials science*, 116, p. 100673. doi:10.1016/j.pmatsci.2020.100673.

Longin, R. (1971) ‘New method of collagen extraction for radiocarbon dating’, *Nature (London)*, 230.5291, pp. 241–42.

Loong, C.-K., Rey, C., Kuhn, L.., Combes, C., Wu, Y., Chen, S.-H. and Glimcher, M.. (2000) ‘Evidence of hydroxyl-ion deficiency in bone apatites: an inelastic neutron-scattering study’, *Bone*. Elsevier Inc, pp. 599–602. doi:10.1016/S8756-3282(00)00273-8.

López-Costas, O., Lantes-Suárez, Ó. and Martínez Cortizas, A. (2016) ‘Chemical compositional changes in archaeological human bones due to diagenesis: Type of bone vs soil environment’, *Journal Of Archaeological Science*, 67, pp. pp43-51. doi:10.1016/j.jas.2016.02.001.

Lozano, L.F., Peña-Rico, M.A., Heredia, A., Ocotlán-Flores, J., Gómez-Cortés, A., Velázquez, R., Belío, I.A. and Bucio, L. (no date) ‘Thermal analysis study of human bone’, *Journal of materials science*, 38(23), pp. 4777–4782. doi:10.1023/A:1027483220584.

Lundy, J.K. (1989) ‘Death, decay and reconstruction: Approaches to archaeology and forensic science’, *Journal of Human Evolution*. Elsevier Ltd, pp. 506–507. doi:10.1016/0047-2484(89)90082-1.

Lyman, R.L. (1994) ‘Vertebrate taphonomy’. Cambridge: Cambridge University Press (Cambridge manuals in archaeology).

Lynch-Aird, J., Moffatt, C. and Simmons, T. (2015) ‘Decomposition Rate and Pattern in

Hanging Pigs', *J Forensic Sci*, 60(5), pp. 1155–1163. doi:10.1111/1556-4029.12796.

Lynn, K.S. and Fairgrieve, S.I. (2009) 'Microscopic Indicators of Axe and Hatchet Trauma in Fleshed and Defleshed Mammalian Long Bones', *Journal of Forensic Sciences*, 54(4), pp. 793–797. doi:10.1111/j.1556-4029.2009.01062.x.

Maiti, G.C. and Freund, F. (1981) 'Incorporation of chlorine into hydroxy-apatite', *Journal of inorganic & nuclear chemistry*, 43(11), pp. 2633–2637. doi:10.1016/0022-1902(81)80589-1.

Mamede, A.P., Gonçalves, D., Marques, M.P.M. and Batista de Carvalho, L.A.E. (2018) 'Burned bones tell their own stories: A review of methodological approaches to assess heat-induced diagenesis', *Applied Spectroscopy Reviews*, 53(8), pp. 603–635. doi:10.1080/05704928.2017.1400442.

Maples, W.R. (1986) 'Trauma analysis by the forensic anthropologist', in Reichs, K.J. (ed.) *Forensic Osteology*. Springfield, IL: CC Thomas, pp. 218–228.

Marchiafava, V., Bonucci, E. and Ascenzi, A. (1974) 'Fungal osteoclasia: a model of dead bone resorption', *Calcified Tissue Research*, 14(1), pp. 195–210. doi:10.1007/BF02060295.

Marín Arroyo, A.., Landete Ruiz, M.., Vidal Bernabeu, G., Seva Román, R., González Morales, M.. and Straus, L.. (2008) 'Archaeological implications of human-derived manganese coatings: a study of blackened bones in El Mirón Cave, Cantabrian Spain', *Journal of archaeological science*, 35(3), pp. 801–813. doi:10.1016/j.jas.2007.06.007.

De Marini, G.F. (1998) *A New and Interesting Description of the Lao Kingdom (1642-1648)*. 1663rd edn. Bangkok: White Lotus Press.

Marques, M.P.M., Mamede, A.P., Vassalo, A.R., Makhoul, C., Cunha, E., Gonçalves, D., Parker, S.F. and Batista de Carvalho, L.A.E. (2018) 'Heat-induced Bone Diagenesis Probed by Vibrational Spectroscopy', *Scientific Reports*, 8(1), pp. 1–13. doi:10.1038/s41598-018-34376-w.

Márquez-Grant, N., Schotsmans, E.M. and Forbes, S. (2017) *Taphonomy of human remains : forensic analysis of the dead and the depositional environment*. Chichester, England (Ebook central).

Mata Tutor, P., Benito Sánchez, M., Villoria Rojas, C., Muñoz García, A., Pérez Guzmán, I. and Márquez-Grant, N. (2021) 'Cut or burnt? – Categorizing morphological characteristics of heat-induced fractures and sharp force trauma', *Legal Medicine (Tokyo, Japan)*, 50, pp. 101868–101868. doi:10.1016/j.legalmed.2021.101868.

Mata Tutor, P., Márquez-Grant, N., Villoria Rojas, C., Muñoz García, A., Pérez Guzmán, I. and Benito Sánchez, M. (2021) 'Through fire and flames: post-burning survival and detection of dismemberment-related toolmarks in cremated cadavers', *International Journal of Legal Medicine*, 135(3), pp. 801–815. doi:10.1007/s00414-020-02447-1.

Matuszewski, S., Hall, M.J.R., Moreau, G., Schoenly, K.G., Tarone, A.M. and Villet, M.H. (2020) 'Pigs vs people: the use of pigs as analogues for humans in forensic entomology and taphonomy research', *International journal of legal medicine*, 134(2), pp. 793–810. doi:10.1007/s00414-019-02074-5.

Mayer, I., Schlam, R. and Featherstone, J.D.. (1997) 'Magnesium-containing carbonate apatites', *Journal of inorganic biochemistry*, 66(1), pp. 1–6. doi:10.1016/S0162-0134(96)00145-6.

Mayne Correia, P. (1997) ‘Fire modification of bone: a review of the literature’, in Haglund, W. and Sorg, M. (eds) *Forensic Taphonomy: The Post Mortem Fate of Human Remains*. Boca Raton, FL: CRC Press, pp. 275–293.

Mayne, P.M. (1990) *The identification of precremation trauma in cremated bone*. University of Alberta.

Mckinley, J. (1994) *The Anglo-Saxon cemetery at Spong Hill, North Elmham. Part VIII: the cremations*, *East Anglian Archaeol*. Norfolk, Museums Service.

Mckinley, J. (1999) ‘Excavations at Ham Hill, Montacute, Somerset 1994 and 1998’, *Somerset Archaeol Natur Hist*, 142(77–137).

Mckinley, J. (2000) ‘Human bone’, in Lawson, A.J. (ed.) *Potterne 1982–5 animal husbandry in later prehistoric Wessex*. Wessex Ach. Salisbory: Trust for Wessex Archaeology, pp. 95–101.

Mckinley, J. (2008) ‘Human remains and diet’, in Mercer, R. and Healy, F. (eds) *Hambledon Hill, Dorset, England, Volumes 1 and 2 -- Excavation and survey of a Neolithic Monument Complex and its Surrounding Landscape*. Swindon: JSTOR, pp. 477–535.

McKinley, J.I. (1997) ‘Bronze Age “Barrows” and Funerary Rites and Rituals of Cremation’, *Proceedings of the Prehistoric Society*, 63, pp. 129–145. doi:10.1017/S0079497X00002401.

McKinley, J.I. (2000) ‘Cremation burials’, in Barber, B. and Bowsher, D. (eds) *The eastern cemetery of Roman London: Excavations 1983-90 MoLAS Mon. 4*. London: Museum of London Archaeology Service, pp. 254–277.

McKinley, J.I. (2004) ‘Compiling a skeletal inventory: cremated human bone’, in Brickley, M. and McKinley, J.I. (eds) *Guidelines to the Standards for Recording Human Remains*. no 7, pp. 9–13.

Mckinnon, M., Henneberg, M., Simpson, E. and Higgins, D. (2020) ‘A comparison of crystal structure in fresh, burned and archaic bone – Implications for forensic sampling’, *Forensic Science International*, 313, p. 110328. doi:10.1016/j.forsciint.2020.110328.

McMahon, S., Anderson, R.P., Saupe, E.E. and Briggs, D.E.G. (2016) ‘Experimental evidence that clay inhibits bacterial decomposers; implications for preservation of organic fossils’, *Geology (Boulder)*, 44(10), pp. 867–870. doi:10.1130/G38454.1.

Merbs, C.F. (1967) ‘Cremated Human Remains from Point of Pines, Arizona: A New Approach’, *American antiquity*, 32(4), pp. 498–506. doi:10.2307/2694077.

Metzler-Zens, N., Metzler-Zens, J., Méniel, P., Bis, R., Gaeng, C. and Villemeur, I. (1999) ‘Lamadelaine: Une Nécropole de l’Oppidum du Titelberg’, *g. Luxembourg: Dossiers d’Archeologie du Musée National d’Histoire et d’Art*, 6.

Miles, C.A. and Ghelashvili, M. (1999) ‘Polymer-in-a-Box Mechanism for the Thermal Stabilization of Collagen Molecules in Fibers’, *Biophysical journal*, 76(6), pp. 3243–3252. doi:10.1016/S0006-3495(99)77476-X.

Miles, C.A., Sionkowska, A., Hulin, S.L., Sims, T.J., Avery, N.C. and Bailey, A.J. (2000) ‘Identification of an Intermediate State in the Helix-Coil Degradation of Collagen by Ultraviolet Light’, *The Journal of biological chemistry*, 275(42), pp. 33014–33020. doi:10.1074/jbc.M002346200.

Millard, A. (1993) *Diagenesis of archaeological bone : the case of uranium uptake*. DPhil thesis, University of Oxford.

Millard, A.R. (2001) 'Deterioration of Bone', in Brothwell, D.R. and Pollard, A.M. (eds) *Handbook of Archaeological Sciences*. Chichester: Wiley.

Millard, A.R. and Hedges, R.E.. (1996) 'A diffusion-adsorption model of uranium uptake by archaeological bone', *Geochimica et cosmochimica acta*, 60(12), pp. 2139–2152. doi:10.1016/0016-7037(96)00050-6.

Miller, L.M., Vairavamurthy, V., Chance, M.R., Mendelsohn, R., Paschalis, E.P., Betts, F. and Boskey, A.L. (2001) 'In situ analysis of mineral content and crystallinity in bone using infrared micro-spectroscopy of the ν 4 PO 43− vibration', *Biochimica et biophysica acta. General subjects*, 1527(1), pp. 11–19. doi:10.1016/S0304-4165(01)00093-9.

Mkukuma, L., Skakle, J., Gibson, I., Imrie, C., Aspden, R. and Hukins, D. (2004) 'Effect of the Proportion of Organic Material in Bone on Thermal Decomposition of Bone Mineral: An Investigation of a Variety of Bones from Different Species Using Thermogravimetric Analysis coupled to Mass Spectrometry, High-Temperature X-ray Diffraction', *Calcified Tissue International*, 75(4), pp. 321–328. doi:10.1007/s00223-004-0199-5.

Moraitis, K. and Spiliopoulou, C. (2006) 'Identification and differential diagnosis of perimortem blunt forcetrauma in tubular long bones', *Forensic Science, Medicine, and Pathology*, 2(4), pp. 221–229.

Morales, N.S., Catella, L., Oliva, F., Sarmiento, P.L. and Barrientos, G. (2018) 'Journal of Archaeological Science : Reports A SEM-based assessment of bioerosion in Late Holocene faunal bone assemblages from the southern Pampas of Argentina', *Journal of Archaeological Science: Reports*, 18, pp. 782–791. doi:10.1016/j.jasrep.2017.07.012.

Muñoz, M., Villar, I. and García-erce, J.A. (2009) 'An update on iron physiology', *World Journal of Gastroenterology*, 15(37), pp. 4617–4626. doi:10.3748/wjg.15.4617.

Munro, L.E., Longstaffe, F.J. and White, C.D. (2007) 'Burning and boiling of modern deer bone: Effects on crystallinity and oxygen isotope composition of bioapatite phosphate', *Palaeogeography, Palaeoclimatology, Palaeoecology*, 249(1–2), pp. 90–102. doi:10.1016/j.palaeo.2007.01.011.

Murphy, E. (2003) 'Funerary Processing of the Dead in Prehistoric Ireland', *Archaeology Ireland*, 17, pp. 13–15.

Nagy, G., Lorand, T., Patonai, Z., Montsko, G., Bajnoczky, I., Marcsik, A. and Mark, L. (2008) 'Analysis of pathological and non-pathological human skeletal remains by FT-IR spectroscopy', *Forensic Science International*, 175(1), pp. 55–60. doi:10.1016/j.forsciint.2007.05.008.

Nelson, R. (1992) 'A Microscopic Comparison of Fresh and Burned Bone', *Journal of Forensic Sciences*, 37(4), pp. 1055–1060.

Neuman, W.F. and Weikel Jr, J.H. (1955) 'Recrystallization in bone mineral', *Annals of the New York Academy of Sciences*, 60(5), pp. 685–695. doi:10.1111/j.1749-6632.1955.tb40059.x.

Ngailo, E.K. (2020) *Contributions to linear discriminant analysis with applications to growth curves*. PhD thesis, Linköping University.

Niblett, R. (1999) *The excavation of a ceremonial site at Folly Lane, Verulamium*. London: Society for the Promotion of Roman Studies (Britannia monograph series ; no.14).

Nicholson, R.A. (1993) 'A morphological investigation of burnt animal bone and an evaluation of its utility in archaeology', *Journal of Archaeological Science*, 20(4), pp. 411–428. doi:10.1006/jasc.1993.1025.

Nielsen-Marsh, C.M. and Hedges, R.E.. (2002) 'Patterns of Diagenesis in Bone I: The Effects of Site Environments', *Journal of Archaeological Science*, 27(12), pp. 1139–1150. doi:10.1006/jasc.1999.0537.

Nielsen-Marsh, C.M., Smith, C.I., Jans, M.M.E., Nord, A., Kars, H. and Collins, M.J. (2007) 'Bone diagenesis in the European Holocene II : taphonomic and environmental considerations', *Journal of Archaeological Science*, 34(9), pp. 1523–1531. doi:10.1016/j.jas.2006.11.012.

Olive, D.J. (2017) *Linear regression*. Cham, Switzerland.

Olsen, J., Heinemeier, J., Bennike, P., Krause, C., Margrethe Hornstrup, K. and Thrane, H. (2008) 'Characterisation and blind testing of radiocarbon dating of cremated bone', *Journal of Archaeological Science*, 35(3), pp. 791–800. doi:10.1016/j.jas.2007.06.011.

Olszta, M.J., Chengm, X., Jee, S.S., Kumar, R., Kim, Y.Y., Kaufman, M.J., Douglas, E.P. and Gower, L.B. (2007) 'Bone structure and formation: a new perspective', *Materials Science and Engineering*, R 58, pp. 77–116.

Ortner, D. (2008) 'Differential Diagnosis of Skeletal Injuries', in Kimmerle, E. and Baraybar, J. (eds) *Skeletal Trauma: Identification of Injuries Resulting from Human Rights Abuse andArmed Conflict*. Boca Raton, FL: CRC Press, pp. 21–87.

Palmer, L.C., Newcomb, C.J., Kaltz, S.R., Spoerke, E.D. and Stupp, S.I. (2008) 'Biomimetic Systems for Hydroxyapatite Mineralization Inspired By Bone and Enamel', *Chemical reviews*, 108(11), pp. 4754–4783. doi:10.1021/cr8004422.

Parker, R.B., Toots, H. and Murphy, J.. (1974) 'Leaching of sodium from skeletal parts during fossilization', *Geochimica et cosmochimica acta*, 38(8), pp. 1317–1321. doi:10.1016/0016-7037(74)90125-2.

Parker, S. (2007) *The Human Body*. London: DK Publishing.

Pasteris, J.D., Wopenka, B., Freeman, J.J., Rogers, K., Valsami-Jones, E., van der Houwen, J.A.. and Silva, M.J. (2004) 'Lack of OH in nanocrystalline apatite as a function of degree of atomic order: implications for bone and biomaterials', *Biomaterials*, 25(2), pp. 229–238. doi:10.1016/S0142-9612(03)00487-3.

Pate, F.D. and Hutton, J.T. (1988) 'The use of soil chemistry data to address post-mortem diagenesis in bone mineral', *Journal of Archaeological Science*, 15(6), pp. 729–739. doi:10.1016/0305-4403(88)90062-3.

Pearce, A.I., Richards, R.G., Milz, S., Schneider, E. and Pearce, S.G. (2007) 'Animal models for implant biomaterial research in bone: A review', *European Cells and Materials*, 13(0), pp. 1–10. doi:10.22203/eCM.v013a01.

Pearson, K. (1901) 'On Lines and Planes of Closest Fit to Systems of Points in Space', *Philosophical Magazine*, 2(11), pp. 559–572.

Pechal, J.L., Crippen, T.L., Tarone, A.M., Lewis, A.J., Tomberlin, J.K. and Benbow, M.E. (2013) 'Microbial community functional change during vertebrate carrion decomposition', *PLoS ONE*. Public Library of Science (PLoS), p. e79035. doi:10.1371/journal.pone.0079035.

Penkman, K.E.., Kaufman, D.., Maddy, D. and Collins, M.. (2008) 'Closed-system behaviour of the intra-crystalline fraction of amino acids in mollusc shells', *Quaternary geochronology*, 3(1–2), pp. 2–25. doi:10.1016/j.quageo.2007.07.001.

Person, A., Bocherens, H., Mariotti, A. and Renard, M. (1996) 'Diagenetic evolution and experimental heating of bone phosphate', *Palaeogeography, Palaeoclimatology, Palaeoecology*, 126(1), pp. 135–149. doi:10.1016/S0031-0182(97)88906-7.

Pesko, B.K., Weidt, S., McLaughlin, M., Wescott, D.J., Torrance, H., Burgess, K. and Burchmore, R. (2020) 'Postmortomics: The Potential of Untargeted Metabolomics to Highlight Markers for Time Since Death', *Omics (Larchmont, N.Y.)*, 24(11), pp. 649–659. doi:10.1089/omi.2020.0084.

Pesquero, M.D., Bell, L.S., Fernández-Jalvo, Y., Pesquero, M.D., Bell, L.S. and Fernández-jalvo, Y. (2018) 'Skeletal modification by microorganisms and their environments', *Historical Biology*, 2963, pp. 1–12. doi:10.1080/08912963.2017.1371713.

Piekarski, K. (1970) 'Fracture of Bone', *Journal of Applied Physics*, 41(1), pp. 215–223. doi:10.1063/1.1658323.

Piepenbrink, H. (1986) 'Two examples of biogenous dead bone decomposition and their consequences for taphonomic interpretation', *Journal of Archaeological Science*. Elsevier Ltd, pp. 417–430. doi:10.1016/0305-4403(86)90012-9.

Piepenbrink, H. and Schutkowski, H. (1987) 'Decomposition of skeletal remains in desert dry soil A roentgenological study', *Human Evolution*, 2(6), pp. 481–491. doi:10.1007/BF02437423.

Piga, G., Gonçalves, D., Thompson, T.J.U., Brunetti, A., Malgosa, A. and Enzo, S. (2016) 'Understanding the Crystallinity Indices Behavior of Burned Bones and Teeth by ATR-IR and XRD in the Presence of Bioapatite Mixed with Other Phosphate and Carbonate Phases', *International Journal of Spectroscopy*, p. 9. doi:10.1155/2016/4810149.

Piga, G., Malgosa, A., Thompson, T.J.U. and Enzo, S. (2008) 'A new calibration of the XRD technique for the study of archaeological burned human remains', *Journal of Archaeological Science*, 35(8), pp. 2171–2178. doi:10.1016/j.jas.2008.02.003.

Piga, G., Thompson, T.J.U., Malgosa, A. and Enzo, S. (2009) 'The potential of X-ray diffraction in the analysis of burned remains from forensic contexts', *Journal of Forensic Sciences*, 54(3), pp. 534–539. doi:10.1111/j.1556-4029.2009.01037.x.

Piggott, S. (1962) *The West Kennet Long Barrow excavations 1955-56*, *Ministry of Works Archaeol Rep*.

Pleshko, N., Boskey, A. and Mendelsohn, R. (1991) 'Novel infrared spectroscopic method for the determination of crystallinity of hydroxyapatite minerals', *Biophysical Journal*, 60(4), pp. 786–793. doi:10.1016/S0006-3495(91)82113-0.

Pokines, J.T. and Symes, S.A. (2014) *Manual of forensic taphonomy*. Boca Raton: CRC Press/Taylor & Francis Group.

Pope, E.J. (2007) 'The effects of fire on human remains: Characteristics of taphonomy and

trauma', 3292654, p. 525. Available at: http://0-search.proquest.com.wam.leeds.ac.uk/docview/304896784?accountid=14664%5Cnhttp://openurl.ac.uk/?genre=dissertations+%26+theses&issn=&title=The+effects+of+fire+on+human+remains%3A+Characteristics+of+taphonomy+and+trauma&volume=&issue=&date=2007-01-.

Pope, E.J. and Smith, O.C. (2004) 'Identification of traumatic injury in burned cranial bone: an experimental approach.', *Journal of forensic sciences*, 49(3), pp. 431–440. doi:10.1520/JFS2003286.

Poppa, P., Porta, D., Gibelli, D., Mazzucchi, A., Brandone, A., Grandi, M. and Cattaneo, C. (2011) 'Detection of Blunt, Sharp Force and Gunshot Lesions on Burnt Remains: A Cautionary Note', *The American journal of forensic medicine and pathology*, 32(3), pp. 275–279.

Posner, A.S. (1985) 'The mineral of bone', *Clinical orthopaedics and related research*, (200), pp. 87–99. doi:10.1097/00003086-198511000-00018.

Praprotnik, M. and Janežič, D. (2005) 'Molecular dynamics integration and molecular vibrational theory. III. The infrared spectrum of water', *The Journal of Chemical Physics*, 17, p. 174102.

Pringle, J.K., Jervis, J.R., Hansen, J.D., Jones, G.M., Cassidy, N.J. and Cassella, J.P. (2012) 'Geophysical Monitoring of Simulated Clandestine Graves Using Electrical and Ground-Penetrating Radar Methods: 0-3вЂґYears After Burial', *J Forensic Sci*. Received 4, 57(6), pp. 1467–1486. doi:10.1111/j.1556-4029.2012.02151.x.

Procopio, N. and Buckley, M. (2017) 'Minimizing Laboratory-Induced Decay in Bone Proteomics', *Journal of proteome research*, 16(2), pp. 447–458. doi:10.1021/acs.jproteome.6b00564.

Procopio, N., Ghignone, S., Voyron, S., Chiapello, M., Williams, A., Chamberlain, A., Mello, A. and Buckley, M. (2020) 'Soil Fungal Communities Investigated by Metabarcoding Within Simulated Forensic Burial Contexts', *Frontiers in microbiology*, 11, pp. 1686–1686. doi:10.3389/fmicb.2020.01686.

Procopio, N., Ghignone, S., Williams, A., Chamberlain, A., Mello, A. and Buckley, M. (2019) 'Metabarcoding to investigate changes in soil microbial communities within forensic burial contexts', *Forensic science international : genetics*, 39, pp. 73–85. doi:10.1016/j.fsigen.2018.12.002.

Pyle, J.M., Spear, F.S. and Wark, D.A. (2002) 'Electron microprobe analysis of REE in apatite, monazite and xenotime: Protocols and pitfalls', *Reviews in Mineralogy and Geochemistry*, 48, pp. 337–362.

Quarta, G., Calcagnile, L., D'Elia, M., Maruccio, L., Gaballo, V. and Caramia, A. (2013) 'A combined PIXE–PIGE approach for the assessment of the diagenetic state of cremated bones submitted to AMS radiocarbon dating', *Nuclear instruments & methods in physics research. Section B, Beam interactions with materials and atoms*, 294, pp. 221–225. doi:10.1016/j.nimb.2012.06.014.

Quatrehomme, G., Bolla, M., Muller, M., Rocca, J., Grévin, G., Bailet, P. and Ollier, A. (1998) 'Experimental Single Controlled Study of Burned Bones: Contribution of Scanning Electron Microscopy', *Journal of Forensic Sciences*, 43(2), pp. 417–422.

Raff, E.C., Schollaert, K.L., Nelson, D.E., Donoghue, P.C.J., Thomas, C.-W., Turner, F.R., Stein, B.D., Dong, X., Bengtson, S., Huldtgren, T., Stampanoni, M., Chongyu, Y. and Raff, R.A. (2008) 'Embryo Fossilization Is a Biological Process Mediated by Microbial Biofilms', *Proceedings of the National Academy of Sciences - PNAS*, 105(49), pp. 19360–19365. doi:10.1073/pnas.0810106105.

Randolph-Quinney, P. (2014a) 'Burnt Human Remains Part 1 -- Fire Dynamics and Body Recovery', in Mallet, X., Blythe, T., and Berry, R. (eds) *Advances in Forensic Human Identification*. New York: CRC Press, pp. 127–144.

Randolph-Quinney, P. (2014b) 'Burnt Human Remains Part 2 - Identification and Laboratory Analysis', in Mallet, X., Blythe, T., and Berry, R. (eds) *Advances in Forensic Human Identification*. New York: CRC Press, pp. 145–164.

Raspanti, M., Guizzardi, S., De Pasquale, V., Martini, D. and Ruggeri, A. (1994) 'Ultrastructure of heat-deproteinated compact bone', *Biomaterials*, 15(6), pp. 433–437. doi:10.1016/0142-9612(94)90222-4.

Raynaud, S., Champion, E., Bernache-Assollant, D. and Thomas, P. (2002) 'Calcium phosphate apatites with variable Ca/P atomic ratio I. Synthesis, characterisation and thermal stability of powders', *Biomaterials*, 23(4), pp. 1065–1072. doi:10.1016/S0142-9612(01)00218-6.

Reidsma, F.., van Hoesel, A., van Os, B.J.., Megens, L. and Braadbaart, F. (2016) 'Charred bone : Physical and chemical changes during laboratory simulated heating under reducing conditions and its relevance for the study of fire use in archaeology', *Journal of Archaeological Science:Reports*, 10, pp. 282–292. doi:10.1016/j.jasrep.2016.10.001.

Renfrew, C. (1979) *Investigations in Orkney*. London: The Society of Antiquaries of London.

Rey, C., Collins, B., Goehl, T., Dickson, I.R. and Glimcher, M.J. (1989) 'The carbonate environment in bone mineral: a resolution-enhanced Fourier transform infrared spectroscopy study', *Calcified tissue international*, 45(3), pp. 157–164. doi:10.1007/BF02556059.

Rey, C., Combes, C., Drouet, C. and Glimcher, M.J. (2009) 'Bone mineral: Update on chemical composition and structure', *Osteoporosis International*, 20(6), pp. 1013–1021. doi:10.1007/s00198-009-0860-y.

Rey, C., Combes, C., Drouet, C., Lebugle, A., Sfihi, H. and Barroug, A. (2007) 'Nanocrystalline apatites in biological systems: characterisation, structure and properties', *Materialwissenschaft und Werkstofftechnik*, 38(12), pp. 996–1002. doi:10.1002/mawe.200700229.

Rey, C., Combes, C., Drouet, C., Sfihi, H. and Barroug, A. (2007) 'Physico-chemical properties of nanocrystalline apatites: Implications for biominerals and biomaterials', *Materials Science & Engineering C*, 27(2), pp. 198–205. doi:10.1016/j.msec.2006.05.015.

Rey, C., Miquel, J.., Facchini, L., Legrand, A.. and Glimcher, M.. (1995) 'Hydroxyl groups in bone mineral', *Bone*, 16(5), pp. 583–586. doi:10.1016/8756-3282(95)00101-I.

Rey, C., Renugopalakrishnan, V., Collins, B. and Glimcher, M.J. (1991) 'Fourier transform infrared spectroscopic study of the carbonate ions in bone mineral during aging.', *Calcified tissue international*, 49, pp. 251–258. doi:10.1007/BF02556214.

Rey, C., Shimizu, M., Collins, B. and Glimcher, M. (1990) 'Resolution-enhanced fourier transform infrared spectroscopy study of the environment of phosphate ions in the early

deposits of a solid phase of calcium-phosphate in bone and enamel, and their evolution with age. I: Investigations in the v 4 PO 4 domain', *Calcified Tissue International*, 46(6), pp. 384–394. doi:10.1007/BF02554969.

Richards, C. (1988) 'Altered images: a re-examination of Neolithic mortuary practices in Orkney', in Barrett, J. and Kinnes, I. (eds) *The Archaeology of Context in the Neolithic and Bronze Age: Recent Trends*. Sheffield: Department of Archaeology and Prehistory, Sheffield University, pp. 42–55.

Rinaldi, R. and Llovet, X. (2015) 'Electron Probe Microanalysis: A Review of the Past, Present, and Future', *Microscopy And Microanalysis*, 21(5), pp. pp1053-1069. doi:10.1017/S1431927615000409.

Rogers, K.. and Daniels, P. (2002) 'An X-ray diffraction study of the effects of heat treatment on bone mineral microstructure', *Biomaterials*, 23(12), pp. 2577–2585. doi:10.1016/S0142-9612(01)00395-7.

Rogers, K. and Zioupos, P. (1999) 'The Bone Tissue of the Rostrum of a Mesoplodon Densirostris Whale: a Mammalian Biomineral Demonstrating Extreme Texture', *Journal of Materials Science Letters*, 18(8), pp. 651–654. doi:10.1023/A:1006615422214.

Roux, G.A.D.T. (1887) 'Contribution à l'étude clinique et thérapeutique des taenias de l'homme. Gabriel Roux'. Lyon: Faculte de medecine et de pharmacie de Lyon.

Sauer, N. (2003) 'The Timing of Injuries and Manner of Death: Distinguishing Among Antemortem, Perimortem, and Postmortem Trauma BT - Forensic Osteology', *Forensic Osteology*, pp. 321–331. Available at: papers2://publication/uuid/A330E30C-EA34-4274-9020-834F7F7F4C5F.

Sauer, N.J. (1998) 'The timing of injuries and manner of death: distinguishing among antemortem, perimortem and postmortem trauma', in Reichs, K.J. (ed.) *Forensic Osteology: Advances in the Identification of Human Remains*. 2nd edn. Springfield, IL: Charles C. Thomas, pp. 321–332.

Saville, P.A., Hainsworth, S. V. and Rutty, G.N. (2007) 'Cutting crime: The analysis of the "uniqueness" of saw marks on bone', *International Journal of Legal Medicine*, 121(5), pp. 349–357. doi:10.1007/s00414-006-0120-z.

Scharlotta, I., Goriunova, O.I. and Weber, A. (2013) 'Micro-sampling of human bones for mobility studies: diagenetic impacts and potentials for elemental and isotopic research', *Journal of Archaeological Science*, 40(12), pp. 4509–4527. doi:10.1016/j.jas.2013.07.014.

Scherrer, P. (1918) 'Bestimmung der Grösse und der inneren Struktur von Kolloidteilchen mittels Röntgenstrahlen', *Nachr. Ges. Wiss.*, 26, pp. 98–100.

Schiegl, S., Goldberg, P., Pfretzschner, H.-U. and Conard, N.J. (2003) 'Paleolithic burnt bone horizons from the Swabian Jura: Distinguishing betweenin situ fireplaces and dumping areas', *Geoarchaeology*, 18(5), pp. 541–565. doi:10.1002/gea.10080.

Schmidt, C. and Symes, S. (2005) 'Beyond Recognition: The Analysis of Burned Human Remains', in *74th Annual Meeting of the American Association of Physical Anthropology*. Milwaukee, WI.

Schmidt, C.W. and Symes, S.A. (2015) *The Analysis of Burned Human Remains*. 2nd ed. Atlas of Surgical Pathology.

Schroeter, E.R. and Cleland, T.P. (2016) ‘Glutamine deamidation: an indicator of antiquity, or preservational quality?’, *Rapid communications in mass spectrometry*, 30(2), pp. 251–255. doi:10.1002/rcm.7445.

Schulting, R., Sheridan, A., Crozier, R. and Murphy, E. (2010) ‘Revisiting Quanterness: New AMS dates and stable isotope data from an Orcadian chamber tomb’, *Proceedings of the Society of Antiquaries of Scotland*, 140, pp. 1–50.

Schulting, R.J. (2012) ‘Skeletal evidence for interpersonal violence’, in Schulting, R.J. and Fibiger, L. (eds) *Sticks, Stones, and Broken Bones: Neolithic Violence in a European Perspective*. Oxford: Oxford University Press.

Schultz, J.J., Warren, M.W. and Krigbaum, J.S. (2008) ‘Analysis of human cremains: gross and chemical methods’, in Schmidt, C.W. and Symes, S.A. (eds) *The Analysis of Burned Human Remains*. London : Academic Press, pp. 75–94.

Schutkowski, H., Herrmann, B. and Grupe, G. (1999) ‘Diet , Status and Decomposition at Weingarten : Trace Element and Isotope Analyses on Early Mediaeval Skeletal Material’, pp. 675–685.

Shahack-Gross, R., Bar-Yosef, O. and Weiner, S. (1997) ‘Black-Coloured Bones in Hayonim Cave, Israel: Differentiating Between Burning and Oxide Staining’, *Journal of Archaeological Science*, 24(5), pp. 439–446.

Shi, J., Klocke, A., Zhang, M. and Bismayer, U. (2005) ‘Thermally-induced structural modification of dental enamel apatite; decomposition and transformation of carbonate groups’, *European journal of mineralogy (Stuttgart)*, 17(5), pp. 769–775. doi:10.1127/0935-1221/2005/0017-0769.

Shipman, P., Foster, G. and Schoeninger, M. (1984) ‘Burnt bones and teeth: an experimental study of color, morphology, crystal structure and shrinkage’, *Journal of Archaeological Science*, 11(4), pp. 307–325. doi:10.1016/0305-4403(84)90013-X.

Simpson, J.., Penkman, K.E.., Demarchi, B., Koon, H., Collins, M.., Thomas-Oates, J., Shapiro, B., Stark, M. and Wilson, J. (2016) ‘The effects of demineralisation and sampling point variability on the measurement of glutamine deamidation in type I collagen extracted from bone’, *Journal of archaeological science*, 69, pp. 29–38. doi:10.1016/j.jas.2016.02.002.

Skinner, H.C.W. (2015) ‘The Web of Magnesium’, *International Geology Review*, 47(11), pp. 1111–1119. doi:10.2747/0020-6814.47.11.1111.

Smith, C.I., Chamberlain, A.T., Riley, M.S., Stringer, C. and Collins, M.J. (2003) ‘The thermal history of human fossils and the likelihood of successful DNA amplification’, *Journal of Human Evolution*, 45(3), pp. 203–217. doi:10.1016/S0047-2484(03)00106-4.

Smith, M. and Brickley, M. (2009) *People of the Long Barrows: Life, Death and Burial in the Earlier Neolithic*. Stroud.

Snoeck, C., Lee-Thorp, J., Schulting, R., de Jong, J., Debouge, W. and Mattielli, N. (2015) ‘Calcined bone provides a reliable substrate for strontium isotope ratios as shown by an enrichment experiment’, *Rapid communications in mass spectrometry*, 29(1), pp. 107–114. doi:10.1002/rcm.7078.

Snoeck, C., Lee-Thorp, J.A. and Schulting, R.J. (2014) ‘From bone to ash: Compositional and structural changes in burned modern and archaeological bone’, *Palaeogeography, Palaeoclimatology, Palaeoecology*, 416, pp. 55–68. doi:10.1016/j.palaeo.2014.08.002.

Snoeck, C., Schulting, R.J., Lee-Thorp, J.A., Lebon, M. and Zazzo, A. (2016) ‘Impact of heating conditions on the carbon and oxygen isotope composition of calcined bone’, *Journal of Archaeological Science*, 65, pp. 32–43. doi:10.1016/j.jas.2015.10.013.

Sorg, M.H. (2019) ‘Differentiating trauma from taphonomic alterations’, *Forensic science international*, 302, pp. 109893–109893. doi:10.1016/j.forsciint.2019.109893.

Spennemann, D.H.R. and Colley, S.M. (1989) ‘Fire in a Pit: the effects of burning on faunal remains’, *Archaeozoologia*, 3, pp. 51–64.

Spitz, W.U. (1993) ‘Thermal Injuries’, in Spitz, W.U. (ed.) *Medicolegal Investigations of Death*. third. Springfield, IL: Charles C. Thomas, pp. 413–443.

Sponheimer, M. and Lee-Thorp, J.A. (1999) ‘Isotopic evidence for the diet of an early hominid, Australopithecus africanus’, *Science (New York, N.Y.)*, 283(5400), p. 368. doi:10.1126/science.283.5400.368.

Sponheimer, M., Ryder, C.M., Fewlass, H., Smith, E.K., Pestle, W.J. and Talamo, S. (2019) ‘Saving Old Bones: a non-destructive method for bone collagen prescreening’, *Scientific reports*, 9(1), pp. 13928–7. doi:10.1038/s41598-019-50443-2.

Squires, K., Errickson, D. and MΓŸrquez-Grant, N. (2020) *Ethical approaches to human remains : a global challenge in bioarchaeology and forensic anthropology*. Corrected. Cham, Switzerland: Springer Nature Switzerland.

Squires, K.E., Thompson, T.J.U., Islam, M. and Chamberlain, A. (2011) ‘The application of histomorphometry and Fourier Transform Infrared Spectroscopy to the analysis of early Anglo-Saxon burned bone’, *Journal of Archaeological Science*, 38(9), pp. 2399–2409. doi:10.1016/j.jas.2011.04.025.

Stathopoulou, E.T., Psycharis, V., Chryssikos, G.D., Gionis, V. and Theodorou, G. (2008) ‘Bone diagenesis: New data from infrared spectroscopy and X-ray diffraction’, *Palaeogeography, Palaeoclimatology, Palaeoecology*, 266(3–4), pp. 168–174. doi:10.1016/j.palaeo.2008.03.022.

Steinberg, S.M. and Bada, J.L. (1983) ‘Peptide Decomposition in the Neutral pH Region via the Formation of Diketopiperazines’, *The Journal of Organic Chemistry*, 48(13), pp. 2295–2298.

Stevens, J. (2002) *Applied multivariate statistics for the social sciences*. 4th ed. Mahwah, N.J. ; London: Erlbaum.

Stiner, M.C., Kuhn, S.L., Weiner, S. and Bar-Yosef, O. (1995) ‘Differential Burning, Recrystallization, and Fragmentation of Archaeological Bone’, *Journal of Archaeological Science*, 22(2), pp. 223–237. doi:10.1006/jasc.1995.0024.

Stratton, S.U. and Beattie, O.B. (1999) ‘Mass disasters: comment and discussion regarding the Hinton Train collision of 1986’, in Fairgrieve, S.I. (ed.) *Forensic Osteological Analysis: A Book of Case Studies*. Springfield, IL: Charles C Thomas, pp. 267–286.

Van Strydonck, M., Boudin, M., Hoefkens, M. and De Mulder, G. (2005) ‘14C-dating of cremated bones, why does it work’, *Lunula. Archaeologia protohistorica*, 13, pp. 3–10.

Strydonck, M. Van, Boudin, M. and Mulder, G. De (2010) ‘The Carbon Origin of Structural Carbonate in Bone Apatite of Cremated Bones’, *Radiocarbon*, 52(2), pp. 578–586. doi:10.1017/S0033822200045616.

Subira, M.E. and Malgosa, A. (1993) 'The effect of cremation on the study of trace elements', *International Journal of Osteoarchaeology*, 3(2), pp. 115–118. doi:10.1002/oa.1390030208.

Supova, M. (2014) 'Isolation and Preparation of Nanoscale Bioapatites from Natural Sources: A Review', *Journal of Nanoscience and Nanotechnology*, 14, pp. 546–563.

Symes, S., Williams, J., Murray, E., Hoffman, J., Holland, T., Saul, J., Saul, F. and Pope, E. (2002) 'Taphonomic Context of Sharp-Force Trauma in Suspected Cases of Human Mutilation and Dismemberment', in Haglund, W. and Sorg, M. (eds) *Advances in Forensic Taphonomy:Method, Theory, and Archaeological Perspectives*. Boca Raton, FL: CRC Press, pp. 403–434.

Symes, S.A., Dirkmaat, D.C., Ousley, S., Chapman, E. and Cabo, L. (2012) *Recovery and Interpretation of Burned Human Remains*. Available at: https://www.ncjrs.gov/App/AbstractDB/AbstractDBDetails.aspx?id=260003.

Symes, S.A., L'Abbé, E.N., Pokines, J.T., Messer, D., Stromquist, A. and Keough, N. (2014) 'Thermal Alteration to Bone', in Symes, S.A. and Pokines, J. (eds) *Manual of forensic taphonomy*. Boca Raton, FL: CRC Press/Taylor & Francis Group, pp. 367–402.

Symes, S.A., Rainwater, C.W., Chapman, E.N., Gipson, D.R. and Piper, A.L. (2008) 'Patterned thermal destruction of human remains in a forensic setting', in Schmidt, C.W. and Symes, S.A. (eds) *The Analysis of Burned Human Remains*. CRC Press. Boca Raton, pp. 15–55.

Szpak, P., Metcalfe, J.Z. and Macdonald, R.A. (2017) 'Best practices for calibrating and reporting stable isotope measurements in archaeology', *Journal of archaeological science, reports*, 13, pp. 609–616. doi:10.1016/j.jasrep.2017.05.007.

Taylor, M.E., Morecroft, M.D. and Oliver, H.R. (2011) 'The Physical Environment', *Wytham Woods* [Preprint]. Oxford University Press. doi:10.1093/acprof:osobl/9780199605187.003.0002.

Taylor, M.G., Parker, S.F., Simkiss, K. and Mitchell, P.C.H. (2001) 'Bone mineral: evidence for hydroxy groups by inelastic neutron scattering', *Physical Chemistry Chemical Physics*, pp. 1514–1517. doi:10.1039/b005666i.

Termine, J.D. (1972) 'Mineral chemistry and skeletal biology', *Clinical orthopaedics and related research*, 85, pp. 207–241. doi:10.1097/00003086-197206000-00036.

Terwiel, B.J. (1975) *Monks and Magic: An Analysis of Religious Ceremonies in Central Thailand*. London: Curzon Press.

Théry-Parisot, I. (2002) 'Fuel Management (Bone and Wood) During the Lower Aurignacian in the Pataud Rock Shelter (Lower Palaeolithic, Les Eyzies de Tayac, Dordogne, France). Contribution of Experimentation', *Journal of Archaeological Science*, 29(12), pp. 1415–1421. doi:10.1006/jasc.2001.0781.

Thompson, T.J.., Islam, M., Piduru, K. and Marcel, A. (2011) 'An investigation into the internal and external variables acting on crystallinity index using Fourier Transform Infrared Spectroscopy on unaltered and burned bone', *Palaeogeography, palaeoclimatology, palaeoecology*, 299(1–2), pp. 168–174. doi:10.1016/j.palaeo.2010.10.044.

Thompson, T.J.U. (2004) 'Recent advances in the study of burned bone and their implications for forensic anthropology', *Forensic Science International*, 146(SUPPL.), pp.

203–205. doi:10.1016/j.forsciint.2004.09.063.

Thompson, T.J.U. (2005) ‘Heat-induced dimensional changes in bone and their consequences for forensic anthropology’, *Journal of Forensic Sciences*, 50, pp. 185–193.

Thompson, T.J.U. (2015) *The archaeology of cremation : burned human remains in funerary studies*. Oxford, England ; Philadelphia, Pennsylvania.

Thompson, T.J.U., Gauthier, M. and Islam, M. (2009) ‘The application of a new method of Fourier Transform Infrared Spectroscopy to the analysis of burned bone’, *Journal of Archaeological Science*, 36(3), pp. 910–914. doi:10.1016/j.jas.2008.11.013.

Thompson, T.J.U. and Inglis, J. (2009) ‘Differentiation of serrated and non-serrated blades from stab marks in bone’, *International Journal of Legal Medicine*, 123(2), pp. 129–135. doi:10.1007/s00414-008-0275-x.

Thompson, T.J.U., Islam, M. and Bonniere, M. (2013) ‘A new statistical approach for determining the crystallinity of heat-altered bone mineral from FTIR spectra.(Report)’, *Journal of Archaeological Science*, 40(1), p. 416.

Tjelldén, A.K.E., Kristiansen, S.M., Birkedal, H. and Jans, M.M.E. (2018) ‘The pattern of human bone dissolution—A histological study of Iron Age warriors from a Danish wetland site’, *International Journal of Osteoarchaeology*, 28(4), pp. 407–418. doi:10.1002/oa.2666.

Trueman, C.N.., Behrensmeyer, A.K., Tuross, N. and Weiner, S. (2004) ‘Mineralogical and compositional changes in bones exposed on soil surfaces in Amboseli National Park, Kenya: diagenetic mechanisms and the role of sediment pore fluids’, *Journal of Archaeological Science*, 31(6), pp. 721–739. doi:10.1016/j.jas.2003.11.003.

Trueman, C.N. (1999) ‘Rare Earth Element Geochemistry and Taphonomy of Terrestrial Vertebrate Assemblages’, *PALAIOS*, 14(6), pp. 555–568. doi:10.2307/3515313.

Trueman, C.N. (2013) ‘Chemical taphonomy of biomineralized tissues’, *Palaeontology*, 56(3), pp. 475–486. doi:10.1111/pala.12041.

Trueman, C.N. and Martill, D.M. (2002) ‘The long–term survival of bone: the role of bioerosion’, *Archaeometry*. Oxford, UK and Boston, USA: Blackwell Publishers Ltd, pp. 371–382. doi:10.1111/1475-4754.t01-1-00070.

Trueman, C.N., Privat, K. and Field, J. (2008) ‘Why do crystallinity values fail to predict the extent of diagenetic alteration of bone mineral?’, *Palaeogeography, Palaeoclimatology, Palaeoecology*, 266(3–4), pp. 160–167. doi:10.1016/j.palaeo.2008.03.038.

Trueman, C.N. and Tuross, N. (2002) ‘Trace Elements in Recent and Fossil Bone Apatite’, *Reviews in Mineralogy and Geochemistry*, 48(1), pp. 489–521. doi:10.2138/rmg.2002.48.13.

Turner-Walker, G. (2007) ‘The Chemical and Microbial Degradation of Bones and Teeth’, in Pinhasi, R. and Mays, S. (eds) *Advances in Human Palaeopathology*. John Wiley & Sons, Ltd, pp. 3–13. doi:10.1002/9780470724187.ch1.

Turner-Walker, Gordon (2012) ‘Early bioerosion in skeletal tissues : Persistence through deep time Early bioerosion in skeletal tissues : persistence through deep time’, *Neues Jahrbuch fur Geologie und Palaontologie-Abhandlungen* [Preprint], (August 2012). doi:10.1127/0077-7749/2012/0253.

Turner-Walker, G. (2012) ‘Early bioerosion in skeletal tissues: persistence through deep

time', *Neues Jahrbuch fur Geologie und Palaontologie-Abhandlungen*, 265(2), pp. 165–183.

Turner-Walker, G. (2019) 'Light at the end of the tunnels ? The origins of microbial bioerosion in mineralised collagen', *Palaeogeography, Palaeoclimatology, Palaeoecology*, 529(June 2018), pp. 24–38. doi:10.1016/j.palaeo.2019.05.020.

Turner-Walker, G. and Jans, M. (2008) 'Reconstructing taphonomic histories using histological analysis', *Palaeogeography , Palaeoclimatology , Palaeoecology*, 266(3), pp. 227–35. doi:10.1016/j.palaeo.2008.03.024.

Turner-Walker, G. and Peacock, E.E. (2008) 'Preliminary results of bone diagenesis in Scandinavian bogs', *Palaeogeography, palaeoclimatology, palaeoecology*, 266(3), pp. 151–159. doi:10.1016/j.palaeo.2008.03.027.

Turner-Walker, G. and Syversen, U. (2002) 'Quantifying histological changes in archaeological bones using BSE-SEM image analysis', *Archaeometry*, 44(3), pp. 461–468. doi:10.1111/1475-4754.t01-1-00078.

Turner, B. and Wiltshire, P. (1999) 'Experimental validation of forensic evidence : a study of the decomposition of buried pigs in a heavy clay soil', 101, pp. 113–122.

Ubelaker, D.H. (2009) 'The forensic evaluation of burned skeletal remains: A synthesis', *Forensic Science International*, 183(1–3), pp. 1–5. doi:10.1016/j.forsciint.2008.09.019.

Ubelaker, D.H. (2015) 'Case applications of recent research on thermal effects on the skeleton', in Thompson, T. (ed.) *The Archaeology of Cremation: burned human remains in funerary studies*, pp. 213–227.

Ubelaker, D.H. and Adams, B.J. (1995) 'Differentiation of perimortem and postmortem trauma using taphonomic indicators', *Journal of Forensic Sciences*, 40(3), pp. 509–512.

Upton, R.N., Checinska Sielaff, A., Hofmockel, K.S., Xu, X., Polley, H.W. and Wilsey, B.J. (2020) 'Soil depth and grassland origin cooperatively shape microbial community co-occurrence and function', *Ecosphere (Washington, D.C)*, 11(1), pp. 1–20. doi:10.1002/ecs2.2973.

Van Vark, G.N. (1970) *Some Statistical Procedures for the Investigation of Prehistoric Human Skeletal Material.* Groningen: Rijksuniversiteit te Groningen.

Végh, E. and Rando, C. (2017) 'Effects of Heat as a Taphonomic Agent on Kerf Dimensions', *Archaeological and Environmental Forensic Science*, 1(2), pp. 105–118.

Végh, E.I., Czermak, A., Márquez-Grant, N. and Schulting, R.J. (2021) 'Assessing the reliability of microbial bioerosion features in burnt bones: A novel approach using feature-labelling in histotaphonomical analysis', *Journal of archaeological science : Reports*, 37, p. 102906. doi:10.1016/j.jasrep.2021.102906.

Végh, E.I., Márquez-Grant, N. and Schulting, R.J. (2022) 'Physicochemical Changes in Bone Bioapatite During the Late Postmortem Interval Pre- and Post-Burning', *Applied spectroscopy*, pp. 37028221085600–37028221085600. doi:10.1177/00037028221085600.

Walden, S.J., Mulville, J., Rowlands, J.P. and Evans, S.L. (2018) 'An Analysis of Systematic Elemental Changes in Decomposing Bone', *Journal of Forensic Sciences*, 63(1), pp. 207–213. doi:10.1111/1556-4029.13480.

Walker, P.L., Miller, K.W.P. and Richman, R. (2008) 'Time, temperature, and oxygen

availability: an experimental study of the effects of environmental conditions on the color and organic content of cremated bone', in Schmidt, C. and Symes, S.A. (eds) *The Analysis of Burned Human Remains*. 1st edn. San Diego: Academic Press, pp. 129–xi.

Walshaw, R. (2018) 'Electron probe microanalysis (EPMA) in the Earth Sciences', in Kearns, S.L. (ed.) *Book of Tutorials and Abstracts. Microbeam Analysis in the Earth Sciences, 13th EMAS Regional Workshop*. University of Bristol, Bristol, pp. 93–102.

Waltenberger, L. and Schutkowski, H. (2017) 'Effects of heat on cut mark characteristics', *Forensic Science International*, 271, pp. 49–58. doi:10.1016/j.forsciint.2016.12.018.

Walters, M. a., Leung, Y.C., Blumenthal, N.C., LeGeros, R.Z. and Konsker, K. a. (1990) 'A raman and infrared spectroscopic investigation of biological hydroxyapatite', *Journal of Inorganic Biochemistry*, 39(3), pp. 193–200. doi:10.1016/0162-0134(90)84002-7.

Wang, X.-Y., Zuo, Y., Huang, D., Hou, X.-D. and LI, Y.-B. (2010) 'Comparative Study on Inorganic Composition and Crystallographic Properties of Cortical and Cancellous Bone', *Biomedical and Environmental Sciences*, 23(6), pp. 473–480. doi:10.1016/S0895-3988(11)60010-X.

Ward, S.M. and Tayles, N. (2015) 'The Use of Ethnographic Information in Cremation Studies: A Southeast Asian Example', in Schmidt, C.W. and Symes, S.A. (eds) *The Analysis of Burned Human Remains*. 2nd edn. Amsterdam: Academic Press, Elservier, pp. 381–402.

Warren, B.E. (1941) 'X-Ray Diffraction in Random Layer Lattices', *Physical Review*, 59(9), pp. 693–698.

Waterman, D.M., Wells, C. and Northover, J.P. (1978) 'The Excavation of a Court Cairn at Tully County Fermanagh', *Ulster Journal of Archaeology*, 41, pp. 3–14.

Wedel, V.L. (2014) *Broken bones : anthropological analysis of blunt force trauma*. Second edition. Springfield, Illinois.

Wedl, C. (1864) 'Über einen im Zahnbein und Knochen keimenden Pilz', *Sitzungsberichte der Kaiserlichen Akademie der Wissenschaften zu Wien, Mathematisch-Naturwissenschaftliche Classe*, 50(1), pp. 171–193.

Weiner, S. and Bar-Yosef, O. (1990) 'States of preservation of bones from prehistoric sites in the Near East: A survey', *Journal of Archaeological Science*, 17(2), pp. 187–196. doi:10.1016/0305-4403(90)90058-D.

Wells, C. (1978) 'Notes on Cremated Bones from Tully Court Cairn', *Ulster Journal of Archaeology*, 41, pp. 13–14.

Wells, L.H. (1962) 'Report on the inhumation burials from the West Kennet barrow', *Piggott*, pp. 79–89.

Wheatley, B. (2008) 'Perimortem or Postmortem Bone Fractures? An Experimental Study of Fracture Patterns in Deer Femora', *Journal of Forensic Sciences*, 53(1), pp. 69–72.

White, E.M. and Hannus, L.A. (1983) 'Chemical Weathering of Bone in Archaeological Soils', *American antiquity*, 48(2), pp. 316–322. doi:10.2307/280453.

White, L. and Booth, T.J. (2014) 'The origin of bacteria responsible for bioerosion to the internal bone microstructure: Results from experimentally-deposited pig carcasses', *Forensic Science International*, 239, pp. 92–102. doi:10.1016/j.forsciint.2014.03.024.

White, T.D. (2000) *Human Osteology*. 2nd edn. San Diego: Academic Press.

White, T.D. and Folkens, P.A. (2005) *The human bone manual*. Burlington, Mass: London: Elsevier.

Whyte, T. (2001) 'Distinguishing remains of human cremations from burned animal bones', *Journal of Field Archaeology*, 28, pp. 437–448.

Wieberg, D.A.M. and Wescott, D.J. (2008) 'Estimating the timing of long bone fractures: Correlation between the postmortem interval, bone moisture content, and blunt force trauma fracture characteristics', *Journal of Forensic Sciences*, 53(5), pp. 1028–1034. doi:10.1111/j.1556-4029.2008.00801.x.

Williams, C.T. (1988) 'Alteration of Chemical Composition of Fossil Bones by Soil Processes and Groundwater', in G., G. and B., H. (eds) *Trace Elements in Environmental History. Proceedings in Life Sciences*. Springer, Berlin, pp. 27–40. doi:https://doi.org/10.1007/978-3-642-73297-3_3.

Wilson, A.S., Janaway, R.C., Holland, A.D., Dodson, H.I., Baran, E., Pollard, A.M., Tobin, D.J., Sciences, A. and Bd, W.Y. (2007) 'Modelling the buried human body environment in upland climes using three contrasting field sites', 169, pp. 6–18. doi:10.1016/j.forsciint.2006.07.023.

Wilson, J., van Doorn, N.L. and Collins, M.J. (2012) 'Assessing the Extent of Bone Degradation Using Glutamine Deamidation in Collagen', *Analytical chemistry (Washington)*, 84(21), pp. 9041–9048. doi:10.1021/ac301333t.

de Winter, N.J., Snoeck, C., Schulting, R., Fernández-Crespo, T. and Claeys, P. (2019) 'High-resolution trace element distributions and models of trace element diffusion in enamel of Late Neolithic/Early Chalcolithic human molars from the Rioja Alavesa region (north-central Spain) help to separate biogenic from diagenetic trends', *Palaeogeography, palaeoclimatology, palaeoecology*, 532, p. 109260. doi:10.1016/j.palaeo.2019.109260.

Wong, D. (1998) 'Mon Music for Thai Deaths: Ethnicity and Status in Thai Urban Funerals', *Asian folklore studies*, 57(1), pp. 99–130. doi:10.2307/1178999.

Woodman, J., Shinn, W., Urban, R. and Galante, J. (1984) 'Electron microprobe analysis of metal ion transport in cortical bone', *Journal of Biomedical Materials Research*, 18(4), p. 463. doi:10.1002/jbm.820180412.

Wopenka, B. and Pasteris, J.D. (2005) 'A mineralogical perspective on the apatite in bone', *Materials Science and Engineering*, C 25, pp. 131–143.

Wright, L.E. and Schwarcz, H.P. (1996) 'Infrared and Isotopic Evidence for Diagenesis of Bone Apatite at Dos Pilas, Guatemala: Palaeodietary Implications', *Journal of Archaeological Science*, 23(6), pp. 933–944. doi:10.1006/jasc.1996.0087.

Yao, F., LeGeros, J.P. and LeGeros, R.Z. (2009) 'Simultaneous incorporation of carbonate and fluoride in synthetic apatites: Effect on crystallographic and physico-chemical properties', *Acta biomaterialia*, 5(6), pp. 2169–2177. doi:10.1016/j.actbio.2009.02.007.

Yoder, C.H., Bollmeyer, M.M., Stepien, K.R. and Dudrick, R.N. (2012) 'The effect of incorporated carbonate and sodium on the IR spectra of A- and AB-type carbonated apatites', *American Mineralogist*, 104(6), pp. 869–877. doi:10.2138/am-2019-6800.

Yoo, D.S., Cho, J.S., Chung, Y.-C. and Rhee, S.-H. (2021) 'Defect structures of sodium and

chloride co-substituted hydroxyapatite and its osseointegration capacity', *Journal of Materials Science*, 56(9), pp. 5493–5508. doi:10.1007/s10853-020-05645-9.

Yoshino, M., Kimijima, T., Miyasaka, S., Sato, H. and Seta, S. (1991) 'Microscopical study on estimation of time since death in skeletal remains', *Forensic Science International*, 49(2), pp. 143–158. doi:10.1016/0379-0738(91)90074-S.

Yravedra, J., García-Vargas, E., Maté-González, M.Á., Aramendi, J., Palomeque-González, J.F., Vallés-Iriso, J., Matesanz-Vicente, J., González-Aguilera, D. and Domínguez-Rodrigo, M. (2017) 'The use of Micro-Photogrammetry and Geometric Morphometrics for identifying carnivore agency in bone assemblages', *Journal of Archaeological Science:Reports*, 14, pp. 106–115. doi:10.1016/j.jasrep.2017.05.043.

Zapanta Legeros, R. (1981) 'Apatites in biological systems', *Progress in crystal growth and characterization*, 4(1–2), pp. 1–45. doi:10.1016/0146-3535(81)90046-0.

Zazzo, A., Lécuyer, C., Mariotti, A., Jiang, M., Terra, J., Rossi, A.M., Morales, M.A., Baggio Saitovitch, E.M., Ellis, D.E., Caruso, V., Marinoni, N., Diella, V., Berna, F., Cantaluppi, M., Mancini, L., *et al.* (2020) '(formula presented) substitution in hydroxyapatite: Theory and experiment', *Physical Review B - Condensed Matter and Materials Physics*, 2148(1), pp. 87–100. doi:10.1016/j.jasrep.2020.102333.

Zazzo, A. and Saliège, J.-F. (2011) 'Radiocarbon dating of biological apatites: A review', *Palaeogeography, Palaeoclimatology, Palaeoecology*, 310(1), pp. 52–61. doi:10.1016/j.palaeo.2010.12.004.

Zazzo, A., Saliège, J.-F., Person, A. and Boucher, H. (2009) 'Radiocarbon Dating of Calcined Bones: Where Does the Carbon Come from?', *Radiocarbon*, 51(2), pp. 601–611. doi:10.1017/S0033822200055958.

Zioupos, Peter, Currey, J.D. and Casinos, A. (1999) 'Exploring the Effects of Hypermineralisation in Bone Tissue by Using an Extreme Biological Example', *Connective Tissue Research*, 41(3), pp. 229–248. doi:10.3109/03008200009005292.

Zioupos, P., Currey, J.D. and Hamer, A.J. (1999) 'The role of collagen in the declining mechanical properties of aging human cortical bone', *Journal of Biomedical Materials Research*, 45(4), pp. 108–116. doi:10.1002/(SICI)1097-4636(199905)45:2<108::AID-JBM5>3.0.CO;2-A.

Appendixes

Appendix A: Proof-of-Concept Study

This small study served as a proof-of-concept study prior to the other experiments in the thesis (Chapters III, IV, and V). The methodologies used are thoroughly described in this small study. Bones from differing diagenetic histories and postmortem intervals (5,5 ka to fresh) were burnt in an Anagama kiln. This type of kiln was chosen because it is operated outdoors and thus fleshed tibiae could be placed inside, unlike in furnaces in a laboratory setting. This pre-study was useful for a number of reasons. First, it showed that burning in a kiln with constant temperatures at around 500°C does not result in the recrystallisation of the apatite phase, thus outdoor fires with more variable temperatures were used for the main experiments. Second, the study demonstrated that only a PMI of 4 years is enough to cause changes in the bone's molecular structure. Third, that looking at substitutions of elements can be of potential use in diagenesis studies, which would be of the highest importance if they survive burning. And finally, it demonstrated that only the fresh bones showed thumbnail fractures and only 4 years of PMI is sufficient for this feature to be absent.

A.1 Introduction

Major complications in the analysis of human remains include distinguishing between injuries inflicted perimortem and those that occur well after death fresh, as well as recognising trauma features on burnt bones. This study investigated sharp force trauma (SFT) manually inflicted on bones at different stages of decomposition and weathering, particularly the possibility of determining the time of trauma infliction relative to the burning event. The first aim was to analyse whether post-mortem or taphonomic alterations to bone, which might appear as SFT, can be mistaken as trauma inflicted on fresh, or 'perimortem', remains. Secondly, it aimed to examine the physicochemical changes and macro- and microscopic alterations on burnt bones and to answer whether it is possible to determine their original state

prior to the fire event. The results of this study contribute to understanding the effects of heat-induced changes and to the recognition of osteogenic reactions for applications both in osteoarchaeology and forensic anthropology.

A.2 Materials and Methods

The bones used for the control study included bones from different original conditions comprised of: (1) one fully fleshed pig tibia (C5); (2) one partially de-fleshed but still fresh pig tibia (C4); (3) two de-fleshed pig tibiae which have weathered outdoors for 4 years (C1, C3); (4) and one 5.5ka archaeological cattle rib bone (C2). The fresh tibiae were kept in a freezer from the time of collection until the time of transportation (approximately 70 h) to the kiln site. They were out of the freezer for approximately 1 hour wrapped in plastic and in aluminium foil for transportation. C1 and C3 displayed lipid retention along the diaphysis, furrows and scalloped edges from animal gnawing (Pokines and Symes, 2014).

Three types of trauma were inflicted on each bone: a non-serrated, single edged knife, a partially serrated knife, and a flint blade. These lesions were inflicted on all samples from all experiments, as described in Chapter VI. All incisions were on one side of the bone (Fig. 33) except the fully fleshed one. It was impossible to see where the trauma was inflicted on the fleshed limb (C5) and the flint cutmarks were produced on the opposite side of C5. The non-serrated knife was used to cut through the skin, subcutaneous fat, flesh, and tendons carefully to access the bone and then the right type of instrument was used to cut the bone. Once all SFT was inflicted, a centimetre-thick sample was taken from the distal end of each bone with a butcher's saw and a hacksaw for further analyses. These two weapons were only used to take samples and the imprint they left on the bones were not investigated further.

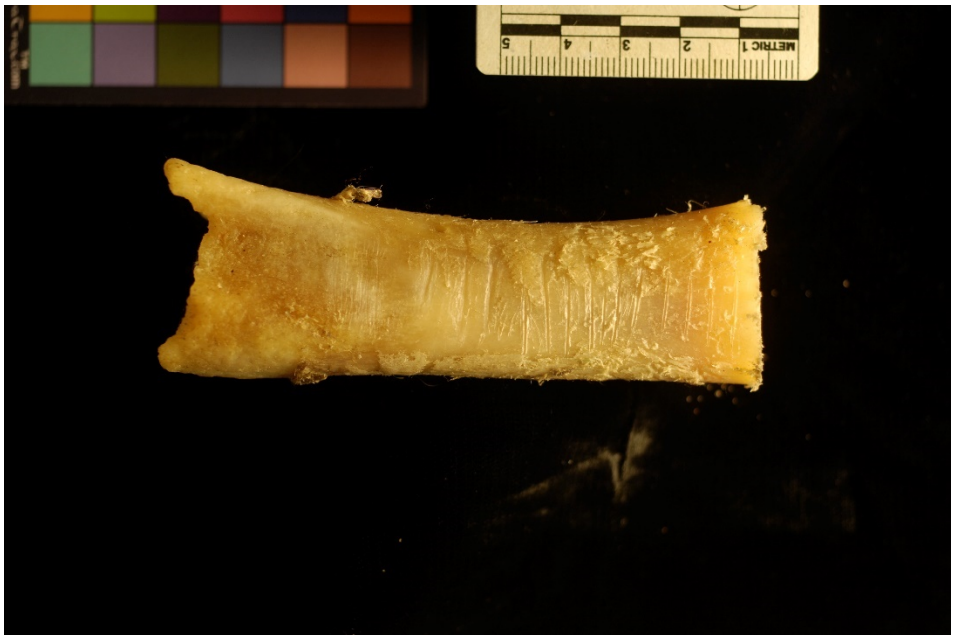


Figure 33 – Example of the SFT present on a four-year weathered bone (C1). Weapons used from right to left: non-serrated knife, partially serrated knife, flint blade (five incisions per weapon).

A.2.1 Controlled Heating in Kiln

The differentially decomposed and processed legs were placed into a Japanese-style brick anagama ceramics kiln provided to the researcher by the Anagama Project at Wytham Woods, Oxfordshire. The kiln had two openings on the sides with shelves into which another brick with the bones could be slid inside (Fig. 34). A thermocouple was fixed on the partially defleshed bone (Fig. 35) in order to measure the bone's temperature rather than the overall heat in the kiln, as it has been shown that the temperature of the fire or heat source is not representative of the temperature the bone suffers (Fairgrieve, 2008) and there are misalignments of temperatures and corresponding changes in some previous papers.



Figure 34 – The ceramics kiln used for the control experiment.



Figure 35 – The thermocouple is fixed onto the bone kept in place by the bricks. The bricks also served an insulating purpose to keep the heat inside the kiln.

The kiln used was 6 m long and 1.5 m wide and was fuelled by soft wood. The temperature at the front of the kiln was 1023°C, but the bones were placed at the cooler end of the furnace, so results and temperatures could be replicated in an outdoor fire. The kiln was already at the desired temperature when the legs were placed in. Temperatures were recorded every 15 minutes with the thermocouple. The bone's temperature fluctuated between 437°C and 536°C with a mean temperature of 515°C throughout the 2 hours and 45 minutes they were in the kiln. Previous literature suggests that fat on fleshed remains ignits at around 700 °C, and below this temperature the bone's crystal structure is less affected by heat (Ellingham *et al.*, 2016). Ten minutes after the bones were placed into the kiln white smoke came out from the

small openings on the kiln for approximately 5 minutes. This smoke turned black and continued to be released for over an hour. The legs were examined every 30 mins as the researcher's intention was to take them out whenever all bones appear fully calcined marked by their overall white colour to ensure all bones' constant post-burnt state. After an hour of heating the two 4-year-weathered bones (C1, C3) were already completely white, while the flesh on the bone surface of C5 was blazing with the bone marrow almost completely leached out (Fig. 35). Once bones were removed, they were carefully packed and transported to the laboratory for further analysis.



Figure 36 – The fully fleshed bone (C5) blazes after an hour in the kiln.

The methods to examine the bones throughout this study included the imaging techniques (photography, light microscopy, SEM), ImageJ software for quantitative analysis, FTIR-ATR, XRD, and data analysis and visualisation in Python programming language. This section describes the methodology used to determine qualitative feature characteristics, quantitative changes to cutmarks, surface micromorphology, crystal structure changes, and the way heat-induced fractures were classified.

A.2.2.1 Macroscopic Image Acquisition

A Nikon D2Xs camera fitted with a 60mm Nikon macro lens was used for the photographs. Images were taken of the instruments, and the bones pre- and post-burning. Where it was necessary, putty was used to adjust the samples to make sure the bones' surfaces were perpendicular to the lens's surface. A spirit level was also used on each bone's surfaces to establish they were perpendicular to the camera's lens. Where applicable, an X-Rite ColorChecker Classic Chart was included on the images. The scale was elevated to the same level as the bones' surface where the cutmarks were present to ensure the distances on the scale appear 'real size' compared to the cutmarks. A monopod was used to assure that the camera was stabilised while taking photographs and to eliminate vibration during image capturing. The objects were lit from only one side and the same light was reflected back from the other side with a white paper card. Images were then imported and corrected, and the raw files were converted to PNG. Edges of the cutmarks were possible to recognise in the new file format after zooming in.

Photographs during the experiments were taken by a Nikon Coolpix 510 camera fitted with a "bridge" lens. It was set to Creative Automatic Mode ('CA') in macro mode when the object was close to the lens. This mode allowed the researcher to focus on the area of interest. 'Macro' mode was set for very close photographs of cutmarks, and the flash was turned off for each image.

A.2.2.2 Light Microscopy

Optical light microscopy is perhaps the most often used research tool in imaging. A Wild Photomacroscope (Wild Heerbrugg, Heerbrugg, Switzerland) light microscope was used to observe the pre- and post-burnt cutmarks and bone surfaces. Images were taken with a LMscope, VTC4x2 (LCMOS, Brunel Microscopes Ltd., Chippenham, UK) USB camera

together with ToupView 3.7 (ToupTek Photonics, Zhejiang, China) software. Lighting was optimised using an external lighting source with a wide dynamic range designed to give a choice of high or low intensity illumination at high or low magnifications, respectively. The lowest magnification was set up (6.3x) after calibration in order to visualise larger areas of the cutmarks. Images were later stitched together with Image Composite Editor 2.0.3 (Microsoft, Redmond, Washington, USA). A scale of 1 mm was placed on each image with the ToupView software and exported to a PNG file format.

A.2.2.3 Scanning Electron Microscopy

A Hitachi SU3500 scanning electron microscope (SEM; Hitachi, Chiyoda, Japan) was used at the Forensic Institute of Cranfield University (Defence Academy of the United Kingdom) to acquire detailed images of the post-burnt bone lesions and the bones' surface. SEM has been suggested to give the most precise information regarding the morphology of cutmarks and bone micromorphology (Bartelink *et al.*, 2001; Alunni-Perret *et al.*, 2005; Saville *et al.*, 2007; Bello and Soligo, 2008; Thompson and Inglis, 2009). There was no carbon or gold coating, or any special preparation necessary because the SEM used was environmental (Goldstein *et al.*, 2003). Variable pressure (VP-SEM) mode with 15.0 kV beam energy and 80Pa were used for image acquisition. The SEM was designed to have a working distance of 5 mm at each sample. Bone surfaces and cutmarks were imaged under varying magnification. Each cutmark was observed at least twice: one wider image with lower magnification at 35x-60x and a close up of the walls and the floor at around 210x magnification. Brightness and contrast were adjusted to ensure that kerf walls are as clear and visible as possible, since walls exhibit many qualitative features. When special or unusual features were present, multiple images were taken. The images were saved in TIFF file format.

Qualitative analyses were carried out on the different features of the kerfs, the heat-induced fragmentation pattern, and on the bone surface. Examination of kerf and trauma features and the bone surface were executed on the light microscopy and SEM images, as these provided much more detail than the macroscopic photographs.

A.2.3.1 Kerf Feature Analysis

The SFT was examined for features for two reasons: (1) to find diagnostic features between 'perimortem' (or green bone) and postmortem (or dry bone) injuries to the bone before and after burning; (2) to differentiate between the instruments used after burning, such as the partially serrated knife, flint blade, and non-serrated knife. To inform on the timing of trauma infliction features on the differentially weathered kerfs were observed, which were previously proposed by the literature (Symes *et al.*, 2002; Sauer, 2003; Ortner, 2008), while the features chosen to differentiate between the instrument used were followed after Crowder and colleagues (2013). These features are in Table 17. The total number of cutmarks exhibiting the feature per type of weapon per cutmark was recorded.

Green Bone Features	**Dry Bone Features**	**Features for Weapon Classification**
Irregular kerf edges	Regular shaped cuts	Striations: fine/coarse/fine and coarse/none
Curling or uplifting at kerf edges	Sharp edged kerf	Kerf margin deformation
Splintering at kerf breaks	Discoloured kerf	Exit scraping or trailing scratches
		Clumping on floor

Table 17 – Qualitative Features examined on the cutmarks for diagnostic features of timing ('perimortem' vs postmortem trauma) and for instrument classification.

A.2.3.2 Heat-Induced Fractures

Heat-induced fractures examined include longitudinal fractures, transverse fractures, curved transverse (thumbnail) fractures, step fractures, patina, delamination, splintering, and warping. These fractures were examined with the naked eye and light microscopy. Their presence or absence and the number of times it occurred per bone were recorded.

Due to the scarcity of parallel studies in the literature, a new scoring system was created to quantify the severity of the fractures on the scale of 6. It was developed on the basis of Behrensmeyer's (Behrensmeyer, 1978) scale of the severity of bone weathering, but it was based on the findings of the this study. The description of the scores are the following:

1: There is no macroscopic fragmentation present on the bone. Microscopic superficial fractures or occasional delamination might be present. The bone is intact. There might be some colour change on some parts of the bone.

2: The bone is intact. Superficial fractures are present, but no penetrating cracks along the shaft. Patches of delamination might be present.

3: The bone is cracked, fissured, or fractured. It shows penetrating cracks, but they do not split the shaft (long bone, as per the study). There might be additional superficial fractures, delamination, and warping. In long bones the epiphyses are missing.

4: Bone is fractured into larger pieces. In case of long bones, the epiphyses are completely separated from the diaphysis. Other cracks and superficial fractures are present.

5: In long bones, one side of the diaphysis might be intact but are not fully connected to the other side circumferentially. The epiphyses might be broken into two pieces. Major damage to the bone shaft. Delamination is evident on the bone surface.

6: Bone is shattered. The epiphyses are separated into more than two pieces. More than half of the bone is present only in splinters.

A.2.4 Analytical Techniques

The samples underwent preparation, as discussed in chapter IV, for the analytical laboratory analyses of the powdered bones before and after the fire events.

A.2.4.1 Fourier Transform Infrared Spectroscopy (FTIR)

Fourier Transform Infrared Spectroscopy (FTIR) in attenuated total reflection (ATR) mode was used as described in Chapter II and IV. Ratios used included the crystallinity index/splitting factor (IRSF), amide I, II, III, amide to phosphate ratio (APR), carbonate to phosphate ratio (C/P), carbonate A and B ratio (C/C), carbonate B to phosphate (BPI), and maturity from $_{v1, v3}(PO_4^{3-})$ peaks.

A.2.4.2 X-ray Diffraction (XRD)

X-ray diffraction (XRD) is used to assess the structure and composition of crystalline samples in different materials. It is a commonly used technique in analysing heat-damaged osseous material for different purposes. It has been utilised to differentiate burnt human bone from animal bone based on the inter-species variation in the lattice parameters of the bone crystals (Beckett *et al.*, 2011; Greenwood *et al.*, 2013), to determine the maximum temperature at which bone was burnt at (Shipman *et al.*, 1984; Piga *et al.*, 2008, 2009), and in bone diagenesis studies (Stathopoulou *et al.*, 2008; Trueman *et al.*, 2008). It is evident then that this analytical technique was chosen for this study, also because it allows the researcher to compare the morphological changes and associate it with the microstructural changes of the bone. XRD application within this study is aimed to identify changes in the coherence lengths (crystal size and strain) in the differently decomposed bone samples before and after burning. XRD works by shooting elastic scattering X-rays at the atoms within each defined unit of the material at different angles.

A.2.4.2.1 XRD Data Acquisition

The powdered samples (approximately 0.5-1 g per sample) were placed into separate back-filled sample holders or onto low background scatting sample holders (depending on the amount of sample available). These were then loaded into a carousel and placed inside a PANalytical X'pert PRO Multi-Purpose X-ray diffractometer (Malvern Instruments Ltd., Malvern, UK) and Cu Kα radiation with a PIXcel strip detector. Each sample was run for one hour and the results were then collected by the equipment's detector. Bruker Topas XRD (version 4.1, 2008, Bruker, Billarica, Massachusetts, USA) software was used for fitting lattice parameters and individual peaks of diffraction profiles. All scans used a 10° - 80° 2θ range.

Lattice parameters were inspected to detect any chemical modification of the mineral phase due to ionic exchanges. As the program refined the spectra, it plotted a line representing hydroxyapatite (HAp) in order to match it with the detected structure. Once it reached 3 to 4 decimals for the 'a' and 'c' positions, the line fitting was stopped. If the values in these positions showed values that were too far off from normal HAp (i.e. 'a' = 9.432 and 'c'= 6.881) than these samples were run again in the XRD for a longer period to reach better results. This is because when the diffractogram is too noisy, it is not possible to refine both lattice parameters and sample displacement. When better results were not reached by rerunning the samples for longer and it still appeared noisy with bad refinements done by the program, internal standards were used on the bone by being doped with silicone (5-8%). Once ran again, it was refined based on the silicone peaks to produce a less noisy diffractogram. These values were recorded in an Excel sheet with the sample displacement values, which defines what the sample's position is compared to where it meant to be (0 is ideal). Sample displacement was refined and the data was corrected according to conventional XRD analysis (Warren, 1941). Images of the plotted structures were then copied to the clipboard as a metafile and saved in MS Word

(Microsoft, Redmond, Washington, USA). Although, the software shows a value under 'crystal size', it is not a true representation of the size of the crystals, since includes a scaling factor. Then, for each sample the lattice positions, area, the left and right full width half maximum (FWHM)[7], and the left and right Lorentzian at <002>, <004>, <030>, <210> were recorded with their respective error ranges for future calculations. EVA software (DIFFRAC.EVA, Bruker, Billerica, Massachusetts, USA) was used to plot the data acquired from the same bone pre- and post-burning onto the same graph.

When peak data represented additional phases, Crystallographica Search-Match (Oxford Cryosystems, Oxford, UK) was used. This software is a search-match program that searches algorithms for multiple-phase identification from raw and/or peak data and compares them to the International Centre for Diffraction Data's PDF databases. Once the program is running, it goes through the spectrum and shows what chemical modifications are present at which domains. Restrictions of compounds (Ca, P, H, O) were added in order to get more HAp phases in the results. This was necessary, because some peaks or elements were so nanocrystalline that they did not show up as primary results on the pre-burnt samples. In other words, if the peak had very low intensity, it was not possible to see it on the data. The phases that the program picked up were then saved with their international fraction (PDF) number. The microstructural changes found with XRD were than cross-checked using SEM.

A.2.4.2.2 Coherence Lengths: Crystal Size and Strain Calculations

Coherence length (CL) expresses the crystallite size and its defects, such as the strain and disorder in the crystal lattice. Exact crystal size, if it is not a single crystal consisting of only one domain, on its own is not possible to access with XRD.

[7] FWHM is the width of the diffraction peak at the half-way height between the background and the maximum peak in radians (Langford and Wilson, 1978).

CL of all samples were calculated with the aim to investigate the changes to the bones' crystal structure, namely the size and strain of the hydroxyapatite crystal. Crystallite size is the cube root of the volume of the crystallite assuming all crystallites in the material are same sized and shaped (Scherrer, 1918; Langford and Wilson, 1978). The CLs were calculated by measuring the peaks at <002>, <004>, <030>, and <210> on each diffractogram. For each of these indices the position, area, FWHM left, FWHM right, Lorentzian (Lor.) left, and Lor. right of the peaks were recorded with their respective error ranges. In order to get the measurements for <030> and <210>, first another sample had to be analysed by the software, which has been heated for higher temperatures, so it had stronger peaks, to align and find the three peaks. CLs were calculated from the Scherrer equation (Scherrer, 1918):

$$CL(2\theta) = \frac{k\lambda}{\beta cos\theta}$$

Where 'k', or the Scherrer constant, is the shape factor [=0.89 for spherical crystals (Greenwood *et al.*, 2013)]; $'\lambda'$ is the wavelength, which is always the same for CuKα (1.54 Å); 'β' = (FWHM left + FWHM right) – β_{irf}, where 'β_{irf}' is the instrumental factor, in this analysis the DWHM of the NIST SRM64C silicon standard diffraction (used in order to correct for instrumental broadening); and 'Cosθ' is the Bragg angle/angle of diffraction (Langford and Wilson, 1978; Greenwood *et al.*, 2013). One of the reasons that it is not possible to calculate crystal size from the Scherrer Equation is that is uses the FWHM, which is affected by not only the crystal size but by the structural strain.

A.2.4.2.3 Lattice Parameter

The lattice parameter gives the values of the physical dimensions of the unit cells (the smallest repeating unit) in the crystal structure. Lattice parameters were calculated in order to attempt to identify the changes that occurred in the microstructure. The investigation of specific

substitutions in the crystal lattice is not of interest of this thesis, but the *effects* of these substitutions on the crystallites. Therefore, the pre-burnt bones at different stages of decomposition were compared and visually plotted and then the pre-burnt and post-burnt samples lattice parameters were compared at all positions.

A.2.5 Data Management and Statistical Analyses

Acquired data from the different parts of the study were always recorded in MS Excel and converted to a CSV file to be able to load it into other programs. The visual examination of results and data analyses were done in Python programming language in Jupyter notebook environment.

A.3 Results

A.3.1 Sharp Force Trauma Features

Qualitative microscopic features were analysed to help in instrument class identification, which included striation quality[8], quantity, and spacing on both the walls and floor of the kerf (Fig. 37 and 38), kerf margin deformation, exit scraping or trailing scratches, and clumping[9] on the floor of the cutmarks (Fig. 39 and Fig. 40).

[8] Striation quality refers to whether the observed striations were fine, coarse, both or none, and whether they were regularly spaced (patterns) or not (Crowder, Rainwater and Fridie, 2013, 1120-1121)

[9] Clumping, as a feature on cutmarks was introduced to ease the classification. It refers to kerfs, which show clumped bone residue on the floor.

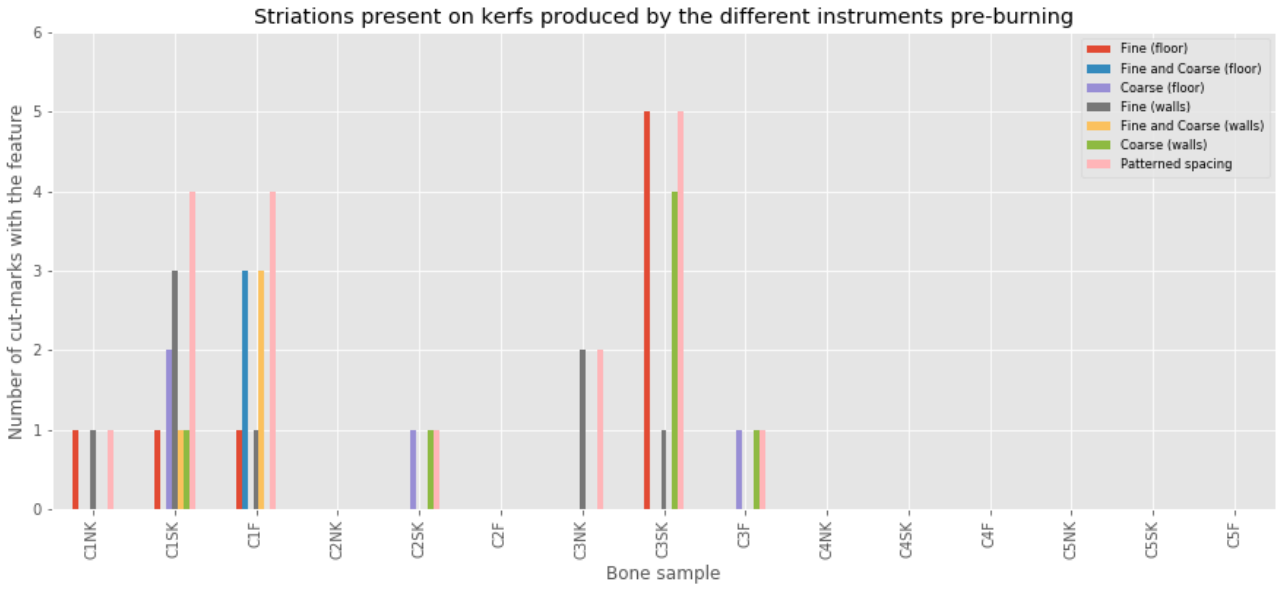


Figure 37 -- The striations noted on the pre-burnt cutmarks. It was not possible to observe striations on the kerfs of partially fleshed and fully fleshed bones, because these were hidden by soft tissue. (Notation: C1 and C3: 5-year PMI bones; C2: 5.5 kya bone; C4: fresh defleshed bone; C5: fresh fleshed bone; NK= non-serrated knife; SK= partially-serrated knife; F=flint blade).

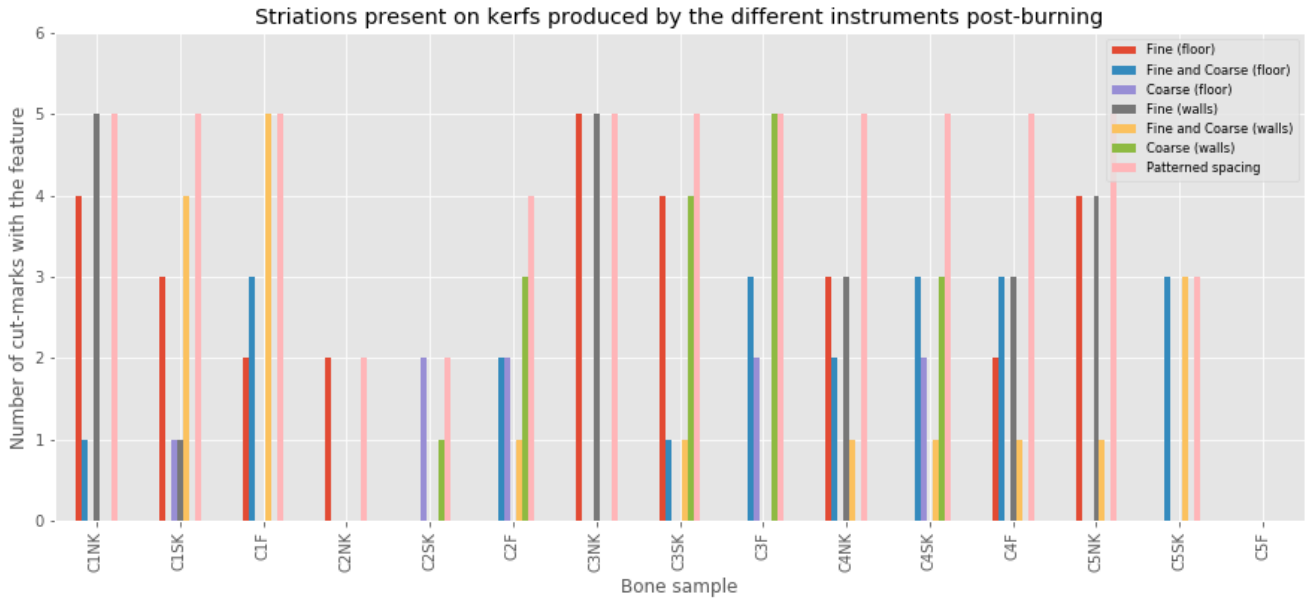


Figure 38 – Striation features observed on the post-burnt kerfs (notation: C1 and C3: 5-year PMI bones; C2: 5.5 kya bone; C4: fresh defleshed bone; C5: fresh fleshed bone; NK= non-serrated knife; SK= partially-serrated knife; F=flint blade).

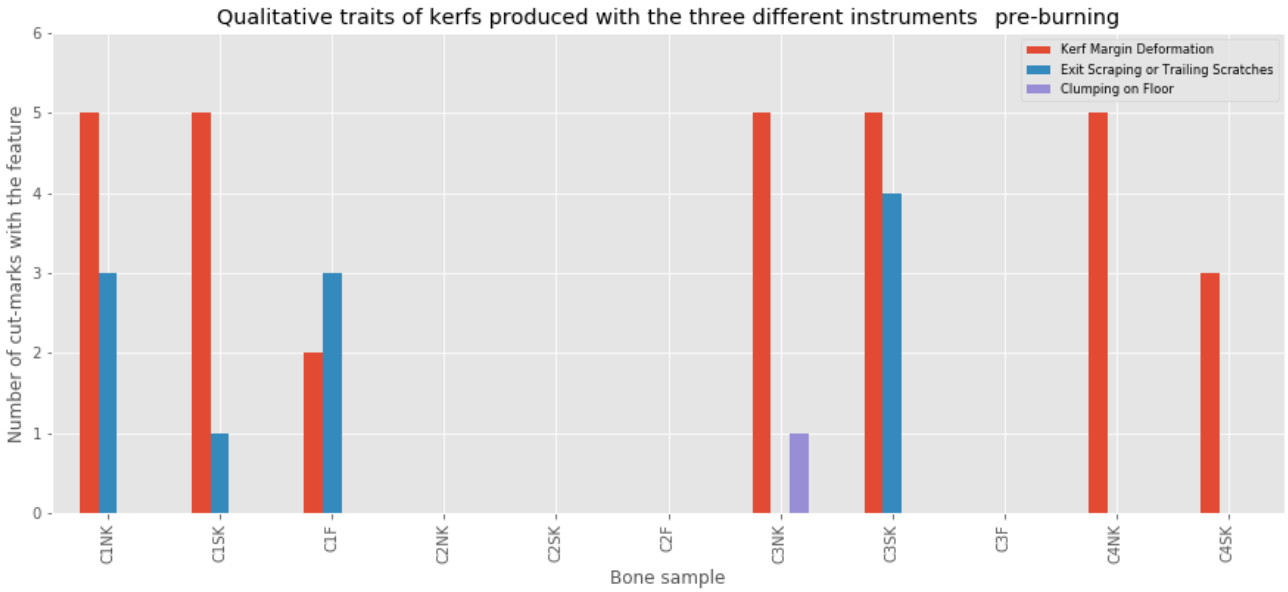


Figure 39 – Qualitative traits observed on the unburnt control kerfs (Notation: C1 and C3: 5-year PMI bones; C2: 5.5 kya bone; C4: fresh defleshed bone; C5: fresh fleshed bone; NK= non-serrated knife; SK= partially-serrated knife; F=flint blade).

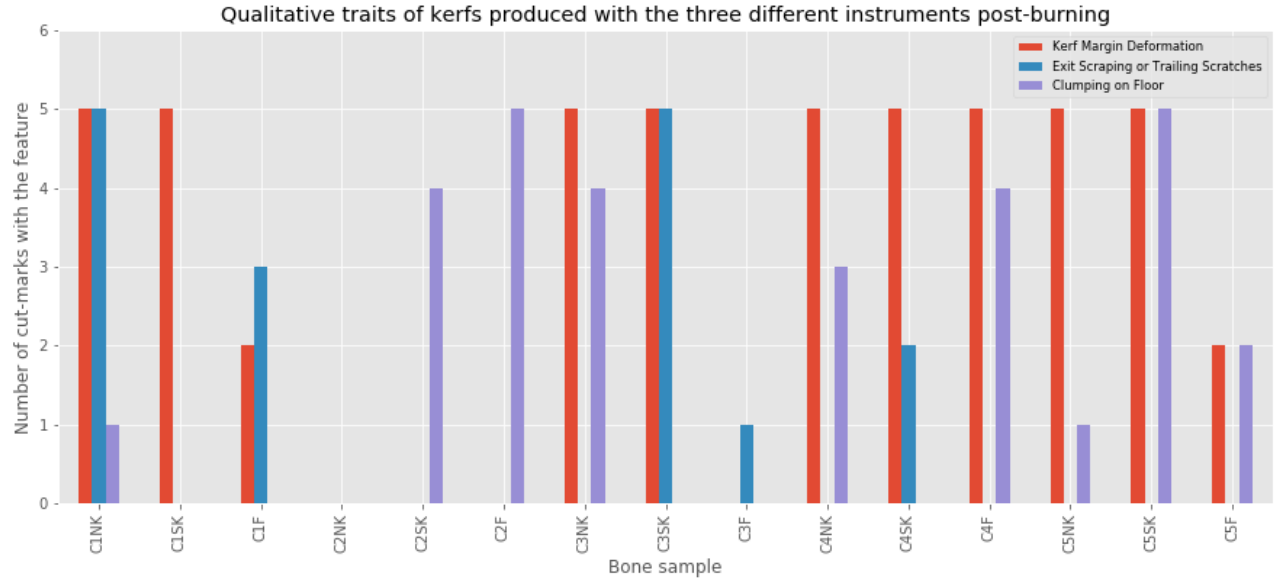


Figure 40 – The qualitative features observed on the burnt control cutmarks (Notation: C1 and C3: 5-year PMI bones; C2: 5.5 kya bone; C4: fresh defleshed bone; C5: fresh fleshed bone; NK= non-serrated knife; SK= partially-serrated knife; F=flint blade).

Striations were more visible on the kerfs post-burning. The 'fine and coarse', and 'coarse' striations on walls were only present when the partially-serrated knife (SK) or the flint blade (F) were used. The kerf margin deformation stayed constant pre- and post-burning. In general, features were more visible post-burning than before the heat was introduced, which aligns with previous research (Végh and Rando, 2017).

Results of the qualitative features that might identify the original condition of the body when the trauma was inflicted can be seen in Fig. 41 for peri-mortem SFT features and Fig. 42 for post-mortem features. The archaeological bone (C2) was the only bone that showed post-mortem SFT features from all the weapons used before burning and the two 4-year weathered bones (C1, C3) showed such features when the flint blade was used for trauma infliction. This might be because the bones were generally dried at the edges where the flint was used towards the proximal ends. Irregular edges were the most common green bone feature in all samples, except the archaeological one, which did not exhibit any macroscopic fracture.

Longitudinal, transverse, step fractures, and delamination was possible to observe on all modern bones (Table 18). The archaeological bone (C2) showed no macroscopic fractures. Thumbnail or curved transverse fractures were only visible on the fresh bones (C4 and C5).

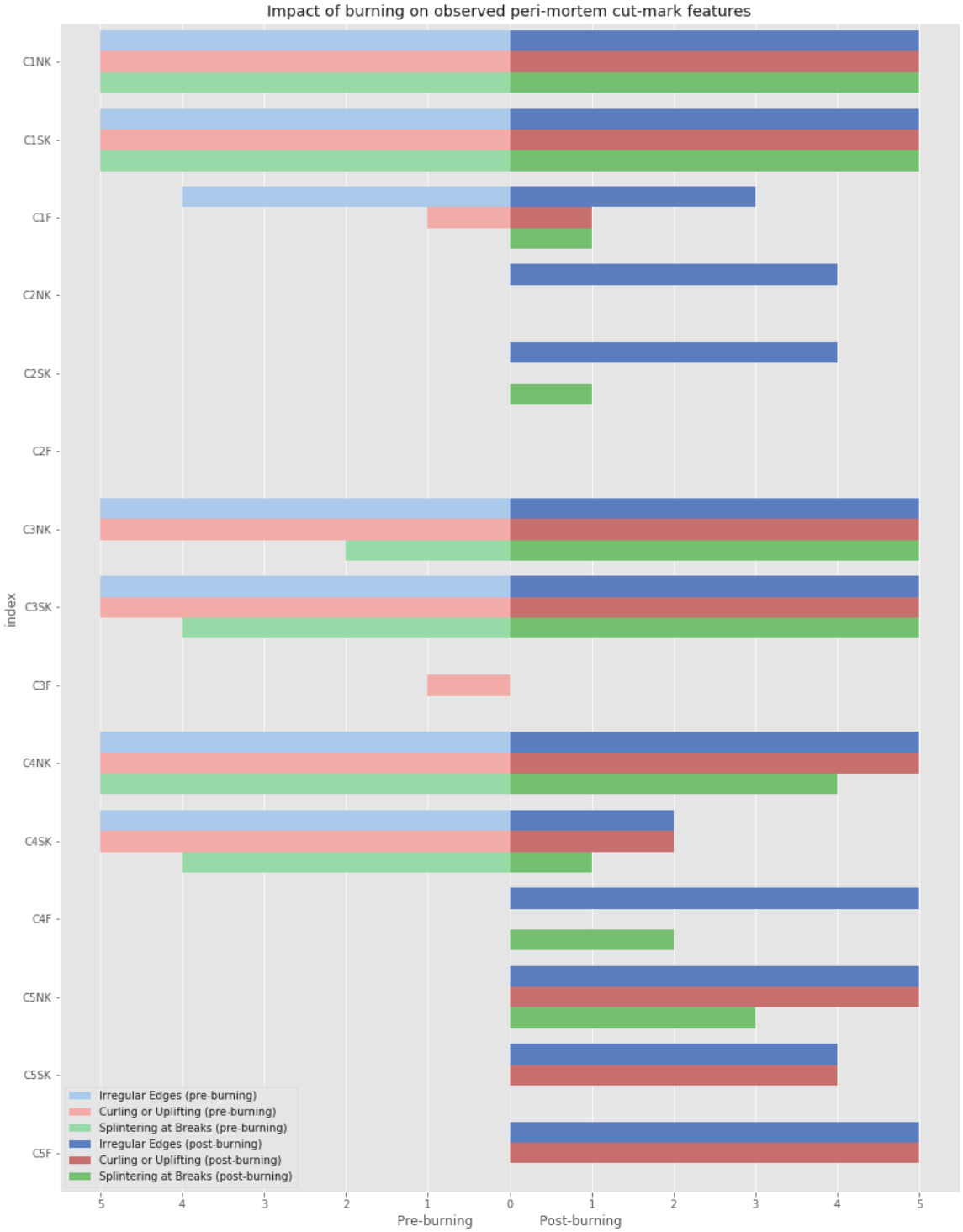


Figure 41 – Graph showing the presence or absence of the peri-mortem features observed on the cutmarks proposed by the literature. The left side shows the presence of these features on the cutmarks before burning, and the right side shows the same features post-burning. (Notation: C1 and C3: 5-year PMI bones; C2: 5.5 kya bone; C4: fresh defleshed bone; C5: fresh fleshed bone; NK= non-serrated knife; SK= partially-serrated knife; F=flint blade).

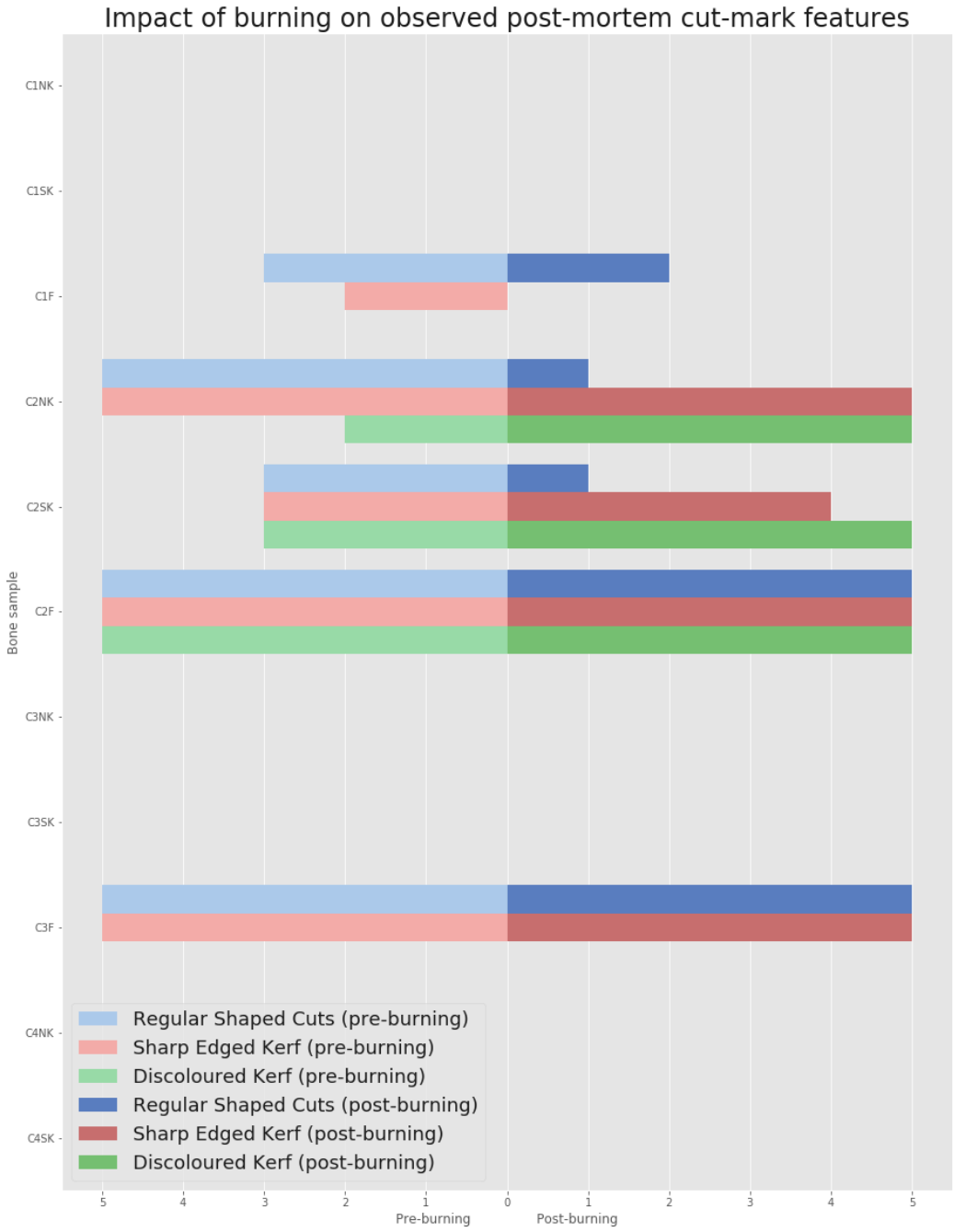


Figure 42 - Graph showing the presence or absence of the peri-mortem features observed on the cutmarks proposed by the literature. The left side shows the presence of these features on the cutmarks before burning, and the right side shows the same features post-burning. (Notation: C1 and C3: 5-year PMI bones; C2: 5.5 kya bone; C4: fresh defleshed bone; C5: fresh fleshed bone; NK= non-serrated knife; SK= partially-serrated knife; F=flint blade).

Fracture type (Macroscopic)	5500-year-old (C2)	4-year-weathered (C1)	4-year-weathered (C3)	Fresh, partially defleshed (C4)	Fresh, fleshed (C5)
Longitudinal	N	Y	Y	Y	Y
Transverse	N	Y	Y	Y	Y
Thumbnail (curved transverse)	N	N	N	Y	Y
Step	N	Y	Y	Y	Y
Patina	N	N	N	N	N
Delamination	N	Y	Y	Y	Y
Splintering	N	N	Y	Y	Y
Warping*	N	N	N	N/A	Y

Table 18 – Table summarising the presence of absence of the macroscopic heat related fractures on the bones involved in the control study.

A.3.2 Infrared Spectroscopy

The calculated ratios from the powdered samples are presented in Table 19. The crystallinity index (IRSF) for all pre-burnt bones was in the range of value for modern natural bone calculated from the FTIR spectra. IRSF increases when the crystal structure becomes more ordered (Thompson *et al.*, 2009; Ellingham *et al.*, 2016). Crystals progress naturally towards a more ordered state very slowly after death through different diagenetic pathways. It is observable that the archaeological bone's IRSF value was the highest before burning. This bone's IRSF value increased the least (from 2.77 to 3.14), while the two freshest bones' (C4 and C5) IRSF values were the highest post-burning (from 2.27 to 4.63 and 4.20, respectively), suggesting that the flesh acted as fuel and so these bones were exposed to higher temperatures than the other ones. The two 4-year weathered bones' IRSF increased more than the archaeological bone but did not reach as high values as the two freshest bones. This suggests that even such short times of decomposition (4 years) is enough to alter the IRSF, affecting the post-burnt values as well. The fresh, partially defleshed (C4) bone doubled its IRSF value after heating and suffered the largest breakage of the collagen intermolecular cross links at amide I

band peaks. In other words, the bones with higher original pre-burnt collagen content (C4, C5), measured from APR, the higher the IRSF values post-burning.

Sample	IRSF		C/P		C/C		APR		BPI		Maturity	
	Pre-burn	Post-burn	Pre-burn	Post-burn	Pre-burn	Post-burn	Pre-burn	Post-burn	Pre-burn	Post-burn	Pre-burn	Post-burn
C1	2.47	3.88	0.53	0.22	1.01	1.43	1.229	1.488	1.115	0.905	1.053	0.827
C2	2.77	3.14	0.3	0.19	0.94	0.98	0.471	0.951	0.619	0.506	1.398	N/A
C3	2.61	3.52	0.35	1.12	1.12	1.51	1.041	0.96	0.742	0.463	0.936	0.834
C4	2.27	4.63	0.72	0.04	1.08	1.12	1.47	0.521	1.238	2.225	1.074	0.053
C5	2.27	4.2	0.72	0.11	1.08	1.36	1.47	0.225	1.238	0.298	1.074	0.926

Table 19 – The investigated FTIR ratios in the pre- and post-burnt bones.

The bone apatite maturity ratios showed that the fresher the bones, the more values decreased with heating. For example, the archaeological bone (C2) did not present either of the peaks necessary for maturity estimation (Fredericks *et al.*, 2012). C/C increased post-burning due to either the loss of B-type carbonates or the increase in A-type carbonates (Holcomb and Younger, 1980; Snoeck *et al.*, 2014).

A.3.3 X-ray Diffraction

Table 20 shows the coherence length, which exhibits both the crystal size and its strain, values for the pre- and post-burnt bones. The fully fleshed bone's (C5) CL increased the most in value (by 19.73 nm), with the largest change at <030> lattice of the HAp crystal (Fig. 42), followed by the two 4-year-weathered bone (C1, C5) and then the partially fleshed bone (C4). It was not yet possible to extract data from the archaeological bone, because an additional quartz (SiO_2) phase blocked the software in recognising the <002> peak and fitted the line on the additional phase instead of the hydroxyapatite. Adjustments need to be made before this

bone's crystal structure can be analysed through XRD. Only C2 presented an additional α SiO_2 in its lattice structure (Fig. 43).

The Williamson-Hall technique (Dorset, 1998) was applied to calculate crystal sizes in Python. Only C4 and C5 produced acceptable results because HAp is a very anisotropic material, so attempting to compare several crystallographic directions at once produced inaccurate results. Thus, only <002> and <004> was used for the crystal size calculations. However, when only the <00l> crystallography was used, only two points were produced for the linear regression, which naturally produces a perfect fit for a line. Thus, native biological HAp only has a few good quality reflections for size and strain separation resulting in a determination of only the 'c' lattice parameters, which is insufficient for crystal size determination.

Coherence Length (CL, in Å)								
HAp Miller indices	**C1**		**C3**		**C4**		**C5**	
	Pre-burn	**Post-burn**	**Pre-burn**	**Post-burn**	**Pre-burn**	**Post-burn**	**Pre-burn**	**Post-burn**
<002>	21.60	42.60	22.5	18.00	23.80	36.30	23.80	52.70
<004>	15.80	31.00	12.00	17.90	16.80	14.70	16.80	52.60
<030>	6.37	29.70	5.58	35.90	7.94	28.90	7.94	50.80
<210>	9.89	29.20	7.57	39.80	11.20	36.3	11.20	49.90

Table 20 – Coherence lengths in Å from the XRD data in the pre- and post-burnt bones.

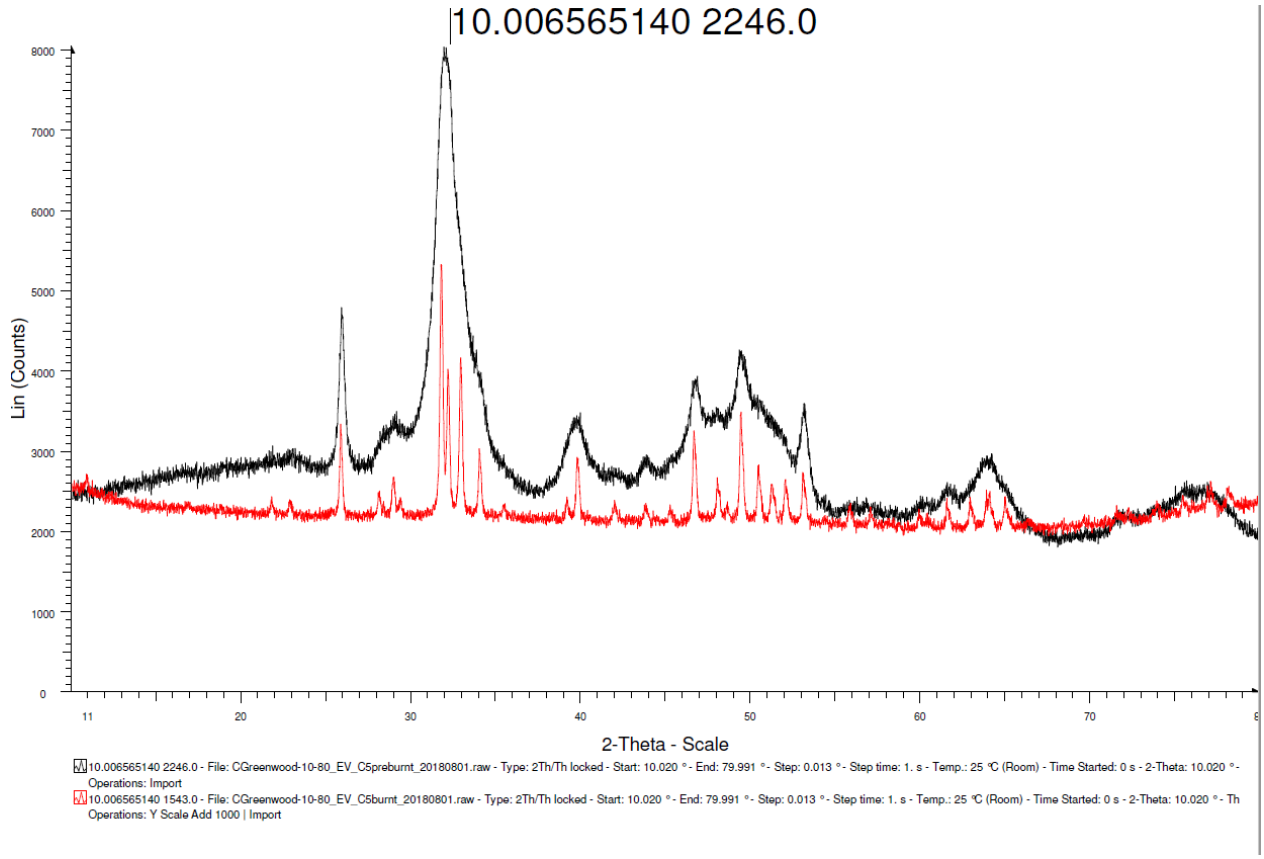


Figure 43 – XRD results of the fleshed bone (C5) pre-burnt (black line) and post-burnt (red line). Note the sharper peaks in values post-burning, representing a more crystalline state of hydroxyapatite.

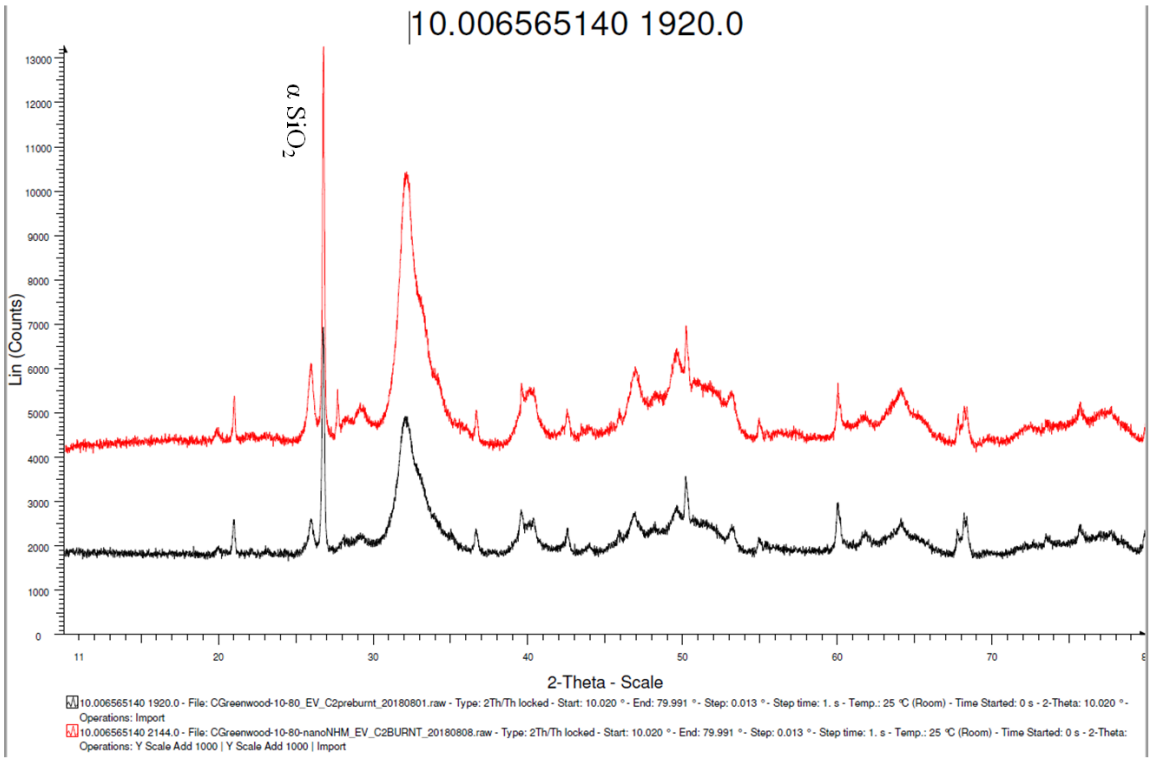


Figure 44 – The X-ray diffractrogram of the 5.5 ka archaeological cow bone (C2). Red = post-burnt, black = pre-burnt. Note the additional SiO_2 phase.

A.4 Discussion and Conclusion

The 'timing specific' features of SFT inflicted on differently decomposed bones survive post-burning. It was not possible to distinguish the pre-burnt preservation of the bones based on only the 'perimortem' features of the cut-marks. Features of the kerfs, which might help in instrument classification, became more visible after burning. Although C1 retained the most collagen intermolecular cross-links (amide I, II, III) pre-burning, no thumbnail fractures or warping was detected on this bone. Meanwhile, the bones covered by different amounts of soft tissues exhibited these heat-induced changes and fractured severely. Amide peaks were still detected in all bones post-burning, suggesting that none of the bones fully calcined. Recrystallisation probably did not happen in the fresher bones (C1, C3, C4, C5). Changes in crystallinity happen very slowly after death, as the crystal structure of bone alters to a more ordered composition with increased crystal size (Munro *et al.*, 2007; Olsen *et al.*, 2008; Thompson *et al.*, 2009). By contrast, burning causes instant recrystallisation above approximately 650 °C (Munro *et al.*, 2007). The freshest bones (C4, C5) possessed the lowest crystallinity index pre-burning and the highest one's post-burning, while the archaeological bone's CI hardly changed. This suggests that the fat ignited and caused increased temperatures on these bones. The 4-year weathered bones' values demonstrate that even such short decaying time is sufficient to alter the crystallinity index. C4 lost the most collagen post-burning, while C5's crystal growth is the most significant. The Williamson-Hall plot might be unapplicable to the decaying bones to calculate crystal size.

This study examines both the decay- and heat-induced changes caused to bone, as well as the timing of cutmarks produced, which were introduced on the bones at their original state of decomposition, post-burning. For many years, cremated bones in archaeology were not seen

as a valuable source of information, because of the difficulty of analysing them and the lack of appropriate technology. This study served as a proof-of-concept for further experimental studies on the determination of the pre-burning condition of bone. The clear differences between the fresh and the 4-year PMI bones demonstrate that these changes are potentially present in only 1-year of PMI as well. If a methodology could be developed to help to establish the approximate states of human remains prior to the fire event, it could give a rise to the re-examination of cremated bones kept in museums' and Universities' storage facilities by osteologists. The questions this study attempts to answer, like the classification of the decompositional state of the body at the time of burning and the timing of trauma infliction in relation to the timing of the fire event, is of great interest in forensic cases[10], in the field of biological anthropology, and in funerary archaeology.

[10] Information acquired from a personal conversation with L. Ainscough, Reporting Forensic Officer in anthropology and archaeology at Cellmark Forensic Services, UK.

Appendix B: Végh, E. I., *et al.,* 2021. Assessing the reliability of microbial bioerosion features in burnt bones: A novel approach using feature-labelling in histotaphonomical analysis. Journal of Archaeological Science:Reports 37, 102906.

Appendix B: Végh, E. I., *et al.,* 2022. Physicochemical Changes in Bone Bioapatite During the Late Postmortem Interval Pre- and Post-Burning. *Applied Spectroscopy.* https://doi.org/10.1177/00037028221085600

Journal of Archaeological Science: Reports 37 (2021) 102906

Contents lists available at ScienceDirect

Journal of Archaeological Science: Reports

journal homepage: www.elsevier.com/locate/jasrep

Assessing the reliability of microbial bioerosion features in burnt bones: A novel approach using feature-labelling in histotaphonomical analysis

Emese I. Végh [a,*], Andrea Czermak [a], Nicholas Márquez-Grant [b], Rick J. Schulting [a]

[a] Research Laboratory for Archaeology and the History of Art, School of Archaeology, University of Oxford, UK
[b] Cranfield Forensic Institute, Cranfield University, Defence Academy of the United Kingdom, UK

ARTICLE INFO

Keywords:
Microbial bioerosion
Burning
Bone
Cremation
Taphonomy

ABSTRACT

Objectives: Recent histotaphonomic studies have focused on the presence of features thought to be caused either by bacteria (microscopic focal destruction/MFD and cyanobacterial tunnelling) or fungal (Wedl tunnelling types 1 and 2) attack on unburnt bone. Identifying these characteristics on burnt bones could indicate the state of decomposition before burning, with important repercussions for both archaeological and forensic contexts.
Materials and Methods: Fleshed pig (Sus scrofa, N = 25) tibiae were left exposed on a field, then collected at 14-, 34-, 91-, 180-, 365-day intervals before being burnt in an outdoor fire (≤750 °C). Fresh (fleshed) legs (N = 10) acted as unburnt and burnt controls. Thin sections were examined using transmitted light microscopy and backscattered scanning electron microscopy. Diagenetic traits were quantitatively and systematically assessed by a novel data labelling application developed for this study.
Results: Features meeting the published characteristics of microbial bioerosion ('Wedl tunnelling', 'lamellate' and 'budded MFD') were significantly correlated with time since deposition on the unburnt bones. Only budded MFD increased significantly over time in the burnt groups. However, the presence features meeting the published characteristics of Wedl 2 tunnelling were present on the fresh burnt bones, indicating that they are an artefact.
Discussion: The presence of many features seemingly indistinguishable from those caused by bioerosion on the freshly burnt control bones suggests that burning is not only able to conceal features thought to be the result of bioerosion but can produce them as well. Thus, such features are not a reliable indication of bioerosion. Budded MFD may be a viable indicator but more research is required.

1. Introduction

Understanding early postmortem changes to the body is of interest in many fields, including archaeology, physical anthropology, forensic science, palaeobiology, and palaeontology. Deciphering early bone diagenesis and shedding light on the processes that lead to fossilisation presents a challenge, one that is further exacerbated when bone is subjected to cremation. Identifying bioerosion on burnt bones would open the possibility of establishing whether a body had gone through a decomposition phase with soft tissue still present prior to burning. This research aims to investigate whether bioerosion features can be used as an indication of decomposition on burnt bones, which has implications to understanding funerary practices in the archaeological record as well as understanding the sequence of events leading to deposition in forensic investigations.

Burning of the body can occur either when the body is fully fleshed (e.g. homicide, suicide, accidental fires, cremation) or once it has decomposed to different degrees (e.g. burning to conceal evidence of homicide, cremation, accidental fires, freeing up space in a cemetery) in both archaeological and forensic contexts. Early studies mainly focused on establishing whether bone was at either of the two extremes – fleshed or dry – of the spectrum when burnt (Baby, 1954; Binford, 1963; Buikstra and Swegle, 1989; Etxeberria, 1994; Spennemann and Colley, 1989; Whyte, 2001). The methods employed were primarily macroscopic, recording the presence of warping and of thumbnail fractures (Buikstra and Swegle, 1989; Spennemann and Colley, 1989; Whyte, 2001). However, this has been shown to be relate primarily to collagen content (Gonçalves et al., 2011). Currently, it remains challenging to identify the body's state of decomposition before burning.

A reliable method of establishing the body's stage of decomposition

* Corresponding author at: Research Laboratory for Archaeology and the History of Art, School of Archaeology, University of Oxford, Dyson Perrins Building, South Parks Road, Oxford OX1 3QY, United Kingdom.
E-mail address: emese.vegh@wolfson.ox.ac.uk (E.I. Végh).

https://doi.org/10.1016/j.jasrep.2021.102906
Received 15 January 2021; Received in revised form 23 February 2021; Accepted 24 February 2021
Available online 22 March 2021
2352-409X/© 2021 Elsevier Ltd. All rights reserved.

at the point of burning would help determine whether this occurred immediately or sometime after death. In archaeology, the interaction between anthropogenic and natural processes is vital to understand human behaviour connected to past funerary rites. For example, it has been suggested that at some Neolithic and Bronze Age sites in Ireland, including the passage tombs of the Boyne Valley and Fourknocks, as well as Kilgreany cave (Waterman, 1978; Dowd, 2008; Cooney et al., 2014), human remains were either passively or actively excarnated before inhumation and cremation. At other Irish sites, such as Tully, the excavators claimed that the bodies were burnt with full soft tissue coverage (Wells, 1978). These claims were based on supposedly diagnostic fracture patterns, which, as noted above, may be problematic.

There are a few cases discussed in the forensic anthropological literature in which a single individual has been found partially burnt (Bontrager and Nawrocki, 2008; Garrido-Varas and Intriago-Leiva, 2015). The postmortem intervals were established using both the signs of carnivore gnawing and patterned thermal destruction. However, usually only fragmented calcined remains are encountered. Thus, there is a need for better and more accurate methods of determining the stage of decomposition from a single burnt skeletal fragment.

Bone is a complex, composite material, which undergoes diagenetic alterations post-deposition. Three distinct diagenetic pathways can be distinguished (Collins et al., 2002): (1) chemical degradation of the organic component (collagen hydrolysis); (2) chemical degradation of the inorganic phase (bioapatite dissolution); and (3) microbial degradation of both phases (Child, 1995; Hedges and Millard, 1995; Millard, 2001; Collins et al., 2002; Nielsen-Marsh and Hedges, 2002; Turner-Walker and Jans, 2008; Kontopoulos et al., 2016; Huisman et al., 2017). Pathway 3 presumably happens either (1) rapidly after death as it is thought to be linked to putrefaction processes involving soft tissues (Collins et al., 2002; Jans, 2005; Fernández-Jalvo et al., 2010; Huisman et al., 2017) or (2) by soil bacteria post-deposition (Turner-Walker, 2012, 2019; Kendall et al., 2018). This study focuses on this pathway's (i.e. microbial degradation) supposedly diagnostic features in an effort to shed light on the early postmortem history of the remains.

Histotaphonomy, the taphonomy of bone at the microstructural level, has been often employed by researchers to investigate the biological deterioration of bone (e.g. White and Booth, 2014; Kontopoulos et al., 2016). Many studies use features of bacterial attack on unburnt bones to inform on the initial postmortem period of the body (Child, 1995; Jans et al., 2004; Nielsen-Marsh et al., 2007; Hollund et al., 2012, 2014; White and Booth, 2014). Whether the origin of the bioerosive bacteria is endogenous or exogenous, most studies focus on archaeological bone (Jans et al., 2002; Turner-Walker and Jans, 2008; Brönnimann et al., 2018), and some on recent bone (Yoshino et al., 1991; White and Booth, 2014; Kontopoulos et al., 2016; Lemmers et al., 2020). Furthermore, to our knowledge there have only been two studies on histotaphonomic features on burnt bones (Grévin et al., 1991; Lemmers et al., 2020). Grévin et al. (1991) reported that human bones from a Late Bronze Age site at Pincevent, France, had been buried for weeks to months prior to cremation based on microradiographs showing 'typical' postmortem bacterial attack. Recently, Lemmers et al. (2020) proposed that bioerosion features survive in burnt bones and can be readily distinguished from alterations in the microstructure caused by burning.

All scholarship agrees that there is a need for more experimental histological studies. This paper aims to assess whether bioerosion features are useful indicators of decomposition in burnt bones.

1.1. Histotaphonomic features in bone

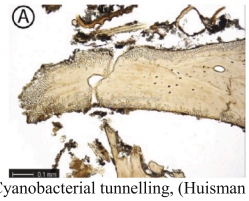
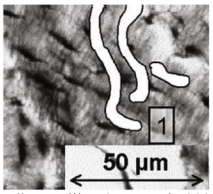
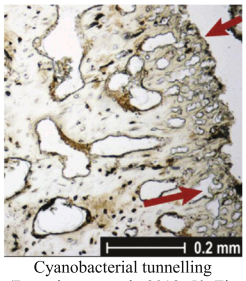
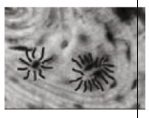
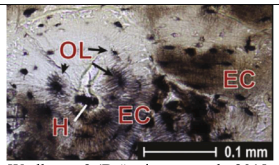
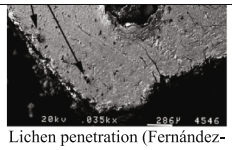
The specific causative agents of microstructural changes are poorly known, but mainly they are attributed to bacteria, fungi, or marine based organisms (Bell, 2012a). Microbiological decay of the body commences soon after death. Bacteria and fungi alter hard tissues by entering through bone's vasculature (Bell et al., 1996; Millard, 2001). The bacterial flora in the gut initially affect the bone from the endosteal surface, while exogenous bacteria from the environment (e.g. soil) attack the bone from the periosteal surface (Hackett, 1981; Jans, 2008; Daniel and Chin, 2010; Boaks et al., 2014; White and Booth, 2014; Kontopoulos et al., 2016).

Table 1
Microbial bioerosion features, their thought to be causative agents, contexts and environments in the literature.

Feature	Appearance	Causative agent	Context and Environment
Microscopic Focal Destruction (MFD)	Linear, Budded, or Lamellate structures around Haversian canals	Endogenous bacteria (Bell et al., 1996; Jans et al., 2004; Jans, 2013; Nielsen-Marsh et al., 2007; Trueman and Martill, 2002; White and Booth, 2014) Soil bacteria (Turner-Walker, 2014; Grine et al., 2015; Kontopoulos et al., 2016; Kendall et al., 2018; Morales et al., 2018)	Terrestrial
Wedl tunnelling	Dendritic structures	Fungi (Hackett, 1981; Bell et al., 1991; Trueman and Martill, 2002)	Marine (Garland, 1987; Millard, 1993) Terrestrial: surface exposed and/or buried de-fleshed bones (Trueman and Martill, 2002; Jans, 2008; Brönnimann et al., 2018) Oxygenated, wet environments in neutral to acidic soils (Huisman et al., 2009, 2017)
Wedl type 2/ Enlarged canaliculi/ enlarged osteocyte lacunae/Non-Wedl MFD	Enlarged canaliculi, resembling a spider-like structure	Fungi (Trueman and Martill, 2002; Kontopoulos et al., 2016, 2019) Bacteria (White and Booth, 2014; Booth and Madgwick, 2016)	Terrestrial
Cyanobacterial tunnelling	Tunnelling from periosteal surface of bone	Bacteria (Bell et al., 1991; Jans, 2008; Bell, 2012a; Turner-Walker, 2012, 2014)	Marine- or fresh water (Bell et al., 1991; Jans, 2008; Bell, 2012a; Turner-Walker, 2012, 2014)

Morphological changes to bone resulting from bioerosion was first described by Wedl (1864) and Roux (1887), and subsequently by Hackett (1981) and Garland (1987). These changes include (1) small channels (Wedl, 1864) caused by fungi (Roux, 1887), (2) microscopic focal destruction (MFD), which can be linear longitudinal, lamellate, or budded (Hackett, 1981), and (3) other types of diagenetic changes, such as reduction in birefringence, inclusions, and infiltrations (Garland, 1987). Hedges et al. (1995) developed the *Oxford Histological Index* (OHI) to approximate the preservation of bone histology. The OHI is still used in bone histology studies, providing an ordinal scale assessment of the degree to which bone is affected by bioerosion. We build on this here

Table 2
Identical histotaphonomic features named differently across the literature.

Feature	Different naming of the features across the literature			
	 Cyanobacterial tunnelling, (Huisman et al., 2017, 20, Fig 4.A)	 Wedl tunnelling (Jans et al., 2004, 89, Fig 1)	 Cyanobacterial tunnelling (Brönnimann et al., 2018, 50, Fig 4G)	 Wedl tunnelling – no scale provided, x170 (Hackett, 1981, 251, Fig 2)
	 Wedl type 2 (Brönnimann et al., 2018, 50, Fig 4E)	 Expanded osteocytic lacunae and canaliculi due to environmental infiltration (Tjelldén et al. 2018, 412, Fig. 6)	 Lichen penetration (Fernández-Jalvo et al., 2010, 74, Fig 7.4)	

by including a quantitative assessment of the percentage of the bone affected.

More recent research has focused mainly on the presence of MFD, Wedl tunnelling, Wedl type 2, and cyanobacterial tunnelling on unburnt bone (see Table 1).

Diagenetic features on bones are usually studied under either transmitted light microscopy (Jans et al., 2002, 2004; Jans, 2005; Tjelldén et al., 2018) or electron microscopy (Bell et al., 1991; Bell, 2012b; Turner-Walker, 2014), with a few studies employing both methods (Huisman et al., 2017; Turner-Walker, 2019). General changes in bone microstructure due to bacterial attack manifest in demineralised (darker) and adjacent hypermineralised (brighter) areas on the back-scattered scanning electron microscope (BSEM), which recently has been proposed to be a more effective means of identifying bioerosion features (Turner-Walker, 2019).

Complicating discussion of histotaphonomical features is the fact that morphologically identical or similar features have been given different terms in the literature (see Table 2). For example, the same dendritic features often called Wedl tunnels (Brönnimann et al., 2018), are also called as non-Wedl MFD (Fernández-Jalvo et al., 2010), Wedl type 2 (Trueman and Martill, 2002; Brönnimann et al., 2018), lichen penetration (Fernández-Jalvo et al., 2010), and early stage of non-Wedl MFD (White and Booth, 2014). This distinction is crucial, since for example Wedl tunnelling are thought to be caused by fungi from the burial environment (Fernández-Jalvo et al., 2010; Brönnimann et al., 2018), while non-Wedl MFD have been attributed to bacterial activity, most often from the gut (Bell et al., 1996; Jans et al., 2004; Jans, 2013; Nielsen-Marsh et al., 2007; Trueman and Martill, 2002; White and Booth, 2014). The present study uses the terminology outlined by Brönnimann et al. (2018) because of its clear illustrations and descriptions.

1.2. Histology of burnt bone

The primary focus of burnt bone histology studies has been on estimating fire temperature and duration (Herrmann, 1976, 1977; Nicholson, 1993; Holden et al., 1995a, 1995b; Quatrehomme et al., 1998; Ubelaker, 2009; Absolonova et al., 2013; Imaizumi et al., 2014; Cambra-Moo et al., 2017) or on species identification (Cattaneo et al., 1999) using histomorphometry or histomorphology (Table 3). There is a considerable disagreement between different authors on when, and if, identifiable histological changes take place. The histological structure of bone has been variously reported to be nearly identical to that of unburnt bone when burnt under 600 °C (Bradtmiller and Buikstra, 1984), 700 °C (Herrmann, 1977), 900 °C (Squires et al., 2011), or 1200 °C (Cattaneo et al., 1999). However, it is unknown whether these were bone or air temperatures, which might be a source of discrepancy. Other complicating factors include the method of burning (e.g., furnace or natural fire), the type, size, and state of the bone, and the presence/absence of soft tissues.

The primary focus of burnt bone histology studies has been on estimating fire temperature and duration (Herrmann, 1976, 1977; Nicholson, 1993; Holden et al., 1995a, 1995b; Quatrehomme et al., 1998; Ubelaker, 2009; Absolonova et al., 2013; Imaizumi et al., 2014; Cambra-Moo et al., 2017) or on species identification (Cattaneo et al., 1999) using histomorphometry or histomorphology (Table 3). There is a considerable disagreement between different authors on when, and if, identifiable histological changes take place. The histological structure of bone has been variously reported to be nearly identical to that of unburnt bone when burnt under 600 °C (Bradtmiller and Buikstra, 1984), 700 °C (Herrmann, 1977), 900 °C (Squires et al., 2011), or 1200 °C (Cattaneo et al., 1999). However, it is unknown whether these were bone or air temperatures, which might be a source of discrepancy. Other complicating factors include the method of burning (e.g., furnace or natural fire), the type, size, and state of the bone, and the presence/absence of soft tissues.

Investigating histomorphological changes due to burning are essential to the current study, because these can influence the appearance of microbial bioerosion and hence their recognition to identify the post-mortem stage at which the bones were burnt.

Table 3
Histomorphometric and histomorphology changes of burnt bone in the literature.

Temperature (°C)	Histomorphometric Changes	Histomorphology Changes
500	Increase in size and number of cracks due to differential shrinkage of bone tissues (Imaizumi et al., 2014)	Cracking, minute fissures, separation of the osteons from interstitial lamellae (Imaizumi et al., 2014)
<600	No change, identical to unburnt bones (Absolonova et al., 2013)	
	No cracking with minimal carbon deposits (Hanson and Cain, 2007)	
	Microfeatures identifiable, but less well preserved (Carroll and Squires, 2020)	
600	Increase in osteon size diameter (Bradtmiller and Buikstra, 1984)	Individual lamellae often indistinguishable (Nelson, 1992)
	Haversian canals increased in size while the osteon's diameter decreased (Nelson, 1992)	Histological structures disappear with extensive carbon deposits (Hanson and Cain, 2007)
<700	No change, identical to unburnt bones (Herrmann, 1976, 1977)	
	Cracks present outwards of vascular canals (Hanson and Cain, 2007)	
700–800	Structural changes occur (Herrmann, 1976, 1977; Hummel and Schutkowski, 1986; Absolonova et al., 2013)	
800	No changes below, shrinkage above (Van Vark, 1970)	No major changes below (Van Vark, 1970)
	No significant shrinkage (Cattaneo et al., 1999)	Lamellar structure of bone is lost (Holden et al., 1995b)
900	Microstructural changes occur (Squires et al., 2011)	Haversian and Volkmann's canals cannot be distinguished, no microstructure preserved (Squires et al., 2011)
		Granular surface appears (Castillo et al., 2013)
		700–900 °C: Degeneration of microscopic structures (<60% of area, Carroll and Squires, 2020)
1000	Shrinkage occurs (Cattaneo et al., 1999)	Haversian canals survive, while Volkmann's canals, circumferential lamellae, resorption cavities are hard to differentiate (Absolonova et al., 2013)
		Few misshapen Haversian canals survive, but 86.3% of sample area show complete fusion of hydroxyapatite (Carroll and Squires, 2020)
1200	Microstructural changes start to occur (Cattaneo et al., 1999)	
1400		Haversian Canals and osteocyte lacunae indistinguishable (Holden et al., 1995b)
1600	All structural features are completely destroyed (Holden et al., 1995b; Fairgrieve, 2008)	

2. Materials and methods

2.1. Experiment

Fleshed *Sus scrofa domesticus* (pig) tibiae were sourced from a local butcher, euthanised at 18 months. All limbs were kept in a freezer at –18 °C until collection. Pigs, in addition to being easily sourced, have been widely utilised as a substitute for human bodies in decomposition, fire, and histology studies (Forbes et al., 2005; Lynn and Fairgrieve, 2009; Thompson and Inglis, 2009; Bonney et al., 2011; Symes et al., 2012; White and Booth, 2014; Kontopoulos et al., 2016). There is an ongoing discussion on how appropriate pigs are as human analogues (Matuszewski et al. 2020), but they are considered to be reasonable proxies in many respects, including bone macro- and microstructure, remodelling, mineral concentration and density, as well as gut microbiota (Turner and Wiltshire, 1999; Forbes et al., 2005; Pearce et al., 2007; Wilson et al., 2007; Feng and Jasiuk, 2011; Hollund et al., 2014; White and Booth, 2014; Kontopoulos et al., 2016). Long bones were chosen for the study because of their common use in histological studies, their large cortical bone area, and their survival rate (Booth and Madgwick, 2016).



Fig. 1. Burning of the 14- and 34-day postmortem bones on the pyre. Upper image was taken subsequently after the ignition of the fire, while the lower was taken when the bones have calcined. All outdoor fires were executed in the same manner. The pyres were built on a flat clearing, using bricks to provide support for a wire mesh holding the bones, as well as partial protection from the wind. While offering less control over temperature rather than a furnace, the use of an outdoor fire better reflects real-world conditions due to the more variable temperatures of the fire, and the influence of the wind. Each fire was built and maintained in the same manner, using a mixture of hard and soft woods as fuel. [PRINT IN COLOUR]

The pig tibiae (N = 25) were left to decay for 14, 34, 91, 180, and 365 days prior to burning on an outdoor fire. Fresh fleshed bones (N = 10) served as unburnt and burnt control samples. The first round of fleshed tibiae were sub-aerially deposited on an open grassland area at Wytham Woods, Oxfordshire, England, in June 2018 and between February and June 2019. The exposed tibiae were protected from scavengers with a cage covered by layers of iron mesh. Scavenging produced tooth marks on nearly all bones, but only a few bones were completely removed from the cage (one of the 180-day and four of the 365-day postmortem bones).

Wytham Woods is located in a temperate climate with moderate to high rainfall averaging 717 mm, with monthly mean temperatures ranging from 1.6 °C in January to 20.3 °C in July with a long-term annual mean of 10.0 °C (Taylor et al., 2011). At collection bones were

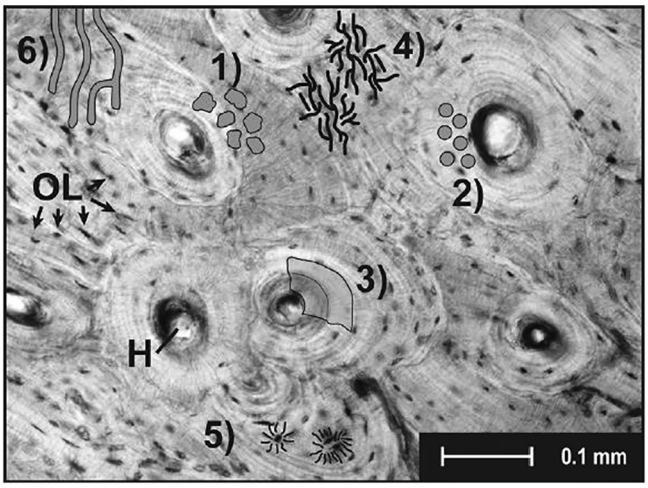


Fig. 2. Criteria for labelling microbial bioerosion from Brönnimann et al., 2018. 1) Budded MFD; 2) Linear longitudinal MFD; 3) Lamellate MFD; 4) Wedl tunnelling; 5) Wedl 2; 6) Cyanobacterial tunnelling (Brönnimann et al., 2018, 46, Fig. 4). Features that appeared to be similar to linear MFD were not labelled in this study, because they were caused by burning. [PERMISSION REQUESTED FROM ELSEVIER FOR IMAGE ON 12/04/2020]

partially covered by the soil, which may have instigated exogenous bioerosion. Soil pH range from 3 to 7 (Taylor et al., 2011).

Pyres were built and maintained in the same manner (Fig. 1), each fire lasting 2.5–3 h, until the bones calcined (Fig. 1). Bone temperatures were monitored by a thermocouple, averaging 553 °C, with a recorded maximum of 751 °C. Maximum fire temperatures reached 995 °C. The bones were left to cool and subsequently collected for transport.

2.2. Analysis

Unburnt samples were defatted in a 2:1 chloroform:methanol mixture for between 8 and 20 weeks, in order to remove fat infilling the pores of bone tissues. Samples were taken before and after burning from the minimum diameter of the tibiae diaphyses. Samples were embedded undecalcified in transparent epoxy cold mounting resin and a catalyst (Spectrographic Ltd., Leeds, UK), in order to impregnate the bones within a solid medium to facilitate sectioning for microscopical analysis (Garland, 1987). The resin blocks (N = 56) were then placed into a desiccator with vacuum pump to inhibit bubble formation. Two transverse thin sections (~50–70 μm) were cut from each sample using a Buehler saw fitted with a diamond blade (Buehler, Lake Bluff, IL, USA) and subsequently fixed onto glass slides using Eukitt mounting medium (Merck, Darmstadt, Germany) and covered with microscope glass slides.

The slides were examined under a Leica DM 2500 P transmission light microscopy with (Leica, Wetzlar, Germany) using normal and polarised light at 50x, 100x, and 400x magnification. Each sample was composed of three to five images, which were taken across the bone with a USB camera (Brunel Microscopes Ltd., Chippenham, UK) per thin section at 50x magnification to represent bone from the periosteal to the endosteal surfaces, through the mid-cortical region for quantitative analysis. Higher magnification images were taken to observe and document more closely the features of interest.

Diagenetic traits on the optical microscopy images (N = 270) were quantitatively assessed by calculating the percentage of areas affected by diagenetic and/or heat-induced features. This was done by a human observer clicking on the features present on each block (N = 27,000) of randomly selected images in a data labelling application built for this study in Python (Flask web framework) and Javascript (jQuery library) programming languages. Each image (at 50x magnification) was divided into 100 equal blocks. The random selection of images across all samples by the application excluded bias in labelling, hence the samples were examined 'blind'. Results were automatically saved into a database recording whether a feature was present or absent within a block. The cumulative score of the 100 blocks estimates the proportion of the initial image that contains a given feature. Features (Fig. 2) were labelled according to descriptions in Brönnimann et al. (2018, 46, Fig. 1), which are in turn based on figures in Jans et al. (2004, 89, Fig. 1) and Hackett (1981, 250, Fig. 1). Features were initially labelled according to their closest comparanda in the literature, with no presuppositions being made regarding the veracity of the labels. This usage is indicated by single quotation marks. Some features were more variable in appearance than those discussed in the literature. For example, the label 'cyanobacterial tunnelling' was applied when the tunnels looked the most like the image in Brönnimann et al. (2018) taking into account tunnel diameters (Fig. 3) after re-examination of all images by the same researcher (EIV).

The prevalence of features on unburnt and burnt bones was then statistically analysed using Jupyter notebook in Python programming language (Pandas, Matplotlib, Seaborn, SciPy, and Numpy libraries). Linear regression was used to measure the strength of the relationship between the presence (in percentage) of each taphonomic feature and the length of the postmortem period before and after burning, with statistical significance assessed by associated p-values ($\alpha = 0.05$). The null hypothesis was that the presence (in %) of a given feature per bone does not increase with the postmortem interval. The coefficient of variation (CV) was used to assess the dispersion of the features in different decompositional stages and burning status.

Validation of whether or not features were due to bioerosion was then undertaken using a BSEM detector in the electron microprobe. The contrast on the images resulting from demineralised and hypermineralised areas can be used to identify bioerosion (Turner-Walker, 2019). The resin blocks were ground with carborundum paper of progressively finer grit size (800, 1200, 2500). The blocks were then

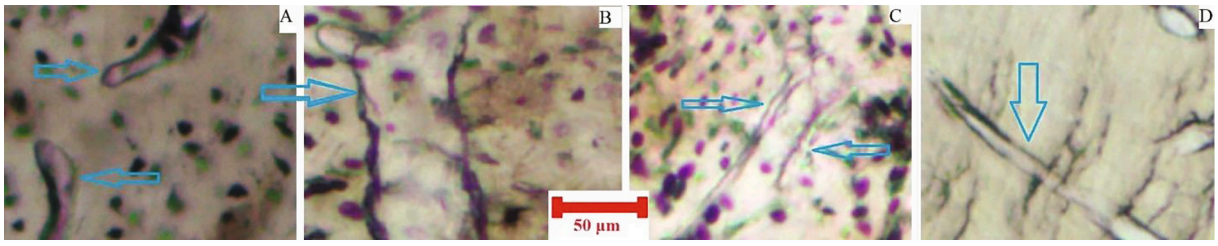


Fig. 3. Variation of features appearing to be tunnels in the different samples. **A** and **B** are of Volkmann's canals, **C** and **D** are unidentified channels and hence were labelled having the appearance of features consistent with 'cyanobacterial tunnelling', even though there is no clear indication of cyanobacteria being present in a terrestrial context, and the tunnel in **D** appears to be connected to a Haversian canal. The features are indicated by the blue arrows. Note the differences in the width of the tunnels. In the literature, maximum tunnel diameters caused by microorganisms have been reported to be between 0.1 and 2.0 μm (terrestrial), 7–18 μm (freshwater), and 5–19 μm (marine, Pesquero et al., 2018). Here, diameters under 20 μm were considered to be 'cyanobacterial tunnelling', while > 20 μm were classed as Volkmann's canals. (Transmitted light microscopy, 50x, from left to right: WSF2D2W5_unburnt, WSF2D2W5_burnt, WSF1D1M2_unburnt, WSF1D1M2_burnt). [PRINT IN COLOUR]

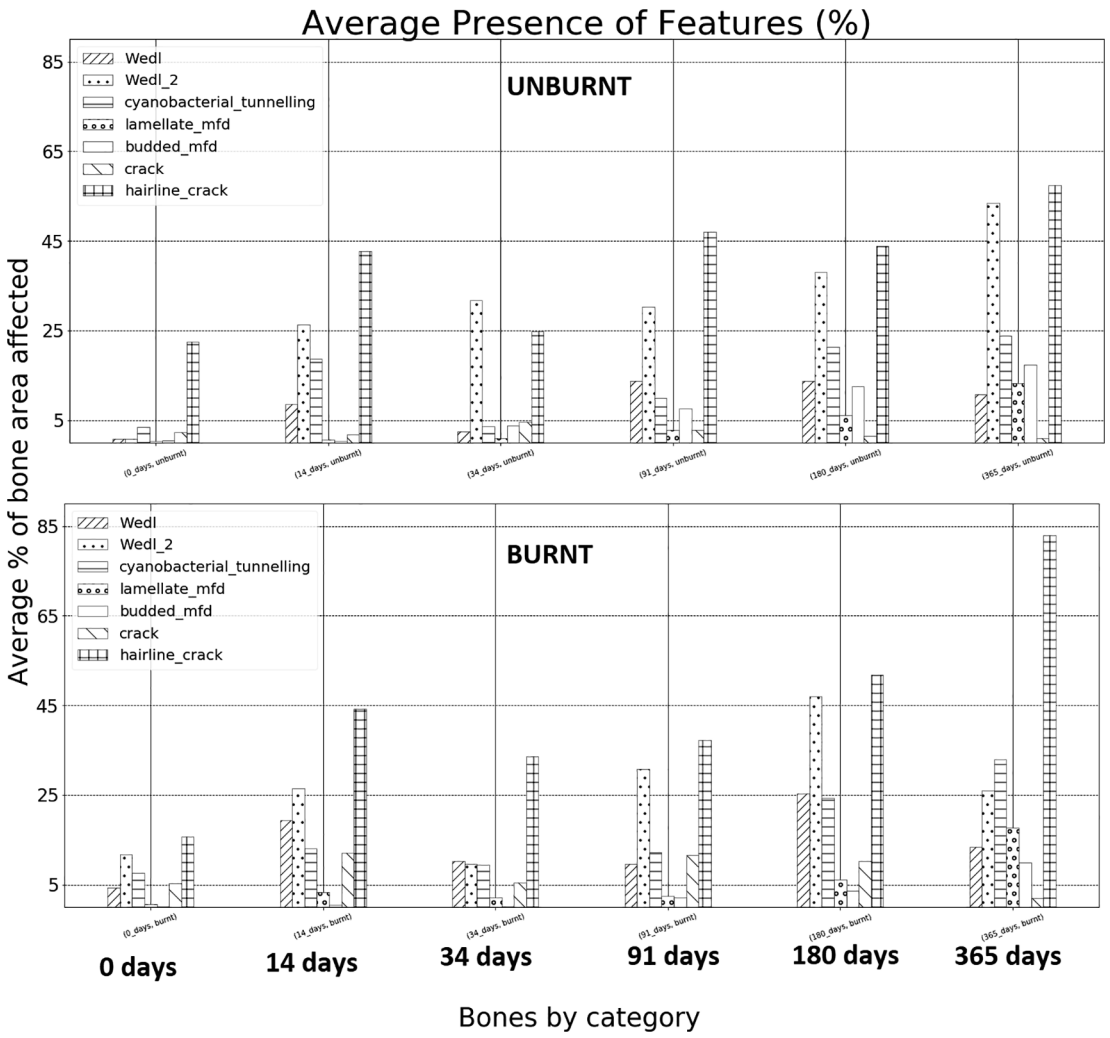


Fig. 4. The average presence of the taphonomic features at each stage of decomposition before (upper) and after (lower) burning.

polished on a Buehler wheel and a satin woven acetate polishing cloth (DP-Dac, Struers A/S) using 3 μm and 1 μm monocrystalline diamond paste and suspension (DP-Paste M, Struers A/S and MetaDi, Buehler, respectively) for 30 and 5 min, respectively. The mounts were cleaned in an ultra-sonic bath in petroleum ether (40°-60 °C). Samples were carbon-coated using a carbon evaporation coater (HHV Auto 360), the carbon acting as a conductive layer to prevent charging.

3. Results

The percentage of given features present for each decompositional stage before and after burning is shown in Fig 4. The most common taphonomic features affecting the largest percentage of the bone areas were hairline cracks and those similar to what has been described in the literature as 'Wedl type 2′. The latter feature was absent from the unburnt fresh/control group but was present on the freshly burnt controls. 'Wedl 2′ was also present after only 2 weeks of deposition on both the unburnt (26.32%) and burnt (26.43%) groups. After 1 year, this feature was present on over half of the areas investigated (53.5%).

The unburnt control group presented a very small number of 'Wedl tunnelling' (0.75%), 'Wedl 2′ (0.75%), 'lamellate' (0.25%) and 'budded MFD' (0.50%) and tunnels resembling 'cyanobacterial tunnelling' (3.5%). These are attributed to human labelling errors, and quantify labelling error, which is negligible for almost all categories, due to the impossibility of bioerosion being present on the control bones. As cyanobacterial tunnelling cannot be present on these bones, they are almost certainly mislabelled Volkmann's canals. Hairline cracks are abundant on this group (22.5%). This group should not show any sign of microbial bioerosion, since the pigs were dismembered shortly after death and were not exposed to soil. Conversely, the burnt fresh/control group exhibited significantly higher percentages of features consistence with 'Wedl tunnelling' (4.25%), 'Wedl 2′ (11.68%) and tunnels resembling 'cyanobacterial tunnelling' (7.56%) as identified in the literature.

Diagenetic features increase for all bone categories after burning in all decompositional stages. There was a moderate positive linear correlation between time passed since deposition and percentage of the presence of 'Wedl tunnelling' ($r = 0.442$, $p < 0.0001$), 'lamellate MFD' ($r = 0.493$, $p < 0.001$), 'budded MFD' ($r = 0.531$, $p < 0.001$) on the

Table 4
Correlation Coefficient ('r') and p-value ('p') for each analysed feature on the unburnt and burnt bones. H_0 = Presence (in %) of X feature per bone does not increase with postmortem time period. ** indicates significant p-values.

Feature	r unburnt	p unburnt	r burnt	p burnt
Wedl tunnelling	0.442	0.00009**	−0.016	0.886
Wedl 2	0.170	0.151	0.254	0.012**
Cyanobacterial tunnelling	−0.204	0.084	0.114	0.312
Lamellate mfd	0.493	0.00001**	0.091	0.412
Budded mfd	0.531	0.000001**	0.296	0.006**
Crack	0.064	0.591	0.184	0.095
Hairline crack	0.278	0.017**	0.159	0.150

Table 5
Coefficients of variation for each feature on the grouped samples by postmortem period and state of burning.

Coefficient of Variation (CV)								
Bones		Wedl	Wedl_2	Cyanobacterial tunnelling	Lamellate MFD	Budded MFD	Cracks	Hairline cracks
0 days	unburnt	1.27	0.66	0.82	2.00	1.15	0.75	0.50
	burnt	1.37	1.71	1.00	1.83	2.73	0.89	1.18
14 days	unburnt	0.72	0.52	0.56	1.36	2.07	1.82	0.30
	burnt	1.15	0.94	0.63	1.00	4.00	0.68	0.61
34 days	unburnt	1.24	0.64	0.73	1.10	1.33	0.94	0.60
	burnt	0.80	1.05	0.71	1.73	2.07	0.74	0.57
91 days	unburnt	0.49	0.70	0.60	0.95	0.98	1.20	0.24
	burnt	1.22	0.94	1.16	1.37	2.21	1.10	0.78
180 days	unburnt	0.43	0.64	0.40	0.55	0.67	1.40	0.31
	burnt	0.93	0.35	0.45	0.87	0.60	0.79	0.45
365 days	unburnt	0.80	0.51	0.36	0.25	0.50	2.00	0.27
	burnt	0.60	0.78	0.50	0.11	0.26	1.00	0.02

Table 6
Analysis of compositional images.

Decompositional stage	State	Contrast difference present? (trabecular, mid-cortical, periosteal)	Tunnels/cracks with hypermineralised rims?
Fresh	unburnt	No	No
Fresh	burnt	Yes	No
2 weeks	unburnt	No	No
2 weeks	burnt	Yes	Not generally, except 1
1 month	unburnt	No	Yes
1 month	burnt	No	No
3 months	unburnt	No	Yes, around tunnels/ cracks and Wedl 2/ MFD
3 months	burnt	Yes	No
6 months	unburnt	No	No
6 months	burnt	Yes	No
12 months	unburnt	No	No
12 months	burnt	Yes	No, but grey colour around tunnels

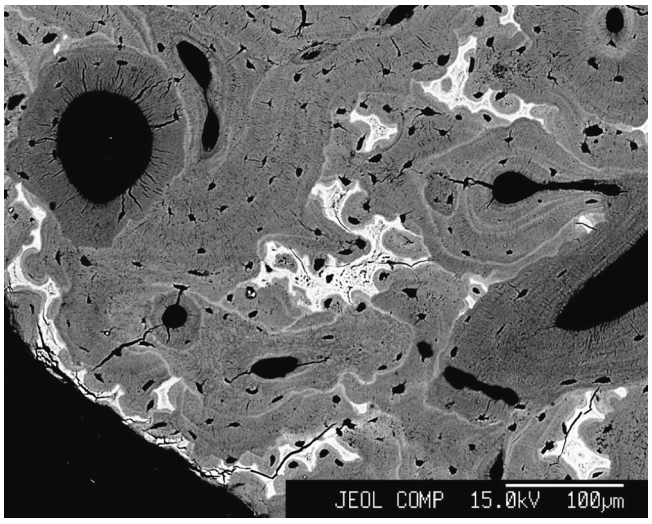


Fig. 5. Backscattered electron image of one of the 1-month postmortem unburnt bones (WSF5D1M3_unburnt). Note the brighter (hypermineralised) areas around the black (demineralised) 'tunnels' toward the lower end of the image. These bright areas are in fact not due to bioerosion, but to heavy mineral loading in growing individuals where osteonal bone has not replaced the primary lamellar bone.

unburnt bones, while hairline cracks ($r = 0.278$, $p < 0.017$), showed a weaker correlation with time, though it remained significant (Table 4). Weak but significant correlations were observed for 'Wedl 2′ ($r = 0.254$, $p < 0.012$) and 'budded MFD' ($r = 0.296$, $p < 0.006$) in burnt bones.

The coefficient of variation (CV) shows that hairline cracks had the lowest variability between samples of the same decompositional stage (Table 5), while 'lamellate' and 'budded MFD' showed the greatest variability. In general, features were less variable pre-burning than post-burning. The 91 days unburnt, 180 and 365 days postmortem unburnt and burnt bones had the lowest CV scores across all features. The 14-day burnt bones with features recalling 'budded MFD' (2.73) showed the highest variability.

The BSEM images (Table 6) present bioerosion-like hypermineralised 'tunnels', which are due to heavy mineral loading in growing individuals (Fig. 5), and thus not the result of bioerosion. A small number of images indicate initial stages of bacterial attack on some of the exposed unburnt bones, for instance one of the 3-months exposed unburnt bones (Fig. 6). Bioerosion was not present on any of the burnt samples. Generally, contrast varied across the burnt bones, while there was no significant difference across the unburnt bones.

4. Discussion

Three features associated in the literature with microbial bioerosion are present on the burnt fresh/control group but absent on the fresh unburnt group. The clear implication is that, despite their apparent similarity, these are not bioerosional features but are instead artefacts induced by burning. The feature labelled as 'Wedl type 2′ appears on 11.68% of the areas affected on the burnt fresh/control bones (Fig. 7). The frequency of 'Wedl 2′ shows a statistically significant relationship with postmortem time interval only in the burnt samples. This feature has been alternatively interpreted as an indication of bioerosion caused by fungi (Trueman and Martill, 2002), but the aetiology of enlarged lacunae and canaliculi is uncertain and has also been associated with staining, mineral infiltration, and burning (White and Booth, 2014; Hanson and Cain, 2017). Supporting this, it was found there that these are in fact carbonised osteocyte cells trapped in the canaliculi due to burning (Fig. 8.). This observation challenges the interpretation of the cremated remains reported by Grévin et al. (1991), where researchers noted these enlarged canaliculi (referred to here as 'Wedl 2′) to be the sign of a delay of weeks to months before cremation. The high variance (CV = 1.71) of 'Wedl 2′ presence on the freshly burnt samples further suggests that the feature was produced by fire.

The frequency of features labelled as 'Wedl tunnelling', and 'lamellate MFD' increase significantly with decay time on unburnt bones, and although they were present, they showed no correlation with time since deposition in the burnt groups. Wedl tunnelling is thought to be attributed to surface exposed and/or buried de-fleshed bones from terrestrial environments (Trueman and Martill, 2002; Jans, 2008;

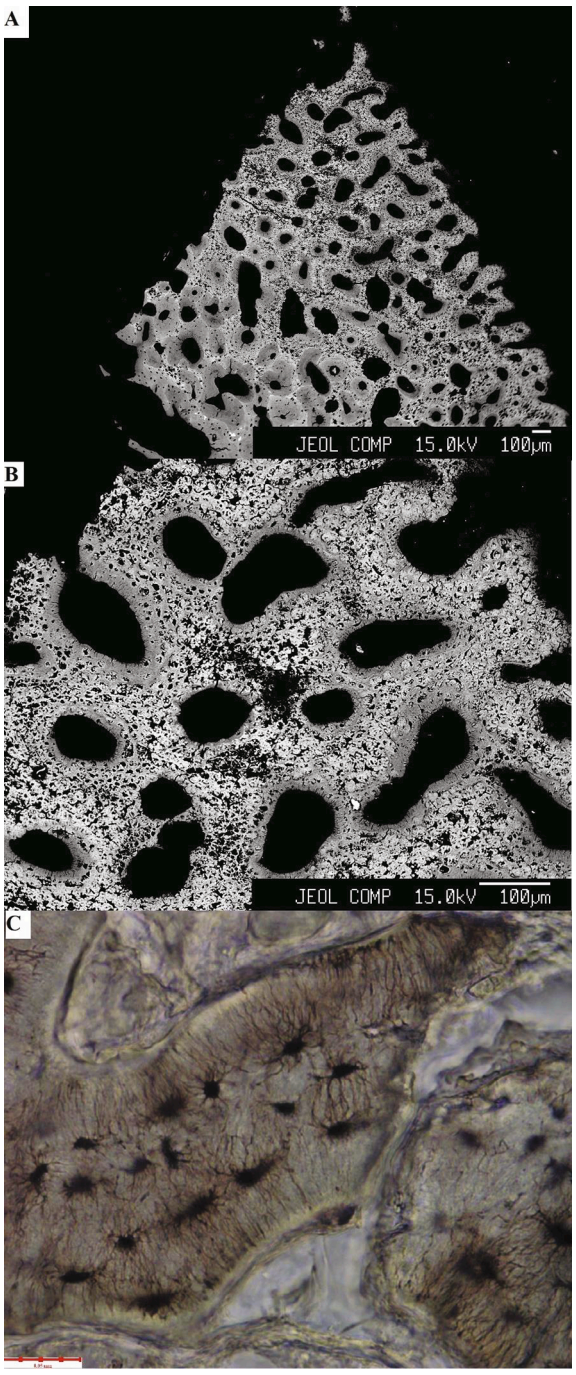


Fig. 6. **A** and **B:** Backscattered electron image of 3-month postmortem unburnt bone (WSF3D3M3_unburnt). Note the accumulation of darker (demineralised) circular areas (appearing to be 'Wedl 2′ or enlarged canaliculi, but probably naturally demineralised primary bone with microcracks) with bright (hyper-mineralised) areas around. **C:** Transmitted light microscopy image of a thin section from the same sample (WSF3D3M3_unburnt) at 400x magnification.

Brönnimann et al., 2018) and should only happen in oxygenated wet environments in neutral to acidic soils (Huisman et al., 2009, 2017). Most bones were covered by soft tissue to different degrees. Less soft tissue coverage means bone desiccation begins earlier, which might limit the intensity of bioerosion (Jans et al., 2004; Nielsen-Marsh et al., 2007). Although the 1-month postmortem unburnt bones were much less affected by 'Wedl tunnelling', the other groups with soft tissues were more affected by this feature. Therefore, no difference was found in bones with remnants of soft tissues and de-fleshed (by scavenging) bones

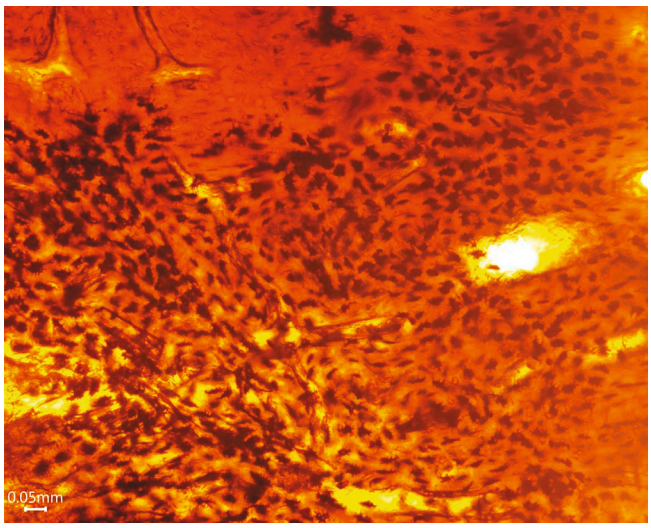


Fig. 7. Staining of the osteocyte-canalicular network that appears to be Wedl type 2 on one of the fresh burnt control bones (SWF1FR2_burnt_1). The tunnels were labelled 'blind' as 'cyanobacterial tunnelling', but these are Volkmann's canals. Neither of these features should be present on freshly burnt bones. Transmission light microscopy, 100x magnification. [PRINT IN COLOUR]

in the mean bone areas affected by 'Wedl tunnelling'. Sub-aerial exposure, the water-logged soil, and the pH (3–7; Farmer, 1995) suggest Wedl tunnelling should be present (Huisman et al., 2009, 2017), but the fact that it was more frequent in the burnt than in the unburnt bones suggests that similar features are not due to fungal activity and can be produced by burning.

Although the literature suggests that MFD might indicate an endogenous source of bacteria, here it can be ruled out. 'Budded MFD' was the only feature to consistently show a statistically significant correlation with time since deposition for both the unburnt and burnt groups. Post-burning this relationship becomes less robust, suggesting that these features are more likely to be lost or at least become less visible through burning. In addition, this was the least reliably present on all bones, followed by 'lamellate MFD'. 'Budded MFD' (Fig. 9) appeared on the unburnt bones after just 34 days, but it was rarely observed on the same burnt group (0.19%), increasing slightly in the 3-month postmortem group (2.14%). Its presence reaches 10% after a year of decomposition post-burning, suggesting that 'budded MFD' can also be produced by burning.

If bone colonization by microorganism occurs and manifests as budded MFD, it must happen before burning, because this destroys the organic component on which bacteria feed (Grévin et al., 1991). The seasonality of functional activity of microbial communities associated with putrefaction has been investigated (Pechal et al., 2013). It was noted that the carbon consumption of bacterial communities in bone was the highest in Spring, when the 1- and 3-month postmortem bones were placed in the cage. The appearance of budded MFD after just 1-month postmortem would conventionally be attributed to endogenous bacteria that spread through the bone's vasculature causing bioerosion; however, since the pigs were dismembered shortly after death and frozen until they were deposited in the cages, endogenous bacteria as a source can be excluded. Although time is thought to be the least important factor in bioerosion (Piepenbrink, 1986; Piepenbrink and Schutkowski, 1987; Bell et al., 1996), it is likely that soil bacteria attacks bone over a longer timescale when bones are buried, especially given that organics (i.e., collagen) can survive for millennia. It has been shown that microbial extracellular enzyme activity for carbon cycling enzymes significantly increases in soil closer to the surface (Upton et al., 2019). Thus, the pig legs in this experiment, lying on and partially submerged in the soil, were arguably exposed to more soil microorganisms than if they

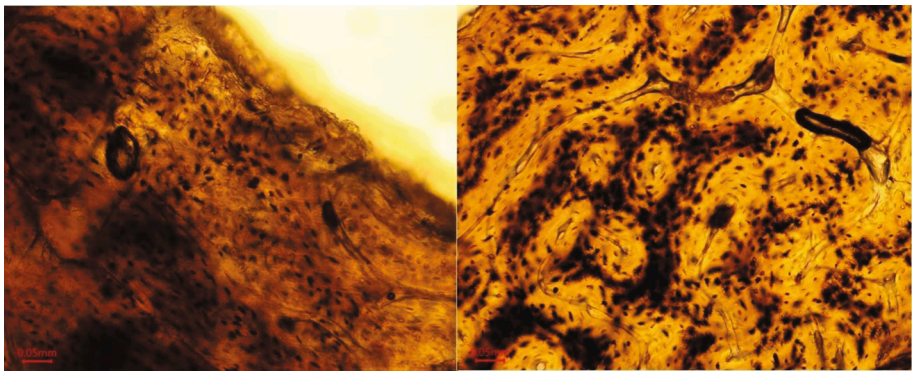


Fig. 8. Staining that appears to be 'Wedl 2′. While it is restricted to some canaliculi on the unburnt 6-months postmortem section (left), it affects all osteons on the same burnt bone (right). 'Wedl type 2′ features are probably due to discolouration on the freshly burnt bones. The source of discolouration can be: (1) sooting from combustion gasses infiltrating the osteocyte-canalicular network after most of the organic matter has burnt out; or (2) iron, manganese, or other metal ions infiltrating the osteocyte-canalicular network prior to burning and then reduced to darker species, such as manganese dioxide or magnetite, when the bones were burnt. While the pig tibiae were not buried, those that were exposed for sufficiently long did become partly covered in soil, which may have presented the opportunity for the infiltration of metal ions. (Sample WSF5D6M1_1, transmission light microscopy, 100x magnification). [PRINT IN COLOUR]

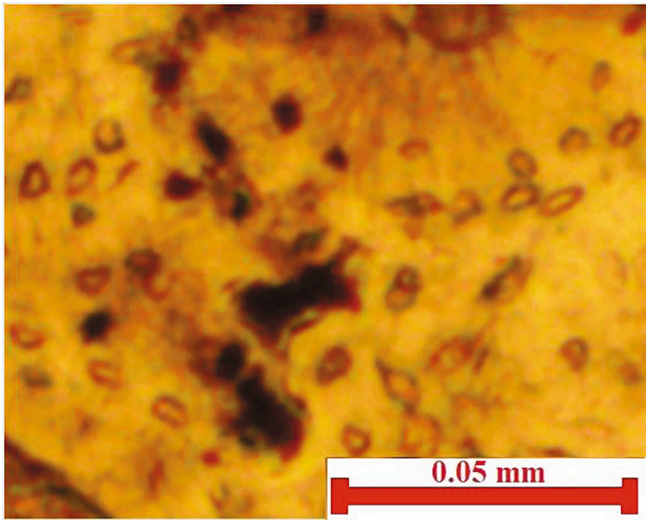


Fig. 9. Features resembling 'budded MFD' from a 6-months postmortem burnt bone (WSF5D6M3_burnt). Transmitted light microscopy, 50x.

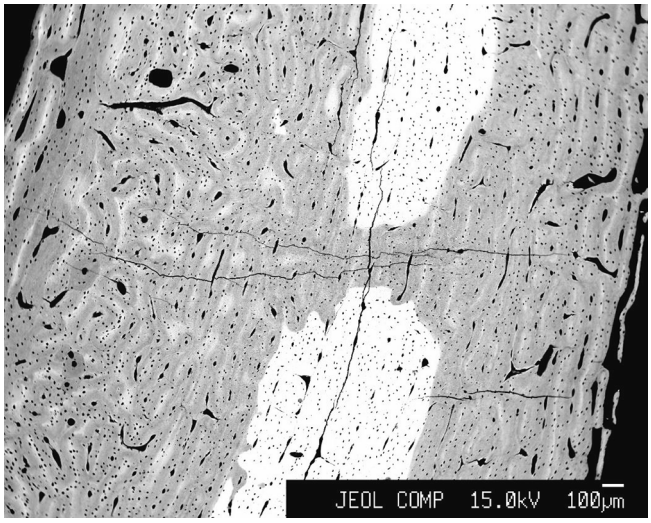


Fig. 10. Contrast differences due to burning of a 6-month decayed bone sample (WSF5D6M1_burnt). Note the central mineralised areas. (Electron microprobe, backscatter electron detector image.)

would have been buried. Although the types of soil bacteria are environment-specific such that the bioerosion features might manifest differently at various locations, a large-scale study carried out by Brönnimann et al. (2018) did not find any relationship between sediment type and intensity of microbial bioerosion.

Previous studies found that the first microscopic changes due to burning appear at varying temperatures ranging from 600 to 1200 °C. It is unknown where these temperatures were measured (bone or air in furnace). In this study maximum mean bone temperatures reached ≤ 750 °C, while fire temperatures were as high as 995 °C. If burnt and unburnt bone microstructure is indeed indistinguishable at these temperatures, it is possible that these subtle microscopic changes (e.g. 'Wedl 2′ and 'MFD') caused by burning are mistaken for bioerosion features. In general, the presence/absence of features on unburnt bones was less variable than on burnt bones, meaning not all the bones are affected the same way by fire. Variations might be due to the movement of the wind, flame height, soft tissue coverage, and this variation might not be present when bones are burnt in a furnace. Thus, it is argued here that experiments conducted on an outdoor fire give a better indication of real-life conditions in both forensic and archaeological cases than bones burnt in a furnace.

Squires et al. (2011) noted that bones cremated at temperatures between 600 and 900 °C should have very few, if any, Volkmann's canals surviving. Conversely, it is argued here that Volkmann's canals do survive 'intense cremation', as they were observed on all burnt bones. They were recorded on 3.5% of fresh, unburnt samples, giving an indication of their expected frequency. The fact that the bones were deposited in a terrestrial context – and hence not exposed to cyanobacteria – further suggests that these features are mostly Volkmann's canals, which can assume a variety of forms depending on the angles at which the bone is sectioned, and so may be responsible for this discrepancy.

Hairline cracks are most probably due to the contraction and expansion of bone attributable to weather changes, explaining the feature's positive correlation with longer decay times in the unburnt groups, which disappeared post-burning. Cracks are considered to be indications of collagen degradation (Huisman et al., 2017), but no statistically significant increase was observed with time of deposition. Neither feature appears to be a useful indicator for degradation in the bones, not least because the preparation of thin sections and/or burning can cause them. The black enlarged lacunae and canaliculi may be present because of carbon incorporation into the uneven surfaces of bone.

Demineralised and hypermineralised foci were sometimes present on the BSEM images of the unburnt bones. However, these foci did not resemble tunnels on BSEM images published by Fernández-Jalvo et al. (2010) and Turner-Walker (2019). Bright, heavily mineralised areas on the unburnt bones (e.g. Fig. 5) may instead relate to the structure of bone

in young individuals, in which osteonal bone has not yet replaced the primary lamellar bone, producing a mixture of darker, less dense (younger) and heavier mineralised (older) areas (Boskey and Coleman, 2010), which can be mistaken for tunnelling. Hypermineralised areas with a less diffused degradation pattern than has been previously documented (Turner-Walker and Syversen, 2002; Turner-Walker and Peacock, 2008) suggest early bacterial bioerosion in some of the 3-months postmortem unburnt bones. All bioerosion-like features were obliterated through the burning process (Fig. 10). Therefore, BSEM is not a useful technique for identification of bioerosion features on burnt bones.

This study was conducted simultaneously with another recent study by Lemmers et al. (2020), with similar overall aims and methods. Although they suggest that bioerosion lesions have the potential to act as a proxy for the pre-burnt condition of the body, the opposite is suggested here. The cause of this discrepancy might be that in the current study fresh, fleshed tibiae were burnt as controls, while the freshest bones in Lemmers et al.'s (2020) study were > 3 years postmortem and may have been embalmed with a decomposition accelerator compound. In our study features indistinguishable from bioerosional features as described in the literature appeared on the fresh burnt controls, suggesting that they were produced by burning.

Limitations of the present study include the use of pigs as a proxy for humans and their young age (18 months), which might make them more susceptible to bioerosion due to the higher amount of organic matter in the bones. The data from the 1-year postmortem group are based on two samples, because the rest were removed by scavengers during the exposure phase. It was not possible to get access to a microtome, so thin sections were cut with a Buehler saw, producing a less consistent thickness across samples. All labelling was executed by one researcher (EIV) and due to the sheer number of blocks (N = 27,000) some may have been incorrectly labelled. Balanced against this is the consistency in approach to identification that this permitted. Finally, the bones were not exposed to endogenous bioerosion, which should be the focus of future studies.

5. Conclusions

This study aimed to establish the utility of diagenetic features as a proxy for the body's state of decomposition prior to incineration. Ours is the first histotaphonomic study to apply a data labelling application, built for this purpose, to statistically assess bioerosion. We highlight the inconsistency in the literature concerning the naming of diagenetic features and their considered aetiologies. Although most recent literature is concerned with what the source of bacteria is (i.e. endogenous or exogenous), verification of which of these features are in fact caused by microbial bioerosion is more urgent. Our results showed that Wedl tunnelling, Wedl 2, and lamellate MFD are not reliable indicators of decomposition because similar features appear on freshly burnt bones, and thus can be caused by other factors, such as burning. Budded MFD was the only feature that showed a statistically significant increase in bone areas affected on both the unburnt and burnt groups. However, burning considerably reduced the visibility of this feature. Features labelled here as similar to 'cyanobacterial tunnelling' were in fact probably Volkmann's canals, which survived cremation on all bones. Hairline cracks did not appear to be informative on decay. Although BSEM is a useful tool in bioerosion studies in unburnt bones, it cannot be used on burnt bones. In summary, it can be argued that microbial bioerosion features are not accurate proxies for the body's pre-burning condition and caution should be practised when identifying these in bones in both forensic and archaeological contexts.

CRediT authorship contribution statement

Emese I. Végh: Conceptualization, Data curation, Formal analysis, Funding acquisition, Investigation, Methodology, Project administration, Resources, Software, Validation, Visualization, Writing - original draft, Writing - review & editing. **Andrea Czermak:** Conceptualization, Data curation, Formal analysis, Methodology, Validation, Visualization. **Nicholas Márquez-Grant:** Conceptualization, Supervision, Validation, Writing - review & editing. **Rick J. Schulting:** Conceptualization, Data curation, Funding acquisition, Investigation, Resources, Supervision, Validation, Writing - review & editing.

Acknowledgements

The study was supported by the Meyerstein Foundation, School of Archaeology, University of Oxford. We would like to thank Prof. Robert Hedges for his insights into the study and Dr Victoria Smith for her help on the electron microprobe. We would also like to thank Mr Kevin Lemagnen for his help and support while developing the data labelling application. We thank the anonymous reviewers for their careful reading, valuable comments, and improvements made to the paper.

Funding

This work was supported by the Meyerstein Foundation, School of Archaeology, University of Oxford.

References

Absolonova, K., Veleminsky, P., Dobisikova, M., Beran, M., Zocova, J., 2013. Histological estimation of age at death from the compact bone of burned and unburned human ribs. J. Forensic Sci. 58, S135–S145. https://doi.org/10.1111/j.1556-4029.2012.02303.x.

Baby, R.S., 1954. Hopewell cremation practices. Papers in Archaeology. Ohio Historical Society, pp. 1–7.

Bell, L.S., 2012a. Histotaphonomy. In: Crowder, C., Stout, S. (Eds.), Bone Histology: An Anthropological Perspective. Taylor and Francis, Boca Raton, FL, pp. 241–251.

Bell, L.S., 2012b. Identifying postmortem microstructural change to skeletal and dental tissues using backscattered electron imaging. In: Bell, L.S. (Ed.), Forensic Microscopy for Skeletal Tissues. Humana Press, pp. 173–190.

Bell, L.S., Boyde, A., Jones, S.J., 1991. Diagenetic alteration to teeth in situ illustrated by backscattered electron imaging: diagenetic alteration to teeth by BSE. Scanning 13 (2), 173–183. https://doi.org/10.1002/sca.4950130204.

Bell, L.S., Skinner, M.F., Jones, S.J., 1996. The speed of post mortem change to the human skeleton and its taphonomic significance. Forensic Sci. Int. 82 (2), 129–140. https://doi.org/10.1016/0379-0738(96)01984-6.

Binford, L.R., 1963. An analysis of cremations from three Michigan sites. Wisconsin Archaeol. 44, 98–110.

Boaks, A., Siwek, D., Mortazavi, F., 2014. The temporal degradation of bone collagen: a histochemical approach. Forensic Sci. Int. 240, 104–110. https://doi.org/10.1016/j.forsciint.2014.04.008.

Bonney, H., Colston, B.J., Goodman, A.M., 2011. Regional variation in the mechanical properties of cortical bone from the porcine femur. Med. Eng. Phys. 33 (4), 513–520. https://doi.org/10.1016/j.medengphy.2010.12.002.

Bontrager, A.B., Nawrocki, S.P., 2008. Cremains from the Fox Hollow Farm serial homicide site. In: C.W. Schmidt, S.A. Symes (Eds.), The Analysis of Burned Human Remains. London, Academic Press, pp. 211–226.

Booth, T.J., Madgwick, R., 2016. New evidence for diverse secondary burial practices in Iron Age Britain: a histological case study. J. Archaeol. Sci. 67, 14–24. https://doi.org/10.1016/j.jas.2016.01.010.

Boskey, A.L., Coleman, R., 2010. Aging and bone. J. Dent. Res. 89 (12), 1333–1348. https://doi.org/10.1177/0022034510377791.

Bradtmiller, B., Buikstra, J.E., 1984. Effects of burning on human bone microstructure: a preliminary study. J. Forensic Sci. 29 (2), 11701J. https://doi.org/10.1520/JFS11701J.

Brönnimann, D., Portmann, C., Pichler, S.L., Booth, T.J., Röder, B., Vach, W., Schibler, J., Rentzel, P., 2018. Contextualising the dead – combining geoarchaeology and osteoanthropology in a new multi-focus approach in bone histotaphonomy. J. Archaeol. Sci. 98, 45–58. https://doi.org/10.1016/j.jas.2018.08.005.

Buikstra, J.E., Swegle, M., 1989. Bone modification due to burning: experimental evidence. In: Bonnichsen, R., Sorg, M. (Eds.), Bone Modification. The Centre for the Study of the First Americans, College Station, TX, pp. 247–258.

Cambra-Moo, O., Barroso Bermejo, R., García Gil, O., Bueno Ramírez, P., Rascón Pérez, J., González Martín, A., Rietveld, H.M., 2017. The effect of soft tissue on temperature estimation from burnt bone using Fourier Transform Infrared Spectroscopy. J. Forensic Sci. 35 (1), 1–8.

Carroll, E.L., Squires, K.E., 2020. Burning by numbers: a pilot study using quantitative petrography in the analysis of heat-induced alteration in burned bone. Int. J. Osteoarchaeol. 30 (5), 691–699. https://doi.org/10.1002/oa.2902.

Fernández Castillo, R., Ubelaker, D.H., Acosta, J.A.L., de la Rosa, R.J.E., Garcia, I.G., 2013. Effect of temperature on bone tissue: histological changes. J. Forensic Sci. 58 (3), 578–582. https://doi.org/10.1111/1556-4029.12093.

Cattaneo, C., DiMartino, S., Scali, S., Craig, O.E., Grandi, M., Sokol, R.J., 1999. Determining the human origin of fragments of burnt bone: a comparative study of histological, immunological and DNA techniques. Forensic Sci. Int. 102 (2-3), 181–191. https://doi.org/10.1016/S0379-0738(99)00059-6.

Child, A.M., 1995. Towards and understanding of the microbial decomposition of archaeological bone in the burial environment. J. Archaeol. Sci. 22 (2), 165–174. https://doi.org/10.1006/jasc.1995.0018.

Cooney, G., Quinn, C.P., Kuijt, Ian, 2014. Transformation by Fire. Tucson, University of Arizona Press.

Collins, M.J., Nielsen–Marsh, C.M., Hiller, J., Smith, C.I., Roberts, J.P., Prigodich, R.V., et al., 2002. The survival of organic matter in bone: a review. Archaeometry, 44(3), 383–394.

Daniel, J.C., Chin, K., 2010. The role of bacterially mediated precipitation in the permineralization of bone. Palaios. Sepm (Soc. Sedim. Geol.) 25(7/8), 507–516.

Dowd, Marion A., 2008. The use of caves for funerary and ritual practices in Neolithic Ireland. Antiquity 82 (316), 305–317. https://doi.org/10.1017/S0003598X00096824.

Etxeberria, F., 1994. Aspectos macroscópicos del hueso sometido al fuego: revisión de las cremaciones descritas en el País Vasco desde la arqueología. Munibe 46, 111–116.

Fairgrieve, S.I., 2008. Forensic cremation recovery and analysis. Boca Raton, FL, CRC Press.

Farmer, Andrew M., 1995. Soil chemistry change in a lowland english deciduous Woodland 1974–1991. Water Air Soil Pollut. 85 (2), 677–682. https://doi.org/10.1007/BF00476907.

Feng, Liang, Jasiuk, Iwona, 2011. Multi-scale characterization of swine femoral cortical bone. J. Biomech. 44 (2), 313–320. https://doi.org/10.1016/j.jbiomech.2010.10.011.

Fernández-Jalvo, Yolanda, Andrews, Peter, Pesquero, Dolores, Smith, Colin, Marín-Monfort, Dolores, Sánchez, Begoña, Geigl, Eva-Maria, Alonso, Antonio, 2010. Early bone diagenesis in temperate environments. Palaeogeogr. Palaeoclimatol. Palaeoecol. 288 (1-4), 62–81. https://doi.org/10.1016/j.palaeo.2009.12.016.

Forbes, Shari L., Stuart, Barbara H., Dent, Boyd B., 2005. The effect of the method of burial on adipocere formation. Forensic Sci. Int. 154 (1), 44–52. https://doi.org/10.1016/j.forsciint.2004.09.109.

Garland, A.N., 1987. A histological study of archaeological bone decomposition. In: Boddington, A., Garland, A.N., Janaway, R.C. (Eds.), Death, Decay, and Reconstruction: Approaches to Archaeology and Forensic Science. Manchester University Press, Manchester, pp. 109–126.

Garrido-Varas, C., Intriago-Leiva, M., 2015. The interpretation and reconstruction of the post-mortem events in a case of scattered burned remains in Chile. In: Thompson, T. (Ed.), The Archaeology of Cremation: Burned Human Remains in Funerary Studies. Oxbow Books, Havertown, pp. 227–242.

Gonçalves, D., Thompson, T.J.U., Cunha, E., 2011. Implications of heat-induced changes in bone on the interpretation of funerary behaviour and practice. J. Archaeol. Sci. 38 (6), 1308–1313. https://doi.org/10.1016/j.jas.2011.01.006.

Grévin, Gilles, Baud, Charles-A., Susini, Alberto, 1991. Etude anthropologique et paléopathologique d'un adulte inhumé puis incinéré provenant du site de Pincevent (Seine-et-Marne). bmsap 2 (3), 77–87. https://doi.org/10.3406/bmsap.1990.1745.

Grine, Frederick E., Bromage, Timothy G., Daegling, David J., Burr, David B., Brain, Charles K., 2015. Microbial osteolysis in an Early Pleistocene hominin (Paranthropus robustus) from Swartkrans, South Africa. J. Hum. Evol. 85, 126–135. https://doi.org/10.1016/j.jhevol.2015.05.004.

Hackett, C.J., 1981. Microscopial focal destruction (Tunnels) in exhumed human bones. Med. Sci. Law 21 (4), 243–265.

Hanson, M., Cain, C.R., 2007. Examining histology to identify burned bone. J. Archaeol. Sci. 34 (11), 1902–1913.

Hedges, Robert E.M., Millard, Andrew R., 1995. Bones and groundwater: towards the modelling of diagenetic processes. J. Archaeol. Sci. 22 (2), 155–164. https://doi.org/10.1006/jasc.1995.0017.

Hedges, Robert E.M., Millard, Andrew R., Pike, A.W.G., 1995. Measurements and relationships of diagenetic alteration of bone from three archaeological sites. J. Archaeol. Sci. 22 (2), 201–209. https://doi.org/10.1006/jasc.1995.0022.

Herrmann, B., 1976. Neuere Ergebnisse zur Beurteilung menschilcher Brandknochen. Z. Rechtsmedizin 17, 191–200.

Herrmann, B., 1977. On histological investigations of cremated human remains. J. Hum. Evol. 6 (2), 101–103. https://doi.org/10.1016/S0047-2484(77)80112-7.

Holden, J.L., Phakey, P.P., Clement, J.G., 1995a. Scanning electron microscope observations of heat-treated human bone. Forensic Sci. Int. 74 (1-2), 29–45. https://doi.org/10.1016/0379-0738(95)01735-2.

Holden, J.L., Clement, J.G., Phakey, P.P., 1995b. Age and temperature related changes to the ultrastructure and composition of human bone mineral. J. Bone Miner. Res. 10 (9), 1400–1409. https://doi.org/10.1002/jbmr.5650100918.

Hollund, H.I., Jans, M.M.E., Collins, M.J., Kars, H., Joosten, I., Kars, S.M., 2012. What happened here? Bone histology as a tool in decoding the postmortem histories of archaeological bone from Castricum, The Netherlands. Int. J. Osteoarchaeol. 22 (5), 537–548.

Hollund, Hege I, Jans, M.M.E., Kars, H., 2014. How are teeth better than bone? An investigation of dental tissue diagenesis and state of preservation at a histological scale (with photo catalogue). Internet Archaeol. 36.

Huisman, D.J., Raemaekers, D.C.M., Jongmans, A.G., 2009. Investigating Early Neolithic land use in Swifterbant (NL) using micromorphological techniques. Catena 78 (3), 185e197.

Huisman, Hans, Ismail-Meyer, Kristin, Sageidet, Barbara M., Joosten, Ineke, 2017. Micromorphological indicators for degradation processes in archaeological bone from temperate European wetland sites. J. Archaeol. Sci. 85, 13–29. https://doi.org/10.1016/j.jas.2017.06.016.

Hummel, S., Schutkowski, H., 1986. Bedeutungen für die Leichenbranddiagnose. Mit 4 Abbildungen und 1 Tabelle im Text. Zeitschrift für Morphologie und. Anthropologie 77 (1), 1–9.

Imaizumi, K., Taniguchi, K., Ogawa, Y., 2014. DNA survival and physical and histological properties of heat-induced alterations in burnt bones. Int. J. Legal Med. 128 (3), 439–446. https://doi.org/10.1007/s00414-014-0988-y.

Jans, M.M.E., Nielsen-Marsh, C.M., Smith, C.I., Collins, M.J., Kars, H., 2004. Characterisation of microbial attack on archaeological bone. J. Archaeol. Sci. 31 (1), 87–95. https://doi.org/10.1016/j.jas.2003.07.007.

Jans, M.M.E., Kars, H., Nielsen-Marsh, C.M., Smith, C.I., Nord, A.G., Arthur, P., Earl, N., 2002. In situ preservation of archaeological bone: a histological study within a multidisciplinary approach. Archaeometry 44 (3), 343–352. https://doi.org/10.1111/1475-4754.t01-1-00067.

Jans, M.M.E., 2005. Histological Characterisation of Diagenetic Alteration of Archaeological Bone (Unpublished doctoral dissertation). Institute for Geo and Bioarchaeology, Amsterdam.

Jans, M.M.E., 2008. Microbial bioerosion of bone - a review. In: M. Wisshak, L. Tapanila (Eds.), Current Developments in Bioerosion. Berlin, Heidelberg, Springer, pp. 397–493.

Jans, M.M.E., 2013. Microscopic destruction of bone. In: Pokines, J.T., Symes, S.A. (Eds.), Manual of Forensic Taphonomy. CRC Press, Taylor and Francis Group, pp. 19–35.

Kendall, Christopher, Eriksen, Anne Marie Høier, Kontopoulos, Ioannis, Collins, Matthew J., Turner-Walker, Gordon, 2018. Diagenesis of archaeological bone and tooth. Palaeogeogr. Palaeoclimatol. Palaeoecol. 491, 21–37. https://doi.org/10.1016/j.palaeo.2017.11.041.

Kontopoulos, Ioannis, Penkman, Kirsty, Liritzis, Ioannis, Collins, Matthew J., 2019. Bone diagenesis in a Mycenaean secondary burial (Kastrouli, Greece). Archaeol. Anthropol. Sci. 11 (10), 5213–5230. https://doi.org/10.1007/s12520-019-00853-0.

Kontopoulos, I., Nystrom, P., White, L., 2016. Experimental taphonomy: post-mortem microstructural modifications in sus scrofa domesticus bone. Forensic Sci. Int. 266 (April 2019), 320–328.

Lemmers, S.A.M., Gonçalves, Cunha, E.D., Vassalo, A.R., Appleby, J., 2020. Burned fleshed or dry ? The potential of bioerosion to determine the pre-burning condition of human remains. J. Archaeol. Method Theory.

Lynn, K.S., Fairgrieve, S.I., 2009. Microscopic indicators of axe and hatchet trauma in fleshed and defleshed mammalian long bones. J. Forensic Sci. 54(4), 793–797.

Millard, A., 1993. Diagenesis of archaeological bone: the case of uranium uptake. (Unpublished doctoral thesis) University of Oxford: Research Laboratory for Archaeology and the History of Art.

Matuszewski, S., Moreau, G., Schoenley, K.G., Tarone, A.M., Villet, M.H., 2020. Pigs vs people: the use of pigs as analogues for humans in forensic entomology and taphonomy research. Int. J. Legal Med. 134 (2), 793–810.

Millard, A.R., 2001. Deterioration of bone. In: Brothwell, D.R., Pollard, A.M. (Eds.), Handbook of Archaeological Sciences. J. Wiley, Chichester; New York, pp. 637–647.

Morales, N.S., Catella, L., Oliva, F., Sarmiento, P.L., Barrientos, G., 2018. A SEM-based assessment of bioerosion in Late Holocene faunal bone assemblages from the southern Pampas of Argentina. J. Archaeolog. Sci.: Rep. 18, 782–791.

Nelson, R., 1992. A microscopic comparison of fresh and burned bone. J. Forensic Sci. 37 (4), 1055–1060.

Nicholson, Rebecca A., 1993. A morphological investigation of burnt animal bone and an evaluation of its utility in archaeology. J. Archaeol. Sci. 20 (4), 411–428. https://doi.org/10.1006/jasc.1993.1025.

Nielsen-Marsh, Christina M, Hedges, Robert E.M, 2002. Patterns of diagenesis in bone I: the effects of site environments. J. Archaeol. Sci. 27 (12), 1139–1150. https://doi.org/10.1006/jasc.1999.0537.

Nielsen-Marsh, C.M., Smith, C.I., Jans, M.M.E., Nord, A., Kars, H., Collins, M.J., 2007. Bone diagenesis in the European Holocene II : taphonomic and environmental considerations. J. Archaeol. Sci. 34 (9), 1523–1531.

Pearce, A.I., Richards, R.G., Milz, S., Schneider, E., Pearce, S.G., 2007. Animal models for implant biomaterial research in bone: a review. Eur. Cells Mater. 13(0), 1–10. https://doi.org/10.22203/eCM.v013a01.

Pechal, J.L., Tawni L. Crippen, Aaron M. Tarone, Andrew J. Lewis, Jeffery K. Tomberlin, M. Eric Benbow, 2013. Microbial community functional change during vertebrate carrion decomposition. PLoS ONE 8(11), e79035.

Pesquero, M.D., Bell, L.S., Fernández-jalvo, Y., Pesquero, M.D., Bell, L.S., Fernández-jalvo, Y., 2018. Skeletal modification by microorganisms and their environments. Hist. Biol. 2963, 1–12. https://doi.org/10.1080/08912963.2017.1371713.

Piepenbrink, Hermann, 1986. Two examples of biogenous dead bone decomposition and their consequences for taphonomic interpretation. J. Archaeol. Sci. 13 (5), 417–430. https://doi.org/10.1016/0305-4403(86)90012-9.

Piepenbrink, H., Schutkowski, H., 1987. Decomposition of skeletal remains in desert dry soil a roentgenological study. Hum. Evol. 2 (6), 481–491. https://doi.org/10.1007/BF02437423.

Quatrehomme, Gérald, Bolla, Marc, Muller, Michèle, Rocca, Jean-Paul, Grévin, Gilles, Bailet, Paul, Ollier, Amédeé, 1998. Experimental single controlled study of burned bones: contribution of scanning electron microscopy. J. Forensic Sci. 43 (2), 16160J. https://doi.org/10.1520/JFS16160J.

Roux, G.A.D.T., 1887. Contribution à l'étude clinique et thérapeutique des taenias de l'homme (Unpublished doctoral thesis). University of Lyon, Lyon, France.

Spennemann, D.H.R., Colley, S.M., 1989. Fire in a Pit: the effects of burning on faunal remains. Archaeozoologia 3, 51–64.

Squires, Kirsty E., Thompson, Tim J.U., Islam, Meez, Chamberlain, Andrew, 2011. The application of histomorphometry and Fourier Transform Infrared Spectroscopy to the analysis of early Anglo-Saxon burned bone. J. Archaeol. Sci. 38 (9), 2399–2409. https://doi.org/10.1016/j.jas.2011.04.025.

Symes, A.S., Dirkmaat, D.C., Ousley, S., Chapman, E., Cabo, L., 2012.s Recovery and Interpretation of Burned Human Remains. NIJ Report. National Institute of Justice Available at https://www.ncjrs.gov/pdffiles1/nij/grants/237966.pdf (20/04/2016).

Taylor, M.E., Morecroft, M.D., Oliver, H.R., 2011. The Physical Environment. Oxford University Press, Wytham Woods.

Thompson, T.J.U., Inglis, J., 2009. Differentiation of serrated and non-serrated blades from stab marks in bone. Int. J. Legal Med. 123 (2), 129–135. https://doi.org/10.1007/s00414-008-0275-x.

Tjelldén, A.K.E., Kristiansen, S.M., Birkedal, H., Jans, M.M.E., 2018. The pattern of human bone dissolution-a histological study of Iron Age warriors from a Danish wetland site. Int. J. Osteoarchaeol. 28 (4), 407–418. https://doi.org/10.1002/oa.2666.

Trueman, C.N., Martill, D.M., 2002. The long-term survival of bone: the role of bioerosion. Archaeometry 44 (3), 371–382. https://doi.org/10.1111/1475-4754.t01-1-00070.

Turner, B., Wiltshire, P., 1999. Experimental validation of forensic evidence: a study of the decomposition of buried pigs in a heavy clay soil. Forensic Sci. Int. 101, 113–122.

Turner-Walker, Gordon, 2012. Early bioerosion in skeletal tissues: persistence through deep timeEarly bioerosion in skeletal tissues: persistence through deep time. njgpa 265 (2), 165–183. https://doi.org/10.1127/0077-7749/2012/0253.

Turner-Walker, G., 2014. The chemical and microbial degradation of bones and teeth. In: Pinhasi, R., Mays, S. (Eds.), Advances in Human Palaeopathology. John Wiley and Sons, pp. 3–29.

Turner-Walker, G., 2019. Light at the end of the tunnels ? The origins of microbial bioerosion in mineralised collagen. Palaeogeogr. Palaeoclimatol. Palaeoecol. 529, 24–38.

Turner-Walker, G., Syversen, U., 2002. Quantifying histological changes in archaeological bones using BSE-SEM image analysis. Archaeometry 44 (3), 461–468. https://doi.org/10.1111/1475-4754.t01-1-00078.

Turner-Walker, Gordon, Jans, Miranda, 2008. Reconstructing taphonomic histories using histological analysis. Palaeogeogr. Palaeoclimatol. Palaeoecol. 266 (3-4), 227–235. https://doi.org/10.1016/j.palaeo.2008.03.024.

Turner-Walker, Gordon, Peacock, Elizabeth E., 2008. Preliminary results of bone diagenesis in Scandinavian bogs. Palaeogeogr. Palaeoclimatol. Palaeoecol. 266 (3-4), 151–159. https://doi.org/10.1016/j.palaeo.2008.03.027.

Ubelaker, Douglas H., 2009. The forensic evaluation of burned skeletal remains: a synthesis. Forensic Sci. Int. 183 (1-3), 1–5. https://doi.org/10.1016/j.forsciint.2008.09.019.

Upton, Racheal N., Checinska Sielaff, Aleksandra, Hofmockel, Kirsten S., Xu, Xia, Polley, H. Wayne, Wilsey, Brian J., 2020. Soil depth and grassland origin cooperatively shape microbial community co-occurrence and function. Ecosphere 11 (1). https://doi.org/10.1002/ecs2.2973.

Van Vark, G.N., 1970. Some Statistical Procedures for the Investigation of Prehistoric Human Skeletal Material. Rijksuniversiteir te Groningen, Groningen.

Waterman, D.M., 1978. The excavation of a court cairn at Tully, Co. Fermanagh. Ulster J. Archaeol. 41, 3–14.

Wedl, C., 1864. Über einen im Zahnbein und Knochen keimenden Pilz. Sitzungsberichte Der Kaiserlichen Akademie Der Wissenschaften Zu Wien. Mathematisch-Naturwissenschaftliche Classe 50 (1), 171–193.

Wells, C., 1978. Notes on cremated bones from Tully court cairn. Ulster J. Archaeol. 41, 13–14.

White, Lorraine, Booth, Thomas J., 2014. The origin of bacteria responsible for bioerosion to the internal bone microstructure: results from experimentally-deposited pig carcasses. Forensic Sci. Int. 239, 92–102. https://doi.org/10.1016/j.forsciint.2014.03.024.

Whyte, Thomas R., 2001. Distinguishing remains of human cremations from burned animal bones. J. Field Archaeol. 28 (3-4), 437–448. https://doi.org/10.1179/jfa.2001.28.3-4.437.

Wilson, Andrew S., Janaway, Robert C., Holland, Andrew D., Dodson, Hilary I., Baran, Eve, Pollard, A. Mark, Tobin, Desmond J., 2007. Modelling the buried human body environment in upland climes using three contrasting field sites. Forensic Sci. Int. 169 (1), 6–18. https://doi.org/10.1016/j.forsciint.2006.07.023.

Yoshino, Mineo, Kimijima, Tetsuo, Miyasaka, Sachio, Sato, Hajime, Seta, Sueshige, 1991. Microscopical study on estimation of time since death in skeletal remains. Forensic Sci. Int. 49 (2), 143–158. https://doi.org/10.1016/0379-0738(91)90074-S.

Submitted Manuscript

Applied Spectroscopy

Applied Spectroscopy
2022, Vol. 0(0) 1–20
© The Author(s) 2022
Article reuse guidelines:
sagepub.com/journals-permissions
DOI: 10.1177/00037028221085600
journals.sagepub.com/home/asp
SAGE

Physicochemical Changes in Bone Bioapatite During the Late Postmortem Interval Pre- and Post-Burning

Emese I. Végh[1,*], Nicholas Márquez-Grant[2], and Rick J. Schulting[1]

Abstract

Postmortem chemical transformation of bone bioapatite can take place during early diagenesis, resulting in a more thermodynamically stable mineral phase. This paper examines the impact of a one year postmortem interval on unburnt and burnt bone's structural and chemical alterations. This question is of importance for the reconstruction of funerary practices involving cremation in the archaeological record, as well as forensic anthropological investigations. Fleshed pig (*Sus scrofa*) tibiae were left exposed in a field, then collected at 14, 34, 91, 180, and 365 days intervals prior to being burnt in an outdoor fire (≤750 °C bone temperature). Fresh (fleshed) tibiae acted as unburnt and burnt controls. Also included in the study were two cremated human bone fragments from Middle–Late Neolithic (ca. 3300–2500 BCE) Ireland. Samples were analyzed for major and trace elements using an electron microprobe wavelength dispersive analyzer and molecular structures using Fourier transform infrared spectroscopy. Linear regression, principal component analysis, linear discriminant analysis, and multivariate analysis of variance were performed for statistical analysis. Results indicate that the concentrations of elements associated with extracellular fluid (K, Na, and Cl) change with the postmortem interval (PMI) and survive burning. K values under 0.07 ± 0.01 wt% in the inner and mid-cortical zones of burnt bones suggest that bones were not burnt immediately after death. Using this criterion, results from the archaeological samples would indicate a PMI of at least weeks to months prior to cremation. Ca, P, Fe, Al, Si, and Sr are not significantly altered with burning, and Fe, Al, Si, and Sr are also unaffected by the PMI. In unburnt bones increased crystallinity and carbonate loss are detectable in <1 year, but both are obscured by burning. Structurally, the carbonate to phosphate ratio (C/P), the phosphate high temperature, and cyanamide to phosphate (CN/P) are the most useful ratios for discriminating between unburnt and burnt bones.

Keywords

Cremation, electron microprobe, Fourier transform infrared, Fourier transform infrared spectroscopy, taphonomy, potassium

Date received: 24 November 2021; accepted: 9 February 2022

Introduction

Thermally altered human bones occur in both forensic and archaeological contexts. Burnt bones can result from accidental fires or arson, or to mask the victim's identity as well as the cause and manner of death in a homicide case.[1] Since antiquity, cremation has been a common funerary practice in many cultures, though there are often questions regarding the state of the corpse at the time of burning. In several tombs and burials of Neolithic, Bronze, and Iron Age Ireland,[2–5] Scotland,[6,7] England,[8–11] and France,[12] for example, human remains may have been excarnated before cremation, while in other cases bodies seem to have been burned soon after death.[3–5] Some of this interpretation is based on heat-induced fracture patterns including thumbnail fractures and warping, associated with the burning of fresh bones in early studies.[13–18] However, more recent research has shown that these fractures do not depend on the presence of soft tissues, but rather on collagen content and distribution.[19,20] Recent attempts to identify bone decomposition prior to burning through histotaphonomical analysis[21] may be unreliable.[22] Identifying when burning took place after death presents a challenge, one addressed here through a study of the

[1]Research Laboratory for Archaeology and the History of Art, University of Oxford, Oxford, Oxfordshire, UK
[2]Defence Academy of the United Kingdom, Cranfield Forensic Institute, Cranfield University, Cranfield, Bedford, UK

Corresponding author:
*Emese I. Végh, Research Laboratory for Archaeology and the History of Art, Wolfson College, Linton Rd, Oxford, Oxfordshire OX2 6UD, UK.
Email: emese.vegh@wolfson.ox.ac.uk

physicochemical changes of bones pre- and post-burning up to one year post-deposition.

If changes in elemental concentrations to bone are detectable after a short period of deposition/postmortem interval (PMI; in the current study two weeks to one year) and they survive burning, it can be hypothesized that it is possible to inform on the pre-burning condition, that is, on whether bodies were fresh or partly decomposed when burnt. Although effects of diagenesis on the elemental concentration had been investigated,[23–25] no studies have examined these changes after exposure to heat. Therefore, this study aims to assess the potential of compositional and structural changes in unburnt and burnt bone to help distinguish between fresh and variably taphonomically altered bones within a defined post-mortem interval. The results of this experiment are compared to the chemical composition of archaeological (Neolithic) cremated bones. Our hypothesis based on previous studies (e.g., Keenan and Engel,[24] Walden et al.[25]) is that these changes can occur weeks following deposition by the loss of endogenous elements in vivo and from the uptake of exogenous elements from the environment. We further hypothesize that these changes will be observed in the burnt bones since inorganic mass loss is negligible in bones burnt at up to 900 °C.[26]

Taphonomic Alterations to the Elemental Concentration and Structure of Bone

Bone is a composite material consisting of ~55–70 wt% mineral, ~20–35 wt% organic carbon, and ~10–15% water.[27–29] Hydroxyapatite [HAp, $Ca_{10}(PO_4)_6(OH)_2$] is the basis of all biologically formed apatite, while bioapatite [$(Ca,Mg,Na)_{10-x}[(PO_4)_{6-x}(CO_3)_x](OH)_{2-x}$] is a carbonate-containing variety of HAp, which forms the inorganic component of bone.[28,30,31] Bioapatite is chemically more complex than HAp; it is non-stoichiometric, and can incorporate a wide variety of elements into its structure.[28,31–33]

The chemical profile of bone (Table S1, Supplemental Material) results from the combination of the pre-mortem (e.g., diet and inhalation) and postmortem (e.g., degradation and soil) incorporation and release of elements. However, it is modified by taphonomic (post-mortem) factors, which can be natural (e.g., weathering, mineral replacement, and microbial attack) or anthropogenically induced (e.g., inhumation, subaerial exposure, disarticulation and defleshing, and burning).[34] Early decomposition includes the hydrolysis of collagen, and the first biological, chemical, and structural changes to bioapatite.[35,36] Bioerosion causes increased surface areas which either encourages mineral dissolution or enhances the movement of ions and substitutions, eventually leading to a more thermodynamically stable mineral phase.[37] Organic loss has been associated with increased ion transport[36,37] due to the open pore spaces between the mineral phase, facilitating the movement of fluids, microorganisms, and dissolved ions,[35] unless pore spaces are blocked by ingress of trace elements from the environment.[38] Fossils, the resulting mineral phase from late diagenesis, have a wide variety of substitutions, but most commonly have F- and Ca-enriched apatite phases[35,39,40] or CO_3^{2-} loss.[41] An experiment in which modern bones were exposed for up to 30 years on soil surfaces in Kenya showed that crystal sizes increase in number and size with time.[42]

Bone composition is susceptible to changes as soon as bone is exposed to the environment, which has been documented in unburnt modern,[24,25] archaeological,[43] and fossil bone,[37] but regarded as negligible.[44] Bioapatite can accommodate various substitutions at every site of the crystal lattice, which makes it one of the most diverse minerals.[24,45] Cations (metals) substitute for Ca(I) and Ca(II),[46] while anions for phosphates, carbonates, and hydroxyls. Trace elemental uptake due to ion exchange can occur after one week, while after a year a more thermodynamically stable mineralogical phase shift to F- and Fe-enriched apatite phases can be seen.[24] Non-uniform, nonlinear increases (Mn, Fe, Ca, and F) and decreases (Cl and Na) were also seen in bone buried >1 year. However, the calcium to phosphate ratio (Ca/P) remains constant during putrefaction,[47,48] while a decrease of carbonate to phosphate (C/P) has been identified after burial for one year. The latter is due to either carbonate loss (A and B), increased phosphate content, or the loss of organic material in bone.[24]

Much of the work on trace element uptake into bone has revolved around rare earth elements and uranium,[49–51] which are taken up by bioapatite over 10^3–10^6 years post-mortem.[50] In modern bone, Ca, P (from bioapatite), Fe, Na, K (associated with bodily fluids), F, Mg, Al, Si, Cl, and Mn (associated with trace elements from soil) are usually studied. Fe, Al, and Mn are often abundant in weathered soils but are less likely to enter into solution.[52] If this does occur, Al and Mn do not only affect the outermost layers of bone, but are measurable as contaminants in the mid-cortical region in archaeological bone.[53] Fe is stored in vivo in blood, bodily organs,[25,54] with a minuscule amount being surface-bound in bone.[47,54] The decrease of Na and K has been linked to the dehydration of bone during decomposition.[25] Mg is surface-bound in bioapatite, and although it has been shown not to be much affected by diagenesis, very small amounts can be incorporated into the bioapatite lattice.[25] In buried bone cations diffuse inward toward the pores from the outer cortex.[51] Adsorption will cease once equilibrium is reached with the surrounding pore waters,[55] also evidenced by the slowing and halting of trace element leaching during fossilization.[56] The rate of approaching equilibrium with pore waters is dependent on the element concentration, mobility in the environment, and the adsorption coefficient (i.e., a constant relating to the speed a molecule will bind to the surface of bioapatite at defined conditions).[51,55]

Heat Changes to the Physicochemical Structure of Bone

Generally, heat-induced changes in bone go through the following stages: (i) dehydration of the bone with the breakage

of hydroxyl bonds and water removal; (ii) organic component (lipids and proteins) decomposition around 400–500 °C; (iii) inversion, marked by carbonate loss (CO_3^{2-} disappears completely at ~ 700 °C); and (iv) fusion of the crystals (>700 °C) when the crystallites grow in size and OH^- and PO_4^{2-} rearranges within the pores which are now vacant of organics and water.[19,57]

Many studies have investigated the elemental compositional changes of burnt bone in archaeological and experimental contexts,[32,43,58–61] and for biomaterials research (e.g., Holden et al.,[62] Rogers and Daniels[63]). During the burning process, bone is susceptible to chemical substitutions.[64] Although in theory, most inorganic elements in bone should not change at temperatures possible to reach in an outdoor fire, the inorganic mass loss has been shown to fluctuate around 2.8 wt% independent from temperature during heating up to 900 °C.[26] Various heat-induced elemental changes have been documented (Table S2, Supplemental Material).

The main structural changes observed include the reordering of phosphate, the decrease/loss of carbonate, and increased crystallinity,[26,60,65] which start to occur at 600/700 °C.[26,66,67] Extensions to the α-lattice and changes to the c-lattice parameters are accompanied by the release of lattice carbonate and possibly water, which results in an increase in crystal size and crystallinity.[68] At temperatures around 730 °C, a new phase of beta-tricalcium-phosphate (β-TCP) appears in bioapatite, which remains stable at high temperatures.[69] The appearance of β-TCP signals the thermal decomposition of the apatite phase, which happens due to non-stoichiometric substitutions/P ratio (i.e., <1.67).[69,70] Another secondary phase by-product is CaO, which appears at >700 °C [71] is due to the thermal decomposition of $CaCO_3$.[72]

As regards diagenetic processes, most research has investigated chemical changes to bone post-burning and after deposition,[43,58] which was thought to be similar in cremated bone as in unburnt bone in earlier research.[49,58] However, these studies were observational with no controls,[49] and only referring to calcium.[58] Bioapatite is less reactive post-deposition in an archaeological timescale[42,73] and especially after burning because the crystals transform into a more stable thermodynamic phase[74]; thus, the inorganic structure seems to remain stable post-burning. The amount of organic material in bone prior to burning appears to affect thermal decomposition as traced through OH^-, carbonate (type A and B), β-TCP, tetracalcium phosphate (TetCP), loss of CO_2 and water content,[75] and presence of cyanamide.[74]

Materials and methods

The material and experimental protocol employed here follows that of a parallel study,[22] which examined the histotaphonomic features in unburnt and burnt bones to inform on the PMI. Fleshed pig (*Sus scrofa domesticus)* tibiae (N = 22) were allowed to decay exposed within a cage for 14 (N = 5), 34 (N = 5), 91 (N = 5), 180 (N = 5), and 365 (N = 2) days prior to burning on an outdoor fire in Wytham Woods, Oxfordshire, UK. Fresh pig tibiae (N = 10) served as controls throughout the study, without being exposed. Over time the exposed bones became partially submerged in soil and vegetation; however, experimental studies have found no significant differences in elemental concentrations in buried and surface-exposed bones.[25]

Wytham Woods is located in a temperate climate with annual precipitation averaging 717 mm and mean winter and summer temperatures of 1.6 °C and 20.3 °C, respectively. Soil pH ranges widely from 3 to 7.[76] Bones were burnt on an outdoor fire, which was executed in the same manner with each event lasting from 2.5–3 h until the bones were deemed to be fully calcined based on their appearance. A thermocouple was used to directly monitor bone temperature, with a mean of 553 °C and a recorded maximum of 751 °C.[22]

Bone samples were taken from diaphyses before and after burning to maintain consistency with other studies of elemental concentration.[25] The unburnt samples were defatted in a 2:1 chloroform:methanol mixture. The composition and atomic-level structure of the bones were analyzed from: (i) polished resin blocks using wavelength-dispersive X-ray spectroscopy (WDS) on an electron microprobe (EMP) and (ii) powders using Fourier transform infrared spectroscopy (FT-IR) in attenuated total reflection (ATR) mode. Electron microprobe wavelength dispersive allows spatially resolved analysis of a single bone. This approach is essential since the outer layer of the bone may have a different distribution of elements than the mid- or inner cortical bone adjacent to the medullary cavity (cf. Gallello et al.[43]). FT-IR has been used previously to determine bone composition (organic and inorganic) and bone structure, such as the infrared splitting factor (IRSF), which provides insights into bone crystallinity (e.g., Keenan and Engel,[24] Snoeck et al.[74]).

Additionally, two cremated human bone fragments from burials 1 and 7 at a Middle/Late Neolithic (ca. 3300–2500 cal BCE) stone circle in Kiltierney, Co. Fermanagh, Northern Ireland,[77] were included. The fragments presented thumbnail fractures, suggestive of high bone collagen content at the time of burning.[20] They were analyzed with EMP, to compare their bone chemistry to the experimental results.

Fourier Transform Infrared Spectroscopy

Fourier transform IR was used to retrieve structural and molecular information from the unburnt and burnt bones. This has been frequently used to investigate both the diagenetic pathways in osseous material,[78–80] to differentiate between heated bone at low, medium, and high temperatures,[81,82] and to characterize modern and archaeological burnt bone.[74,83] ATR was chosen instead of KBr discs, as it has been shown to provide more reliable measurements and fewer chemical modifications.[79,81,84,85]

The powdered pre- and post-burnt samples were measured with a Cary 600 series FT-IR spectrometer 5.3 (Agilent Technologies, USA). A diamond crystal accessory was utilized with an operational range of 30,000 to 200 cm^{-1}. Resolution Pro FT-IR software (Agilent Technologies, Santa Clara, California, USA) was used for automatic software correction and for generating the backgrounds and the raw data for each sample. After the spectrometer was aligned, a resolution of 4 cm^{-1} was chosen. Sixty-four scans were taken of each sample with scan range set between 4000 and 400 cm^{-1}, which represents mid-IR spectrum analysis. The background was measured after at least every second sample. Before the sample was placed on the accessory, the live spectrum was monitored to ensure no background noise. Baseline corrections were made at around 450, 800, 900, and 1200 cm^{-1}. The calculated ratios included those from the literature: the crystallinity index/splitting factor (IRSF),[20,60,66,86] amide to phosphate (APR),[87] carbonate (type B) to phosphate (C/P), amount of type B carbonate (BPI),[81] type A carbonate to phosphate (API),[81,88] type B to type A carbonates (C/C), cyanamide to phosphate (CN/P),[74] carbonyl to carbonate (CO/CO_3), amide I to phosphate (N/P) ratios, and the phosphate high temperature (PHT)[67] (Table S3, Supplemental Material). Additionally, the presence of β-TCP was noted when present as a peak at 1123 cm^{-1} and as a shoulder at 547 cm^{-1}.[89] Presence of β-TCP implies that burnt bone reached >700 °C. If this β-TCP peak is present at 1123 cm^{-1}, IRSF loses its usefulness in estimating crystallinity. It was also suggested that the presence of this peak might be associated with Mg substitution for Ca in the bone.[89] Type A carbonates (~1540 cm^{-1}) were not evaluated in unburnt bone because its peak overlaps with amide II.[88] However, it was included in the burnt bone spectra evaluations because organics were removed by heating. The peak heights were evaluated by observing the maximum height from the data at around the associated absorbance using Jupyter notebook in Python programming language. If a slight frequency shift was present (±5 cm^{-1}), the maximum height between this interval was recorded for the ratio calculations and the extent of shift noted.

Electron Microprobe Analysis

A total of 58 unburnt and burnt bone fragments were embedded undecalcified into epoxy cold mounting resin and a catalyst (Spectrographic Ltd., UK) and placed under vacuum in a desiccator to ensure diffusion of the resin into bone pores. Mounted blocks were then ground with carbon papers of progressively finer grit size (800, 1200, and 2500) using a grinding and lapping machine (Buehler, USA). The blocks were then polished on a Buehler wheel using 3 mm diamond paste (DP-Paste M, Struers A/S) and a satin woven acetate polishing cloth (DP-Dac, Struers A/S) for 30 min following another 5 min cycle using another polishing cloth with 1 mm monocrystalline diamond suspension (MetaDi, Buehler). The mounts were cleaned in an ultrasonic water bath after each phase, then finished with another round of ultrasonic bath in petroleum ether (40–60 °C, analytical reagent grade, Fisher Scientific). Samples were carbon-coated using a carbon evaporation coater (HHV Auto 360), the carbon acting as a conductive layer to prevent charging.

Major and trace element compositions were determined using a wavelength-dispersive Jeol JXA-8200 electron microprobe at the Research Laboratory for Archaeology and the History of Art, University of Oxford, UK. An accelerating voltage of 15 kV, 10 nA beam current, and 10 μm beam were used to analyze the polished samples. Peak count times were 30 s for P, Al, Na, Si, K, and Ca; 40 s for Cl; and 60 s for Mg, Sr, Fe, and Mn. Background counts were collected for half the peak count time either side of the peak.[90] The microprobe was calibrated using a range of mineral standards, with accuracy verified by analyzing apatite secondary standards (Durango, Bamble, and Wilberforce)[91] and previously analyzed secondary bone standards provided by the Directorate Earth and History of Life, Royal Belgian Institute of Natural Sciences, at the start of every run. Reference materials were within ±1 standard deviation of the preferred values.[92] Analytical errors of the electron microprobe analysis (EMPA) and detection limits for the measured elements are provided in Table I. K and Mg were in much higher concentration in the samples than in the secondary standards, meaning that their error rates presented a lower value. Thus, the standard deviation percentage (SD%) was measured for these elements which were 37.87 SD% for K and 3.83 SD% for Mg. A total of 617 measurements were taken from the outer cortical layer (OC), mid-cortical region (MC), inner cortical layer (IC), and around vascular canals (HC) on the transverse bone sections. This excludes 82 points that were removed from the dataset because the sum of elements was less than expected in bone (total elements measured <50%) due to errors in locating and focusing the electron beam.

Statistical Analysis

The absorption peaks, ratios from the FT-IR, and the elemental concentration EMPA data were analyzed using Python programming language. Descriptive statistics and linear regression were used to measure the strength of the relationship between the measured changes and the PMI in both the unburnt and burnt bones, with statistical significance assessed by associated p-values ($\alpha = 0.05$). The null hypothesis was that parameter X does not increase with PMI. The coefficient of variation (CV) was used to evaluate the scattering of parameters in each group with different PMI and burning status.

Principal component analysis (PCA) and linear discriminant analysis (LDA) were used to identify the main elements of interest and FT-IR ratios were used to differentiate between PMI groups and burning states. LDA was a better statistical model for the purposes of this study. A priori categories in this

Table I. The coefficient of variation and detection limits of the measured major and trace elements in the secondary standards.

Element	Secondary standards	Confidence interval (CV)	Detection limit
P	Bamble, DURANGO, Bone	0.79	0.07
Na	Bamble, Durango, Bone	6.90	0.02
Cl	Bamble, Durango, Bone	3.49	0.01
K	Bone	17.22 (SD%: 37.87)	0.01
Fe	Bamble, Durango, Bone	33.99	0.01
Al	Wilberforce	1.71	0.03
Si	Bamble, Durango, Wilberforce	16.81	0.04
Sr	Bamble, Durango, Wilberforce, Bone	57.62	0.03
Mn	Bamble, Durango, Wilberforce, Bone	65.20	0.01
Mg	Bamble, Wilberforce, Bone	2.82 (SD%: 3.83%)	0.02
Ca	Bamble, Durango, Bone	0.51	0.01

study were state (unburnt versus burnt), PMI (0–365 days), and zone (outer-, mid-, inner-cortical, and around vascular canals). The confidence score of each sample determined the parameter based on which they were placed into one of these categories. Multivariate analysis of variance (MANOVA) was used to examine for statistical differences on one dependent variable (PMI) by independent grouping variables (EMPA and FT-IR datasets) in Statsmodels Python library. This was coupled with pairwise post hoc multivariate comparison testing (MCT) to identify which specific groups significantly differed from one another.

Datapoints below detection points (Table IV) were entered as 0.00 in the EMPA data. Both FT-IR and EMPA dataframes were scaled for the analyses using Scikit-Learn Python library. All data analyses were performed in Jupyter Notebook in Python programming language.

Results

Fourier transform infrared spectroscopy Results

The spectra of unburnt and burnt bone were investigated in different regions and their associated changes were noted as a function of length of PMI and burning (Fig. 1; Table II). A change in the intensity of peaks from 0 to 365 days PMI groups were found at several frequencies.

The majority of the mean IRSF values for the unburnt bones ranged between 2.88 and 3.30, with the exception of the 365 days bone (5.04) (Table S4). There was an increase in all mean IRSF values post-burning (37.77–57.27%) across all groups, except for the 365 days PMI sample, which decreased by 5.35%. In unburnt bone, the 365 days group's high IRSF value was significantly different than all other PMI group (Table III). CV values showed very low variation across samples within the same PMI groups. IRSF gives an indication of highest reached temperature and cremation efficiency, due to increased crystallinity values. The sequence of crystallinity of the PMI groups is: 91 > 0 > 180 & 365 > 34 > 14 days. This sequence does not follow the PMI order and it is likely due to the variation in burning conditions (e.g., temperature, duration, and position in the pyre), which are the dominant factors affecting crystallinity.

The results of the linear regression (Table III) show that there was a strong positive linear correlation between IRSF and time since deposition in unburnt bone ($r = 0.856$, $p < 0.029$). This increase in structural ordering suggests the early post-mortem recrystallization of bioapatite is already measurable in the first year of PMI. BPI was negatively correlated with PMIs in unburnt bone ($r = -0.876$, $p < 0.022$) (Table III). Although there was no linear change in any of the proposed parameters for PMI estimation in the burnt bone, MANOVA and MCT revealed that IRSF, C/C, and CO/CO_3 ratios were significantly different in various PMI groups in burnt bone, as well as IRSF, BPI, C/C, and PHT in unburnt bone (Table III).

Unburnt bone at 0 and 91 days PMI displayed an extra shoulder at 1123 cm^{-1}, which is assigned for either β-TCP or Mg substitution.[89] All burnt bone had an extra peak at 1100–1080 cm^{-1}, except the 34 day post-mortem group. No burnt bone displayed a shoulder at 547 cm^{-1}, but it was a common feature in the unburnt bone, intensity ranging from strong (365 days) to very weak (0 days), which translation band also suggest Mg–OH substitutions.[102] Mg shows a non-uniform, nonlinear increase in the unburnt bone through the PMI in the EMPA data.

Principal component analysis indicated that the ratios explained 81.67% of the variance in the dataset with the first (PC1) and second (PC2) principal components accounting for 66.67% and 15.00%, respectively. Loadings show that all ratios contributed to PC1, with IRSF (0.74), BPI (0.35), and CO/CO_3 (0.33) being the largest (Fig. 2), while the main contributors to discrimination by LDA was C/P for burnt bone and PHT and CN/P for unburnt bone (Figure S1, Supplemental Material). Both PCA and LDA differentiated between unburnt and burnt bone, but not between PMI groups.

WDS-EMP Results

The WDS-EMP data were analyzed spatially for major and trace elemental concentration (Table S5) of unburnt and burnt bone at different PMIs. Variations in elemental concentrations

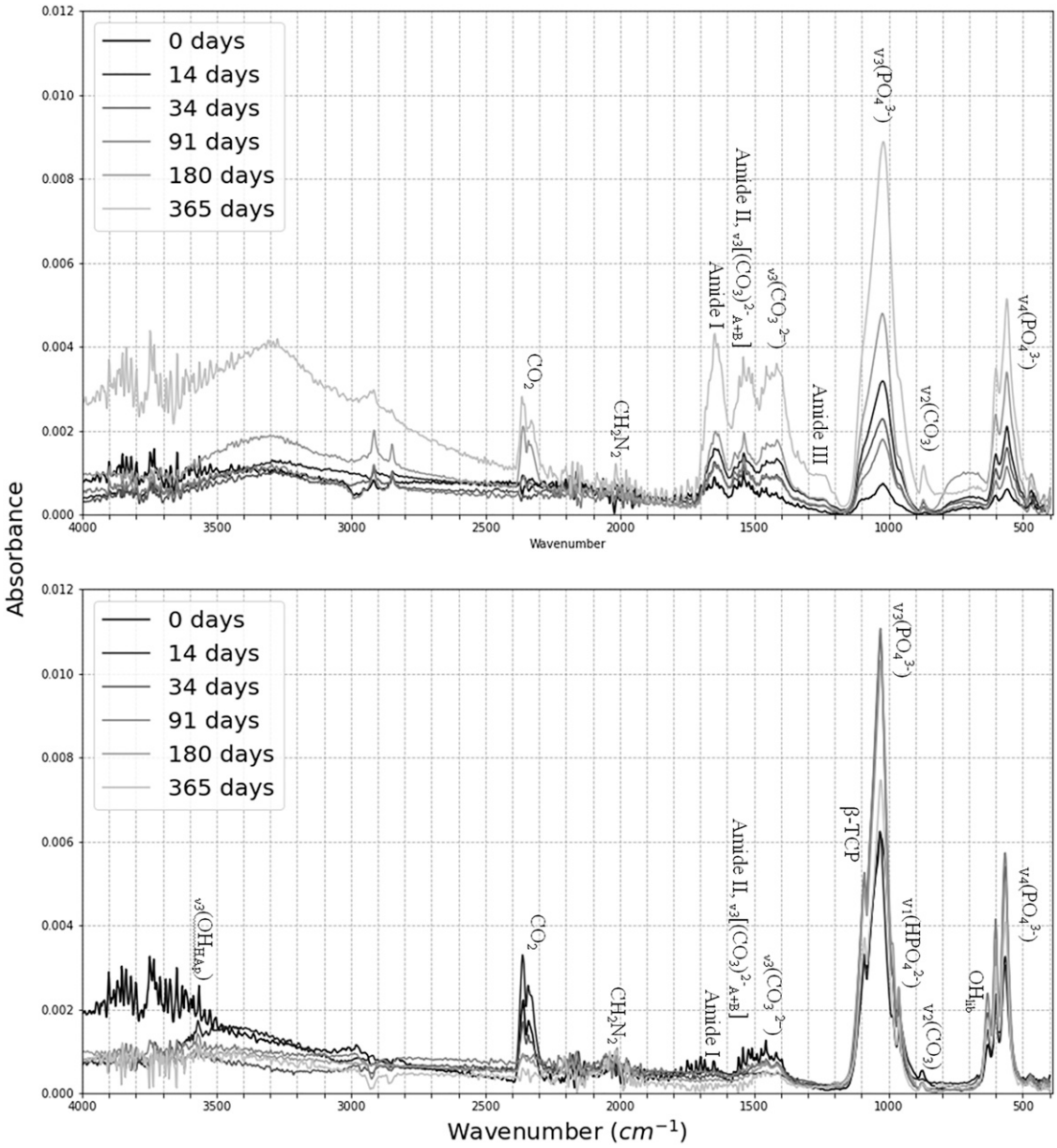


Figure 1. The FT-IR spectra of the means of each PMI group before (upper image) and after (lower image) burning. Labeled are the peak assignments of interest.

as a function of time in the experimental bone are visualized in Fig. 3. The most highly variable zones in unburnt bone across all elements were the OC (0.60) and HC (0.50), while IC (0.49) and MC (0.46) were the lowest. The mid-cortical and the inner cortical zones showed the lowest variability across all samples.

In the archaeological cremated bone (KILT) P and Ca remained relatively stable in all zones, while K, Fe, Al, Si, Sr, Mn, and Mg display very high values in the outer cortical layers, suggesting diffusion of elements from the soil (Fig. 4). The highest CV scores were recorded for Sr, especially in the outer cortical layers (Fig. 5).

Linear regression analysis (Table IV) shows that only K, Mn, and Mg in unburnt bone and Na, Cl, and K in burnt bone changed in a linear fashion with time. K was the only element that decreased both in the unburnt and burnt bone sections overall, and separately in the IC and HC zones. There were no significant trends in the Ca/P ratios and all zones presented similar values (between 1.23 and 1.29) while the archaeological samples were insignificantly higher (1.35).

The PCA showed that the first principal component (PC1) explained 93.49% of the variance and the second principal component (PC2) explained 4.19%, with the key

Table II. Identified zones of interest and their associated absorption changes on the unburnt and burnt bones.

Wavenumber (cm^{-1})	Functional group	Mode	Bone samples	
			Unburnt	Burnt
3570	Apatitic hydroxyl groups ($_{versus}OH^-$)	OH stretching[57,93]	N/A	Intensity decreases with longer PMI
3600–2700	Organic fraction and water[94]	C–H and O–H stretching [95]	Convoluted bands, no peaks	N/A
2400–2300	(atmospheric) CO_2	C≡O stretching[96]	Doublet of bands (traces of CO_2 from atmosphere)	Doublet of bands (traces of CO_2 from atmosphere)
2010	Cyanamide (CH_2N_2) [74,97]	C–N stretching	Weak peak present, highest in 365 day group	Weak peak present, highest in 365 day group
1660	Amide I[57] (C=O) and water	C–O stretching and H–O–H bending	Decreases with longer PMI	Very weak bands: highest 0 day group, lowest 365 day
1550	Amide II[57] (N–H)	N–H bending	Decreases with longer PMI	Very weak bands: highest 0 day group, lowest 365 day
1250	Amide III[57] (N–H)	N–H bending	Shoulder on all groups, except a very weak peak in the 0 day group	N/A
1600–1300	Stretching modes of carbonate ions[94,98]	C–O stretching	Three broad bands with additional peaks; highest: 365 day, lowest: 0 day, mixed in between	Weak bands, highest; 0 day, lowest: 14 day
1415	B type carbonates $_{v3}(CO_3^{2-})_B$[98,99]	C–O stretching	Highest of the carbonate peaks, highest in 365 day, lowest in 0 day	Weak peaks: highest in 0 day, lowest in 365 day
1540	A type carbonates $_{v3}(CO_3^{2-})_A$[98]	C–O stretching	Overlaps with amide II	Weak peaks: 0 days highest, 365 days lowest
1123	Extra peak, due to appearance of β-TCP[89]	P–O stretching (anti-symmetric (ν3))	No extra peak. Shoulder on the 0 and 91 day groups.	Extra peak around 1080–1090 cm^{-1} on all groups except 34 day group
960–1200	$_{v1,\ v3}$ (PO_4^{3-})[57]	P–O stretching (symmetric (ν1) and anti-symmetric (ν3))	No peaks, shoulders. Most intense: 365 day, least intense: 0 day	Present. Highest intensity: 0, 91, 180 day; weakest: 14 day
872–879	Carbonates (three sub-bands): type A, type B, "labile" $_{v2}(CO_3)$ [86,94,100]	out-of-plane bending C–O	Present, but as a convolution of the three sub-bands. Highest: 365 day, weakest: 0 day. All the rest are clustered around the same absorbance value.	Present, but as a convolution of the three sub-bands. Decreases with longer PMI. Most intense: 0 day > 14 day. Other groups: clustered around the same lower value
640–620	Apatitic hydroxyl groups[57,101]	(OH) librational	N/A	Present. Intensity of peak: 91 > 34 > 180 > 365 >14 > 0 day
600–500	$_{v4}(PO_4^{3-})$[98,99]	P–O bending	Two peaks ($_{v3}$ splitting). Most intense: 365 days, least intense: 0 days	Three peaks ($_{v3}$ splitting and OH_{lib} band). $_{v3}$ intensity: 91 > 34 > 180 > 365 > 0 > 14 days
547	Shoulder, due to appearance of β-TCP[89]	P–O bending[98,99]	Present on all. 365 days: strong, 180 days: moderate, 91-, 34-, and 14 days: weak, 0 days: very weak	N/A

discriminators being Ca and P (Fig. 2). LDA was used to reduce the features (elements), classify samples, and subsequently visualizing the classification according to the defined categories (state, PMI, and zone). When the data were transformed into a two-feature (unburnt versus burnt) linear discriminant dataset, the two states were clearly differentiated (Fig. 6a). LDA did not clearly differentiate between the PMI groups, with slightly more separation of PMIs in unburnt bone (Fig. 6b). MANOVA and MCT showed that P, Na, Cl, K, Mn, Mg, and Ca were significantly associated with burning, while

Table III. Linear regression and multivariate comparison test (MCT) on the Fy-IR dataset. Correlation coefficient (*r*) and *p*-value (*p*) for each analyzed FT-IR parameter on the unburnt and burnt bone in the linear regression section. H_0 = X parameter does not increase with postmortem time period.

	Linear Regression				Multivariate comparison of means test		
	Unburnt[a]		Burnt		PMI (PR>F)		
FT-IR parameters	r	*p*	r	*p*	Unburnt	Burnt	State (PR>F)
IRSF	0.856	**0.029**	0.2	0.704	**0.000002**	**0.014**	**0.001**
C/P	–0.531	0.278	–0.557	0.251	0.505	0.561	**0.001**
BPI	–0.876	**0.022**	–0.619	0.19	**0.006**	0.638	**0.001**
API	N/A	N/A	–0.631	0.179	N/A	0.667	N/A
CO3/P	0.269	0.606	–0.049	0.926	N/A	N/A	N/A
C/C	0.08	0.879	0.096	0.855	**0.034**	**0.003**	**0.024**
CN/P	–0.701	0.12	–0.039	0.941	0.535	0.316	**0.003**
CO/CO3	–0.655	0.158	–0.519	0.29	0.16	**0.003**	**0.005**
PHT	0.679	0.138	–0.159	0.763	**0.032**	0.055	**0.001**
N/P	–0.46	0.357	–0.508	0.303	N/A	N/A	N/A
APR	–0.542	0.267	–0.492	0.321	N/A	N/A	N/A

[a]Items in bold indicate significant *p*-values. The MCT section shows the results of the MANOVA and multivariate comparison testing on the established FT-IR ratios as a function of state (unburnt versus burnt) and time.

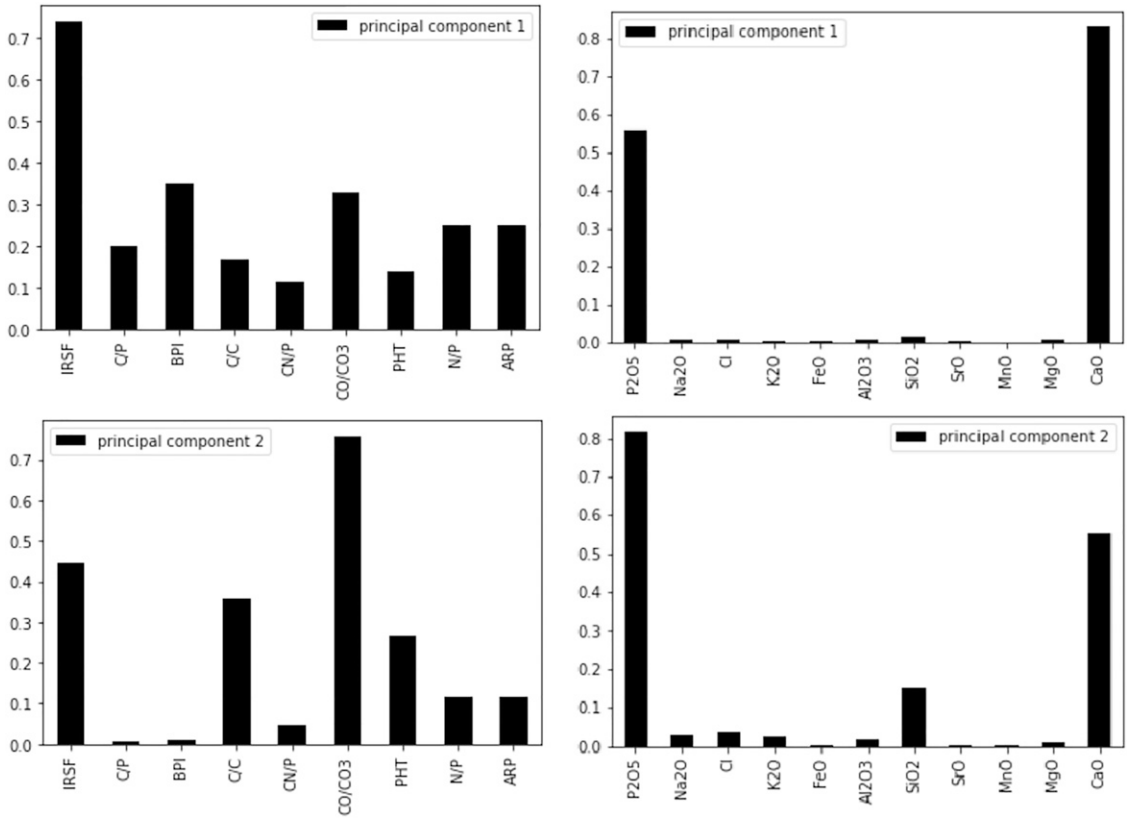


Figure 2. Loadings of the principal component analysis when using both the FT-IR and EMP dataset.

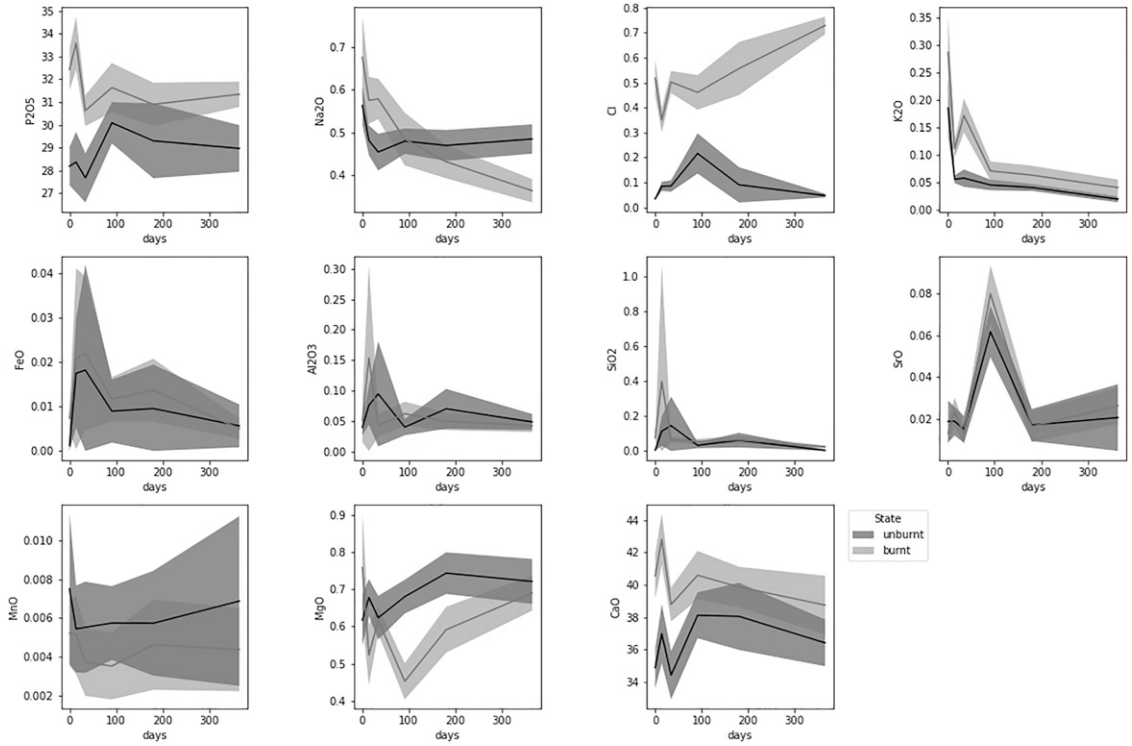


Figure 3. Average elemental concentration (wt %) of the experimental bones using the electron microprobe analysis data. Mean ± 2 standard errors for each measured element as a function of time in unburnt (blue) and burnt (orange) bone.

Fe, Si, Sr, and Al were not (Table IV). An overall significant difference was observed between PMI groups in Cl, K, Sr, and Mg levels in unburnt bone, and in P, Na, Cl, K, Sr, Mg, and Ca values in burnt bone (Table IV). The fresh group differed significantly in K values from all other PMI groups in both unburnt and burnt bone by MANOVA and MCT.

Discussion

This study on the early diagenesis and burning of bioapatite has shown that both structural and chemical changes are observable after only one-year PMI. Potassium elemental concentration decreased with PMI and survived burning, making it the best discriminator between bone burnt fresh and partially decomposed. This decrease compared to experimental bone suggests that endogenous K had decayed prior to cremation in the Neolithic bone, thus the bodies might have been left to decompose prior to further funerary treatment. While decrease in carbonates and increase in crystallinity were documented in only one year of surface exposure, these were masked by burning. Ca, P, Fe, Al, Si, and Sr did not significantly change with heat-treatment and Fe, Al, Si, and Sr were not associated with time since deposition either.

Crystallinity increases in a linear fashion with PMI in unburnt bone and burnt bone shows higher crystallinity compared to unburnt bone. This agrees with the literature (e.g., Thompson et al.[67] and Snoeck et al.[74]), except the 365 day burnt group where results show a slight decrease, which may be the result of the already higher crystallinity of the bone or small-scale temperature variation across individual bones. The lack of linear increase in burnt bone crystallinity with time suggests that burning overrides the increase in IRSF due to early diagenesis in the first six months of the PMI. As crystallinity increased, carbonate content decreased in a linear fashion in the unburnt bone, in line with other studies.[24,103] Keenan and Engel[24] documented significant carbonate loss at three years PMI, with insignificant decrease after one year but increase compared to that value in two years, while here A and B carbonates to phosphate ratios showed a significant linear decrease throughout only a year PMI. However, B type carbonates only significantly changed prior to three months PMI compared to the 365 days group. Burning, again, obscured the effects of early diagenesis of carbonate loss.

β-TCP signals the thermal decomposition of the apatite phase and should be detectable in bones burnt at >700 °C,[69,70,104] which was reached in this study for a short duration. There is an extra peak at ~1100–1080 cm^{-1} on all burnt bone spectra, which might be due to a shift in the spectra and might still represent β-TCP. However, the lack of a shoulder at 547 cm^{-1} suggests otherwise. Surprisingly, all unburnt bone displayed a shoulder at 547 cm^{-1}. These shoulders cannot be due to β-TCP in unburnt bone but are

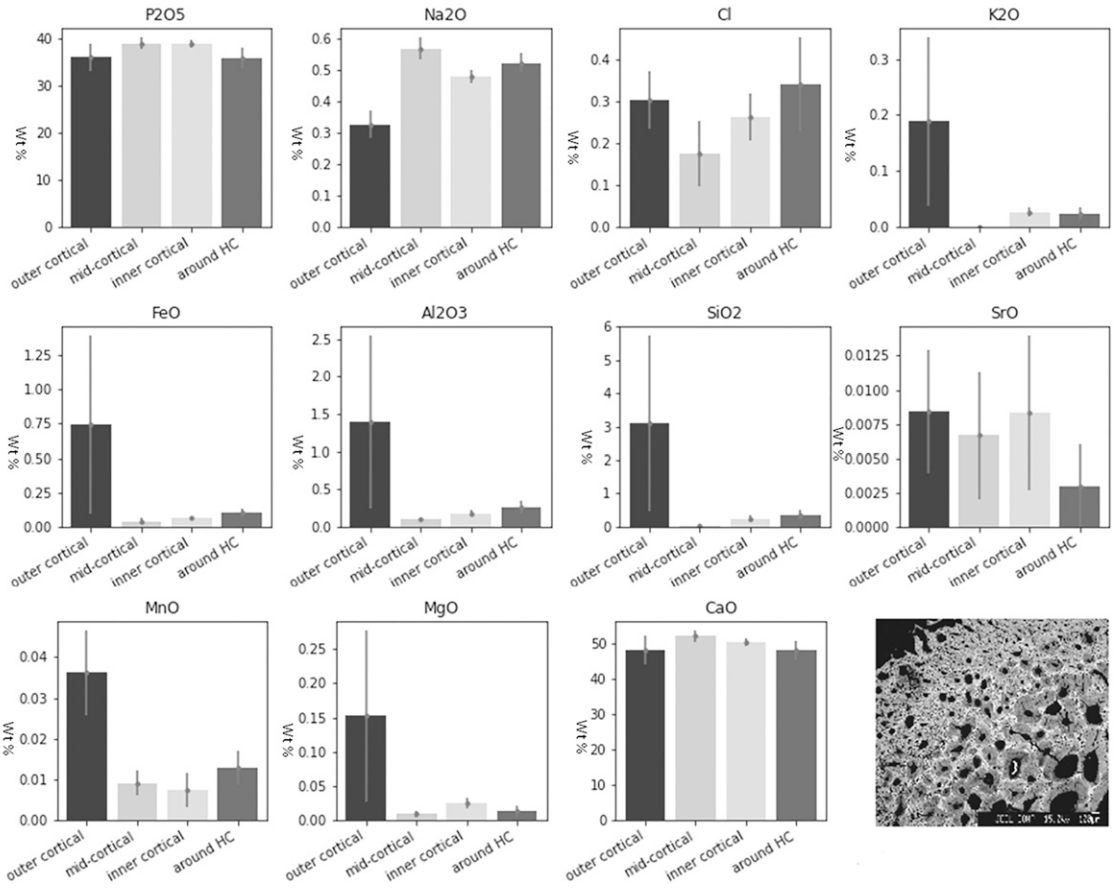


Figure 4. Average elemental concentration (wt %) of the Neolithic cremated human remains for each zone. Mean ±2 standard errors for each measured major and trace element in archaeological cremated bone. The backscattered electron microscopy (BSEM) image represents an example of a bone cross section.

probably due Mg substitutions for Ca.[89] However, there were no outstanding elevated levels of Mg in the unburnt bone (unburnt mean Mg levels ranged between 0.01 and 0.82 wt%). Mg values in all zones are slightly higher in the 180- and 365 days groups than those with shorter PMIs, suggesting a non-uniform, nonlinear increase. However, Mg values were highly variable in burnt bone. With a melting point of 650 °C, this might be due to the burning efficiency of the different fire events. Therefore, β-TCP as a thermal decomposition product might not have occurred, but Mg ions might have increased despite its reduced competitiveness in substituting due to the crystal lattices' more accommodating nature for sodium and potassium.[105] Another possibility is that β-TCP did appear as a thermal decomposition product, but post-cooling it was not possible to detect, as it is not thermally stable.[106]

As the bones were burnt in an outdoor fire, burning efficiency was variable. Burning efficiency could be estimated for the different PMI groups from the N/P ratios and IRSF. The sequence from highly efficient to less efficient from N/P was 91- and 180 days > 365 days > 34 days > 0 days > 14 days, while from IRSF data it was 91 days > 0 days > 180- and 365 days > 34 days > 14 days. The differing placement of the 0 days group in the two sequences might be due to the placement of the different fat-content of the individual fresh legs, since fat acts as a fuel during burning, increasing temperature when more fat is present and resulting in higher crystallinity. MANOVA results confirmed that all FT-IR ratios designed to assess cremation efficiency[19,67,81] differ significantly in unburnt and burnt bone. In both cases, the 91 days group was the most efficiently cremated and the 14 days group the least. This might explain why only the 14 days and the 0 days groups showed significantly different values in P in burnt bone. Ca and P, the two major elements in bone, were otherwise insignificant in both the unburnt and burnt groups. Sr was significantly different in the most efficiently burnt group (91 days) than in all others, but this difference was present in its unburnt state as well; thus, it was not due to burning.

Other than Mn, the increase in all other element's atomic percentage is higher in burnt 0 days (fresh) bone than in unburnt fresh bone. However, it appears this is due to the decrease in organic content and thus does not essentially

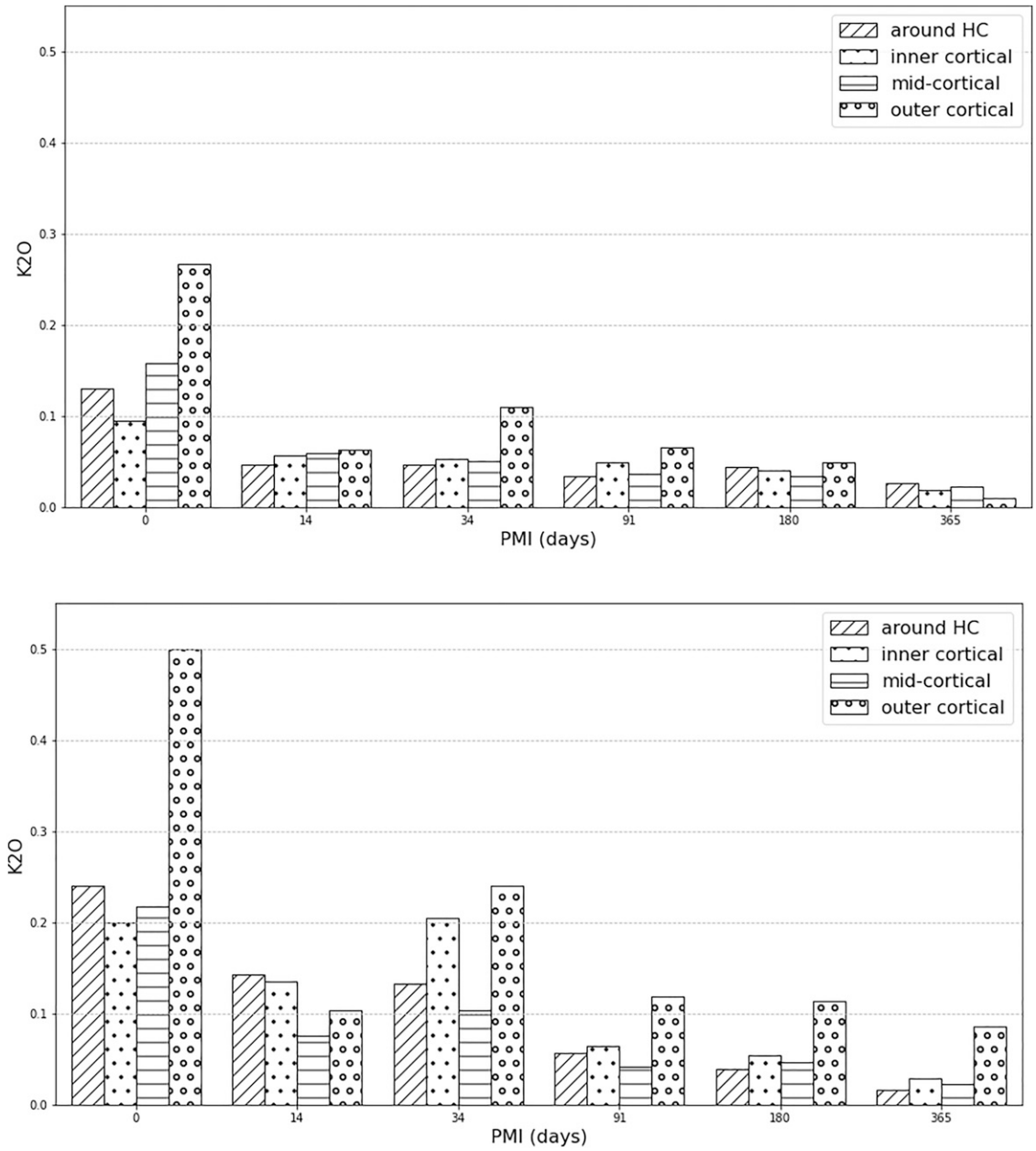


Figure 5. Potassium wt% content in experimental unburnt (upper) and burnt (lower) bone by zone.

indicate a real increase in the mineral phase. Ca, P, Fe, Al, Si, and Sr changes through the PMI stages in the same fashion in unburnt and burnt bone, meaning they are not highly affected by burning at ≤750 °C and their amount in burnt bone is representative of their pre-burnt levels. The results for Sr agree with those of Snoeck et al.,[74] who did not find changes in Sr isotopic signals following experimental cremation. Fe showed an initial increase at 14 days PMI and a sharp decrease thereafter, which is due to soft tissue putrefaction and aligns with the literature.[25]

Only three elements (K, Na, Cl) were found to be affected by time since deposition in the first year PMI. Potassium and sodium are associated with moisture in bone and their decrease signifies dehydration.[25] Here, potassium was the most useful element in differentiating between fresh (0 days) and all other PMI groups in unburnt bone. In addition, K showed an overall linear decrease in both unburnt and burnt bone area for all zones combined. The unburnt group's potassium values suggest rapid depletion of K in two weeks (from mean 0.16 wt% to mean 0.06 wt%), after which depletion slowed down.

Table IV. Linear regression and multivariate comparison test on the electron microprobe analysis data. Correlation Coefficient (*r*) and *p*-value (*p*) are given for each analyzed element in unburnt and burnt bone for the linear regression. H_0 = X parameter does not increase with postmortem time period.

		Linear regression				Multivariate comparison test (MCT)		
		Unburnt		Burnt		PMI		
Element	Location	*r*	*p*	*r*	*p*	Unburnt	Burnt	State
P_2O_5	OC	0.602	0.206	0.204	0.699	0.419	**0.000	**0.001
	MC	0.246	0.638	–0.276	0.597			
	IC	0.217	0.68	–0.572	0.236			
	HC	0.063	0.905	–0.428	0.397			
	All	0.277	0.19	–0.284	0.179			
Na_2O	OC	–0.172	0.745	–0.676	0.141	0.061	**0.000	**0.001
	MC	–0.436	0.388	–0.873	**0.023			
	IC	0.561	0.247	–0.889	**0.018			
	HC	0.236	0.652	–0.872	**0.023			
	All	–0.051	0.813	–0.744	**0.000			
Cl	OC	–0.397	0.436	0.830	**0.041	**0.000	**0.000	**0.001
	MC	–0.099	0.852	0.702	0.120			
	IC	–0.142	0.789	0.843	**0.035			
	HC	–0.009	0.986	0.801	0.055			
	All	–0.162	0.449	0.690	**0.000			
K_2O	OC	–0.655	0.158	–0.54	0.269	**6.05E-26	**9.15E-23	**0.001
	MC	–0.603	0.205	–0.666	0.149			
	IC	–0.834	**0.039	–0.810	**0.050			
	HC	–0.551	0.257	–0.804	0.054			
	All	–0.552	**0.005	–0.578	**0.003			
FeO	OC	–0.413	0.416	–0.397	0.436	0.767	0.302	0.839
	MC	0.614	0.195	–0.097	0.855			
	IC	–0.153	0.773	0.011	0.983			
	HC	–0.493	0.321	–0.395	0.438			
	All	–0.160	0.454	–0.251	0.238			
Al_2O_3	OC	–0.304	0.558	–0.027	0.96	0.633	0.209	0.900
	MC	–0.497	0.316	0.502	0.311			
	IC	–0.441	0.382	0.690	0.129			
	HC	0.715	0.111	–0.423	0.403			
	All	–0.127	0.555	–0.171	0.424			
SiO_2	OC	–0.498	0.315	–0.780	0.067	0.283	0.493	0.497
	MC	–0.584	0.223	–0.519	0.291			
	IC	–0.391	0.443	–0.507	0.304			
	HC	–0.045	0.932	–0.370	0.470			
	All	–0.242	0.255	–0.206	0.335			
SrO	OC	0.178	0.736	0.025	0.963	**0.000	**3.03E-32	0.470
	MC	–0.255	0.625	0.215	0.682			
	IC	0.086	0.872	–0.052	0.922			
	HC	0.128	0.809	0.023	0.966			
	All	0.027	0.899	0.054	0.804			
MnO	OC	0.637	0.173	–0.473	0.344	0.952	0.692	**0.031
	MC	–0.873	**0.023	0.123	0.817			
	IC	–0.567	0.241	0.137	0.795			
	HC	0.523	0.287	–0.085	0.872			
	All	0.127	0.553	–0.062	0.772			
MgO	OC	0.709	0.115	0.182	0.731	**0.048	**0.000	**0.003
	MC	0.402	0.429	0.621	0.189			
	IC	0.780	0.068	–0.418	0.409			
	HC	0.480	0.335	0.379	0.458			
	All	0.456	**0.025	0.138	0.52			

(continued)

Table IV. (continued)

		Linear regression				Multivariate comparison test (MCT)		
		Unburnt		Burnt		PMI		
Element	Location	*r*	*p*	*r*	*p*	Unburnt	Burnt	State
CaO	OC	0.753	0.084	0.642	0.169	0.089	**0.001	**0.001
	MC	0.137	0.795	–0.555	0.253			
	IC	0.078	0.884	–0.668	0.147			
	HC	0.071	0.894	–0.637	0.174			
	All	0.286	0.176	–0.354	0.090			

** Indicates significant *p*-values. HC = around vascular canals; OC = outer cortical; MC = mid-cortical; IC = inner cortical zones. In the multivariate comparison test, *p*-values are derived from both MANOVA and multivariate comparison testing.

Environmental factors might have altered the rate of depletion in the OC and IC zones. After 34 days, bone had a higher K-value in the OC zones, which coincides with the time at which the specimens started to be noticeably partially submerged into the soil. The burnt experimental bone always had higher K-levels than unburnt but followed the same pattern of depletion. Although KOH has a relatively low melting point (360 °C), it was found in apatitic aorta deposits burnt at 720 °C,[107] suggesting that it is bound to the crystal. K was previously found to be localized in the removed organic bone material[108] and was suggested to be present mainly in a labile state, meaning it is localized on the mineral crystal surface with low migration activity.[107] However, the latter study's limitations included a more limited detection limit of EDS and the inability to evaluate the contributions to the labile fraction corresponding to surface-localized water-soluble compounds related to the organic matrix. Since organic material was removed by burning in the present study's bones, meaning that the oxidation of carbon was complete (assessed by the white color of calcined bones without black ash/carbon left behind), but K was still detectable by EMPA, it is possible that K integrates into the crystal lattice. The 0 days burnt bioapatite samples always had K-values ≥0.20 wt%, while after 14 days this decreased to <0.14 wt% in all areas. The OC zones also showed depletion but at a slower rate than other areas. After three months, all K concentrations at IC, MC, and HC zones were ≤0.06 wt% and <12 wt% at OC areas. Thus, K-levels of <0.07 ± 0.001 wt% in the inner and mid-cortical zones, and around vascular canals of burnt bone suggest that the corpse was not burnt immediately after death, but after around three months. The outer cortical zones might show higher K concentrations due to uptake of potassium from the soil. It has to be noted that these bones were surface exposed, and that dehydration would be expected to be slower had they been buried. In the Neolithic human bone fragments, endogenous K was below detection limit in the mid-cortical bone sections. Exogenous K (mean 0.08 wt%) from the soil might have diffused into the OC layers and to a lesser degree from the IC end and through the HC zones. Since bioapatite is less susceptible to changes post-burning, due to increased crystallinity,[42,73,74,109] this might mean that potassium essentially depleted in the Neolithic samples prior to cremation. Therefore, these bodies might have been left to decompose prior to cremation, to a degree that endogenous potassium was no longer present. Based on the experimental results of this study, in which K-values were never below the detection point at any zone, the postmortem interval prior to cremation in the archaeological bone can be suggested to have been >1 year.

Sodium is also associated with extracellular fluid in the body.[25] The 0 days burnt group showed higher values than the unburnt group, which agrees with Ellingham et al.[48] In the experimental burnt samples there was a slight decrease between the 0 days (0.54 wt%) and 14 days (0.46 wt%) groups, after which it remained stable (0.45–0.48 wt%). Previously, Na was shown to have a tendency of mass transfer, leaving the crystals at 720 °C and increasing at 760 °C, which was suggested to be due to the reversible exchange of CO_3^{2-}.[107] Here, Na showed a linear decrease with time in heated bones. The decrease of Na in the EMPA data is confirmed and supported by the decrease of CO_3 ions in the FT-IR data.[110] The initial value was 54% lower than in modern human bone reported by Elliott.[28] This discrepancy might be due to inter-species differences in calcium-substituting ions, such as Na, but studies on them are sparse.[111] The Na value of 0.47 wt% for the Neolithic bone is consistent with that of unburnt archaeological bone reported in the literature.[112] The burnt bone demonstrated that MC, IC, and HC zones had similar Na values, while OC zone was depleted. Normally, Na leaches out of the layers of bone closest to the environment over time,[112,113] but these bones were broken. Nevertheless, it seems to explain why the experimental burnt bone had higher Na values in the OC zones one year post-mortem than the archaeological samples.

Chlorine values in burnt bone behaved almost inversely proportional to unburnt bone over time. Cl-enriched phases might appear in early diagenetic bone through the incorporation of Cl^- facilitated by the protonation of hydroxyl ions,[35]

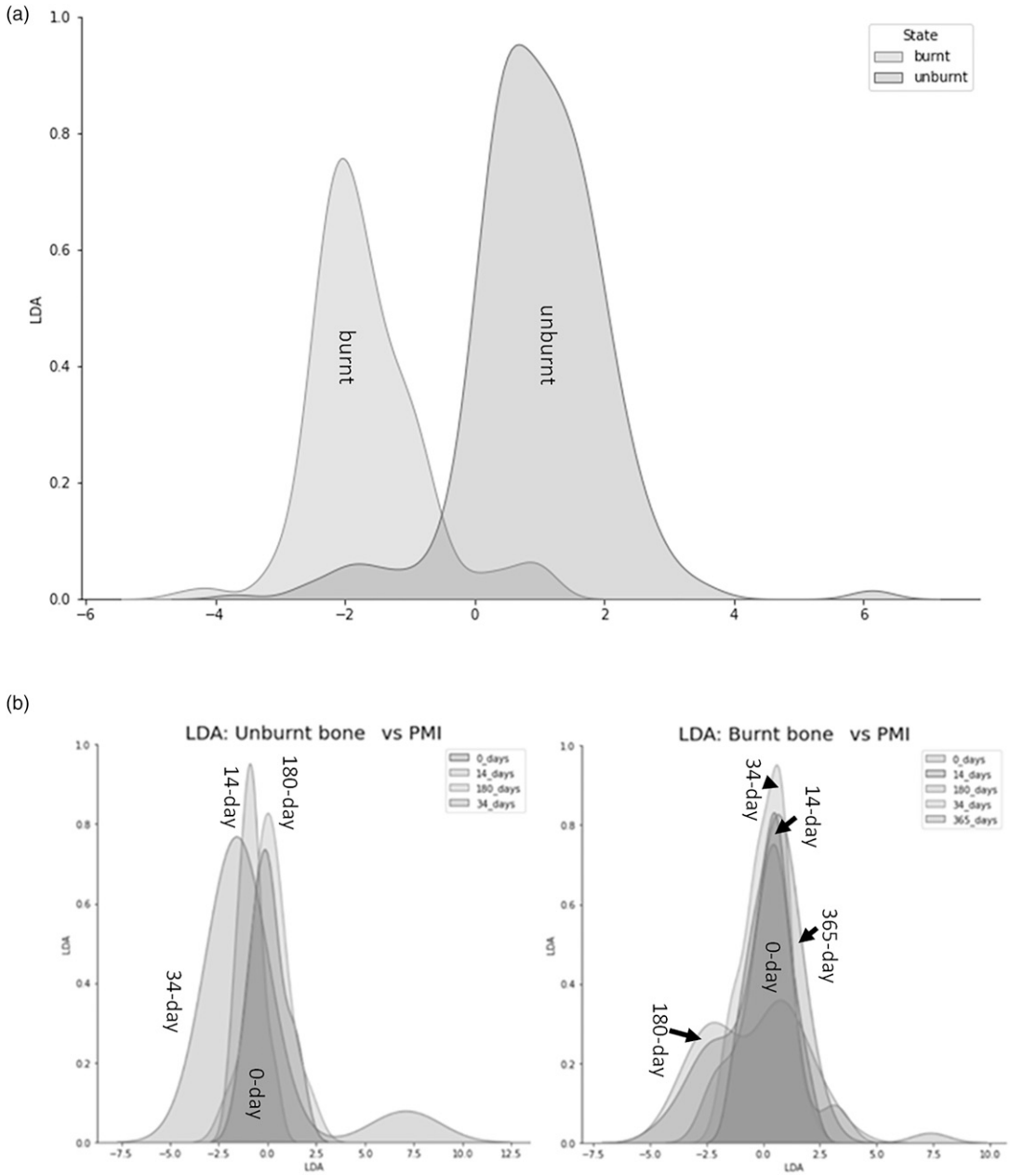


Figure 6. Linear discriminant analysis (LDA) on the electron microprobe analysis dataset. (a) Separation of unburnt and burnt bone by LDA. Contributions: Al_2O_3: 0.244, CaO: -6.882, Cl: 3.216, FeO: 0.07, K_2O: 0.607, MgO: –1.036, MnO: –0.056, Na_2O: –0.545, P_2O5: –3.97, SiO_2: –0.902, SrO: 0.199, Total: 13.08. (b) Clusters created by LDA of the (left) unburnt and (right) burnt PMI groups.

and/or by burning above 600 °C,[114] up to <800 °C in defleshed bone and <900 °C in fleshed bone.[48] OH sites in bone can be substituted with Cl.[110] An OH–Cl peak was observed in the FT-IR spectra of the burnt bones in all PMI groups, suggesting that Cl substitution for OH started in these bones. Our results are supported by the agreement between the EMPA and the FT-IR results and previous studies' results showing Cl incorporation when HAp is heated above 600 °C.[114]

Principal component analysis and LDA formed clearly separate clusters of unburnt and burnt groups but were unable to distinguish between PMI groups. C/P, PHT and CN/P were the main discriminating ratios between the state of bone. Thus, FT-IR is a useful technique in differentiating between unburnt and burnt bone, but it cannot detect early diagenesis up to one year postmortem in burnt bone. The main discriminating chemical elements between unburnt and burnt bone were Ca and Cl by LDA, and Ca and P by PCA.

The Ca/P molar ratios remained fundamentally constant not only during soft tissue putrefaction,[47] but also at one year PMI. The fact that this ratio did not present significant alterations with burning makes it a characteristic signature of bone, further supported by the similar Ca/P ratios of the archaeological and experimental burnt bone. Ratios were much lower than for stoichiometric HAp, due to the lattice housing carbonates and other elements.[28] Both Ca and P remained stable during the entire PMI. For Ca, this agrees with Reidsma et al.,[26] but in contrast to findings by Subirà and Malgosa[58] and McKinnon et al.[71]. Although a decrease in C/P ratio had been documented after one year of burial,[24] here C/P ratios (from the FT-IR dataset) did not change significantly with PMI, suggesting a stable ratio of carbonate to phosphate during the studied PMI in the same unburnt or burnt groups. The discrepancy with Keenan and Engel's[24] results might be due to the fact that their experimental alligator bones had evidence of microbial bioerosion, while this was not present in this study's bones.[22] Nevertheless, time since deposition does not seem to be the driving cause of C/P variation.

The outer cortical layer's highest variation in elements in unburnt bone demonstrates that exogenous elements diffuse into the bone in less than one year and endogenous elements are lost. However, zones around the vascular canals show the most varied elemental chemistry once bone is burnt. The high variability in concentration around osteons aligns with a microsampling study of unburnt bone by Scharlotta et al.[115] which found the presence of diagenetically unaltered zones further from the osteons. K, Si, Al, and Fe were barely detectable in the mid-cortical section in the archaeological bone, while the levels of these elements were high in the OC layers. However, in the experimental bone, the MC section did exhibit changes in elemental concentration with time. In other words, the mid-cortical section is more resistant to diagenesis than other areas of the bone, but it is also taphonomically altered, evidenced in <1 year postmortem.

Conclusion

Fire drastically changes the morphological and chemical profile of bone, making it notoriously difficult to derive information about circumstances surrounding death and deposition or burial of an individual. This includes how cultures treated their dead prior to and during cremation, and how cause and manner of death are identified after burning in forensic cases. Our investigation indicates that crystallinity increases in unburnt bone are detectable during the first year postmortem. B-type carbonate content decreased rapidly in the first three months PMI in unburnt bone, after which it slowed down. Both changes are masked by burning. The thermal decomposition of the apatite phase did not occur post-burning from the lack of β-TCP signals in the IR spectra. The presence of these signals in unburnt bone suggests Mg substitutions, supported by the non-uniform, nonlinear increase of Mg values with time from the EMPA data.

Major (Ca, P) and some trace elements (Fe, Al, Si, and Sr) were not significantly associated with thermal treatment, while Fe, Al, Si, and Sr were not associated with the PMI. K, Na, Mg, and Cl were the only elements associated with time since deposition in the experimental bone. Potassium showed a potential to estimate the late postmortem interval/early diagenesis in both unburnt and burnt bone in the first year postmortem. Potassium rapidly depleted in bone after two weeks and continued to decrease over one year PMI. It is proposed here that if the K-values are under 0.07 ± 0.01 wt% in the inner and mid-cortical zones of burnt bone then they were not burnt subsequently after death, but after at least three months decomposition in a surface exposed environment, or after a few months/years if buried, since burial slows down dehydration. Since K was present in calcined bones, it is proposed here that it might not exclusively be present in the organic phase of bones. In the Neolithic human cremated bones endogenous potassium is below detection limits. Therefore, if the bioapatite crystal structure truly become thermodynamically stable after burning at high temperatures as previous studies indicate,[42,73,74] then it suggests that cremation of these corpses was delayed by at least some weeks following death.

Sodium, which is also associated with the extracellular fluid, rapidly decreased in 2 weeks in both unburnt and burnt bone, after which it remained stable in the former, but continued to decrease at a higher rate in the latter. The decrease of Na in the burnt bones was also confirmed by the decrease of CO_3 ions. The increase of Cl in the burnt bones with time was confirmed by the EMPA data and the start of the Cl substitutions for OH by the OH–Cl peaks in the FT-IR data.

Principal component analysis and LDA were moderately successful at differentiating between unburnt and burnt bone, but not between PMIs of up to one year. C/P, PHT, and CN/P from the FT-IR and Ca, Cl, and P from the EMPA were the best discriminators for unburnt versus burnt state of bone. This study demonstrates that Ca/P molar ratios do not change significantly due to PMI or burning in the experimental and only insignificantly change in the archaeological bone. However, C/P ratios might be dependent on the presence of microbial bioerosion rather than the time since deposition. Elemental chemistry analysis demonstrated that the mid-cortical zone is the least affected by contamination in both a modern and archaeological timescale.

This study has relevance for the assessment of postmortem interval, deposition environment, and time of burning in analysis of archaeological cremated bones and of burnt human remains in forensic cases.

Acknowledgments

We would like to thank Dr Victoria Smith for her help and assistance on the electron microprobe and Sophie Decrée from the Directorate Earth and History of Life, Royal Belgian Institute of Natural Sciences for providing the secondary bone standards for the EMPA

analysis of this study. We would also like to thank the team at Wytham Woods, Oxfordshire, UK for allowing us to conduct the taphonomy experiment and outdoor burning at their site. The Kiltierney samples were provided by the Environment and Heritage Service, Northern Ireland. We would also like to thank the anonymous reviewers for the valuable comments and improvements made to the paper.

Declaration of Conflicting Interests

The author(s) declared no potential conflicts of interest with respect to the research, authorship, and/or publication of this article.

Funding

The author(s) disclosed receipt of the following financial support for the research, authorship, and/or publication of this article: This work was supported by the Meyerstein Foundation, School of Archaeology, University of Oxford.

ORCID iDs

Emese I. Végh https://orcid.org/0000-0002-5871-2815
Rick J. Schulting https://orcid.org/0000-0002-4444-766X

Supplemental Material

All supplemental material mentioned in the text is available in the online version of the journal.

References

1. S.A. Symes, C.W. Rainwater, E.N. Chapman, D.R. Gipson, A.L. Piper. "Patterned Thermal Destruction of Human Remains in a Forensic Setting". In: C.W. Schmidt, S.A. Symes, editors. The Analysis of Burned Human Remains. Boca Raton, Florida: CRC Press, 2008. Chap. 2, Pp. 15–54.
2. D.M. Waterman, C. Wells, J.P. Northover. "The Excavation of a Court Cairn at Tully County Fermanagh". Ulster J. Archaeol. 1978. 41: 3–14.
3. M.A. Dowd. "The Use of Caves for Funerary and Ritual Practices in Neolithic Ireland". Antiquity. 2008. 82(316): 305–317.
4. G. Cooney. "The Role of Cremation in Mortuary Practice in the Irish Neolithic". In: I. Kuijit, editor. Transformation by Fire: The Archaeology of Cremation in Cultural Context. Amerind Studies in Archaeology. Tucson: University of Arizona Press, 2014. Pp. 189–206.
5. C. Wells. "Notes on Cremated Bones from Tully Court Cairn". Ulster J. Archaeol. 1978. 41: 13–14.
6. J.T. Chesterman. "Investigation of the Human Bones from Quanterness". In: C. Renfrew, editor. Investigations in Orkney. London: The Society of Antiquaries of London, 1979. Pp. 97–111.
7. C. Renfrew. Investigations in Orkney. London: The Society of Antiquaries of London, 1979.
8. J.I. McKinley. "Human Remains and Diet". In: R. Mercer, F. Healy, editors. Hambledon Hill, Dorset, England, Volumes 1 and 2: Excavation and Survey of a Neolithic Monument Complex and Its Surrounding Landscape. Swindon: English Heritage, 2008. Pp. 477–535.
9. J.I. McKinley. "Cremation Burials". In: B. Barber, D. Bowsher, editors. The Eastern Cemetery of Roman London: Excavations 1983–1990 MoLAS Monograph 4. London: Museum of London Archaeology Service, 2000. Pp. 254–277.
10. T.J. Booth, J. Brück. "Death is Not the End: Radiocarbon and Histo-Taphonomic Evidence for the Curation and Excarnation of Human Remains in Bronze Age Britain". Antiquity. 2020. 94(377): 1186–1203. doi:10.13184/Aqy.2020.132.
11. G. Carr. "Excarnation to Cremation: Continuity or Change?" In: C. Haselgrove, T. Moore, editors. The Later Iron Age in Britain and Beyond. Oxford: Oxbow, 2007. Chap. 26, Pp. 444–453.
12. G. Grévin, C. Baud, A. Susini. "Etude anthropologique et paléopathologique d'un adulte inhumé puis incinéré provenant du site de Pincevent (Seine-et-Marne)". Bulletins et Mémoires de la Société d'anthropologie de Paris. 1990. 2(3): 77–87.
13. R.S. Baby. Hopewell Cremation Practices. Columus: Ohio Historical Society, 1954. Pp. 1–7.
14. L.R. Binford. "An Analysis of Cremations from Three Michigan Sites". Wisconsin Archaeol. 1963. 44: 98–110.
15. J.E. Buikstra, M. Swegle. "Bone Modification Due to Burning: Experimental Evidence". In: R. Bonnichsen, M. Sorg, editors. Bone Modification. College Station, Texas: The Centre for the Study of the First Americans, 1989. Pp. 247–258.
16. D.H.R. Spennemann, S.M. Colley. "Fire in a Pit: The Effects of Burning on Faunal Remains". Archaeozoologia. 1989. 3(1–2): 51–64.
17. F. Etxeberria. "Aspectos macroscópicos del hueso sometido al fuego: Revisión de las cremaciones descritas en el País Vasco desde La Arqueologia". Munibe Antropologia–Arkeologia. 1994. 46: 111–116.
18. T. Whyte. "Distinguishing Remains of Human Cremations from Burned Animal Bones". J. F. Archaeol. 2001. 28(3–4): 437–448.
19. T.J.U. Thompson. "Heat-Induced Dimensional Changes in Bone and Their Consequences for Forensic Anthropology". J. Forensic Sci 2005. 50(5): 185–193.
20. D. Gonçalves, T.J.U. Thompson, E. Cunha. "Implications of Heat-Induced Changes in Bone on the Interpretation of Funerary Behaviour and Practice". J. Archaeol. Sci. 2011. 38(6): 1308–1313. doi:10.1016/J.Jas.2011.01.006.
21. S.A.M. Lemmers, D. Gonçalves, E. Cunha, A.R. Vassalo, J. Appleby. "Burned Fleshed or Dry? The Potential of Bioerosion to Determine the Pre-Burning Condition of Human Remains". J. Archaeol. Method Theory. 2020. 27: 972–991.
22. E.I. Végh, A. Czermak, N. Márquez-Grant, R.J. Schulting. "Assessing the Reliability of Microbial Bioerosion Features in Burnt Bones: A Novel Approach Using Feature-Labelling in Histotaphonomical Analysis". J. Archaeol. Sci. Reports. 2021. 37: 102906. doi:10.1016/J.Jasrep.2021.102906.
23. M.J. Kohn, R.J. Moses. "Trace Element Diffusivities in Bone Rule Out Simple Diffusive Uptake During Fossilization but Explain In Vivo Uptake and Release". Proc. Natl. Acad. Sci. U.S.A. 2013. 110(2): 419. doi:10.1073/Pnas.1209513110.

24. S.W. Keenan, A.S. Engel. "Early Diagenesis and Recrystallization of Bone". Geochim. Cosmochim. Acta. 2017. 196: 209–223. doi: 10.1016/J.Gca.2016.09.033.
25. S.J. Walden, J. Mulville, J.P. Rowlands, S.L. Evans. "An Analysis of Systematic Elemental Changes in Decomposing Bone". J. Forensic Sci. 2018. 63(1): 207–213. doi:10.1111/1556-4029.13480.
26. F. Reidsma, A. Van Hoesel, B.J. Van Os, L. Megens, F. Braadbaart. "Charred Bone: Physical and Chemical Changes During Laboratory Simulated Heating Under Reducing Conditions and Its Relevance for the Study of Fire Use in Archaeology". J. Archaeol. Sci. Rep. 2016. 10: 282–292. doi:10.1016/J.Jasrep.2016.10.001.
27. K. Rogers, P. Zioupos. "The Bone Tissue of the Rostrum of a Mesoplodon Densirostris Whale: A Mammalian Biomineral Demonstrating Extreme Texture". J. Mater. Sci. Lett. 1999. 18(8): 651–654. doi:10.1023/A:1006615422214.
28. J.C. Elliott. "Calcium Phosphate Biominerals". In: M.J. Kohn, J. Rakovan, J.M. Hughes, editors. Phosphates: Geochemical, Geobiological and Material Importance, Reviews in Mineralogy and Geochemistry, Vol. 48. Washington, DC: Mineralogical Society of America, 2002. Chap. 11, Pp. 427–454.
29. V. Caruso, N. Marinoni, V. Diella, F. Berna, et al. "Bone Diagenesis in Archaeological and Contemporary Human Remains: An Investigation of Bone 3D Microstructure and Minero-Chemical Assessment". Archaeol. Anthropol. Sci. 2020. 12(8): 162. doi:10.1007/S12520-020-01090-6.
30. C. Rey, C. Combes, C. Drouet, A. Lebugle, H. Sfihi, et al. "Nanocrystalline Apatites in Biological Systems: Characterisation, Structure and Properties". Materwiss. Werksttech. 2007. 38(12): 996–1002. doi:10.1002/mawe.200700229.
31. Z. Li, J.D. Pasteris. "Chemistry of Bone Mineral, Based on the Hypermineralized Rostrum of the Beaked Whale Mesoplodon Densirostris". Am. Mineral. Mineralogical Society of America, 2014. 99(4): 645. doi:10.2138/am.2014.4571.
32. E.T. Bergslien, M. Bush, P.J. Bush. "Identification of Cremains Using X-ray Diffraction Spectroscopy and a Comparison to Trace Element Analysis". Forensic Sci. Int. 2008. 175(2–3): 218–226. doi:10.1016/J.Forsciint.2007.07.004.
33. R. Zapanta Legeros. "Apatites in Biological Systems". Prog. Cryst. Growth Charact. 1981. 4(1–2): 1–45. doi:10.1016/0146-3535(81)90046-0.
34. Y. Fernández-Jalvo, P. Andrews. Atlas of Taphonomic Identifications: 1001+ Images of Fossil and Recent Mammal Bone Modification. Dordrecht: Springer, 2016.
35. S.W. Keenan. "From Bone to Fossil: A Review of the Diagenesis of Bioapatite". Am. Mineral. 2016. 101(9): 1943–1951. doi:10.2138/Am-2016-5737.
36. A. Child. "Towards and Understanding of the Microbial Decomposition of Archaeological Bone in the Burial Environment". J. Archaeol. Sci 1995. 22(2): 165–174. doi:10.1006/jasc.1995.0018.
37. S.W. Keenan, A.S. Engel, A. Roy, G. Lisa Bovenkamp-Langlois. "Evaluating the Consequences of Diagenesis and Fossilization on Bioapatite Lattice Structure and Composition". Chem. Geol. 2015. 413: 18–27. doi:10.1016/J.Chemgeo.2015.08.005.
38. M.J. Kohn. "Models of Diffusion-Limited Uptake of Trace Elements in Fossils and Rates of Fossilization". Geochim. Cosmochim. Acta. 2008. 72(15): 3758–3770. doi:10.1016/J.Gca.2008.05.045.
39. M. Sponheimer, J.A. Lee-Thorp. "Isotopic Evidence for the Diet of An Early Hominid, Australopithecus africanus". Science. 1999. 283(5400): 368. doi:10.1126/science.283.5400.368.
40. F. Berna, A. Matthews, S. Weiner. "Solubilities of Bone Mineral from Archaeological Sites: The Recrystallization Window". J. Archaeol. Sci. 2004. 31(7): 867–882. doi:10.1016/j.jas.2003.12.003.
41. L.E. Wright, H.P. Schwarcz. "Infrared and Isotopic Evidence for Diagenesis of Bone Apatite at Dos Pilas, Guatemala: Palaeodietary Implications". J. Archaeol. Sci. 1996. 23(6): 933–944. doi:10.1006/Jasc.1996.0087.
42. C.N. Trueman, A.K. Behrensmeyer, N. Tuross, S. Weiner. "Mineralogical and Compositional Changes in Bones Exposed on Soil Surfaces in Amboseli National Park, Kenya: Diagenetic Mechanisms and the Role of Sediment Pore Fluids". J. Archaeol. Sci. 2004. 31(6): 721–739. doi: 10.1016/J.Jas.2003.11.003.
43. G. Gallello, J. Kuligowski, A. Pastor, A. Diez, J. Bernabeu. "Biological Mineral Content in Iberian Skeletal Cremains for Control of Diagenetic Factors Employing Multivariate Statistics". J. Archaeol. Sci. 2013. 40(5): 2477–2484. doi:10.1016/J.Jas.2013.01.022.
44. H. Schutkowski, B. Herrmann, G. Grupe. "Diet, Status, and Decomposition at Weingarten: Trace Element and Isotope Analyses on Early Mediaeval Skeletal Material". J. Archaeol. Sci. 1999. 26(6): 675–685.
45. S.W. Keenan, A.S. Engel. "Reconstructing Diagenetic Conditions of Bone at the Gray Fossil Site, Tennessee, USA". Palaeogeogr. Palaeoclimatol. Palaeoecol. 2017. 471: 48–57. doi:10.1016/j.palaeo.2017.01.037.
46. A. Zazzo, C. Lécuyer, A. Mariotti, M. Jiang, et al. "(Formula Presented) Substitution in Hydroxyapatite: Theory and Experiment". Phys. Rev. B: Condens. Matter Mater. Phys. 2020. 2148(1): 87–100. doi:10.1016/J.Jasrep.2020.102333.
47. J.A. Ezzo. "Putting the Chemistry Back Into Archaeological Bone Chemistry Analysis: Modeling Potential Palaeodietary Indicators". J. Anth. Arch. 1994. 13: 1–34.
48. S.T.D. Ellingham, T.J.U. Thompson, M. Islam. "Scanning Electron Microscopy–Energy-Dispersive X-ray (SEM/EDX): A Rapid Diagnostic Tool to Aid the Identification of Burnt Bone and Contested Cremains". J. Forensic Sci. 2018. 63(2): 504–510. doi: 10.1111/1556-4029.13541.
49. C.T. Williams. "Alteration of Chemical Composition of Fossil Bones by Soil Processes and Groundwater". In: G. Grupe, B. Herrmann, editors. Trace Elements in Environmental History. Proceedings in Life Sciences: Proceedings of the Symposium Held from June 24th to 26th, 1987, at Göttingen. Berlin; New York: Springer, 1988. Pp. 27–40. doi:10.1007/978-3-642-73297-3_3.
50. C.N. Trueman, N. Tuross. "Trace Elements in Recent and Fossil Bone Apatite". Rev. Mineral. Geochem. 2002. 48(1): 489–521. doi:10.2138/rmg.2002.48.13.

51. C.N. Trueman. "Chemical Taphonomy of Biomineralized Tissues". Palaeontology. 2013. 56(3): 475–486. doi:10.1111/pala.12041.
52. F.D. Pate, J.T. Hutton. "The Use of Soil Chemistry Data to Address Post-Mortem Diagenesis in Bone Mineral". J. Archaeol. Sci. 1988. 15(6): 729–739. doi:10.1016/0305-4403(88)90062-3.
53. J.B. Lambert, L. Xue, J.E. Buikstra. "Inorganic Analysis of Excavated Human Bone After Surface Removal". J. Archaeol. Sci. 1991. 18(3): 363–383. doi:10.1016/0305-4403(91)90072-W.
54. M. Muñoz, I. Villar, J.A. García-Erce. "An Update on Iron Physiology". World J. Gastroenterol. 2009. 15(37): 4617–4626. doi:10.3748/wjg.15.4617.
55. A.R. Millard, R.E. Hedges. "A Diffusion-Adsorption Model of Uranium Uptake by Archaeological Bone". Geochim. Cosmochim. Acta. 1996. 60(12): 2139–2152. doi:10.1016/0016-7037(96)00050-6.
56. N.J. de Winter, C. Snoeck, R. Schulting, T. Fernández-Crespo, P. Claeys. "High-Resolution Trace Element Distributions and Models of Trace Element Diffusion in Enamel of Late Neolithic/Early Chalcolithic Human Molars from the Rioja Alavesa Region (North-Central Spain) Help to Separate Biogenic from Diagenetic Trends". Palaeogeogr. Palaeoclimatol. Palaeoecol. 2019. 532: 109260. doi:10.1016/J.Palaeo.2019.109260.
57. M.P.M. Marques, A.P. Mamede, A.R. Vassalo, C. Makhoul, et al. "Heat-Induced Bone Diagenesis Probed by Vibrational Spectroscopy". Sci. Rep. 2018. 8(1): 1–13. doi:10.1038/S41598-018-34376-W.
58. M.E. Subira, A. Malgosa. "The Effect of Cremation on the Study of Trace Elements". Int. J. Osteoarchaeol. 1993. 3(2): 115–118. doi:10.1002/oa.1390030208.
59. J.J. Schultz, M.W. Warren, J.S. Krigbaum. "Analysis of Human Cremains: Gross and Chemical Methods". In: C.W. Schmidt, S.A. Symes, editors. The Analysis of Burned Human Remains. London: Academic Press, 2008. Chap. 4, Pp. 75–94.
60. M.C. Stiner, S.L. Kuhn, S. Weiner, O. Bar-Yosef. "Differential Burning, Recrystallization, and Fragmentation of Archaeological Bone". J. Archaeol. Sci. 1995. 22(2): 223–237. doi:10.1006/jasc.1995.0024.
61. P. Shipman, G. Foster, M. Schoeninger. "Burnt Bones and Teeth: An Experimental Study of Color, Morphology, Crystal Structure, and Shrinkage". J. Archaeol. Sci. 1984. 11(4): 307–325. doi:10.1016/0305-4403(84)90013-X.
62. J.L. Holden, P.P. Phakey, J.G. Clement. "Scanning Electron Microscope Observations of Heat-Treated Human Bone". Forensic Sci. Int. 1995. 74(1): 29–45. doi:10.1016/0379-0738(95)01735-2.
63. K. Rogers, P. Daniels. "An X-ray Diffraction Study of the Effects of Heat Treatment on Bone Mineral Microstructure". Biomaterials. 2002. 23(12): 2577–2585. doi:10.1016/S0142-9612(01)00395-7.
64. M. Van Strydonck, M. Boudin, G. de Mulder. "The Carbon Origin of Structural Carbonate in Bone Apatite of Cremated Bones". Radiocarbon. 2010. 52(2): 578–586. doi:10.1017/S0033822200045616.
65. J.L. Holden, J.G. Clement, P.P. Phakey. "Age and Temperature Related Changes to the Ultrastructure and Composition of Human Bone Mineral". J. Bone Miner. Res. 1995. 10(9): 1400–1409. doi:10.1002/Jbmr.5650100918.
66. L.E. Munro, F.J. Longstaffe, C.D. White. "Burning and Boiling of Modern Deer Bone: Effects on Crystallinity and Oxygen Isotope Composition of Bioapatite Phosphate". Palaeogeogr. Palaeoclimatol. Palaeoecol. 2007. 249(1–2): 90–102. doi:10.1016/J.Palaeo.2007.01.011.
67. T.J.U. Thompson, M. Islam, M. Bonniere. "A New Statistical Approach for Determining the Crystallinity of Heat-Altered Bone Mineral from FTIR Spectra". J. Archaeol. Sci. 2013. 40(1): 416–422.
68. X.-Y. Wang, Y. Zuo, D. Huang, X.-D. Hou, Y.-B. Li. "Comparative Study on Inorganic Composition and Crystallographic Properties of Cortical and Cancellous Bone". Biomed. Environ. Sci. 2010. 23(6): 473–480. doi:10.1016/S0895-3988(11)60010-X.
69. M. Hidouri, S. Dorozhkin, N. Albeladi. "Thermal Behavior, Sintering and Mechanical Characterization of Multiple Ion-Substituted Hydroxyapatite Bioceramics". J. Inorg. Organomet. Polym. Mater. 2019. 29(1): 87–100. doi:10.1007/S10904-018-0969-6.
70. S. Raynaud, E. Champion, D. Bernache-Assollant, P. Thomas. "Calcium Phosphate Apatites with Variable Ca/P Atomic Ratio I. Synthesis, Characterisation and Thermal Stability of Powders". Biomaterials. 2002. 23(4): 1065–1072. doi:10.1016/S0142-9612(01)00218-6.
71. M. McKinnon, M. Henneberg, E. Simpson, D. Higgins. "A Comparison of Crystal Structure in Fresh, Burned and Archaic Bone: Implications for Forensic Sampling". Forensic Sci. Int. 2020. 313: 110328. doi:10.1016/J.Forsciint.2020.110328.
72. K.S. Karunadasa, C. Manoratne, H.M.T.G. Pitawala, R.M. Rajapakse. "Thermal Decomposition of Calcium Carbonate (Calcite Polymorph) as Examined by In-Situ High-Temperature X-ray Powder Diffraction". J. Phys. Chem. Solids. 2019. 134: 21–28. doi:10.1016/J.Jpcs.2019.05.023.
73. J. Lee-Thorp. "Two Decades of Progress Towards Understanding Fossilization Processes and Isotopic Signals in Calcified Tissue Minerals". Archaeometry. 2002. 44(3): 435–446. doi:10.1111/1475-4754.T01-1-00076.
74. C. Snoeck, J.A. Lee-Thorp, R.J. Schulting. "From Bone to Ash: Compositional and Structural Changes in Burned Modern and Archaeological Bone". Palaeogeogr. Palaeoclimatol. Palaeoecol. 2014. 416: 55–68. doi:10.1016/J.Palaeo.2014.08.002.
75. L. Mkukuma, J. Skakle, I. Gibson, C. Imrie, et al. "Effect of the Proportion of Organic Material in Bone on Thermal Decomposition of Bone Mineral: An Investigation of a Variety of Bones from Different Species Using Thermogravimetric Analysis Coupled to Mass Spectrometry, High-Temperature X-ray Diffraction". Calcif. Tissue Int. 2004. 75(4): 321–328. doi:10.1007/S00223-004-0199-5.
76. M.E. Taylor, M.D. Morecroft, H.R. Oliver. The Physical Environment. Wytham Woods, UK: Oxford University Press, 2011. doi:10.1093/Acprof:Osobl/9780199605187.003.0002.

77. M.J. Daniells, B.B. Williams, R.A. Larmour. "Excavations at Kiltierney Deerpark, County Fermanagh". Ulster J. Archaeol. 1977. 40: 32–41. http://www.jstor.org/stable/20567792
78. C.N. Trueman, K. Privat, J. Field. "Why Do Crystallinity Values Fail to Predict the Extent of Diagenetic Alteration of Bone Mineral?" Palaeogeogr. Palaeoclimatol. Palaeoecol. 2008. 266(3–4): 160–167. doi:10.1016/J.Palaeo.2008.03.038.
79. E.T. Stathopoulou, V. Psycharis, G.D. Chryssikos, V. Gionis, G. Theodorou. "Bone Diagenesis: New Data from Infrared Spectroscopy and X-ray Diffraction". Palaeogeogr. Palaeoclimatol. Palaeoecol. 2008. 266(3–4): 168–174. doi:10.1016/j.palaeo.2008.03.022.
80. C. Rey, V. Renugopalakrishnan, B. Collins, M.J. Glimcher. "Fourier Transform Infrared Spectroscopic Study of the Carbonate Ions in Bone Mineral During Aging." Calcif. Tissue Int. 1991. 49: 251–258. doi:10.1007/bf02556214.
81. T.J.U. Thompson, M. Gauthier, M. Islam. "The Application of a New Method of Fourier Transform Infrared Spectroscopy to the Analysis of Burned Bone". J. Archaeol. Sci. 2009. 36(3): 910–914. doi:10.1016/J.Jas.2008.11.013.
82. S.T.D. Ellingham, T.J.U. Thompson, M. Islam. "The Effect of Soft Tissue on Temperature Estimation from Burnt Bone Using Fourier Transform Infrared Spectroscopy". J. Forensic Sci. 2016. 61(1): 151–159.
83. C. Snoeck, R.J. Schulting, J.A. Lee-Thorp, M. Lebon, A. Zazzo. "Impact of Heating Conditions on the Carbon and Oxygen Isotope Composition of Calcined Bone". J. Archaeol. Sci. 2016. 65: 32–43. doi:10.1016/j.jas.2015.10.013.
84. M.M. Beasley, E.J. Bartelink, L. Taylor, R.M. Miller. "Comparison of Transmission FTIR, ATR, and DRIFT Spectra: Implications for Assessment of Bone Bioapatite Diagenesis". J. Archaeol. Sci. 2014. 46(1): 16–22. doi:10.1016/j.jas.2014.03.008.
85. T.J. Thompson, M. Islam, K. Piduru, A. Marcel. "An Investigation Into the Internal and External Variables Acting on Crystallinity Index Using Fourier Transform Infrared Spectroscopy on Unaltered and Burned Bone". Palaeogeogr. Palaeoclimatol. Palaeoecol. 2011. 299(1–2): 168–174. doi:10.1016/j.palaeo.2010.10.044.
86. T.J.U. Thompson, J. Inglis. "Differentiation of Serrated and Non-Serrated Blades from Stab Marks in Bone". Int. J. Legal Med. 2009. 123(2): 129–135. doi:10.1007/S00414-008-0275-X.
87. J.D. Fredericks, P. Bennett, A. Williams, K.D. Rogers. "FTIR Spectroscopy: A New Diagnostic Tool to Aid DNA Analysis from Heated Bone". Forensic Sci. Int. Genet. 2012. 6(3): 375–380. doi:10.1016/J.Fsigen.2011.07.014.
88. A. Grunenwald, C. Keyser, A. Sautereau, E. Crubézy, et al. "Revisiting Carbonate Quantification in Apatite (Bio)Minerals: A Validated FTIR Methodology". J. Archaeol. Sci 2014. 49: 134–141. doi:10.1016/j.jas.2014.05.004.
89. G. Piga, D. Gonçalves, T.J.U. Thompson, A. Brunetti, et al. "Understanding the Crystallinity Indices Behavior of Burned Bones and Teeth by ATR-IR and XRD in the Presence of Bioapatite Mixed with Other Phosphate and Carbonate Phases". Int. J. Spectrosc. 2016. 2016: 1–9. doi:10.1155/2016/4810149.
90. J.M. Pyle, F.S. Spear, D.A. Wark. "Electron Microprobe Analysis of REE in Apatite, Monazite, and Xenotime: Protocols and Pitfalls". Rev. Mineral. Geochem. 2002. 48(1): 337–362. doi:10.2138/rmg.2002.48.8.
91. W.D. Carlson, R.A. Donelick, R.A. Ketcham. "Variability of Apatite Fission-Track Annealing Kinetics: I. Experimental Results". Am. Mineral. 1999. 84(9): 1213–1223. doi:10.2138/am-1999-0901.
92. K.P. Jochum, B. Stoll, K. Herwig, M. Willbold, et al. "MPI-DING Reference Glasses for in Situ Microanalysis: New Reference Values for Element Concentrations and Isotope Ratios". Geochemistry, Geophys. Geosystems. 2006. 7(2): Q02008. 10.1029/2005gc001060.
93. D. Goodman. "Encyclopedia of Analytical Chemistry: Applications, Theory, and Instrumentation". CHOICE Curr. Rev. Acad. Books. 2001. 39(2): 287.
94. D.W. Holcomb, R.A. Younger. "Thermal Decomposition of Human Tooth Enamel". Calcif. Tissue Int. 1980. 31(1): 198–201.
95. M. Praprotnik, D. Janežič. "Molecular Dynamics Integration and Molecular Vibrational Theory. III. The Infrared Spectrum of Water". J. Chem. Phys. 2005. 122(17): 174102.
96. P.A. Gerakines, W.A. Schutte, J.M. Greenberg, E.F. Dishoeck. "The Infrared Band Strengths of H_2O, CO, and CO_2 in Laboratory Simulations of Astrophysical Ice Mixtures". Astron. Astrophys. 1995. 296: 810–818.
97. S.E.P. Dowker, J.C. Elliott. "Infrared Adsorption Bands from NCO^- and NCN^{2-} in Heated Carbonate-Containing Apatites Prepared in the Presence of NH_4+ Ions". Calcif. Tissue Int. 1979. 29: 177–178.
98. R.Z. Legeros, O.R. Trautz, E. Klein, J.P. Legeros. "Two Types of Carbonate Substitution in the Apatite Structure". Experientia. 1969. 25(1): 5–7. doi:10.1007/bf01903856.
99. R.Z. LeGeros, J.P. LeGeros. "Carbonate Analyses of Synthetic, Mineral, and Biological Apatites". J. Dent. Res. 1983. 62(2 Suppl): 259.
100. C. Rey, B. Collins, T. Goehl, I.R. Dickson, M.J. Glimcher. "The Carbonate Environment in Bone Mineral: A Resolution-Enhanced Fourier Transform Infrared Spectroscopy Study". Calcif. Tissue Int. 1989. 45(3): 157–164. doi:10.1007/BF02556059.
101. A.P. Mamede, D. Gonçalves, M.P.M. Marques, L.A.E. Batista de Carvalho. "Burned Bones Tell Their Own Stories: A Review of Methodological Approaches to Assess Heat-Induced Diagenesis". Appl. Spectrosc. Rev. 2018. 53(8): 603–635. doi:10.1080/05704928.2017.1400442.
102. J.T. Kloprogge, L. Hickey, R.L. Frost. "FT-Raman and FT-IR Spectroscopic Study of Synthetic Mg/Zn/Al-Hydrotalcites". J. Raman Spectrosc. 2004. 35(11): 967–974. doi:10.1002/Jrs.1244.
103. L.M. Miller, V. Vairavamurthy, M.R. Chance, R. Mendelsohn, et al. "In Situ Analysis of Mineral Content and Crystallinity in Bone Using Infrared Micro-Spectroscopy of the ν4 PO_4^{3-} Vibration". Biochim. Biophys. Acta. Gen. Subj. 2001. 1527(1): 11–19. doi:10.1016/S0304-4165(01)00093-9.

104. G. Piga, T.J.U. Thompson, A. Malgosa, S. Enzo. "The Potential of X-ray Diffraction in the Analysis of Burned Remains from Forensic Contexts". J. Forensic Sci. 2009. 54(3): 534–539. doi:10.1111/J.1556-4029.2009.01037.X.
105. S. Beckett. Inter-Species Variation in Bone Mineral. [Doctoral Thesis]. Shrivenham, United Kingdom: Cranfield University, 2009.
106. C. Greenwood, K. Rogers, S. Beckett, J. Clement. "Initial Observations of Dynamically Heated Bone". Cryst. Res. Technol. 2013. 48(12): 1073–1082. doi:10.1002/crat.201300254.
107. S.N. Danilchenko, A.N. Kalinkevich, R.A. Moskalenko, V.N. Kuznetsov, et al. "Structural and Crystal-Chemical Characteristics of the Apatite Deposits from Human Aortic Walls". Interv. Med. Appl. Sci. 2018. 10(2): 110–119. doi:10.1556/1646.10.2018.24.
108. D.A. Bushinsky, K.L. Gavrilov, J.M. Chabala, R. Levi-Setti. "Contribution of Organic Material to the Ion Composition of Bone". J. Bone Miner. Res. 2000. 15(10): 2026–2032. doi:10.1359/Jbmr.2000.15.10.2026.
109. G. Gallo, M. Fyhrie, C. Paine, S.V. Ushakov, et al. "Characterization of Structural Changes in Modern and Archaeological Burnt Bone: Implications for Differential Preservation Bias". PLoS One. 2021. 16(7): E0254529–E0254529. doi:10.1371/journal.pone.0254529.
110. D.S. Yoo, J.S. Cho, Y.-C. Chung, S.-H. Rhee. "Defect Structures of Sodium and Chloride Co-Substituted Hydroxyapatite and Its Osseointegration Capacity". J. Mater. Sci 2021. 56(9): 5493–5508. doi:10.1007/S10853-020-05645-9.
111. S. Beckett, K.D. Rogers, J.G. Clement. "Inter-Species Variation in Bone Mineral Behavior Upon Heating". J. Forensic Sci. 2011. 56(3): 571–579. doi:10.1111/J.1556-4029.2010.01690.X.
112. J.B. Lambert, S. Vlasak, C.B. Szpunar, J.E. Buikstra. "Bone Diagenesis and Dietary Analysis". J. Hum. Evol. 1985. 14(5): 477–482. doi:10.1016/S0047-2484(85)80026-9.
113. R.B. Parker, H. Toots, J. Murphy. "Leaching of Sodium from Skeletal Parts During Fossilization". Geochim. Cosmochim. Acta. 1974. 38(8): 1317–1321. doi:10.1016/0016-7037(74)90125-2.
114. G.C. Maiti, F. Freund. "Incorporation of Chlorine into Hydroxy-Apatite". J. Inorg. Nucl. Chem. 1981. 43(11): 2633–2637. doi:10.1016/0022-1902(81)80589-1.
115. I. Scharlotta, O.I. Goriunova, A. Weber. "Micro-Sampling of Human Bones for Mobility Studies: Diagenetic Impacts and Potentials for Elemental and Isotopic Research". J. Archaeol. Sci 2013. 40(12): 4509–4527. doi:10.1016/j.jas.2013.07.014.

Appendix C: Histology Dataset

Please find the histology images attached in the electronic file (Appendix_C).

Appendix C.1: Dataset Generated from the Data Labelling Application

Image name	Block reference	Wedl	Wedl_2	cyanobacterial_tunnelling	lamellate_mfd	budded_mfd	crack	hairline_crack
WSF3D1M3_UNBURNT_1_50X_4	x7_y0.png	FALSE	FALSE	FALSE	FALSE	FALSE	FALSE	TRUE
WSF3D1M1_BURNT_50X_3	x7_y5.png	FALSE	FALSE	FALSE	FALSE	FALSE	FALSE	FALSE
WSF3D1M1_BURNT_50X_12	x3_y4.png	FALSE	FALSE	FALSE	FALSE	FALSE	FALSE	FALSE
WSF3D1M1_BURNT_50X_7	x0_y6.png	FALSE	FALSE	FALSE	TRUE	FALSE	FALSE	FALSE
WSF3D1M4_NO2_BURNT_50X_3	x2_y7.png	FALSE	FALSE	FALSE	FALSE	FALSE	FALSE	FALSE
WSF3D1M2_BURNT_50X_5	x8_y1.png	FALSE	FALSE	FALSE	FALSE	FALSE	FALSE	FALSE
WSF3D1M2_BURNT_50X_3	x6_y6.png	FALSE	FALSE	TRUE	FALSE	FALSE	FALSE	FALSE
SWF2FR4_BURNT_50X	x4_y7.png	FALSE	FALSE	FALSE	FALSE	FALSE	FALSE	FALSE
SWF1_BURNT_4_50X_1	x1_y6.png	FALSE	FALSE	FALSE	FALSE	FALSE	FALSE	FALSE
WS Fresh	x7_y6.png	FALSE	FALSE	FALSE	FALSE	FALSE	FALSE	FALSE
WSF3D1M3_BURNT_50X_1	x0_y6.png	FALSE	FALSE	FALSE	FALSE	FALSE	FALSE	FALSE
WSF3D1M4_NO2_BURNT_50X_3	x7_y8.png	FALSE	FALSE	FALSE	FALSE	FALSE	FALSE	FALSE
WSF3D1M1_BURNT_50X_8	x4_y6.png	FALSE	FALSE	FALSE	FALSE	FALSE	FALSE	TRUE
WSF3D1M1_BURNT_50X_9	x5_y7.png	FALSE	FALSE	FALSE	FALSE	FALSE	FALSE	FALSE
WSF3D1M4_BURNT_50X_2	x8_y7.png	FALSE	FALSE	FALSE	FALSE	FALSE	FALSE	FALSE
WSF3D1M3_UNBURNT_1_50X_3	x8_y9.png	FALSE	FALSE	FALSE	FALSE	FALSE	FALSE	FALSE
SWF1FR2_BURNT_50X_3	x1_y4.png	FALSE	FALSE	FALSE	FALSE	FALSE	FALSE	FALSE
WS Fresh_50X_1	x1_y1.png	FALSE	FALSE	FALSE	FALSE	FALSE	FALSE	FALSE
WSF3D1M5_SMALLPIECE_BURNT_50X_3	x3_y3.png	FALSE	FALSE	FALSE	FALSE	FALSE	FALSE	TRUE

WSF3D1M5_SMALLPIECE_BURNT_50X_3	x8_y1.png	FALSE	FALSE	FALSE	FALSE	FALSE	FALSE	TRUE
WSF3D1M3_UNBURNT_1_50X_4	x3_y9.png	FALSE	TRUE	FALSE	FALSE	FALSE	FALSE	FALSE
WSF3D1M1_BURNT_50X_4	x8_y4.png	FALSE	FALSE	FALSE	FALSE	FALSE	FALSE	TRUE
WSF3D1M4_NO2_BURNT_50X_1	x7_y9.png	FALSE	FALSE	FALSE	FALSE	FALSE	FALSE	FALSE
WSF3D1M3_UNBURNT_1_50X_3	x1_y3.png	FALSE	TRUE	FALSE	FALSE	FALSE	FALSE	FALSE
WS Fresh_50X_3	x3_y0.png	FALSE	FALSE	FALSE	FALSE	FALSE	FALSE	FALSE
SWF1_BURNT_4_50X_1	x7_y3.png	FALSE	FALSE	FALSE	FALSE	FALSE	FALSE	FALSE
SWF1_BURNT_3_50X_1	x1_y9.png	FALSE	FALSE	FALSE	FALSE	FALSE	FALSE	FALSE
WSF3D1M3_BURNT_50X_3	x9_y6.png	FALSE	FALSE	FALSE	FALSE	FALSE	FALSE	TRUE
WS Fresh_50X_2	x6_y6.png	FALSE	FALSE	FALSE	FALSE	FALSE	FALSE	FALSE
WSF3D1M4_BURNT_50X_3	x8_y7.png	FALSE	FALSE	FALSE	FALSE	FALSE	FALSE	TRUE
SWF2FR1_BURNT_2_5X_2	x2_y6.png	FALSE	FALSE	FALSE	FALSE	FALSE	FALSE	FALSE
WSF3D1M1_BURNT_50X_3	x5_y0.png	FALSE	FALSE	FALSE	FALSE	FALSE	FALSE	FALSE
WSF3D1M2_BURNT_50X_1	x1_y9.png	FALSE	FALSE	FALSE	FALSE	FALSE	FALSE	FALSE
WSF3D1M5_SMALLPIECE_BURNT_50X_3	x3_y9.png	FALSE	FALSE	FALSE	FALSE	FALSE	FALSE	FALSE
WSF3D1M5_SMALLPIECE_BURNT_50X_3	x1_y3.png	FALSE	FALSE	FALSE	FALSE	FALSE	FALSE	TRUE
SWF1FR2_BURNT_50X_3	x6_y4.png	FALSE	TRUE	FALSE	FALSE	FALSE	FALSE	FALSE
SWF1_BURNT_5_50X_1	x4_y3.png	FALSE	FALSE	FALSE	FALSE	FALSE	FALSE	FALSE
WSF3D1M3_UNBURNT_1_50X_4	x1_y4.png	FALSE	TRUE	FALSE	FALSE	FALSE	FALSE	FALSE
WSF3D1M1_BURNT_50X_9	x3_y7.png	FALSE	FALSE	FALSE	FALSE	FALSE	FALSE	FALSE
WSF3D1M4_NO2_BURNT_50X_2	x2_y5.png	FALSE	FALSE	FALSE	FALSE	FALSE	FALSE	FALSE

WS Fresh_50X_1	x6_y1.png	FALSE	FALSE	FALSE	FALSE	FALSE	FALSE	FALSE
SWF1FR2_BURNT_50X_1	x9_y5.png	FALSE	FALSE	FALSE	FALSE	FALSE	FALSE	FALSE
WSF3D1M3_UNBURNT_1_50X_4	x5_y4.png	FALSE	FALSE	FALSE	FALSE	FALSE	FALSE	FALSE
WSF3D1M1_BURNT_50X_10	x1_y3.png	FALSE	FALSE	FALSE	FALSE	FALSE	FALSE	FALSE
WS Fresh_50X_1	x7_y5.png	FALSE	FALSE	FALSE	FALSE	FALSE	FALSE	FALSE
WS Fresh_50X_3	x5_y5.png	FALSE	FALSE	FALSE	FALSE	FALSE	FALSE	FALSE
WS Fresh_50X_3	x5_y7.png	FALSE	FALSE	FALSE	FALSE	FALSE	FALSE	FALSE
SWF2FR1_BURNT_2_5X_2	x8_y3.png	FALSE	FALSE	FALSE	FALSE	FALSE	FALSE	FALSE
WSF3D1M5_BURNT_50X_3	x3_y0.png	FALSE	FALSE	FALSE	FALSE	FALSE	FALSE	FALSE
WS Fresh_50X_1	x9_y6.png	FALSE	FALSE	FALSE	FALSE	FALSE	FALSE	FALSE
SWF2FR1_BURNT_1_5X_2	x2_y0.png	FALSE	FALSE	FALSE	FALSE	FALSE	FALSE	FALSE
WSF3D1M3_UNBURNT_1_50X_3	x3_y7.png	FALSE	FALSE	FALSE	FALSE	FALSE	FALSE	FALSE
WSF3D1M2_BURNT_50X_1	x5_y7.png	FALSE	FALSE	FALSE	FALSE	FALSE	FALSE	FALSE
WSF3D1M3_UNBURNT_1_50X_3	x0_y1.png	FALSE	FALSE	FALSE	FALSE	FALSE	FALSE	FALSE
WSF3D1M3_UNBURNT_1_50X_3	x0_y1.png	FALSE	FALSE	FALSE	FALSE	FALSE	FALSE	FALSE
SWF1FR2_BURNT_50X_1	x6_y7.png	FALSE	FALSE	FALSE	FALSE	FALSE	FALSE	FALSE
WSF3D1M1_BURNT_50X_8	x3_y1.png	FALSE	FALSE	FALSE	FALSE	FALSE	TRUE	FALSE
WSF3D1M2_BURNT_50X_3	x3_y2.png	FALSE	FALSE	FALSE	FALSE	FALSE	FALSE	FALSE
WSF3D1M5_SMALLPIECE_BURNT_50X_3	x8_y0.png	FALSE	FALSE	FALSE	FALSE	FALSE	FALSE	TRUE
SWF2FR1_BURNT_1_5X_2	x4_y7.png	FALSE	FALSE	FALSE	FALSE	FALSE	FALSE	FALSE
WSF3D1M3_BURNT_50X_1	x8_y8.png	FALSE	FALSE	FALSE	FALSE	FALSE	FALSE	FALSE
WS Fresh_50X_3	x2_y5.png	FALSE	FALSE	FALSE	FALSE	FALSE	FALSE	FALSE

SWF1FR2_BURNT_50X_3	x0_y8.png	FALSE	FALSE	FALSE	FALSE	FALSE	FALSE	FALSE
WSF3D1M1_BURNT_50X_5	x5_y5.png	FALSE	FALSE	FALSE	FALSE	FALSE	FALSE	FALSE
WSF3D1M5_BURNT_50X_1	x4_y8.png	FALSE	FALSE	FALSE	FALSE	FALSE	FALSE	FALSE
WSF3D1M1_BURNT_50X_5	x3_y6.png	FALSE	FALSE	FALSE	FALSE	FALSE	FALSE	FALSE
SWF1_BURNT_5_50X_2	x8_y0.png	FALSE	FALSE	FALSE	FALSE	FALSE	FALSE	FALSE
WSF3D1M5_SMALLPIECE_BURNT_50X_3	x0_y5.png	FALSE	FALSE	FALSE	FALSE	FALSE	FALSE	FALSE
WSF3D1M2_BURNT_50X_5	x1_y8.png	FALSE	FALSE	FALSE	FALSE	FALSE	FALSE	FALSE
SWF1_BURNT_4_50X_2	x8_y4.png	FALSE	FALSE	FALSE	FALSE	FALSE	FALSE	FALSE
WS Fresh_50X_1	x6_y0.png	FALSE	FALSE	FALSE	FALSE	FALSE	FALSE	FALSE
WS Fresh_50X_3	x7_y2.png	FALSE	FALSE	FALSE	FALSE	FALSE	FALSE	TRUE
WSF3D1M1_BURNT_50X_8	x0_y1.png	FALSE	TRUE	FALSE	FALSE	FALSE	FALSE	FALSE
WSF3D1M5_UNBURNT_1_50X_1	x7_y1.png	FALSE	FALSE	FALSE	FALSE	FALSE	FALSE	TRUE
WSF3D1M3_UNBURNT_2_50X_1	x9_y2.png	FALSE	TRUE	FALSE	FALSE	FALSE	FALSE	FALSE
WSF3D1M1_BURNT_50X_8	x2_y9.png	FALSE	FALSE	TRUE	FALSE	FALSE	FALSE	FALSE
WSF3D1M5_SMALLPIECE_BURNT_50X_3	x4_y9.png	FALSE	FALSE	FALSE	FALSE	FALSE	FALSE	FALSE
WSF3D1M4_BURNT_50X_1	x3_y7.png	FALSE	TRUE	FALSE	FALSE	FALSE	FALSE	FALSE
WSF3D1M5_UNBURNT_1_50X_1	x5_y5.png	FALSE	FALSE	FALSE	FALSE	FALSE	FALSE	FALSE
WSF3D1M3_UNBURNT_1_50X_4	x1_y8.png	FALSE	FALSE	FALSE	FALSE	FALSE	FALSE	FALSE
WSF3D1M3_BURNT_50X_3	x6_y4.png	FALSE	FALSE	FALSE	FALSE	FALSE	FALSE	FALSE
SWF1_BURNT_4_50X_3	x4_y5.png	FALSE	FALSE	FALSE	FALSE	FALSE	FALSE	FALSE
WSF3D1M5_BURNT_50X_1	x2_y5.png	FALSE	FALSE	FALSE	FALSE	FALSE	FALSE	FALSE

WSF3D1M5_BURNT_50X_2	x6_y1.png	FALSE	FALSE	FALSE	FALSE	FALSE	FALSE	FALSE
SWF2FR1_BURNT_2_5X_2	x3_y4.png	FALSE	FALSE	FALSE	FALSE	FALSE	FALSE	FALSE
WSF3D1M1_BURNT_50X_6	x5_y4.png	FALSE	FALSE	TRUE	FALSE	FALSE	FALSE	FALSE
WSF3D1M1_BURNT_50X_5	x3_y3.png	FALSE	FALSE	FALSE	FALSE	FALSE	FALSE	FALSE
WSF3D1M4_NO2_BURNT_50X_2	x9_y8.png	FALSE	FALSE	FALSE	FALSE	FALSE	FALSE	FALSE
WSF3D1M1_BURNT_50X_5	x8_y5.png	FALSE	FALSE	FALSE	FALSE	FALSE	FALSE	FALSE
WSF3D1M1_BURNT_50X_2	x0_y1.png	FALSE	FALSE	FALSE	FALSE	FALSE	FALSE	FALSE
WSF3D1M1_BURNT_50X_3	x5_y5.png	FALSE	TRUE	FALSE	FALSE	FALSE	FALSE	FALSE
SWF1_BURNT_5_50X_1	x5_y7.png	FALSE	FALSE	FALSE	FALSE	FALSE	FALSE	FALSE
WSF3D1M1_BURNT_50X_10	x3_y3.png	FALSE	FALSE	FALSE	FALSE	FALSE	FALSE	FALSE
SWF2FR1_BURNT_2_5X_2	x7_y9.png	FALSE	FALSE	FALSE	FALSE	FALSE	FALSE	FALSE
SWF1_BURNT_5_50X_3	x5_y7.png	FALSE	FALSE	FALSE	FALSE	FALSE	FALSE	FALSE
WSF3D1M4_NO2_BURNT_50X_3	x2_y4.png	FALSE	FALSE	FALSE	FALSE	FALSE	FALSE	FALSE
SWF1_BURNT_4_50X_2	x0_y4.png	FALSE	FALSE	FALSE	FALSE	FALSE	FALSE	FALSE
WSF3D1M2_BURNT_50X_3	x2_y5.png	FALSE	FALSE	TRUE	FALSE	FALSE	FALSE	TRUE
SWF1_BURNT_4_50X_1	x5_y6.png	FALSE	FALSE	FALSE	FALSE	FALSE	FALSE	FALSE
WSF3D1M4_BURNT_50X_3	x4_y2.png	FALSE	TRUE	FALSE	FALSE	FALSE	FALSE	FALSE
WSF3D1M1_BURNT_50X_7	x4_y7.png	FALSE	FALSE	TRUE	FALSE	FALSE	FALSE	FALSE
WSF3D1M2_BURNT_50X_3	x8_y9.png	FALSE	FALSE	FALSE	FALSE	FALSE	FALSE	TRUE
WS Fresh	x0_y6.png	FALSE	FALSE	FALSE	FALSE	FALSE	FALSE	FALSE
WSF3D1M5_BURNT_50X_3	x3_y8.png	FALSE	FALSE	FALSE	FALSE	FALSE	FALSE	FALSE

WSF3D1M2_BURNT_50X_1	x3_y6.png	FALSE	FALSE	FALSE	FALSE	FALSE	FALSE	FALSE
WSF3D1M1_BURNT_50X_4	x5_y9.png	FALSE	FALSE	FALSE	FALSE	FALSE	FALSE	TRUE
SWF1FR2_BURNT_50X_2	x7_y7.png	FALSE	TRUE	FALSE	FALSE	FALSE	FALSE	FALSE
WSF3D1M5_BURNT_50X_1	x3_y8.png	FALSE	FALSE	FALSE	FALSE	FALSE	FALSE	FALSE
SWF1_BURNT_5_50X_2	x2_y6.png	FALSE	FALSE	FALSE	FALSE	FALSE	FALSE	TRUE
WS Fresh_50X_3	x1_y6.png	FALSE	FALSE	FALSE	FALSE	FALSE	FALSE	FALSE
WSF3D1M1_BURNT_50X_6	x2_y4.png	FALSE	TRUE	FALSE	FALSE	FALSE	FALSE	FALSE
WSF3D1M4_BURNT_50X_3	x5_y9.png	FALSE	FALSE	FALSE	FALSE	FALSE	FALSE	TRUE
SWF1_BURNT_4_50X_1	x5_y9.png	FALSE	FALSE	FALSE	FALSE	FALSE	FALSE	FALSE
WSF3D1M4_NO2_BURNT_50X_3	x3_y3.png	FALSE	FALSE	FALSE	FALSE	FALSE	FALSE	FALSE
WSF3D1M3_BURNT_50X_2	x3_y9.png	FALSE	FALSE	FALSE	FALSE	FALSE	FALSE	FALSE
WSF3D1M1_BURNT_50X_4	x1_y6.png	FALSE	FALSE	FALSE	FALSE	FALSE	FALSE	FALSE
WSF3D1M5_UNBURNT_1_50X_1	x4_y0.png	FALSE	FALSE	FALSE	FALSE	FALSE	FALSE	FALSE
WSF3D1M3_BURNT_50X_1	x2_y1.png	FALSE	FALSE	FALSE	FALSE	FALSE	FALSE	FALSE
WSF3D1M3_UNBURNT_1_50X_5	x5_y7.png	FALSE	TRUE	FALSE	FALSE	FALSE	FALSE	FALSE
WSF3D1M5_BURNT_50X_1	x2_y2.png	FALSE	FALSE	FALSE	FALSE	FALSE	FALSE	FALSE
SWF1FR2_BURNT_50X_3	x8_y0.png	FALSE	FALSE	TRUE	FALSE	FALSE	FALSE	FALSE
WSF3D1M3_UNBURNT_1_50X_3	x9_y0.png	FALSE	FALSE	FALSE	FALSE	FALSE	FALSE	FALSE
SWF2FR1_BURNT_1_5X	x0_y8.png	FALSE	FALSE	FALSE	FALSE	FALSE	FALSE	FALSE
SWF2FR1_BURNT_1_5X	x7_y9.png	FALSE	FALSE	FALSE	FALSE	FALSE	FALSE	FALSE
WSF3D1M2_BURNT_50X_4	x1_y5.png	FALSE	FALSE	FALSE	FALSE	FALSE	FALSE	TRUE

WSF3D1M1_BURNT_50X_4	x5_y5.png	FALSE	TRUE	FALSE	FALSE	FALSE	FALSE	FALSE
WSF3D1M4_BURNT_50X_2	x8_y4.png	FALSE	FALSE	FALSE	FALSE	FALSE	TRUE	TRUE
WSF3D1M3_UNBURNT_2_50X_1	x5_y3.png	FALSE	FALSE	FALSE	FALSE	FALSE	FALSE	FALSE
WSF3D1M5_BURNT_50X_3	x7_y0.png	FALSE	FALSE	FALSE	FALSE	FALSE	FALSE	FALSE
SWF1_BURNT_4_50X_3	x0_y2.png	FALSE	FALSE	FALSE	FALSE	FALSE	FALSE	FALSE
WSF3D1M2_BURNT_50X_3	x6_y0.png	FALSE	FALSE	TRUE	FALSE	FALSE	FALSE	FALSE
WSF3D1M1_BURNT_50X_8	x9_y9.png	FALSE	FALSE	FALSE	FALSE	FALSE	FALSE	FALSE
SWF2FR4_BURNT_50X	x5_y1.png	FALSE	FALSE	TRUE	FALSE	FALSE	FALSE	FALSE
WSF3D1M5_BURNT_50X_3	x6_y2.png	FALSE	FALSE	FALSE	FALSE	FALSE	FALSE	FALSE
WSF3D1M2_BURNT_50X_5	x5_y9.png	FALSE	FALSE	TRUE	FALSE	FALSE	FALSE	TRUE
WSF3D1M1_BURNT_50X_2	x5_y3.png	FALSE	TRUE	FALSE	FALSE	FALSE	FALSE	FALSE
WSF3D1M2_BURNT_50X_6	x5_y3.png	FALSE	FALSE	FALSE	FALSE	FALSE	FALSE	FALSE
WSF3D1M1_BURNT_50X_3	x3_y0.png	FALSE	FALSE	FALSE	FALSE	FALSE	FALSE	FALSE
WSF3D1M2_BURNT_50X_5	x2_y6.png	FALSE	FALSE	TRUE	FALSE	FALSE	FALSE	FALSE
SWF1FR2_BURNT_50X_4	x4_y0.png	FALSE	FALSE	FALSE	FALSE	FALSE	FALSE	FALSE
WSF3D1M1_BURNT_50X	x5_y4.png	FALSE	TRUE	FALSE	FALSE	FALSE	FALSE	FALSE
WSF3D1M1_BURNT_50X_6	x8_y5.png	FALSE	FALSE	FALSE	FALSE	FALSE	FALSE	FALSE
WSF3D1M1_BURNT_50X_10	x9_y2.png	FALSE	FALSE	TRUE	TRUE	FALSE	FALSE	FALSE
SWF2FR1_BURNT_2_5X_2	x8_y7.png	FALSE	FALSE	FALSE	FALSE	FALSE	FALSE	FALSE
WSF3D1M1_BURNT_50X_5	x0_y3.png	FALSE	TRUE	FALSE	FALSE	FALSE	FALSE	FALSE

WSF3D1M1_BURNT_50X_7	x9_y1.png	FALSE	FALSE	FALSE	FALSE	FALSE	FALSE	TRUE
WSF3D1M4_NO2_BURNT_50X_1	x8_y5.png	FALSE	FALSE	TRUE	FALSE	FALSE	FALSE	FALSE
WSF3D1M3_UNBURNT_2_50X_1	x7_y6.png	FALSE	TRUE	FALSE	FALSE	FALSE	FALSE	TRUE
SWF1FR2_BURNT_50X_3	x8_y5.png	FALSE	TRUE	FALSE	TRUE	FALSE	FALSE	TRUE
WS Fresh	x6_y8.png	FALSE	FALSE	FALSE	FALSE	FALSE	FALSE	FALSE
WSF3D1M4_NO2_BURNT_50X_3	x7_y0.png	FALSE	FALSE	FALSE	FALSE	FALSE	FALSE	FALSE
WSF3D1M3_BURNT_50X_3	x4_y9.png	FALSE	FALSE	FALSE	FALSE	FALSE	FALSE	FALSE
SWF1_BURNT_4_50X_3	x3_y1.png	FALSE	FALSE	FALSE	FALSE	FALSE	FALSE	FALSE
WSF3D1M4_NO2_BURNT_50X_3	x0_y5.png	FALSE	FALSE	FALSE	FALSE	FALSE	TRUE	FALSE
WSF3D1M4_NO2_BURNT_50X_2	x5_y7.png	FALSE	FALSE	FALSE	FALSE	FALSE	FALSE	TRUE
SWF1_BURNT_3_50X_1	x6_y8.png	FALSE	FALSE	FALSE	FALSE	FALSE	FALSE	FALSE
WSF3D1M3_UNBURNT_1_50X_4	x3_y5.png	FALSE	TRUE	FALSE	FALSE	FALSE	FALSE	FALSE
WSF3D1M1_BURNT_50X_3	x1_y2.png	FALSE	FALSE	FALSE	FALSE	FALSE	FALSE	FALSE
WSF3D1M2_BURNT_50X_3	x7_y7.png	FALSE	FALSE	FALSE	FALSE	FALSE	FALSE	TRUE
WSF3D1M3_BURNT_50X_3	x5_y4.png	FALSE	FALSE	TRUE	FALSE	FALSE	FALSE	TRUE
WS Fresh_50X_1	x3_y9.png	FALSE	FALSE	FALSE	FALSE	FALSE	FALSE	FALSE
WSF3D1M1_BURNT_50X_3	x7_y8.png	FALSE	FALSE	FALSE	FALSE	FALSE	FALSE	FALSE
WSF3D1M1_BURNT_50X_6	x9_y0.png	FALSE	FALSE	FALSE	FALSE	FALSE	FALSE	FALSE
WSF3D1M5_BURNT_50X_1	x3_y5.png	FALSE	FALSE	FALSE	FALSE	FALSE	FALSE	FALSE
SWF1_BURNT_5_50X_3	x1_y1.png	FALSE	FALSE	FALSE	FALSE	FALSE	FALSE	FALSE
WSF3D1M2_BURNT_50X_6	x8_y7.png	FALSE	FALSE	FALSE	FALSE	FALSE	FALSE	FALSE

WSF3D1M2_BURNT_50X_2	x8_y4.png	FALSE	FALSE	FALSE	FALSE	FALSE	FALSE	FALSE
WSF3D1M2_BURNT_50X_6	x1_y2.png	TRUE	FALSE	FALSE	FALSE	FALSE	FALSE	FALSE
WSF3D1M3_BURNT_50X_1	x5_y5.png	FALSE	FALSE	FALSE	FALSE	FALSE	FALSE	FALSE
WSF3D1M5_BURNT_50X_2	x6_y8.png	FALSE	FALSE	FALSE	FALSE	FALSE	FALSE	FALSE
WSF3D1M3_UNBURNT_1_50X_1	x8_y0.png	FALSE	FALSE	FALSE	FALSE	FALSE	FALSE	FALSE
WSF3D1M5_SMALLPIECE_BURNT_50X_4	x3_y5.png	FALSE	FALSE	FALSE	FALSE	FALSE	FALSE	FALSE
SWF2FR1_BURNT_2_5X_2	x0_y1.png	FALSE	FALSE	FALSE	FALSE	FALSE	FALSE	FALSE
SWF2FR1_BURNT_2_5X_2	x6_y0.png	FALSE	FALSE	FALSE	FALSE	FALSE	FALSE	FALSE
WSF3D1M4_NO2_BURNT_50X_2	x5_y1.png	FALSE	FALSE	FALSE	FALSE	FALSE	FALSE	FALSE
WS Fresh_50X_2	x6_y8.png	FALSE	FALSE	FALSE	FALSE	FALSE	FALSE	FALSE
SWF1FR2_BURNT_50X_1	x7_y9.png	FALSE	TRUE	FALSE	FALSE	FALSE	FALSE	FALSE
WSF3D1M3_UNBURNT_2_50X_1	x1_y4.png	FALSE	TRUE	TRUE	FALSE	FALSE	FALSE	FALSE
WSF3D1M1_BURNT_50X	x0_y2.png	FALSE	FALSE	FALSE	FALSE	FALSE	FALSE	TRUE
WSF3D1M4_BURNT_50X_2	x2_y2.png	FALSE	FALSE	FALSE	FALSE	FALSE	FALSE	TRUE
WSF3D1M5_SMALLPIECE_BURNT_50X_3	x3_y8.png	FALSE	FALSE	FALSE	FALSE	FALSE	FALSE	FALSE
WSF3D1M1_BURNT_50X_8	x2_y3.png	FALSE	FALSE	FALSE	FALSE	FALSE	FALSE	TRUE
WSF3D1M3_BURNT_50X_1	x9_y4.png	FALSE	FALSE	FALSE	FALSE	FALSE	FALSE	FALSE
WSF3D1M1_BURNT_50X_2	x7_y0.png	FALSE	FALSE	TRUE	FALSE	FALSE	FALSE	FALSE
SWF1FR2_BURNT_50X_3	x0_y1.png	FALSE	FALSE	FALSE	FALSE	FALSE	FALSE	FALSE
WSF3D1M4_BURNT_50X_2	x1_y3.png	TRUE	FALSE	FALSE	FALSE	FALSE	FALSE	FALSE

WSF3D1M3_BURNT_50X_2	x0_y2.png	TRUE	FALSE	FALSE	FALSE	FALSE	FALSE	FALSE
WSF3D1M2_BURNT_50X_4	x7_y8.png	FALSE	FALSE	TRUE	FALSE	FALSE	FALSE	FALSE
WSF3D1M5_BURNT_50X_3	x5_y4.png	FALSE	FALSE	FALSE	FALSE	FALSE	FALSE	FALSE
WSF3D1M1_BURNT_50X_3	x2_y1.png	TRUE	FALSE	FALSE	FALSE	FALSE	FALSE	FALSE
WSF3D1M5_SMALLPIECE_BURNT_50X_4	x7_y5.png	FALSE	FALSE	FALSE	FALSE	FALSE	FALSE	FALSE
WSF3D1M3_BURNT_50X_1	x7_y6.png	FALSE	FALSE	FALSE	FALSE	FALSE	FALSE	FALSE
WSF3D1M2_BURNT_50X_2	x4_y0.png	FALSE	FALSE	TRUE	FALSE	FALSE	FALSE	FALSE
WSF3D1M2_BURNT_50X_2	x0_y7.png	FALSE	TRUE	FALSE	FALSE	FALSE	FALSE	FALSE
WSF3D1M4_BURNT_50X_4	x4_y8.png	FALSE	FALSE	TRUE	TRUE	FALSE	FALSE	FALSE
SWF2FR1_BURNT_2_5X_1	x1_y8.png	FALSE	FALSE	FALSE	FALSE	FALSE	TRUE	FALSE
SWF1_BURNT_4_50X_3	x9_y5.png	FALSE	FALSE	FALSE	FALSE	FALSE	FALSE	FALSE
SWF1FR2_BURNT_50X_3	x6_y2.png	TRUE	FALSE	FALSE	FALSE	FALSE	FALSE	FALSE
WSF3D1M3_UNBURNT_1_50X_5	x1_y2.png	FALSE	FALSE	TRUE	FALSE	FALSE	FALSE	FALSE
WSF3D1M2_BURNT_50X_3	x8_y3.png	FALSE	FALSE	FALSE	FALSE	FALSE	FALSE	FALSE
WSF3D1M5_BURNT_50X_2	x2_y0.png	FALSE	FALSE	FALSE	FALSE	FALSE	FALSE	FALSE
WSF3D1M2_BURNT_50X_1	x8_y7.png	FALSE	FALSE	TRUE	FALSE	FALSE	FALSE	FALSE
WSF3D1M3_BURNT_50X_1	x3_y4.png	FALSE	FALSE	TRUE	FALSE	FALSE	FALSE	FALSE
WSF3D1M3_BURNT_50X_3	x6_y2.png	FALSE	FALSE	FALSE	FALSE	FALSE	FALSE	FALSE
SWF2FR1_BURNT_1_5X	x3_y2.png	FALSE	FALSE	FALSE	FALSE	FALSE	FALSE	FALSE
SWF2FR1_BURNT_2_5X_1	x5_y2.png	FALSE	FALSE	FALSE	FALSE	FALSE	FALSE	FALSE

WSF3D1M2_BURNT_50X_1	x6_y9.png	FALSE	FALSE	TRUE	FALSE	FALSE	FALSE	FALSE
WSF3D1M2_BURNT_50X_3	x0_y7.png	FALSE	FALSE	TRUE	FALSE	FALSE	FALSE	FALSE
WSF3D1M4_BURNT_50X_3	x0_y6.png	FALSE	FALSE	FALSE	FALSE	FALSE	FALSE	TRUE
SWF2FR1_BURNT_1_5X	x1_y2.png	FALSE	FALSE	FALSE	FALSE	FALSE	FALSE	FALSE
WSF3D1M3_BURNT_50X_3	x5_y8.png	FALSE	FALSE	FALSE	FALSE	FALSE	FALSE	FALSE
SWF1_BURNT_5_50X_2	x9_y0.png	FALSE	FALSE	FALSE	FALSE	FALSE	FALSE	FALSE
WS Fresh	x1_y0.png	FALSE	FALSE	FALSE	FALSE	FALSE	FALSE	FALSE
WSF3D1M4_BURNT_50X_2	x2_y0.png	TRUE	FALSE	FALSE	FALSE	FALSE	FALSE	FALSE
WSF3D1M4_NO2_BURNT_50X_3	x2_y2.png	FALSE	FALSE	FALSE	FALSE	FALSE	FALSE	FALSE
WSF3D1M1_BURNT_50X_8	x1_y6.png	FALSE	FALSE	TRUE	FALSE	FALSE	FALSE	FALSE
WS Fresh_50X_1	x2_y3.png	FALSE	FALSE	FALSE	FALSE	FALSE	FALSE	FALSE
WSF3D1M1_BURNT_50X_10	x0_y0.png	FALSE	FALSE	FALSE	FALSE	FALSE	FALSE	FALSE
SWF1_BURNT_4_50X_3	x9_y3.png	FALSE	FALSE	FALSE	FALSE	FALSE	FALSE	FALSE
WSF3D1M4_BURNT_50X_1	x0_y6.png	FALSE	FALSE	FALSE	FALSE	FALSE	FALSE	FALSE
WSF3D1M3_UNBURNT_1_50X_4	x6_y1.png	FALSE	FALSE	FALSE	FALSE	FALSE	FALSE	FALSE
WSF3D1M1_BURNT_50X_2	x2_y7.png	FALSE	FALSE	TRUE	FALSE	FALSE	FALSE	FALSE
WSF3D1M3_UNBURNT_1_50X_3	x5_y3.png	FALSE	FALSE	FALSE	FALSE	FALSE	FALSE	FALSE
WSF3D1M3_UNBURNT_1_50X_4	x7_y2.png	FALSE	FALSE	FALSE	FALSE	FALSE	FALSE	FALSE
SWF1_BURNT_4_50X_2	x0_y0.png	FALSE	FALSE	FALSE	FALSE	FALSE	FALSE	FALSE
WSF3D1M4_NO2_BURNT_50X_1	x3_y9.png	FALSE	FALSE	FALSE	FALSE	FALSE	FALSE	FALSE
WSF3D1M1_BURNT_50X_5	x8_y0.png	FALSE	FALSE	FALSE	FALSE	FALSE	FALSE	FALSE

WSF3D1M1_BURNT_50X_3	x1_y1.png	FALSE	FALSE	FALSE	FALSE	FALSE	FALSE	TRUE
WSF3D1M4_NO2_BURNT_50X_2	x7_y4.png	FALSE	FALSE	TRUE	FALSE	FALSE	FALSE	FALSE
WSF3D1M1_BURNT_50X_9	x3_y8.png	FALSE	FALSE	FALSE	FALSE	FALSE	FALSE	TRUE
WSF3D1M2_BURNT_50X_4	x2_y4.png	FALSE	FALSE	FALSE	FALSE	FALSE	FALSE	FALSE
WSF3D1M1_BURNT_50X_3	x9_y4.png	FALSE	FALSE	FALSE	FALSE	FALSE	FALSE	FALSE
SWF1_BURNT_4_50X_3	x3_y3.png	FALSE	FALSE	FALSE	FALSE	FALSE	FALSE	FALSE
WSF3D1M2_BURNT_50X_1	x9_y2.png	FALSE	FALSE	TRUE	FALSE	FALSE	FALSE	FALSE
WSF3D1M4_NO2_BURNT_50X_1	x6_y8.png	FALSE	FALSE	FALSE	FALSE	FALSE	FALSE	FALSE
WSF3D1M4_BURNT_50X_3	x3_y4.png	TRUE	FALSE	FALSE	FALSE	FALSE	FALSE	FALSE
WSF3D1M5_UNBURNT_1_50X_1	x1_y4.png	FALSE	FALSE	FALSE	FALSE	FALSE	FALSE	FALSE
WSF3D1M4_BURNT_50X_2	x7_y4.png	TRUE	FALSE	FALSE	FALSE	FALSE	FALSE	FALSE
SWF1_BURNT_4_50X_2	x0_y7.png	FALSE	FALSE	FALSE	FALSE	FALSE	FALSE	FALSE
WSF3D1M2_BURNT_50X_1	x9_y7.png	FALSE	FALSE	FALSE	FALSE	FALSE	FALSE	FALSE
SWF2FR1_BURNT_2_5X_1	x2_y1.png	FALSE	FALSE	FALSE	FALSE	FALSE	FALSE	FALSE
WSF3D1M2_BURNT_50X_2	x3_y9.png	FALSE	FALSE	FALSE	FALSE	FALSE	FALSE	TRUE
WSF3D1M1_BURNT_50X_3	x1_y4.png	FALSE	FALSE	FALSE	FALSE	FALSE	FALSE	FALSE
WSF3D1M1_BURNT_50X_9	x9_y4.png	FALSE	FALSE	FALSE	FALSE	FALSE	FALSE	FALSE
WSF3D1M5_BURNT_50X_3	x2_y9.png	FALSE	FALSE	FALSE	FALSE	FALSE	FALSE	TRUE
WSF3D1M1_BURNT_50X_10	x8_y5.png	FALSE	FALSE	FALSE	FALSE	FALSE	FALSE	FALSE

WSF3D1M3_BURNT_50X_1	x9_y1.png	FALSE	FALSE	FALSE	FALSE	FALSE	FALSE	FALSE
WSF3D1M1_BURNT_50X_9	x5_y1.png	TRUE	FALSE	FALSE	FALSE	FALSE	FALSE	TRUE
WSF3D1M3_UNBURNT_2_50X_1	x1_y5.png	FALSE	FALSE	FALSE	FALSE	FALSE	FALSE	FALSE
WSF3D1M5_SMALLPIECE_BURNT_50X_4	x1_y1.png	FALSE	FALSE	FALSE	FALSE	FALSE	FALSE	FALSE
WSF3D1M4_BURNT_50X_4	x8_y2.png	FALSE	FALSE	FALSE	FALSE	FALSE	FALSE	TRUE
WSF3D1M5_SMALLPIECE_BURNT_50X_4	x0_y7.png	FALSE	FALSE	FALSE	FALSE	FALSE	FALSE	FALSE
WSF3D1M2_BURNT_50X_3	x7_y4.png	FALSE	FALSE	TRUE	FALSE	FALSE	FALSE	FALSE
WSF3D1M5_BURNT_50X_3	x7_y6.png	FALSE	FALSE	FALSE	FALSE	FALSE	FALSE	FALSE
SWF1_BURNT_3_50X_1	x5_y1.png	FALSE	FALSE	FALSE	FALSE	FALSE	FALSE	FALSE
SWF1FR2_BURNT_50X_3	x9_y6.png	TRUE	FALSE	FALSE	FALSE	FALSE	FALSE	FALSE
WS Fresh_50X_1	x0_y8.png	FALSE	FALSE	FALSE	FALSE	FALSE	FALSE	FALSE
WSF3D1M4_NO2_BURNT_50X_2	x8_y5.png	FALSE	FALSE	FALSE	FALSE	FALSE	FALSE	FALSE
WSF3D1M4_NO2_BURNT_50X_2	x9_y2.png	FALSE	FALSE	FALSE	FALSE	FALSE	FALSE	FALSE
WSF3D1M4_NO2_BURNT_50X_2	x4_y9.png	FALSE	FALSE	FALSE	FALSE	FALSE	FALSE	FALSE
WSF3D1M5_BURNT_50X_1	x6_y8.png	FALSE	FALSE	FALSE	FALSE	FALSE	FALSE	FALSE
SWF1_BURNT_3_50X_1	x7_y7.png	FALSE	FALSE	FALSE	FALSE	FALSE	FALSE	FALSE
WSF3D1M1_BURNT_50X	x1_y2.png	FALSE	FALSE	FALSE	FALSE	FALSE	FALSE	FALSE
WS Fresh_50X_2	x7_y0.png	FALSE	FALSE	TRUE	FALSE	FALSE	FALSE	FALSE
SWF1_BURNT_4_50X_3	x2_y2.png	FALSE	FALSE	FALSE	FALSE	FALSE	FALSE	FALSE
WSF3D1M5_UNBURNT_1_50X_1	x6_y5.png	FALSE	TRUE	FALSE	FALSE	FALSE	FALSE	FALSE
WSF3D1M4_NO2_BURNT_50X_1	x3_y0.png	FALSE	FALSE	FALSE	FALSE	FALSE	FALSE	FALSE

SWF2FR1_BURNT_2_5X_2	x3_y6.png	FALSE	FALSE	FALSE	FALSE	FALSE	FALSE	FALSE
SWF1_BURNT_5_50X_2	x1_y2.png	TRUE	FALSE	FALSE	FALSE	FALSE	FALSE	FALSE
WSF3D1M5_SMALLPIECE_BURNT_50X_3	x0_y1.png	FALSE	FALSE	FALSE	FALSE	FALSE	FALSE	FALSE
WSF3D1M2_BURNT_50X_3	x7_y5.png	FALSE	FALSE	FALSE	FALSE	FALSE	TRUE	FALSE
WSF3D1M4_NO2_BURNT_50X_2	x9_y5.png	FALSE	FALSE	FALSE	FALSE	FALSE	FALSE	FALSE
WSF3D1M2_BURNT_50X_1	x5_y6.png	FALSE	FALSE	TRUE	FALSE	FALSE	FALSE	FALSE
SWF1FR2_BURNT_50X_1	x4_y5.png	FALSE	FALSE	FALSE	FALSE	FALSE	FALSE	FALSE
SWF2FR1_BURNT_2_5X_2	x0_y2.png	FALSE	FALSE	FALSE	FALSE	FALSE	FALSE	FALSE
WSF3D1M5_SMALLPIECE_BURNT_50X_4	x9_y6.png	FALSE	FALSE	FALSE	FALSE	FALSE	FALSE	FALSE
WSF3D1M5_BURNT_50X_3	x9_y7.png	FALSE	FALSE	FALSE	FALSE	FALSE	FALSE	FALSE
WS Fresh_50X_2	x5_y9.png	FALSE	FALSE	FALSE	FALSE	FALSE	FALSE	TRUE
SWF1_BURNT_5_50X_2	x7_y8.png	FALSE	FALSE	FALSE	FALSE	FALSE	FALSE	TRUE
WSF3D1M1_BURNT_50X_2	x3_y3.png	FALSE	TRUE	FALSE	FALSE	FALSE	FALSE	FALSE
SWF1_BURNT_5_50X_2	x8_y6.png	FALSE	FALSE	FALSE	FALSE	FALSE	FALSE	TRUE
WS Fresh	x0_y0.png	FALSE	FALSE	FALSE	FALSE	FALSE	FALSE	FALSE
WSF3D1M1_BURNT_50X_10	x4_y5.png	FALSE	FALSE	TRUE	FALSE	FALSE	FALSE	FALSE
WSF3D1M1_BURNT_50X_6	x3_y9.png	TRUE	FALSE	FALSE	FALSE	FALSE	FALSE	FALSE
SWF1_BURNT_3_50X_1	x3_y1.png	FALSE	FALSE	FALSE	FALSE	FALSE	TRUE	FALSE
SWF1_BURNT_4_50X_3	x6_y5.png	FALSE	FALSE	TRUE	FALSE	FALSE	FALSE	FALSE
WSF3D1M1_BURNT_50X_5	x1_y7.png	TRUE	FALSE	FALSE	FALSE	FALSE	FALSE	FALSE
WSF3D1M2_BURNT_50X_1	x2_y7.png	FALSE	FALSE	TRUE	FALSE	FALSE	FALSE	FALSE
SWF1_BURNT_4_50X_2	x5_y3.png	FALSE	FALSE	FALSE	FALSE	FALSE	FALSE	FALSE

SWF1FR2_BURNT_50X_4	x8_y0.png	FALSE	TRUE	FALSE	FALSE	FALSE	FALSE	FALSE
WSF3D1M2_BURNT_50X_2	x3_y3.png	FALSE	FALSE	FALSE	FALSE	FALSE	FALSE	FALSE
WSF3D1M3_UNBURNT_1_50X_1	x0_y2.png	FALSE	TRUE	FALSE	FALSE	FALSE	FALSE	FALSE
WSF3D1M2_BURNT_50X_3	x9_y4.png	FALSE	FALSE	FALSE	FALSE	FALSE	FALSE	FALSE
WSF3D1M4_BURNT_50X_2	x3_y6.png	FALSE	FALSE	FALSE	TRUE	FALSE	FALSE	FALSE
WSF3D1M3_UNBURNT_1_50X_3	x7_y4.png	FALSE	FALSE	FALSE	FALSE	FALSE	FALSE	FALSE
WSF3D1M4_NO2_BURNT_50X_1	x3_y8.png	FALSE	FALSE	FALSE	FALSE	FALSE	FALSE	FALSE
SWF1FR2_BURNT_50X_1	x0_y5.png	FALSE	FALSE	FALSE	FALSE	FALSE	FALSE	TRUE
SWF1_BURNT_5_50X_1	x9_y6.png	FALSE	FALSE	FALSE	FALSE	FALSE	FALSE	FALSE
SWF1FR2_BURNT_50X_3	x9_y3.png	FALSE	TRUE	FALSE	FALSE	FALSE	FALSE	FALSE
WSF3D1M4_BURNT_50X_4	x0_y3.png	TRUE	FALSE	FALSE	FALSE	FALSE	FALSE	FALSE
WSF3D1M1_BURNT_50X_5	x0_y5.png	FALSE	FALSE	FALSE	FALSE	FALSE	FALSE	FALSE
SWF1_BURNT_5_50X_2	x6_y1.png	FALSE	FALSE	FALSE	FALSE	FALSE	FALSE	FALSE
SWF1_BURNT_5_50X_1	x6_y8.png	TRUE	FALSE	FALSE	FALSE	FALSE	FALSE	FALSE
WS Fresh_50X_3	x8_y1.png	FALSE	FALSE	FALSE	FALSE	FALSE	FALSE	FALSE
WSF3D1M5_SMALLPIECE_BURNT_50X_3	x4_y2.png	TRUE	FALSE	FALSE	FALSE	FALSE	FALSE	FALSE
WSF3D1M1_BURNT_50X	x2_y9.png	FALSE	FALSE	TRUE	FALSE	FALSE	FALSE	FALSE
WSF3D1M1_BURNT_50X_2	x2_y5.png	FALSE	FALSE	FALSE	FALSE	FALSE	FALSE	FALSE
WSF3D1M3_BURNT_50X_1	x0_y3.png	FALSE	FALSE	FALSE	FALSE	FALSE	FALSE	FALSE
WSF3D1M4_NO2_BURNT_50X_3	x1_y3.png	FALSE	FALSE	FALSE	FALSE	FALSE	FALSE	FALSE
SWF1_BURNT_4_50X_1	x2_y8.png	FALSE	FALSE	FALSE	FALSE	FALSE	FALSE	FALSE
SWF1_BURNT_4_50X_1	x1_y0.png	FALSE	FALSE	FALSE	FALSE	FALSE	FALSE	FALSE

WSF3D1M1_BURNT_50X_10	x0_y6.png	FALSE	FALSE	TRUE	FALSE	FALSE	FALSE	FALSE
WSF3D1M1_BURNT_50X_10	x0_y6.png	FALSE	FALSE	TRUE	FALSE	FALSE	FALSE	FALSE
WSF3D1M1_BURNT_50X_10	x0_y6.png	FALSE	FALSE	TRUE	FALSE	FALSE	FALSE	FALSE
WSF3D1M1_BURNT_50X_10	x0_y6.png	FALSE	FALSE	TRUE	FALSE	FALSE	FALSE	FALSE
WSF3D1M1_BURNT_50X_10	x0_y6.png	FALSE	FALSE	TRUE	FALSE	FALSE	FALSE	FALSE
SWF1FR2_BURNT_50X_4	x1_y7.png	FALSE	TRUE	FALSE	FALSE	FALSE	FALSE	FALSE
SWF1_BURNT_4_50X_2	x4_y1.png	FALSE	FALSE	FALSE	FALSE	FALSE	FALSE	FALSE
SWF1_BURNT_4_50X_2	x4_y1.png	FALSE	FALSE	FALSE	FALSE	FALSE	FALSE	FALSE
SWF1FR2_BURNT_50X_4	x6_y3.png	FALSE	FALSE	FALSE	FALSE	FALSE	FALSE	TRUE
SWF1_BURNT_5_50X_1	x8_y7.png	FALSE	FALSE	FALSE	FALSE	FALSE	TRUE	FALSE
WSF3D1M1_BURNT_50X_9	x7_y5.png	FALSE	FALSE	FALSE	FALSE	FALSE	FALSE	TRUE
WSF3D1M4_NO2_BURNT_50X_3	x2_y1.png	FALSE	FALSE	FALSE	FALSE	FALSE	FALSE	FALSE
WS Fresh_50X_1	x2_y4.png	FALSE	FALSE	FALSE	FALSE	FALSE	FALSE	FALSE
WSF3D1M3_UNBURNT_1_50X_3	x5_y1.png	FALSE	TRUE	FALSE	FALSE	FALSE	FALSE	TRUE
WSF3D1M1_BURNT_50X_8	x9_y2.png	FALSE	FALSE	FALSE	FALSE	FALSE	FALSE	TRUE
WSF3D1M3_UNBURNT_1_50X_1	x9_y1.png	FALSE	FALSE	TRUE	FALSE	FALSE	FALSE	FALSE
SWF2FR1_BURNT_1_5X_2	x0_y2.png	FALSE	FALSE	FALSE	FALSE	FALSE	FALSE	FALSE
WSF3D1M4_BURNT_50X_3	x9_y6.png	FALSE	TRUE	FALSE	FALSE	FALSE	FALSE	FALSE
WSF3D1M3_UNBURNT_1_50X_5	x2_y2.png	FALSE	TRUE	FALSE	FALSE	FALSE	FALSE	FALSE
SWF1_BURNT_5_50X_1	x2_y5.png	FALSE	FALSE	FALSE	FALSE	FALSE	FALSE	TRUE
WSF3D1M1_BURNT_50X_7	x6_y2.png	FALSE	FALSE	FALSE	FALSE	FALSE	FALSE	FALSE

WSF3D1M1_BURNT_50X_10	x8_y0.png	FALSE	FALSE	TRUE	FALSE	FALSE	FALSE	TRUE
WSF3D1M1_BURNT_50X_10	x2_y5.png	FALSE	FALSE	FALSE	FALSE	FALSE	FALSE	TRUE
WSF3D1M1_BURNT_50X_2	x1_y6.png	FALSE	TRUE	FALSE	FALSE	FALSE	FALSE	FALSE
SWF1_BURNT_3_50X_1	x2_y7.png	FALSE	FALSE	FALSE	FALSE	FALSE	FALSE	FALSE
WSF3D1M4_NO2_BURNT_50X_3	x1_y6.png	FALSE	FALSE	FALSE	FALSE	FALSE	FALSE	FALSE
WSF3D1M1_BURNT_50X_12	x5_y3.png	FALSE	FALSE	FALSE	FALSE	FALSE	FALSE	FALSE
SWF2FR1_BURNT_2_5X_2	x4_y4.png	FALSE	FALSE	FALSE	FALSE	FALSE	FALSE	FALSE
WS Fresh_50X_3	x0_y7.png	FALSE	FALSE	FALSE	FALSE	FALSE	FALSE	FALSE
WSF3D1M5_SMALLPIECE_BURNT_50X_4	x1_y2.png	FALSE	FALSE	FALSE	FALSE	FALSE	FALSE	FALSE
WSF3D1M4_NO2_BURNT_50X_1	x9_y5.png	FALSE	FALSE	TRUE	FALSE	FALSE	FALSE	FALSE
WS Fresh	x5_y0.png	FALSE	FALSE	FALSE	FALSE	FALSE	FALSE	FALSE
WSF3D1M3_UNBURNT_1_50X_5	x9_y8.png	FALSE	TRUE	FALSE	FALSE	FALSE	FALSE	FALSE
WSF3D1M1_BURNT_50X_10	x1_y8.png	FALSE	FALSE	FALSE	FALSE	FALSE	FALSE	FALSE
SWF1_BURNT_4_50X_3	x3_y2.png	FALSE	FALSE	TRUE	FALSE	FALSE	FALSE	FALSE
WSF3D1M3_UNBURNT_2_50X_1	x7_y2.png	FALSE	TRUE	FALSE	FALSE	FALSE	FALSE	FALSE
SWF1FR2_BURNT_50X_2	x8_y3.png	FALSE	TRUE	FALSE	FALSE	FALSE	FALSE	FALSE
SWF1FR2_BURNT_50X_2	x5_y6.png	FALSE	TRUE	FALSE	FALSE	FALSE	FALSE	FALSE
SWF1_BURNT_4_50X_1	x6_y2.png	FALSE	FALSE	FALSE	FALSE	FALSE	FALSE	FALSE
WSF3D1M2_BURNT_50X_3	x3_y1.png	FALSE	FALSE	FALSE	FALSE	FALSE	FALSE	TRUE
WSF3D1M4_BURNT_50X_2	x6_y2.png	FALSE	FALSE	FALSE	FALSE	FALSE	FALSE	TRUE
WSF3D1M3_BURNT_50X_2	x6_y5.png	FALSE	TRUE	FALSE	FALSE	FALSE	FALSE	TRUE

WSF3D1M2_BURNT_50X_1	x7_y7.png	FALSE	FALSE	TRUE	FALSE	FALSE	FALSE	FALSE
WSF3D1M4_BURNT_50X_2	x0_y1.png	FALSE	FALSE	FALSE	FALSE	FALSE	FALSE	FALSE
WSF3D1M1_BURNT_50X_4	x3_y7.png	FALSE	FALSE	FALSE	FALSE	FALSE	TRUE	TRUE
WSF3D1M3_BURNT_50X_3	x5_y0.png	FALSE	FALSE	FALSE	FALSE	FALSE	TRUE	FALSE
WSF3D1M4_BURNT_50X_2	x9_y7.png	FALSE	FALSE	TRUE	FALSE	FALSE	FALSE	TRUE
SWF1_BURNT_5_50X_2	x5_y6.png	FALSE	FALSE	TRUE	FALSE	FALSE	FALSE	TRUE
WSF3D1M2_BURNT_50X_1	x4_y6.png	FALSE	FALSE	TRUE	FALSE	FALSE	FALSE	FALSE
SWF2FR4_BURNT_50X	x6_y9.png	FALSE	FALSE	FALSE	FALSE	FALSE	FALSE	FALSE
WSF3D1M5_SMALLPIECE_BURNT_50X_4	x9_y2.png	FALSE	FALSE	FALSE	FALSE	FALSE	FALSE	FALSE
WSF3D1M5_BURNT_50X_1	x6_y9.png	FALSE	FALSE	FALSE	FALSE	FALSE	FALSE	FALSE
WSF3D1M1_BURNT_50X_6	x5_y1.png	FALSE	FALSE	FALSE	FALSE	FALSE	FALSE	FALSE
SWF2FR1_BURNT_1_5X_2	x4_y4.png	FALSE	FALSE	FALSE	FALSE	FALSE	FALSE	FALSE
SWF1FR2_BURNT_50X_1	x2_y5.png	FALSE	FALSE	FALSE	FALSE	FALSE	FALSE	TRUE
WSF3D1M2_BURNT_50X_3	x2_y6.png	FALSE	FALSE	FALSE	FALSE	FALSE	FALSE	FALSE
SWF2FR1_BURNT_1_5X	x4_y6.png	FALSE	FALSE	FALSE	FALSE	FALSE	FALSE	FALSE
WSF3D1M1_BURNT_50X_9	x4_y0.png	FALSE	FALSE	FALSE	FALSE	FALSE	FALSE	TRUE
WSF3D1M3_UNBURNT_1_50X_3	x0_y2.png	FALSE	TRUE	FALSE	FALSE	FALSE	FALSE	TRUE
SWF1_BURNT_5_50X_3	x1_y0.png	FALSE	FALSE	FALSE	FALSE	FALSE	FALSE	FALSE
WSF3D1M4_NO2_BURNT_50X_2	x8_y9.png	FALSE	FALSE	FALSE	FALSE	FALSE	FALSE	FALSE
WSF3D1M3_BURNT_50X_2	x3_y5.png	FALSE	FALSE	FALSE	FALSE	FALSE	FALSE	TRUE
WSF3D1M1_BURNT_50X_10	x6_y5.png	FALSE	FALSE	FALSE	FALSE	FALSE	FALSE	FALSE

SWF2FR1_BURNT_2_5X_2	x1_y4.png	FALSE	FALSE	TRUE	FALSE	FALSE	FALSE	FALSE
WSF3D1M3_UNBURNT_1_50X_5	x7_y8.png	FALSE	FALSE	FALSE	FALSE	FALSE	FALSE	FALSE
WSF3D1M3_UNBURNT_1_50X_4	x0_y6.png	FALSE	TRUE	FALSE	FALSE	FALSE	FALSE	FALSE
SWF1_BURNT_4_50X_1	x8_y5.png	FALSE	FALSE	FALSE	FALSE	FALSE	FALSE	FALSE
WS Fresh	x9_y3.png	FALSE	FALSE	FALSE	FALSE	FALSE	FALSE	FALSE
SWF2FR4_BURNT_50X	x0_y9.png	FALSE	FALSE	FALSE	FALSE	FALSE	FALSE	FALSE
WSF3D1M5_BURNT_50X_2	x3_y4.png	FALSE	FALSE	FALSE	FALSE	FALSE	FALSE	FALSE
WSF3D1M1_BURNT_50X_10	x5_y0.png	FALSE	FALSE	FALSE	FALSE	FALSE	FALSE	FALSE
SWF1_BURNT_3_50X_1	x1_y6.png	FALSE	FALSE	FALSE	FALSE	FALSE	FALSE	FALSE
WSF3D1M5_BURNT_50X_2	x9_y4.png	FALSE	FALSE	FALSE	FALSE	FALSE	FALSE	FALSE
WSF3D1M1_BURNT_50X_2	x3_y5.png	FALSE	TRUE	FALSE	FALSE	FALSE	FALSE	FALSE
WSF3D1M4_BURNT_50X_3	x3_y1.png	FALSE	TRUE	FALSE	FALSE	FALSE	FALSE	TRUE
SWF1FR2_BURNT_50X_1	x2_y6.png	FALSE	TRUE	FALSE	FALSE	FALSE	FALSE	FALSE
WSF3D1M4_BURNT_50X_4	x9_y0.png	FALSE	FALSE	FALSE	FALSE	FALSE	FALSE	TRUE
WSF3D1M2_BURNT_50X_4	x7_y1.png	FALSE	FALSE	TRUE	FALSE	FALSE	FALSE	FALSE
WS Fresh_50X_3	x1_y4.png	FALSE	FALSE	TRUE	FALSE	FALSE	FALSE	FALSE
SWF1_BURNT_4_50X_2	x7_y7.png	FALSE	FALSE	FALSE	FALSE	FALSE	FALSE	FALSE
SWF1_BURNT_5_50X_2	x1_y6.png	FALSE	FALSE	TRUE	FALSE	FALSE	FALSE	FALSE
WSF3D1M4_NO2_BURNT_50X_1	x2_y9.png	FALSE	FALSE	FALSE	FALSE	FALSE	FALSE	FALSE
WSF3D1M3_BURNT_50X_1	x9_y9.png	TRUE	FALSE	FALSE	FALSE	FALSE	FALSE	FALSE
WSF3D1M3_UNBURNT_1_50X_3	x4_y7.png	FALSE	TRUE	FALSE	FALSE	TRUE	FALSE	FALSE
WSF3D1M5_BURNT_50X_3	x3_y4.png	FALSE	FALSE	FALSE	FALSE	FALSE	FALSE	FALSE

SWF1_BURNT_4_50X_2	x2_y5.png	FALSE	FALSE	FALSE	FALSE	FALSE	FALSE	FALSE
SWF2FR1_BURNT_1_5X_2	x2_y4.png	FALSE	FALSE	FALSE	FALSE	FALSE	FALSE	FALSE
WSF3D1M1_BURNT_50X_12	x8_y4.png	FALSE	FALSE	TRUE	FALSE	FALSE	FALSE	FALSE
SWF1_BURNT_4_50X_2	x0_y5.png	FALSE	FALSE	FALSE	FALSE	FALSE	FALSE	FALSE
WSF3D1M2_BURNT_50X_6	x5_y5.png	TRUE	FALSE	FALSE	FALSE	FALSE	FALSE	FALSE
WSF3D1M1_BURNT_50X_7	x6_y7.png	FALSE	FALSE	FALSE	FALSE	FALSE	FALSE	TRUE
WSF3D1M1_BURNT_50X_10	x4_y0.png	FALSE	FALSE	FALSE	FALSE	FALSE	FALSE	FALSE
WSF3D1M3_UNBURNT_2_50X_1	x6_y2.png	FALSE	TRUE	FALSE	FALSE	FALSE	FALSE	FALSE
WSF3D1M4_NO2_BURNT_50X_1	x1_y2.png	FALSE	FALSE	FALSE	FALSE	FALSE	FALSE	FALSE
WSF3D1M1_BURNT_50X_6	x4_y3.png	FALSE	FALSE	FALSE	FALSE	FALSE	FALSE	FALSE
WSF3D1M1_BURNT_50X_9	x1_y6.png	FALSE	FALSE	FALSE	FALSE	FALSE	FALSE	TRUE
WS Fresh	x2_y3.png	FALSE	FALSE	FALSE	FALSE	FALSE	FALSE	FALSE
SWF1_BURNT_5_50X_2	x7_y1.png	FALSE	FALSE	FALSE	FALSE	FALSE	FALSE	FALSE
SWF1_BURNT_5_50X_1	x9_y9.png	FALSE	FALSE	FALSE	FALSE	FALSE	FALSE	FALSE
SWF2FR1_BURNT_1_5X_2	x3_y7.png	FALSE	FALSE	FALSE	FALSE	FALSE	FALSE	FALSE
WSF3D1M2_BURNT_50X_5	x6_y4.png	FALSE	FALSE	FALSE	FALSE	FALSE	FALSE	FALSE
WSF3D1M2_BURNT_50X_5	x9_y2.png	TRUE	FALSE	FALSE	FALSE	FALSE	FALSE	FALSE
WSF3D1M4_BURNT_50X_4	x7_y6.png	FALSE	TRUE	FALSE	FALSE	FALSE	FALSE	TRUE
WS Fresh_50X_2	x7_y6.png	FALSE	FALSE	TRUE	FALSE	FALSE	FALSE	FALSE
SWF2FR1_BURNT_1_5X	x3_y3.png	FALSE	FALSE	FALSE	FALSE	FALSE	FALSE	FALSE
WSF3D1M3_BURNT_50X_3	x3_y7.png	FALSE	FALSE	TRUE	FALSE	FALSE	FALSE	FALSE

SWF2FR1_BURNT_1_5X_2	x0_y0.png	FALSE	FALSE	FALSE	FALSE	FALSE	FALSE	FALSE
WSF3D1M3_BURNT_50X_3	x5_y7.png	FALSE	FALSE	FALSE	FALSE	FALSE	FALSE	FALSE
SWF2FR1_BURNT_2_5X_1	x3_y4.png	FALSE	FALSE	FALSE	FALSE	FALSE	FALSE	FALSE
WS Fresh_50X_2	x0_y0.png	FALSE	FALSE	FALSE	FALSE	FALSE	FALSE	TRUE
SWF1_BURNT_5_50X_3	x9_y9.png	FALSE	FALSE	FALSE	FALSE	FALSE	FALSE	FALSE
SWF1FR2_BURNT_50X_3	x9_y7.png	FALSE	FALSE	FALSE	FALSE	FALSE	FALSE	FALSE
WSF3D1M2_BURNT_50X_1	x5_y0.png	TRUE	FALSE	FALSE	FALSE	FALSE	FALSE	FALSE
SWF2FR1_BURNT_2_5X_2	x9_y9.png	FALSE	FALSE	FALSE	FALSE	FALSE	FALSE	FALSE
WSF3D1M3_BURNT_50X_3	x0_y6.png	FALSE	FALSE	FALSE	FALSE	FALSE	FALSE	FALSE
WSF3D1M1_BURNT_50X_7	x8_y2.png	FALSE	FALSE	FALSE	FALSE	FALSE	FALSE	TRUE
SWF1FR2_BURNT_50X_4	x1_y9.png	FALSE	TRUE	FALSE	FALSE	FALSE	FALSE	FALSE
WSF3D1M2_BURNT_50X_5	x3_y1.png	TRUE	FALSE	FALSE	FALSE	FALSE	FALSE	FALSE
WSF3D1M3_UNBURNT_1_50X_5	x5_y3.png	FALSE	FALSE	FALSE	FALSE	FALSE	FALSE	FALSE
WSF3D1M2_BURNT_50X_4	x1_y6.png	FALSE	FALSE	FALSE	FALSE	FALSE	FALSE	FALSE
WSF3D1M5_UNBURNT_1_50X_1	x3_y5.png	FALSE	FALSE	FALSE	FALSE	FALSE	TRUE	TRUE
SWF2FR1_BURNT_1_5X	x8_y3.png	FALSE	FALSE	FALSE	FALSE	FALSE	FALSE	FALSE
SWF1_BURNT_4_50X_3	x7_y4.png	FALSE	FALSE	FALSE	FALSE	FALSE	FALSE	FALSE
WSF3D1M2_BURNT_50X_2	x8_y8.png	FALSE	FALSE	TRUE	FALSE	FALSE	FALSE	TRUE
WSF3D1M5_BURNT_50X_2	x6_y9.png	FALSE	FALSE	FALSE	FALSE	FALSE	FALSE	FALSE
WSF3D1M5_BURNT_50X_2	x8_y9.png	FALSE	FALSE	FALSE	FALSE	FALSE	FALSE	FALSE
WSF3D1M3_UNBURNT_2_50X_1	x8_y6.png	FALSE	TRUE	FALSE	FALSE	FALSE	FALSE	FALSE

WSF3D1M2_BURNT_50X_3	x9_y1.png	FALSE	FALSE	TRUE	FALSE	FALSE	FALSE	FALSE
WSF3D1M1_BURNT_50X_12	x5_y0.png	FALSE	FALSE	FALSE	FALSE	FALSE	FALSE	FALSE
SWF1FR2_BURNT_50X_1	x6_y4.png	FALSE	FALSE	FALSE	FALSE	FALSE	TRUE	FALSE
SWF1FR2_BURNT_50X_1	x3_y5.png	FALSE	FALSE	FALSE	FALSE	FALSE	FALSE	TRUE
WSF3D1M1_BURNT_50X_4	x3_y1.png	FALSE	FALSE	FALSE	FALSE	FALSE	FALSE	FALSE
SWF2FR1_BURNT_2_5X_2	x7_y0.png	FALSE	FALSE	FALSE	FALSE	FALSE	FALSE	FALSE
WSF3D1M1_BURNT_50X_10	x1_y6.png	FALSE	FALSE	FALSE	FALSE	FALSE	FALSE	TRUE
WSF3D1M3_UNBURNT_1_50X_3	x9_y7.png	FALSE	FALSE	FALSE	FALSE	FALSE	FALSE	TRUE
WSF3D1M5_SMALLPIECE_BURNT_50X_4	x8_y5.png	FALSE	FALSE	FALSE	FALSE	FALSE	FALSE	FALSE
SWF2FR1_BURNT_1_5X_2	x4_y8.png	FALSE	FALSE	FALSE	FALSE	FALSE	FALSE	FALSE
WSF3D1M3_UNBURNT_1_50X_4	x5_y3.png	FALSE	FALSE	FALSE	FALSE	FALSE	FALSE	FALSE
WSF3D1M3_UNBURNT_1_50X_5	x7_y9.png	FALSE	FALSE	FALSE	FALSE	FALSE	FALSE	FALSE
WSF3D1M1_BURNT_50X_2	x7_y3.png	FALSE	FALSE	FALSE	FALSE	FALSE	FALSE	FALSE
WSF3D1M5_SMALLPIECE_BURNT_50X_3	x6_y5.png	FALSE	FALSE	TRUE	FALSE	FALSE	FALSE	FALSE
WSF3D1M2_BURNT_50X_1	x8_y0.png	TRUE	FALSE	FALSE	FALSE	FALSE	FALSE	FALSE
SWF1_BURNT_4_50X_1	x3_y8.png	FALSE	FALSE	FALSE	FALSE	FALSE	FALSE	FALSE
WSF3D1M4_BURNT_50X_4	x1_y9.png	FALSE	FALSE	FALSE	FALSE	FALSE	FALSE	FALSE
SWF1FR2_BURNT_50X_3	x0_y3.png	FALSE	FALSE	FALSE	FALSE	FALSE	FALSE	FALSE
WSF3D1M1_BURNT_50X_9	x7_y8.png	FALSE	FALSE	FALSE	FALSE	FALSE	FALSE	FALSE
WSF3D1M5_SMALLPIECE_BURNT_50X_3	x9_y8.png	FALSE	FALSE	FALSE	FALSE	FALSE	FALSE	FALSE
WS Fresh_50X_1	x1_y2.png	FALSE	FALSE	FALSE	FALSE	FALSE	FALSE	FALSE

SWF1FR2_BURNT_50X_4	x3_y1.png	FALSE	FALSE	TRUE	FALSE	FALSE	FALSE	TRUE
WSF3D1M2_BURNT_50X_6	x6_y1.png	FALSE	FALSE	FALSE	FALSE	FALSE	FALSE	FALSE
WSF3D1M3_UNBURNT_1_50X_3	x5_y4.png	FALSE	FALSE	TRUE	FALSE	FALSE	FALSE	FALSE
WSF3D1M5_UNBURNT_1_50X_1	x3_y1.png	FALSE	FALSE	FALSE	FALSE	FALSE	FALSE	FALSE
SWF1_BURNT_4_50X_3	x5_y0.png	FALSE	FALSE	FALSE	FALSE	FALSE	FALSE	FALSE
WS Fresh_50X_3	x2_y0.png	FALSE	FALSE	FALSE	FALSE	FALSE	FALSE	FALSE
WSF3D1M4_NO2_BURNT_50X_1	x8_y9.png	FALSE	FALSE	FALSE	FALSE	FALSE	FALSE	FALSE
WSF3D1M5_BURNT_50X_1	x2_y7.png	FALSE	FALSE	FALSE	FALSE	FALSE	FALSE	FALSE
WSF3D1M3_BURNT_50X_2	x8_y1.png	FALSE	FALSE	FALSE	FALSE	FALSE	FALSE	FALSE
WSF3D1M3_BURNT_50X_3	x0_y5.png	FALSE	FALSE	FALSE	FALSE	FALSE	FALSE	FALSE
SWF1_BURNT_5_50X_3	x8_y5.png	FALSE	FALSE	FALSE	FALSE	FALSE	FALSE	FALSE
WSF3D1M5_BURNT_50X_2	x5_y2.png	FALSE	FALSE	FALSE	FALSE	FALSE	FALSE	FALSE
WSF3D1M1_BURNT_50X_2	x9_y0.png	FALSE	FALSE	FALSE	FALSE	FALSE	FALSE	FALSE
SWF1_BURNT_4_50X_1	x6_y9.png	FALSE	FALSE	FALSE	FALSE	FALSE	FALSE	FALSE
WSF3D1M1_BURNT_50X_12	x8_y1.png	FALSE	FALSE	FALSE	FALSE	FALSE	FALSE	FALSE
WS Fresh_50X_2	x9_y8.png	FALSE	FALSE	FALSE	FALSE	FALSE	FALSE	FALSE
WSF3D1M3_UNBURNT_1_50X_3	x9_y9.png	FALSE	FALSE	TRUE	FALSE	FALSE	FALSE	FALSE
WSF3D1M4_BURNT_50X_4	x1_y0.png	TRUE	FALSE	FALSE	FALSE	FALSE	FALSE	FALSE
WSF3D1M3_UNBURNT_1_50X_3	x8_y4.png	FALSE	FALSE	FALSE	FALSE	FALSE	FALSE	FALSE
WSF3D1M1_BURNT_50X_6	x5_y5.png	FALSE	FALSE	FALSE	FALSE	FALSE	FALSE	FALSE
SWF2FR1_BURNT_1_5X_2	x6_y9.png	FALSE	FALSE	FALSE	FALSE	FALSE	FALSE	FALSE

WSF3D1M3_UNBURNT_1_50X_3	x5_y9.png	FALSE	FALSE	FALSE	FALSE	FALSE	FALSE	FALSE
WSF3D1M2_BURNT_50X_4	x6_y3.png	FALSE	FALSE	FALSE	FALSE	FALSE	FALSE	FALSE
SWF1_BURNT_4_50X_1	x5_y7.png	FALSE	FALSE	FALSE	FALSE	FALSE	FALSE	FALSE
WS Fresh	x8_y8.png	FALSE	FALSE	FALSE	FALSE	FALSE	FALSE	FALSE
WSF3D1M1_BURNT_50X_6	x9_y2.png	FALSE	FALSE	FALSE	FALSE	FALSE	FALSE	FALSE
WSF3D1M3_UNBURNT_1_50X_3	x7_y1.png	FALSE	FALSE	TRUE	FALSE	FALSE	FALSE	FALSE
WS Fresh_50X_3	x6_y1.png	FALSE	FALSE	FALSE	FALSE	FALSE	FALSE	FALSE
WSF3D1M1_BURNT_50X_10	x9_y9.png	FALSE	FALSE	FALSE	FALSE	FALSE	FALSE	FALSE
SWF1_BURNT_5_50X_3	x8_y1.png	FALSE	FALSE	FALSE	FALSE	FALSE	FALSE	FALSE
WSF3D1M5_BURNT_50X_1	x5_y4.png	FALSE	FALSE	FALSE	FALSE	FALSE	FALSE	FALSE
WSF3D1M1_BURNT_50X_8	x9_y3.png	FALSE	FALSE	FALSE	FALSE	FALSE	FALSE	FALSE
WSF3D1M2_BURNT_50X_5	x4_y5.png	FALSE	FALSE	TRUE	FALSE	FALSE	FALSE	FALSE
WSF3D1M1_BURNT_50X_8	x4_y4.png	FALSE	FALSE	FALSE	FALSE	FALSE	FALSE	TRUE
SWF1FR2_BURNT_50X_1	x0_y2.png	FALSE	TRUE	FALSE	FALSE	FALSE	FALSE	FALSE
SWF1FR2_BURNT_50X_3	x5_y5.png	FALSE	TRUE	TRUE	FALSE	FALSE	FALSE	FALSE
WSF3D1M4_BURNT_50X_1	x0_y3.png	FALSE	FALSE	TRUE	FALSE	FALSE	FALSE	FALSE
SWF1FR2_BURNT_50X_2	x5_y8.png	FALSE	TRUE	TRUE	FALSE	FALSE	FALSE	FALSE
WSF3D1M1_BURNT_50X	x0_y5.png	FALSE	FALSE	TRUE	FALSE	FALSE	FALSE	FALSE
WSF3D1M5_SMALLPIECE_BURNT_50X_3	x0_y4.png	FALSE	FALSE	FALSE	FALSE	FALSE	FALSE	FALSE
WSF3D1M1_BURNT_50X_9	x6_y1.png	FALSE	TRUE	FALSE	FALSE	FALSE	FALSE	FALSE
WSF3D1M3_UNBURNT_1_50X_1	x5_y3.png	FALSE	TRUE	FALSE	FALSE	FALSE	FALSE	FALSE
WSF3D1M3_BURNT_50X_1	x7_y8.png	FALSE	FALSE	FALSE	FALSE	FALSE	FALSE	FALSE

WS Fresh	x0_y7.png	FALSE	FALSE	FALSE	FALSE	FALSE	FALSE	FALSE
WSF3D1M4_BURNT_50X_3	x4_y7.png	FALSE	TRUE	FALSE	FALSE	FALSE	FALSE	FALSE
WSF3D1M5_BURNT_50X_2	x7_y6.png	FALSE	FALSE	FALSE	FALSE	FALSE	FALSE	FALSE
WSF3D1M1_BURNT_50X_5	x1_y5.png	FALSE	TRUE	FALSE	FALSE	FALSE	FALSE	FALSE
WSF3D1M3_UNBURNT_2_50X_1	x6_y6.png	FALSE	TRUE	FALSE	FALSE	FALSE	FALSE	FALSE
WS Fresh	x7_y5.png	FALSE	FALSE	FALSE	FALSE	FALSE	FALSE	FALSE
WS Fresh_50X_1	x8_y1.png	FALSE	FALSE	FALSE	FALSE	FALSE	FALSE	FALSE
WSF3D1M1_BURNT_50X_5	x4_y6.png	FALSE	FALSE	FALSE	FALSE	FALSE	FALSE	FALSE
SWF1_BURNT_4_50X_1	x9_y1.png	FALSE	FALSE	FALSE	FALSE	FALSE	FALSE	FALSE
SWF1_BURNT_4_50X_3	x8_y1.png	FALSE	FALSE	FALSE	FALSE	FALSE	FALSE	FALSE
SWF2FR1_BURNT_2_5X_2	x7_y2.png	FALSE	FALSE	FALSE	FALSE	FALSE	FALSE	FALSE
WSF3D1M2_BURNT_50X_2	x2_y6.png	FALSE	FALSE	FALSE	FALSE	FALSE	FALSE	FALSE
WSF3D1M1_BURNT_50X_2	x2_y8.png	FALSE	FALSE	FALSE	FALSE	FALSE	FALSE	TRUE
WSF3D1M1_BURNT_50X_9	x9_y7.png	FALSE	FALSE	FALSE	FALSE	FALSE	FALSE	FALSE
SWF1_BURNT_5_50X_2	x4_y8.png	FALSE	FALSE	FALSE	FALSE	FALSE	FALSE	TRUE
WSF3D1M5_SMALLPIECE_BURNT_50X_4	x2_y8.png	FALSE	FALSE	FALSE	FALSE	FALSE	FALSE	FALSE
SWF2FR1_BURNT_1_5X_2	x3_y8.png	FALSE	FALSE	FALSE	FALSE	FALSE	FALSE	FALSE
WSF3D1M3_UNBURNT_1_50X_1	x7_y7.png	FALSE	TRUE	FALSE	FALSE	FALSE	FALSE	FALSE
WSF3D1M4_NO2_BURNT_50X_1	x4_y0.png	FALSE	FALSE	FALSE	FALSE	FALSE	FALSE	FALSE
SWF2FR4_BURNT_50X	x3_y7.png	FALSE	FALSE	FALSE	FALSE	FALSE	FALSE	FALSE
SWF1FR2_BURNT_50X_3	x7_y1.png	FALSE	FALSE	TRUE	FALSE	FALSE	FALSE	FALSE
WSF3D1M1_BURNT_50X_6	x2_y7.png	FALSE	FALSE	FALSE	FALSE	FALSE	FALSE	TRUE

SWF2FR4_BURNT_50X	x0_y0.png	FALSE	FALSE	FALSE	FALSE	FALSE	FALSE	FALSE
SWF2FR1_BURNT_2_5X_1	x7_y9.png	FALSE	FALSE	FALSE	FALSE	FALSE	FALSE	FALSE
WSF3D1M2_BURNT_50X_3	x7_y1.png	FALSE	FALSE	TRUE	FALSE	FALSE	FALSE	FALSE
SWF1_BURNT_5_50X_2	x5_y3.png	FALSE	FALSE	FALSE	FALSE	FALSE	FALSE	FALSE
SWF1_BURNT_5_50X_1	x2_y0.png	FALSE	FALSE	FALSE	FALSE	FALSE	FALSE	FALSE
SWF1FR2_BURNT_50X_4	x0_y7.png	FALSE	TRUE	FALSE	FALSE	FALSE	FALSE	FALSE
WSF3D1M1_BURNT_50X_5	x1_y0.png	FALSE	FALSE	FALSE	FALSE	FALSE	FALSE	FALSE
WSF3D1M4_BURNT_50X_2	x6_y7.png	FALSE	FALSE	FALSE	TRUE	FALSE	FALSE	FALSE
SWF2FR4_BURNT_50X	x3_y9.png	FALSE	FALSE	FALSE	FALSE	FALSE	FALSE	FALSE
WSF3D1M4_BURNT_50X_3	x9_y5.png	FALSE	FALSE	FALSE	FALSE	FALSE	FALSE	FALSE
WSF3D1M1_BURNT_50X_10	x6_y9.png	FALSE	FALSE	FALSE	FALSE	FALSE	FALSE	FALSE
WS Fresh	x2_y6.png	FALSE	FALSE	FALSE	FALSE	FALSE	FALSE	FALSE
WSF3D1M3_UNBURNT_1_50X_5	x1_y4.png	FALSE	FALSE	FALSE	FALSE	FALSE	FALSE	FALSE
WSF3D1M1_BURNT_50X_2	x4_y9.png	TRUE	FALSE	FALSE	FALSE	FALSE	FALSE	FALSE
WSF3D1M4_NO2_BURNT_50X_1	x7_y6.png	FALSE	FALSE	FALSE	FALSE	FALSE	FALSE	FALSE
WSF3D1M4_NO2_BURNT_50X_3	x9_y0.png	FALSE	FALSE	FALSE	FALSE	FALSE	FALSE	FALSE
WSF3D1M5_BURNT_50X_2	x3_y7.png	FALSE	FALSE	FALSE	FALSE	FALSE	FALSE	FALSE
SWF1_BURNT_4_50X_2	x9_y0.png	FALSE	FALSE	FALSE	FALSE	FALSE	FALSE	FALSE
SWF2FR1_BURNT_2_5X_1	x3_y3.png	FALSE	FALSE	FALSE	FALSE	FALSE	FALSE	FALSE
WSF3D1M3_BURNT_50X_3	x3_y1.png	FALSE	FALSE	FALSE	FALSE	FALSE	FALSE	FALSE
WS Fresh	x4_y9.png	FALSE	FALSE	FALSE	FALSE	FALSE	FALSE	FALSE
SWF1FR2_BURNT_50X_2	x5_y9.png	FALSE	FALSE	FALSE	FALSE	FALSE	FALSE	FALSE

SWF1FR2_BURNT_50X_3	x4_y8.png	FALSE	FALSE	FALSE	FALSE	FALSE	FALSE	FALSE
WSF3D1M1_BURNT_50X	x2_y8.png	FALSE	TRUE	FALSE	FALSE	FALSE	FALSE	FALSE
WSF3D1M2_BURNT_50X_6	x1_y1.png	FALSE	FALSE	FALSE	FALSE	FALSE	FALSE	FALSE
WSF3D1M5_UNBURNT_1_50X_1	x8_y7.png	FALSE	FALSE	FALSE	FALSE	FALSE	FALSE	FALSE
WSF3D1M2_BURNT_50X_3	x8_y8.png	FALSE	FALSE	FALSE	FALSE	FALSE	TRUE	FALSE
SWF2FR4_BURNT_50X	x4_y4.png	FALSE	FALSE	FALSE	FALSE	FALSE	FALSE	FALSE
SWF1FR2_BURNT_50X_3	x3_y0.png	FALSE	FALSE	FALSE	FALSE	FALSE	FALSE	FALSE
SWF2FR1_BURNT_1_5X	x1_y0.png	FALSE	FALSE	FALSE	FALSE	FALSE	FALSE	FALSE
SWF1_BURNT_4_50X_2	x7_y8.png	FALSE	FALSE	FALSE	FALSE	FALSE	FALSE	FALSE
WSF3D1M3_UNBURNT_1_50X_5	x4_y9.png	FALSE	FALSE	FALSE	FALSE	FALSE	FALSE	FALSE
WSF3D1M3_BURNT_50X_1	x6_y2.png	FALSE	FALSE	TRUE	FALSE	FALSE	FALSE	FALSE
SWF1FR2_BURNT_50X_4	x4_y3.png	FALSE	FALSE	FALSE	FALSE	FALSE	FALSE	FALSE
WSF3D1M3_UNBURNT_1_50X_3	x9_y3.png	FALSE	FALSE	FALSE	FALSE	FALSE	FALSE	FALSE
WSF3D1M1_BURNT_50X_10	x4_y9.png	FALSE	FALSE	FALSE	FALSE	FALSE	FALSE	FALSE
WSF3D1M3_UNBURNT_1_50X_1	x3_y1.png	FALSE	TRUE	FALSE	FALSE	FALSE	FALSE	FALSE
WSF3D1M2_BURNT_50X_6	x0_y5.png	TRUE	TRUE	FALSE	FALSE	FALSE	FALSE	FALSE
WSF3D1M2_BURNT_50X_6	x3_y8.png	FALSE	FALSE	FALSE	FALSE	FALSE	FALSE	FALSE
WSF3D1M4_NO2_BURNT_50X_2	x4_y0.png	FALSE	FALSE	FALSE	FALSE	FALSE	FALSE	FALSE
SWF1_BURNT_5_50X_1	x2_y8.png	FALSE	FALSE	FALSE	FALSE	FALSE	FALSE	FALSE
WSF3D1M2_BURNT_50X_2	x6_y4.png	FALSE	FALSE	FALSE	FALSE	FALSE	FALSE	FALSE
WSF3D1M1_BURNT_50X_8	x5_y3.png	FALSE	FALSE	FALSE	FALSE	FALSE	TRUE	FALSE
WSF3D1M1_BURNT_50X_9	x5_y9.png	FALSE	FALSE	FALSE	FALSE	FALSE	FALSE	FALSE

WSF3D1M5_BURNT_50X_2	x9_y0.png	FALSE	FALSE	FALSE	FALSE	FALSE	FALSE	FALSE
WSF3D1M1_BURNT_50X	x6_y8.png	FALSE	TRUE	FALSE	FALSE	FALSE	FALSE	FALSE
SWF2FR1_BURNT_1_5X_2	x6_y1.png	FALSE	FALSE	FALSE	FALSE	FALSE	FALSE	FALSE
WSF3D1M5_BURNT_50X_1	x6_y0.png	FALSE	FALSE	TRUE	FALSE	FALSE	FALSE	FALSE
SWF2FR4_BURNT_50X	x3_y1.png	FALSE	FALSE	FALSE	FALSE	FALSE	FALSE	FALSE
WSF3D1M2_BURNT_50X_6	x8_y8.png	FALSE	FALSE	FALSE	FALSE	FALSE	FALSE	FALSE
SWF1_BURNT_5_50X_3	x7_y7.png	FALSE	FALSE	FALSE	FALSE	FALSE	FALSE	FALSE
SWF1_BURNT_5_50X_1	x5_y0.png	FALSE	FALSE	FALSE	FALSE	FALSE	FALSE	FALSE
WS Fresh_50X_3	x3_y3.png	FALSE	FALSE	FALSE	FALSE	FALSE	FALSE	FALSE
WSF3D1M1_BURNT_50X_3	x0_y6.png	FALSE	FALSE	FALSE	FALSE	FALSE	FALSE	FALSE
WSF3D1M2_BURNT_50X_5	x3_y7.png	FALSE	FALSE	FALSE	FALSE	FALSE	FALSE	TRUE
SWF1FR2_BURNT_50X_3	x8_y6.png	FALSE	TRUE	FALSE	FALSE	FALSE	FALSE	FALSE
WSF3D1M1_BURNT_50X_7	x7_y8.png	FALSE	FALSE	FALSE	FALSE	FALSE	FALSE	FALSE
SWF1_BURNT_5_50X_3	x2_y3.png	TRUE	FALSE	FALSE	FALSE	FALSE	FALSE	FALSE
SWF2FR1_BURNT_2_5X_2	x5_y6.png	FALSE	FALSE	FALSE	FALSE	FALSE	FALSE	FALSE
WSF3D1M5_BURNT_50X_3	x2_y0.png	FALSE	FALSE	FALSE	FALSE	FALSE	FALSE	FALSE
SWF1FR2_BURNT_50X_4	x6_y9.png	FALSE	FALSE	FALSE	FALSE	FALSE	TRUE	FALSE
SWF1FR2_BURNT_50X_3	x4_y6.png	FALSE	FALSE	FALSE	FALSE	FALSE	FALSE	FALSE
SWF1_BURNT_4_50X_1	x6_y7.png	FALSE	FALSE	FALSE	FALSE	FALSE	FALSE	FALSE
SWF2FR1_BURNT_1_5X	x7_y4.png	FALSE	FALSE	FALSE	FALSE	FALSE	FALSE	FALSE
WSF3D1M2_BURNT_50X_4	x3_y3.png	FALSE	FALSE	FALSE	FALSE	FALSE	FALSE	FALSE
WSF3D1M1_BURNT_50X_3	x7_y9.png	FALSE	FALSE	FALSE	FALSE	FALSE	FALSE	FALSE
SWF2FR1_BURNT_2_5X_2	x3_y7.png	FALSE	FALSE	FALSE	FALSE	FALSE	FALSE	FALSE

WSF3D1M2_BURNT_50X_2	x7_y0.png	FALSE	FALSE	FALSE	FALSE	FALSE	FALSE	FALSE
WSF3D1M3_BURNT_50X_2	x4_y2.png	FALSE	FALSE	FALSE	FALSE	FALSE	FALSE	TRUE
WSF3D1M4_NO2_BURNT_50X_1	x5_y0.png	FALSE	FALSE	TRUE	FALSE	FALSE	FALSE	FALSE
WSF3D1M5_SMALLPIECE_BURNT_50X_3	x1_y1.png	FALSE	FALSE	FALSE	FALSE	FALSE	FALSE	FALSE
WSF3D1M1_BURNT_50X_3	x9_y3.png	FALSE	FALSE	FALSE	FALSE	FALSE	FALSE	FALSE
WSF3D1M5_BURNT_50X_2	x1_y9.png	FALSE	FALSE	FALSE	FALSE	FALSE	FALSE	FALSE
WSF3D1M1_BURNT_50X_3	x3_y1.png	FALSE	FALSE	FALSE	FALSE	FALSE	FALSE	TRUE
SWF1_BURNT_5_50X_2	x6_y7.png	FALSE	FALSE	FALSE	FALSE	FALSE	FALSE	FALSE
WSF3D1M3_UNBURNT_1_50X_4	x8_y0.png	FALSE	FALSE	TRUE	FALSE	FALSE	FALSE	FALSE
WSF3D1M1_BURNT_50X_9	x6_y8.png	FALSE	FALSE	FALSE	FALSE	FALSE	FALSE	FALSE
WS Fresh_50X_3	x5_y0.png	TRUE	FALSE	FALSE	FALSE	FALSE	FALSE	FALSE
SWF1_BURNT_5_50X_1	x7_y3.png	FALSE	FALSE	FALSE	FALSE	FALSE	FALSE	TRUE
WSF3D1M2_BURNT_50X_5	x1_y6.png	FALSE	FALSE	FALSE	FALSE	FALSE	FALSE	FALSE
WSF3D1M5_BURNT_50X_1	x3_y9.png	FALSE	FALSE	FALSE	FALSE	FALSE	FALSE	FALSE
WSF3D1M5_BURNT_50X_3	x6_y3.png	FALSE	FALSE	FALSE	FALSE	FALSE	FALSE	FALSE
WSF3D1M5_BURNT_50X_3	x7_y9.png	FALSE	FALSE	FALSE	FALSE	FALSE	TRUE	FALSE
WSF3D1M5_BURNT_50X_3	x4_y5.png	FALSE	FALSE	FALSE	FALSE	FALSE	FALSE	FALSE
WSF3D1M2_BURNT_50X_2	x1_y2.png	FALSE	FALSE	TRUE	FALSE	FALSE	FALSE	FALSE
WS Fresh_50X_2	x8_y8.png	FALSE	FALSE	FALSE	FALSE	FALSE	TRUE	FALSE
WSF3D1M1_BURNT_50X_8	x9_y1.png	FALSE	FALSE	FALSE	FALSE	FALSE	FALSE	FALSE

WSF3D1M3_BURNT_50X_2	x0_y3.png	FALSE	FALSE	FALSE	FALSE	FALSE	TRUE	FALSE
WSF3D1M2_BURNT_50X_5	x6_y6.png	FALSE	FALSE	FALSE	FALSE	FALSE	FALSE	FALSE
WSF3D1M4_NO2_BURNT_50X_3	x7_y2.png	FALSE	FALSE	FALSE	FALSE	FALSE	FALSE	FALSE
WSF3D1M1_BURNT_50X_9	x9_y6.png	FALSE	FALSE	FALSE	FALSE	FALSE	FALSE	FALSE
WSF3D1M4_BURNT_50X_3	x2_y9.png	FALSE	FALSE	FALSE	FALSE	FALSE	FALSE	FALSE
SWF1_BURNT_5_50X_2	x4_y3.png	FALSE	FALSE	FALSE	FALSE	FALSE	FALSE	FALSE
WSF3D1M4_BURNT_50X_3	x7_y0.png	FALSE	FALSE	TRUE	FALSE	FALSE	FALSE	FALSE
WSF3D1M1_BURNT_50X_7	x9_y8.png	FALSE	FALSE	FALSE	FALSE	FALSE	FALSE	FALSE
SWF2FR1_BURNT_1_5X	x7_y1.png	FALSE	FALSE	FALSE	FALSE	FALSE	FALSE	FALSE
WS Fresh_50X_1	x2_y7.png	FALSE	FALSE	FALSE	FALSE	FALSE	FALSE	FALSE
WS Fresh_50X_1	x5_y2.png	FALSE	FALSE	FALSE	FALSE	FALSE	FALSE	FALSE
SWF1_BURNT_4_50X_2	x3_y5.png	FALSE	FALSE	FALSE	FALSE	FALSE	FALSE	FALSE
SWF1_BURNT_5_50X_2	x6_y2.png	FALSE	FALSE	FALSE	FALSE	FALSE	FALSE	FALSE
SWF2FR1_BURNT_1_5X	x8_y5.png	FALSE	FALSE	FALSE	FALSE	FALSE	FALSE	FALSE
WSF3D1M1_BURNT_50X_7	x7_y2.png	FALSE	FALSE	FALSE	FALSE	FALSE	FALSE	FALSE
WSF3D1M5_BURNT_50X_3	x9_y9.png	FALSE	FALSE	FALSE	FALSE	FALSE	FALSE	FALSE
SWF2FR1_BURNT_1_5X_2	x8_y4.png	FALSE	FALSE	FALSE	FALSE	FALSE	FALSE	FALSE
WSF3D1M3_UNBURNT_1_50X_4	x5_y2.png	FALSE	FALSE	FALSE	FALSE	FALSE	FALSE	FALSE
WSF3D1M4_NO2_BURNT_50X_1	x5_y1.png	FALSE	FALSE	FALSE	FALSE	FALSE	FALSE	FALSE
WSF3D1M1_BURNT_50X_5	x7_y2.png	FALSE	FALSE	FALSE	FALSE	FALSE	FALSE	FALSE
WSF3D1M5_BURNT_50X_2	x1_y0.png	FALSE	FALSE	FALSE	FALSE	FALSE	FALSE	FALSE
WS Fresh_50X_2	x9_y7.png	FALSE	FALSE	FALSE	FALSE	FALSE	FALSE	FALSE

WS Fresh_50X_2	x6_y4.png	FALSE	FALSE	FALSE	FALSE	FALSE	FALSE	FALSE
SWF1FR2_BURNT_50X_3	x1_y2.png	FALSE	FALSE	FALSE	FALSE	FALSE	FALSE	FALSE
SWF2FR1_BURNT_2_5X_2	x4_y0.png	FALSE	FALSE	FALSE	FALSE	FALSE	FALSE	FALSE
WSF3D1M4_NO2_BURNT_50X_2	x3_y0.png	FALSE	FALSE	FALSE	FALSE	FALSE	FALSE	FALSE
SWF1_BURNT_5_50X_2	x5_y1.png	FALSE	FALSE	FALSE	FALSE	FALSE	FALSE	FALSE
WSF3D1M4_BURNT_50X_2	x6_y6.png	FALSE	TRUE	FALSE	FALSE	FALSE	FALSE	FALSE
WSF3D1M4_NO2_BURNT_50X_3	x9_y8.png	FALSE	FALSE	FALSE	FALSE	FALSE	FALSE	FALSE
SWF1_BURNT_5_50X_1	x6_y9.png	FALSE	FALSE	FALSE	FALSE	FALSE	FALSE	FALSE
WS Fresh_50X_1	x0_y7.png	FALSE	FALSE	FALSE	FALSE	FALSE	FALSE	FALSE
WSF3D1M3_UNBURNT_1_50X_5	x3_y4.png	FALSE	FALSE	FALSE	FALSE	FALSE	FALSE	FALSE
SWF1_BURNT_5_50X_3	x9_y7.png	FALSE	FALSE	FALSE	FALSE	FALSE	FALSE	FALSE
WSF3D1M4_BURNT_50X_3	x6_y3.png	FALSE	FALSE	FALSE	FALSE	FALSE	FALSE	FALSE
WSF3D1M4_BURNT_50X_3	x5_y2.png	FALSE	FALSE	FALSE	FALSE	FALSE	TRUE	FALSE
SWF1_BURNT_3_50X_1	x3_y4.png	FALSE	FALSE	FALSE	FALSE	FALSE	FALSE	FALSE
SWF1_BURNT_3_50X_1	x5_y5.png	FALSE	FALSE	FALSE	FALSE	FALSE	TRUE	FALSE
WSF3D1M1_BURNT_50X_7	x7_y3.png	FALSE	FALSE	FALSE	FALSE	FALSE	FALSE	FALSE
SWF1FR2_BURNT_50X_4	x0_y4.png	FALSE	FALSE	TRUE	FALSE	FALSE	FALSE	FALSE
WSF3D1M1_BURNT_50X_3	x6_y1.png	FALSE	FALSE	TRUE	FALSE	FALSE	FALSE	FALSE
WSF3D1M2_BURNT_50X_1	x2_y4.png	FALSE	FALSE	FALSE	FALSE	FALSE	FALSE	FALSE
WSF3D1M3_UNBURNT_1_50X_1	x4_y9.png	FALSE	TRUE	FALSE	FALSE	FALSE	FALSE	FALSE
SWF1_BURNT_4_50X_2	x6_y5.png	FALSE	FALSE	FALSE	FALSE	FALSE	FALSE	FALSE
WS Fresh_50X_3	x8_y2.png	FALSE	FALSE	FALSE	FALSE	FALSE	FALSE	FALSE
WSF3D1M1_BURNT_50X_12	x3_y9.png	FALSE	FALSE	FALSE	FALSE	FALSE	FALSE	FALSE

SWF1_BURNT_3_50X_1	x4_y9.png	FALSE	FALSE	FALSE	FALSE	FALSE	FALSE	TRUE
WSF3D1M3_BURNT_50X_3	x3_y5.png	FALSE	FALSE	FALSE	FALSE	FALSE	TRUE	TRUE
WSF3D1M2_BURNT_50X_5	x7_y7.png	FALSE	FALSE	FALSE	FALSE	FALSE	FALSE	FALSE
WSF3D1M5_BURNT_50X_2	x0_y0.png	FALSE	FALSE	FALSE	FALSE	FALSE	FALSE	FALSE
WSF3D1M1_BURNT_50X_10	x0_y5.png	FALSE	FALSE	FALSE	FALSE	FALSE	FALSE	FALSE
WSF3D1M1_BURNT_50X_2	x5_y8.png	FALSE	FALSE	FALSE	FALSE	FALSE	FALSE	FALSE
WSF3D1M2_BURNT_50X_4	x0_y1.png	FALSE	FALSE	FALSE	FALSE	FALSE	FALSE	FALSE
WSF3D1M1_BURNT_50X_6	x3_y2.png	FALSE	FALSE	FALSE	FALSE	FALSE	FALSE	TRUE
WSF3D1M5_SMALLPIECE_BURNT_50X_4	x3_y3.png	FALSE	FALSE	FALSE	FALSE	FALSE	FALSE	FALSE
SWF2FR1_BURNT_1_5X	x7_y7.png	FALSE	FALSE	FALSE	FALSE	FALSE	FALSE	FALSE
WSF3D1M5_BURNT_50X_1	x5_y5.png	FALSE	FALSE	FALSE	FALSE	FALSE	FALSE	FALSE
SWF2FR1_BURNT_1_5X_2	x9_y1.png	FALSE	FALSE	FALSE	FALSE	FALSE	FALSE	FALSE
SWF2FR1_BURNT_1_5X	x5_y1.png	FALSE	FALSE	FALSE	FALSE	FALSE	FALSE	FALSE
SWF2FR1_BURNT_2_5X_2	x3_y8.png	FALSE	FALSE	FALSE	FALSE	FALSE	TRUE	FALSE
SWF1_BURNT_3_50X_1	x0_y6.png	FALSE	FALSE	FALSE	FALSE	FALSE	FALSE	FALSE
WSF3D1M1_BURNT_50X_9	x5_y3.png	TRUE	FALSE	FALSE	FALSE	FALSE	FALSE	FALSE
WSF3D1M1_BURNT_50X_10	x2_y8.png	FALSE	FALSE	FALSE	FALSE	FALSE	FALSE	FALSE
WSF3D1M1_BURNT_50X_4	x6_y0.png	FALSE	FALSE	FALSE	FALSE	FALSE	FALSE	TRUE
SWF1FR2_BURNT_50X_2	x4_y1.png	FALSE	TRUE	FALSE	FALSE	FALSE	FALSE	FALSE
WSF3D1M5_BURNT_50X_3	x9_y5.png	FALSE	FALSE	FALSE	FALSE	FALSE	FALSE	FALSE
WSF3D1M3_UNBURNT_1_50X_3	x6_y2.png	FALSE	FALSE	FALSE	FALSE	FALSE	FALSE	FALSE

WSF3D1M4_NO2_BURNT_50X_3	x2_y0.png	FALSE	FALSE	FALSE	FALSE	FALSE	TRUE	FALSE
WSF3D1M5_SMALLPIECE_BURNT_50X_3	x2_y0.png	FALSE	FALSE	FALSE	FALSE	FALSE	FALSE	FALSE
WSF3D1M5_BURNT_50X_1	x4_y1.png	FALSE	FALSE	FALSE	FALSE	FALSE	TRUE	FALSE
WS Fresh_50X_3	x5_y1.png	FALSE	FALSE	FALSE	FALSE	FALSE	FALSE	TRUE
WSF3D1M3_BURNT_50X_2	x2_y0.png	FALSE	FALSE	FALSE	FALSE	FALSE	FALSE	FALSE
WSF3D1M3_UNBURNT_1_50X_4	x2_y7.png	FALSE	TRUE	FALSE	FALSE	FALSE	FALSE	FALSE
WSF3D1M2_BURNT_50X_1	x7_y4.png	FALSE	FALSE	TRUE	FALSE	FALSE	FALSE	FALSE
SWF2FR1_BURNT_2_5X_1	x8_y2.png	FALSE	FALSE	FALSE	FALSE	FALSE	FALSE	FALSE
WS Fresh	x5_y8.png	FALSE	FALSE	FALSE	FALSE	FALSE	FALSE	FALSE
WSF3D1M1_BURNT_50X_10	x5_y5.png	FALSE	FALSE	FALSE	FALSE	FALSE	FALSE	FALSE
SWF2FR1_BURNT_2_5X_2	x8_y9.png	FALSE	FALSE	FALSE	FALSE	FALSE	FALSE	FALSE
SWF1_BURNT_4_50X_2	x7_y5.png	FALSE	FALSE	FALSE	FALSE	FALSE	FALSE	FALSE
WSF3D1M1_BURNT_50X_10	x7_y8.png	FALSE	FALSE	FALSE	FALSE	FALSE	FALSE	FALSE
WSF3D1M4_NO2_BURNT_50X_3	x3_y9.png	FALSE	FALSE	FALSE	FALSE	FALSE	FALSE	FALSE
WSF3D1M3_UNBURNT_1_50X_4	x5_y1.png	FALSE	FALSE	FALSE	FALSE	FALSE	FALSE	FALSE
WSF3D1M1_BURNT_50X_7	x0_y0.png	FALSE	FALSE	FALSE	FALSE	FALSE	FALSE	FALSE
WSF3D1M4_NO2_BURNT_50X_2	x3_y8.png	FALSE	FALSE	FALSE	FALSE	FALSE	FALSE	FALSE
SWF2FR1_BURNT_1_5X	x5_y7.png	FALSE	FALSE	FALSE	FALSE	FALSE	FALSE	FALSE
WSF3D1M4_BURNT_50X_1	x9_y7.png	FALSE	FALSE	FALSE	FALSE	FALSE	FALSE	TRUE
WSF3D1M2_BURNT_50X_4	x4_y6.png	FALSE	FALSE	FALSE	FALSE	FALSE	FALSE	FALSE
SWF1FR2_BURNT_50X_4	x1_y0.png	FALSE	FALSE	FALSE	FALSE	FALSE	FALSE	FALSE

WSF3D1M3_UNBURNT_1_50X_3	x4_y2.png	FALSE	FALSE	TRUE	FALSE	FALSE	FALSE	FALSE
WS Fresh_50X_1	x0_y4.png	FALSE	FALSE	FALSE	FALSE	FALSE	FALSE	FALSE
WSF3D1M4_NO2_BURNT_50X_3	x6_y7.png	FALSE	FALSE	FALSE	FALSE	FALSE	FALSE	FALSE
WSF3D1M5_BURNT_50X_1	x1_y3.png	FALSE	FALSE	FALSE	FALSE	FALSE	FALSE	FALSE
SWF2FR1_BURNT_1_5X	x5_y6.png	FALSE	FALSE	FALSE	FALSE	FALSE	FALSE	FALSE
WSF3D1M3_BURNT_50X_3	x1_y6.png	FALSE	FALSE	FALSE	FALSE	FALSE	TRUE	FALSE
WSF3D1M1_BURNT_50X_4	x4_y8.png	FALSE	TRUE	FALSE	FALSE	FALSE	FALSE	FALSE
WSF3D1M2_BURNT_50X_2	x4_y3.png	FALSE	TRUE	FALSE	FALSE	FALSE	FALSE	FALSE
WSF3D1M5_BURNT_50X_1	x2_y6.png	FALSE	FALSE	FALSE	FALSE	FALSE	FALSE	FALSE
WSF3D1M2_BURNT_50X_2	x6_y9.png	FALSE	FALSE	FALSE	FALSE	FALSE	FALSE	FALSE
WSF3D1M1_BURNT_50X_10	x3_y4.png	FALSE	FALSE	FALSE	FALSE	FALSE	FALSE	FALSE
WSF3D1M2_BURNT_50X_3	x5_y3.png	FALSE	FALSE	FALSE	FALSE	FALSE	FALSE	FALSE
WSF3D1M4_BURNT_50X_4	x3_y9.png	FALSE	FALSE	FALSE	FALSE	FALSE	FALSE	TRUE
SWF1_BURNT_5_50X_1	x7_y8.png	FALSE	FALSE	FALSE	FALSE	FALSE	FALSE	TRUE
WSF3D1M5_UNBURNT_1_50X_1	x4_y8.png	FALSE	FALSE	FALSE	FALSE	FALSE	FALSE	FALSE
SWF2FR1_BURNT_2_5X_2	x4_y2.png	FALSE	FALSE	FALSE	FALSE	FALSE	FALSE	FALSE
WSF3D1M2_BURNT_50X_3	x0_y0.png	FALSE	FALSE	FALSE	FALSE	FALSE	FALSE	FALSE
SWF1_BURNT_5_50X_1	x0_y2.png	FALSE	FALSE	FALSE	FALSE	FALSE	FALSE	FALSE
WSF3D1M1_BURNT_50X_4	x7_y5.png	FALSE	FALSE	FALSE	FALSE	FALSE	FALSE	FALSE
WSF3D1M4_BURNT_50X_2	x0_y3.png	FALSE	FALSE	FALSE	FALSE	FALSE	FALSE	FALSE

WSF3D1M5_BURNT_50X_1	x4_y9.png	FALSE	FALSE	FALSE	FALSE	FALSE	FALSE	FALSE
WSF3D1M5_SMALLPIECE_BURNT_50X_3	x7_y2.png	FALSE	FALSE	FALSE	FALSE	FALSE	FALSE	TRUE
WSF3D1M1_BURNT_50X	x1_y4.png	FALSE	FALSE	FALSE	FALSE	FALSE	FALSE	FALSE
WSF3D1M1_BURNT_50X_5	x3_y7.png	FALSE	FALSE	FALSE	FALSE	FALSE	FALSE	FALSE
SWF2FR1_BURNT_2_5X_2	x3_y2.png	FALSE	FALSE	FALSE	FALSE	FALSE	FALSE	FALSE
WSF3D1M5_BURNT_50X_1	x8_y9.png	FALSE	FALSE	FALSE	FALSE	FALSE	FALSE	FALSE
WSF3D1M2_BURNT_50X_4	x8_y4.png	FALSE	FALSE	FALSE	FALSE	FALSE	FALSE	FALSE
WSF3D1M1_BURNT_50X_5	x4_y8.png	FALSE	FALSE	FALSE	FALSE	FALSE	FALSE	FALSE
SWF1_BURNT_4_50X_1	x5_y3.png	FALSE	FALSE	FALSE	FALSE	FALSE	FALSE	FALSE
WS Fresh	x2_y2.png	FALSE	FALSE	FALSE	FALSE	FALSE	FALSE	FALSE
WSF3D1M2_BURNT_50X_2	x1_y7.png	FALSE	FALSE	FALSE	FALSE	FALSE	FALSE	FALSE
SWF1_BURNT_3_50X_1	x3_y9.png	FALSE	FALSE	FALSE	FALSE	FALSE	FALSE	FALSE
WSF3D1M1_BURNT_50X_3	x2_y4.png	FALSE	FALSE	FALSE	FALSE	FALSE	FALSE	FALSE
WS Fresh	x7_y9.png	FALSE	FALSE	FALSE	FALSE	FALSE	FALSE	FALSE
WSF3D1M1_BURNT_50X_5	x2_y7.png	FALSE	FALSE	TRUE	FALSE	FALSE	FALSE	FALSE
WSF3D1M3_BURNT_50X_1	x2_y3.png	FALSE	FALSE	FALSE	FALSE	FALSE	FALSE	FALSE
SWF2FR1_BURNT_1_5X_2	x3_y2.png	FALSE	FALSE	FALSE	FALSE	FALSE	FALSE	FALSE
WSF3D1M1_BURNT_50X_9	x8_y1.png	FALSE	FALSE	FALSE	FALSE	FALSE	FALSE	FALSE
WS Fresh	x3_y8.png	FALSE	FALSE	FALSE	FALSE	FALSE	FALSE	FALSE
WSF3D1M1_BURNT_50X_6	x8_y2.png	FALSE	FALSE	FALSE	FALSE	FALSE	FALSE	FALSE
WSF3D1M3_BURNT_50X_1	x6_y5.png	TRUE	FALSE	FALSE	FALSE	FALSE	FALSE	FALSE

WSF3D1M3_UNBURNT_2_50X_1	x1_y2.png	TRUE	TRUE	FALSE	FALSE	FALSE	FALSE	FALSE
SWF2FR1_BURNT_2_5X_2	x1_y6.png	FALSE	FALSE	FALSE	FALSE	FALSE	FALSE	FALSE
WS Fresh_50X_2	x7_y4.png	FALSE	FALSE	FALSE	FALSE	FALSE	FALSE	FALSE
WSF3D1M5_SMALLPIECE_BURNT_50X_4	x0_y1.png	FALSE	FALSE	FALSE	FALSE	FALSE	FALSE	FALSE
WSF3D1M1_BURNT_50X_3	x8_y5.png	FALSE	FALSE	FALSE	FALSE	FALSE	FALSE	FALSE
WSF3D1M1_BURNT_50X_2	x2_y2.png	FALSE	FALSE	FALSE	FALSE	FALSE	FALSE	FALSE
WSF3D1M3_BURNT_50X_2	x5_y1.png	TRUE	FALSE	FALSE	FALSE	FALSE	FALSE	FALSE
WSF3D1M4_NO2_BURNT_50X_2	x1_y6.png	FALSE	FALSE	FALSE	FALSE	FALSE	FALSE	FALSE
WSF3D1M3_BURNT_50X_2	x7_y1.png	FALSE	FALSE	FALSE	FALSE	FALSE	FALSE	FALSE
WSF3D1M1_BURNT_50X_3	x2_y5.png	FALSE	FALSE	FALSE	FALSE	FALSE	FALSE	FALSE
WSF3D1M5_BURNT_50X_1	x4_y3.png	FALSE	FALSE	FALSE	FALSE	FALSE	FALSE	FALSE
WSF3D1M1_BURNT_50X_4	x3_y2.png	FALSE	FALSE	FALSE	FALSE	FALSE	FALSE	FALSE
SWF1FR2_BURNT_50X_1	x9_y9.png	FALSE	FALSE	FALSE	FALSE	FALSE	FALSE	FALSE
SWF2FR4_BURNT_50X	x4_y8.png	FALSE	FALSE	FALSE	FALSE	FALSE	FALSE	FALSE
WSF3D1M1_BURNT_50X_5	x2_y2.png	FALSE	FALSE	FALSE	FALSE	FALSE	FALSE	FALSE
WSF3D1M4_NO2_BURNT_50X_1	x1_y5.png	FALSE	FALSE	FALSE	FALSE	FALSE	FALSE	FALSE
WSF3D1M3_BURNT_50X_1	x8_y1.png	FALSE	FALSE	TRUE	FALSE	FALSE	FALSE	FALSE
WSF3D1M5_UNBURNT_1_50X_1	x3_y2.png	FALSE	FALSE	FALSE	FALSE	FALSE	FALSE	FALSE
WSF3D1M5_BURNT_50X_1	x4_y6.png	FALSE	FALSE	FALSE	FALSE	FALSE	FALSE	FALSE
WSF3D1M4_BURNT_50X_1	x3_y2.png	FALSE	FALSE	FALSE	FALSE	FALSE	FALSE	FALSE

SWF1FR2_BURNT_50X_4	x4_y5.png	FALSE	FALSE	FALSE	FALSE	FALSE	FALSE	FALSE
SWF2FR1_BURNT_2_5X_1	x0_y4.png	FALSE	FALSE	FALSE	FALSE	FALSE	FALSE	FALSE
WSF3D1M1_BURNT_50X	x1_y3.png	FALSE	FALSE	FALSE	FALSE	FALSE	FALSE	FALSE
SWF1_BURNT_4_50X_3	x7_y3.png	FALSE	FALSE	FALSE	FALSE	FALSE	FALSE	FALSE
WSF3D1M2_BURNT_50X_3	x5_y1.png	FALSE	FALSE	FALSE	FALSE	FALSE	FALSE	FALSE
SWF1_BURNT_5_50X_2	x7_y6.png	FALSE	FALSE	FALSE	FALSE	FALSE	FALSE	FALSE
WSF3D1M1_BURNT_50X_9	x8_y0.png	FALSE	FALSE	FALSE	FALSE	FALSE	FALSE	FALSE
WSF3D1M4_NO2_BURNT_50X_3	x1_y5.png	FALSE	FALSE	FALSE	FALSE	FALSE	FALSE	FALSE
WSF3D1M2_BURNT_50X_1	x7_y1.png	FALSE	FALSE	FALSE	FALSE	FALSE	FALSE	FALSE
SWF1_BURNT_3_50X_1	x3_y6.png	FALSE	FALSE	FALSE	FALSE	FALSE	FALSE	FALSE
SWF1FR2_BURNT_50X_4	x4_y4.png	FALSE	FALSE	TRUE	FALSE	FALSE	FALSE	FALSE
WSF3D1M4_BURNT_50X_3	x7_y7.png	FALSE	FALSE	FALSE	FALSE	FALSE	FALSE	FALSE
WSF3D1M5_BURNT_50X_2	x9_y8.png	FALSE	FALSE	FALSE	FALSE	FALSE	FALSE	FALSE
WSF3D1M4_NO2_BURNT_50X_2	x4_y6.png	FALSE	FALSE	TRUE	FALSE	FALSE	FALSE	FALSE
WSF3D1M3_BURNT_50X_3	x3_y6.png	FALSE	FALSE	FALSE	FALSE	FALSE	FALSE	TRUE
WSF3D1M1_BURNT_50X_2	x9_y3.png	FALSE	FALSE	FALSE	FALSE	FALSE	FALSE	FALSE
WSF3D1M2_BURNT_50X_5	x5_y6.png	FALSE	FALSE	FALSE	FALSE	FALSE	FALSE	TRUE
WS Fresh_50X_2	x1_y0.png	FALSE	FALSE	FALSE	FALSE	FALSE	FALSE	FALSE
SWF2FR4_BURNT_50X	x0_y4.png	FALSE	FALSE	FALSE	FALSE	FALSE	FALSE	FALSE
WSF3D1M4_BURNT_50X_3	x0_y1.png	FALSE	FALSE	FALSE	FALSE	FALSE	FALSE	FALSE
WSF3D1M4_BURNT_50X_3	x7_y5.png	TRUE	FALSE	FALSE	FALSE	FALSE	FALSE	FALSE
SWF2FR1_BURNT_1_5X_2	x4_y9.png	FALSE	FALSE	FALSE	FALSE	FALSE	FALSE	FALSE

SWF1_BURNT_4_50X_1	x9_y0.png	FALSE	FALSE	FALSE	FALSE	FALSE	FALSE	FALSE
WSF3D1M1_BURNT_50X_8	x5_y6.png	TRUE	FALSE	FALSE	FALSE	FALSE	FALSE	FALSE
WSF3D1M4_NO2_BURNT_50X_1	x3_y4.png	FALSE	FALSE	FALSE	FALSE	FALSE	FALSE	FALSE
SWF2FR1_BURNT_1_5X	x7_y6.png	FALSE	FALSE	FALSE	FALSE	FALSE	FALSE	FALSE
SWF1_BURNT_5_50X_3	x9_y3.png	FALSE	FALSE	FALSE	FALSE	FALSE	FALSE	TRUE
WS Fresh_50X_2	x1_y4.png	FALSE	FALSE	FALSE	FALSE	FALSE	FALSE	FALSE
WSF3D1M3_UNBURNT_2_50X_1	x4_y0.png	FALSE	TRUE	FALSE	FALSE	FALSE	FALSE	FALSE
SWF1_BURNT_5_50X_3	x2_y0.png	FALSE	FALSE	FALSE	FALSE	FALSE	FALSE	FALSE
WSF3D1M1_BURNT_50X_10	x1_y0.png	FALSE	FALSE	FALSE	FALSE	FALSE	FALSE	FALSE
SWF2FR1_BURNT_1_5X_2	x7_y1.png	FALSE	FALSE	FALSE	FALSE	FALSE	FALSE	FALSE
WSF3D1M2_BURNT_50X_2	x6_y8.png	FALSE	FALSE	FALSE	FALSE	FALSE	FALSE	FALSE
WSF3D1M3_BURNT_50X_3	x2_y4.png	FALSE	FALSE	FALSE	FALSE	FALSE	FALSE	FALSE
WSF3D1M1_BURNT_50X_8	x3_y3.png	FALSE	FALSE	FALSE	FALSE	FALSE	FALSE	TRUE
WSF3D1M5_SMALLPIECE_BURNT_50X_3	x5_y9.png	FALSE	FALSE	FALSE	FALSE	FALSE	FALSE	FALSE
WSF3D1M1_BURNT_50X_10	x1_y7.png	FALSE	FALSE	FALSE	FALSE	FALSE	FALSE	TRUE
SWF1_BURNT_5_50X_1	x6_y3.png	FALSE	FALSE	FALSE	FALSE	FALSE	FALSE	TRUE
SWF1_BURNT_4_50X_2	x9_y6.png	FALSE	FALSE	FALSE	FALSE	FALSE	FALSE	FALSE
WSF3D1M1_BURNT_50X_7	x5_y5.png	TRUE	FALSE	FALSE	FALSE	FALSE	FALSE	FALSE
WSF3D1M1_BURNT_50X_12	x0_y6.png	FALSE	FALSE	FALSE	FALSE	FALSE	FALSE	FALSE
WSF3D1M4_BURNT_50X_3	x9_y7.png	FALSE	FALSE	FALSE	FALSE	FALSE	FALSE	TRUE
SWF2FR4_BURNT_50X	x0_y5.png	FALSE	FALSE	FALSE	FALSE	FALSE	FALSE	FALSE
WSF3D1M4_BURNT_50X_4	x2_y4.png	FALSE	FALSE	FALSE	FALSE	FALSE	FALSE	TRUE

WSF3D1M1_BURNT_50X_4	x1_y5.png	FALSE	TRUE	FALSE	FALSE	FALSE	FALSE	FALSE
WSF3D1M1_BURNT_50X_5	x8_y4.png	FALSE	FALSE	FALSE	FALSE	FALSE	FALSE	FALSE
WSF3D1M1_BURNT_50X_5	x3_y5.png	FALSE	FALSE	FALSE	FALSE	FALSE	FALSE	TRUE
WSF3D1M3_BURNT_50X_2	x5_y6.png	FALSE	FALSE	FALSE	FALSE	FALSE	FALSE	TRUE
WSF3D1M4_BURNT_50X_4	x0_y5.png	FALSE	FALSE	FALSE	FALSE	FALSE	FALSE	FALSE
WS Fresh_50X_3	x4_y4.png	FALSE	FALSE	FALSE	FALSE	FALSE	FALSE	FALSE
SWF1FR2_BURNT_50X_1	x0_y0.png	FALSE	FALSE	FALSE	FALSE	FALSE	FALSE	TRUE
SWF1_BURNT_4_50X_1	x9_y2.png	FALSE	FALSE	FALSE	FALSE	FALSE	FALSE	FALSE
SWF2FR1_BURNT_2_5X_1	x0_y7.png	FALSE	FALSE	FALSE	FALSE	FALSE	FALSE	FALSE
WSF3D1M4_BURNT_50X_1	x2_y7.png	FALSE	FALSE	FALSE	FALSE	FALSE	FALSE	TRUE
WSF3D1M1_BURNT_50X	x6_y0.png	FALSE	FALSE	FALSE	FALSE	FALSE	FALSE	FALSE
WSF3D1M2_BURNT_50X_6	x2_y5.png	FALSE	FALSE	FALSE	FALSE	FALSE	FALSE	TRUE
WSF3D1M2_BURNT_50X_5	x9_y5.png	FALSE	FALSE	FALSE	FALSE	FALSE	FALSE	FALSE
WSF3D1M1_BURNT_50X_9	x8_y4.png	FALSE	FALSE	FALSE	FALSE	FALSE	FALSE	FALSE
WSF3D1M3_UNBURNT_2_50X_1	x2_y8.png	FALSE	FALSE	FALSE	FALSE	FALSE	FALSE	FALSE
WSF3D1M2_BURNT_50X_3	x1_y3.png	FALSE	FALSE	FALSE	FALSE	FALSE	FALSE	FALSE
SWF1_BURNT_3_50X_1	x3_y8.png	FALSE	FALSE	FALSE	FALSE	FALSE	FALSE	FALSE
WSF3D1M1_BURNT_50X_12	x9_y7.png	FALSE	FALSE	FALSE	FALSE	FALSE	FALSE	FALSE
WSF3D1M2_BURNT_50X_5	x9_y9.png	FALSE	FALSE	FALSE	FALSE	FALSE	FALSE	FALSE
WSF3D1M4_BURNT_50X_4	x2_y2.png	FALSE	FALSE	FALSE	FALSE	FALSE	FALSE	FALSE
WSF3D1M4_BURNT_50X_4	x1_y3.png	FALSE	FALSE	FALSE	FALSE	FALSE	FALSE	TRUE

WSF3D1M5_UNBURNT_1_50X_1	x9_y7.png	FALSE	FALSE	FALSE	FALSE	FALSE	FALSE	FALSE
WSF3D1M2_BURNT_50X_3	x7_y9.png	FALSE	FALSE	FALSE	FALSE	FALSE	FALSE	FALSE
WSF3D1M4_BURNT_50X_4	x1_y7.png	FALSE	FALSE	FALSE	FALSE	FALSE	FALSE	TRUE
WSF3D1M5_SMALLPIECE_BURNT_50X_3	x5_y2.png	FALSE	FALSE	FALSE	FALSE	FALSE	FALSE	TRUE
WS Fresh_50X_1	x7_y1.png	FALSE	FALSE	FALSE	FALSE	FALSE	FALSE	FALSE
SWF1_BURNT_5_50X_3	x7_y3.png	FALSE	FALSE	FALSE	FALSE	FALSE	FALSE	FALSE
SWF1FR2_BURNT_50X_3	x2_y5.png	FALSE	TRUE	FALSE	FALSE	FALSE	FALSE	FALSE
SWF2FR1_BURNT_1_5X	x2_y9.png	FALSE	FALSE	FALSE	FALSE	FALSE	FALSE	FALSE
SWF1_BURNT_4_50X_3	x2_y3.png	FALSE	FALSE	FALSE	FALSE	FALSE	FALSE	FALSE
WSF3D1M3_UNBURNT_1_50X_4	x2_y2.png	FALSE	TRUE	FALSE	FALSE	FALSE	FALSE	FALSE
WSF3D1M5_BURNT_50X_3	x3_y9.png	FALSE	FALSE	FALSE	FALSE	FALSE	FALSE	FALSE
WSF3D1M5_BURNT_50X_1	x6_y7.png	FALSE	FALSE	FALSE	FALSE	FALSE	FALSE	FALSE
WSF3D1M1_BURNT_50X_7	x8_y1.png	FALSE	FALSE	FALSE	FALSE	FALSE	FALSE	TRUE
WSF3D1M3_UNBURNT_1_50X_4	x0_y2.png	FALSE	TRUE	FALSE	FALSE	FALSE	FALSE	FALSE
WSF3D1M2_BURNT_50X_3	x3_y7.png	FALSE	FALSE	FALSE	FALSE	FALSE	FALSE	FALSE
WSF3D1M1_BURNT_50X_4	x2_y7.png	FALSE	FALSE	FALSE	FALSE	FALSE	FALSE	FALSE
WSF3D1M1_BURNT_50X_10	x7_y3.png	FALSE	FALSE	FALSE	FALSE	FALSE	FALSE	FALSE
WS Fresh_50X_1	x8_y6.png	FALSE	FALSE	FALSE	FALSE	FALSE	FALSE	FALSE
WSF3D1M4_BURNT_50X_4	x5_y0.png	FALSE	FALSE	FALSE	FALSE	FALSE	TRUE	FALSE
SWF1_BURNT_5_50X_2	x6_y5.png	FALSE	FALSE	FALSE	FALSE	FALSE	FALSE	FALSE
WSF3D1M1_BURNT_50X_2	x8_y8.png	FALSE	FALSE	FALSE	FALSE	FALSE	FALSE	FALSE

WSF3D1M5_BURNT_50X_2	x0_y3.png	FALSE	FALSE	FALSE	FALSE	FALSE	FALSE	FALSE
WSF3D1M2_BURNT_50X_3	x5_y6.png	FALSE	FALSE	TRUE	FALSE	FALSE	FALSE	FALSE
WSF3D1M2_BURNT_50X_1	x3_y7.png	FALSE	FALSE	FALSE	FALSE	FALSE	FALSE	FALSE
WS Fresh_50X_3	x2_y1.png	FALSE	FALSE	FALSE	FALSE	FALSE	FALSE	FALSE
WSF3D1M5_BURNT_50X_3	x3_y2.png	FALSE	FALSE	FALSE	FALSE	FALSE	FALSE	FALSE
WSF3D1M3_UNBURNT_1_50X_3	x6_y7.png	FALSE	FALSE	FALSE	FALSE	FALSE	FALSE	FALSE
WSF3D1M3_UNBURNT_2_50X_1	x4_y3.png	FALSE	TRUE	FALSE	FALSE	FALSE	FALSE	FALSE
SWF2FR1_BURNT_1_5X	x3_y8.png	FALSE	FALSE	FALSE	FALSE	FALSE	FALSE	FALSE
WSF3D1M1_BURNT_50X_3	x6_y2.png	FALSE	FALSE	FALSE	FALSE	FALSE	FALSE	TRUE
WSF3D1M1_BURNT_50X_7	x8_y7.png	FALSE	FALSE	FALSE	FALSE	FALSE	FALSE	FALSE
SWF2FR4_BURNT_50X	x5_y0.png	FALSE	FALSE	FALSE	FALSE	FALSE	FALSE	FALSE
WSF3D1M2_BURNT_50X_1	x0_y8.png	FALSE	FALSE	FALSE	FALSE	FALSE	FALSE	TRUE
WSF3D1M3_UNBURNT_1_50X_3	x6_y3.png	FALSE	FALSE	FALSE	FALSE	FALSE	FALSE	FALSE
WSF3D1M4_BURNT_50X_4	x7_y5.png	FALSE	FALSE	FALSE	FALSE	FALSE	FALSE	TRUE
WSF3D1M3_BURNT_50X_3	x8_y8.png	FALSE	FALSE	FALSE	FALSE	FALSE	FALSE	TRUE
WSF3D1M2_BURNT_50X_2	x8_y0.png	FALSE	FALSE	FALSE	FALSE	FALSE	FALSE	FALSE
WSF3D1M2_BURNT_50X_1	x5_y9.png	FALSE	FALSE	FALSE	FALSE	FALSE	FALSE	FALSE
SWF1_BURNT_3_50X_1	x0_y2.png	FALSE	FALSE	FALSE	FALSE	FALSE	FALSE	FALSE
SWF2FR1_BURNT_1_5X_2	x7_y7.png	FALSE	FALSE	FALSE	FALSE	FALSE	TRUE	FALSE
WSF3D1M3_UNBURNT_1_50X_5	x8_y7.png	FALSE	FALSE	FALSE	FALSE	FALSE	FALSE	TRUE

WSF3D1M2_BURNT_50X_3	x4_y6.png	FALSE	FALSE	FALSE	FALSE	FALSE	FALSE	FALSE
WSF3D1M3_UNBURNT_1_50X_3	x8_y2.png	FALSE	FALSE	FALSE	FALSE	FALSE	FALSE	TRUE
WSF3D1M4_BURNT_50X_2	x6_y8.png	FALSE	TRUE	FALSE	FALSE	FALSE	FALSE	FALSE
WSF3D1M2_BURNT_50X_5	x6_y5.png	FALSE	FALSE	FALSE	FALSE	FALSE	FALSE	FALSE
WSF3D1M5_BURNT_50X_2	x6_y3.png	FALSE	FALSE	TRUE	FALSE	FALSE	FALSE	FALSE
SWF2FR4_BURNT_50X	x3_y0.png	FALSE	FALSE	FALSE	FALSE	FALSE	FALSE	FALSE
SWF2FR1_BURNT_1_5X_2	x7_y0.png	FALSE	FALSE	FALSE	FALSE	FALSE	FALSE	FALSE
WS Fresh_50X_2	x7_y9.png	FALSE	FALSE	FALSE	FALSE	FALSE	FALSE	FALSE
WSF3D1M5_BURNT_50X_2	x8_y5.png	FALSE	FALSE	FALSE	FALSE	FALSE	FALSE	FALSE
SWF1_BURNT_4_50X_2	x5_y6.png	FALSE	FALSE	FALSE	FALSE	FALSE	FALSE	FALSE
WSF3D1M1_BURNT_50X_7	x2_y0.png	FALSE	FALSE	FALSE	FALSE	FALSE	FALSE	FALSE
WSF3D1M3_BURNT_50X_3	x6_y7.png	FALSE	FALSE	FALSE	FALSE	FALSE	FALSE	TRUE
SWF1_BURNT_4_50X_3	x0_y3.png	FALSE	FALSE	FALSE	FALSE	FALSE	FALSE	FALSE
SWF2FR1_BURNT_2_5X_1	x5_y0.png	FALSE	FALSE	FALSE	FALSE	FALSE	FALSE	FALSE
SWF1_BURNT_4_50X_3	x0_y8.png	FALSE	FALSE	FALSE	FALSE	FALSE	FALSE	FALSE
WSF3D1M2_BURNT_50X_3	x2_y0.png	FALSE	FALSE	FALSE	FALSE	FALSE	FALSE	FALSE
WSF3D1M5_SMALLPIECE_BURNT_50X_4	x8_y9.png	FALSE	FALSE	FALSE	FALSE	FALSE	FALSE	TRUE
SWF1FR2_BURNT_50X_2	x6_y6.png	FALSE	TRUE	FALSE	FALSE	FALSE	FALSE	FALSE
WSF3D1M1_BURNT_50X_4	x5_y4.png	FALSE	FALSE	FALSE	FALSE	FALSE	FALSE	FALSE
WSF3D1M1_BURNT_50X_6	x4_y5.png	FALSE	FALSE	FALSE	FALSE	FALSE	FALSE	FALSE
WSF3D1M1_BURNT_50X_6	x8_y0.png	FALSE	FALSE	FALSE	FALSE	FALSE	FALSE	FALSE

WSF3D1M3_UNBURNT_1_50X_1	x5_y8.png	FALSE	TRUE	FALSE	FALSE	FALSE	FALSE	FALSE
WSF3D1M1_BURNT_50X_8	x4_y2.png	FALSE	FALSE	FALSE	FALSE	FALSE	FALSE	FALSE
WSF3D1M1_BURNT_50X_8	x5_y9.png	FALSE	FALSE	FALSE	FALSE	FALSE	FALSE	FALSE
WSF3D1M2_BURNT_50X_3	x5_y2.png	FALSE	FALSE	FALSE	FALSE	FALSE	FALSE	TRUE
SWF1_BURNT_5_50X_2	x9_y3.png	FALSE	FALSE	FALSE	FALSE	FALSE	FALSE	TRUE
SWF1FR2_BURNT_50X_2	x2_y8.png	FALSE	FALSE	FALSE	FALSE	FALSE	FALSE	FALSE
WSF3D1M1_BURNT_50X	x4_y7.png	FALSE	FALSE	FALSE	TRUE	FALSE	FALSE	FALSE
WSF3D1M2_BURNT_50X_1	x7_y9.png	TRUE	FALSE	FALSE	FALSE	FALSE	FALSE	FALSE
WSF3D1M3_BURNT_50X_2	x1_y9.png	FALSE	FALSE	FALSE	FALSE	FALSE	FALSE	FALSE
SWF2FR4_BURNT_50X	x7_y1.png	FALSE	FALSE	FALSE	FALSE	FALSE	FALSE	FALSE
SWF1FR2_BURNT_50X_4	x6_y5.png	TRUE	TRUE	FALSE	FALSE	FALSE	FALSE	FALSE
SWF1_BURNT_5_50X_2	x5_y9.png	TRUE	FALSE	FALSE	FALSE	FALSE	FALSE	FALSE
WSF3D1M3_BURNT_50X_3	x8_y4.png	FALSE	FALSE	FALSE	FALSE	FALSE	FALSE	FALSE
WSF3D1M5_BURNT_50X_3	x8_y4.png	FALSE	FALSE	FALSE	FALSE	FALSE	FALSE	FALSE
WSF3D1M4_BURNT_50X_3	x6_y8.png	FALSE	TRUE	FALSE	FALSE	FALSE	FALSE	FALSE
WS Fresh_50X_1	x7_y0.png	FALSE	FALSE	FALSE	FALSE	FALSE	FALSE	TRUE
WSF3D1M1_BURNT_50X_5	x6_y7.png	FALSE	FALSE	FALSE	FALSE	FALSE	FALSE	FALSE
SWF2FR4_BURNT_50X	x5_y2.png	FALSE	FALSE	FALSE	FALSE	FALSE	FALSE	FALSE
WSF3D1M3_UNBURNT_2_50X_1	x7_y4.png	FALSE	TRUE	FALSE	TRUE	FALSE	FALSE	FALSE
WSF3D1M2_BURNT_50X_1	x8_y3.png	FALSE	TRUE	FALSE	FALSE	FALSE	FALSE	FALSE
WSF3D1M4_NO2_BURNT_50X_2	x2_y2.png	FALSE	FALSE	FALSE	FALSE	FALSE	FALSE	FALSE
SWF1_BURNT_5_50X_3	x7_y4.png	FALSE	FALSE	FALSE	FALSE	FALSE	FALSE	FALSE

WSF3D1M2_BURNT_50X_6	x7_y9.png	TRUE	FALSE	FALSE	FALSE	FALSE	FALSE	FALSE
SWF1FR2_BURNT_50X_3	x2_y1.png	FALSE	FALSE	FALSE	FALSE	FALSE	FALSE	FALSE
SWF1_BURNT_4_50X_2	x7_y4.png	FALSE	FALSE	FALSE	FALSE	FALSE	FALSE	FALSE
WSF3D1M1_BURNT_50X_6	x4_y1.png	FALSE	TRUE	FALSE	FALSE	FALSE	FALSE	FALSE
WSF3D1M3_UNBURNT_1_50X_4	x2_y1.png	FALSE	TRUE	FALSE	FALSE	FALSE	FALSE	FALSE
WSF3D1M1_BURNT_50X_10	x0_y4.png	FALSE	TRUE	FALSE	FALSE	FALSE	FALSE	FALSE
WSF3D1M4_NO2_BURNT_50X_2	x4_y2.png	FALSE	FALSE	FALSE	FALSE	FALSE	FALSE	FALSE
WSF3D1M3_UNBURNT_1_50X_5	x0_y3.png	FALSE	TRUE	FALSE	FALSE	FALSE	FALSE	FALSE
WSF3D1M3_BURNT_50X_2	x7_y0.png	FALSE	FALSE	FALSE	FALSE	FALSE	FALSE	FALSE
WSF3D1M2_BURNT_50X_2	x0_y1.png	FALSE	FALSE	FALSE	FALSE	FALSE	FALSE	FALSE
WSF3D1M1_BURNT_50X_2	x2_y0.png	FALSE	FALSE	FALSE	FALSE	FALSE	FALSE	FALSE
SWF2FR4_BURNT_50X	x1_y3.png	FALSE	FALSE	FALSE	FALSE	FALSE	FALSE	FALSE
WSF3D1M5_UNBURNT_1_50X_1	x7_y8.png	FALSE	FALSE	FALSE	FALSE	FALSE	FALSE	FALSE
WSF3D1M3_UNBURNT_1_50X_5	x7_y4.png	FALSE	TRUE	FALSE	FALSE	FALSE	FALSE	FALSE
WSF3D1M3_BURNT_50X_2	x1_y3.png	FALSE	FALSE	FALSE	FALSE	FALSE	FALSE	FALSE
WSF3D1M2_BURNT_50X_3	x6_y9.png	FALSE	FALSE	FALSE	FALSE	FALSE	FALSE	TRUE
WSF3D1M4_NO2_BURNT_50X_2	x1_y0.png	FALSE	FALSE	FALSE	FALSE	FALSE	FALSE	FALSE
WSF3D1M1_BURNT_50X_6	x8_y4.png	FALSE	FALSE	FALSE	FALSE	FALSE	FALSE	FALSE
WSF3D1M1_BURNT_50X_7	x8_y4.png	FALSE	FALSE	FALSE	FALSE	FALSE	FALSE	FALSE
WSF3D1M1_BURNT_50X_6	x3_y6.png	FALSE	FALSE	FALSE	FALSE	FALSE	FALSE	FALSE

SWF2FR1_BURNT_2_5X_2	x2_y5.png	FALSE	FALSE	FALSE	FALSE	FALSE	FALSE	FALSE
WSF3D1M4_NO2_BURNT_50X_3	x8_y7.png	FALSE	FALSE	FALSE	FALSE	FALSE	FALSE	FALSE
WSF3D1M4_BURNT_50X_3	x2_y1.png	FALSE	FALSE	FALSE	FALSE	FALSE	FALSE	FALSE
WSF3D1M4_NO2_BURNT_50X_1	x3_y3.png	FALSE	FALSE	FALSE	FALSE	FALSE	FALSE	FALSE
SWF1_BURNT_5_50X_2	x6_y9.png	FALSE	FALSE	FALSE	FALSE	FALSE	FALSE	TRUE
WSF3D1M1_BURNT_50X_8	x4_y9.png	FALSE	FALSE	FALSE	FALSE	FALSE	FALSE	FALSE
WSF3D1M5_UNBURNT_1_50X_1	x8_y6.png	FALSE	FALSE	FALSE	FALSE	FALSE	FALSE	FALSE
WSF3D1M4_BURNT_50X_1	x1_y1.png	FALSE	TRUE	FALSE	FALSE	FALSE	FALSE	FALSE
SWF1FR2_BURNT_50X_4	x1_y1.png	FALSE	FALSE	FALSE	FALSE	FALSE	FALSE	TRUE
WSF3D1M5_BURNT_50X_2	x8_y0.png	FALSE	FALSE	FALSE	FALSE	FALSE	FALSE	FALSE
SWF1FR2_BURNT_50X_3	x7_y3.png	FALSE	FALSE	FALSE	FALSE	FALSE	FALSE	FALSE
SWF2FR1_BURNT_2_5X_1	x9_y6.png	FALSE	FALSE	FALSE	FALSE	FALSE	FALSE	FALSE
WSF3D1M5_BURNT_50X_1	x5_y0.png	FALSE	FALSE	FALSE	FALSE	FALSE	FALSE	FALSE
WSF3D1M3_UNBURNT_1_50X_3	x7_y8.png	FALSE	TRUE	FALSE	FALSE	FALSE	FALSE	FALSE
SWF1_BURNT_4_50X_1	x7_y2.png	FALSE	FALSE	FALSE	FALSE	FALSE	FALSE	FALSE
WSF3D1M4_BURNT_50X_1	x3_y4.png	TRUE	FALSE	FALSE	FALSE	FALSE	FALSE	FALSE
SWF1_BURNT_5_50X_2	x8_y4.png	FALSE	FALSE	FALSE	FALSE	FALSE	FALSE	TRUE
WSF3D1M4_NO2_BURNT_50X_3	x9_y2.png	FALSE	FALSE	FALSE	FALSE	FALSE	FALSE	TRUE
SWF2FR1_BURNT_1_5X_2	x8_y6.png	FALSE	FALSE	FALSE	FALSE	FALSE	FALSE	FALSE
WSF3D1M5_SMALLPIECE_BURNT_50X_4	x3_y6.png	FALSE	FALSE	FALSE	FALSE	FALSE	FALSE	FALSE
SWF1FR2_BURNT_50X_4	x5_y8.png	FALSE	TRUE	FALSE	FALSE	FALSE	FALSE	FALSE

WSF3D1M2_BURNT_50X_1	x0_y4.png	FALSE	FALSE	FALSE	FALSE	FALSE	FALSE	FALSE
WSF3D1M3_UNBURNT_1_50X_5	x6_y6.png	FALSE	TRUE	FALSE	FALSE	FALSE	FALSE	FALSE
SWF1FR2_BURNT_50X_1	x3_y9.png	FALSE	TRUE	FALSE	FALSE	FALSE	FALSE	FALSE
WSF3D1M3_BURNT_50X_3	x6_y3.png	FALSE	FALSE	FALSE	FALSE	FALSE	FALSE	TRUE
WSF3D1M5_SMALLPIECE_BURNT_50X_3	x6_y0.png	FALSE	FALSE	FALSE	FALSE	FALSE	FALSE	TRUE
WSF3D1M4_NO2_BURNT_50X_3	x8_y5.png	FALSE	FALSE	FALSE	FALSE	FALSE	FALSE	FALSE
WSF3D1M5_SMALLPIECE_BURNT_50X_3	x4_y7.png	FALSE	FALSE	FALSE	FALSE	FALSE	FALSE	FALSE
WSF3D1M1_BURNT_50X_7	x0_y1.png	FALSE	TRUE	FALSE	TRUE	FALSE	FALSE	TRUE
WSF3D1M3_UNBURNT_1_50X_4	x6_y9.png	FALSE	TRUE	FALSE	FALSE	FALSE	FALSE	FALSE
WSF3D1M5_UNBURNT_1_50X_1	x6_y4.png	FALSE	FALSE	TRUE	FALSE	FALSE	FALSE	FALSE
WSF3D1M3_UNBURNT_1_50X_1	x8_y6.png	FALSE	TRUE	FALSE	FALSE	FALSE	FALSE	FALSE
WSF3D1M5_SMALLPIECE_BURNT_50X_4	x0_y9.png	FALSE	FALSE	FALSE	FALSE	FALSE	FALSE	FALSE
WSF3D1M5_BURNT_50X_3	x2_y3.png	FALSE	FALSE	FALSE	FALSE	FALSE	FALSE	FALSE
SWF1FR2_BURNT_50X_2	x0_y1.png	FALSE	TRUE	FALSE	FALSE	FALSE	FALSE	FALSE
SWF2FR1_BURNT_1_5X	x0_y4.png	FALSE	FALSE	FALSE	FALSE	FALSE	FALSE	FALSE
WSF3D3M4_BURNT_50X_1_4	x2_y0.png	FALSE	FALSE	FALSE	FALSE	FALSE	FALSE	FALSE
WSF3D3M4_BURNT_50X_1_2	x8_y6.png	FALSE	FALSE	FALSE	FALSE	FALSE	FALSE	FALSE
WSF3D3M4_BURNT_50X_1_1	x1_y4.png	FALSE	FALSE	FALSE	FALSE	FALSE	FALSE	FALSE
SWF1FR2_BURNT_50X_1	x8_y1.png	FALSE	FALSE	FALSE	FALSE	FALSE	FALSE	FALSE
WSF3D3M4_BURNT_50X_1_5	x1_y5.png	FALSE	FALSE	FALSE	FALSE	FALSE	FALSE	FALSE

WSF3D3M2_BURNT_100X_1_1	x9_y8.png	FALSE	FALSE	FALSE	FALSE	FALSE	FALSE	TRUE
SWF1_BURNT_5_50X_2	x3_y5.png	FALSE	FALSE	FALSE	FALSE	FALSE	FALSE	TRUE
WSF3D1M4_BURNT_50X_1	x2_y1.png	FALSE	TRUE	FALSE	FALSE	FALSE	FALSE	FALSE
SWF2FR4_BURNT_50X	x2_y0.png	FALSE	FALSE	FALSE	FALSE	FALSE	FALSE	FALSE
WSF3D1M2_BURNT_50X_2	x2_y3.png	FALSE	FALSE	FALSE	FALSE	FALSE	FALSE	FALSE
WSF3D1M4_NO2_BURNT_50X_3	x5_y3.png	FALSE	TRUE	FALSE	FALSE	FALSE	FALSE	FALSE
WSF3D1M3_UNBURNT_1_50X_4	x6_y5.png	FALSE	FALSE	FALSE	FALSE	FALSE	FALSE	FALSE
WSF3D1M4_NO2_BURNT_50X_1	x0_y8.png	FALSE	FALSE	FALSE	FALSE	FALSE	FALSE	TRUE
WSF3D1M5_BURNT_50X_2	x4_y2.png	FALSE	FALSE	FALSE	FALSE	FALSE	FALSE	FALSE
SWF2FR1_BURNT_2_5X_2	x1_y2.png	FALSE	FALSE	FALSE	FALSE	FALSE	FALSE	FALSE
WSF3D3M4_BURNT_50X_1_1	x5_y9.png	FALSE	FALSE	FALSE	FALSE	FALSE	TRUE	FALSE
WSF3D1M1_BURNT_50X_5	x5_y9.png	FALSE	TRUE	FALSE	FALSE	FALSE	FALSE	FALSE
WS Fresh_50X_2	x6_y7.png	FALSE	TRUE	FALSE	FALSE	FALSE	FALSE	FALSE
WS Fresh_50X_1	x5_y4.png	FALSE	TRUE	FALSE	FALSE	FALSE	FALSE	FALSE
WSF3D1M1_BURNT_50X	x2_y2.png	FALSE	TRUE	FALSE	FALSE	FALSE	FALSE	TRUE
WSF3D1M5_BURNT_50X_2	x2_y5.png	FALSE	FALSE	FALSE	FALSE	FALSE	FALSE	FALSE
SWF2FR1_BURNT_1_5X	x2_y8.png	FALSE	FALSE	FALSE	FALSE	FALSE	FALSE	FALSE
WSF3D1M1_BURNT_50X_8	x7_y1.png	FALSE	FALSE	FALSE	FALSE	FALSE	FALSE	FALSE
WSF3D1M4_NO2_BURNT_50X_2	x0_y4.png	TRUE	FALSE	FALSE	FALSE	FALSE	FALSE	FALSE
WSF3D3M2_BURNT_50X_1_1	x2_y8.png	FALSE	FALSE	FALSE	FALSE	FALSE	FALSE	FALSE
WSF3D1M3_UNBURNT_1_50X_1	x3_y7.png	FALSE	TRUE	FALSE	FALSE	FALSE	FALSE	FALSE

SWF1_BURNT_4_50X_2	x5_y8.png	FALSE	FALSE	FALSE	FALSE	FALSE	FALSE	FALSE
WSF3D1M3_UNBURNT_1_50X_5	x4_y6.png	FALSE	FALSE	FALSE	FALSE	FALSE	FALSE	FALSE
WS Fresh_50X_3	x8_y8.png	FALSE	FALSE	FALSE	FALSE	FALSE	FALSE	TRUE
WSF3D1M2_BURNT_50X_3	x1_y1.png	TRUE	FALSE	FALSE	FALSE	FALSE	FALSE	TRUE
WSF3D1M3_UNBURNT_2_50X_1	x4_y6.png	FALSE	TRUE	FALSE	FALSE	FALSE	FALSE	FALSE
SWF2FR1_BURNT_1_5X	x2_y4.png	FALSE	FALSE	FALSE	FALSE	FALSE	FALSE	FALSE
WSF3D1M5_BURNT_50X_2	x5_y4.png	FALSE	FALSE	TRUE	FALSE	FALSE	FALSE	FALSE
WSF3D3M4_BURNT_50X_1_6	x3_y3.png	FALSE	FALSE	FALSE	FALSE	FALSE	FALSE	FALSE
WSF3D3M1_BURNT_50X_1	x3_y5.png	FALSE	TRUE	FALSE	FALSE	FALSE	FALSE	FALSE
WSF3D1M3_UNBURNT_1_50X_4	x4_y8.png	FALSE	TRUE	FALSE	FALSE	FALSE	FALSE	FALSE
WSF3D3M1_BURNT_50X_1_2	x1_y5.png	FALSE	TRUE	FALSE	FALSE	FALSE	FALSE	FALSE
WSF3D3M4_BURNT_50X_1_3	x4_y1.png	FALSE	FALSE	FALSE	TRUE	FALSE	FALSE	FALSE
WSF3D1M1_BURNT_50X_8	x3_y5.png	TRUE	TRUE	FALSE	FALSE	FALSE	FALSE	TRUE
WSF3D3M4_BURNT_50X_1_5	x0_y7.png	FALSE	TRUE	FALSE	FALSE	FALSE	FALSE	FALSE
WS Fresh_50X_1	x4_y1.png	FALSE	FALSE	FALSE	FALSE	FALSE	FALSE	FALSE
WSF3D3M4_BURNT_50X_1_6	x8_y5.png	FALSE	TRUE	FALSE	FALSE	FALSE	FALSE	TRUE
WSF3D3M2_BURNT_50X_1_3	x5_y1.png	FALSE	TRUE	FALSE	FALSE	FALSE	FALSE	TRUE
WSF3D1M5_BURNT_50X_2	x7_y7.png	FALSE	FALSE	FALSE	FALSE	FALSE	FALSE	FALSE
SWF1_BURNT_4_50X_1	x2_y4.png	FALSE	FALSE	FALSE	FALSE	FALSE	FALSE	FALSE
WSF3D1M5_BURNT_50X_3	x6_y1.png	FALSE	FALSE	FALSE	FALSE	FALSE	FALSE	FALSE
WSF3D1M2_BURNT_50X_4	x9_y1.png	FALSE	FALSE	FALSE	FALSE	FALSE	FALSE	FALSE

WSF3D1M5_BURNT_50X_1	x1_y8.png	FALSE	FALSE	FALSE	FALSE	FALSE	FALSE	FALSE
WSF3D3M2_BURNT_100X_1_1	x6_y5.png	FALSE	TRUE	FALSE	FALSE	FALSE	FALSE	FALSE
SWF1_BURNT_5_50X_1	x8_y4.png	FALSE	FALSE	TRUE	FALSE	FALSE	FALSE	FALSE
WSF3D1M3_BURNT_50X_1	x7_y7.png	FALSE	FALSE	FALSE	FALSE	FALSE	FALSE	TRUE
WSF3D1M3_UNBURNT_2_50X_1	x4_y9.png	FALSE	TRUE	FALSE	FALSE	FALSE	FALSE	FALSE
WSF3D1M4_BURNT_50X_4	x7_y0.png	FALSE	FALSE	TRUE	FALSE	FALSE	FALSE	FALSE
WS Fresh_50X_2	x8_y9.png	FALSE	FALSE	FALSE	FALSE	FALSE	FALSE	FALSE
WSF3D1M1_BURNT_50X_9	x0_y1.png	FALSE	FALSE	FALSE	FALSE	FALSE	FALSE	FALSE
WSF3D1M1_BURNT_50X_9	x2_y4.png	FALSE	FALSE	FALSE	FALSE	FALSE	FALSE	FALSE
SWF1FR2_BURNT_50X_2	x8_y2.png	FALSE	TRUE	FALSE	FALSE	FALSE	FALSE	TRUE
WSF3D1M1_BURNT_50X_5	x3_y4.png	FALSE	FALSE	FALSE	TRUE	FALSE	FALSE	FALSE
WS Fresh_50X_2	x1_y1.png	FALSE	FALSE	FALSE	FALSE	FALSE	FALSE	FALSE
WSF2D2W5_BURNT_50X_1_3	x6_y3.png	FALSE	TRUE	FALSE	FALSE	FALSE	FALSE	FALSE
WSF3D3M4_BURNT_50X_1_4	x6_y4.png	FALSE	FALSE	FALSE	FALSE	FALSE	FALSE	FALSE
WSF2D2W5_BURNT_50X_1_2	x9_y2.png	FALSE	FALSE	FALSE	FALSE	FALSE	FALSE	FALSE
WSF3D1M1_BURNT_50X_2	x4_y7.png	FALSE	TRUE	FALSE	FALSE	FALSE	FALSE	TRUE
WSF3D1M1_BURNT_50X_7	x1_y2.png	FALSE	FALSE	FALSE	FALSE	FALSE	FALSE	TRUE
WSF3D3M1_BURNT_50X_1_3	x7_y7.png	FALSE	FALSE	FALSE	FALSE	FALSE	FALSE	FALSE
WSF3D3M1_BURNT_50X_1_2	x1_y4.png	FALSE	FALSE	FALSE	FALSE	FALSE	FALSE	FALSE
WSF3D3M4_BURNT_50X_1_6	x4_y9.png	FALSE	FALSE	FALSE	FALSE	FALSE	FALSE	FALSE

WSF3D1M2_BURNT_50X_2	x5_y4.png	FALSE	FALSE	FALSE	FALSE	FALSE	FALSE	TRUE
WSF3D3M4_BURNT_50X_1_3	x5_y9.png	FALSE	FALSE	FALSE	FALSE	FALSE	FALSE	TRUE
WSF3D1M2_BURNT_50X_6	x6_y4.png	FALSE	FALSE	FALSE	FALSE	FALSE	FALSE	FALSE
WSF3D1M3_BURNT_50X_3	x0_y9.png	FALSE	FALSE	FALSE	FALSE	FALSE	FALSE	FALSE
WSF3D3M4_BURNT_50X_1_3	x8_y2.png	FALSE	FALSE	FALSE	FALSE	FALSE	FALSE	FALSE
WSF3D1M2_BURNT_50X_3	x1_y8.png	FALSE	FALSE	TRUE	FALSE	FALSE	FALSE	FALSE
SWF2FR1_BURNT_1_5X	x4_y4.png	FALSE	FALSE	FALSE	FALSE	FALSE	FALSE	FALSE
SWF1_BURNT_5_50X_3	x9_y4.png	FALSE	FALSE	FALSE	FALSE	FALSE	FALSE	FALSE
WSF3D1M5_BURNT_50X_1	x4_y7.png	FALSE	FALSE	FALSE	FALSE	FALSE	FALSE	FALSE
WSF3D1M1_BURNT_50X_5	x1_y3.png	FALSE	TRUE	FALSE	FALSE	FALSE	FALSE	FALSE
WSF3D1M1_BURNT_50X	x0_y6.png	TRUE	FALSE	FALSE	FALSE	FALSE	FALSE	FALSE
WSF3D1M2_BURNT_50X_2	x2_y1.png	FALSE	FALSE	FALSE	FALSE	FALSE	FALSE	FALSE
WSF3D3M1_BURNT_50X_1_2	x6_y6.png	FALSE	FALSE	FALSE	FALSE	FALSE	FALSE	FALSE
WSF3D1M1_BURNT_50X_6	x4_y9.png	FALSE	FALSE	FALSE	FALSE	FALSE	FALSE	TRUE
WSF3D3M4_BURNT_50X_1_2	x8_y3.png	FALSE	TRUE	FALSE	FALSE	FALSE	FALSE	FALSE
WSF3D1M4_BURNT_50X_4	x6_y9.png	FALSE	FALSE	FALSE	FALSE	FALSE	FALSE	TRUE
WSF3D1M4_BURNT_50X_4	x5_y2.png	FALSE	FALSE	FALSE	FALSE	FALSE	FALSE	TRUE
WSF3D3M4_BURNT_50X_1_6	x1_y7.png	FALSE	TRUE	FALSE	FALSE	FALSE	FALSE	FALSE
WSF3D1M2_BURNT_50X_5	x9_y1.png	FALSE	FALSE	FALSE	FALSE	FALSE	FALSE	FALSE
WSF3D1M1_BURNT_50X_4	x1_y0.png	FALSE	FALSE	FALSE	FALSE	FALSE	TRUE	FALSE

WSF3D3M2_BURNT_100X_1_1	x5_y4.png	FALSE	TRUE	FALSE	FALSE	FALSE	FALSE	FALSE
WSF3D1M5_UNBURNT_1_50X_1	x2_y4.png	FALSE	FALSE	FALSE	FALSE	FALSE	FALSE	TRUE
WSF3D3M1_BURNT_50X_1_2	x2_y3.png	FALSE	FALSE	FALSE	FALSE	FALSE	FALSE	FALSE
WSF3D1M3_BURNT_50X_2	x7_y9.png	FALSE	FALSE	FALSE	FALSE	FALSE	TRUE	TRUE
WSF3D1M3_BURNT_50X_3	x4_y2.png	FALSE	FALSE	FALSE	FALSE	FALSE	TRUE	FALSE
SWF1_BURNT_4_50X_1	x2_y5.png	FALSE	FALSE	FALSE	FALSE	FALSE	TRUE	FALSE
SWF1_BURNT_4_50X_1	x2_y5.png	FALSE	FALSE	FALSE	FALSE	FALSE	TRUE	FALSE
SWF1_BURNT_4_50X_3	x0_y6.png	FALSE	FALSE	FALSE	FALSE	FALSE	FALSE	FALSE
SWF1_BURNT_4_50X_2	x9_y1.png	FALSE	FALSE	FALSE	FALSE	FALSE	FALSE	FALSE
SWF2FR1_BURNT_2_5X_1	x1_y3.png	FALSE	FALSE	FALSE	FALSE	FALSE	FALSE	FALSE
WSF3D1M2_BURNT_50X_2	x5_y5.png	FALSE	FALSE	FALSE	FALSE	FALSE	FALSE	FALSE
WSF3D3M1_BURNT_50X_1_2	x2_y4.png	FALSE	FALSE	FALSE	FALSE	FALSE	FALSE	FALSE
WSF3D3M4_BURNT_50X_1_3	x0_y9.png	FALSE	FALSE	FALSE	FALSE	FALSE	FALSE	FALSE
WSF3D1M5_UNBURNT_1_50X_1	x1_y0.png	FALSE	TRUE	FALSE	FALSE	FALSE	FALSE	TRUE
WSF3D1M3_UNBURNT_2_50X_1	x6_y0.png	FALSE	TRUE	FALSE	FALSE	FALSE	FALSE	FALSE
SWF2FR4_BURNT_50X	x5_y8.png	FALSE	FALSE	FALSE	FALSE	FALSE	FALSE	FALSE
WSF2D2W5_BURNT_50X_2_1	x1_y9.png	FALSE	FALSE	FALSE	FALSE	FALSE	FALSE	FALSE
WSF3D1M2_BURNT_50X_4	x8_y0.png	FALSE	FALSE	TRUE	FALSE	FALSE	FALSE	FALSE
WS Fresh	x4_y2.png	FALSE	FALSE	FALSE	FALSE	FALSE	FALSE	TRUE
WSF3D1M1_BURNT_50X_12	x4_y9.png	FALSE	FALSE	FALSE	FALSE	FALSE	FALSE	FALSE
WSF3D3M4_BURNT_50X_1_3	x8_y0.png	FALSE	FALSE	FALSE	FALSE	FALSE	FALSE	FALSE

SWF1_BURNT_4_50X_2	x1_y7.png	FALSE	FALSE	FALSE	FALSE	FALSE	FALSE	FALSE
WSF3D1M1_BURNT_50X_5	x6_y4.png	FALSE	FALSE	FALSE	FALSE	FALSE	FALSE	FALSE
WSF3D1M1_BURNT_50X_3	x3_y8.png	FALSE	FALSE	FALSE	FALSE	FALSE	FALSE	FALSE
WSF3D1M3_UNBURNT_1_50X_5	x1_y6.png	FALSE	TRUE	FALSE	FALSE	FALSE	FALSE	FALSE
WSF3D1M3_BURNT_50X_2	x3_y2.png	FALSE	FALSE	FALSE	FALSE	FALSE	FALSE	FALSE
WSF2D2W5_BURNT_50X_1	x5_y0.png	FALSE	FALSE	FALSE	FALSE	FALSE	FALSE	FALSE
WSF3D1M3_UNBURNT_1_50X_1	x2_y9.png	FALSE	TRUE	FALSE	FALSE	FALSE	FALSE	TRUE
SWF1_BURNT_5_50X_2	x3_y3.png	FALSE	TRUE	FALSE	FALSE	FALSE	FALSE	TRUE
WSF3D1M5_SMALLPIECE_BURNT_50X_4	x6_y1.png	FALSE	FALSE	FALSE	FALSE	FALSE	FALSE	FALSE
WSF2D2W5_BURNT_50X_1	x1_y1.png	FALSE	FALSE	FALSE	FALSE	FALSE	FALSE	FALSE
WSF3D1M3_BURNT_50X_2	x1_y6.png	FALSE	FALSE	FALSE	FALSE	FALSE	TRUE	TRUE
WSF3D1M3_UNBURNT_1_50X_4	x6_y0.png	FALSE	FALSE	FALSE	FALSE	FALSE	FALSE	FALSE
WSF3D1M3_BURNT_50X_2	x1_y7.png	FALSE	FALSE	FALSE	FALSE	FALSE	TRUE	TRUE
SWF1_BURNT_5_50X_3	x7_y6.png	FALSE	FALSE	FALSE	FALSE	FALSE	FALSE	FALSE
WS Fresh_50X_2	x9_y9.png	FALSE	FALSE	FALSE	FALSE	FALSE	FALSE	FALSE
WSF3D1M1_BURNT_50X	x8_y7.png	FALSE	FALSE	FALSE	FALSE	FALSE	FALSE	FALSE
WSF3D3M1_BURNT_50X_1_3	x3_y9.png	FALSE	FALSE	TRUE	FALSE	FALSE	FALSE	FALSE
WSF3D3M2_BURNT_50X_1_1	x6_y0.png	FALSE	FALSE	FALSE	FALSE	FALSE	FALSE	FALSE
WSF3D1M4_NO2_BURNT_50X_1	x7_y3.png	FALSE	FALSE	FALSE	FALSE	FALSE	FALSE	FALSE
WSF3D1M3_BURNT_50X_3	x4_y0.png	FALSE	FALSE	FALSE	FALSE	FALSE	FALSE	FALSE
WSF3D1M4_NO2_BURNT_50X_2	x3_y4.png	FALSE	FALSE	FALSE	FALSE	FALSE	FALSE	FALSE

WSF3D3M1_BURNT_50X_1_4	x2_y4.png	FALSE	FALSE	FALSE	FALSE	FALSE	FALSE	FALSE
WSF3D1M1_BURNT_50X_7	x8_y3.png	FALSE	FALSE	FALSE	FALSE	FALSE	FALSE	FALSE
WSF3D3M4_BURNT_50X_1_5	x5_y7.png	FALSE	TRUE	FALSE	FALSE	FALSE	FALSE	FALSE
WSF3D3M1_BURNT_50X_1_2	x7_y5.png	FALSE	FALSE	FALSE	FALSE	FALSE	FALSE	FALSE
WSF3D1M1_BURNT_50X_12	x1_y1.png	FALSE	FALSE	FALSE	FALSE	FALSE	FALSE	FALSE
WSF3D1M1_BURNT_50X_2	x2_y9.png	FALSE	FALSE	FALSE	FALSE	FALSE	FALSE	TRUE
WSF3D1M1_BURNT_50X_4	x5_y1.png	FALSE	TRUE	FALSE	FALSE	FALSE	FALSE	FALSE
WSF3D1M4_NO2_BURNT_50X_2	x8_y0.png	FALSE	FALSE	FALSE	FALSE	FALSE	FALSE	FALSE
SWF1_BURNT_4_50X_1	x8_y6.png	FALSE	FALSE	FALSE	FALSE	FALSE	FALSE	FALSE
WSF3D3M4_BURNT_50X_1_3	x1_y1.png	FALSE	FALSE	FALSE	FALSE	FALSE	FALSE	FALSE
WSF3D1M1_BURNT_50X_3	x4_y6.png	FALSE	TRUE	FALSE	FALSE	FALSE	TRUE	FALSE
SWF1_BURNT_5_50X_1	x7_y5.png	TRUE	FALSE	FALSE	FALSE	FALSE	FALSE	FALSE
WS Fresh	x0_y1.png	FALSE	FALSE	FALSE	FALSE	FALSE	FALSE	FALSE
SWF1_BURNT_4_50X_1	x5_y0.png	FALSE	FALSE	FALSE	FALSE	FALSE	FALSE	FALSE
WSF2D2W5_BURNT_50X_1_2	x8_y2.png	FALSE	TRUE	FALSE	FALSE	FALSE	TRUE	FALSE
WSF3D3M1_BURNT_50X_1_4	x3_y1.png	FALSE	FALSE	FALSE	FALSE	FALSE	FALSE	FALSE
WSF2D2W5_BURNT_50X_1	x2_y0.png	FALSE	FALSE	FALSE	FALSE	FALSE	FALSE	FALSE
WS Fresh_50X_2	x7_y1.png	FALSE	FALSE	TRUE	FALSE	FALSE	FALSE	FALSE
WSF2D2W5_BURNT_50X_2_2	x4_y4.png	TRUE	TRUE	FALSE	FALSE	FALSE	FALSE	FALSE
WSF3D1M2_BURNT_50X_1	x2_y9.png	FALSE	FALSE	FALSE	FALSE	FALSE	FALSE	FALSE
SWF1_BURNT_5_50X_2	x3_y8.png	TRUE	FALSE	FALSE	FALSE	FALSE	FALSE	FALSE

WSF3D1M5_SMALLPIECE_BURNT_50X_3	x4_y0.png	FALSE	FALSE	FALSE	FALSE	FALSE	FALSE	TRUE
WSF3D3M4_BURNT_50X_1_6	x9_y2.png	FALSE	FALSE	FALSE	FALSE	FALSE	FALSE	FALSE
WSF3D3M2_BURNT_50X_1_2	x0_y4.png	FALSE	FALSE	FALSE	FALSE	FALSE	FALSE	TRUE
SWF1_BURNT_5_50X_1	x6_y1.png	TRUE	FALSE	FALSE	FALSE	FALSE	FALSE	FALSE
WS Fresh_50X_3	x7_y0.png	FALSE	FALSE	FALSE	FALSE	FALSE	FALSE	FALSE
SWF1_BURNT_5_50X_3	x8_y8.png	FALSE	FALSE	FALSE	FALSE	FALSE	FALSE	FALSE
SWF2FR1_BURNT_1_5X	x2_y1.png	FALSE	FALSE	FALSE	FALSE	FALSE	FALSE	FALSE
SWF2FR1_BURNT_1_5X_2	x1_y5.png	FALSE	FALSE	FALSE	FALSE	FALSE	FALSE	FALSE
WSF3D1M2_BURNT_50X_5	x5_y0.png	FALSE	FALSE	FALSE	FALSE	FALSE	FALSE	TRUE
WSF3D1M4_NO2_BURNT_50X_1	x9_y2.png	FALSE	FALSE	FALSE	FALSE	FALSE	FALSE	FALSE
WS Fresh_50X_3	x4_y5.png	FALSE	FALSE	FALSE	FALSE	FALSE	FALSE	FALSE
WSF2D2W5_BURNT_50X_1_3	x0_y9.png	FALSE	FALSE	FALSE	FALSE	FALSE	FALSE	FALSE
WSF3D1M4_BURNT_50X_4	x5_y1.png	TRUE	TRUE	FALSE	FALSE	FALSE	FALSE	FALSE
WSF3D1M3_UNBURNT_1_50X_4	x2_y4.png	FALSE	TRUE	FALSE	FALSE	FALSE	FALSE	FALSE
WSF3D1M1_BURNT_50X_10	x7_y0.png	FALSE	FALSE	FALSE	FALSE	FALSE	FALSE	FALSE
WSF3D1M1_BURNT_50X_10	x7_y6.png	FALSE	FALSE	FALSE	FALSE	FALSE	FALSE	TRUE
WSF3D1M2_BURNT_50X_4	x4_y5.png	FALSE	FALSE	FALSE	FALSE	FALSE	FALSE	TRUE
WSF3D1M1_BURNT_50X_2	x0_y4.png	FALSE	FALSE	FALSE	FALSE	FALSE	FALSE	FALSE
WSF3D1M2_BURNT_50X_5	x5_y8.png	FALSE	FALSE	FALSE	FALSE	FALSE	FALSE	FALSE
WSF3D3M2_BURNT_50X_1_2	x7_y6.png	FALSE	TRUE	FALSE	FALSE	FALSE	FALSE	FALSE
WSF3D1M3_BURNT_50X_1	x1_y4.png	FALSE	FALSE	FALSE	FALSE	FALSE	FALSE	TRUE

WS Fresh_50X_1	x9_y5.png	FALSE	FALSE	FALSE	FALSE	FALSE	FALSE	FALSE
WSF3D1M3_UNBURNT_1_50X_3	x5_y7.png	FALSE	FALSE	FALSE	FALSE	FALSE	FALSE	FALSE
WSF3D3M1_BURNT_50X_1_4	x4_y6.png	FALSE	FALSE	FALSE	FALSE	FALSE	FALSE	FALSE
SWF2FR1_BURNT_1_5X_2	x5_y4.png	FALSE	FALSE	FALSE	FALSE	FALSE	FALSE	FALSE
SWF2FR1_BURNT_2_5X_2	x0_y4.png	FALSE	FALSE	FALSE	FALSE	FALSE	FALSE	FALSE
WSF3D1M4_NO2_BURNT_50X_2	x6_y6.png	FALSE	FALSE	FALSE	FALSE	FALSE	FALSE	FALSE
WSF3D3M2_BURNT_50X_1_3	x0_y8.png	FALSE	FALSE	FALSE	FALSE	FALSE	FALSE	TRUE
WS Fresh	x4_y0.png	FALSE	FALSE	FALSE	FALSE	FALSE	FALSE	FALSE
WSF3D3M2_BURNT_100X_1_1	x9_y6.png	FALSE	FALSE	FALSE	FALSE	FALSE	FALSE	FALSE
WSF3D3M4_BURNT_50X_1_6	x8_y3.png	FALSE	FALSE	FALSE	FALSE	FALSE	FALSE	FALSE
WSF3D3M1_BURNT_50X_1_3	x6_y5.png	FALSE	FALSE	FALSE	FALSE	FALSE	FALSE	FALSE
WSF3D3M2_BURNT_50X_1_3	x0_y3.png	FALSE	FALSE	TRUE	FALSE	FALSE	FALSE	FALSE
WSF3D1M4_BURNT_50X_1	x4_y1.png	FALSE	TRUE	FALSE	FALSE	FALSE	FALSE	FALSE
WSF3D3M4_BURNT_50X_1_5	x6_y6.png	FALSE	TRUE	FALSE	FALSE	FALSE	FALSE	FALSE
SWF1FR2_BURNT_50X_1	x9_y0.png	FALSE	FALSE	FALSE	FALSE	FALSE	FALSE	FALSE
WSF3D3M4_BURNT_50X_1_1	x1_y8.png	FALSE	FALSE	FALSE	FALSE	FALSE	FALSE	FALSE
WSF3D1M1_BURNT_50X	x2_y7.png	TRUE	TRUE	FALSE	FALSE	FALSE	FALSE	FALSE
WSF3D1M3_UNBURNT_1_50X_4	x5_y6.png	FALSE	TRUE	FALSE	FALSE	FALSE	FALSE	FALSE
WSF3D1M1_BURNT_50X_7	x5_y6.png	FALSE	FALSE	FALSE	FALSE	FALSE	FALSE	FALSE
WSF3D3M4_BURNT_50X_1_3	x1_y0.png	FALSE	FALSE	FALSE	FALSE	FALSE	FALSE	FALSE

WSF3D3M2_BURNT_50X_1_2	x5_y0.png	FALSE	FALSE	FALSE	FALSE	FALSE	FALSE	FALSE
WSF3D3M4_BURNT_50X_1_6	x0_y4.png	FALSE	FALSE	FALSE	FALSE	FALSE	FALSE	FALSE
WSF3D1M4_NO2_BURNT_50X_1	x8_y6.png	FALSE	FALSE	FALSE	FALSE	FALSE	FALSE	FALSE
WSF3D1M3_BURNT_50X_3	x4_y6.png	FALSE	FALSE	FALSE	FALSE	FALSE	FALSE	TRUE
WSF3D1M3_BURNT_50X_3	x8_y7.png	FALSE	FALSE	FALSE	FALSE	FALSE	FALSE	FALSE
WSF3D1M1_BURNT_50X_7	x9_y5.png	TRUE	FALSE	FALSE	FALSE	FALSE	FALSE	FALSE
WSF3D3M4_BURNT_50X_1_1	x4_y2.png	TRUE	FALSE	FALSE	FALSE	FALSE	FALSE	FALSE
WSF3D1M4_BURNT_50X_4	x2_y8.png	FALSE	FALSE	FALSE	FALSE	FALSE	TRUE	FALSE
SWF2FR1_BURNT_2_5X_2	x1_y9.png	FALSE	FALSE	FALSE	FALSE	FALSE	FALSE	FALSE
WSF3D1M1_BURNT_50X_5	x0_y4.png	FALSE	TRUE	FALSE	FALSE	FALSE	FALSE	FALSE
WSF3D1M4_BURNT_50X_2	x7_y3.png	FALSE	FALSE	FALSE	TRUE	FALSE	FALSE	FALSE
WSF3D1M5_BURNT_50X_3	x3_y5.png	FALSE	FALSE	FALSE	FALSE	FALSE	FALSE	FALSE
WSF3D1M1_BURNT_50X_8	x9_y8.png	FALSE	FALSE	FALSE	FALSE	FALSE	TRUE	FALSE
WSF3D3M1_BURNT_50X_1_3	x2_y5.png	FALSE	FALSE	FALSE	FALSE	FALSE	FALSE	FALSE
WSF3D1M2_BURNT_50X_6	x6_y2.png	FALSE	FALSE	FALSE	FALSE	FALSE	FALSE	FALSE
WSF3D3M4_BURNT_50X_1_2	x2_y7.png	FALSE	FALSE	FALSE	FALSE	FALSE	FALSE	FALSE
WSF3D3M1_BURNT_50X_1_3	x5_y4.png	FALSE	FALSE	FALSE	FALSE	FALSE	FALSE	FALSE
SWF2FR1_BURNT_2_5X_1	x7_y1.png	FALSE	FALSE	FALSE	FALSE	FALSE	FALSE	FALSE
WSF3D1M5_SMALLPIECE_BURNT_50X_4	x7_y9.png	FALSE	FALSE	FALSE	FALSE	FALSE	FALSE	FALSE

WS Fresh_50X_2	x9_y1.png	FALSE	FALSE	FALSE	FALSE	FALSE	FALSE	FALSE
WSF3D1M4_NO2_BURNT_50X_3	x0_y7.png	FALSE	FALSE	FALSE	FALSE	FALSE	FALSE	FALSE
WSF2D2W5_BURNT_50X_2_1	x4_y8.png	FALSE	FALSE	TRUE	FALSE	FALSE	FALSE	FALSE
WSF3D3M4_BURNT_50X_1_6	x9_y3.png	FALSE	FALSE	FALSE	FALSE	FALSE	FALSE	FALSE
WSF3D1M2_BURNT_50X_6	x0_y4.png	TRUE	TRUE	FALSE	FALSE	FALSE	FALSE	FALSE
WSF2D2W5_BURNT_50X_1_2	x8_y7.png	TRUE	TRUE	FALSE	FALSE	FALSE	FALSE	FALSE
WSF3D1M1_BURNT_50X_4	x2_y1.png	FALSE	FALSE	FALSE	FALSE	FALSE	TRUE	FALSE
WSF3D1M1_BURNT_50X	x1_y8.png	FALSE	TRUE	FALSE	FALSE	FALSE	FALSE	FALSE
WSF3D1M2_BURNT_50X_1	x5_y5.png	TRUE	FALSE	FALSE	FALSE	FALSE	FALSE	FALSE
WSF3D1M3_UNBURNT_1_50X_5	x9_y4.png	FALSE	TRUE	FALSE	FALSE	FALSE	FALSE	FALSE
WSF3D3M1_BURNT_50X_1_2	x0_y3.png	FALSE	FALSE	FALSE	FALSE	FALSE	FALSE	FALSE
WSF2D2W5_BURNT_50X_2_1	x7_y4.png	TRUE	FALSE	FALSE	FALSE	FALSE	FALSE	FALSE
WSF3D1M3_BURNT_50X_3	x5_y1.png	TRUE	FALSE	FALSE	FALSE	FALSE	FALSE	FALSE
WSF3D1M1_BURNT_50X_7	x1_y0.png	FALSE	FALSE	FALSE	FALSE	FALSE	FALSE	FALSE
WSF3D3M2_BURNT_50X_1_3	x2_y9.png	FALSE	TRUE	FALSE	FALSE	FALSE	FALSE	FALSE
WS Fresh_50X_2	x6_y2.png	FALSE	FALSE	FALSE	FALSE	FALSE	FALSE	FALSE
WSF3D1M4_BURNT_50X_3	x2_y7.png	FALSE	FALSE	FALSE	FALSE	FALSE	FALSE	TRUE
WSF3D3M4_BURNT_50X_1_5	x8_y6.png	FALSE	FALSE	FALSE	FALSE	FALSE	FALSE	FALSE
SWF1_BURNT_4_50X_3	x3_y6.png	FALSE	FALSE	FALSE	FALSE	FALSE	FALSE	FALSE
SWF1_BURNT_4_50X_2	x8_y1.png	FALSE	FALSE	FALSE	FALSE	FALSE	FALSE	FALSE
SWF1_BURNT_5_50X_3	x1_y6.png	FALSE	FALSE	FALSE	FALSE	FALSE	FALSE	TRUE

WSF3D1M5_BURNT_50X_1	x9_y7.png	FALSE	FALSE	FALSE	FALSE	FALSE	FALSE	FALSE
WSF3D1M5_BURNT_50X_1	x9_y6.png	FALSE	FALSE	TRUE	FALSE	FALSE	FALSE	FALSE
WSF3D3M4_BURNT_50X_1_1	x1_y3.png	FALSE	FALSE	FALSE	FALSE	FALSE	FALSE	FALSE
SWF1_BURNT_5_50X_2	x6_y3.png	TRUE	FALSE	FALSE	FALSE	FALSE	FALSE	FALSE
SWF1_BURNT_4_50X_3	x7_y0.png	FALSE	FALSE	FALSE	FALSE	FALSE	FALSE	FALSE
WSF3D1M4_BURNT_50X_1	x3_y8.png	FALSE	TRUE	FALSE	TRUE	FALSE	FALSE	TRUE
WSF3D1M3_BURNT_50X_3	x7_y5.png	TRUE	FALSE	FALSE	FALSE	FALSE	FALSE	FALSE
SWF1_BURNT_4_50X_2	x6_y2.png	FALSE	FALSE	FALSE	FALSE	FALSE	FALSE	FALSE
SWF1_BURNT_4_50X_1	x1_y9.png	FALSE	FALSE	FALSE	FALSE	FALSE	FALSE	FALSE
WS Fresh_50X_2	x1_y2.png	FALSE	FALSE	FALSE	FALSE	FALSE	FALSE	FALSE
WSF3D3M1_BURNT_50X_1_3	x0_y6.png	FALSE	FALSE	FALSE	FALSE	FALSE	FALSE	FALSE
WSF3D1M4_NO2_BURNT_50X_1	x5_y3.png	FALSE	TRUE	TRUE	FALSE	FALSE	FALSE	FALSE
WSF3D3M4_BURNT_50X_1_1	x4_y1.png	FALSE	FALSE	FALSE	FALSE	FALSE	TRUE	TRUE
SWF2FR4_BURNT_50X	x8_y5.png	FALSE	FALSE	FALSE	FALSE	FALSE	FALSE	FALSE
WSF3D1M5_UNBURNT_1_50X_1	x2_y2.png	FALSE	TRUE	FALSE	FALSE	FALSE	FALSE	TRUE
SWF1FR2_BURNT_50X_4	x7_y9.png	FALSE	FALSE	FALSE	FALSE	FALSE	FALSE	FALSE
WSF3D3M1_BURNT_50X_1_2	x2_y0.png	FALSE	FALSE	FALSE	FALSE	FALSE	FALSE	FALSE
WSF3D3M2_BURNT_100X_1_1	x7_y9.png	FALSE	TRUE	TRUE	FALSE	FALSE	FALSE	FALSE
WSF3D1M1_BURNT_50X	x1_y7.png	TRUE	FALSE	FALSE	FALSE	FALSE	FALSE	FALSE
WSF3D1M4_BURNT_50X_2	x5_y4.png	TRUE	TRUE	FALSE	FALSE	FALSE	FALSE	FALSE
WSF3D1M1_BURNT_50X	x2_y4.png	FALSE	FALSE	TRUE	FALSE	FALSE	FALSE	FALSE
WSF3D3M2_BURNT_50X_1_2	x9_y8.png	FALSE	FALSE	FALSE	FALSE	FALSE	TRUE	FALSE

WSF3D1M1_BURNT_50X	x7_y8.png	FALSE	TRUE	TRUE	FALSE	FALSE	FALSE	FALSE
WSF3D1M1_BURNT_50X_12	x3_y6.png	FALSE	FALSE	TRUE	FALSE	FALSE	FALSE	FALSE
WSF3D1M3_UNBURNT_1_50X_4	x8_y6.png	FALSE	FALSE	FALSE	FALSE	FALSE	FALSE	FALSE
WS Fresh_50X_3	x3_y5.png	FALSE	FALSE	FALSE	FALSE	FALSE	FALSE	FALSE
SWF2FR1_BURNT_2_5X_1	x0_y9.png	FALSE	FALSE	FALSE	FALSE	FALSE	FALSE	FALSE
WSF3D1M1_BURNT_50X_4	x1_y1.png	FALSE	TRUE	FALSE	FALSE	FALSE	FALSE	FALSE
WSF3D1M4_NO2_BURNT_50X_2	x0_y1.png	FALSE	FALSE	FALSE	FALSE	FALSE	FALSE	FALSE
WSF3D1M1_BURNT_50X_4	x0_y7.png	FALSE	FALSE	FALSE	FALSE	FALSE	FALSE	TRUE
WSF3D1M4_NO2_BURNT_50X_1	x2_y8.png	FALSE	FALSE	FALSE	FALSE	FALSE	FALSE	FALSE
SWF2FR1_BURNT_1_5X	x8_y9.png	FALSE	FALSE	FALSE	FALSE	FALSE	FALSE	FALSE
WSF3D1M1_BURNT_50X_4	x7_y7.png	FALSE	TRUE	FALSE	FALSE	FALSE	FALSE	FALSE
SWF2FR1_BURNT_1_5X_2	x7_y2.png	FALSE	FALSE	FALSE	FALSE	FALSE	FALSE	FALSE
WS Fresh_50X_2	x2_y1.png	TRUE	FALSE	FALSE	FALSE	FALSE	FALSE	FALSE
WS Fresh_50X_3	x1_y2.png	FALSE	TRUE	FALSE	FALSE	FALSE	FALSE	FALSE
WSF3D1M4_NO2_BURNT_50X_2	x0_y3.png	TRUE	FALSE	FALSE	FALSE	FALSE	FALSE	FALSE
WSF3D1M4_BURNT_50X_4	x8_y6.png	TRUE	TRUE	FALSE	FALSE	FALSE	FALSE	FALSE
WSF3D3M2_BURNT_50X_1_1	x6_y9.png	FALSE	FALSE	FALSE	FALSE	FALSE	FALSE	TRUE
WSF3D1M3_BURNT_50X_3	x9_y9.png	TRUE	FALSE	FALSE	FALSE	FALSE	FALSE	FALSE
WS Fresh_50X_2	x5_y6.png	TRUE	FALSE	FALSE	FALSE	FALSE	FALSE	FALSE
WSF3D1M5_SMALLPIECE_BURNT_50X_4	x1_y9.png	FALSE	FALSE	FALSE	FALSE	FALSE	FALSE	FALSE
WSF2D2W5_BURNT_50X_2_1	x0_y1.png	FALSE	FALSE	FALSE	FALSE	FALSE	FALSE	FALSE

WSF3D1M5_SMALLPIECE_BURNT_50X_3	x6_y2.png	TRUE	FALSE	FALSE	FALSE	FALSE	FALSE	FALSE
WSF3D1M3_UNBURNT_1_50X_5	x4_y2.png	FALSE	TRUE	FALSE	FALSE	FALSE	FALSE	FALSE
WSF3D1M2_BURNT_50X_6	x4_y8.png	FALSE	FALSE	FALSE	FALSE	FALSE	FALSE	FALSE
WSF3D1M5_BURNT_50X_1	x8_y6.png	FALSE	FALSE	FALSE	FALSE	FALSE	TRUE	FALSE
WSF3D1M4_BURNT_50X_3	x8_y5.png	TRUE	TRUE	FALSE	FALSE	FALSE	FALSE	FALSE
WSF3D3M1_BURNT_50X_1	x2_y1.png	FALSE	FALSE	TRUE	FALSE	FALSE	FALSE	FALSE
SWF2FR1_BURNT_2_5X_2	x4_y1.png	FALSE	FALSE	FALSE	FALSE	FALSE	FALSE	FALSE
WSF3D1M5_SMALLPIECE_BURNT_50X_3	x4_y6.png	FALSE	FALSE	FALSE	FALSE	FALSE	FALSE	FALSE
WSF3D1M1_BURNT_50X_7	x2_y9.png	FALSE	FALSE	FALSE	FALSE	FALSE	TRUE	TRUE
WSF3D1M4_BURNT_50X_3	x5_y5.png	TRUE	FALSE	FALSE	FALSE	TRUE	FALSE	FALSE
WSF3D3M2_BURNT_50X_1_2	x2_y3.png	FALSE	TRUE	FALSE	FALSE	FALSE	FALSE	TRUE
WS Fresh_50X_1	x8_y8.png	FALSE	TRUE	FALSE	FALSE	FALSE	FALSE	FALSE
WSF3D1M3_UNBURNT_1_50X_3	x8_y3.png	FALSE	TRUE	FALSE	FALSE	FALSE	FALSE	FALSE
SWF2FR1_BURNT_2_5X_1	x3_y1.png	FALSE	FALSE	FALSE	FALSE	FALSE	FALSE	FALSE
WS Fresh_50X_2	x4_y6.png	FALSE	FALSE	FALSE	FALSE	FALSE	FALSE	FALSE
WSF3D3M1_BURNT_50X_1_4	x0_y5.png	FALSE	TRUE	FALSE	FALSE	FALSE	FALSE	FALSE
WSF3D1M4_BURNT_50X_3	x8_y0.png	FALSE	FALSE	FALSE	FALSE	FALSE	FALSE	TRUE
SWF1_BURNT_5_50X_3	x9_y2.png	FALSE	FALSE	FALSE	FALSE	FALSE	FALSE	FALSE
WSF3D1M5_SMALLPIECE_BURNT_50X_4	x6_y5.png	FALSE	FALSE	FALSE	FALSE	FALSE	FALSE	FALSE
WSF3D1M1_BURNT_50X_9	x5_y8.png	FALSE	FALSE	FALSE	FALSE	FALSE	FALSE	FALSE

WS Fresh	x3_y5.png	FALSE	FALSE	FALSE	FALSE	FALSE	FALSE	FALSE
SWF1_BURNT_4_50X_1	x2_y1.png	FALSE	FALSE	FALSE	FALSE	FALSE	FALSE	TRUE
WSF3D3M1_BURNT_50X_1_4	x6_y7.png	FALSE	FALSE	FALSE	FALSE	FALSE	FALSE	TRUE
WSF3D1M2_BURNT_50X_6	x4_y6.png	TRUE	TRUE	FALSE	FALSE	FALSE	FALSE	FALSE
WSF2D2W5_BURNT_50X_1	x8_y3.png	FALSE	FALSE	FALSE	FALSE	FALSE	FALSE	TRUE
WSF3D1M3_UNBURNT_1_50X_5	x8_y8.png	FALSE	TRUE	FALSE	FALSE	FALSE	FALSE	FALSE
SWF2FR1_BURNT_1_5X	x7_y5.png	FALSE	FALSE	FALSE	FALSE	FALSE	FALSE	FALSE
WSF3D3M1_BURNT_50X_1_2	x2_y5.png	FALSE	TRUE	FALSE	FALSE	FALSE	FALSE	FALSE
SWF2FR4_BURNT_50X	x6_y0.png	FALSE	FALSE	FALSE	FALSE	FALSE	FALSE	FALSE
WSF3D1M3_UNBURNT_1_50X_3	x8_y7.png	FALSE	TRUE	FALSE	FALSE	FALSE	FALSE	TRUE
WSF3D1M5_BURNT_50X_3	x0_y9.png	FALSE	FALSE	FALSE	FALSE	FALSE	FALSE	FALSE
WSF3D3M4_BURNT_50X_1_2	x9_y8.png	FALSE	FALSE	FALSE	FALSE	FALSE	FALSE	FALSE
WSF3D1M1_BURNT_50X_8	x8_y7.png	FALSE	FALSE	FALSE	FALSE	FALSE	FALSE	FALSE
WSF3D3M2_BURNT_50X_1_3	x6_y0.png	FALSE	FALSE	TRUE	FALSE	FALSE	FALSE	TRUE
SWF1_BURNT_4_50X_2	x4_y6.png	FALSE	FALSE	FALSE	FALSE	FALSE	FALSE	FALSE
SWF1FR2_BURNT_50X_3	x5_y1.png	FALSE	FALSE	FALSE	FALSE	FALSE	FALSE	TRUE
SWF2FR1_BURNT_2_5X_1	x9_y1.png	FALSE	FALSE	FALSE	FALSE	FALSE	FALSE	FALSE
WSF3D1M5_BURNT_50X_1	x8_y5.png	FALSE	FALSE	FALSE	FALSE	FALSE	FALSE	FALSE
WSF3D3M4_BURNT_50X_1_5	x7_y5.png	FALSE	TRUE	TRUE	FALSE	FALSE	FALSE	FALSE
SWF1_BURNT_5_50X_2	x5_y7.png	FALSE	FALSE	FALSE	FALSE	FALSE	FALSE	TRUE
WSF3D1M4_BURNT_50X_3	x6_y1.png	FALSE	TRUE	FALSE	FALSE	FALSE	FALSE	TRUE

WSF3D3M4_BURNT_50X_1_3	x9_y8.png	FALSE	FALSE	FALSE	FALSE	FALSE	FALSE	FALSE
WSF3D1M3_UNBURNT_1_50X_3	x2_y1.png	FALSE	TRUE	FALSE	FALSE	FALSE	FALSE	TRUE
WSF3D1M2_BURNT_50X_4	x7_y2.png	FALSE	FALSE	FALSE	FALSE	FALSE	FALSE	FALSE
WSF3D3M1_BURNT_50X_1_3	x5_y3.png	FALSE	FALSE	FALSE	FALSE	FALSE	FALSE	FALSE
WSF3D1M4_NO2_BURNT_50X_2	x2_y0.png	FALSE	FALSE	FALSE	FALSE	FALSE	FALSE	FALSE
WSF3D1M1_BURNT_50X_3	x8_y4.png	FALSE	FALSE	FALSE	FALSE	FALSE	FALSE	TRUE
WSF3D1M3_UNBURNT_1_50X_1	x2_y0.png	FALSE	TRUE	FALSE	FALSE	FALSE	FALSE	FALSE
WSF3D3M4_BURNT_50X_1_4	x3_y2.png	FALSE	FALSE	FALSE	FALSE	FALSE	FALSE	FALSE
WSF3D3M4_BURNT_50X_1_6	x9_y0.png	FALSE	FALSE	FALSE	FALSE	FALSE	FALSE	FALSE
WSF3D1M4_BURNT_50X_2	x1_y7.png	FALSE	FALSE	FALSE	FALSE	FALSE	FALSE	FALSE
WS Fresh_50X_1	x5_y8.png	FALSE	TRUE	FALSE	FALSE	FALSE	FALSE	FALSE
WS Fresh	x3_y0.png	FALSE	FALSE	FALSE	FALSE	FALSE	FALSE	FALSE
WSF3D3M1_BURNT_50X_1	x7_y1.png	FALSE	FALSE	FALSE	FALSE	FALSE	FALSE	FALSE
WSF3D1M3_UNBURNT_1_50X_5	x1_y8.png	FALSE	FALSE	FALSE	FALSE	FALSE	FALSE	FALSE
WSF3D1M3_UNBURNT_1_50X_1	x1_y8.png	FALSE	TRUE	FALSE	FALSE	FALSE	FALSE	FALSE
WSF3D1M5_UNBURNT_1_50X_1	x8_y8.png	FALSE	FALSE	FALSE	FALSE	FALSE	FALSE	FALSE
WS Fresh	x8_y7.png	FALSE	FALSE	FALSE	FALSE	FALSE	FALSE	FALSE
WS Fresh_50X_2	x9_y5.png	FALSE	FALSE	FALSE	FALSE	FALSE	FALSE	FALSE
WSF3D1M3_BURNT_50X_3	x8_y5.png	TRUE	FALSE	FALSE	FALSE	FALSE	FALSE	TRUE
SWF2FR1_BURNT_2_5X_1	x2_y2.png	FALSE	FALSE	FALSE	FALSE	FALSE	FALSE	FALSE
WS Fresh_50X_1	x6_y4.png	FALSE	TRUE	FALSE	FALSE	FALSE	FALSE	TRUE

SWF1FR2_BURNT_50X_3	x7_y4.png	FALSE	TRUE	FALSE	FALSE	FALSE	FALSE	FALSE
WS Fresh_50X_1	x9_y7.png	FALSE	FALSE	FALSE	FALSE	FALSE	FALSE	FALSE
WS Fresh_50X_1	x9_y7.png	FALSE	FALSE	FALSE	FALSE	FALSE	FALSE	FALSE
SWF2FR1_BURNT_2_5X_1	x5_y4.png	FALSE	FALSE	FALSE	FALSE	FALSE	FALSE	FALSE
SWF2FR1_BURNT_1_5X_2	x6_y8.png	FALSE	FALSE	FALSE	FALSE	FALSE	FALSE	FALSE
WSF3D1M2_BURNT_50X_5	x1_y9.png	FALSE	FALSE	FALSE	FALSE	FALSE	FALSE	FALSE
WSF3D1M2_BURNT_50X_5	x7_y1.png	FALSE	FALSE	FALSE	FALSE	FALSE	FALSE	FALSE
WSF3D1M2_BURNT_50X_1	x5_y1.png	FALSE	FALSE	FALSE	FALSE	FALSE	FALSE	TRUE
WSF3D3M4_BURNT_50X_1_3	x4_y0.png	FALSE	FALSE	FALSE	FALSE	FALSE	FALSE	FALSE
SWF1FR2_BURNT_50X_4	x9_y0.png	FALSE	TRUE	FALSE	FALSE	FALSE	FALSE	TRUE
WSF3D1M3_UNBURNT_1_50X_5	x6_y4.png	FALSE	TRUE	FALSE	FALSE	FALSE	FALSE	FALSE
WSF2D2W5_BURNT_50X_1	x2_y4.png	FALSE	FALSE	FALSE	FALSE	FALSE	FALSE	FALSE
WSF3D3M1_BURNT_50X_1_2	x0_y5.png	FALSE	TRUE	FALSE	FALSE	FALSE	FALSE	FALSE
WS Fresh	x6_y7.png	FALSE	FALSE	FALSE	FALSE	FALSE	FALSE	TRUE
WSF3D1M1_BURNT_50X	x7_y3.png	FALSE	TRUE	FALSE	FALSE	FALSE	FALSE	FALSE
WSF3D3M4_BURNT_50X_1_6	x1_y8.png	FALSE	FALSE	FALSE	FALSE	FALSE	FALSE	FALSE
SWF2FR4_BURNT_50X	x3_y8.png	FALSE	FALSE	FALSE	FALSE	FALSE	FALSE	FALSE
WSF3D3M1_BURNT_50X_1_3	x7_y3.png	FALSE	FALSE	FALSE	FALSE	FALSE	FALSE	FALSE
WSF3D3M4_BURNT_50X_1_6	x9_y8.png	FALSE	FALSE	FALSE	FALSE	FALSE	FALSE	FALSE
WS Fresh	x0_y4.png	FALSE	TRUE	FALSE	FALSE	FALSE	FALSE	TRUE
WSF3D1M4_NO2_BURNT_50X_1	x3_y7.png	FALSE	FALSE	FALSE	FALSE	FALSE	FALSE	FALSE
WSF3D1M5_BURNT_50X_2	x8_y1.png	TRUE	FALSE	FALSE	FALSE	FALSE	FALSE	FALSE

SWF2FR1_BURNT_1_5X	x3_y7.png	FALSE	FALSE	FALSE	FALSE	FALSE	FALSE	FALSE
WSF3D1M4_BURNT_50X_2	x6_y4.png	TRUE	TRUE	FALSE	FALSE	FALSE	TRUE	FALSE
SWF1FR2_BURNT_50X_2	x5_y7.png	FALSE	TRUE	FALSE	FALSE	FALSE	FALSE	FALSE
SWF1_BURNT_5_50X_2	x4_y0.png	FALSE	FALSE	FALSE	FALSE	FALSE	FALSE	FALSE
WSF3D1M1_BURNT_50X_3	x6_y5.png	FALSE	FALSE	FALSE	FALSE	FALSE	FALSE	FALSE
WSF3D3M1_BURNT_50X_1_4	x0_y3.png	FALSE	TRUE	FALSE	FALSE	FALSE	FALSE	FALSE
SWF1_BURNT_4_50X_1	x7_y4.png	FALSE	FALSE	FALSE	FALSE	FALSE	FALSE	FALSE
SWF2FR1_BURNT_1_5X_2	x9_y5.png	FALSE	FALSE	FALSE	FALSE	FALSE	FALSE	FALSE
WSF3D1M5_UNBURNT_1_50X_1	x3_y0.png	FALSE	TRUE	FALSE	FALSE	FALSE	FALSE	FALSE
WSF3D1M1_BURNT_50X_7	x4_y6.png	FALSE	FALSE	FALSE	FALSE	FALSE	FALSE	TRUE
WSF3D1M3_UNBURNT_2_50X_1	x2_y9.png	FALSE	TRUE	FALSE	FALSE	FALSE	FALSE	FALSE
SWF2FR1_BURNT_1_5X_2	x6_y2.png	FALSE	FALSE	FALSE	FALSE	FALSE	FALSE	FALSE
WSF3D3M4_BURNT_50X_1_3	x1_y9.png	FALSE	FALSE	FALSE	FALSE	FALSE	FALSE	FALSE
WS Fresh_50X_2	x4_y7.png	FALSE	TRUE	FALSE	FALSE	FALSE	FALSE	FALSE
WSF3D1M4_BURNT_50X_2	x2_y1.png	FALSE	FALSE	FALSE	FALSE	FALSE	FALSE	FALSE
WSF3D1M1_BURNT_50X_9	x9_y8.png	FALSE	FALSE	FALSE	FALSE	FALSE	FALSE	FALSE
WSF3D1M1_BURNT_50X_9	x8_y3.png	FALSE	FALSE	FALSE	FALSE	FALSE	FALSE	TRUE
SWF1FR2_BURNT_50X_2	x3_y6.png	FALSE	TRUE	FALSE	FALSE	FALSE	FALSE	FALSE
WSF3D1M3_BURNT_50X_3	x1_y5.png	FALSE	FALSE	FALSE	FALSE	FALSE	FALSE	FALSE
WSF3D3M4_BURNT_50X_1_3	x3_y4.png	FALSE	TRUE	FALSE	FALSE	FALSE	FALSE	FALSE
SWF1_BURNT_5_50X_3	x2_y1.png	FALSE	FALSE	FALSE	FALSE	FALSE	FALSE	FALSE
SWF1_BURNT_4_50X_3	x0_y1.png	FALSE	FALSE	FALSE	FALSE	FALSE	FALSE	FALSE

WSF3D1M3_UNBURNT_1_50X_1	x5_y1.png	FALSE	TRUE	FALSE	FALSE	FALSE	FALSE	FALSE
WSF3D1M5_BURNT_50X_3	x4_y6.png	FALSE	FALSE	FALSE	FALSE	FALSE	FALSE	FALSE
WSF3D1M1_BURNT_50X_4	x0_y4.png	FALSE	TRUE	FALSE	FALSE	FALSE	FALSE	FALSE
WSF2D2W5_BURNT_50X_2_2	x0_y1.png	TRUE	FALSE	FALSE	FALSE	FALSE	FALSE	FALSE
SWF1FR2_BURNT_50X_3	x0_y7.png	FALSE	FALSE	FALSE	FALSE	FALSE	TRUE	FALSE
WSF3D1M5_UNBURNT_1_50X_1	x2_y0.png	FALSE	TRUE	FALSE	FALSE	FALSE	FALSE	TRUE
WSF3D1M2_BURNT_50X_4	x7_y0.png	FALSE	FALSE	FALSE	FALSE	FALSE	FALSE	FALSE
WSF3D3M1_BURNT_50X_1_2	x1_y3.png	FALSE	FALSE	FALSE	FALSE	FALSE	FALSE	FALSE
WSF3D3M2_BURNT_50X_1_3	x5_y4.png	TRUE	TRUE	FALSE	FALSE	FALSE	FALSE	FALSE
WSF3D1M3_UNBURNT_1_50X_5	x6_y3.png	FALSE	TRUE	FALSE	FALSE	FALSE	FALSE	FALSE
WSF3D1M3_UNBURNT_1_50X_3	x1_y7.png	FALSE	TRUE	FALSE	FALSE	FALSE	FALSE	FALSE
SWF2FR1_BURNT_2_5X_1	x3_y7.png	FALSE	FALSE	FALSE	FALSE	FALSE	FALSE	FALSE
SWF1_BURNT_4_50X_2	x9_y7.png	FALSE	FALSE	FALSE	FALSE	FALSE	FALSE	FALSE
SWF1FR2_BURNT_50X_2	x5_y2.png	FALSE	TRUE	FALSE	FALSE	FALSE	FALSE	TRUE
SWF2FR1_BURNT_1_5X_2	x5_y2.png	FALSE	FALSE	FALSE	FALSE	FALSE	FALSE	FALSE
SWF1_BURNT_4_50X_2	x5_y0.png	FALSE	FALSE	FALSE	FALSE	FALSE	FALSE	FALSE
SWF2FR1_BURNT_2_5X_2	x2_y0.png	FALSE	FALSE	TRUE	FALSE	FALSE	FALSE	FALSE
WSF2D2W5_BURNT_50X_2_2	x6_y6.png	TRUE	FALSE	FALSE	FALSE	FALSE	FALSE	FALSE
WSF3D3M1_BURNT_50X_1_3	x0_y9.png	FALSE	TRUE	FALSE	FALSE	FALSE	FALSE	FALSE
WSF3D1M3_UNBURNT_1_50X_5	x9_y1.png	FALSE	TRUE	FALSE	FALSE	FALSE	FALSE	FALSE

WSF3D3M4_BURNT_50X_1_3	x5_y5.png	FALSE	TRUE	FALSE	FALSE	FALSE	FALSE	FALSE
WSF3D1M5_SMALLPIECE_BURNT_50X_3	x0_y2.png	FALSE	TRUE	FALSE	FALSE	FALSE	FALSE	TRUE
WSF3D3M1_BURNT_50X_1_2	x6_y5.png	FALSE	FALSE	FALSE	FALSE	FALSE	FALSE	FALSE
WSF3D1M1_BURNT_50X_7	x7_y6.png	FALSE	FALSE	FALSE	FALSE	FALSE	FALSE	FALSE
WSF3D1M3_UNBURNT_1_50X_3	x6_y5.png	FALSE	TRUE	FALSE	FALSE	FALSE	FALSE	FALSE
WSF3D1M4_BURNT_50X_1	x8_y1.png	FALSE	FALSE	FALSE	FALSE	FALSE	FALSE	TRUE
WSF3D1M3_UNBURNT_1_50X_1	x7_y0.png	FALSE	TRUE	FALSE	FALSE	FALSE	FALSE	FALSE
SWF1FR2_BURNT_50X_4	x0_y3.png	FALSE	FALSE	TRUE	FALSE	FALSE	FALSE	FALSE
SWF1_BURNT_4_50X_1	x5_y1.png	FALSE	FALSE	FALSE	FALSE	FALSE	FALSE	FALSE
WSF3D3M2_BURNT_100X_1_1	x2_y4.png	FALSE	TRUE	FALSE	FALSE	FALSE	FALSE	TRUE
WSF3D1M5_BURNT_50X_3	x2_y8.png	FALSE	FALSE	FALSE	FALSE	FALSE	FALSE	TRUE
SWF1_BURNT_5_50X_2	x0_y1.png	FALSE	FALSE	FALSE	FALSE	TRUE	FALSE	FALSE
WSF3D1M3_BURNT_50X_1	x3_y7.png	TRUE	FALSE	FALSE	FALSE	FALSE	FALSE	FALSE
WSF3D1M1_BURNT_50X_8	x7_y2.png	FALSE	FALSE	FALSE	FALSE	TRUE	FALSE	FALSE
SWF1_BURNT_4_50X_1	x8_y2.png	FALSE	FALSE	FALSE	FALSE	FALSE	FALSE	FALSE
WSF3D1M3_UNBURNT_2_50X_1	x6_y7.png	FALSE	TRUE	FALSE	FALSE	FALSE	FALSE	FALSE
WSF3D1M4_BURNT_50X_2	x2_y9.png	FALSE	FALSE	FALSE	FALSE	FALSE	FALSE	TRUE
WSF2D2W5_BURNT_50X_2_1	x3_y5.png	TRUE	FALSE	FALSE	FALSE	FALSE	FALSE	TRUE
WSF2D2W5_BURNT_50X_1_3	x0_y4.png	FALSE	FALSE	TRUE	FALSE	FALSE	FALSE	TRUE
WSF3D1M5_BURNT_50X_1	x0_y9.png	FALSE	FALSE	FALSE	FALSE	FALSE	FALSE	FALSE

WSF2D2W5_BURNT_50X_1_3	x5_y8.png	FALSE	FALSE	FALSE	FALSE	FALSE	FALSE	FALSE
WSF3D3M4_BURNT_50X_1_4	x7_y8.png	FALSE	FALSE	FALSE	FALSE	FALSE	FALSE	FALSE
WSF3D3M1_BURNT_50X_1	x2_y8.png	FALSE	FALSE	FALSE	FALSE	FALSE	FALSE	FALSE
WSF3D1M1_BURNT_50X_4	x5_y3.png	FALSE	FALSE	FALSE	FALSE	FALSE	TRUE	FALSE
WSF3D1M2_BURNT_50X_3	x6_y2.png	FALSE	FALSE	FALSE	FALSE	FALSE	FALSE	FALSE
WSF3D3M1_BURNT_50X_1_4	x8_y1.png	FALSE	FALSE	FALSE	FALSE	FALSE	FALSE	FALSE
WSF3D1M2_BURNT_50X_2	x4_y9.png	FALSE	FALSE	FALSE	FALSE	FALSE	FALSE	FALSE
WSF3D1M3_BURNT_50X_3	x4_y3.png	FALSE	FALSE	TRUE	FALSE	FALSE	FALSE	TRUE
WSF3D1M4_BURNT_50X_4	x3_y1.png	FALSE	FALSE	FALSE	FALSE	FALSE	FALSE	TRUE
WSF3D1M1_BURNT_50X_6	x9_y3.png	FALSE	TRUE	FALSE	FALSE	FALSE	FALSE	FALSE
WSF3D3M1_BURNT_50X_1_4	x3_y6.png	FALSE	FALSE	FALSE	FALSE	FALSE	FALSE	FALSE
WSF3D1M1_BURNT_50X_3	x1_y5.png	FALSE	FALSE	FALSE	FALSE	FALSE	FALSE	FALSE
WS Fresh	x9_y0.png	FALSE	FALSE	FALSE	FALSE	FALSE	FALSE	FALSE
WSF3D1M3_UNBURNT_2_50X_1	x7_y8.png	FALSE	TRUE	FALSE	FALSE	FALSE	FALSE	FALSE
WSF2D2W5_BURNT_50X_2_1	x3_y4.png	TRUE	FALSE	FALSE	FALSE	FALSE	FALSE	FALSE
SWF1_BURNT_5_50X_1	x0_y0.png	FALSE	FALSE	FALSE	FALSE	FALSE	FALSE	FALSE
WSF2D2W5_BURNT_50X_1_2	x0_y5.png	TRUE	TRUE	FALSE	FALSE	FALSE	FALSE	FALSE
WSF3D1M4_NO2_BURNT_50X_1	x0_y5.png	FALSE	FALSE	FALSE	FALSE	FALSE	FALSE	FALSE
WSF3D3M4_BURNT_50X_1_1	x0_y0.png	FALSE	TRUE	FALSE	FALSE	FALSE	FALSE	TRUE

WSF3D1M2_BURNT_50X_1	x0_y6.png	TRUE	FALSE	FALSE	FALSE	FALSE	FALSE	FALSE
WSF3D1M3_UNBURNT_1_50X_3	x7_y5.png	FALSE	TRUE	TRUE	FALSE	FALSE	FALSE	FALSE
WSF3D3M4_BURNT_50X_1_2	x3_y8.png	FALSE	FALSE	FALSE	FALSE	FALSE	FALSE	FALSE
SWF1_BURNT_5_50X_2	x0_y5.png	TRUE	FALSE	TRUE	FALSE	FALSE	FALSE	FALSE
WSF3D3M1_BURNT_50X_1_2	x5_y2.png	FALSE	TRUE	FALSE	FALSE	FALSE	FALSE	FALSE
WSF3D3M2_BURNT_50X_1_1	x5_y5.png	FALSE	FALSE	FALSE	FALSE	FALSE	FALSE	FALSE
WSF3D3M4_BURNT_50X_1_1	x0_y6.png	FALSE	FALSE	FALSE	FALSE	FALSE	FALSE	FALSE
WSF3D1M1_BURNT_50X_12	x1_y5.png	FALSE	FALSE	FALSE	FALSE	FALSE	TRUE	FALSE
WSF3D1M5_BURNT_50X_3	x3_y6.png	FALSE	FALSE	FALSE	TRUE	FALSE	FALSE	FALSE
WSF3D1M4_NO2_BURNT_50X_2	x1_y3.png	FALSE	FALSE	FALSE	FALSE	FALSE	FALSE	FALSE
SWF1_BURNT_5_50X_2	x8_y5.png	FALSE	FALSE	TRUE	FALSE	FALSE	FALSE	FALSE
WSF3D3M2_BURNT_100X_1_1	x9_y0.png	FALSE	TRUE	FALSE	FALSE	TRUE	FALSE	TRUE
WS Fresh	x1_y8.png	FALSE	FALSE	FALSE	FALSE	FALSE	FALSE	FALSE
SWF2FR1_BURNT_1_5X_2	x3_y5.png	FALSE	FALSE	FALSE	FALSE	FALSE	FALSE	FALSE
WSF3D1M3_UNBURNT_1_50X_3	x4_y5.png	FALSE	TRUE	FALSE	FALSE	FALSE	FALSE	FALSE
WS Fresh	x2_y7.png	FALSE	TRUE	FALSE	FALSE	FALSE	FALSE	FALSE
WSF3D3M4_BURNT_50X_1_5	x6_y4.png	FALSE	TRUE	FALSE	FALSE	FALSE	FALSE	FALSE
WSF3D3M4_BURNT_50X_1_6	x4_y6.png	FALSE	TRUE	FALSE	FALSE	FALSE	FALSE	FALSE
WSF3D3M2_BURNT_50X_1_2	x3_y2.png	FALSE	TRUE	TRUE	FALSE	FALSE	FALSE	FALSE
WSF3D3M1_BURNT_50X_1_4	x8_y8.png	FALSE	FALSE	FALSE	FALSE	FALSE	FALSE	FALSE

WSF3D1M3_BURNT_50X_1	x2_y5.png	FALSE	FALSE	TRUE	FALSE	FALSE	FALSE	FALSE
WSF3D1M4_BURNT_50X_3	x5_y6.png	FALSE	TRUE	FALSE	FALSE	FALSE	FALSE	TRUE
WSF3D3M2_BURNT_100X_1_1	x2_y8.png	FALSE	TRUE	FALSE	TRUE	FALSE	FALSE	FALSE
WSF2D2W5_UNBURNT_1_50X_3	x6_y8.png	FALSE	TRUE	FALSE	FALSE	FALSE	FALSE	FALSE
WSF2D2W3_UNBURNT_1_50X_1	x6_y5.png	FALSE	TRUE	FALSE	FALSE	FALSE	FALSE	FALSE
WSF2D2W5_UNBURNT_1_50X_2	x0_y2.png	FALSE	TRUE	FALSE	FALSE	FALSE	FALSE	FALSE
WSF3D1M2_BURNT_50X_1	x4_y0.png	FALSE	TRUE	TRUE	FALSE	FALSE	FALSE	FALSE
WSF2D2W1_UNBURNT_3_50X_1	x3_y0.png	FALSE	FALSE	FALSE	FALSE	FALSE	FALSE	TRUE
WSF2D2W1_UNBURNT_2_50X_1	x5_y2.png	FALSE	TRUE	FALSE	FALSE	FALSE	FALSE	FALSE
WSF3D3M3_UNBURNT_1_50X_4	x0_y0.png	TRUE	FALSE	FALSE	FALSE	FALSE	FALSE	FALSE
WSF3D3M1_BURNT_50X_1_4	x9_y1.png	FALSE	FALSE	FALSE	FALSE	FALSE	FALSE	FALSE
WS Fresh_50X_1	x7_y3.png	FALSE	FALSE	FALSE	FALSE	FALSE	FALSE	FALSE
WSF3D1M2_BURNT_50X_6	x9_y4.png	FALSE	TRUE	FALSE	FALSE	FALSE	FALSE	FALSE
WSF3D1M3_BURNT_50X_1	x1_y1.png	FALSE	FALSE	FALSE	FALSE	FALSE	TRUE	TRUE
WSF3D3M4_BURNT_50X_1_6	x1_y9.png	FALSE	FALSE	FALSE	FALSE	FALSE	FALSE	FALSE
WSF3D3M4_BURNT_50X_1_1	x4_y7.png	FALSE	FALSE	FALSE	FALSE	FALSE	TRUE	FALSE
WSF3D1M5_SMALLPIECE_BURNT_50X_3	x6_y8.png	FALSE	FALSE	FALSE	FALSE	FALSE	FALSE	FALSE
WSF2D2W1_UNBURNT_1_50X_1	x2_y2.png	FALSE	TRUE	FALSE	FALSE	FALSE	FALSE	FALSE
WSF3D1M1_BURNT_50X_3	x6_y7.png	TRUE	TRUE	FALSE	FALSE	FALSE	FALSE	FALSE

WSF3D1M4_BURNT_50X_3	x1_y7.png	TRUE	FALSE	FALSE	FALSE	FALSE	FALSE	FALSE
WSF3D3M4_BURNT_50X_1_5	x6_y5.png	FALSE	TRUE	TRUE	FALSE	FALSE	FALSE	FALSE
WSF3D3M1_BURNT_50X_1_3	x4_y9.png	FALSE	FALSE	FALSE	FALSE	FALSE	FALSE	FALSE
SWF2FR1_BURNT_2_5X_1	x1_y9.png	FALSE	FALSE	FALSE	FALSE	FALSE	FALSE	FALSE
WS Fresh_50X_1	x2_y6.png	FALSE	FALSE	FALSE	FALSE	FALSE	FALSE	FALSE
WSF3D1M4_NO2_BURNT_50X_3	x5_y6.png	TRUE	FALSE	FALSE	FALSE	FALSE	FALSE	FALSE
WSF3D3M2_BURNT_100X_1_1	x6_y2.png	FALSE	TRUE	FALSE	FALSE	FALSE	FALSE	FALSE
WSF3D1M1_BURNT_50X_5	x8_y3.png	FALSE	FALSE	FALSE	FALSE	FALSE	FALSE	FALSE
WSF2D2W5_BURNT_50X_2_2	x7_y7.png	TRUE	FALSE	FALSE	FALSE	FALSE	FALSE	TRUE
WSF2D2W1_UNBURNT_3_50X_3	x2_y0.png	FALSE	FALSE	FALSE	FALSE	FALSE	FALSE	FALSE
WSF3D3M4_BURNT_50X_1_6	x6_y9.png	FALSE	FALSE	FALSE	FALSE	FALSE	FALSE	FALSE
WSF3D1M1_BURNT_50X_10	x6_y6.png	TRUE	FALSE	FALSE	FALSE	FALSE	FALSE	FALSE
WSF3D1M2_BURNT_50X_1	x8_y2.png	FALSE	FALSE	FALSE	FALSE	FALSE	FALSE	FALSE
WSF2D2W1_UNBURNT_3_50X_1	x2_y0.png	FALSE	FALSE	FALSE	FALSE	FALSE	FALSE	FALSE
WSF3D3M3_UNBURNT_1_50X_5	x2_y8.png	TRUE	TRUE	FALSE	FALSE	FALSE	FALSE	FALSE
WSF3D1M3_UNBURNT_2_50X_1	x3_y0.png	FALSE	TRUE	FALSE	FALSE	FALSE	FALSE	FALSE
SWF2FR1_BURNT_1_5X_2	x7_y6.png	FALSE	FALSE	TRUE	FALSE	FALSE	FALSE	FALSE
WSF2D2W1_UNBURNT_2_50X_1	x7_y6.png	FALSE	TRUE	FALSE	FALSE	FALSE	FALSE	FALSE
WSF2D2W5_UNBURNT_2_50X_3	x9_y6.png	FALSE	FALSE	FALSE	TRUE	FALSE	FALSE	TRUE

WSF3D3M3_UNBURNT_1_50X_5	x1_y1.png	FALSE	FALSE	FALSE	FALSE	FALSE	FALSE	TRUE
WSF3D3M4_BURNT_50X_1_4	x4_y0.png	FALSE	FALSE	FALSE	FALSE	FALSE	FALSE	FALSE
WSF3D3M3_UNBURNT_1_50X_5	x2_y2.png	FALSE	TRUE	FALSE	FALSE	FALSE	FALSE	FALSE
WSF3D1M4_BURNT_50X_3	x6_y7.png	TRUE	TRUE	FALSE	TRUE	FALSE	FALSE	FALSE
WSF3D1M4_BURNT_50X_1	x0_y4.png	FALSE	FALSE	FALSE	FALSE	TRUE	FALSE	FALSE
WSF3D1M1_BURNT_50X_8	x0_y9.png	FALSE	FALSE	FALSE	FALSE	FALSE	FALSE	FALSE
WSF3D3M3_UNBURNT_1_50X_3	x6_y7.png	TRUE	TRUE	FALSE	FALSE	FALSE	FALSE	FALSE
WSF2D2W3_UNBURNT_1_50X_1	x3_y6.png	TRUE	TRUE	FALSE	FALSE	FALSE	FALSE	FALSE
WS Fresh_50X_3	x9_y8.png	FALSE	FALSE	FALSE	FALSE	FALSE	FALSE	FALSE
WSF3D1M4_BURNT_50X_1	x8_y6.png	FALSE	FALSE	FALSE	FALSE	FALSE	FALSE	TRUE
WSF2D2W5_UNBURNT_1_50X_2	x3_y0.png	FALSE	TRUE	FALSE	FALSE	FALSE	FALSE	FALSE
WSF2D2W5_BURNT_50X_1_3	x4_y0.png	FALSE	FALSE	FALSE	FALSE	FALSE	FALSE	FALSE
WSF3D3M2_BURNT_50X_1_3	x9_y7.png	FALSE	FALSE	FALSE	FALSE	FALSE	FALSE	FALSE
WSF2D2W5_UNBURNT_2_50X_2	x4_y2.png	TRUE	TRUE	FALSE	FALSE	FALSE	FALSE	FALSE
WSF3D3M4_BURNT_50X_1_1	x9_y5.png	FALSE	FALSE	FALSE	FALSE	FALSE	TRUE	FALSE
WSF3D3M2_BURNT_100X_1_1	x0_y0.png	FALSE	FALSE	FALSE	FALSE	FALSE	FALSE	FALSE
WSF3D3M4_BURNT_50X_1_3	x4_y5.png	FALSE	TRUE	FALSE	FALSE	FALSE	FALSE	FALSE
WSF3D1M4_NO2_BURNT_50X_2	x6_y0.png	FALSE	FALSE	FALSE	FALSE	FALSE	FALSE	FALSE
SWF2FR1_BURNT_2_5X_2	x6_y2.png	FALSE	FALSE	FALSE	FALSE	FALSE	FALSE	FALSE

WSF3D1M3_UNBURNT_2_50X_1	x1_y0.png	FALSE	TRUE	FALSE	FALSE	FALSE	FALSE	FALSE
SWF1FR2_BURNT_50X_2	x7_y6.png	FALSE	TRUE	FALSE	TRUE	FALSE	FALSE	FALSE
WS Fresh	x1_y4.png	FALSE	FALSE	FALSE	FALSE	FALSE	FALSE	TRUE
WSF3D1M3_UNBURNT_1_50X_1	x0_y6.png	FALSE	TRUE	FALSE	FALSE	FALSE	FALSE	FALSE
WSF3D1M2_BURNT_50X_6	x0_y0.png	TRUE	FALSE	TRUE	FALSE	FALSE	FALSE	TRUE
WSF3D1M5_BURNT_50X_3	x0_y2.png	FALSE	FALSE	FALSE	FALSE	FALSE	FALSE	FALSE
WSF2D2W3_UNBURNT_1_50X_4	x3_y8.png	TRUE	TRUE	FALSE	FALSE	FALSE	FALSE	FALSE
WSF2D2W1_UNBURNT_3_50X_2	x4_y0.png	FALSE	TRUE	FALSE	FALSE	FALSE	FALSE	FALSE
WSF3D3M3_UNBURNT_1_50X_1	x3_y6.png	FALSE	FALSE	FALSE	FALSE	FALSE	FALSE	FALSE
WSF3D3M4_BURNT_50X_1_1	x8_y6.png	FALSE	FALSE	TRUE	FALSE	FALSE	FALSE	FALSE
SWF1_BURNT_5_50X_2	x5_y0.png	FALSE	FALSE	FALSE	FALSE	FALSE	FALSE	FALSE
WSF3D3M4_BURNT_50X_1_6	x8_y1.png	FALSE	FALSE	FALSE	FALSE	FALSE	FALSE	FALSE
WSF3D1M1_BURNT_50X_3	x1_y0.png	FALSE	FALSE	FALSE	FALSE	FALSE	FALSE	TRUE
SWF2FR1_BURNT_2_5X_1	x1_y1.png	FALSE	FALSE	FALSE	FALSE	FALSE	FALSE	FALSE
WSF3D3M3_UNBURNT_1_50X_4	x0_y5.png	FALSE	FALSE	FALSE	FALSE	FALSE	FALSE	FALSE
WSF3D1M2_BURNT_50X_5	x2_y0.png	FALSE	FALSE	FALSE	FALSE	FALSE	FALSE	FALSE
WSF2D2W5_BURNT_50X_1	x4_y0.png	FALSE	FALSE	FALSE	FALSE	FALSE	FALSE	FALSE
WSF3D1M3_UNBURNT_1_50X_1	x2_y8.png	FALSE	TRUE	FALSE	FALSE	FALSE	FALSE	FALSE
WSF3D1M4_BURNT_50X_2	x8_y0.png	FALSE	TRUE	FALSE	FALSE	FALSE	FALSE	TRUE
WSF2D2W5_BURNT_50X_1_2	x5_y7.png	TRUE	TRUE	FALSE	FALSE	FALSE	FALSE	FALSE

WS Fresh_50X_3	x2_y9.png	FALSE	FALSE	FALSE	FALSE	FALSE	FALSE	FALSE
WSF2D2W1_UNBURNT_1_50X_1	x6_y6.png	FALSE	TRUE	FALSE	FALSE	FALSE	FALSE	FALSE
WSF3D1M4_BURNT_50X_1	x3_y6.png	FALSE	TRUE	FALSE	TRUE	FALSE	FALSE	FALSE
WS Fresh_50X_3	x6_y9.png	FALSE	FALSE	FALSE	FALSE	FALSE	FALSE	FALSE
WS Fresh	x0_y2.png	FALSE	TRUE	FALSE	FALSE	FALSE	FALSE	TRUE
WSF2D2W1_UNBURNT_1_50X_2	x0_y5.png	FALSE	FALSE	FALSE	FALSE	FALSE	FALSE	FALSE
SWF1_BURNT_4_50X_3	x2_y8.png	FALSE	FALSE	FALSE	FALSE	FALSE	FALSE	FALSE
SWF1_BURNT_4_50X_2	x3_y4.png	FALSE	FALSE	FALSE	FALSE	FALSE	FALSE	FALSE
WSF3D1M5_SMALLPIECE_BURNT_50X_3	x8_y6.png	TRUE	FALSE	FALSE	FALSE	FALSE	FALSE	FALSE
SWF1FR2_BURNT_50X_4	x8_y5.png	FALSE	TRUE	FALSE	FALSE	FALSE	FALSE	FALSE
WSF2D2W3_UNBURNT_1_50X_1	x3_y5.png	FALSE	TRUE	TRUE	FALSE	FALSE	FALSE	FALSE
WSF2D2W1_UNBURNT_1_50X_2	x6_y2.png	FALSE	TRUE	FALSE	FALSE	FALSE	FALSE	FALSE
WSF3D1M5_UNBURNT_1_50X_1	x4_y1.png	FALSE	TRUE	FALSE	FALSE	FALSE	FALSE	FALSE
WSF2D2W1_UNBURNT_1_50X_1	x5_y8.png	FALSE	TRUE	FALSE	FALSE	FALSE	FALSE	FALSE
WSF3D1M1_BURNT_50X_9	x3_y4.png	TRUE	FALSE	FALSE	FALSE	FALSE	FALSE	TRUE
WSF3D3M2_BURNT_50X_1_3	x4_y6.png	TRUE	TRUE	FALSE	FALSE	FALSE	FALSE	FALSE
WS Fresh_50X_2	x3_y9.png	FALSE	FALSE	FALSE	FALSE	FALSE	FALSE	FALSE
SWF1_BURNT_5_50X_2	x9_y5.png	FALSE	FALSE	TRUE	FALSE	FALSE	FALSE	FALSE
WSF2D2W1_UNBURNT_1_50X_1	x0_y4.png	FALSE	TRUE	FALSE	FALSE	FALSE	FALSE	FALSE
WSF3D3M1_BURNT_50X_1_2	x9_y6.png	FALSE	FALSE	TRUE	FALSE	FALSE	FALSE	FALSE
WSF2D2W5_BURNT_50X_2_2	x5_y5.png	FALSE	FALSE	TRUE	FALSE	FALSE	FALSE	FALSE
WSF3D3M2_BURNT_50X_1_1	x8_y1.png	FALSE	FALSE	FALSE	FALSE	FALSE	FALSE	FALSE

WSF3D1M1_BURNT_50X_3	x6_y6.png	FALSE	TRUE	FALSE	FALSE	FALSE	FALSE	TRUE
SWF2FR1_BURNT_2_5X_2	x6_y5.png	FALSE	FALSE	FALSE	FALSE	FALSE	FALSE	FALSE
WSF2D2W5_UNBURNT_1_50X_3	x6_y3.png	FALSE	TRUE	FALSE	FALSE	FALSE	FALSE	FALSE
WSF3D1M3_BURNT_50X_2	x4_y5.png	TRUE	TRUE	TRUE	FALSE	FALSE	FALSE	FALSE
WSF3D3M3_UNBURNT_1_50X_1	x7_y8.png	FALSE	TRUE	TRUE	FALSE	FALSE	FALSE	FALSE
SWF1_BURNT_4_50X_2	x4_y7.png	FALSE	FALSE	FALSE	FALSE	FALSE	FALSE	FALSE
WSF2D2W1_UNBURNT_1_50X_1	x1_y8.png	TRUE	TRUE	FALSE	FALSE	FALSE	FALSE	FALSE
WSF3D1M4_BURNT_50X_3	x1_y9.png	TRUE	FALSE	FALSE	FALSE	FALSE	FALSE	FALSE
SWF1FR2_BURNT_50X_3	x5_y8.png	FALSE	FALSE	FALSE	FALSE	FALSE	FALSE	FALSE
WSF3D1M5_SMALLPIECE_BURNT_50X_3	x9_y4.png	TRUE	FALSE	FALSE	FALSE	FALSE	FALSE	FALSE
WSF3D1M1_BURNT_50X_10	x2_y4.png	FALSE	FALSE	FALSE	FALSE	FALSE	FALSE	FALSE
WSF3D3M4_BURNT_50X_1_5	x4_y9.png	FALSE	FALSE	FALSE	FALSE	FALSE	FALSE	FALSE
WSF2D2W5_BURNT_50X_1_3	x3_y3.png	TRUE	FALSE	TRUE	FALSE	FALSE	FALSE	FALSE
WSF2D2W5_UNBURNT_1_50X_1	x4_y4.png	FALSE	TRUE	TRUE	FALSE	FALSE	FALSE	FALSE
WSF3D1M4_BURNT_50X_4	x8_y4.png	TRUE	FALSE	FALSE	FALSE	FALSE	FALSE	FALSE
WSF3D3M3_UNBURNT_1_50X_5	x9_y6.png	TRUE	TRUE	FALSE	FALSE	FALSE	FALSE	FALSE
WSF3D1M2_BURNT_50X_2	x2_y2.png	TRUE	FALSE	FALSE	FALSE	FALSE	FALSE	FALSE
WSF2D2W5_UNBURNT_2_50X_2	x9_y5.png	FALSE	TRUE	TRUE	FALSE	FALSE	FALSE	FALSE
SWF1FR2_BURNT_50X_2	x3_y7.png	FALSE	TRUE	FALSE	FALSE	FALSE	FALSE	TRUE
SWF2FR1_BURNT_2_5X_1	x6_y3.png	FALSE	FALSE	FALSE	FALSE	FALSE	FALSE	FALSE

WSF3D1M2_BURNT_50X_6	x0_y1.png	FALSE	FALSE	FALSE	FALSE	FALSE	FALSE	TRUE
WSF2D2W5_UNBURNT_2_50X_3	x7_y4.png	FALSE	TRUE	FALSE	FALSE	FALSE	FALSE	TRUE
SWF1FR2_BURNT_50X_3	x1_y1.png	FALSE	FALSE	FALSE	FALSE	FALSE	FALSE	FALSE
WS Fresh_50X_3	x9_y0.png	FALSE	FALSE	FALSE	FALSE	FALSE	FALSE	FALSE
WSF2D2W5_UNBURNT_2_50X_2	x9_y2.png	TRUE	TRUE	FALSE	FALSE	FALSE	FALSE	FALSE
WSF2D2W5_UNBURNT_2_50X_2	x0_y4.png	FALSE	TRUE	FALSE	FALSE	FALSE	FALSE	TRUE
WSF3D1M3_UNBURNT_1_50X_1	x4_y1.png	FALSE	TRUE	FALSE	FALSE	FALSE	FALSE	TRUE
WSF3D1M3_UNBURNT_2_50X_1	x2_y4.png	FALSE	TRUE	FALSE	FALSE	FALSE	FALSE	FALSE
WSF2D2W1_UNBURNT_1_50X_3	x5_y5.png	TRUE	TRUE	FALSE	FALSE	FALSE	FALSE	FALSE
WSF2D2W5_BURNT_50X_2_1	x0_y9.png	FALSE	FALSE	FALSE	FALSE	FALSE	FALSE	FALSE
WSF3D1M3_BURNT_50X_2	x3_y3.png	FALSE	FALSE	FALSE	FALSE	FALSE	FALSE	FALSE
WSF3D3M1_BURNT_50X_1_3	x8_y9.png	FALSE	FALSE	FALSE	FALSE	FALSE	FALSE	FALSE
WSF2D2W1_UNBURNT_1_50X_3	x2_y7.png	FALSE	TRUE	TRUE	FALSE	FALSE	FALSE	FALSE
SWF1_BURNT_5_50X_2	x2_y8.png	TRUE	FALSE	FALSE	FALSE	FALSE	FALSE	FALSE
WSF2D2W5_UNBURNT_2_50X_4	x8_y2.png	FALSE	TRUE	FALSE	FALSE	FALSE	FALSE	TRUE
SWF1FR2_BURNT_50X_4	x4_y8.png	FALSE	TRUE	FALSE	TRUE	FALSE	FALSE	FALSE
WSF3D1M1_BURNT_50X_8	x1_y7.png	TRUE	FALSE	TRUE	FALSE	FALSE	FALSE	FALSE
SWF1FR2_BURNT_50X_4	x5_y1.png	FALSE	FALSE	FALSE	FALSE	FALSE	FALSE	FALSE
WSF3D3M2_BURNT_50X_1_2	x2_y9.png	TRUE	TRUE	FALSE	FALSE	FALSE	FALSE	FALSE
WSF2D2W1_UNBURNT_3_50X_1	x3_y8.png	FALSE	TRUE	FALSE	FALSE	FALSE	FALSE	FALSE
SWF2FR1_BURNT_2_5X_1	x1_y6.png	FALSE	FALSE	FALSE	FALSE	FALSE	FALSE	FALSE

WSF3D1M1_BURNT_50X_6	x3_y5.png	FALSE	FALSE	FALSE	FALSE	FALSE	FALSE	FALSE
WS Fresh_50X_2	x0_y6.png	FALSE	TRUE	FALSE	FALSE	FALSE	FALSE	FALSE
WSF3D3M2_BURNT_50X_1_2	x3_y3.png	TRUE	TRUE	FALSE	FALSE	FALSE	FALSE	FALSE
SWF1_BURNT_4_50X_3	x0_y0.png	FALSE	FALSE	FALSE	FALSE	FALSE	FALSE	FALSE
SWF1_BURNT_3_50X_1	x4_y8.png	TRUE	FALSE	FALSE	FALSE	FALSE	FALSE	FALSE
WSF3D1M1_BURNT_50X_8	x4_y8.png	FALSE	FALSE	FALSE	FALSE	FALSE	FALSE	FALSE
WSF3D1M4_NO2_BURNT_50X_1	x9_y1.png	FALSE	FALSE	FALSE	FALSE	FALSE	FALSE	FALSE
WSF3D1M3_UNBURNT_1_50X_4	x9_y9.png	TRUE	TRUE	FALSE	FALSE	FALSE	FALSE	FALSE
WSF2D2W1_UNBURNT_3_50X_1	x9_y6.png	FALSE	TRUE	TRUE	FALSE	FALSE	FALSE	FALSE
SWF1_BURNT_5_50X_2	x0_y7.png	FALSE	FALSE	TRUE	FALSE	FALSE	FALSE	FALSE
WSF2D2W1_UNBURNT_1_50X_3	x1_y1.png	FALSE	FALSE	FALSE	FALSE	FALSE	FALSE	TRUE
WSF2D2W5_BURNT_50X_1_3	x0_y7.png	FALSE	FALSE	FALSE	FALSE	FALSE	FALSE	FALSE
WSF2D2W5_UNBURNT_2_50X_1	x3_y4.png	TRUE	TRUE	FALSE	FALSE	FALSE	FALSE	FALSE
WSF2D2W3_UNBURNT_1_50X_3	x8_y9.png	TRUE	FALSE	FALSE	FALSE	FALSE	FALSE	FALSE
WS Fresh	x5_y5.png	FALSE	TRUE	FALSE	FALSE	FALSE	FALSE	FALSE
WSF3D3M4_BURNT_50X_1_2	x1_y3.png	FALSE	FALSE	FALSE	FALSE	FALSE	TRUE	FALSE
WSF2D2W1_UNBURNT_2_50X_1	x7_y0.png	FALSE	TRUE	TRUE	FALSE	FALSE	FALSE	FALSE
WSF2D2W5_UNBURNT_1_50X_2	x6_y9.png	FALSE	TRUE	FALSE	FALSE	FALSE	FALSE	FALSE
WSF2D2W5_UNBURNT_2_50X_1	x3_y9.png	TRUE	FALSE	FALSE	FALSE	FALSE	FALSE	TRUE
WSF2D2W1_UNBURNT_3_50X_2	x7_y4.png	FALSE	TRUE	FALSE	FALSE	FALSE	FALSE	FALSE
WSF3D1M4_NO2_BURNT_50X_1	x9_y8.png	FALSE	FALSE	TRUE	FALSE	FALSE	FALSE	FALSE

WSF3D1M4_NO2_BURNT_50X_3	x8_y2.png	FALSE	FALSE	FALSE	FALSE	FALSE	FALSE	FALSE
WSF3D1M1_BURNT_50X_4	x5_y0.png	TRUE	FALSE	FALSE	FALSE	FALSE	FALSE	FALSE
WSF2D2W5_UNBURNT_2_50X_1	x0_y9.png	TRUE	TRUE	FALSE	FALSE	FALSE	FALSE	FALSE
WSF2D2W5_BURNT_50X_2_2	x3_y1.png	TRUE	FALSE	FALSE	FALSE	FALSE	FALSE	TRUE
WSF2D2W1_UNBURNT_2_50X_1	x8_y3.png	FALSE	TRUE	TRUE	FALSE	FALSE	FALSE	FALSE
WSF3D1M4_BURNT_50X_4	x5_y7.png	TRUE	TRUE	FALSE	FALSE	FALSE	FALSE	FALSE
WSF3D3M4_BURNT_50X_1_5	x9_y1.png	TRUE	FALSE	FALSE	FALSE	FALSE	FALSE	FALSE
WSF3D3M2_BURNT_50X_1_1	x4_y1.png	FALSE	FALSE	FALSE	FALSE	FALSE	FALSE	FALSE
WSF3D3M4_BURNT_50X_1_1	x2_y0.png	FALSE	FALSE	FALSE	FALSE	FALSE	TRUE	FALSE
WSF3D3M3_UNBURNT_1_50X_3	x6_y0.png	TRUE	TRUE	FALSE	FALSE	FALSE	FALSE	FALSE
WSF2D2W1_UNBURNT_2_50X_2	x6_y9.png	FALSE	TRUE	FALSE	FALSE	FALSE	FALSE	FALSE
WSF2D2W1_UNBURNT_3_50X_3	x7_y8.png	FALSE	TRUE	FALSE	FALSE	FALSE	FALSE	FALSE
WSF3D3M1_BURNT_50X_1_2	x9_y3.png	FALSE	TRUE	FALSE	FALSE	FALSE	FALSE	FALSE
WSF3D1M3_BURNT_50X_3	x2_y7.png	FALSE	FALSE	TRUE	FALSE	FALSE	FALSE	FALSE
SWF1_BURNT_5_50X_2	x3_y9.png	TRUE	FALSE	FALSE	FALSE	FALSE	TRUE	FALSE
WSF3D3M4_BURNT_50X_1_3	x3_y1.png	FALSE	TRUE	TRUE	FALSE	FALSE	FALSE	FALSE
WSF3D1M3_BURNT_50X_3	x5_y6.png	FALSE	FALSE	TRUE	FALSE	FALSE	FALSE	FALSE
WSF2D2W3_UNBURNT_1_50X_3	x6_y7.png	FALSE	TRUE	TRUE	FALSE	FALSE	FALSE	TRUE
WSF3D1M5_BURNT_50X_1	x6_y6.png	FALSE	FALSE	FALSE	FALSE	FALSE	FALSE	FALSE

WSF3D3M1_BURNT_50X_1_2	x5_y5.png	FALSE	FALSE	FALSE	FALSE	FALSE	FALSE	FALSE
WSF3D1M1_BURNT_50X_12	x5_y1.png	FALSE	FALSE	FALSE	FALSE	FALSE	TRUE	FALSE
WS Fresh	x3_y2.png	FALSE	FALSE	FALSE	FALSE	FALSE	FALSE	FALSE
SWF1_BURNT_4_50X_1	x9_y8.png	FALSE	FALSE	FALSE	FALSE	FALSE	FALSE	FALSE
WSF2D2W3_UNBURNT_1_50X_4	x4_y9.png	TRUE	TRUE	TRUE	FALSE	FALSE	FALSE	FALSE
WSF3D1M2_BURNT_50X_5	x7_y5.png	FALSE	FALSE	FALSE	FALSE	FALSE	FALSE	FALSE
WSF3D1M3_BURNT_50X_3	x4_y1.png	FALSE	FALSE	FALSE	FALSE	FALSE	TRUE	FALSE
WSF3D1M4_BURNT_50X_1	x7_y4.png	TRUE	FALSE	FALSE	FALSE	FALSE	FALSE	FALSE
WSF3D1M3_BURNT_50X_2	x8_y4.png	TRUE	FALSE	FALSE	FALSE	FALSE	FALSE	FALSE
WSF3D3M2_BURNT_100X_1_1	x1_y3.png	FALSE	FALSE	FALSE	FALSE	FALSE	FALSE	FALSE
WSF2D2W3_UNBURNT_1_50X_3	x1_y8.png	TRUE	FALSE	FALSE	TRUE	FALSE	FALSE	FALSE
WSF3D3M4_BURNT_50X_1_2	x6_y4.png	FALSE	TRUE	FALSE	TRUE	FALSE	FALSE	FALSE
WSF3D3M4_BURNT_50X_1_4	x8_y1.png	FALSE	FALSE	FALSE	FALSE	FALSE	FALSE	FALSE
WSF3D1M5_SMALLPIECE_BURNT_50X_4	x4_y7.png	FALSE	FALSE	FALSE	FALSE	FALSE	FALSE	FALSE
WSF3D3M1_BURNT_50X_1_4	x2_y2.png	FALSE	FALSE	FALSE	FALSE	FALSE	FALSE	FALSE
SWF1_BURNT_5_50X_2	x4_y7.png	FALSE	FALSE	FALSE	FALSE	FALSE	FALSE	FALSE
WSF2D2W5_BURNT_50X_2_2	x8_y2.png	TRUE	FALSE	TRUE	FALSE	FALSE	FALSE	FALSE
WSF3D3M3_UNBURNT_1_50X_2	x6_y2.png	FALSE	FALSE	FALSE	FALSE	FALSE	FALSE	FALSE
WSF3D1M4_NO2_BURNT_50X_3	x0_y8.png	FALSE	FALSE	FALSE	FALSE	FALSE	FALSE	FALSE
SWF1FR2_BURNT_50X_3	x8_y4.png	FALSE	TRUE	FALSE	FALSE	FALSE	FALSE	FALSE

WSF3D1M1_BURNT_50X_12	x5_y5.png	FALSE	FALSE	FALSE	FALSE	FALSE	FALSE	FALSE
WSF2D2W5_UNBURNT_1_50X_3	x6_y2.png	FALSE	TRUE	TRUE	FALSE	FALSE	FALSE	FALSE
SWF1_BURNT_4_50X_1	x3_y7.png	FALSE	FALSE	FALSE	FALSE	FALSE	FALSE	FALSE
SWF1_BURNT_4_50X_2	x8_y6.png	FALSE	FALSE	FALSE	FALSE	FALSE	FALSE	FALSE
WSF2D2W1_UNBURNT_3_50X_1	x0_y5.png	FALSE	FALSE	FALSE	FALSE	FALSE	FALSE	FALSE
WSF3D3M4_BURNT_50X_1_5	x1_y1.png	FALSE	FALSE	FALSE	FALSE	FALSE	FALSE	FALSE
WSF3D3M3_UNBURNT_1_50X_5	x9_y0.png	FALSE	FALSE	FALSE	FALSE	FALSE	FALSE	FALSE
WSF3D3M1_BURNT_50X_1_4	x9_y3.png	FALSE	FALSE	FALSE	FALSE	FALSE	FALSE	FALSE
WSF3D1M3_BURNT_50X_1	x4_y0.png	FALSE	FALSE	FALSE	FALSE	FALSE	FALSE	TRUE
WSF3D1M2_BURNT_50X_1	x2_y8.png	FALSE	FALSE	FALSE	FALSE	FALSE	FALSE	FALSE
WSF2D2W5_UNBURNT_2_50X_4	x1_y8.png	TRUE	TRUE	FALSE	FALSE	FALSE	FALSE	TRUE
WSF3D3M2_BURNT_100X_1_1	x5_y7.png	FALSE	TRUE	FALSE	FALSE	FALSE	FALSE	FALSE
WSF3D3M4_BURNT_50X_1_4	x9_y6.png	FALSE	FALSE	FALSE	FALSE	FALSE	FALSE	FALSE
WSF3D1M4_BURNT_50X_4	x0_y7.png	FALSE	FALSE	FALSE	FALSE	FALSE	FALSE	FALSE
WSF2D2W5_UNBURNT_2_50X_1	x1_y2.png	TRUE	FALSE	TRUE	FALSE	FALSE	FALSE	FALSE
WSF3D1M1_BURNT_50X_2	x9_y5.png	FALSE	FALSE	FALSE	FALSE	FALSE	FALSE	FALSE
WS Fresh	x0_y9.png	FALSE	TRUE	FALSE	FALSE	FALSE	FALSE	FALSE
SWF1_BURNT_5_50X_1	x4_y1.png	FALSE	FALSE	FALSE	FALSE	FALSE	FALSE	FALSE
WSF3D1M2_BURNT_50X_1	x5_y8.png	TRUE	FALSE	TRUE	FALSE	FALSE	FALSE	FALSE
WSF2D2W1_UNBURNT_2_50X_3	x3_y6.png	FALSE	TRUE	FALSE	FALSE	FALSE	FALSE	FALSE

WSF3D3M1_BURNT_50X_1_2	x7_y9.png	FALSE	FALSE	FALSE	FALSE	FALSE	TRUE	FALSE
WSF3D1M3_UNBURNT_1_50X_1	x1_y6.png	FALSE	TRUE	FALSE	FALSE	FALSE	FALSE	FALSE
WSF3D3M2_BURNT_50X_1_3	x2_y7.png	FALSE	TRUE	FALSE	FALSE	FALSE	FALSE	FALSE
WSF2D2W1_UNBURNT_1_50X_3	x6_y3.png	FALSE	TRUE	FALSE	FALSE	FALSE	FALSE	TRUE
WSF3D3M2_BURNT_100X_1_1	x8_y5.png	TRUE	FALSE	TRUE	FALSE	FALSE	FALSE	FALSE
WSF3D1M3_BURNT_50X_3	x6_y6.png	FALSE	FALSE	TRUE	FALSE	FALSE	FALSE	FALSE
WSF2D2W1_UNBURNT_2_50X_3	x1_y2.png	FALSE	TRUE	TRUE	FALSE	FALSE	FALSE	FALSE
WSF3D1M3_UNBURNT_1_50X_3	x1_y5.png	FALSE	TRUE	FALSE	FALSE	FALSE	FALSE	FALSE
WSF3D1M5_BURNT_50X_1	x8_y7.png	FALSE	FALSE	FALSE	FALSE	FALSE	FALSE	FALSE
WSF3D1M1_BURNT_50X_8	x0_y2.png	TRUE	FALSE	FALSE	FALSE	FALSE	FALSE	TRUE
WSF2D2W1_UNBURNT_2_50X_3	x5_y5.png	FALSE	TRUE	FALSE	FALSE	FALSE	FALSE	FALSE
SWF1FR2_BURNT_50X_1	x5_y3.png	TRUE	FALSE	FALSE	FALSE	FALSE	FALSE	TRUE
WSF2D2W5_BURNT_50X_1	x4_y9.png	FALSE	FALSE	FALSE	FALSE	FALSE	FALSE	FALSE
WSF2D2W1_UNBURNT_1_50X_3	x5_y3.png	TRUE	TRUE	FALSE	FALSE	FALSE	FALSE	FALSE
SWF1_BURNT_4_50X_2	x6_y1.png	FALSE	FALSE	FALSE	FALSE	FALSE	FALSE	FALSE
WSF2D2W1_UNBURNT_2_50X_3	x0_y8.png	FALSE	TRUE	TRUE	FALSE	FALSE	FALSE	FALSE
WSF3D3M3_UNBURNT_1_50X_1	x5_y9.png	TRUE	FALSE	FALSE	FALSE	FALSE	FALSE	FALSE
WSF2D2W3_UNBURNT_1_50X_3	x5_y6.png	TRUE	TRUE	FALSE	FALSE	FALSE	FALSE	FALSE
WSF2D2W5_UNBURNT_1_50X_2	x0_y1.png	FALSE	TRUE	TRUE	FALSE	FALSE	FALSE	FALSE

WSF3D1M2_BURNT_50X_4	x0_y4.png	FALSE	FALSE	FALSE	FALSE	FALSE	FALSE	TRUE
WSF3D1M4_NO2_BURNT_50X_3	x0_y2.png	FALSE	FALSE	FALSE	FALSE	FALSE	FALSE	FALSE
WSF3D1M1_BURNT_50X_12	x7_y7.png	FALSE	FALSE	FALSE	FALSE	FALSE	FALSE	FALSE
SWF2FR1_BURNT_1_5X	x4_y9.png	FALSE	FALSE	FALSE	FALSE	FALSE	FALSE	FALSE
SWF1FR2_BURNT_50X_1	x7_y2.png	TRUE	FALSE	FALSE	FALSE	FALSE	FALSE	FALSE
WSF2D2W5_UNBURNT_2_50X_2	x9_y9.png	FALSE	TRUE	TRUE	FALSE	FALSE	FALSE	FALSE
WSF3D1M1_BURNT_50X_12	x9_y6.png	FALSE	FALSE	FALSE	FALSE	FALSE	FALSE	FALSE
SWF1_BURNT_5_50X_1	x5_y6.png	FALSE	FALSE	TRUE	FALSE	FALSE	FALSE	FALSE
WSF2D2W1_UNBURNT_2_50X_1	x2_y8.png	FALSE	TRUE	FALSE	FALSE	FALSE	FALSE	TRUE
WSF2D2W5_BURNT_50X_2_1	x7_y2.png	TRUE	FALSE	FALSE	FALSE	FALSE	FALSE	FALSE
WSF2D2W3_UNBURNT_1_50X_3	x4_y3.png	FALSE	TRUE	FALSE	FALSE	FALSE	FALSE	FALSE
WSF3D1M1_BURNT_50X_4	x9_y0.png	FALSE	FALSE	FALSE	FALSE	FALSE	FALSE	FALSE
WSF3D1M3_UNBURNT_1_50X_4	x5_y0.png	FALSE	TRUE	TRUE	FALSE	FALSE	FALSE	FALSE
WSF3D3M4_BURNT_50X_1_5	x9_y0.png	FALSE	FALSE	FALSE	FALSE	FALSE	FALSE	FALSE
WSF3D1M3_UNBURNT_2_50X_1	x6_y8.png	FALSE	TRUE	FALSE	FALSE	FALSE	FALSE	FALSE
WSF2D2W3_UNBURNT_1_50X_3	x3_y7.png	FALSE	TRUE	TRUE	FALSE	FALSE	FALSE	FALSE
WSF2D2W1_UNBURNT_1_50X_2	x9_y1.png	FALSE	TRUE	FALSE	FALSE	FALSE	FALSE	FALSE
WSF2D2W5_BURNT_50X_1_2	x5_y1.png	TRUE	TRUE	FALSE	FALSE	FALSE	FALSE	FALSE
WSF3D1M4_NO2_BURNT_50X_2	x7_y3.png	TRUE	FALSE	TRUE	FALSE	FALSE	FALSE	FALSE
WSF3D1M1_BURNT_50X_2	x1_y3.png	TRUE	TRUE	FALSE	FALSE	FALSE	FALSE	FALSE

WSF3D1M2_BURNT_50X_5	x0_y6.png	TRUE	FALSE	FALSE	FALSE	FALSE	FALSE	FALSE
SWF1_BURNT_3_50X_1	x8_y0.png	FALSE	FALSE	FALSE	FALSE	FALSE	FALSE	FALSE
WSF3D3M4_BURNT_50X_1_1	x0_y4.png	FALSE	FALSE	FALSE	FALSE	FALSE	FALSE	FALSE
WSF3D1M4_NO2_BURNT_50X_1	x7_y0.png	FALSE	FALSE	FALSE	FALSE	FALSE	FALSE	FALSE
WSF3D3M4_BURNT_50X_1_6	x7_y0.png	FALSE	FALSE	FALSE	FALSE	FALSE	FALSE	FALSE
WSF3D1M4_BURNT_50X_3	x3_y9.png	TRUE	FALSE	FALSE	FALSE	FALSE	FALSE	FALSE
WSF3D1M1_BURNT_50X_4	x4_y6.png	FALSE	TRUE	FALSE	TRUE	FALSE	FALSE	FALSE
WSF3D1M1_BURNT_50X_9	x5_y4.png	TRUE	FALSE	FALSE	FALSE	FALSE	FALSE	TRUE
WSF2D2W3_UNBURNT_1_50X_1	x1_y8.png	TRUE	TRUE	FALSE	FALSE	FALSE	FALSE	FALSE
WSF2D2W1_UNBURNT_2_50X_1	x0_y2.png	FALSE	FALSE	FALSE	FALSE	FALSE	FALSE	TRUE
WS Fresh_50X_1	x6_y5.png	FALSE	FALSE	FALSE	FALSE	FALSE	FALSE	FALSE
SWF1_BURNT_3_50X_1	x1_y8.png	FALSE	FALSE	FALSE	FALSE	FALSE	FALSE	FALSE
WSF3D1M1_BURNT_50X_5	x5_y4.png	FALSE	FALSE	FALSE	FALSE	FALSE	FALSE	FALSE
WSF2D2W3_UNBURNT_1_50X_3	x8_y6.png	FALSE	TRUE	FALSE	FALSE	FALSE	FALSE	FALSE
SWF2FR1_BURNT_1_5X_2	x8_y7.png	FALSE	FALSE	FALSE	FALSE	FALSE	FALSE	FALSE
WSF3D3M3_UNBURNT_1_50X_5	x8_y2.png	TRUE	FALSE	FALSE	FALSE	FALSE	FALSE	FALSE
WSF3D3M4_BURNT_50X_1_5	x5_y3.png	FALSE	TRUE	FALSE	FALSE	FALSE	FALSE	FALSE
WSF2D2W1_UNBURNT_2_50X_1	x9_y2.png	FALSE	TRUE	FALSE	FALSE	FALSE	FALSE	FALSE
WSF2D2W5_BURNT_50X_2_2	x5_y0.png	TRUE	FALSE	FALSE	FALSE	FALSE	TRUE	FALSE
WS Fresh	x7_y8.png	FALSE	FALSE	FALSE	FALSE	FALSE	FALSE	FALSE

WSF3D1M1_BURNT_50X_3	x9_y6.png	FALSE	FALSE	FALSE	FALSE	FALSE	FALSE	FALSE
WSF2D2W5_UNBURNT_2_50X_3	x6_y0.png	FALSE	TRUE	TRUE	FALSE	FALSE	FALSE	FALSE
WSF3D1M3_BURNT_50X_1	x1_y6.png	FALSE	FALSE	FALSE	FALSE	FALSE	FALSE	FALSE
WSF2D2W5_UNBURNT_1_50X_2	x1_y9.png	TRUE	FALSE	FALSE	FALSE	FALSE	FALSE	TRUE
SWF1FR2_BURNT_50X_2	x1_y5.png	FALSE	TRUE	FALSE	FALSE	FALSE	FALSE	TRUE
WSF3D1M4_BURNT_50X_4	x9_y8.png	FALSE	TRUE	FALSE	FALSE	FALSE	FALSE	FALSE
WSF2D2W5_UNBURNT_1_50X_2	x8_y0.png	FALSE	FALSE	FALSE	FALSE	FALSE	FALSE	FALSE
SWF1_BURNT_5_50X_1	x0_y3.png	FALSE	FALSE	FALSE	FALSE	FALSE	FALSE	FALSE
WSF3D1M1_BURNT_50X_2	x0_y3.png	FALSE	FALSE	FALSE	FALSE	FALSE	TRUE	FALSE
SWF1FR2_BURNT_50X_2	x0_y8.png	FALSE	FALSE	TRUE	FALSE	FALSE	FALSE	FALSE
WSF2D2W3_UNBURNT_1_50X_2	x6_y7.png	TRUE	FALSE	FALSE	FALSE	FALSE	FALSE	FALSE
WSF3D3M1_BURNT_50X_1_3	x0_y4.png	FALSE	FALSE	FALSE	FALSE	FALSE	FALSE	FALSE
WSF3D1M3_BURNT_50X_3	x0_y2.png	TRUE	FALSE	FALSE	FALSE	FALSE	FALSE	FALSE
WSF3D1M3_UNBURNT_1_50X_4	x5_y8.png	FALSE	TRUE	FALSE	FALSE	FALSE	FALSE	FALSE
WS Fresh	x6_y5.png	FALSE	FALSE	FALSE	FALSE	FALSE	FALSE	FALSE
WSF3D1M3_UNBURNT_2_50X_1	x5_y0.png	FALSE	TRUE	TRUE	FALSE	FALSE	FALSE	FALSE
WSF3D3M2_BURNT_100X_1_1	x3_y5.png	TRUE	TRUE	FALSE	FALSE	FALSE	FALSE	FALSE
WSF2D2W3_UNBURNT_1_50X_2	x6_y5.png	TRUE	TRUE	FALSE	FALSE	FALSE	FALSE	FALSE
WSF2D2W5_UNBURNT_2_50X_1	x5_y3.png	FALSE	TRUE	FALSE	FALSE	FALSE	FALSE	FALSE
SWF1FR2_BURNT_50X_1	x5_y0.png	FALSE	FALSE	FALSE	FALSE	FALSE	FALSE	FALSE
WSF2D2W5_BURNT_50X_2_2	x1_y5.png	FALSE	FALSE	TRUE	FALSE	FALSE	FALSE	FALSE

WSF3D1M5_UNBURNT_1_50X_1	x1_y5.png	TRUE	TRUE	TRUE	FALSE	FALSE	FALSE	FALSE
WSF2D2W5_UNBURNT_2_50X_2	x7_y5.png	FALSE	TRUE	TRUE	FALSE	FALSE	FALSE	FALSE
WSF3D1M5_SMALLPIECE_BURNT_50X_4	x1_y5.png	FALSE	FALSE	FALSE	FALSE	FALSE	FALSE	FALSE
WSF2D2W5_BURNT_50X_2_1	x9_y3.png	TRUE	FALSE	FALSE	FALSE	FALSE	FALSE	FALSE
SWF2FR1_BURNT_2_5X_1	x5_y1.png	FALSE	FALSE	FALSE	FALSE	FALSE	FALSE	FALSE
WS Fresh_50X_3	x5_y8.png	FALSE	FALSE	FALSE	FALSE	FALSE	TRUE	FALSE
WSF2D2W1_UNBURNT_3_50X_2	x6_y6.png	FALSE	TRUE	FALSE	FALSE	FALSE	FALSE	FALSE
WSF2D2W3_UNBURNT_1_50X_2	x0_y6.png	TRUE	FALSE	FALSE	FALSE	FALSE	FALSE	FALSE
WSF3D1M3_BURNT_50X_1	x7_y9.png	FALSE	FALSE	FALSE	FALSE	FALSE	FALSE	FALSE
WSF3D1M1_BURNT_50X_3	x2_y3.png	FALSE	FALSE	FALSE	FALSE	FALSE	FALSE	FALSE
WSF3D1M4_NO2_BURNT_50X_2	x4_y7.png	FALSE	FALSE	FALSE	FALSE	FALSE	FALSE	FALSE
SWF1_BURNT_3_50X_1	x4_y2.png	TRUE	FALSE	FALSE	FALSE	FALSE	FALSE	FALSE
WSF2D2W3_UNBURNT_1_50X_3	x7_y6.png	FALSE	TRUE	FALSE	FALSE	FALSE	FALSE	TRUE
WSF3D1M2_BURNT_50X_3	x4_y0.png	FALSE	FALSE	FALSE	FALSE	FALSE	FALSE	TRUE
SWF2FR4_BURNT_50X	x2_y6.png	FALSE	FALSE	FALSE	FALSE	FALSE	FALSE	FALSE
WSF3D3M2_BURNT_50X_1_1	x7_y8.png	FALSE	FALSE	FALSE	FALSE	FALSE	FALSE	FALSE
SWF1FR2_BURNT_50X_3	x9_y5.png	FALSE	TRUE	FALSE	TRUE	FALSE	FALSE	FALSE
WSF3D1M2_BURNT_50X_4	x7_y4.png	FALSE	FALSE	TRUE	FALSE	FALSE	FALSE	FALSE
SWF1FR2_BURNT_50X_4	x7_y6.png	FALSE	TRUE	FALSE	FALSE	FALSE	FALSE	FALSE
WSF3D1M2_BURNT_50X_3	x3_y9.png	FALSE	FALSE	FALSE	FALSE	FALSE	FALSE	FALSE
WSF2D2W5_BURNT_50X_2_1	x8_y8.png	TRUE	FALSE	FALSE	FALSE	FALSE	FALSE	FALSE

WSF2D2W5_UNBURNT_1_50X_1	x0_y9.png	TRUE	TRUE	FALSE	FALSE	FALSE	FALSE	FALSE
WSF2D2W5_BURNT_50X_2_1	x0_y3.png	TRUE	FALSE	FALSE	FALSE	FALSE	FALSE	FALSE
WSF2D2W1_UNBURNT_1_50X_3	x5_y9.png	FALSE	TRUE	FALSE	FALSE	FALSE	FALSE	FALSE
WSF3D3M3_UNBURNT_1_50X_3	x7_y9.png	TRUE	TRUE	FALSE	FALSE	FALSE	FALSE	FALSE
SWF2FR4_BURNT_50X	x0_y7.png	FALSE	FALSE	FALSE	FALSE	FALSE	FALSE	FALSE
SWF1_BURNT_3_50X_1	x4_y0.png	FALSE	FALSE	FALSE	FALSE	FALSE	FALSE	FALSE
WSF2D2W1_UNBURNT_1_50X_2	x5_y9.png	TRUE	TRUE	FALSE	FALSE	FALSE	FALSE	FALSE
WSF2D2W5_BURNT_50X_2_1	x8_y6.png	TRUE	FALSE	FALSE	FALSE	FALSE	FALSE	FALSE
WSF3D1M5_SMALLPIECE_BURNT_50X_3	x8_y3.png	FALSE	FALSE	FALSE	FALSE	FALSE	FALSE	TRUE
WSF3D1M5_SMALLPIECE_BURNT_50X_4	x8_y0.png	FALSE	FALSE	FALSE	FALSE	FALSE	FALSE	FALSE
WSF3D1M2_BURNT_50X_4	x6_y6.png	FALSE	FALSE	FALSE	FALSE	FALSE	FALSE	FALSE
SWF1_BURNT_4_50X_1	x4_y7.png	FALSE	FALSE	FALSE	FALSE	FALSE	FALSE	FALSE
WSF2D2W1_UNBURNT_2_50X_2	x3_y2.png	FALSE	TRUE	FALSE	FALSE	FALSE	FALSE	FALSE
WS Fresh_50X_1	x2_y1.png	FALSE	FALSE	FALSE	FALSE	FALSE	FALSE	TRUE
WSF2D2W3_UNBURNT_1_50X_3	x2_y8.png	TRUE	TRUE	FALSE	FALSE	FALSE	FALSE	TRUE
WSF2D2W5_UNBURNT_1_50X_2	x2_y1.png	FALSE	TRUE	TRUE	FALSE	FALSE	FALSE	FALSE
WSF3D1M3_UNBURNT_1_50X_4	x1_y1.png	FALSE	TRUE	FALSE	FALSE	FALSE	FALSE	FALSE
SWF1_BURNT_5_50X_3	x9_y8.png	FALSE	FALSE	FALSE	FALSE	FALSE	FALSE	FALSE
WSF3D3M4_BURNT_50X_1_3	x3_y6.png	FALSE	TRUE	FALSE	FALSE	FALSE	FALSE	FALSE
WSF2D2W5_UNBURNT_2_50X_1	x5_y8.png	FALSE	TRUE	FALSE	FALSE	FALSE	FALSE	TRUE
WSF2D2W5_UNBURNT_2_50X_1	x5_y8.png	FALSE	TRUE	FALSE	FALSE	FALSE	FALSE	TRUE

SWF1FR2_BURNT_50X_4	x1_y3.png	FALSE	FALSE	FALSE	FALSE	FALSE	FALSE	TRUE
WSF2D2W1_UNBURNT_3_50X_1	x1_y4.png	FALSE	FALSE	TRUE	FALSE	FALSE	FALSE	TRUE
WSF2D2W5_UNBURNT_2_50X_2	x3_y3.png	FALSE	TRUE	TRUE	FALSE	FALSE	FALSE	FALSE
WSF3D1M5_BURNT_50X_3	x2_y7.png	FALSE	FALSE	FALSE	FALSE	FALSE	FALSE	FALSE
WSF3D1M4_BURNT_50X_3	x1_y6.png	TRUE	FALSE	FALSE	FALSE	FALSE	FALSE	FALSE
WSF2D2W1_UNBURNT_1_50X_2	x0_y9.png	TRUE	FALSE	FALSE	FALSE	FALSE	FALSE	FALSE
WSF3D3M4_BURNT_50X_1_6	x1_y2.png	FALSE	FALSE	FALSE	FALSE	FALSE	FALSE	FALSE
WSF3D1M4_BURNT_50X_4	x3_y6.png	FALSE	TRUE	FALSE	FALSE	TRUE	FALSE	TRUE
WSF3D1M1_BURNT_50X	x9_y7.png	TRUE	FALSE	FALSE	FALSE	FALSE	FALSE	FALSE
SWF1FR2_BURNT_50X_3	x3_y8.png	FALSE	FALSE	FALSE	FALSE	FALSE	TRUE	TRUE
WSF2D2W5_UNBURNT_1_50X_3	x0_y3.png	TRUE	TRUE	FALSE	FALSE	FALSE	FALSE	FALSE
WSF2D2W1_UNBURNT_1_50X_3	x6_y8.png	TRUE	FALSE	FALSE	FALSE	FALSE	FALSE	TRUE
WSF2D2W1_UNBURNT_2_50X_1	x2_y7.png	TRUE	TRUE	FALSE	FALSE	FALSE	FALSE	FALSE
WSF2D2W5_UNBURNT_1_50X_2	x3_y3.png	TRUE	TRUE	FALSE	FALSE	FALSE	FALSE	FALSE
SWF1FR2_BURNT_50X_1	x7_y6.png	TRUE	FALSE	FALSE	FALSE	FALSE	FALSE	TRUE
WSF3D3M1_BURNT_50X_1_4	x9_y0.png	FALSE	FALSE	FALSE	FALSE	FALSE	FALSE	FALSE
WSF3D3M2_BURNT_50X_1_2	x3_y8.png	TRUE	TRUE	FALSE	FALSE	FALSE	FALSE	FALSE
WSF3D1M2_BURNT_50X_5	x2_y5.png	FALSE	FALSE	FALSE	FALSE	FALSE	FALSE	FALSE
WSF2D2W1_UNBURNT_3_50X_1	x4_y9.png	FALSE	TRUE	FALSE	FALSE	FALSE	FALSE	FALSE
SWF2FR1_BURNT_2_5X_1	x6_y1.png	FALSE	FALSE	TRUE	FALSE	FALSE	FALSE	FALSE
WS Fresh	x8_y2.png	FALSE	FALSE	FALSE	FALSE	FALSE	FALSE	FALSE

WSF3D3M3_UNBURNT_1_50X_4	x5_y0.png	TRUE	FALSE	FALSE	FALSE	FALSE	FALSE	TRUE
WSF3D1M2_BURNT_50X_6	x5_y2.png	FALSE	FALSE	FALSE	FALSE	FALSE	FALSE	FALSE
WSF3D3M4_BURNT_50X_1_6	x8_y0.png	FALSE	FALSE	FALSE	FALSE	FALSE	FALSE	FALSE
WSF3D1M5_SMALLPIECE_BURNT_50X_4	x2_y0.png	FALSE	FALSE	FALSE	FALSE	FALSE	FALSE	FALSE
WSF2D2W3_UNBURNT_1_50X_3	x6_y5.png	TRUE	TRUE	FALSE	FALSE	FALSE	FALSE	FALSE
SWF2FR1_BURNT_1_5X_2	x1_y9.png	FALSE	FALSE	FALSE	FALSE	FALSE	FALSE	FALSE
WSF2D2W1_UNBURNT_3_50X_1	x5_y0.png	FALSE	FALSE	FALSE	FALSE	FALSE	FALSE	FALSE
WSF3D3M4_BURNT_50X_1_4	x0_y7.png	FALSE	FALSE	FALSE	FALSE	FALSE	FALSE	FALSE
WSF3D3M4_BURNT_50X_1_6	x2_y0.png	FALSE	FALSE	FALSE	FALSE	FALSE	FALSE	FALSE
WSF3D1M3_BURNT_50X_2	x5_y2.png	FALSE	TRUE	FALSE	FALSE	TRUE	FALSE	TRUE
WSF3D1M3_BURNT_50X_3	x9_y3.png	TRUE	FALSE	TRUE	FALSE	FALSE	TRUE	FALSE
WSF2D2W3_UNBURNT_1_50X_2	x2_y1.png	TRUE	TRUE	FALSE	FALSE	FALSE	FALSE	FALSE
WSF3D1M1_BURNT_50X_10	x4_y2.png	FALSE	FALSE	FALSE	FALSE	FALSE	TRUE	TRUE
WSF2D2W1_UNBURNT_2_50X_3	x0_y9.png	TRUE	TRUE	FALSE	FALSE	TRUE	FALSE	FALSE
WSF2D2W1_UNBURNT_2_50X_3	x6_y9.png	FALSE	TRUE	FALSE	FALSE	FALSE	FALSE	FALSE
WSF2D2W1_UNBURNT_1_50X_3	x8_y1.png	TRUE	TRUE	FALSE	FALSE	FALSE	FALSE	FALSE
WSF2D2W5_UNBURNT_2_50X_1	x1_y4.png	TRUE	TRUE	TRUE	FALSE	FALSE	FALSE	FALSE
WSF3D3M4_BURNT_50X_1_2	x0_y4.png	FALSE	FALSE	FALSE	FALSE	FALSE	FALSE	FALSE
WSF3D1M5_SMALLPIECE_BURNT_50X_4	x4_y3.png	FALSE	FALSE	FALSE	FALSE	FALSE	FALSE	FALSE

WSF2D2W5_UNBURNT_1_50X_3	x8_y0.png	TRUE	TRUE	FALSE	FALSE	FALSE	FALSE	FALSE
WSF2D2W5_UNBURNT_1_50X_1	x8_y5.png	FALSE	TRUE	FALSE	FALSE	FALSE	FALSE	FALSE
WSF2D2W3_UNBURNT_1_50X_2	x8_y7.png	TRUE	TRUE	FALSE	FALSE	TRUE	FALSE	FALSE
WSF3D1M3_BURNT_50X_2	x5_y5.png	TRUE	TRUE	FALSE	FALSE	FALSE	FALSE	FALSE
SWF1FR2_BURNT_50X_3	x8_y8.png	FALSE	FALSE	FALSE	FALSE	FALSE	TRUE	FALSE
WSF2D2W3_UNBURNT_1_50X_4	x0_y2.png	TRUE	TRUE	FALSE	FALSE	FALSE	FALSE	FALSE
WSF3D1M4_BURNT_50X_3	x8_y6.png	TRUE	FALSE	FALSE	FALSE	FALSE	FALSE	FALSE
SWF2FR1_BURNT_2_5X_2	x5_y7.png	FALSE	FALSE	FALSE	FALSE	FALSE	FALSE	FALSE
WSF2D2W3_UNBURNT_1_50X_3	x1_y6.png	TRUE	TRUE	FALSE	FALSE	FALSE	FALSE	FALSE
WSF3D1M1_BURNT_50X_10	x3_y1.png	FALSE	FALSE	FALSE	FALSE	FALSE	FALSE	FALSE
WSF3D1M3_UNBURNT_1_50X_1	x9_y9.png	TRUE	TRUE	FALSE	FALSE	FALSE	FALSE	FALSE
WSF3D1M1_BURNT_50X_12	x4_y3.png	FALSE	FALSE	FALSE	FALSE	FALSE	FALSE	FALSE
WSF3D1M5_SMALLPIECE_BURNT_50X_3	x9_y2.png	TRUE	FALSE	FALSE	FALSE	FALSE	FALSE	FALSE
WSF3D1M1_BURNT_50X_7	x6_y8.png	FALSE	FALSE	FALSE	FALSE	FALSE	TRUE	FALSE
WSF3D1M2_BURNT_50X_5	x3_y0.png	TRUE	FALSE	FALSE	FALSE	FALSE	FALSE	FALSE
WSF3D1M1_BURNT_50X_7	x3_y8.png	TRUE	FALSE	FALSE	FALSE	FALSE	FALSE	FALSE
WSF3D3M2_BURNT_100X_1_1	x7_y6.png	FALSE	TRUE	FALSE	FALSE	FALSE	FALSE	TRUE
WSF3D1M3_UNBURNT_1_50X_3	x4_y8.png	FALSE	TRUE	FALSE	FALSE	FALSE	FALSE	FALSE
SWF1_BURNT_5_50X_1	x4_y7.png	TRUE	FALSE	TRUE	FALSE	FALSE	FALSE	FALSE

WSF2D2W1_UNBURNT_3_50X_1	x2_y4.png	FALSE	FALSE	FALSE	FALSE	FALSE	FALSE	FALSE
WSF3D1M2_BURNT_50X_2	x0_y2.png	FALSE	FALSE	FALSE	FALSE	FALSE	FALSE	FALSE
WSF2D2W1_UNBURNT_2_50X_1	x1_y0.png	TRUE	FALSE	FALSE	FALSE	FALSE	FALSE	FALSE
WSF3D3M4_BURNT_50X_1_6	x6_y6.png	FALSE	TRUE	FALSE	FALSE	FALSE	FALSE	FALSE
WSF2D2W5_BURNT_50X_2_1	x5_y6.png	FALSE	FALSE	TRUE	FALSE	FALSE	FALSE	TRUE
SWF1FR2_BURNT_50X_3	x3_y7.png	FALSE	TRUE	FALSE	FALSE	FALSE	FALSE	FALSE
WSF3D1M5_SMALLPIECE_BURNT_50X_4	x8_y1.png	FALSE	FALSE	FALSE	FALSE	FALSE	TRUE	FALSE
WSF2D2W5_UNBURNT_2_50X_2	x2_y1.png	TRUE	TRUE	FALSE	FALSE	FALSE	FALSE	FALSE
WSF3D1M4_BURNT_50X_2	x5_y2.png	FALSE	TRUE	FALSE	TRUE	FALSE	FALSE	FALSE
WSF2D2W1_UNBURNT_2_50X_3	x1_y5.png	FALSE	TRUE	FALSE	FALSE	FALSE	FALSE	FALSE
WSF3D1M1_BURNT_50X_5	x1_y6.png	FALSE	TRUE	FALSE	FALSE	FALSE	FALSE	FALSE
WSF3D1M1_BURNT_50X_9	x1_y5.png	FALSE	FALSE	FALSE	FALSE	FALSE	FALSE	FALSE
WSF3D3M1_BURNT_50X_1_3	x3_y3.png	FALSE	FALSE	FALSE	FALSE	FALSE	FALSE	FALSE
WSF3D3M3_UNBURNT_1_50X_4	x2_y0.png	TRUE	FALSE	FALSE	FALSE	FALSE	FALSE	FALSE
WSF3D3M2_BURNT_50X_1_2	x4_y2.png	FALSE	TRUE	FALSE	FALSE	FALSE	FALSE	FALSE
WS Fresh_50X_1	x5_y5.png	FALSE	FALSE	FALSE	FALSE	FALSE	FALSE	FALSE
SWF1FR2_BURNT_50X_4	x5_y9.png	FALSE	TRUE	FALSE	FALSE	FALSE	TRUE	TRUE
WSF3D1M4_BURNT_50X_2	x4_y3.png	TRUE	FALSE	FALSE	FALSE	FALSE	FALSE	TRUE
SWF2FR1_BURNT_2_5X_1	x7_y3.png	FALSE	FALSE	FALSE	FALSE	FALSE	FALSE	FALSE
WSF3D1M1_BURNT_50X_3	x1_y6.png	FALSE	FALSE	FALSE	FALSE	FALSE	FALSE	FALSE

SWF1FR2_BURNT_50X_4	x8_y7.png	FALSE	TRUE	TRUE	FALSE	FALSE	FALSE	FALSE
WSF3D3M4_BURNT_50X_1_6	x3_y9.png	FALSE	FALSE	FALSE	FALSE	FALSE	FALSE	FALSE
SWF1_BURNT_5_50X_2	x8_y9.png	TRUE	FALSE	FALSE	FALSE	FALSE	FALSE	FALSE
WSF3D1M1_BURNT_50X_6	x0_y6.png	FALSE	TRUE	FALSE	FALSE	FALSE	FALSE	FALSE
SWF1_BURNT_5_50X_2	x7_y0.png	FALSE	FALSE	FALSE	FALSE	FALSE	FALSE	FALSE
WSF2D2W5_BURNT_50X_1_3	x1_y0.png	FALSE	TRUE	FALSE	FALSE	FALSE	FALSE	FALSE
WSF2D2W1_UNBURNT_2_50X_2	x3_y0.png	TRUE	TRUE	FALSE	FALSE	FALSE	FALSE	FALSE
WSF2D2W5_BURNT_50X_2_1	x8_y7.png	TRUE	FALSE	FALSE	FALSE	FALSE	FALSE	FALSE
WSF3D1M3_UNBURNT_1_50X_4	x2_y6.png	FALSE	TRUE	FALSE	FALSE	FALSE	FALSE	FALSE
SWF1FR2_BURNT_50X_3	x1_y6.png	FALSE	TRUE	FALSE	FALSE	FALSE	TRUE	TRUE
WSF3D1M2_BURNT_50X_4	x9_y2.png	FALSE	FALSE	FALSE	FALSE	FALSE	FALSE	FALSE
WSF3D1M2_BURNT_50X_5	x0_y2.png	TRUE	FALSE	FALSE	FALSE	FALSE	FALSE	FALSE
WSF2D2W5_UNBURNT_2_50X_1	x8_y0.png	FALSE	FALSE	FALSE	FALSE	FALSE	TRUE	FALSE
SWF2FR4_BURNT_50X	x8_y3.png	FALSE	FALSE	FALSE	FALSE	FALSE	FALSE	FALSE
WSF3D3M2_BURNT_50X_1_3	x4_y7.png	FALSE	TRUE	TRUE	FALSE	FALSE	TRUE	FALSE
WSF3D3M4_BURNT_50X_1_2	x0_y6.png	FALSE	FALSE	FALSE	FALSE	FALSE	FALSE	FALSE
SWF1FR2_BURNT_50X_3	x8_y2.png	FALSE	FALSE	FALSE	FALSE	FALSE	FALSE	FALSE
WSF3D1M1_BURNT_50X_5	x2_y9.png	TRUE	FALSE	FALSE	FALSE	FALSE	FALSE	FALSE
WSF3D1M2_BURNT_50X_6	x5_y0.png	TRUE	FALSE	FALSE	FALSE	FALSE	FALSE	FALSE
WSF3D1M1_BURNT_50X_3	x1_y9.png	FALSE	FALSE	FALSE	FALSE	FALSE	FALSE	FALSE
WSF3D3M3_UNBURNT_1_50X_3	x3_y8.png	FALSE	FALSE	FALSE	FALSE	FALSE	FALSE	FALSE

WSF3D3M1_BURNT_50X_1_4	x3_y9.png	FALSE	FALSE	FALSE	FALSE	FALSE	FALSE	FALSE
WSF3D1M5_BURNT_50X_3	x5_y0.png	FALSE	FALSE	FALSE	FALSE	FALSE	FALSE	FALSE
WSF2D2W5_BURNT_50X_1_3	x9_y3.png	FALSE	FALSE	FALSE	FALSE	FALSE	FALSE	TRUE
WSF3D3M4_BURNT_50X_1_6	x0_y1.png	FALSE	FALSE	FALSE	FALSE	FALSE	FALSE	FALSE
WSF2D2W1_UNBURNT_3_50X_1	x7_y6.png	FALSE	TRUE	FALSE	FALSE	TRUE	FALSE	TRUE
WSF3D1M1_BURNT_50X_7	x7_y0.png	TRUE	FALSE	FALSE	FALSE	FALSE	FALSE	FALSE
SWF2FR1_BURNT_1_5X	x3_y6.png	FALSE	FALSE	FALSE	FALSE	FALSE	FALSE	FALSE
WSF3D1M3_BURNT_50X_1	x1_y7.png	FALSE	FALSE	TRUE	FALSE	FALSE	FALSE	FALSE
WSF2D2W3_UNBURNT_1_50X_4	x1_y3.png	TRUE	TRUE	FALSE	FALSE	FALSE	FALSE	TRUE
WSF2D2W1_UNBURNT_3_50X_3	x8_y7.png	FALSE	TRUE	FALSE	FALSE	FALSE	FALSE	FALSE
WSF2D2W5_BURNT_50X_2_1	x5_y5.png	TRUE	FALSE	FALSE	FALSE	FALSE	FALSE	FALSE
WSF2D2W1_UNBURNT_2_50X_3	x2_y0.png	FALSE	TRUE	TRUE	FALSE	FALSE	FALSE	FALSE
WSF3D3M4_BURNT_50X_1_6	x7_y6.png	FALSE	TRUE	FALSE	FALSE	FALSE	FALSE	FALSE
WSF3D1M4_NO2_BURNT_50X_2	x8_y2.png	FALSE	FALSE	FALSE	FALSE	FALSE	FALSE	TRUE
WSF3D3M3_UNBURNT_1_50X_5	x8_y3.png	TRUE	TRUE	FALSE	FALSE	FALSE	FALSE	FALSE
WSF3D1M3_UNBURNT_1_50X_3	x8_y0.png	TRUE	FALSE	FALSE	FALSE	FALSE	FALSE	FALSE
WSF3D3M4_BURNT_50X_1_4	x8_y2.png	FALSE	FALSE	FALSE	FALSE	FALSE	FALSE	FALSE
WSF3D3M3_UNBURNT_1_50X_1	x2_y8.png	FALSE	FALSE	FALSE	FALSE	FALSE	FALSE	TRUE
WSF3D3M4_BURNT_50X_1_1	x1_y1.png	FALSE	FALSE	FALSE	FALSE	FALSE	TRUE	FALSE

WSF3D1M3_BURNT_50X_3	x7_y7.png	FALSE	FALSE	FALSE	FALSE	FALSE	FALSE	TRUE
WSF3D1M3_UNBURNT_1_50X_1	x0_y3.png	FALSE	TRUE	FALSE	FALSE	FALSE	FALSE	FALSE
WSF3D3M1_BURNT_50X_1_4	x3_y4.png	FALSE	FALSE	FALSE	FALSE	FALSE	FALSE	FALSE
SWF1FR2_BURNT_50X_2	x3_y0.png	FALSE	TRUE	FALSE	FALSE	FALSE	FALSE	FALSE
WSF3D3M3_UNBURNT_1_50X_2	x9_y8.png	TRUE	FALSE	FALSE	FALSE	FALSE	FALSE	FALSE
SWF1FR2_BURNT_50X_2	x3_y1.png	TRUE	TRUE	FALSE	FALSE	FALSE	FALSE	FALSE
WSF3D3M2_BURNT_50X_1_3	x1_y4.png	TRUE	TRUE	TRUE	FALSE	FALSE	FALSE	FALSE
WSF2D2W1_UNBURNT_3_50X_1	x3_y6.png	FALSE	TRUE	FALSE	FALSE	FALSE	FALSE	FALSE
WSF2D2W1_UNBURNT_2_50X_2	x9_y1.png	FALSE	TRUE	FALSE	FALSE	FALSE	FALSE	FALSE
WSF2D2W5_UNBURNT_2_50X_4	x6_y0.png	TRUE	TRUE	FALSE	FALSE	FALSE	FALSE	FALSE
SWF2FR1_BURNT_1_5X_2	x9_y6.png	FALSE	FALSE	FALSE	FALSE	FALSE	FALSE	FALSE
WSF3D3M4_BURNT_50X_1_3	x2_y7.png	TRUE	TRUE	FALSE	FALSE	FALSE	FALSE	FALSE
WSF3D1M1_BURNT_50X_6	x2_y0.png	FALSE	TRUE	FALSE	FALSE	FALSE	FALSE	FALSE
WSF3D3M2_BURNT_50X_1_2	x9_y3.png	FALSE	TRUE	FALSE	FALSE	FALSE	FALSE	TRUE
WSF3D3M3_UNBURNT_1_50X_5	x9_y4.png	TRUE	FALSE	FALSE	FALSE	TRUE	FALSE	FALSE
WSF3D3M3_UNBURNT_1_50X_1	x2_y5.png	FALSE	TRUE	FALSE	FALSE	FALSE	FALSE	TRUE
WSF3D1M3_BURNT_50X_1	x5_y6.png	TRUE	FALSE	FALSE	FALSE	FALSE	FALSE	FALSE
WSF2D2W1_UNBURNT_3_50X_3	x6_y8.png	TRUE	TRUE	FALSE	FALSE	FALSE	FALSE	FALSE
SWF2FR4_BURNT_50X	x1_y6.png	FALSE	FALSE	FALSE	FALSE	FALSE	FALSE	FALSE
WSF3D1M3_UNBURNT_1_50X_3	x2_y3.png	FALSE	TRUE	FALSE	FALSE	FALSE	FALSE	FALSE

WSF2D2W1_UNBURNT_2_50X_3	x0_y1.png	FALSE	TRUE	TRUE	FALSE	TRUE	FALSE	FALSE
WSF3D1M5_BURNT_50X_3	x8_y1.png	FALSE	FALSE	FALSE	FALSE	FALSE	FALSE	TRUE
WSF3D3M4_BURNT_50X_1_6	x9_y6.png	FALSE	TRUE	FALSE	FALSE	FALSE	FALSE	FALSE
WSF3D1M4_NO2_BURNT_50X_3	x6_y6.png	FALSE	FALSE	FALSE	FALSE	FALSE	TRUE	TRUE
WSF3D1M1_BURNT_50X_7	x5_y1.png	TRUE	FALSE	FALSE	FALSE	FALSE	FALSE	TRUE
SWF2FR1_BURNT_2_5X_1	x8_y5.png	FALSE	FALSE	FALSE	FALSE	FALSE	FALSE	FALSE
WSF2D2W1_UNBURNT_1_50X_2	x4_y2.png	FALSE	TRUE	TRUE	FALSE	FALSE	FALSE	FALSE
WSF3D3M4_BURNT_50X_1_6	x2_y6.png	FALSE	TRUE	FALSE	TRUE	FALSE	FALSE	FALSE
WSF3D1M1_BURNT_50X_5	x4_y5.png	TRUE	FALSE	FALSE	FALSE	FALSE	FALSE	FALSE
SWF2FR1_BURNT_2_5X_2	x2_y8.png	FALSE	FALSE	FALSE	FALSE	FALSE	FALSE	FALSE
WSF2D2W5_UNBURNT_2_50X_2	x7_y8.png	FALSE	TRUE	TRUE	FALSE	FALSE	FALSE	TRUE
SWF1_BURNT_5_50X_1	x5_y3.png	TRUE	TRUE	FALSE	FALSE	FALSE	FALSE	FALSE
WSF3D3M3_UNBURNT_1_50X_1	x5_y1.png	TRUE	FALSE	TRUE	FALSE	FALSE	FALSE	FALSE
WSF3D1M1_BURNT_50X	x2_y5.png	FALSE	FALSE	FALSE	FALSE	FALSE	FALSE	FALSE
WSF3D3M2_BURNT_50X_1_1	x8_y7.png	FALSE	FALSE	FALSE	FALSE	FALSE	FALSE	FALSE
SWF1FR2_BURNT_50X_2	x2_y1.png	FALSE	FALSE	TRUE	FALSE	FALSE	FALSE	FALSE
WSF2D2W5_UNBURNT_2_50X_3	x9_y4.png	TRUE	TRUE	FALSE	FALSE	FALSE	FALSE	FALSE
SWF1FR2_BURNT_50X_3	x2_y6.png	TRUE	TRUE	FALSE	FALSE	FALSE	FALSE	FALSE
SWF1_BURNT_5_50X_1	x0_y1.png	FALSE	FALSE	FALSE	FALSE	FALSE	FALSE	FALSE
WSF3D3M4_BURNT_50X_1_5	x3_y4.png	FALSE	FALSE	FALSE	FALSE	FALSE	FALSE	FALSE
SWF2FR1_BURNT_1_5X_2	x5_y6.png	FALSE	FALSE	FALSE	FALSE	FALSE	FALSE	FALSE

WSF3D1M1_BURNT_50X_4	x9_y3.png	FALSE	FALSE	FALSE	FALSE	FALSE	FALSE	FALSE
WSF3D1M1_BURNT_50X_6	x5_y3.png	TRUE	FALSE	FALSE	FALSE	FALSE	FALSE	FALSE
WSF2D2W5_UNBURNT_1_50X_2	x8_y1.png	TRUE	TRUE	FALSE	FALSE	FALSE	FALSE	FALSE
WSF3D1M1_BURNT_50X_8	x5_y4.png	FALSE	FALSE	FALSE	FALSE	FALSE	TRUE	TRUE
WSF3D3M3_UNBURNT_1_50X_5	x2_y4.png	FALSE	TRUE	FALSE	FALSE	FALSE	FALSE	FALSE
WSF3D1M2_BURNT_50X_5	x7_y2.png	TRUE	FALSE	FALSE	FALSE	FALSE	FALSE	FALSE
WSF3D3M4_BURNT_50X_1_5	x2_y8.png	TRUE	FALSE	FALSE	FALSE	FALSE	TRUE	TRUE
WS Fresh	x7_y1.png	FALSE	FALSE	FALSE	FALSE	FALSE	FALSE	FALSE
WSF3D1M1_BURNT_50X_8	x7_y0.png	FALSE	TRUE	FALSE	FALSE	FALSE	FALSE	FALSE
SWF1_BURNT_4_50X_1	x7_y8.png	FALSE	FALSE	FALSE	FALSE	FALSE	FALSE	FALSE
WSF2D2W5_UNBURNT_2_50X_3	x4_y9.png	TRUE	TRUE	FALSE	FALSE	FALSE	TRUE	FALSE
WSF3D3M3_UNBURNT_1_50X_4	x0_y4.png	FALSE	FALSE	FALSE	FALSE	FALSE	FALSE	TRUE
WS Fresh_50X_2	x4_y3.png	FALSE	FALSE	FALSE	FALSE	FALSE	FALSE	FALSE
WSF3D1M2_BURNT_50X_4	x3_y7.png	FALSE	FALSE	FALSE	FALSE	FALSE	FALSE	FALSE
WSF3D1M4_NO2_BURNT_50X_3	x6_y9.png	FALSE	FALSE	FALSE	FALSE	FALSE	FALSE	FALSE
WSF3D3M1_BURNT_50X_1_4	x3_y0.png	FALSE	FALSE	FALSE	FALSE	FALSE	FALSE	FALSE
WSF3D3M1_BURNT_50X_1_4	x8_y2.png	FALSE	FALSE	FALSE	FALSE	FALSE	FALSE	FALSE
WSF3D1M3_UNBURNT_1_50X_1	x6_y6.png	FALSE	TRUE	FALSE	FALSE	FALSE	FALSE	FALSE
WSF3D3M4_BURNT_50X_1_6	x7_y2.png	FALSE	FALSE	FALSE	FALSE	FALSE	FALSE	FALSE
SWF1FR2_BURNT_50X_1	x5_y2.png	FALSE	TRUE	FALSE	FALSE	FALSE	FALSE	TRUE

WSF3D1M1_BURNT_50X_10	x8_y8.png	FALSE	FALSE	FALSE	FALSE	FALSE	FALSE	TRUE
WSF2D2W1_UNBURNT_3_50X_2	x0_y2.png	FALSE	FALSE	FALSE	FALSE	FALSE	FALSE	TRUE
SWF1_BURNT_4_50X_2	x5_y4.png	FALSE	TRUE	FALSE	FALSE	FALSE	FALSE	FALSE
WSF3D1M2_BURNT_50X_1	x2_y0.png	FALSE	FALSE	FALSE	FALSE	FALSE	FALSE	TRUE
SWF1_BURNT_5_50X_1	x9_y8.png	FALSE	FALSE	FALSE	FALSE	FALSE	FALSE	FALSE
WSF2D2W1_UNBURNT_3_50X_1	x7_y0.png	FALSE	FALSE	FALSE	FALSE	FALSE	FALSE	FALSE
WSF2D2W1_UNBURNT_2_50X_3	x2_y1.png	FALSE	TRUE	FALSE	FALSE	FALSE	FALSE	FALSE
WSF2D2W1_UNBURNT_1_50X_2	x7_y3.png	FALSE	TRUE	FALSE	FALSE	FALSE	FALSE	FALSE
WSF3D1M3_UNBURNT_2_50X_1	x1_y1.png	FALSE	TRUE	FALSE	FALSE	FALSE	FALSE	FALSE
SWF1_BURNT_5_50X_3	x9_y5.png	FALSE	FALSE	FALSE	FALSE	FALSE	FALSE	FALSE
WS Fresh_50X_2	x3_y4.png	FALSE	FALSE	FALSE	FALSE	TRUE	FALSE	FALSE
WSF3D1M1_BURNT_50X_5	x9_y4.png	FALSE	FALSE	FALSE	FALSE	FALSE	FALSE	FALSE
WSF3D1M4_NO2_BURNT_50X_2	x9_y7.png	FALSE	FALSE	FALSE	FALSE	FALSE	FALSE	FALSE
WSF3D3M3_UNBURNT_1_50X_3	x4_y1.png	FALSE	TRUE	FALSE	FALSE	FALSE	FALSE	TRUE
WSF2D2W1_UNBURNT_3_50X_1	x5_y7.png	FALSE	TRUE	FALSE	FALSE	FALSE	FALSE	TRUE
WSF2D2W5_BURNT_50X_2_1	x4_y6.png	FALSE	FALSE	FALSE	FALSE	FALSE	FALSE	TRUE
WSF2D2W3_UNBURNT_1_50X_4	x8_y7.png	TRUE	TRUE	FALSE	FALSE	FALSE	FALSE	FALSE
WSF3D1M5_BURNT_50X_2	x1_y7.png	FALSE	FALSE	FALSE	FALSE	FALSE	FALSE	FALSE
WSF3D1M1_BURNT_50X	x8_y5.png	FALSE	TRUE	FALSE	FALSE	FALSE	FALSE	TRUE
WSF3D1M1_BURNT_50X_2	x7_y1.png	FALSE	FALSE	FALSE	FALSE	FALSE	FALSE	FALSE
SWF2FR4_BURNT_50X	x8_y8.png	FALSE	FALSE	FALSE	FALSE	FALSE	FALSE	FALSE

WSF3D3M4_BURNT_50X_1_4	x7_y6.png	FALSE	FALSE	FALSE	FALSE	FALSE	FALSE	FALSE
WSF3D3M4_BURNT_50X_1_5	x9_y2.png	TRUE	FALSE	FALSE	FALSE	FALSE	FALSE	FALSE
WSF3D1M2_BURNT_50X_1	x6_y0.png	TRUE	FALSE	FALSE	FALSE	FALSE	FALSE	FALSE
WSF3D1M5_SMALLPIECE_BURNT_50X_3	x6_y9.png	FALSE	FALSE	FALSE	FALSE	FALSE	FALSE	TRUE
WSF3D1M1_BURNT_50X_10	x0_y8.png	TRUE	FALSE	FALSE	FALSE	FALSE	FALSE	FALSE
SWF2FR1_BURNT_1_5X_2	x6_y0.png	FALSE	FALSE	FALSE	FALSE	FALSE	FALSE	FALSE
WSF3D1M4_BURNT_50X_4	x5_y9.png	TRUE	FALSE	FALSE	FALSE	FALSE	FALSE	TRUE
WSF3D1M5_BURNT_50X_3	x9_y8.png	FALSE	FALSE	FALSE	FALSE	FALSE	FALSE	FALSE
WSF3D3M4_BURNT_50X_1_3	x3_y0.png	FALSE	FALSE	TRUE	FALSE	FALSE	FALSE	FALSE
WSF2D2W5_UNBURNT_2_50X_2	x6_y6.png	FALSE	TRUE	FALSE	FALSE	FALSE	FALSE	TRUE
WSF3D1M3_UNBURNT_1_50X_4	x3_y3.png	FALSE	TRUE	FALSE	FALSE	FALSE	FALSE	FALSE
WSF3D1M4_NO2_BURNT_50X_3	x0_y0.png	FALSE	FALSE	FALSE	FALSE	FALSE	FALSE	FALSE
SWF2FR1_BURNT_1_5X_2	x8_y0.png	FALSE	FALSE	FALSE	FALSE	FALSE	FALSE	FALSE
WSF3D1M3_UNBURNT_2_50X_1	x8_y1.png	FALSE	TRUE	FALSE	FALSE	FALSE	FALSE	FALSE
WSF2D2W5_BURNT_50X_1_2	x7_y3.png	FALSE	TRUE	FALSE	TRUE	FALSE	FALSE	FALSE
WS Fresh_50X_3	x3_y8.png	FALSE	TRUE	FALSE	FALSE	FALSE	FALSE	FALSE
SWF2FR1_BURNT_2_5X_2	x5_y2.png	FALSE	FALSE	FALSE	FALSE	FALSE	FALSE	FALSE
SWF1FR2_BURNT_50X_3	x1_y9.png	FALSE	FALSE	FALSE	FALSE	FALSE	FALSE	FALSE
WSF3D1M1_BURNT_50X_7	x3_y0.png	FALSE	TRUE	FALSE	FALSE	FALSE	FALSE	FALSE

WSF3D3M1_BURNT_50X_1_4	x6_y6.png	FALSE	FALSE	FALSE	FALSE	FALSE	FALSE	FALSE
SWF1_BURNT_5_50X_3	x9_y0.png	FALSE	FALSE	FALSE	FALSE	FALSE	FALSE	FALSE
WSF3D1M1_BURNT_50X_9	x2_y8.png	FALSE	FALSE	FALSE	FALSE	FALSE	FALSE	FALSE
WSF3D1M4_NO2_BURNT_50X_1	x2_y2.png	FALSE	FALSE	FALSE	FALSE	FALSE	TRUE	FALSE
SWF2FR1_BURNT_1_5X	x5_y9.png	FALSE	FALSE	FALSE	FALSE	FALSE	FALSE	FALSE
WSF3D3M3_UNBURNT_1_50X_1	x2_y3.png	FALSE	TRUE	FALSE	FALSE	FALSE	FALSE	FALSE
WSF3D3M3_UNBURNT_1_50X_1	x9_y8.png	FALSE	FALSE	FALSE	FALSE	FALSE	FALSE	FALSE
SWF1_BURNT_4_50X_1	x0_y3.png	FALSE	FALSE	FALSE	FALSE	FALSE	FALSE	FALSE
WSF3D3M2_BURNT_50X_1_1	x8_y3.png	FALSE	FALSE	FALSE	FALSE	FALSE	FALSE	FALSE
WSF2D2W3_UNBURNT_1_50X_2	x5_y0.png	TRUE	TRUE	FALSE	FALSE	FALSE	FALSE	FALSE
WSF2D2W5_BURNT_50X_1	x5_y9.png	FALSE	FALSE	FALSE	FALSE	FALSE	TRUE	TRUE
WSF3D3M4_BURNT_50X_1_1	x5_y6.png	FALSE	FALSE	TRUE	FALSE	FALSE	FALSE	FALSE
SWF1FR2_BURNT_50X_4	x3_y2.png	FALSE	FALSE	TRUE	FALSE	FALSE	FALSE	TRUE
WSF2D2W5_UNBURNT_1_50X_2	x3_y2.png	FALSE	TRUE	TRUE	FALSE	FALSE	FALSE	FALSE
WSF3D3M3_UNBURNT_1_50X_1	x4_y2.png	TRUE	TRUE	FALSE	FALSE	FALSE	FALSE	FALSE
SWF2FR1_BURNT_2_5X_1	x4_y4.png	FALSE	FALSE	FALSE	FALSE	FALSE	FALSE	FALSE
SWF2FR1_BURNT_1_5X	x6_y4.png	FALSE	FALSE	FALSE	FALSE	FALSE	FALSE	FALSE
WSF3D3M4_BURNT_50X_1_5	x5_y6.png	FALSE	TRUE	FALSE	TRUE	FALSE	FALSE	TRUE
WSF2D2W5_BURNT_50X_1_2	x4_y1.png	FALSE	TRUE	FALSE	FALSE	FALSE	FALSE	TRUE
WSF3D1M5_BURNT_50X_2	x1_y5.png	FALSE	FALSE	FALSE	FALSE	FALSE	FALSE	FALSE
WSF2D2W5_BURNT_50X_1_3	x0_y8.png	FALSE	FALSE	FALSE	FALSE	FALSE	FALSE	FALSE

WSF3D1M2_BURNT_50X_6	x4_y4.png	FALSE	FALSE	FALSE	FALSE	FALSE	FALSE	FALSE
WSF2D2W1_UNBURNT_3_50X_2	x2_y8.png	FALSE	TRUE	FALSE	FALSE	FALSE	FALSE	FALSE
WSF3D1M5_UNBURNT_1_50X_1	x4_y2.png	FALSE	FALSE	FALSE	FALSE	FALSE	TRUE	TRUE
WSF2D2W5_BURNT_50X_1_3	x2_y0.png	FALSE	FALSE	TRUE	FALSE	FALSE	FALSE	FALSE
WSF3D1M2_BURNT_50X_1	x9_y9.png	FALSE	TRUE	TRUE	FALSE	FALSE	FALSE	FALSE
WSF3D3M4_BURNT_50X_1_4	x6_y3.png	FALSE	FALSE	FALSE	FALSE	FALSE	FALSE	FALSE
WSF3D3M3_UNBURNT_1_50X_3	x2_y6.png	FALSE	FALSE	FALSE	FALSE	FALSE	FALSE	FALSE
WSF2D2W5_BURNT_50X_2_1	x1_y0.png	TRUE	FALSE	FALSE	FALSE	FALSE	FALSE	FALSE
SWF1_BURNT_3_50X_1	x4_y6.png	FALSE	FALSE	FALSE	FALSE	FALSE	TRUE	FALSE
WSF3D3M4_BURNT_50X_1_2	x7_y2.png	TRUE	TRUE	FALSE	FALSE	FALSE	FALSE	FALSE
WSF2D2W5_UNBURNT_2_50X_2	x7_y2.png	TRUE	TRUE	FALSE	FALSE	FALSE	FALSE	FALSE
WSF3D3M3_UNBURNT_1_50X_5	x0_y0.png	FALSE	FALSE	FALSE	FALSE	FALSE	FALSE	FALSE
WSF3D1M3_BURNT_50X_2	x0_y4.png	FALSE	FALSE	FALSE	FALSE	FALSE	FALSE	TRUE
WSF3D1M5_SMALLPIECE_BURNT_50X_3	x6_y1.png	TRUE	FALSE	FALSE	FALSE	FALSE	FALSE	FALSE
WSF3D1M3_UNBURNT_1_50X_4	x1_y3.png	FALSE	TRUE	FALSE	FALSE	FALSE	FALSE	FALSE
WSF2D2W5_UNBURNT_2_50X_2	x2_y0.png	TRUE	FALSE	FALSE	FALSE	FALSE	FALSE	FALSE
WSF3D3M4_BURNT_50X_1_4	x3_y9.png	FALSE	FALSE	FALSE	FALSE	FALSE	FALSE	FALSE
WSF3D3M3_UNBURNT_1_50X_2	x6_y7.png	TRUE	FALSE	FALSE	FALSE	FALSE	FALSE	FALSE
WSF3D3M2_BURNT_100X_1_1	x2_y7.png	FALSE	TRUE	FALSE	FALSE	FALSE	FALSE	FALSE

WSF3D3M3_UNBURNT_1_50X_3	x6_y4.png	FALSE	TRUE	TRUE	FALSE	FALSE	FALSE	FALSE
WSF2D2W5_UNBURNT_2_50X_4	x9_y2.png	FALSE	TRUE	TRUE	FALSE	FALSE	FALSE	FALSE
WSF3D3M3_UNBURNT_1_50X_2	x5_y3.png	FALSE	FALSE	FALSE	FALSE	TRUE	FALSE	TRUE
SWF1_BURNT_4_50X_3	x8_y0.png	FALSE	FALSE	FALSE	FALSE	FALSE	FALSE	FALSE
WSF3D1M1_BURNT_50X_8	x6_y2.png	FALSE	TRUE	FALSE	FALSE	FALSE	TRUE	TRUE
WSF2D2W3_UNBURNT_1_50X_4	x0_y4.png	TRUE	FALSE	FALSE	FALSE	TRUE	FALSE	TRUE
WSF3D1M4_BURNT_50X_4	x2_y0.png	TRUE	TRUE	FALSE	FALSE	FALSE	FALSE	FALSE
WSF2D2W5_UNBURNT_2_50X_2	x2_y6.png	TRUE	TRUE	FALSE	FALSE	FALSE	FALSE	FALSE
WSF3D3M4_BURNT_50X_1_1	x0_y2.png	FALSE	FALSE	FALSE	FALSE	FALSE	TRUE	FALSE
WSF3D3M1_BURNT_50X_1_4	x3_y3.png	FALSE	FALSE	FALSE	FALSE	FALSE	FALSE	FALSE
WSF3D1M1_BURNT_50X_6	x6_y7.png	FALSE	FALSE	FALSE	FALSE	FALSE	FALSE	FALSE
WSF3D1M4_BURNT_50X_1	x3_y9.png	TRUE	TRUE	FALSE	FALSE	FALSE	FALSE	FALSE
SWF1FR2_BURNT_50X_4	x3_y5.png	FALSE	FALSE	FALSE	FALSE	FALSE	FALSE	TRUE
WS Fresh_50X_1	x0_y1.png	FALSE	FALSE	FALSE	FALSE	TRUE	FALSE	FALSE
WSF2D2W1_UNBURNT_3_50X_3	x7_y9.png	TRUE	TRUE	FALSE	FALSE	FALSE	FALSE	FALSE
WS Fresh_50X_1	x2_y2.png	TRUE	FALSE	FALSE	FALSE	FALSE	FALSE	FALSE
WSF2D2W3_UNBURNT_1_50X_3	x6_y3.png	FALSE	TRUE	TRUE	FALSE	FALSE	FALSE	FALSE
SWF2FR1_BURNT_2_5X_1	x2_y8.png	FALSE	FALSE	FALSE	FALSE	FALSE	TRUE	FALSE
WSF2D2W5_BURNT_50X_2_1	x3_y0.png	TRUE	FALSE	FALSE	FALSE	FALSE	FALSE	FALSE
WSF2D2W1_UNBURNT_2_50X_1	x9_y7.png	FALSE	TRUE	FALSE	FALSE	FALSE	FALSE	FALSE

WSF3D1M1_BURNT_50X_8	x8_y8.png	FALSE	FALSE	FALSE	FALSE	FALSE	FALSE	FALSE
WSF3D1M4_BURNT_50X_1	x8_y5.png	TRUE	FALSE	FALSE	FALSE	FALSE	FALSE	FALSE
WSF3D3M2_BURNT_50X_1_3	x7_y8.png	FALSE	FALSE	TRUE	FALSE	FALSE	FALSE	FALSE
WSF3D1M1_BURNT_50X_3	x0_y7.png	TRUE	FALSE	FALSE	FALSE	FALSE	FALSE	FALSE
WSF3D3M3_UNBURNT_1_50X_3	x3_y2.png	FALSE	TRUE	FALSE	FALSE	FALSE	FALSE	TRUE
WSF3D3M4_BURNT_50X_1_6	x5_y5.png	FALSE	TRUE	FALSE	FALSE	FALSE	FALSE	FALSE
WSF3D3M2_BURNT_50X_1_1	x4_y2.png	TRUE	TRUE	FALSE	FALSE	FALSE	TRUE	FALSE
WSF2D2W5_UNBURNT_2_50X_1	x1_y1.png	TRUE	TRUE	FALSE	FALSE	FALSE	FALSE	FALSE
WSF2D2W5_UNBURNT_1_50X_1	x6_y9.png	FALSE	TRUE	FALSE	FALSE	FALSE	FALSE	FALSE
WSF3D1M3_UNBURNT_1_50X_4	x4_y3.png	FALSE	TRUE	FALSE	FALSE	FALSE	FALSE	FALSE
WSF3D1M4_BURNT_50X_4	x9_y4.png	FALSE	FALSE	FALSE	TRUE	FALSE	FALSE	TRUE
WSF3D1M5_SMALLPIECE_BURNT_50X_4	x8_y6.png	FALSE	FALSE	FALSE	FALSE	FALSE	FALSE	FALSE
WSF3D1M4_NO2_BURNT_50X_3	x9_y7.png	FALSE	FALSE	TRUE	FALSE	FALSE	FALSE	FALSE
WSF2D2W1_UNBURNT_2_50X_3	x9_y2.png	FALSE	TRUE	FALSE	FALSE	FALSE	FALSE	TRUE
WSF3D3M4_BURNT_50X_1_5	x9_y7.png	FALSE	FALSE	FALSE	FALSE	FALSE	FALSE	FALSE
WSF3D3M1_BURNT_50X_1_2	x0_y6.png	FALSE	TRUE	FALSE	FALSE	FALSE	FALSE	FALSE
WSF3D1M1_BURNT_50X_7	x2_y6.png	TRUE	TRUE	FALSE	FALSE	FALSE	FALSE	FALSE
WSF3D3M2_BURNT_50X_1_3	x1_y0.png	FALSE	FALSE	TRUE	FALSE	FALSE	TRUE	FALSE
SWF2FR1_BURNT_1_5X	x1_y3.png	FALSE	FALSE	FALSE	FALSE	FALSE	FALSE	FALSE

WSF3D1M5_UNBURNT_1_50X_1	x5_y0.png	FALSE	TRUE	FALSE	FALSE	FALSE	FALSE	TRUE
WSF3D3M2_BURNT_50X_1_2	x4_y6.png	TRUE	FALSE	TRUE	TRUE	FALSE	FALSE	FALSE
WSF2D2W3_UNBURNT_1_50X_2	x4_y8.png	FALSE	TRUE	FALSE	FALSE	FALSE	FALSE	TRUE
WSF3D1M5_SMALLPIECE_BURNT_50X_4	x6_y0.png	FALSE	FALSE	FALSE	FALSE	FALSE	FALSE	FALSE
WSF3D1M5_BURNT_50X_2	x0_y9.png	FALSE	FALSE	FALSE	FALSE	FALSE	TRUE	FALSE
WSF3D1M2_BURNT_50X_3	x9_y7.png	TRUE	FALSE	FALSE	TRUE	FALSE	TRUE	TRUE
WSF2D2W5_UNBURNT_1_50X_3	x8_y4.png	FALSE	TRUE	TRUE	FALSE	FALSE	FALSE	TRUE
WSF3D1M4_BURNT_50X_2	x0_y2.png	FALSE	FALSE	FALSE	FALSE	FALSE	FALSE	FALSE
WSF3D1M1_BURNT_50X_7	x8_y6.png	FALSE	FALSE	FALSE	FALSE	FALSE	FALSE	FALSE
WSF3D1M2_BURNT_50X_1	x1_y1.png	FALSE	FALSE	FALSE	FALSE	FALSE	FALSE	FALSE
WSF2D2W5_BURNT_50X_1	x8_y4.png	FALSE	FALSE	FALSE	FALSE	FALSE	FALSE	FALSE
WSF3D1M2_BURNT_50X_5	x9_y6.png	FALSE	FALSE	FALSE	FALSE	FALSE	FALSE	FALSE
WSF3D1M1_BURNT_50X_2	x1_y1.png	FALSE	FALSE	FALSE	FALSE	FALSE	TRUE	TRUE
SWF1FR2_BURNT_50X_3	x5_y6.png	FALSE	TRUE	TRUE	TRUE	FALSE	FALSE	FALSE
WSF3D1M3_BURNT_50X_1	x3_y2.png	FALSE	FALSE	FALSE	FALSE	FALSE	FALSE	TRUE
SWF2FR1_BURNT_2_5X_1	x9_y3.png	FALSE	FALSE	FALSE	FALSE	FALSE	FALSE	FALSE
WSF3D1M1_BURNT_50X_9	x2_y1.png	FALSE	FALSE	FALSE	FALSE	TRUE	FALSE	TRUE
WSF3D1M3_UNBURNT_1_50X_4	x8_y1.png	FALSE	TRUE	FALSE	FALSE	FALSE	FALSE	TRUE
WSF3D1M3_BURNT_50X_3	x9_y5.png	FALSE	FALSE	TRUE	TRUE	FALSE	FALSE	FALSE

WSF3D1M4_NO2_BURNT_50X_1	x2_y5.png	FALSE	FALSE	FALSE	FALSE	FALSE	FALSE	FALSE
WSF3D1M4_BURNT_50X_1	x9_y3.png	TRUE	FALSE	FALSE	FALSE	FALSE	FALSE	FALSE
WSF2D2W5_UNBURNT_2_50X_4	x7_y4.png	FALSE	TRUE	FALSE	FALSE	FALSE	FALSE	FALSE
WSF3D1M4_NO2_BURNT_50X_1	x4_y5.png	FALSE	TRUE	FALSE	FALSE	FALSE	FALSE	TRUE
WSF2D2W5_UNBURNT_2_50X_3	x7_y7.png	FALSE	TRUE	FALSE	TRUE	FALSE	FALSE	TRUE
WSF3D3M3_UNBURNT_1_50X_3	x9_y0.png	FALSE	FALSE	FALSE	FALSE	FALSE	FALSE	FALSE
WSF3D1M5_BURNT_50X_1	x8_y4.png	FALSE	FALSE	FALSE	FALSE	FALSE	FALSE	FALSE
WSF3D3M4_BURNT_50X_1_2	x2_y0.png	TRUE	TRUE	FALSE	FALSE	FALSE	FALSE	FALSE
WSF3D1M1_BURNT_50X	x9_y6.png	TRUE	FALSE	FALSE	FALSE	FALSE	FALSE	FALSE
WSF3D1M2_BURNT_50X_1	x3_y4.png	FALSE	TRUE	FALSE	FALSE	FALSE	FALSE	FALSE
WSF2D2W5_UNBURNT_1_50X_1	x7_y2.png	TRUE	TRUE	FALSE	FALSE	FALSE	FALSE	FALSE
SWF1_BURNT_4_50X_1	x1_y2.png	FALSE	FALSE	FALSE	FALSE	FALSE	FALSE	FALSE
WSF2D2W5_UNBURNT_2_50X_2	x0_y0.png	TRUE	TRUE	FALSE	FALSE	FALSE	FALSE	TRUE
WSF3D3M1_BURNT_50X_1_2	x1_y1.png	TRUE	FALSE	FALSE	FALSE	FALSE	TRUE	FALSE
SWF1FR2_BURNT_50X_2	x3_y4.png	FALSE	TRUE	FALSE	FALSE	FALSE	FALSE	FALSE
SWF2FR4_BURNT_50X	x4_y5.png	FALSE	FALSE	FALSE	FALSE	FALSE	FALSE	FALSE
WSF3D1M4_NO2_BURNT_50X_2	x7_y7.png	FALSE	FALSE	FALSE	FALSE	FALSE	FALSE	TRUE
WSF3D3M4_BURNT_50X_1_1	x4_y8.png	FALSE	FALSE	FALSE	FALSE	FALSE	FALSE	FALSE
SWF2FR1_BURNT_2_5X_2	x1_y8.png	FALSE	FALSE	FALSE	FALSE	FALSE	FALSE	FALSE
WSF2D2W5_BURNT_50X_1_3	x5_y3.png	FALSE	TRUE	FALSE	FALSE	FALSE	FALSE	FALSE
WS Fresh_50X_1	x8_y2.png	FALSE	TRUE	FALSE	FALSE	FALSE	FALSE	TRUE

WSF3D1M4_BURNT_50X_3	x8_y3.png	FALSE	FALSE	FALSE	FALSE	FALSE	FALSE	TRUE
WSF3D1M2_BURNT_50X_2	x5_y9.png	FALSE	FALSE	TRUE	FALSE	FALSE	FALSE	FALSE
SWF2FR4_BURNT_50X	x9_y7.png	FALSE	FALSE	FALSE	FALSE	FALSE	FALSE	FALSE
WSF2D2W5_UNBURNT_2_50X_2	x2_y5.png	FALSE	TRUE	TRUE	FALSE	FALSE	FALSE	FALSE
WSF2D2W5_UNBURNT_2_50X_3	x1_y4.png	TRUE	TRUE	FALSE	FALSE	FALSE	FALSE	FALSE
WSF3D1M1_BURNT_50X	x3_y4.png	FALSE	TRUE	FALSE	FALSE	FALSE	FALSE	FALSE
WSF3D3M4_BURNT_50X_1_1	x7_y6.png	FALSE	FALSE	TRUE	FALSE	FALSE	TRUE	FALSE
WSF2D2W3_UNBURNT_1_50X_2	x3_y0.png	TRUE	TRUE	FALSE	FALSE	FALSE	FALSE	FALSE
SWF1_BURNT_5_50X_1	x0_y5.png	TRUE	FALSE	FALSE	FALSE	FALSE	FALSE	FALSE
WSF2D2W5_UNBURNT_2_50X_1	x7_y4.png	FALSE	TRUE	TRUE	FALSE	FALSE	FALSE	FALSE
WSF3D1M4_NO2_BURNT_50X_2	x5_y0.png	FALSE	FALSE	FALSE	FALSE	FALSE	FALSE	TRUE
WSF3D1M2_BURNT_50X_4	x6_y8.png	FALSE	FALSE	FALSE	FALSE	FALSE	FALSE	FALSE
SWF1FR2_BURNT_50X_1	x8_y8.png	FALSE	FALSE	FALSE	FALSE	FALSE	FALSE	FALSE
WS Fresh_50X_2	x0_y7.png	FALSE	FALSE	FALSE	FALSE	FALSE	FALSE	FALSE
WSF3D3M1_BURNT_50X_1_2	x0_y1.png	FALSE	FALSE	FALSE	FALSE	FALSE	FALSE	FALSE
WSF3D1M1_BURNT_50X_8	x0_y6.png	FALSE	TRUE	FALSE	FALSE	FALSE	FALSE	TRUE
WSF2D2W1_UNBURNT_3_50X_2	x8_y3.png	FALSE	TRUE	FALSE	FALSE	FALSE	FALSE	TRUE
WSF3D3M4_BURNT_50X_1_5	x3_y9.png	FALSE	FALSE	FALSE	FALSE	FALSE	FALSE	FALSE
SWF1FR2_BURNT_50X_2	x2_y5.png	FALSE	TRUE	TRUE	FALSE	FALSE	FALSE	FALSE
SWF1_BURNT_3_50X_1	x8_y6.png	FALSE	FALSE	FALSE	FALSE	FALSE	TRUE	FALSE
WSF3D1M1_BURNT_50X_10	x6_y7.png	FALSE	FALSE	FALSE	FALSE	FALSE	FALSE	TRUE

WSF2D2W3_UNBURNT_1_50X_1	x1_y2.png	FALSE	TRUE	TRUE	FALSE	FALSE	FALSE	TRUE
WS Fresh	x6_y6.png	FALSE	FALSE	FALSE	FALSE	FALSE	FALSE	FALSE
SWF1_BURNT_5_50X_1	x2_y3.png	TRUE	FALSE	TRUE	FALSE	FALSE	FALSE	FALSE
WSF3D1M3_BURNT_50X_1	x6_y4.png	FALSE	FALSE	FALSE	FALSE	FALSE	FALSE	TRUE
WSF2D2W1_UNBURNT_2_50X_2	x7_y4.png	FALSE	TRUE	FALSE	FALSE	FALSE	FALSE	TRUE
WSF2D2W1_UNBURNT_2_50X_1	x0_y7.png	FALSE	TRUE	TRUE	FALSE	FALSE	FALSE	FALSE
SWF1FR2_BURNT_50X_4	x6_y7.png	FALSE	TRUE	FALSE	FALSE	FALSE	FALSE	FALSE
WSF3D3M2_BURNT_50X_1_1	x9_y8.png	FALSE	FALSE	FALSE	FALSE	FALSE	FALSE	FALSE
WSF3D3M3_UNBURNT_1_50X_1	x4_y4.png	FALSE	FALSE	TRUE	FALSE	FALSE	FALSE	TRUE
WSF3D3M3_UNBURNT_1_50X_1	x7_y6.png	FALSE	TRUE	FALSE	FALSE	FALSE	FALSE	TRUE
SWF1FR2_BURNT_50X_2	x3_y5.png	FALSE	TRUE	FALSE	FALSE	FALSE	FALSE	FALSE
WSF3D3M4_BURNT_50X_1_2	x3_y6.png	FALSE	FALSE	TRUE	FALSE	FALSE	FALSE	FALSE
WSF2D2W5_UNBURNT_2_50X_1	x8_y4.png	TRUE	TRUE	FALSE	FALSE	FALSE	FALSE	FALSE
WSF3D3M1_BURNT_50X_1	x1_y8.png	FALSE	FALSE	FALSE	FALSE	FALSE	FALSE	FALSE
WSF2D2W1_UNBURNT_3_50X_2	x9_y7.png	FALSE	TRUE	TRUE	FALSE	TRUE	FALSE	FALSE
WSF2D2W1_UNBURNT_2_50X_3	x3_y1.png	FALSE	TRUE	FALSE	TRUE	FALSE	FALSE	FALSE
WS Fresh_50X_1	x9_y8.png	FALSE	TRUE	FALSE	FALSE	FALSE	FALSE	FALSE
SWF1_BURNT_5_50X_1	x3_y0.png	FALSE	FALSE	FALSE	FALSE	FALSE	FALSE	FALSE
WSF3D3M2_BURNT_50X_1_3	x7_y0.png	FALSE	FALSE	FALSE	TRUE	FALSE	FALSE	TRUE
WSF3D1M2_BURNT_50X_3	x4_y5.png	FALSE	FALSE	TRUE	FALSE	FALSE	FALSE	FALSE
WSF3D1M3_BURNT_50X_3	x9_y8.png	TRUE	FALSE	FALSE	FALSE	FALSE	FALSE	FALSE

WSF2D2W5_UNBURNT_1_50X_2	x3_y8.png	FALSE	TRUE	TRUE	FALSE	FALSE	FALSE	FALSE
WSF2D2W3_UNBURNT_1_50X_1	x0_y3.png	TRUE	TRUE	FALSE	FALSE	FALSE	FALSE	FALSE
SWF1_BURNT_5_50X_2	x0_y9.png	FALSE	FALSE	FALSE	FALSE	FALSE	FALSE	TRUE
WSF3D1M1_BURNT_50X_4	x9_y4.png	FALSE	FALSE	FALSE	FALSE	FALSE	FALSE	FALSE
WSF3D3M3_UNBURNT_1_50X_5	x7_y3.png	FALSE	FALSE	FALSE	FALSE	TRUE	TRUE	TRUE
SWF1_BURNT_4_50X_2	x3_y8.png	FALSE	FALSE	FALSE	FALSE	FALSE	FALSE	FALSE
WSF3D1M1_BURNT_50X_3	x5_y2.png	TRUE	FALSE	FALSE	FALSE	FALSE	FALSE	FALSE
WSF3D1M3_UNBURNT_1_50X_3	x6_y1.png	TRUE	TRUE	FALSE	FALSE	FALSE	TRUE	FALSE
WSF2D2W1_UNBURNT_1_50X_1	x8_y0.png	FALSE	TRUE	FALSE	FALSE	FALSE	FALSE	FALSE
WSF3D3M2_BURNT_50X_1_2	x8_y6.png	FALSE	TRUE	TRUE	FALSE	FALSE	FALSE	FALSE
WSF3D3M2_BURNT_100X_1_1	x4_y4.png	TRUE	TRUE	FALSE	FALSE	FALSE	FALSE	FALSE
WSF3D1M4_NO2_BURNT_50X_1	x6_y9.png	FALSE	FALSE	FALSE	FALSE	FALSE	FALSE	FALSE
SWF1FR2_BURNT_50X_4	x0_y2.png	FALSE	FALSE	FALSE	FALSE	FALSE	TRUE	TRUE
SWF1_BURNT_5_50X_1	x0_y4.png	TRUE	FALSE	FALSE	FALSE	FALSE	FALSE	FALSE
WSF3D3M4_BURNT_50X_1_5	x9_y8.png	FALSE	FALSE	FALSE	FALSE	FALSE	FALSE	FALSE
WSF2D2W5_UNBURNT_2_50X_1	x3_y3.png	FALSE	TRUE	TRUE	FALSE	FALSE	FALSE	FALSE
WSF3D1M1_BURNT_50X_4	x8_y2.png	FALSE	FALSE	FALSE	FALSE	FALSE	FALSE	FALSE
WSF3D3M4_BURNT_50X_1_3	x6_y7.png	FALSE	TRUE	FALSE	FALSE	FALSE	FALSE	FALSE
WSF2D2W5_UNBURNT_1_50X_3	x0_y1.png	TRUE	TRUE	FALSE	FALSE	FALSE	FALSE	FALSE
WSF3D1M1_BURNT_50X_12	x7_y3.png	FALSE	FALSE	FALSE	FALSE	FALSE	FALSE	FALSE
SWF1_BURNT_5_50X_3	x4_y7.png	FALSE	FALSE	FALSE	FALSE	FALSE	FALSE	FALSE

WSF2D2W5_BURNT_50X_1_2	x4_y3.png	FALSE	FALSE	FALSE	FALSE	FALSE	FALSE	FALSE
WSF3D1M1_BURNT_50X_5	x5_y6.png	FALSE	FALSE	FALSE	FALSE	FALSE	FALSE	FALSE
WSF2D2W5_UNBURNT_1_50X_1	x9_y0.png	FALSE	FALSE	FALSE	FALSE	FALSE	FALSE	FALSE
WSF3D1M3_UNBURNT_1_50X_3	x4_y0.png	FALSE	TRUE	FALSE	FALSE	FALSE	FALSE	FALSE
WSF3D1M1_BURNT_50X_2	x1_y8.png	FALSE	TRUE	TRUE	FALSE	FALSE	FALSE	FALSE
WSF3D1M3_UNBURNT_2_50X_1	x2_y6.png	FALSE	TRUE	FALSE	FALSE	FALSE	FALSE	FALSE
WSF3D3M3_UNBURNT_1_50X_1	x5_y3.png	FALSE	TRUE	FALSE	FALSE	FALSE	FALSE	TRUE
WSF3D3M3_UNBURNT_1_50X_1	x5_y5.png	TRUE	TRUE	FALSE	FALSE	FALSE	FALSE	TRUE
WSF2D2W5_BURNT_50X_2_2	x5_y9.png	TRUE	FALSE	TRUE	TRUE	FALSE	FALSE	FALSE
WSF3D1M5_SMALLPIECE_BURNT_50X_3	x2_y6.png	TRUE	FALSE	FALSE	FALSE	FALSE	FALSE	FALSE
WSF3D1M2_BURNT_50X_2	x6_y5.png	TRUE	FALSE	FALSE	FALSE	FALSE	FALSE	TRUE
WSF3D1M1_BURNT_50X_7	x2_y8.png	TRUE	TRUE	FALSE	FALSE	FALSE	FALSE	TRUE
WSF3D1M5_UNBURNT_1_50X_1	x1_y7.png	FALSE	TRUE	FALSE	FALSE	FALSE	TRUE	TRUE
WSF2D2W5_UNBURNT_2_50X_4	x2_y1.png	FALSE	TRUE	FALSE	FALSE	FALSE	FALSE	FALSE
WSF3D1M2_BURNT_50X_5	x1_y2.png	TRUE	FALSE	FALSE	FALSE	FALSE	FALSE	FALSE
WSF2D2W1_UNBURNT_2_50X_2	x5_y2.png	FALSE	TRUE	FALSE	FALSE	FALSE	FALSE	FALSE
WSF3D1M4_NO2_BURNT_50X_2	x3_y9.png	FALSE	FALSE	FALSE	FALSE	FALSE	FALSE	FALSE
SWF1FR2_BURNT_50X_1	x5_y7.png	FALSE	TRUE	FALSE	FALSE	FALSE	FALSE	FALSE
WSF2D2W3_UNBURNT_1_50X_3	x7_y2.png	FALSE	TRUE	FALSE	FALSE	FALSE	FALSE	TRUE

WSF2D2W5_UNBURNT_2_50X_1	x9_y2.png	TRUE	TRUE	FALSE	FALSE	FALSE	FALSE	FALSE
WSF3D1M1_BURNT_50X_10	x4_y6.png	FALSE	FALSE	TRUE	FALSE	FALSE	FALSE	FALSE
SWF1_BURNT_4_50X_2	x0_y9.png	FALSE	FALSE	FALSE	FALSE	FALSE	FALSE	FALSE
WSF2D2W1_UNBURNT_3_50X_3	x6_y7.png	FALSE	TRUE	FALSE	FALSE	FALSE	FALSE	FALSE
WSF3D3M2_BURNT_100X_1_1	x5_y2.png	FALSE	TRUE	FALSE	FALSE	FALSE	FALSE	FALSE
WSF3D3M4_BURNT_50X_1_4	x4_y6.png	FALSE	FALSE	FALSE	FALSE	FALSE	FALSE	FALSE
WSF3D3M3_UNBURNT_1_50X_5	x0_y3.png	FALSE	TRUE	FALSE	FALSE	FALSE	FALSE	TRUE
WSF2D2W5_BURNT_50X_1	x1_y3.png	FALSE	FALSE	FALSE	FALSE	FALSE	FALSE	FALSE

Appendix D: EMPA Data

Appendix D.1: EMPA Dataset

The following table includes the data from electron microprobe analysis (EMPA) used for subsequent statistical analyses.

Sample	P2O5	Na2O	Cl	K2O	FeO	Al2O3	SiO2	SrO	MnO	MgO	CaO	Total
WSF3D3M1_BU_1_	27.54	0.21	0.86	0.1	B.D.	B.D.	0.04	0.1	B.D.	0.34	36.39	63.96
WSF3D3M1_BU_2	31.97	0.36	0.84	0.07	B.D.	B.D.	B.D.	0.14	B.D.	0.65	38.22	70.43
WSF3D3M1_BU_3	30.7	0.36	0.84	0.06	B.D.	0.08	B.D.	0.08	0.01	0.67	38.78	69.79
WSF3D3M1_BU_4	30.88	0.49	0.68	0.01	0.02	0.04	0.04	0.16	B.D.	0.27	41.31	72.1
WSF3D3M1_BU_5	31.97	0.37	0.74	0.03	B.D.	0.03	0.15	0.12	B.D.	0.32	35.14	67.05
WSF3D3M1_BU_6	26.01	0.36	1.03	0.03	0.01	B.D.	0.05	0.09	B.D.	0.21	32.23	58.47
WSF3D3M1_BU_7	29.8	0.46	0.91	0.07	B.D.	B.D.	0.04	0.06	B.D.	0.74	37.76	68.09
WSF3D3M1_BU_8	30.6	0.48	0.86	0.03	B.D.	B.D.	0.11	0.07	B.D.	0.64	34.78	65.8
WSF3D3M1_BU_9	29.66	0.49	0.84	0.04	B.D.	0.06	B.D.	0.06	B.D.	0.59	36.02	66.07
WSF3D3M1_BU_10	31.39	0.65	0.68	0.04	B.D.	0.04	B.D.	0.06	B.D.	0.92	39.69	71.69
WSF3D3M1_BU_11	21.99	0.41	1.14	0.03	B.D.	B.D.	0.04	0.08	0.01	0.5	27.61	50.49
WSF3D3M1_BU_12	31.99	0.5	0.71	0.06	B.D.	B.D.	0.06	0.09	0.01	0.47	40.36	72.41
WSF5D6M5_UN_1_	32.82	0.45	0.05	0.03	B.D.	0.07	B.D.	B.D.	B.D.	0.82	42.88	75.33
WSF5D6M5_UN_2	31.96	0.35	0.05	0.04	B.D.	0.05	0.04	0.04	0.01	1	41.79	73.57
WSF5D6M5_UN_3	31.44	0.59	0.07	0.07	B.D.	0.03	0.09	0.04	0.01	0.8	40.93	72.34
WSF5D6M5_UN_4	32.49	0.58	0.05	0.04	B.D.	0.07	0.07	B.D.	B.D.	0.7	43.22	75.43
WSF5D6M5_UN_5	33.07	0.6	0.03	0.03	B.D.	B.D.	0.05	0.06	B.D.	0.7	44.84	77.55
WSF5D6M5_UN_6	32.21	0.55	0.02	0.02	B.D.	0.06	B.D.	B.D.	B.D.	0.78	45.14	77

WSF5D6M5_UN_10	36.75	0.46	0.04	0.03	0.01	0.04	B.D.	B.D.	B.D.	0.91	35.41	71.71
WSF5D6M5_UN_11	34.05	0.58	0.06	0.03	0.01	B.D.	B.D.	0.03	B.D.	0.75	42.83	76.49
WSF2D2W1_BU_1_	32.91	0.4	0.92	0.11	0.01	0.06	0.06	B.D.	B.D.	0.57	35.56	68.76
WSF2D2W1_BU_2	35.5	0.48	0.69	0.16	0.01	B.D.	0.08	B.D.	0.02	0.52	42.89	78.33
WSF2D2W1_BU_3	36.35	0.91	0.66	0.16	B.D.	B.D.	0.1	0.05	B.D.	0.41	40.65	77.29
WSF2D2W1_BU_4	29.32	0.93	0.58	0.11	B.D.	0	B.D.	0	B.D.	0.14	35.51	64.96
WSF2D2W1_BU_5	35.59	0.35	0.54	0.06	0.02	0.08	B.D.	0.03	B.D.	0.2	45.73	80.58
WSF2D2W1_BU_6	36.36	0.33	0.53	0.06	B.D.	0.03	0.05	B.D.	B.D.	0.19	45.68	81.16
WSF2D2W1_BU_7	32.7	0.58	0.84	0.1	0.04	0.06	0.09	0.04	B.D.	0.2	40.91	73.65
WSF2D2W1_BU_8	33.89	0.3	0.73	0.06	B.D.	0.05	B.D.	B.D.	B.D.	0.2	42.89	76.18
WSF2D2W1_BU_9	32.44	0.75	0.81	0.1	B.D.	0.04	B.D.	B.D.	B.D.	0.22	41.15	73.66
WSF2D2W1_BU_10	34.83	0.48	0.6	0.09	B.D.	0.03	B.D.	B.D.	B.D.	0.17	44.89	79.11
WSF2D2W1_BU_11	36.26	1.12	0.58	0.15	B.D.	B.D.	B.D.	B.D.	0.01	0.22	44.28	80.57
WSF2D2W1_BU_12	23.99	1.26	0.53	0.15	0.7	2.86	0.59	B.D.	0.01	0.22	29.49	58.34
WSF3D3M3_UN_1_	30.31	0.47	0.8	0.15	0.04	0.11	0.07	0	0.01	0.8	36.35	67.35
WSF3D3M3_UN_2	31.2	0.5	0.79	0.14	0.02	B.D.	B.D.	0.04	0.01	0.85	38.4	70.19
WSF3D3M3_UN_3	31.26	0.55	0.77	0.14	B.D.	0.1	0.12	B.D.	0.01	0.85	38.62	70.64
WSF3D3M3_UN_4	31.42	0.62	0.67	0.05	B.D.	0.08	0.14	B.D.	0.01	0.77	40.37	72.36
WSF3D3M3_UN_5	37.12	0.68	0.24	0.09	0.01	0.06	0.08	0.03	B.D.	0.82	50.06	87.12

WSF3D3M3_UN_6	32.36	0.7	0.63	0.04	B.D.	0.05	0.13	0.07	B.D.	0.7	41.82	74.64
WSF3D3M3_UN_7	32.67	0.36	0.67	0.07	B.D.	0.03	B.D.	0.08	0.02	0.57	40.63	73.23
WSF3D3M3_UN_8	33.34	0.45	0.7	0.05	B.D.	0.04	B.D.	0.04	0.01	0.53	41.18	74.43
WSF3D3M3_UN_9	33.19	0.36	0.63	0.07	B.D.	0	B.D.	0.05	B.D.	0.52	40.26	73.21
WSF3D3M3_UN_10	31.27	0.48	0.56	0.06	B.D.	0	0.08	B.D.	B.D.	0.76	39.16	70.6
WSF3D3M3_UN_11	32.32	0.55	0.62	0.05	B.D.	0.07	0.04	B.D.	0.01	0.78	40.99	73.57
WSF3D3M3_UN_12	31.21	0.39	0.83	0.06	0.01	0.03	B.D.	B.D.	B.D.	0.72	38.67	70.13
WSF5D6M2_BU_1_	32.73	0.82	0.71	0.36	0.03	0.15	0.13	B.D.	B.D.	0.82	40.72	74.58
WSF5D6M2_BU_2	31.69	0.6	0.7	0.13	B.D.	0.12	B.D.	0.05	B.D.	0.72	38.96	71.17
WSF5D6M2_BU_3	31.72	0.54	0.61	0.13	B.D.	0.06	0.06	B.D.	B.D.	0.81	40.46	72.59
WSF5D6M2_BU_4	30.4	0.53	0.64	0.05	B.D.	0	B.D.	B.D.	B.D.	0.66	40.25	70.78
WSF5D6M2_BU_5	33.57	0.43	0.55	0.04	B.D.	0.03	0.11	0.05	B.D.	0.83	42.9	76.6
WSF5D6M2_BU_6	31.56	0.36	0.55	0.05	0.02	0	0.04	0.05	0.01	0.78	40.68	72.3
WSF5D6M2_BU_7	29.97	0.38	0.78	0.04	0.04	B.D.	0.07	0.07	0.01	0.74	38.07	68.44
WSF5D6M2_BU_8	30.38	0.34	0.74	0.05	0.01	0.04	0.13	B.D.	B.D.	0.85	39.3	70.08
WSF5D6M2_BU_9	30.97	0.35	0.85	0.07	B.D.	B.D.	0	0.04	B.D.	0.79	38.41	69.7
WSF5D6M2_BU_10	29.56	0.28	0.84	0.02	B.D.	0.03	0.05	B.D.	0.02	0.72	36.7	66.52
WSF5D6M2_BU_12	30.69	0.27	0.73	0.04	0.07	0.03	B.D.	0	B.D.	0.73	37.66	68.49
WSF5D6M5_BU_3	32.52	0.52	0.17	0.07	B.D.	B.D.	0.06	0.05	0.02	0.66	41.91	74.19

WSF5D6M5_BU_4	33.34	0.53	0.09	0.03	B.D.	0.09	0.09	B.D.	B.D.	0.71	44.54	77.59
WSF5D6M5_BU_5	33.05	0.55	0.06	0.02	B.D.	0.06	0	B.D.	B.D.	0.72	44.16	76.81
WSF5D6M5_BU_6	28.29	0.48	0.07	0.03	B.D.	0.1	0	B.D.	0.02	0.71	40.24	68.38
WSF5D6M5_BU_7	34.23	0.49	0.08	0.06	0.01	0.07	0.18	B.D.	0.01	0.63	44.8	78.66
WSF5D6M5_BU_8	30.93	0.46	0.1	0.03	B.D.	0.06	0.28	B.D.	0.02	0.45	40.25	70.89
WSF5D6M5_BU_9	32.68	0.53	0.07	0.03	0.02	0.08	0.1	B.D.	0.01	0.61	42.31	74.63
WSF5D6M5_BU_11	32.38	0.48	0.06	0.03	B.D.	0.05	0.05	0.03	0.01	0.77	43.68	75.73
WSF5D6M5_BU_12	29.44	0.51	0.05	0.03	B.D.	B.D.	0.06	B.D.	B.D.	0.7	38.68	67.88
SWF2FR4_BU_1_	34.491769	0.6154	0.397799	0.3203	B.D.	0.1605	B.D.	B.D.	B.D.	0.9517	40.577184	77.51
SWF2FR4_BU_2	33.724282	0.506	0.3790634	0.2334	B.D.	0.1216	B.D.	0.0369	0.0109	0.9192	40.193905	76.13
SWF2FR4_BU_3	34.864226	0.5708	0.41037	0.5963	0.0102	0.0553	0.0518	B.D.	B.D.59	1.0135	40.69822	78.3
SWF2FR4_BU_4	31.737845	0.2475	0.3518666	0.1111	0.0112	0.0321	B.D.	B.D.	B.D.	0.4384	41.031068	74.01
SWF2FR4_BU_5	34.164458	0.6666	0.3506578	0.3268	B.D.	B.D.	0.0838	0.0376	B.D.	0.5231	42.029612	78.21
SWF2FR4_BU_6	34.503055	0.4811	0.3677012	0.3025	B.D.	0.0665	B.D.	B.D.	B.D.	0.6004	41.091586	77.46
SWF2FR4_BU_7	34.830366	0.5888	0.3911509	0.35	B.D.	0.0593	B.D.	B.D.	B.D.	0.905	41.595901	78.74
SWF2FR4_BU_9	33.848434	0.5257	0.4652472	0.3087	B.D.	0.1005	0	B.D.	0.0119	0.8764	40.143474	76.31
SWF2FR4_BU_10	33.758141	0.5891	0.3293839	0.2841	B.D.	0.0377	B.D.	0.0525	B.D.	0.4323	43.118932	78.61
SWF2FR4_BU_11	35.710719	0.5953	0.2916709	0.3012	0.0114	B.D.	0.0695	0.0465	0.0185	0.6845	43.693851	81.45
SWF2FR4_BU_12	34.457909	0.6077	0.3187469	0.299	B.D.	B.D.	0.0411	B.D.	0.011	0.9622	41.172276	77.9

WSF5D6M2_UN_1_	20.338406	0.1202	0.0571738	0.112	0.1757	0.6026	0.7936	0.0362	0.0245	0.2646	26.466451	48.99
WSF5D6M2_UN_2	31.88457	0.451	0.0213948	0.0363	0.0637	0.0539	0.1499	0.0609	B.D.	0.6866	41.333657	74.74
WSF5D6M2_UN_3	33.769428	0.4156	0.0321527	0.0309	B.D.78	0.0714	0.0448	0.0531	0.012	0.9097	44.157821	79.5
WSF5D6M2_UN_4	29.931993	0.5015	0.0430314	0.0466	B.D.	0.0539	0.0616	B.D.	B.D.	0.8219	44.107389	75.57
WSF5D6M2_UN_5	33.385685	0.4596	0.0360207	0.0415	0.0134	0.071	0.0517	B.D.	B.D.	0.9425	44.329288	79.33
WSF5D6M2_UN_6	34.525628	0.4925	0.0159555	0.0304	0.019	0.0628	B.D.	B.D.	B.D.	0.9246	42.967638	79.04
WSF5D6M2_UN_7	35.428554	0.5087	0.0175268	0.0316	B.D.	B.D.	B.D.	B.D.	B.D.	0.759	43.108846	79.88
WSF5D6M2_UN_8	33.938727	0.465	0.0151094	0.0212	B.D.	0.0591	B.D.	B.D.	B.D.	0.71	43.794714	79.01
WSF5D6M2_UN_9	31.196089	0.4577	0.0188565	0.0372	B.D.	0.0562	0.1211	B.D.	B.D.	0.6498	42.816343	75.35
WSF5D6M2_UN_10	29.322518	0.4535	0.0832827	0.0388	B.D.	0.0787	B.D.	B.D.	0.0214	0.8256	41.192449	72.04
WSF5D6M2_UN_11	7.8554552	0.1318	1.3900604	0.0205	B.D.89	0.2852	0.0558	0.0378	B.D.	0.1864	12.244768	22.22
WSF5D6M2_UN_12	33.058374	0.4586	0.0873925	0.0582	B.D.36	0.0683	0.0458	B.D.	B.D.	0.8516	44.329288	78.98
WSF3D1M1_BU_1_	30.112578	0.5939	0.5028392	0.183	0.018	0.042	B.D.	B.D.	B.D.1	0.683	38.267422	70.4
WSF3D1M1_BU_2	30.146438	0.5456	0.4841036	0.1202	B.D.83	0.0728	B.D.	B.D.	B.D.	0.7017	38.650701	70.73
WSF3D1M1_BU_3	27.979416	0.6768	0.5718588	0.2217	B.D.	B.D.	0	B.D.	B.D.	0.6604	35.30205	65.42
WSF3D1M1_BU_4	29.435384	0.775	0.5261681	0.1378	0.0177	B.D.	B.D.	0.0437	B.D.	0.7149	39.044067	70.73
WSF3D1M1_BU_5	30.327023	0.6582	0.4427645	0.1287	0.0147	0.0496	B.D.	B.D.	B.D.	0.7024	39.366828	71.71
WSF3D1M1_BU_6	28.555031	0.5831	0.5446619	0.1244	B.D.	B.D.	B.D.	B.D.	B.D.	0.6746	36.613269	67.16
WSF3D1M1_BU_9	27.415087	0.5107	0.5102126	0.0949	B.D.22	0.0467	B.D.	B.D.	0.015	0.6156	36.088781	65.34

WSF3D1M1_BU_10	26.455728	0.5637	0.5991765	0.1184	0.0152	0.0734	0.0412	B.D.	B.D.	0.6439	34.364024	62.87
WSF3D1M1_BU_11	24.740169	0.4726	0.6584051	0.1149	B.D.	0.0319	B.D.	B.D.	B.D.	0.6926	29.895793	56.64
WSF3D1M1_BU_12	30.022286	0.6486	0.4573903	0.1162	B.D.	0.0723	0.0418	0.0383	B.D.	0.6836	39.639159	71.72
SWF2FR2_BU_2	29.029067	0.6488	0.6299995	0.2158	0.026	B.D.72	B.D.	0.0661	B.D.	0.7365	36.048436	67.43
SWF2FR2_BU_3	29.954566	0.6199	0.4799939	0.1905	B.D.25	0.0589	B.D.	B.D.	0.0105	0.8566	38.912945	71.09
SWF2FR2_BU_4	29.830414	0.5202	0.4536432	0.1166	B.D.	B.D.	B.D.	B.D.	B.D.	0.6375	39.376915	70.95
SWF2FR2_BU_5	30.846205	0.5598	0.4775764	0.0954	B.D.	B.D.73	B.D.	B.D.	B.D.	0.6074	40.052697	72.66
SWF2FR2_BU_6	31.308955	0.5498	0.4020296	0.1025	B.D.52	0.0587	B.D.	B.D.	B.D.	0.442	41.212621	74.1
SWF2FR2_BU_7	29.751408	1.0055	0.4920814	0.1474	B.D.62	B.D.	B.D.	B.D.	0.0108	0.6109	38.983549	71.05
SWF2FR2_BU_8	28.126141	0.6536	0.4849498	0.0809	B.D.18	B.D.	0.0586	B.D.	B.D.	0.5219	38.539752	68.48
SWF2FR2_BU_9	31.986149	0.7905	0.3926014	0.1201	B.D.	0.0697	0.0768	B.D.	B.D.	0.4392	41.263053	75.14
SWF2FR2_BU_10	27.821404	0.8502	0.5070699	0.2263	0.0362	0.0532	0.0493	B.D.	B.D.	0.4618	35.84671	65.86
SWF2FR2_BU_11	29.706262	0.7829	0.4254794	0.1046	0.0116	B.D.	B.D.	0.0375	0.0141	0.4954	38.257335	69.85
SWF2FR2_BU_12	31.48954	0.5902	0.3917553	0.0843	B.D.	0.0317	0.0536	B.D.	0.0183	0.4414	39.951834	73.08
WSF2D2W3_BU_1_	37.855168	0.6766	0.2115309	0.067	0.0152	B.D.	0.1963	0.0578	B.D.	0.9235	51.208145	91.21
WSF2D2W3_BU_2	37.663296	0.4384	0.1185782	0.0574	B.D.	B.D.	0.0662	0.055	B.D.	0.4108	50.59288	89.43
WSF2D2W3_BU_3	36.354053	0.6228	0.2024653	0.055	B.D.57	0.0794	0.0516	B.D.	B.D.	0.2796	48.162082	85.83
WSF2D2W3_BU_4	34.220891	0.6499	0.2820009	0.0588	B.D.	B.D.	B.D.	B.D.	0.0137	0.7381	47.02233	83.05
WSF2D2W3_BU_5	26.895905	0.5887	0.5213331	0.0547	B.D.	0.0459	B.D.	B.D.	B.D.	0.5491	37.026807	65.68

WSF2D2W3_BU_6	38.035753	0.8001	0.1109631	0.0359	B.D.	0.1351	B.D.	0.0398	0.0137	0.6956	51.692287	91.58
WSF2D2W3_BU_7	41.737749	0.4535	0.1193034	0.0928	B.D.26	B.D.9	0.0762	0.0565	B.D.	0.2751	53.921359	96.76
WSF2D2W3_BU_8	39.175697	0.5327	0.1016557	0.0708	B.D.	0.0534	B.D.	0.047	B.D.	0.2719	53.8911	94.17
WSF2D2W3_BU_9	39.830318	0.5881	0.079173	0.0708	B.D.92	B.D.	B.D.	0.0541	B.D.	0.3377	53.285922	94.28
WSF2D2W3_BU_10	35.834871	0.4966	0.2324423	0.0567	B.D.21	0.0493	B.D.	B.D.	B.D.	0.861	46.649137	84.24
WSF2D2W3_BU_12	20.135247	0.4264	0.2985608	0.0628	0.0548	4.49	0.3396	0.0489	0.0226	0.4545	27.939051	54.27
WSF2D2W3_UN_1_	24.333853	0.4421	0.3731406	0.0263	0.0149	B.D.	0.279	B.D.	B.D.	0.4823	33.879881	59.88
WSF2D2W3_UN_3	14.254942	0.1613	0.0408557	0.0758	0.1265	0.1748	1.1949	B.D.	B.D.	0.2329	21.826753	38.09
WSF2D2W3_UN_4	34.68364	0.5912	0.0479873	0.032	B.D.	B.D.	B.D.	0.0362	0.0148	0.7456	45.993527	82.17
WSF2D2W3_UN_5	35.473701	0.5971	0.0337241	0.0432	B.D.	0.1111	0.0748	B.D.	0.0136	0.7821	46.578533	83.71
WSF2D2W3_UN_6	33.442117	0.6299	0.0340867	0.0399	B.D.	0.0302	B.D.	0.0312	B.D.	0.8204	45.216882	80.25
WSF2D2W3_UN_7	29.232225	0.5299	0.0771181	0.0331	B.D.	B.D.	B.D.	B.D.	B.D.	0.6456	41.444606	71.97
WSF2D2W3_UN_8	28.306726	0.53	0.064668	0.0385	B.D.	0.0841	B.D.	B.D.	B.D.	0.6293	38.297681	68
WSF2D2W3_UN_11	28.013276	0.5431	0.0429106	0.0182	0.0171	0.0416	B.D.	B.D.	B.D.	0.5679	36.441801	65.69
WSF2D2W3_UN_12	33.983873	0.3921	0.0372294	B.D.	0.0158	B.D.	B.D.	0.0423	B.D.	0.8582	44.369633	79.73
WSF3D1M5_BU_2	29.954566	0.9493	0.3790634	0.1428	B.D.	B.D.	B.D.	B.D.	B.D.	0.5194	39.6089	71.62
WSF3D1M5_BU_4	32.934222	0.3578	0.3685473	0.0816	0.0139	0.0703	B.D.	B.D.	B.D.	0.4296	43.683765	77.99
WSF3D1M5_BU_5	32.573051	0.5872	0.3170546	0.1245	B.D.	B.D.	B.D.	0.0339	B.D.	0.4471	42.705394	76.8
WSF3D1M5_BU_7	31.297668	0.3706	0.5087621	0.106	B.D.	B.D.	0.0816	B.D.	B.D.	0.5743	41.232794	74.17

WSF3D1M5_BU_8	31.895857	0.4125	0.4243915	0.1361	0.0101	B.D.	0.0489	B.D.	B.D.	0.6083	41.686677	75.23
WSF3D1M5_BU_9	31.444394	0.4006	0.5297943	0.2146	0.0389	0.0801	0.044	B.D.	B.D.	0.6362	41.394175	74.78
WSF3D1M5_BU_11	33.092234	0.4638	0.3685473	0.0976	B.D.82	B.D.	B.D.	B.D.	B.D.	0.4207	43.754369	78.23
WSF3D1M5_BU_12	33.182526	0.4683	0.3113735	0.0952	B.D.	B.D.	0	B.D.	B.D.	0.4382	46.09439	80.63
WSF3D1M4_UN_2	28.39	0.49	0.04	0.1	0.01	0.04	B.D.	B.D.	0.01	0.63	34.09	63.85
WSF3D1M4_UN_3	15.58	0.14	0.47	0.09	0.02	0.06	0.1	0.04	0.01	0.24	19.24	35.99
WSF3D1M4_UN_4	32.62	0.52	0.04	0.06	B.D.	0.03	0.06	B.D.	0.01	0.73	42.31	76.37
WSF3D1M4_UN_5	28.88	0.51	0.03	0.07	B.D.	0.08	0.04	B.D.	B.D.	0.68	38.69	68.97
WSF3D1M4_UN_6	31.97	0.4	0.04	0.07	0.01	0.03	B.D.	B.D.	0.01	0.72	39.91	73.17
WSF3D1M4_UN_7	24.63	0.35	0.05	0.07	0.03	0.09	0.19	B.D.	0.02	0.37	31.09	56.9
WSF3D1M4_UN_8	28.59	0.43	0.04	0.06	0.01	0.06	0.11	B.D.	B.D.	0.51	36.94	66.75
WSF3D1M4_UN_9	26.67	0.45	0.06	0.06	B.D.	0.1	0.06	B.D.	B.D.	0.49	32.73	60.65
WSF3D1M4_UN_10	27.01	0.39	0.05	0.07	0.01	0.08	0.15	0.05	0.01	0.71	33.41	61.93
WSF3D1M4_UN_11	32.17	0.43	0.05	0.08	B.D.	0	B.D.	0.04	B.D.	0.72	40.18	73.68
WSF5D6M3_BU_1_	34.88	0.24	0.54	0.05	0.03	0.03	0.09	B.D.	0.02	0.21	44.54	80.61
WSF5D6M3_BU_2	33.85	0.57	0.55	0.04	B.D.	0.08	B.D.	B.D.	0.01	0.18	43.69	79.03
WSF5D6M3_BU_3	34.02	0.33	0.63	0.05	B.D.	0.04	0.12	B.D.	B.D.	0.34	42.46	77.99
WSF5D6M3_BU_4	30.88	0.51	0.63	0.05	B.D.	0.03	B.D.	B.D.	0.01	0.48	40.9	73.51
WSF5D6M3_BU_5	31.87	0.48	0.55	0.06	B.D.	B.D.	B.D.	0.07	B.D.	0.5	42.37	75.94

WSF5D6M3_BU_6	32.18	0.54	0.53	0.05	B.D.	0	0	B.D.	B.D.	0.24	42.43	75.97
WSF5D6M3_BU_7	27.05	0.36	1.07	0.09	0.07	0.08	0	0.06	B.D.	0.39	33.07	62.25
WSF5D6M3_BU_8	25.22	0.34	1.1	0.09	0.08	0.03	0.13	0.04	0.02	0.45	32.83	60.32
WSF5D6M3_BU_9	25.23	0.31	1.07	0.05	0.02	B.D.	0.07	B.D.	B.D.	0.45	32.91	60.13
WSF5D6M3_BU_12	30.92	0.41	0.62	0.04	B.D.	B.D.	0.09	0.05	B.D.	0.54	41.45	74.14
WSF3D1M1_BU_1_	31.19	0.55	0.88	0.13	B.D.	B.D.	0.04	B.D.	B.D.	0.84	36.87	70.5
WSF3D1M1_BU_2	31.19	0.67	0.94	0.14	B.D.	B.D.	B.D.	B.D.	B.D.	0.82	36.4	70.2
WSF3D1M1_BU_3	29.26	0.56	0.96	0.14	0.01	0.09	0.07	0.05	B.D.	0.84	35.55	67.53
WSF3D1M1_BU_4	31.41	0.66	0.72	0.11	B.D.	0.03	0.06	B.D.	B.D.	0.68	40.62	74.28
WSF3D1M1_BU_5	32.05	0.57	0.74	0.09	B.D.	B.D.	B.D.	B.D.	0.02	0.72	41.17	75.39
WSF3D1M1_BU_6	31.56	0.54	0.75	0.08	0.02	0.06	B.D.	0.03	B.D.	0.67	40.93	74.65
WSF3D1M1_BU_7	35.78	0.35	0.52	0.07	0.03	0.1	0.09	B.D.	B.D.	0.14	45.55	82.62
WSF3D1M1_BU_8	37.45	0.37	0.39	0.09	B.D.	B.D.	0.12	B.D.	B.D.	0.39	47.83	86.67
WSF3D1M1_BU_9	38.31	0.95	0.34	0.14	0.02	0.07	0.09	0.04	B.D.	0.72	47.37	88.06
WSF3D1M1_BU_10	39.76	0.49	0.13	0.07	B.D.	0.1	0.08	B.D.	B.D.	0.37	51.39	92.39
WSF3D1M1_BU_11	28.54	0.69	0.84	0.09	0.01	0.04	B.D.	B.D.	0.01	0.93	34.29	65.44
WSF3D1M1_BU_12	31.84	0.51	0.57	0.12	0.02	0.48	0.16	B.D.	B.D.	0.84	39.54	74.08
WSF2D2W4_BU_1_	32.98	0.76	0.52	0.18	0.01	0.03	0.2	B.D.	B.D.	0.77	38.58	74.03
WSF2D2W4_BU_2	31.71	0.68	0.48	0.18	B.D.	B.D.	0.07	B.D.	B.D.	0.78	38.64	72.56

WSF2D2W4_BU_3	30.97	0.8	0.36	0.22	0.01	0.08	0.38	B.D.	B.D.	0.74	37.19	70.79
WSF2D2W4_BU_4	35.91	0.48	0.22	0.1	B.D.	B.D.	B.D.	0.03	B.D.	0.2	45.93	82.9
WSF2D2W4_BU_5	34.46	0.53	0.33	0.08	B.D.	0.03	0	B.D.	B.D.	0.2	44.12	79.78
WSF2D2W4_BU_6	34.86	0.5	0.29	0.08	0.01	B.D.	B.D.	B.D.	B.D.	0.19	46.2	82.13
WSF2D2W4_BU_7	39.02	0.57	0.17	0.14	0.04	0.03	0.22	B.D.	0.02	0.51	49.25	89.99
WSF2D2W4_BU_8	37.64	0.29	0.18	0.06	B.D.	0.04	0.15	B.D.	B.D.	0.51	50.31	89.16
WSF2D2W4_BU_9	38.56	0.59	0.15	0.12	B.D.	0.06	0.2	0.05	B.D.	0.45	49.18	89.36
WSF2D2W4_BU_10	37.64	0.48	0.19	0.12	0.02	B.D.	0.08	0.06	B.D.	0.25	48.98	87.81
WSF2D2W4_BU_11	21.24	0.31	0.17	0.09	0.02	0.08	23.41	0	B.D.	0.18	33.2	78.71
WSF3D3M3_BU_1_	32.33	0.18	0.39	0.03	B.D.	0.04	0	B.D.	B.D.	0.36	41.09	74.43
WSF3D3M3_BU_2	30.99	0.23	0.35	0.03	0.03	0.08	B.D.	0.05	B.D.	0.38	40.78	72.94
WSF3D3M3_BU_3	33.27	0.35	0.33	0.03	0.1	0.14	0	B.D.	0.02	0.48	42.74	77.47
WSF3D3M3_BU_4	41.23	0.4	0.03	0.03	B.D.	B.D.	B.D.	0.05	B.D.	0.84	54.41	97
WSF3D3M3_BU_5	41.4	0.43	0.02	0.02	0.01	0.06	B.D.	B.D.	B.D.	0.88	54.48	97.31
WSF3D3M3_BU_6	41.03	0.69	0.04	0.06	0.01	0.06	B.D.	B.D.	B.D.	0.89	54.32	97.11
WSF3D3M3_BU_8	33.29	0.4	0.32	0.09	B.D.	0.13	0.05	B.D.	B.D.	0.63	42.2	77.11
WSF3D3M3_BU_9	35.09	0.76	0.27	0.09	0.02	B.D.	0.09	0.06	B.D.	0.81	43.65	80.85
WSF3D3M3_BU_10	10.62	0.21	0.83	0.03	0.01	0.03	B.D.	B.D.	B.D.	0.21	14.81	26.75
WSF3D3M3_BU_11	32.5	0.37	0.16	0.05	0.12	0.33	0.2	0.04	B.D.	0.55	40.16	74.47

WSF3D3M3_BU_12	25.32	0.16	0.28	0.04	0.05	0.13	0.2	B.D.	B.D.	0.4	29.89	56.46
WSF3D3M1_BU_1_	35.5	0.27	0.14	0.32	B.D.	0.04	0.07	0.21	0.01	0.74	48.41	85.7
WSF3D3M1_BU_2	34.27	0.28	0.39	0.11	B.D.	0.08	0.06	0.17	B.D.	0.59	43.25	79.21
WSF3D3M1_BU_3	31.79	0.31	0.44	0.1	0.02	B.D.	B.D.	0.14	B.D.	0.6	40.15	73.56
WSF3D3M1_BU_4	35.52	0.65	0.2	0.08	B.D.	0.05	B.D.	0.11	0.01	0.47	46.49	83.58
WSF3D3M1_BU_5	37.47	0.51	0.15	0.08	B.D.	0.04	0.05	0.16	B.D.	0.52	48.38	87.35
WSF3D3M1_BU_6	35.15	0.41	0.2	0.06	0.03	0.04	B.D.	0.11	0.01	0.38	45.76	82.14
WSF3D3M1_BU_7	33.99	0.3	0.24	0.07	0.01	0.04	0.23	0.14	B.D.	0.47	43.81	79.29
WSF3D3M1_BU_8	32.38	0.61	0.22	0.09	B.D.	B.D.	0.12	0.11	B.D.	0.49	42.31	76.34
WSF3D3M1_BU_9	33.91	0.76	0.28	0.09	0.01	0.09	0.08	0.11	B.D.	0.39	43.25	78.96
WSF3D3M1_BU_10	34.92	0.54	0.18	0.07	0.01	0.14	0.1	0.08	B.D.	0.39	39.95	76.4
WSF3D3M1_BU_11	33.29	0.35	0.29	0.05	B.D.	0.08	0.05	0.1	B.D.	0.3	43.23	77.74
WSF3D3M1_BU_12	32.2	0.37	0.12	0.06	0.01	0.54	0.2	0.17	B.D.	0.73	45.24	79.64
WSF3D3M4_BU_1_	29.82	0.13	0.44	0.04	0.01	B.D.	B.D.	0.06	B.D.	0.17	39.05	69.79
WSF3D3M4_BU_2	25.85	0.26	0.57	0.07	0.03	0.11	0.11	0.06	B.D.	0.3	32.06	59.4
WSF3D3M4_BU_3	27.47	0.14	0.56	0.06	B.D.	B.D.	B.D.	0.06	B.D.	0.28	34.43	63.02
WSF3D3M4_BU_4	35.24	0.57	0.21	0.05	0.01	0	0.11	0.05	B.D.	0.21	45.21	81.66
WSF3D3M4_BU_5	34.65	0.42	0.24	0.04	B.D.	0.05	0.1	0.1	B.D.	0.17	45.29	81.07
WSF3D3M4_BU_6	33.49	0.55	0.29	0.03	0.01	0.05	0	0.09	B.D.	0.19	43.01	77.71

WSF3D3M4_BU_7	25.96	0.54	0.64	0.07	0.01	0	0.11	0.07	B.D.	0.26	33.45	61.11
WSF3D3M4_BU_8	28.43	0.72	0.53	0.07	0.01	0.06	0	0.08	B.D.	0.4	35.06	65.36
WSF3D3M4_BU_9	32.9	0.84	0.38	0.05	B.D.	0.04	0.08	0.11	B.D.	0.33	40.97	75.7
WSF3D3M4_BU_10	32.95	0.63	0.35	0.06	B.D.	0.06	0.04	0.07	B.D.	0.22	42.95	77.33
WSF3D3M4_BU_12	31.39	0.48	0.3	0.04	0.02	0.09	0.07	0.1	B.D.	0.26	37.86	70.61
WSF2D2W4_UN_4	33.17	0.49	0.04	0.08	B.D.	0.08	0.07	0.04	B.D.	0.8	44.8	79.58
WSF2D2W4_UN_5	30.76	0.63	0.08	0.1	B.D.	B.D.	B.D.	B.D.	0.01	0.67	41.98	74.29
WSF2D2W4_UN_6	32	0.64	0.03	0.07	0.03	0.09	0.07	B.D.	B.D.	0.63	44.31	77.86
WSF2D2W4_UN_7	30.4	0.58	0.06	0.09	B.D.	0.25	B.D.	B.D.	B.D.	0.73	39.03	71.15
WSF2D2W4_UN_8	27.94	0.42	0.09	0.07	B.D.	0.47	0.14	B.D.	B.D.	0.68	37.99	67.81
WSF2D2W4_UN_9	31.64	0.58	0.06	0.05	B.D.	0.37	0.08	B.D.	B.D.	0.66	43.23	76.67
WSF2D2W4_UN_10	30.28	0.42	0.06	0.07	0.02	0.14	0.05	0.04	B.D.	0.65	39.51	71.24
WSF2D2W4_UN_12	28.05	0.48	0.07	0.06	B.D.	0.19	B.D.	B.D.	B.D.	0.64	40.26	69.76
WSF2D2W2_UN_4	34.27	0.61	0.09	0.04	B.D.	B.D.	B.D.	B.D.	B.D.	0.66	45.68	81.4
WSF2D2W2_UN_5	34.06	0.52	0.07	0.04	B.D.	B.D.	0.05	B.D.	B.D.	0.66	44.94	80.35
WSF2D2W2_UN_6	33.78	0.57	0.04	0.03	B.D.	B.D.	0	0.03	0.01	0.79	45.7	80.97
WSF2D2W2_UN_7	29.78	0.53	0.04	0.03	B.D.	B.D.	0.05	0.05	0.02	0.71	43.31	74.53
WSF2D2W2_UN_9	28.53	0.04	0.11	0.05	0.24	0.04	0.52	0.08	0.02	0.13	35.5	65.25
WSF2D2W2_UN_11	35.22	0.46	0.06	0.06	0.01	0.04	0.04	B.D.	B.D.	0.94	43.13	79.97

WSF2D2W2_UN_12	34.45	0.54	0.04	0.03	0.02	0.07	B.D.	0.08	0.02	0.77	44.49	80.53
WSF3D3M3_BU_1_	27.15	0.42	0.93	0.53	B.D.	0.08	0.18	0.03	B.D.	0.61	34.75	64.68
WSF3D3M3_BU_2	25.81	0.65	1.15	0.18	0.02	0.15	0.28	B.D.	B.D.	0.55	33.49	62.29
WSF3D3M3_BU_3	28.17	0.42	0.99	0.11	0.01	0.06	B.D.	0.04	B.D.	0.82	37.25	67.87
WSF3D3M3_BU_4	33.32	0.42	0.59	0.04	B.D.	0.03	0.05	B.D.	0.03	0.27	43.89	78.65
WSF3D3M3_BU_5	33.77	0.39	0.51	0.03	0.02	B.D.	B.D.	0.03	0.02	0.23	44.38	79.41
WSF3D3M3_BU_6	32.8	0.33	0.54	0.01	B.D.	0.03	0	B.D.	B.D.	0.24	42.88	76.85
WSF3D3M3_BU_7	32.83	1.02	0.77	0.06	B.D.	0.05	0.1	0.03	0.01	0.33	41.99	77.18
WSF3D3M3_BU_8	32.19	1.13	0.68	0.07	B.D.	0.04	B.D.	B.D.	0.01	0.3	42.15	76.62
WSF3D3M3_BU_9	33.18	0.37	0.62	0.07	0.03	0.12	0	0.04	B.D.	0.12	43.64	78.2
WSF3D3M3_BU_11	31.49	1.6	0.48	0.12	B.D.	0.05	B.D.	B.D.	0.02	0.39	41.52	75.67
WSF3D3M3_BU_12	31.73	1.08	0.67	0.09	0.01	B.D.	0	B.D.	B.D.	0.4	41.28	75.28
WSF3D1M3_BU_1_	29.08	0.88	0.68	0.48	B.D.	B.D.	0.14	B.D.	0.01	0.72	33.9	65.89
WSF3D1M3_BU_2	23.87	0.86	0.71	0.54	0.09	0.21	0.28	B.D.	B.D.	0.6	26.91	54.07
WSF3D1M3_BU_3	26.98	0.79	0.81	0.4	0.01	0.03	0.09	0.03	B.D.	0.62	31.17	60.94
WSF3D1M3_BU_4	30.77	0.5	0.42	0.14	0.02	0.08	0.08	B.D.	0.03	0.56	39.25	71.86
WSF3D1M3_BU_5	31.4	0.43	0.33	0.08	B.D.	0.25	0.09	0.03	B.D.	0.65	39.96	73.21
WSF3D1M3_BU_6	30.37	0.39	0.42	0.06	0.02	B.D.	0.14	0.04	0.01	0.51	38.73	70.71
WSF3D1M3_BU_7	30.1	1.15	0.6	0.48	B.D.	0.09	0.07	0.03	B.D.	0.72	35.94	69.16

WSF3D1M3_BU_8	30.13	0.77	0.71	0.37	B.D.	B.D.	B.D.	0.05	B.D.	0.64	35.73	68.39
WSF3D1M3_BU_9	29.73	0.67	0.59	0.12	0.02	0.03	B.D.	0.04	B.D.	0.71	37.64	69.6
WSF3D1M3_BU_10	29.89	0.53	0.41	0.08	B.D.	B.D.	0.17	0.05	0.01	0.54	38.62	70.3
WSF3D3M3_UN_2	32.09	0.38	0.04	0.04	B.D.	0.03	B.D.	B.D.	B.D.	0.81	38.18	71.63
WSF3D3M3_UN_3	28.9	0.38	0.06	0.02	B.D.	0.04	0.14	0.05	B.D.	0.53	37.88	67.98
WSF3D3M3_UN_4	32.2	0.53	0.05	0.01	B.D.	0.05	B.D.	0.07	0.02	0.7	41.88	75.54
WSF3D3M3_UN_5	33.21	0.56	0.03	0.02	B.D.	0.06	B.D.	0.03	0.01	0.75	44.03	78.73
WSF3D3M3_UN_6	33.07	0.52	0.07	0.02	B.D.	0	B.D.	0.03	0.01	0.82	43.7	78.26
WSF3D3M3_UN_7	30.66	0.59	0.05	0.03	0.01	0.07	B.D.	B.D.	0.01	0.55	40.96	72.96
WSF3D3M3_UN_8	27.95	0.4	0.09	0.02	0.03	0.12	B.D.	0.04	0.01	0.36	36.7	65.73
WSF3D3M3_UN_10	31.42	0.34	0.08	0.02	0.02	0	0.06	0.07	B.D.	0.8	39.82	72.63
WSF3D3M3_UN_12	32.4	0.5	0.06	0.03	B.D.	B.D.	B.D.	B.D.	0.01	0.72	43.01	76.78
WSF3D3M4_UN_2	22.99	0.38	0.11	0.03	0.01	0.08	B.D.	0.07	0.01	0.36	28.72	52.76
WSF3D3M4_UN_4	26.24	0.44	0.31	0.03	B.D.	B.D.	B.D.	0.05	B.D.	0.65	34.39	62.15
WSF3D3M4_UN_5	32.7	0.6	0.03	0.03	0.02	B.D.	B.D.	0.05	B.D.	0.82	44.37	78.64
WSF3D3M4_UN_6	33.09	0.62	0.04	0.03	B.D.	B.D.	B.D.	0.11	B.D.	0.82	44.28	78.99
WSF3D3M4_UN_7	33.59	0.6	0.06	0.03	B.D.	B.D.	B.D.	0.1	0.01	0.77	45.1	80.26
WSF3D3M4_UN_8	31.38	0.5	0.05	0.03	B.D.	B.D.	B.D.	0.07	0.01	0.68	43.93	76.64
WSF3D3M4_UN_9	27.02	0.43	0.06	0.01	0.01	B.D.	B.D.	0.09	B.D.	0.51	38.62	66.78

WSF3D3M4_UN_10	32.41	0.59	0.05	0.03	B.D.	0	B.D.	0.09	B.D.	0.86	41.09	75.13
WSF3D3M4_UN_11	33.71	0.69	0.03	0.03	B.D.	0.04	0	0.04	B.D.	0.92	43.36	78.83
WSF3D3M4_UN_12	33.1	0.55	0.03	0.03	B.D.	0.07	0	0.11	0.01	0.81	43.51	78.22
WSF5D6M4_BU_1_	31.38	0.3	0.83	0.1	0.01	0.05	0.06	B.D.	B.D.	0.51	39.48	72.73
WSF5D6M4_BU_2	30.77	0.28	0.86	0.09	B.D.	0.06	B.D.	B.D.	B.D.	0.55	39.63	72.26
WSF5D6M4_BU_3	32.5	0.5	0.78	0.12	B.D.	0.06	0.22	B.D.	B.D.	0.88	38.86	73.93
WSF5D6M4_BU_4	32.47	0.39	0.65	0.06	0.01	0.06	0	B.D.	B.D.	0.35	40.21	74.23
WSF5D6M4_BU_5	28.92	0.48	0.76	0.07	B.D.	0.03	0	B.D.	B.D.	0.49	38.96	69.73
WSF5D6M4_BU_6	28.14	0.48	0.76	0.05	B.D.	B.D.	B.D.	B.D.	B.D.	0.51	39.15	69.11
WSF5D6M4_BU_7	22.8	0.18	1.15	0.05	0.06	0.08	0.05	0.03	B.D.	0.22	32.8	57.44
WSF5D6M4_BU_8	28	0.4	0.97	0.04	0.04	0.05	B.D.	B.D.	B.D.	0.66	36.84	67.02
WSF5D6M4_BU_10	31.32	0.26	0.13	0.04	0.04	0.22	0.18	B.D.	B.D.	0.34	31.74	64.28
WSF5D6M4_BU_11	39.52	0.55	0.07	0.06	B.D.	0.1	0.05	0.04	B.D.	0.67	51.84	92.88
WSF5D6M4_BU_12	24.87	0.32	0.13	0.05	B.D.	0.08	0.19	0.04	B.D.	0.87	33.72	60.27
WS_FR_UN_1_	26.29	0.72	0.06	0.4	B.D.	0.05	B.D.	0.03	B.D.	0.98	30.88	59.42
WS_FR1_UN_2	27.6	0.67	0.04	0.29	B.D.	0.08	B.D.	0.04	B.D.	0.56	35.27	64.58
WS_FR1_UN_3	25.18	0.63	0.05	0.38	0.02	B.D.	0	B.D.	B.D.	0.62	32.08	59
WS_FR1_UN_4	28.81	0.48	0.02	0.08	B.D.	0.09	B.D.	B.D.	B.D.	0.7	36.7	66.89
WS_FR1_UN_5	30.69	0.61	0.02	0.12	B.D.	0.03	B.D.	B.D.	0.01	0.82	39.81	72.12

WS_FR1_UN_6	27.08	0.54	0.02	0.11	B.D.	0.04	B.D.	B.D.	B.D.	0.73	35.34	63.86
WS_FR1_UN_8	27.72	0.45	0.04	0.09	B.D.	0.06	B.D.	B.D.	B.D.	0.46	34.95	63.77
WS_FR1_UN_9	26.77	0.46	0.04	0.1	B.D.	0.04	B.D.	B.D.	0.02	0.61	33.11	61.21
WS_FR1_UN_10	30.14	0.61	0.03	0.13	B.D.	B.D.	B.D.	0.03	0.02	0.65	37.27	68.91
WS_FR1_UN_11	26.92	0.43	0.03	0.13	B.D.	0.06	B.D.	0.04	0.01	0.47	32.41	60.49
WS_FR1_UN_12	26.55	0.49	0.03	0.13	B.D.	0.03	B.D.	B.D.	0.01	0.55	31.74	59.53
WS_FR1_UN_3_3	27.98	0.68	0.04	0.28	B.D.	0.04	B.D.	B.D.	0.01	0.42	32.99	62.43
WS_FR1_UN_4_4	30.37	0.61	0.03	0.2	B.D.	0.04	0.07	0.04	0.02	0.57	37.96	69.91
WS_FR1_UN_5_5	29.73	0.6	0.04	0.28	B.D.	0.04	B.D.	0.05	0.01	0.57	36.76	68.11
WS_FR1_UN_20	30.04	0.46	0.04	0.13	B.D.	B.D.	B.D.	0.04	B.D.	0.58	35.36	66.71
WS_FR1_UN_21	29.02	0.56	0.02	0.12	B.D.	0.04	B.D.	0.03	0.01	0.58	35.41	65.81
WSF3D1M2_UN_1_	24.68	0.47	0.12	0.3	0.45	1.67	3.17	B.D.	0.01	0.53	30.39	61.79
WSF3D1M2_UN_2	30.41	0.45	0.1	0.05	0.04	0.07	B.D.	0.06	0.01	0.66	38.34	70.22
WSF3D1M2_UN_3	27.99	0.48	0.12	0.01	0.01	0.04	B.D.	B.D.	0.01	0.58	35.33	64.57
WSF3D1M2_UN_4	25.75	0.4	0.06	0.01	B.D.	0.05	B.D.	0.03	B.D.	0.64	31.88	58.82
WSF3D1M2_UN_5	25.72	0.42	0.05	0.02	B.D.	0.07	B.D.	0.03	0.02	0.58	32.33	59.25
WSF3D1M2_UN_6	26.87	0.44	0.09	0.01	0.02	0	B.D.	B.D.	0.01	0.63	32.05	60.15
WSF3D1M2_UN_7	20.65	0.25	0.1	B.D.	B.D.	0.1	B.D.	0.03	B.D.	0.2	25.08	46.41
WSF3D1M2_UN_8	23.29	0.28	0.11	0.01	B.D.	0.09	B.D.	B.D.	0.02	0.28	28.38	52.47

WSF3D1M2_UN_10	27.84	0.39	0.08	B.D.	0.01	B.D.	0.06	B.D.	B.D.	0.51	32.95	61.86
WSF3D1M2_UN_11	33.09	0.81	0.05	0.03	B.D.	0.04	0.12	0.03	B.D.	0.56	44.95	79.68
WSF3D1M2_UN_12	27.8	0.44	0.04	0.01	0.01	0.07	0.05	B.D.	0.02	0.69	34.03	63.16
SW_FRESH1_BU_2	26.69	1.91	0.29	1.96	0.04	0.05	0.09	B.D.	B.D.	0.82	27.48	59.33
SW_FRESH1_BU_4	34.35	1.25	0.71	0.45	0.01	0.03	0.08	0.06	0.01	0.69	41.77	79.41
SW_FRESH1_BU_5	31.86	0.81	0.7	0.34	0.02	0.03	0.04	0.04	0.01	0.54	40.13	74.52
SW_FRESH1_BU_6	32.07	0.97	0.67	0.26	B.D.	0.07	0.07	B.D.	B.D.	0.57	39.58	74.26
SW_FRESH1_BU_7	39.68	0.25	0.09	0.04	0.02	0.06	0.05	B.D.	0.02	0.92	53.08	94.2
SW_FRESH1_BU_8	39.74	0.22	0.07	0.06	0.06	B.D.	0.1	B.D.	B.D.	0.78	53.81	94.84
SW_FRESH1_BU_9	41.19	0.24	0.1	0.11	B.D.	0.05	0.04	0.04	B.D.	0.86	53.36	96.01
SW_FRESH1_BU_12	34.38	1.15	0.46	0.4	B.D.	B.D.	0.04	0.04	B.D.	0.56	42.63	79.67
SW_FRESH1_BU_3_3	32.75	0.54	0.82	0.41	0.02	B.D.	B.D.	B.D.	0.01	0.77	40.49	75.85
SW_FRESH1_BU_5_5	33.97	0.53	0.9	0.39	B.D.	0.05	0.08	0.07	0.01	0.67	40.74	77.4
SW_FRESH1_BU_6_6	32.89	0.44	0.79	0.28	B.D.	B.D.	0.04	0.05	0.01	0.67	42.54	77.72
SW_FRESH1_BU_7_7	25.33	0.36	0.87	0.22	0.01	0.05	B.D.	B.D.	B.D.	0.38	30.4	57.63
SW_FRESH1_BU_8_8	33.33	0.69	0.77	0.41	0.01	B.D.	0.05	B.D.	0.02	0.82	39.86	75.97

SW_FRESH1_BU_9_9	20.97	0.46	0.83	0.21	0.01	B.D.	0.05	B.D.	B.D.	0.5	27.8	50.84
SW_FRESH1_BU_20	37.83	0.41	0.08	0.1	0.01	0.05	B.D.	B.D.	0.01	0.83	52.79	92.1
SW_FRESH1_BU_21	39.76	0.34	0.08	0.03	0.03	B.D.	0.05	B.D.	B.D.	0.77	54.54	95.59
WSF2D2W5_BU_1_	28.87	0.44	0.49	0.07	0.01	B.D.	0.06	0.11	B.D.	0.54	36.38	67
WSF2D2W5_BU_2	28.1	0.44	0.53	0.07	B.D.	0.05	B.D.	0.05	0.01	0.57	33.83	63.69
WSF2D2W5_BU_3	29.98	0.51	0.49	0.09	0.03	0.05	B.D.	B.D.	0.02	0.63	35.35	67.17
WSF2D2W5_BU_4	25.73	0.29	0.48	0.04	B.D.	B.D.	B.D.	B.D.	0.01	0.14	33.48	60.23
WSF2D2W5_BU_5	30.37	0.27	0.34	0.02	0.01	0.05	B.D.	B.D.	0.01	0.12	39.02	70.24
WSF2D2W5_BU_6	32.66	0.23	0.28	0.02	B.D.	0.04	0.04	0.03	B.D.	0.09	41.56	74.96
WSF2D2W5_BU_7	31.29	0.6	0.37	0.14	0.02	0.04	B.D.	B.D.	0.02	0.45	39.05	72.03
WSF2D2W5_BU_8	32.19	0.48	0.34	0.12	B.D.	0.04	0.04	B.D.	B.D.	0.48	40.55	74.24
WSF2D2W5_BU_9	30.69	0.4	0.38	0.12	0.02	0.05	0.05	B.D.	B.D.	0.58	38.33	70.61
WSF2D2W5_BU_10	32.47	0.39	0.29	0.07	B.D.	0.07	0.07	B.D.	B.D.	0.18	39.17	72.71
WSF2D2W5_BU_11	33.4	0.29	0.22	0.04	B.D.	0.06	0.04	B.D.	B.D.	0.2	43.21	77.49
WSF3D1M1_UN_4	25.14	0.34	0.05	0.05	0.02	0.17	0.11	0.05	B.D.	0.45	30.29	56.67
WSF3D1M1_UN_5	31.51	0.57	0.05	0.04	B.D.	0.03	0.04	B.D.	B.D.	0.85	38.5	71.62
WSF3D1M1_UN_6	27.49	0.44	0.09	0.05	B.D.	0.07	0.05	B.D.	B.D.	0.64	32.39	61.23
WSF3D1M1_UN_7	30.96	0.67	0.02	0.06	B.D.	0.04	0.4	B.D.	0.02	0.74	35.11	68.01

WSF3D1M1_UN_8	25.62	0.49	0.09	0.06	0.03	0.14	0.37	B.D.	B.D.	0.61	28.54	55.96
WSF3D1M1_UN_9	30.67	0.07	0.07	0.05	B.D.	0.04	0.32	0.03	B.D.	0.15	37.14	68.54
WSF3D1M1_UN_10	28.98	0.46	0.1	0.05	B.D.	0.08	0.04	B.D.	B.D.	0.82	35.69	66.24
WSF3D1M1_UN_11	28.83	0.38	0.06	0.04	B.D.	0.06	0.05	0.04	B.D.	0.71	35.05	65.23
WSF3D3M1_UN_1_	27.82	0.41	0.03	0.01	B.D.	B.D.	B.D.	0.12	B.D.	0.38	34.42	63.21
WSF3D3M1_UN_2	26.43	0.46	0.06	0.03	B.D.	B.D.	0.05	0.13	B.D.	0.37	34.03	61.58
WSF3D3M1_UN_4	27.99	0.38	0.05	0.06	B.D.	0.07	B.D.	0.09	B.D.	0.74	32.34	61.75
WSF3D3M1_UN_5	26.42	0.43	0.04	0.01	B.D.	B.D.	B.D.	0.09	B.D.	0.68	33.77	61.46
WSF3D3M1_UN_6	29.32	0.51	0.07	0.04	B.D.	0.03	B.D.	0.04	B.D.	0.82	35.81	66.64
WSF3D3M1_UN_7	30.52	0.48	0.08	0.11	B.D.	B.D.	B.D.	0.11	B.D.	0.73	36.5	68.55
WSF3D3M1_UN_8	26.2	0.43	0.09	0.07	0.01	0.05	0.05	0.15	B.D.	0.52	31.69	59.27
WSF3D3M1_UN_10	28.31	0.36	0.06	0.02	B.D.	0.09	0.05	0.09	0.02	0.72	33.08	62.81
WSF3D3M1_UN_11	28.12	0.39	0.05	0.03	B.D.	0.07	B.D.	0.12	B.D.	0.71	33.98	63.49
WSF3D3M1_UN_12	28.61	0.42	0.05	0.02	B.D.	B.D.	B.D.	0.09	B.D.	0.69	31.96	61.86
WSF2D2W5_UN_1_	11.03	0.2	0.1	0.07	0.14	0.61	0.82	B.D.	0.01	0.23	14.52	27.73
WSF2D2W5_UN_4	27.29	0.48	0.05	0.05	B.D.	0.04	B.D.	0.07	B.D.	0.83	34.41	63.24
WSF2D2W5_UN_5	29.16	0.52	0.04	0.05	B.D.	B.D.	B.D.	0.04	B.D.	1	36.95	67.8
WSF2D2W5_UN_6	28.5	0.46	0.05	0.04	0.02	B.D.	B.D.	B.D.	0.01	0.88	35.43	65.45
WSF2D2W5_UN_7	27.82	0.57	0.15	0.07	B.D.	0.05	B.D.	B.D.	B.D.	0.68	36.53	65.9

WSF2D2W5_UN_8	24.52	0.26	0.09	0.02	B.D.	0.06	0.15	B.D.	B.D.	0.31	30.81	56.25
WSF2D2W5_UN_9	28.64	0.57	0.07	0.07	B.D.	0.07	0.06	0.07	B.D.	0.61	36.99	67.15
WSF2D2W5_UN_10	27.9	0.46	0.04	0.05	B.D.	B.D.	B.D.	0.03	B.D.	0.77	37.28	66.57
WSF2D2W5_UN_11	28.84	0.55	0.04	0.09	0.01	0	B.D.	0	0.01	0.75	35.69	65.99
WSF2D2W5_UN_1_1	23.04	0.37	0.27	0.03	0.09	0.06	0.06	0.04	0.01	0.52	28.53	53.02
WSF2D2W5_UN_3_3	29.43	0.42	0.06	0.05	B.D.	0.08	B.D.	B.D.	B.D.	0.79	36.72	67.55
WSF2D2W5_UN_4_4	27.46	0.42	0.07	0.04	B.D.	0.05	0.04	0.03	B.D.	0.81	35.36	64.27
WSF2D2W5_UN_5_5	26.93	0.53	0.06	0.04	B.D.	0.05	B.D.	0.04	B.D.	0.79	34.79	63.26
WSF2D2W5_UN_6_6	30.55	0.62	0.06	0.06	B.D.	0.04	0.04	0.05	B.D.	0.72	37.83	69.97
WSF2D2W5_UN_7_7	29.9	0.67	0.04	0.09	B.D.	B.D.	0.06	B.D.	B.D.	0.75	37.66	69.17
WSF2D2W5_UN_8_8	29.15	0.44	0.08	0.02	B.D.	0.05	0.15	B.D.	0.02	0.51	37.29	67.7
WSF2D2W5_UN_9_9	22.81	0.3	0.28	0.04	B.D.	0.06	0	B.D.	0.01	0.63	28.68	52.8
WSF2D2W5_UN_10_10	25.93	0.44	0.25	0.03	B.D.	0.07	0.06	0.03	0.01	0.51	33.7	61.03
SWF5D1Y1_UN_5	31.7	0.47	0.05	0.02	B.D.	0.05	B.D.	B.D.	B.D.	0.89	38.91	72.14
SWF5D1Y1_UN_6	30.5	0.49	0.04	0.01	B.D.	0.03	B.D.	0.05	B.D.	0.82	39.02	70.94
SWF5D1Y1_UN_7	30.97	0.56	0.04	0.02	0.01	0.06	B.D.	B.D.	0.02	0.87	38.09	70.66
SWF5D1Y1_UN_8	27.16	0.48	0.05	0.01	B.D.	0	B.D.	B.D.	B.D.	0.61	34.75	63.08
SWF5D1Y1_UN_9	26.91	0.43	0.06	0.03	0.02	0.05	B.D.	0.03	B.D.	0.59	34.85	62.96

SWF5D1Y1_UN_9_9	28.16	0.57	0.06	0.03	0.01	0.05	B.D.	B.D.	B.D.	0.68	33.63	63.19
SWF5D1Y1_UN_10	28.68	0.42	0.04	0.01	B.D.	0.04	B.D.	0.04	0.02	0.75	35.26	65.25
SWF5D1Y1_UN_12	31	0.63	0.03	0.04	B.D.	0.07	B.D.	B.D.	0.01	0.76	39.07	71.62
SWF5D1Y2_UN_2	31.1	0.46	0.04	0.01	B.D.	0.06	B.D.	B.D.	B.D.	0.91	39.3	71.88
SWF5D1Y2_UN_3	27.72	0.39	0.04	0.01	0.03	0.08	B.D.	0.05	0.02	0.49	37.56	66.42
SWF5D1Y2_UN_4	30.54	0.44	0.03	0.02	B.D.	0.04	B.D.	B.D.	B.D.	0.61	39.11	70.78
SWF5D1Y2_UN_6	28.26	0.56	0.04	0.04	0.02	B.D.	B.D.	B.D.	0.01	0.69	35.42	65.08
SWF5D1Y2_UN_7	29.67	0.45	0.06	0.03	B.D.	0.03	B.D.	0.11	0.01	0.69	37.32	68.37
SWF5D1Y2_UN_8	23.75	0.4	0.08	0	B.D.	0.07	B.D.	B.D.	B.D.	0.61	28.31	53.25
SWF5D1Y2_UN_9	28.58	0.46	0.07	0.01	B.D.	0.05	B.D.	B.D.	B.D.	0.81	34.78	64.8
SWF5D1Y2_UN_11	28.66	0.54	0.02	0.03	B.D.	0.1	0.05	0.05	0.02	0.76	37.33	67.56
WSF3D1M2_BU_1_	29.2	0.4	0.5	0.18	0.36	0.08	0.14	B.D.	0.01	0.62	37.23	68.72
WSF3D1M2_BU_2	31.1	0.45	0.47	0.2	0.41	0.05	0.04	B.D.	0.02	0.74	40.11	73.59
WSF3D1M2_BU_3	30.77	0.3	0.23	0.09	B.D.	0.05	0.07	0.03	0	0.58	40.04	72.16
WSF3D1M2_BU_4	33.39	0.65	0.21	0.14	B.D.	0	B.D.	0.03	0.01	0.79	40.74	75.99
WSF3D1M2_BU_5	32.18	0.41	0.24	0.06	B.D.	B.D.	0.1	B.D.	B.D.	0.48	40.86	74.33
WSF3D1M2_BU_6	31.88	0.69	0.26	0.1	0.01	B.D.	0.11	B.D.	B.D.	0.64	38.58	72.29
WSF3D1M2_BU_7	28.85	0.4	0.29	0.08	B.D.	B.D.	0.14	B.D.	0.02	0.44	36.16	66.37
WSF3D1M2_BU_8	28.14	0.88	0.57	0.45	B.D.	B.D.	0.08	0.03	0.01	0.76	33.35	64.28

WSF3D1M2_BU_9	29.58	0.98	0.58	0.46	B.D.	0.06	B.D.	B.D.	B.D.	0.76	34.95	67.42
WSF3D1M2_BU_10	28.74	0.91	0.61	0.44	B.D.	B.D.	B.D.	B.D.	B.D.	0.89	33.77	65.4
WSF3D1M2_BU_12	31.4	0.53	0.27	0.09	B.D.	B.D.	0.06	B.D.	B.D.	0.63	40.07	73.06
WSF3D1M1_UN_4	28.73	0.52	0.09	0.07	B.D.	0.04	0	0.04	B.D.	0.8	35.41	65.71
WSF3D1M1_UN_5	28.28	0.54	0.09	0.07	B.D.	B.D.	B.D.	B.D.	B.D.	0.77	35.36	65.15
WSF3D1M1_UN_6	29.39	0.48	0.11	0.08	B.D.	0.05	B.D.	B.D.	0.01	0.74	36.08	66.95
WSF3D1M1_UN_7	26.74	0.57	0.1	0.06	B.D.	0.07	B.D.	0.03	B.D.	0.77	35.47	63.83
WSF3D1M1_UN_8	28.16	0.53	0.08	0.06	B.D.	B.D.	0	B.D.	B.D.	0.79	34.76	64.43
WSF3D1M1_UN_9	28.37	0.65	0.12	0.1	B.D.	B.D.	0.04	0.04	B.D.	0.77	34.16	64.26
WSF3D1M1_UN_10	28.97	0.52	0.12	0.04	B.D.	B.D.	B.D.	0.03	B.D.	0.83	37.54	68.06
WSF3D1M1_UN_11	24.75	0.55	0.11	0.08	B.D.	B.D.	B.D.	B.D.	B.D.	0.83	35.56	61.89
WSF3D1M1_UN_12	28.07	0.53	0.11	0.07	0.01	0.04	B.D.	B.D.	0.01	0.76	36.69	66.32
WSF3D1M4_BU_1_	33.01	0.43	0.45	0.35	0.07	B.D.	0.22	B.D.	B.D.	0.71	42.46	77.72
WSF3D1M4_BU_2	31.92	0.36	0.46	0.3	0.05	0.05	0.21	0.03	0.01	0.57	41.41	75.37
WSF3D1M4_BU_3	31.07	0.45	0.43	0.31	0.02	0.03	0.17	0.03	B.D.	0.59	41.08	74.17
WSF3D1M4_BU_4	31.05	0.48	0.46	0.13	B.D.	B.D.	0.07	B.D.	B.D.	0.48	37.97	70.68
WSF3D1M4_BU_5	30.12	0.39	0.43	0.11	B.D.	0.03	0.09	B.D.	B.D.	0.55	39.23	70.95
WSF3D1M4_BU_6	30.05	0.29	0.43	0.07	0.01	0.03	0.07	B.D.	B.D.	0.38	38.98	70.31
WSF3D1M4_BU_7	28.3	0.5	0.52	0.16	B.D.	B.D.	0.07	B.D.	0.01	0.57	34.86	64.99

WSF3D1M4_BU_8	28.07	0.75	0.53	0.18	B.D.	0.03	0.11	0.05	B.D.	0.57	36.53	66.82
WSF3D1M4_BU_9	28.68	0.38	0.48	0.12	0.04	0.04	B.D.	0.05	0.02	0.56	37.56	67.97
WSF3D1M4_BU_12	30.74	0.55	0.42	0.15	B.D.	0.07	0.13	0.05	0.01	0.5	39.15	71.77
WSF3D1M4_BU_11_11	28.82	0.64	0.44	0.15	B.D.	B.D.	0.12	B.D.	0.01	0.51	37.51	68.22
WSF3D1M4_BU_12_12	30.1	0.68	0.42	0.15	0.01	B.D.	0.06	B.D.	B.D.	0.46	38.08	69.99
SWF2FR3_BU_1_	29.52	0.8	0.67	1.02	B.D.	B.D.	0.18	0.04	B.D.	0.94	31.51	64.67
SWF2FR3_BU_2	27.27	0.65	0.71	0.69	0.01	B.D.	0.12	B.D.	B.D.	0.79	31.7	61.96
SWF2FR3_BU_3	29.57	0.73	0.67	0.74	0.01	0.05	0.14	B.D.	B.D.	0.88	32.33	65.14
SWF2FR3_BU_4	27.32	0.58	0.57	0.2	0.02	0.03	0.05	0.03	B.D.	0.72	34.76	64.27
SWF2FR3_BU_5	29.99	0.5	0.42	0.14	B.D.	B.D.	0.11	B.D.	B.D.	0.74	37.15	69.04
SWF2FR3_BU_6	30.65	0.55	0.4	0.15	0.01	B.D.	0.07	B.D.	B.D.	0.67	38.8	71.32
SWF2FR3_BU_7	32.66	0.57	0.39	0.31	0.01	B.D.	0.12	B.D.	B.D.	0.59	40.06	74.75
SWF2FR3_BU_8	31.79	0.48	0.35	0.27	0.01	B.D.	0.11	0.08	B.D.	0.53	39.91	73.56
SWF2FR3_BU_9	34.07	0.44	0.36	0.11	B.D.	B.D.	0.16	B.D.	B.D.	0.43	41.83	77.41
SWF2FR3_BU_10	34.15	0.34	0.24	0.05	B.D.	B.D.	0.16	B.D.	0.02	0.38	43.3	78.65
SWF2FR3_BU_11	30.37	1.85	0.38	0.24	B.D.	0.05	0.13	B.D.	B.D.	0.64	36.98	70.67
SWF2FR3_BU_12	33.18	0.93	0.29	0.15	B.D.	B.D.	0.11	0	0.01	0.41	41.08	76.18
WSF3D3M2_UN_1_	24.35	0.3	0.08	0.05	0.12	0.13	0.17	0.07	0.01	0.39	30.47	56.15

WSF3D3M2_UN_2	29.45	0.4	0.08	0.05	B.D.	0.04	B.D.	0.09	0.01	0.53	35.05	65.73
WSF3D3M2_UN_3	22.47	0.29	0.1	0.07	0.11	0.21	0.27	0.09	0.02	0.43	28.5	52.57
WSF3D3M2_UN_4	26.31	0.52	0.03	0.04	B.D.	0.03	0.05	0.04	B.D.	0.82	32.15	59.99
WSF3D3M2_UN_5	28.7	0.53	0.03	0.04	B.D.	0.04	B.D.	0.07	0.01	0.8	33.79	64.02
WSF3D3M2_UN_6	27.22	0.51	0.04	0.04	B.D.	B.D.	B.D.	0.13	0.01	0.73	34	62.71
WSF2D2W2_BU_1_	26.42	0.31	0.56	0.07	0.13	0.04	0.07	B.D.	B.D.	0.69	34.13	62.43
WSF2D2W2_BU_3	26.91	0.49	0.46	0.07	0.08	0.05	B.D.	B.D.	0.01	0.68	33.12	61.89
WSF2D2W2_BU_4	30.51	0.3	0.33	0.06	B.D.	0.05	0.07	0.04	B.D.	0.4	39.8	71.56
WSF2D2W2_BU_5	31.38	0.38	0.36	0.05	0.02	B.D.	B.D.	0.05	0.01	0.45	39.45	72.15
WSF2D2W2_BU_6	29.39	0.44	0.43	0.06	B.D.	0.03	B.D.	B.D.	0.01	0.5	37.07	67.96
WSF2D2W2_BU_7	30.35	0.48	0.5	0.29	B.D.	0.03	B.D.	0.06	0.01	0.82	37.6	70.15
WSF2D2W2_BU_9	25.39	0.51	0.63	0.28	0.04	0.03	0.04	B.D.	0.03	0.8	31.33	59.08
WSF2D2W2_BU_10	29.88	0.44	0.45	0.17	B.D.	B.D.	B.D.	B.D.	0.01	0.73	37.6	69.33
WSF2D2W2_BU_11	29.45	0.4	0.48	0.27	B.D.	B.D.	B.D.	B.D.	0.03	0.69	36.39	67.74
WSF2D2W2_BU_12	29.58	0.38	0.35	0.05	B.D.	0.05	B.D.	B.D.	B.D.	0.4	38.38	69.2
WSF2D2W1_UN_1_	23.18	0.4	0.07	0.11	0.04	0.09	0.08	B.D.	0.01	0.61	28.6	53.21
WSF2D2W1_UN_3	15.88	0.3	0.08	0.08	0.12	0.12	1.71	B.D.	0.01	0.3	18.72	37.34
WSF2D2W1_UN_4	27.89	0.63	0.05	0.1	B.D.	0.05	0.05	B.D.	0.03	0.8	35.47	65.07
WSF2D2W1_UN_5	29.98	0.48	0.08	0.12	B.D.	0.03	B.D.	0.04	B.D.	0.83	36.18	67.74

WSF2D2W1_UN_6	27.63	0.62	0.05	0.09	B.D.	B.D.	0.05	0.06	0.03	0.81	34.77	64.1
WSF2D2W1_UN_7	26.24	0.51	0.09	0.07	B.D.	0.06	B.D.	B.D.	0.01	0.75	34.02	61.76
WSF2D2W1_UN_8	26.16	0.53	0.1	0.09	B.D.	0.06	B.D.	B.D.	B.D.	0.8	32.94	60.7
WSF2D2W1_UN_9	29.79	0.52	0.1	0.07	0.01	0.05	B.D.	B.D.	B.D.	0.88	37.37	68.78
WSF2D2W1_UN_10	24.25	0.38	0.13	0.04	B.D.	0.06	0.07	0.03	B.D.	0.56	32.17	57.7
WSF2D2W1_UN_11	28.57	0.42	0.09	0.06	B.D.	B.D.	B.D.	0.04	B.D.	0.81	36.33	66.34
WSF2D2W1_UN_12	28.34	0.49	0.11	0.06	B.D.	0.04	B.D.	B.D.	0.01	0.79	36.34	66.21
WSF3D3M2_BU_1_	33.65	0.38	0.32	0.11	B.D.	0.05	B.D.	0.14	B.D.	0.31	44.28	79.26
WSF3D3M2_BU_2	26.9	0.37	0.22	0.08	B.D.	0.06	0.06	0.05	B.D.	0.29	36	64.03
WSF3D3M2_BU_3	36.03	0.4	0.27	0.1	0.02	0.09	B.D.	0.15	B.D.	0.36	47.55	84.97
WSF3D3M2_BU_7	32.42	0.08	0.28	0.03	0.01	0	B.D.	0.19	B.D.	0.28	42.15	75.46
WSF3D3M2_BU_8	33.35	0.2	0.22	0.05	0.03	0.06	0.07	0.14	B.D.	0.36	44.52	79
WSF3D3M2_BU_9	32.13	0.65	0.3	0.05	0.03	0.08	B.D.	0.14	0.01	0.5	41.26	75.18
WSF3D3M2_BU_10	32.67	0.72	0.32	0.06	0.02	0.11	B.D.	0.13	0.02	0.57	41.32	75.95
WSF3D3M2_BU_11	33.13	0.64	0.24	0.06	0.01	0.19	0.14	0.14	0.02	0.63	44.14	79.36
WSF3D3M2_BU_12	30.58	0.45	0.35	0.05	B.D.	0.07	B.D.	0.09	B.D.	0.45	39.55	71.61
WSF3D3M2_BU_4	32.65	0.66	0.23	0.08	0.01	0.06	0.05	0.17	0.02	0.59	43.36	77.86
WSF3D3M2_BU_6	25.16	0.59	0.16	0.04	B.D.	0	0.05	0.15	B.D.	0.54	32.35	59.04
WSF5D6M4_UN_4	27.66	0.46	0.12	0.03	B.D.	0	0.05	B.D.	B.D.	0.82	35.13	64.29

WSF5D6M4_UN_5	27.3	0.45	0.1	0.03	B.D.	0.03	0.04	B.D.	0.02	0.93	35.69	64.59
WSF5D6M4_UN_6	27.21	0.59	0.08	0.05	B.D.	B.D.	B.D.	B.D.	0.02	0.75	35.28	64.02
WSF5D6M4_UN_10	23.94	0.28	0.04	0.04	B.D.	0.05	B.D.	B.D.	0.01	0.51	29.44	54.35
WSF5D6M1_UN_1_	28.28	0.49	0.04	0.06	B.D.	0.05	B.D.	0.06	0.01	0.61	34.2	63.81
WSF5D6M1_UN_5	29.65	0.57	0.08	0.04	B.D.	0.05	0.06	B.D.	B.D.	0.85	38.05	69.35
WSF5D6M1_UN_6	30.21	0.58	0.09	0.04	B.D.	B.D.	B.D.	B.D.	B.D.	0.87	39.3	71.14
WSF5D6M1_UN_7	30.39	0.58	0.07	0.03	0.02	0.03	B.D.	B.D.	0.02	0.82	39.03	71.03
WSF5D6M1_UN_11	26.56	0.42	0.06	0.04	B.D.	0.08	B.D.	0.06	B.D.	0.83	35.39	63.46
WSF5D6M3_UN_1_	21.98	0.37	0.05	0.03	B.D.	0.12	0.04	B.D.	B.D.	0.51	32.32	55.43
WSF5D6M3_UN_2	28.53	0.41	0.09	0.03	0.04	0.07	0.18	0.04	0.02	0.85	36.2	66.45
WSF5D6M3_UN_3	28.43	0.44	0.07	0.05	0.01	0.06	0.08	B.D.	0.02	0.89	37.64	67.69
WSF5D6M3_UN_4	26.5	0.47	0.08	0.03	B.D.	0.05	0	B.D.	B.D.	0.8	35.72	63.67
WSF5D6M3_UN_5	27.31	0.6	0.05	0.02	B.D.	0.08	0.05	0.03	B.D.	0.7	37.85	66.68
WSF5D6M3_UN_6	28.31	0.52	0.06	0.03	B.D.	0.05	B.D.	B.D.	0.01	0.71	36.5	66.23
WSF5D6M3_UN_8	26.85	0.47	0.07	0.06	B.D.	0.05	0.13	0.04	0.01	0.54	34.17	62.4
WSF5D6M3_UN_9	26.81	0.46	0.08	0.06	B.D.	0.09	0.08	B.D.	B.D.	0.57	31.94	60.12
WSF5D6M3_UN_12	27.95	0.6	0.01	0.1	B.D.	0.03	0.07	0.06	B.D.	0.7	34.32	63.83
SWFR2_BU_1_	34.25	0.64	0.87	0.45	B.D.	0.09	0.17	B.D.	B.D.	0.74	38.74	75.95
SWFR2_BU_2	35.01	2.32	0.64	0.84	0.01	0.05	0.2	B.D.	B.D.	0.99	36	76.06

SWFR2_BU_3	32.6	0.68	0.68	0.28	B.D.	B.D.	0.18	B.D.	0.01	0.73	38.42	73.58
SWFR2_BU_4	34.46	0.56	0.4	0.19	B.D.	B.D.	0.32	0.03	B.D.	0.6	43.03	79.6
SWFR2_BU_5	33.22	0.53	0.42	0.2	B.D.	B.D.	0.33	B.D.	0.01	0.46	42	77.18
SWFR2_BU_6	34.13	0.44	0.4	0.16	0.01	0.03	0.35	B.D.	0.01	0.47	42.07	78.09
SWFR2_BU_7	39.28	0.9	0.16	0.14	B.D.	0.03	0.1	B.D.	B.D.	0.43	52.23	93.28
SWFR2_BU_8	30.4	0.46	0.17	0.18	0.05	0.42	0.13	0.05	0.01	5.36	43.04	80.26
SWFR2_BU_9	39.92	0.55	0.14	0.09	0.01	0.06	0.09	0.05	B.D.	0.27	52.67	93.86
SWFR2_BU_10	37.08	0.5	0.19	0.11	B.D.	0.05	0.08	B.D.	0.02	2	49.15	89.19
SWFR2_BU_11	29.79	0.45	0.17	0.19	0.01	1.21	0.17	B.D.	B.D.	1.91	43.17	77.08
SWFR2_BU_12	38.88	2.26	0.17	0.76	0.01	0.03	0.23	B.D.	B.D.	0.6	49.49	92.43
WSF2D2W1_BU_1_	29.93	0.41	0.35	0.06	B.D.	0.04	0.06	0.07	0.01	0.23	39.17	70.32
WSF2D2W1_BU_2	30.78	0.39	0.39	0.07	B.D.	B.D.	0.09	B.D.	B.D.	0.36	39.23	71.33
WSF2D2W1_BU_3	33.3	0.54	0.31	0.07	B.D.	0.1	0.1	B.D.	B.D.	0.34	41.43	76.2
WSF2D2W1_BU_4	39.17	0.92	0.11	0.09	B.D.	0.04	0.06	0.05	B.D.	0.34	50.26	91.04
WSF2D2W1_BU_5	39.2	0.61	0.13	0.07	B.D.	B.D.	0.07	B.D.	B.D.	0.37	50.06	90.51
WSF2D2W1_BU_6	38.87	0.8	0.13	0.1	0.01	0.03	B.D.	0.05	B.D.	0.41	49.65	90.04
WSF2D2W1_BU_7	40.74	0.86	0.09	0.18	B.D.	0.05	0.04	0.1	B.D.	0.83	51.63	94.51
WSF2D2W1_BU_8	40.27	0.81	0.09	0.18	0.02	0.04	0	0.06	B.D.	1.12	51.49	94.08
WSF2D2W1_BU_9	39.28	0.81	0.1	0.17	0.01	0.06	0.07	0.06	B.D.	0.91	51.41	92.89

WSF2D2W1_BU_10	38.54	0.99	0.19	0.28	0.02	B.D.	0.04	0.06	B.D.	1.6	49.63	91.35
WSF2D2W1_BU_11	38.25	1.09	0.16	0.29	B.D.	B.D.	B.D.	0.07	0.01	1.45	48	89.33
WSF2D2W1_BU_12	35.27	0.81	0.15	0.25	0.04	1.07	0.52	0.03	B.D.	1.53	44.58	84.25
WSF2D2W1_BU_4_4	39.04	0.89	0.1	0.17	B.D.	0.03	B.D.	0.06	0.02	1.02	50.89	92.25
WSF2D2W1_BU_5_5	40.21	0.84	0.08	0.14	0.01	0.06	0.05	B.D.	B.D.	1.06	50.8	93.26
WSF2D2W1_BU_6_6	40.43	0.85	0.06	0.14	0.02	0.08	B.D.	0.06	0.03	1.09	50.76	93.55
SWFR1_BU_1_	32.79	0.64	0.95	0.32	B.D.	0.04	0.07	B.D.	0.01	0.65	37.2	72.67
SWFR1_BU_2	28	0.58	0.99	0.28	B.D.	0.04	0.08	B.D.	0.02	0.6	32.27	62.87
SWFR1_BU_3	32.92	0.61	0.98	0.32	B.D.	0.06	B.D.	B.D.	B.D.	0.74	37.75	73.41
SWFR1_BU_4	31.43	0.17	0.48	0.1	B.D.	B.D.	0.08	B.D.	B.D.	0.57	39.76	72.6
SWFR1_BU_7	30.75	0.85	1.68	0.37	B.D.	0	B.D.	B.D.	B.D.	0.8	38.45	72.92
SWFR1_BU_8	35.88	0.7	1.45	0.27	0.01	0.03	0.09	B.D.	B.D.	0.8	45.76	85.01
SWFR1_BU_7	32.06	0.2	0.47	0.09	B.D.	0.04	0.06	0.05	B.D.	0.57	41.94	75.48
SWFR1_BU_8	27.65	0.76	1.07	0.24	B.D.	0	B.D.	B.D.	0.02	0.68	35.18	65.61
SWFR1_BU_9	28.23	0.79	1.11	0.26	B.D.	B.D.	B.D.	B.D.	0.01	0.73	35.71	66.89
SWFR1_BU_11	23.42	0.48	0.79	0.16	B.D.	B.D.	B.D.	0.03	0.02	0.49	30.87	56.29
SWF5D1Y1_BU_1_	32.88	0.41	0.66	0.16	0.02	0.07	B.D.	B.D.	B.D.	1.04	41.01	76.26
SWF5D1Y1_BU_2	32.93	0.29	0.72	0.1	B.D.	0.04	B.D.	0.05	0.01	0.76	40.4	75.3
SWF5D1Y1_BU_3	32.9	0.23	0.65	0.08	0.02	0.04	B.D.	B.D.	B.D.	0.53	41.91	76.37

SWF5D1Y1_BU_4	33.31	0.35	0.59	0.01	B.D.	0.04	B.D.	0.04	B.D.	0.59	42.23	77.14
SWF5D1Y1_BU_5	32.6	0.35	0.61	0.01	B.D.	B.D.	B.D.	0.07	0.01	0.54	41.5	75.69
SWF5D1Y1_BU_6	30.52	0.33	0.69	B.D.	0.01	0.07	B.D.	0.06	B.D.	0.44	39.51	71.64
SWF5D1Y1_BU_7	33.21	0.37	0.7	0.02	B.D.	0.09	B.D.	B.D.	B.D.	0.52	40.16	75.08
SWF5D1Y1_BU_8	31.97	0.46	0.74	0.04	0.02	B.D.	B.D.	B.D.	B.D.	0.44	40.75	74.41
SWF5D1Y1_BU_9	29.98	0.36	0.84	0.05	0.01	0.06	B.D.	0.07	B.D.	0.4	36.66	68.43
SWF5D1Y1_BU_10	31.84	0.37	0.63	0.01	B.D.	0.05	0.05	0.09	B.D.	0.78	40.62	74.44
SWF5D1Y1_BU_11	33.45	0.39	0.58	0.02	0.01	0.03	0.08	B.D.	0.02	0.97	41.49	77.03
SWF5D1Y1_BU_12	31.49	0.32	0.49	B.D.81	B.D.	0.17	B.D.	B.D.	0.03	0.82	40.5	73.83
SWF5D1Y1_BU_1_1	31.34	0.5	0.74	0.16	0	B.D.	0.07	0.04	B.D.	0.5	41.41	74.77
SWF5D1Y1_BU_2_2	29.84	0.39	0.82	0.16	0.02	B.D.	0.06	0.08	B.D.	0.55	39.93	71.86
SWF5D1Y1_BU_3_3	32.64	0.37	0.71	0.26	0.02	0.05	0.07	0.04	B.D.	0.68	42.38	77.22
SWF5D1Y1_BU_4_4	32.35	0.44	0.55	0.01	0.02	0.08	0.04	B.D.	B.D.	0.75	42.73	76.98
SWF5D1Y1_BU_5_5	32.39	0.34	0.61	B.D.	B.D.	0.05	0.07	0.04	B.D.	0.8	42.19	76.49
SWF5D1Y1_BU_6_6	32.05	0.49	0.62	0.02	B.D.	B.D.	B.D.	B.D.	0.02	0.72	42	75.91
SWF5D1Y1_BU_7_7	29.39	0.29	0.86	0.02	0.01	B.D.	B.D.	B.D.	B.D.	0.4	36.72	67.7
SWF5D1Y1_BU_9_9	27.43	0.26	0.86	B.D.11	B.D.	0.06	0.04	0.03	B.D.	0.44	34.26	63.38
SWF5D1Y1_BU_10_10	26.17	0.17	0.99	B.D.82	B.D.	0.07	0.06	0.04	B.D.	0.55	33.23	61.27

SWF5D1Y1_BU_11_11	28.11	0.22	0.88	B.D.	B.D.	0.04	B.D.	B.D.	B.D.	0.71	35.87	65.84
SWF5D1Y1_BU_12_12	27.52	0.18	0.91	B.D.77	B.D.	0.06	B.D.	0.04	0.01	0.51	35.26	64.51
SWF5D1Y2_BU_1_	33.3	0.32	0.66	0.04	B.D.	0.05	0.04	0	B.D.	0.8	42.08	77.28
SWF5D1Y2_BU_2	33.37	0.41	0.66	0.03	B.D.	B.D.	B.D.	B.D.	0.01	0.9	42.13	77.52
SWF5D1Y2_BU_3	30.74	0.32	0.83	0.03	B.D.	0.06	B.D.	0	B.D.	0.7	39.14	71.81
SWF5D1Y2_BU_4	32.48	0.54	0.54	0.04	B.D.	0.06	B.D.	0.07	B.D.	0.82	41.53	76.08
SWF5D1Y2_BU_5	33.5	0.64	0.48	0.06	0.02	0.06	B.D.	0.08	B.D.	0.77	43.34	78.95
SWF5D1Y2_BU_6	32.71	0.51	0.58	0.05	0.02	0.08	0.07	0.04	0.02	0.78	41.77	76.63
SWF5D1Y2_BU_7	31.15	0.35	0.76	0.05	B.D.	B.D.	B.D.	B.D.	B.D.	0.64	38.66	71.61
SWF5D1Y2_BU_8	28.93	0.3	0.93	0.03	0.01	0.04	0.04	0.05	0.01	0.6	36.21	67.17
SWF5D1Y2_BU_9	30.81	0.44	0.8	0.04	B.D.	0.06	0.09	0.05	0.02	0.63	37.7	70.63
SWF5D1Y2_BU_10	27.56	0.22	0.95	0.02	0.01	B.D.	0.05	B.D.	B.D.	0.63	35.49	64.94
SWF5D1Y2_BU_11	30.89	0.34	0.86	0.04	B.D.	0	0.05	B.D.	B.D.	0.85	38.25	71.26
SWF5D1Y2_BU_12	31.49	0.32	0.89	0.02	B.D.	B.D.	B.D.	B.D.	B.D.	0.87	39.61	73.21
SWF5D1Y2_BU_1_1	33.65	0.43	0.65	0.05	0.02	0.04	0.05	0.06	B.D.	0.85	42.94	78.74
SWF5D1Y2_BU_2_2	32.67	0.33	0.72	0.06	B.D.	B.D.	0.05	0	B.D.	1	40.02	74.87
SWF5D1Y2_BU_3_3	33.88	0.39	0.65	0.05	B.D.	0.05	B.D.	B.D.	0.01	0.77	42.77	78.57
SWF5D1Y2_BU_4_4	30.3	0.48	0.83	0.02	B.D.	B.D.	0.06	B.D.	B.D.	0.7	39.15	71.54

SWF5D1Y2_BU_5_5	30.89	0.48	0.8	0.02	B.D.	0	B.D.	B.D.	B.D.	0.72	40.00	32.92
SWF5D1Y2_BU_6_6	31.83	0.45	0.75	0.03	B.D.	B.D.	B.D.	0.08	0.01	0.73	40.45	74.33
SWF5D1Y2_BU_7_7	32.14	0.34	0.71	0.03	B.D.	0.04	B.D.	0.04	0.01	0.54	39.49	73.34
SWF5D1Y2_BU_8_8	31.6	0.38	0.79	0.04	B.D.	0.07	B.D.	0	B.D.	0.55	38.3	71.73
SWF5D1Y2_BU_9_9	30.45	0.31	0.77	B.D.	B.D.	0.12	B.D.	B.D.	0.01	0.49	37.62	69.77
SWF5D1Y2_BU_10_10	32.79	0.32	0.69	0.02	B.D.	0.07	0.04	B.D.	B.D.	0.77	39.31	73.99
SWF5D1Y2_BU_11_11	27.14	0.26	0.88	0.02	B.D.	0.05	0.04	0.05	B.D.	0.94	33.72	63.1
SWF5D1Y2_BU_12_12	31.82	0.29	0.68	0.02	B.D.	0.06	B.D.	0	0.01	0.82	38.14	71.85
SWF5D1Y2_BU_12_12_12	32.12	0.39	0.7	0.03	B.D.	0.06	B.D.	0.05	B.D.	0.81	39.4	73.56
KILT1_BU_1_	1.48	0.1	0.9	1.95	8.48	15.01	34.47	B.D.	0.1	1.64	1.94	66.06
KILT1_BU_2	38.71	0.55	0.17	B.D.	0.03	0.19	0.05	0	0.01	B.D.	53.13	92.83
KILT1_BU_3	33.79	0.37	0.1	B.D.	0.07	0.13	0.66	B.D.	0.07	B.D.	48.78	83.98
KILT1_BU_4	39.68	0.48	0.08	B.D.	0.05	0.09	0.15	B.D.	0.01	B.D.	52.5	93.04
KILT1_BU_5	39.61	0.45	0.08	B.D.	0.27	0.21	0.08	0	0.02	0.02	53.23	93.97
KILT1_BU_6	41.03	0.52	0.08	B.D.	0.14	0.14	B.D.	B.D.	0.02	0.04	53.94	95.92
KILT1_BU_7	32.97	0.36	0.67	0.02	0.07	0.25	0.31	B.D.	0.02	0.02	43.83	78.53
KILT1_BU_8	33.24	0.43	0.59	0.04	0.08	0.27	0.28	B.D.	B.D.	0.02	43.48	78.43

KILT1_BU_9	38.37	0.44	0.42	0.02	0.06	0.21	0.08	0.05	B.D.	B.D.	48.22	87.84
KILT1_BU_10	41.13	0.57	0.11	B.D.82	0.1	0.19	B.D.	B.D.	0.01	B.D.	54.07	96.18
KILT1_BU_11	39.97	0.58	0.12	0.01	0.08	0.12	0.08	B.D.	0.02	B.D.	53.9	94.89
KILT1_BU_12	40.26	0.53	0.12	0.02	0.29	0.23	0.26	0	0.02	B.D.	52.85	94.58
KILT1_BU_1_1	41.01	0.48	0.09	0.02	0.08	0.14	0.13	B.D.	B.D.	B.D.	53.9	95.84
KILT1_BU_2_2	40.41	0.48	0.08	0.02	0.07	0.12	0.12	B.D.	B.D.	B.D.	53.91	95.19
KILT1_BU_3_3	41.2	0.44	0.08	B.D.	0.04	0.08	0.05	0	0.01	B.D.	54.22	96.14
KILT1_BU_4_4	40.41	0.48	0.1	B.D.	B.D.	0.14	0.05	B.D.	0.01	B.D.	54.36	95.55
KILT1_BU_5_5	41.36	0.5	0.11	B.D.	B.D.	0.19	B.D.	0	B.D.	B.D.	54.42	96.58
KILT1_BU_6_6	40.24	0.54	0.09	B.D.91	B.D.	0.18	0	B.D.	B.D.	B.D.	54.41	95.46
KILT1_BU_7_7	39.48	0.53	0.14	0.07	0.06	0.15	0.13	B.D.	B.D.	0.08	51.63	92.28
KILT1_BU_8_8	39.71	0.49	0.24	0.01	0.05	0.15	0.21	B.D.	B.D.	0.05	51.7	92.63
KILT1_BU_9_9	41.65	0.4	0.17	B.D.	0.09	0.09	0.09	B.D.	B.D.	0.04	53.5	96.02
KILT1_BU_10_10	40.73	0.48	0.13	0.01	0.07	0.09	0.15	0.03	0.02	0.03	53.82	95.56
KILT1_BU_11_11	40.16	0.53	0.09	B.D.	0.05	0.16	B.D.	0.04	0.02	B.D.	54.24	95.29
KILT1_BU_12_12	40.92	0.52	0.11	B.D.	0.05	0.17	0.17	B.D.	B.D.	0	54.21	96.15
KILT7_BU_1_	34.99	0.23	0.59	0.43	0.69	2.18	4.6	B.D.	0.06	0.23	44.45	88.45
KILT7_BU_2	38.62	0.1	0.44	0	0.06	0.05	B.D.	B.D.	0.11	B.D.47	51.01	90.39
KILT7_BU_3	40.29	0.2	0.21	B.D.	B.D.	B.D.	B.D.	0.03	0.03	0	53.39	94.15

KILT7_BU_4	40.48	0.68	0.07	B.D.	0.01	B.D.	0	B.D.	0.02	B.D.	54.52	95.78
KILT7_BU_5	40.55	0.73	0.09	0.01	B.D.	0.05	0.04	B.D.	B.D.	B.D.79	54.27	95.75
KILT7_BU_6	40.67	0.66	0.11	B.D.	0.01	0.04	0.05	B.D.	B.D.	0.05	53.96	95.57
KILT7_BU_7	40.7	0.59	0.16	B.D.	B.D.	0.05	B.D.	B.D.	0.03	B.D.	52.32	93.85
KILT7_BU_8	38.13	0.51	0.29	0.08	0.19	0.57	1.35	B.D.	0	0.06	48.63	89.81
KILT7_BU_9	40.37	0.58	0.17	0.05	0.08	0.12	0.14	B.D.	0.04	B.D.	51.9	93.46
KILT7_BU_10	29.02	0.43	0.85	0.02	0.03	0.25	0.44	B.D.	0.02	B.D.	38.27	69.32
KILT7_BU_11	39.1	0.64	0.18	0	0.02	0	B.D.	B.D.	B.D.	B.D.	52.29	92.23
KILT7_BU_12	22.1	0.33	1.1	0.06	0.13	0.6	0.91	B.D.	0.04	0.04	30.14	55.45
KILT7_BU_1_1	39.2	0.26	0.5	0.02	0.02	0.07	0.11	B.D.	0.04	0.04	52	92.26
KILT7_BU_2_2	38.95	0.26	0.36	B.D.	0.04	0	B.D.	B.D.	B.D.	0.07	51.96	91.63
KILT7_BU_3_3	41.16	0.23	0.32	0.01	0.05	B.D.	B.D.	0.04	0.02	B.D.	53.92	95.75
KILT7_BU_4_4	24.88	0.35	1.03	0.01	B.D.	0.07	0.14	0.03	B.D.	B.D.	33.36	59.88
KILT7_BU_5_5	40.59	0.65	0.13	B.D.	B.D.	0.05	B.D.	0.05	B.D.	B.D.	53.4	94.87
KILT7_BU_6_6	40.01	0.76	0.13	B.D.	B.D.	B.D.	0	B.D.	0.03	B.D.	53.19	94.12
KILT7_BU_7_7	40.38	0.5	0.09	B.D.	B.D.	0.1	0.05	0.05	B.D.	B.D.	54.03	95.22
KILT7_BU_8_8	41.49	0.48	0.09	0.02	0.03	0.05	0.09	B.D.	B.D.	B.D.	53.96	96.21
KILT7_BU_9_9	41.23	0.42	0.12	0.02	0.03	0.15	0.18	B.D.	B.D.	0.03	53.33	95.51
KILT7_BU_10_10	27.95	0.49	0.42	0.12	0.23	0.94	1.46	B.D.	B.D.	0.07	40.93	72.62

KILT7_BU_12_12	37.98	0.64	0.26	B.D.	B.D.	B.D.	B.D.	B.D.	B.D.	B.D.	50.62	89.51

The following table shows the data (spots on bones) removed from the dataset. These were removed because the sum of elements were less than expected in bone (total elements measured <50%) due to errors in locating and focusing the electron beam. The excluded points sum up to 82.

Sample	P2O5	Na2O	Cl	K2O	FeO	Al2O3	SiO2	SrO	MnO	MgO	CaO	Total
WSF5D6M5_UN_7	0.00	0.00	0.00	0.00	0.00	0.01	0.00	0.00	0.01	0.00	0.09	0.11
WSF5D6M5_UN_8	0.00	0.00	2.25	0.00	0.00	0.00	0.03	0.01	0.00	0.00	0.02	2.03
WSF5D6M5_UN_9	0.01	0.00	1.28	0.00	0.01	0.01	0.04	0.00	0.02	0.00	0.11	1.31
WSF5D6M5_UN_12	1.75	0.00	1.19	0.02	0.01	0.01	0.02	0.01	0.00	0.03	5.12	7.89
WSF5D6M5_BU_1	0.00	0.00	1.87	0.00	0.00	0.02	0.07	0.00	0.00	0.00	0.10	1.84
WSF5D6M5_BU_2	0.00	0.01	2.09	0.00	0.00	0.00	0.04	0.02	0.00	0.00	0.09	2.00
SWF2FR4_BU_8	0.52	0.00	1.61	0.00	0.00	0.00	0.01	0.00	0.00	0.00	0.18	2.31
WSF3D1M1_BU_7	0.53	0.00	1.27	0.00	0.01	0.05	0.11	0.04	0.01	0.01	0.07	2.09
WSF3D1M1_BU_8	0.50	0.00	1.35	0.00	0.00	0.00	0.02	0.00	0.00	0.00	0.08	1.95
SWF2FR2_BU_1	0.44	0.00	1.16	0.00	0.00	0.02	0.03	0.00	0.02	0.00	0.02	1.69
WSRF2D2W3_UN_2	0.21	0.01	0.01	0.04	0.08	0.01	0.00	0.01	0.01	0.01	2.97	3.34
WSF2D2W3_UN_9	0.00	0.00	1.72	0.00	0.00	0.00	0.00	0.00	0.00	0.00	0.05	1.78
WSF2D2W3_UN_10	0.05	0.00	0.42	0.01	0.00	0.04	0.05	0.00	0.00	0.00	2.58	3.15
WSF3D1M4_UN_1	0.46	0.00	1.43	0.02	0.01	0.00	0.03	0.00	0.00	0.00	0.19	2.14
WSF3D1M4_UN_12	0.02	0.00	0.01	0.00	0.01	0.04	0.01	0.00	0.00	0.00	0.19	0.28
WSF5D6M3_BU_10	0.04	0.00	2.03	0.01	0.00	0.01	0.02	0.01	0.01	0.00	0.20	2.33
WSF5D6M3_BU_11	0.06	0.00	2.13	0.00	0.00	0.01	0.00	0.00	0.00	0.00	0.22	2.42
WSF3D3M3_BU_7	0.91	0.00	0.00	0.00	0.00	0.03	0.06	0.02	0.00	0.03	1.48	2.53
WSF2D2W4_UN_1	0.28	0.05	1.83	0.29	0.57	1.69	3.35	0.03	0.01	0.07	0.76	8.92
WSF2D2W4_UN_2	0.12	0.00	0.00	0.07	0.01	0.00	0.06	0.02	0.00	0.00	0.19	0.48
WSF3D3M4_BU_11	0.24	0.06	0.03	0.02	0.01	0.08	0.02	0.02	0.00	0.01	0.49	0.97
WSF2D2W2_UN_1	0.05	0.00	0.00	0.00	0.01	0.00	0.01	0.01	0.00	0.00	0.03	0.12
WSF2D2W2_UN_2	0.00	0.00	0.00	0.00	0.00	0.00	0.00	0.00	0.00	0.00	0.00	0.01
WSF3D1M3_BU_11	0.40	0.00	1.65	0.00	0.00	0.00	0.06	0.00	0.00	0.00	0.15	2.26
WSF3D1M3_BU_12	0.40	0.03	1.66	0.00	0.00	0.00	0.02	0.00	0.01	0.00	0.13	2.26
WSF3D3M4_UN_3	0.03	0.00	2.06	0.00	0.00	0.00	0.04	0.00	0.01	0.00	0.12	2.26
WS_Fresh_7	0.54	0.00	1.50	0.00	0.00	0.03	0.02	0.00	0.00	0.00	0.09	2.19
WS_Fresh_16	0.06	0.00	0.00	0.00	0.00	0.01	0.00	0.00	0.00	0.00	0.08	0.15
WS_Fresh_17	0.09	0.00	0.00	0.00	0.00	0.01	0.02	0.00	0.00	0.00	0.11	0.24
WS_Fresh_18	0.01	0.00	0.00	0.01	0.00	0.00	0.02	0.00	0.00	0.01	0.06	0.13
WS_Fresh_19	0.05	0.00	0.01	0.00	0.00	0.01	0.01	0.00	0.00	0.00	0.14	0.23
SW_FRESH1_BU_3	0.09	0.00	0.04	0.01	0.02	0.03	0.01	0.02	0.00	0.00	0.06	0.28
SW_FRESH1_BU_10	0.67	0.00	1.02	0.00	0.00	0.00	0.04	0.01	0.00	0.00	0.14	1.89
SW_FRESH1_BU_14	0.07	0.00	0.01	0.00	0.00	0.01	0.03	0.00	0.00	0.00	0.09	0.21
WSF2D2W5_BU_12	0.83	0.00	1.63	0.01	0.00	0.01	0.00	0.00	0.01	0.00	0.32	2.79
WSF3D1M1_UN_1	0.17	0.15	0.25	0.44	1.34	4.24	1.46	0.00	0.01	0.45	0.59	9.10

WSF3D1M1_UN_2	0.11	0.04	0.12	0.00	0.01	0.38	0.15	0.00	0.01	0.01	0.18	1.01
WSF3D1M1_UN_3	0.12	0.00	0.09	0.01	0.01	0.00	0.11	0.00	0.00	0.00	0.22	0.57
WSD2S2W5_UN_15	0.11	0.09	0.04	0.08	0.06	0.22	0.00	0.01	0.01	0.10	6.49	7.20
WSD2S2W5_UN_22	0.23	0.00	1.65	0.01	0.00	0.00	0.04	0.00	0.00	0.00	1.51	3.45
SWF5D1Y1_UN_1	0.75	0.02	0.02	0.01	0.01	0.07	0.09	0.00	0.00	0.00	0.53	1.49
SWF5D1Y1_UN_2	0.05	0.00	0.00	0.00	0.00	0.01	0.00	0.02	0.00	0.00	0.09	0.17
SWF5D1Y1_UN_3	0.03	0.00	0.01	0.01	0.00	0.01	0.03	0.04	0.01	0.00	0.11	0.24
SWF5D1Y1_UN_4	0.27	0.00	0.65	0.01	0.00	0.01	0.09	0.00	0.00	0.00	0.26	1.28
SWF5D1Y1_UN_2_2	0.09	0.02	0.03	0.02	0.07	0.08	0.03	0.02	0.00	0.01	0.57	0.94
SWF5D1Y1_UN_3_3	0.09	0.00	0.01	0.01	0.04	0.04	0.07	0.01	0.01	0.01	0.17	0.45
WSF3D1M2_BU_12	0.49	0.01	1.06	0.00	0.01	0.00	0.03	0.00	0.00	0.00	0.11	1.72
WSF3D1M1_UN_2	0.57	0.01	0.14	0.06	0.01	0.04	0.10	0.00	0.00	0.04	0.55	1.52
WSF3D1M1_UN_3	0.14	0.00	0.03	0.03	0.13	0.05	0.04	0.01	0.00	0.01	0.18	0.63
WSF3D1M1_UN_2	0.57	0.01	0.14	0.06	0.01	0.04	0.10	0.00	0.00	0.04	0.55	1.52
WSF3D1M1_UN_3	0.14	0.00	0.03	0.03	0.13	0.05	0.04	0.01	0.00	0.01	0.18	0.63
WSF3D1M1_UN_1	0.32	0.01	0.08	0.05	0.06	0.23	0.32	0.00	0.00	0.04	0.28	1.39
WSF3D1M4_BU_10	0.50	0.02	1.37	0.01	0.00	0.00	0.02	0.02	0.00	0.00	0.17	2.11
WSF3D1M4_BU_11	0.53	0.00	1.45	0.00	0.00	0.02	0.01	0.01	0.00	0.00	0.04	2.06
WSF3D3M2_UN_9	1.27	0.05	0.96	0.05	0.07	0.21	0.20	0.01	0.01	0.02	1.59	4.46
WSF2D2W2_BU_2	1.22	0.02	0.01	0.01	0.00	0.04	0.05	0.01	0.00	0.03	1.28	2.66
WSF3D3M2_BU_5	0.08	0.00	0.01	0.01	0.01	0.00	0.02	0.00	0.00	0.00	0.14	0.27
WSF5D6M4_UN_1	7.09	0.11	0.17	0.02	0.06	0.25	1.16	0.00	0.00	0.15	2.18	11.19
WSF5D6M4_UN_2	0.28	0.04	0.23	0.02	0.03	0.02	0.16	0.01	0.02	0.10	3.76	4.66
WSF5D6M4_UN_3	0.00	0.00	0.01	0.00	0.00	0.00	0.01	0.00	0.00	0.00	0.01	0.03
WSF5D6M4_UN_7	0.00	0.00	0.00	0.00	0.01	0.02	0.01	0.00	0.00	0.00	0.06	0.10
WSF5D6M4_UN_8	0.04	0.00	0.00	0.00	0.01	0.00	0.01	0.00	0.00	0.00	0.06	0.12
WSF5D6M4_UN_9	0.07	0.00	0.01	0.00	0.00	0.03	0.05	0.03	0.00	0.00	0.07	0.27
WSF5D6M4_UN_11	0.22	0.00	0.00	0.02	0.00	0.13	0.30	0.00	0.00	0.00	3.87	4.55
WSF5D6M1_UN_4	0.00	0.00	0.00	0.00	0.01	0.00	0.01	0.00	0.00	0.00	0.00	0.03
WSF5D6M1_UN_3	3.83	0.06	0.03	0.02	0.09	0.11	0.20	0.00	0.02	0.04	4.21	8.61
WSF5D6M1_UN_8	0.05	0.00	0.01	0.00	0.00	0.03	0.03	0.02	0.00	0.00	0.25	0.39
WSF5D6M1_UN_9	0.41	0.02	0.00	0.00	0.02	0.02	0.04	0.00	0.00	0.01	1.02	1.54
WSF5D6M1_UN_10	0.12	0.00	0.00	0.01	0.00	0.06	0.00	0.03	0.00	0.00	1.34	1.56
WSF2D2W4_BU_12	5.45	0.20	1.01	0.04	0.00	0.00	0.03	0.02	0.00	0.00	6.55	13.30
WSF5D6M2_BU_11	3.77	0.03	1.44	0.01	0.01	0.06	0.03	0.00	0.01	0.02	9.08	14.02
WSF3D1M5_BU_1_	0.36	0.00	1.67	0.00	0.00	0.00	0.00	0.00	0.00	0.00	0.12	2.15
WSF2D2W2_UN_3	0.38	0.00	0.00	0.01	0.02	0.01	0.14	0.00	0.00	0.00	0.80	1.36

WSF2D2W2_UN_10	5.12	0.00	0.06	0.02	0.11	0.01	0.10	0.00	0.00	0.01	3.98	9.42
WSF3D3M4_UN_1_	0.15	0.03	0.05	0.03	0.02	0.00	0.00	0.01	0.00	0.01	0.28	0.58
WSF3D1M2_UN_9	1.39	0.00	0.79	0.01	0.00	0.06	0.04	0.00	0.01	0.00	3.17	5.48
SW_FRESH1_BU_1_	0.13	0.00	0.02	0.01	0.00	0.00	0.03	0.00	0.00	0.00	0.06	0.25
WSF2D2W5_UN_12	5.93	0.06	1.56	0.00	0.00	0.00	0.02	0.00	0.00	0.12	7.78	15.48
WSF2D2W5_UN_2_2	4.96	0.14	0.07	0.06	0.07	0.05	0.11	0.00	0.01	0.17	10.43	16.05
SWF5D1Y2_UN_1_	0.21	0.00	0.01	0.02	0.01	0.01	0.04	0.01	0.01	0.00	1.35	1.67
SWF5D1Y2_UN_10	10.73	0.20	0.54	0.01	0.03	0.25	0.07	0.00	0.00	0.32	16.35	28.49
WSF3D1M2_BU_11	4.28	0.08	0.05	0.02	0.00	0.01	0.03	0.01	0.00	0.10	5.47	10.06
WSF3D3M2_UN_7	3.72	0.07	0.67	0.02	0.00	0.04	0.14	0.00	0.00	0.06	4.89	9.60
WSF3D3M2_UN_8	11.84	0.19	0.12	0.04	0.03	0.32	0.18	0.03	0.01	0.21	13.50	26.45
WSF3D3M2_UN_10	9.75	0.12	1.03	0.02	0.01	0.03	0.02	0.03	0.00	0.34	11.07	22.41
WSF3D3M2_UN_12	8.52	0.11	0.56	0.02	0.02	0.04	0.05	0.03	0.00	0.18	9.90	19.43
WSF2D2W1_UN_2	10.99	0.25	0.07	0.07	0.06	0.07	0.08	0.00	0.01	0.35	13.46	25.39
WSF5D6M1_UN_2	11.48	0.10	0.10	0.04	0.37	0.10	1.07	0.01	0.02	0.12	8.20	21.60
WSF5D6M1_UN_12	10.19	0.13	0.07	0.02	0.08	0.28	0.25	0.04	0.02	0.21	14.44	25.75
WSF5D6M3_UN_10	10.55	0.10	0.04	0.06	0.01	0.07	0.12	0.00	0.00	0.18	16.30	27.43
WSF2D2W3_BU_11	7.36	0.26	0.40	0.07	0.13	9.20	0.91	0.09	0.02	0.41	12.21	31.07
WSF3D1M5_BU_3	0.44	0.00	1.03	0.01	0.00	0.00	0.01	0.00	0.00	0.00	0.08	1.58
WSF3D1M5_BU_10	3.63	0.10	1.25	0.04	0.02	0.14	0.22	0.01	0.00	0.19	7.32	12.92
WSF2D2W4_UN_3	11.30	0.34	0.03	0.41	0.56	1.98	1.23	0.00	0.00	0.54	14.96	31.36
WSF2D2W4_UN_11	3.78	0.00	1.87	0.01	0.00	0.16	0.04	0.00	0.00	0.04	4.81	10.70
WSF2D2W2_UN_8	12.34	0.00	0.05	0.02	0.26	0.02	0.50	0.04	0.00	0.03	16.60	29.87
WSF3D3M3_UN_1_	14.40	0.21	0.04	0.01	0.02	0.02	0.05	0.02	0.01	0.22	19.19	34.20
WSF5D6M4_BU_9	11.11	0.28	1.65	0.07	0.06	0.04	0.00	0.00	0.00	0.10	18.36	31.67
WSF3D1M1_UN_12	16.91	0.28	0.21	0.03	0.02	0.11	0.03	0.01	0.00	0.39	19.37	37.35
WSF3D1M1_UN_13	14.75	0.16	0.11	0.02	0.04	0.63	0.42	0.08	0.01	0.17	18.50	34.90
WSF3D3M1_UN_3	16.63	0.17	0.51	0.02	0.04	0.04	0.04	0.06	0.03	0.19	20.63	38.35
WSF2D2W5_UN_2	9.27	0.07	0.09	0.05	0.08	0.21	0.16	0.02	0.00	0.21	12.97	23.14
WSF5D6M3_UN_11	14.20	0.07	0.09	0.07	0.00	0.00	0.08	0.04	0.01	0.16	21.68	36.39
WSF5D6M3_UN_7	16.91	0.31	0.13	0.06	0.01	0.02	0.24	0.04	0.00	0.43	21.28	39.45
SWFR1_BU_10	11.19	0.27	0.95	0.06	0.00	0.00	0.03	0.01	0.01	0.42	14.85	27.79

Appendix D.3.1: Bamble, Durango, Wilberforce

Detection limits							0.07	0.02	0.01	0.01	0.01	0.03	0.04	0.03	0.01	0.02	0.01	
Label	**Number**	**Date**	**X**	**Y**	**Z**	**Current**	**P2O5**	**Na2O**	**Cl**	**K2O**	**FeO**	**Al2O3**	**SiO2**	**SrO**	**MnO**	**MgO**	**CaO**	**Total**
Bamble_1	4	Dec 2 20:56 2020	35.5384	14.8413	11.5193	1.025E-08	41.35	0.28	7.38	0.00	0.08	0.08	0.00	0.00	0.00	0.00	52.59	98.55
Bamble_2	5	Dec 2 21:02 2020	35.5281	14.8736	11.5193	1.026E-08	40.88	0.25	7.45	0.00	0.12	0.06	0.03	0.00	0.00	0.00	52.53	98.13
Bamble_3	6	Dec 2 21:07 2020	35.5457	14.9002	11.5193	1.027E-08	40.85	0.25	7.43	0.00	0.10	0.01	0.06	0.04	0.03	0.00	52.39	97.96
Bamble_4	84	Dec 3 04:09 2020	35.5291	14.9492	11.5193	1.056E-08	42.00	0.28	7.46	0.00	0.10	0.03	0.04	0.03	0.00	0.00	52.43	99.13
Bamble_5	85	Dec 3 04:14 2020	35.4959	14.942	11.5193	1.056E-08	41.84	0.26	7.51	0.00	0.10	0.04	0.06	0.01	0.00	0.01	52.84	99.42
Bamble_1	4	Dec 2 20:56 2020	35.5384	14.8413	11.5193	1.025E-08	41.35	0.28	7.38	0.00	0.08	0.08	0.00	0.00	0.00	0.00	52.59	98.55
Bamble_2	5	Dec 2 21:02 2020	35.5281	14.8736	11.5193	1.026E-08	40.88	0.25	7.45	0.00	0.12	0.06	0.03	0.00	0.00	0.00	52.53	98.13
Bamble_3	6	Dec 2 21:07 2020	35.5457	14.9002	11.5193	1.027E-08	40.85	0.25	7.43	0.00	0.10	0.01	0.06	0.04	0.03	0.00	52.39	97.96
Bamble_4	84	Dec 3 04:09 2020	35.5291	14.9492	11.5193	1.056E-08	42.00	0.28	7.46	0.00	0.10	0.03	0.04	0.03	0.00	0.00	52.43	99.13
Bamble_5	85	Dec 3 04:14 2020	35.4959	14.942	11.5193	1.056E-08	41.84	0.26	7.51	0.00	0.10	0.04	0.06	0.01	0.00	0.01	52.84	99.42
							41.38	**0.26**	**7.44**	**0.00**	**0.10**	**0.04**	**0.04**	**0.02**	**0.01**	**0.00**	**52.56**	**98.64**
							0.50	**0.01**	**0.04**	**0.00**	**0.01**	**0.03**	**0.02**	**0.02**	**0.01**	**0.00**	**0.17**	**0.59**

Preferred values							**41.47**	**0.28**	**7.09**		**0.10**		**0.07**	**0.15**	**0.01**	**0.11**	**52.35**
							0.84	**0.01**	**0.03**		**0.01**		**0.22**	**0.03**	**0.01**	**0.11**	**0.62**

Label	**Number**	**Date**	**X**	**Y**	**Z**	**Current**	**P2O5**	**Na2O**	**Cl**	**K2O**	**FeO**	**Al2O3**	**SiO2**	**SrO**	**MnO**	**MgO**	**CaO**	**Total**
Durango_1	1	Dec 2 20:40 2020	39.6627	14.3636	11.4955	1.023E-08	40.22	0.24	0.40	0.00	0.05	0.03	0.39	0.01	0.00	0.00	53.82	92.87
Durango_2	2	Dec 2 20:4	39.6018	14.345	11.497	1.024E-08	40.64	0.14	0.42	0.00	0.03	0.04	0.51	0.00	0.03	0.00	53.72	93.24

		6 2020															
Durango_3	3	Dec 2 20:51 2020	39.5213	14.3516	11.497	1.024E-08	41.05	0.20	0.43	0.00	0.04	0.02	0.51	0.00	0.00	0.00	53.64	93.56
Durango_4	82	Dec 3 03:58 2020	39.3864	14.4068	11.4948	1.056E-08	41.08	0.12	0.45	0.02	0.03	0.04	0.53	0.02	0.01	0.00	54.02	93.99
Durango_5	83	Dec 3 04:03 2020	39.3555	14.4341	11.4948	1.056E-08	42.27	0.12	0.42	0.01	0.02	0.02	0.52	0.04	0.02	0.00	54.88	95.96
Durango_1	1	Dec 2 20:40 2020	39.6627	14.3636	11.4955	1.023E-08	40.22	0.24	0.40	0.00	0.05	0.03	0.39	0.01	0.00	0.00	53.82	92.87
Durango_2	2	Dec 2 20:46 2020	39.6018	14.345	11.497	1.024E-08	40.64	0.14	0.42	0.00	0.03	0.04	0.51	0.00	0.03	0.00	53.72	93.24
Durango_3	3	Dec 2 20:51 2020	39.5213	14.3516	11.497	1.024E-08	41.05	0.20	0.43	0.00	0.04	0.02	0.51	0.00	0.00	0.00	53.64	93.56
Durango_4	82	Dec 3 03:58	39.3864	14.4068	11.4948	1.056E-08	41.08	0.12	0.45	0.02	0.03	0.04	0.53	0.02	0.01	0.00	54.02	93.99

		2020																
Durango_5	83	Dec 3 04:03 2020	39.3555	14.4341	11.4948	1.056E-08	42.27	0.12	0.42	0.01	0.02	0.02	0.52	0.04	0.02	0.00	54.88	95.96
							41.05	**0.16**	**0.43**	**0.01**	**0.04**	**0.03**	**0.49**	**0.01**	**0.01**	**0.00**	**54.01**	**93.92**
							0.72	**0.05**	**0.02**	**0.01**	**0.01**	**0.01**	**0.05**	**0.02**	**0.01**	**0.00**	**0.48**	**1.14**
Preferred values							**40.96**	**0.15**	**0.45**		**0.04**		**0.42**	**0.11**	**0.01**	**0.00**	**54.22**	
							0.56	**0.02**	**0.03**		**0.01**		**0.03**	**0.04**	**0.01**	**0.00**	**0.40**	
Wilberforce_1	7	Dec 2 21:12 2020	32.4891	15.0344	11.5265	1.028E-08	0.00	0.00	0.00	0.00	0.29	0.02	0.02	0.65	0.26	0.42	58.43	59.68
Wilberforce_2	8	Dec 2 21:18 2020	32.4518	15.0636	11.5265	1.027E-08	0.06	0.00	0.00	0.00	0.32	0.01	0.00	0.69	0.23	0.44	58.42	59.75
Wilberforce_3	9	Dec 2 21:23 2020	32.3685	15.115	11.5265	1.029E-08	0.02	0.00	0.01	0.00	0.33	0.00	0.00	0.71	0.26	0.45	58.23	59.60
Wilberforce_4	86	Dec 3 04:19 2020	32.4006	14.9256	11.5265	1.056E-08	0.00	0.00	0.01	0.00	0.33	0.03	0.00	0.61	0.25	0.43	58.76	60.00

Wilberforce_5	87	Dec 3 04:25 2020	32.3695	14.8945	11.5265	1.056E-08	0.00	0.00	0.00	0.00	0.30	0.05	0.03	0.56	0.24	0.42	58.44	59.63
Wilberforce_1	7	Dec 2 21:12 2020	32.4891	15.0344	11.5265	1.028E-08	0.00	0.00	0.00	0.00	0.29	0.02	0.02	0.65	0.26	0.42	58.43	59.68
Wilberforce_2	8	Dec 2 21:18 2020	32.4518	15.0636	11.5265	1.027E-08	0.06	0.00	0.00	0.00	0.32	0.01	0.00	0.69	0.23	0.44	58.42	59.75
Wilberforce_3	9	Dec 2 21:23 2020	32.3685	15.115	11.5265	1.029E-08	0.02	0.00	0.01	0.00	0.33	0.00	0.00	0.71	0.26	0.45	58.23	59.60
Wilberforce_4	86	Dec 3 04:19 2020	32.4006	14.9256	11.5265	1.056E-08	0.00	0.00	0.01	0.00	0.33	0.03	0.00	0.61	0.25	0.43	58.76	60.00
Wilberforce_5	87	Dec 3 04:25 2020	32.3695	14.8945	11.5265	1.056E-08	0.00	0.00	0.00	0.00	0.30	0.05	0.03	0.56	0.24	0.42	58.44	59.63
								0.00		**0.00**		**0.02**	**0.01**	**0.64**	**0.25**	**0.43**		**59.73**
								0		**0.00193953**		**0.01756937**	**0.01433566**	**0.05582656**	**0.01191555**	**0.01371455**		**0.15105555**

Label	Number	Date	X	Y	Z	Current	P2O5	Na2O	Cl	K2O	FeO	Al2O3	CaO	SrO	MnO	MgO	SiO2	Total

Bamble_4	95	Dec 4 03:27 2020	34.905	14.6017	11.4693	1.031E-08	40.97	0.30	7.41	0.00	0.10	0.08	52.60	0.03	0.00	0.00	0.01	101.49
Bamble_5	96	Dec 4 03:32 2020	34.8934	14.578	11.4693	1.031E-08	41.30	0.27	7.37	0.00	0.08	0.05	52.36	0.09	0.00	0.00	0.08	101.59
Bamble_6	97	Dec 4 03:38 2020	34.8769	14.5382	11.4693	1.031E-08	40.68	0.33	6.50	0.00	0.09	0.04	52.75	0.01	0.00	0.00	0.00	100.40
Bamble_7	98	Dec 4 03:43 2020	34.8448	14.5059	11.4693	1.03E-08	40.87	0.29	7.46	0.02	0.07	0.00	52.28	0.00	0.01	0.00	0.02	101.02
BAMBLE_2	2	Dec 3 19:11 2020	35.2659	14.9958	11.4715	1.008E-08	42.26	0.27	7.22	0.02	0.08	0.00	52.38	0.04	0.00	0.00	0.00	102.26
BAMBLE_3	3	Dec 3 19:16 2020	35.2538	14.9594	11.4715	1.009E-08	41.81	0.32	7.23	0.00	0.09	0.04	52.58	0.04	0.00	0.00	0.02	102.13
							41.31	**0.30**	**7.20**	**0.01**	**0.08**	**0.03**	**52.49**	**0.04**	**0.00**	**0.00**	**0.02**	**101.48**
							0.61	**0.03**	**0.35**	**0.01**	**0.01**	**0.03**	**0.18**	**0.03**	**0.00**	**0.00**	**0.03**	**0.69**
							1.47	8.78	4.92	154.97	9.94	88.02	0.34	85.44	124.22	244.95	127.28	0.68
Durango_3	91	Dec 4 03:06 2020	39.9079	15.1652	11.496	1.03E-08	40.67	0.18	0.43	0.00	0.06	0.06	54.02	0.06	0.01	0.00	0.58	96.06
Durango_4	92	Dec 4 03:11 2020	39.8579	15.1571	11.496	1.029E-08	40.70	0.16	0.46	0.00	0.05	0.10	53.97	0.04	0.02	0.00	0.44	95.96
Durango_5	93	Dec 4 03:16 2020	39.7994	15.1571	11.496	1.03E-08	40.47	0.17	0.42	0.00	0.03	0.00	54.21	0.07	0.00	0.00	0.48	95.87
Durango_6	94	Dec 4 03:22 2020	39.8126	15.2064	11.496	1.031E-08	41.12	0.22	0.42	0.00	0.04	0.03	53.80	0.04	0.02	0.00	0.44	96.14
DURANGO_1	4	Dec 3 19:21 2020	39.4917	14.5343	11.493	1.009E-08	41.39	0.18	0.46	0.00	0.03	0.03	54.20	0.03	0.00	0.00	0.48	96.81
DURANGO_2	5	Dec 3 19:27 2020	39.4329	14.55	11.493	1.01E-08	42.23	0.17	0.43	0.00	0.04	0.07	54.57	0.05	0.00	0.00	0.50	98.07

DURANGO_3	6	Dec 3 19:32 2020	39.3136	14.588	11.493	1.011E-08	41.27	0.14	0.45	0.00	0.03	0.08	53.78	0.05	0.02	0.00	0.49	96.30
								0.17		**0.00**	**0.04**	**0.05**		**0.05**	**0.01**	**0.00**	**0.49**	**96.46**
								0.03		**0.00**	**0.01**	**0.03**		**0.01**	**0.01**	**0.00**	**0.05**	**0.77**

Label	Number	Date	X	Y	Z	Current	P2O5	Na2O	Cl	K2O	FeO	Al2O3	SiO2	SrO	MnO	MgO	CaO	Total
Bamble_1	4	Dec 4 16:05 2020	35.6124	15.0148	11.474	1.01E-08	40.76	0.34	6.86	0.00	0.11	0.05	0.00	0.00	0.01	0.00	52.09	100.23
Bamble_2	5	Dec 4 16:11 2020	35.5784	15.046	11.474	1.01E-08	40.90	0.30	6.80	0.00	0.13	0.02	0.00	0.02	0.04	0.00	52.03	100.24
Bamble_3	6	Dec 4 16:16 2020	35.5783	15.0771	11.474	1.01E-08	41.50	0.22	6.82	0.00	0.09	0.09	0.00	0.05	0.02	0.00	52.22	101.01
Bamble_4	91	Dec 4 23:59 2020	35.6124	15.1117	11.474	1.016E-08	42.07	0.29	6.81	0.00	0.08	0.02	0.08	0.00	0.03	0.00	52.09	101.47
Bamble_5	92	Dec 5 00:04 2020	35.5691	15.1118	11.474	1.015E-08	42.32	0.29	6.83	0.00	0.10	0.00	0.04	0.00	0.01	0.00	52.46	102.05
Bamble_6	93	Dec 5 00:10 2020	35.5802	15.0819	11.474	1.016E-08	41.59	0.28	6.75	0.01	0.10	0.03	0.06	0.00	0.01	0.00	52.19	101.02
Bamble_7	94	Dec 5 00:15 2020	35.5021	15.0382	11.474	1.015E-08	41.15	0.32	6.90	0.02	0.09	0.06	0.09	0.00	0.00	0.00	52.07	100.69
							41.47	**0.29**	**6.82**	**0.00**	**0.10**	**0.04**	**0.04**	**0.01**	**0.02**	**0.00**	**52.16**	**100.96**
							0.58	**0.04**	**0.05**	**0.01**	**0.02**	**0.03**	**0.04**	**0.02**	**0.01**	**0.00**	**0.15**	**0.66**
								0.28			**0.10**		**0.07**	**0.15**	**0.01**	**0.11**	**52.35**	
								0.01			**0.01**		**0.22**	**0.03**	**0.01**	**0.11**	**0.62**	
Durango_1	1	Dec 4 15:49 2020	39.2854	14.9588	11.4915	1.008E-08	40.37	0.19	0.44	0.00	0.02	0.07	0.50	0.10	0.02	0.00	54.32	96.03
Durango_2	2	Dec 4 15:55 2020	39.3232	14.8994	11.4915	1.009E-08	40.94	0.20	0.48	0.01	0.03	0.04	0.51	0.10	0.01	0.00	53.60	95.92
Durango_4	95	Dec 5 00:20 2020	39.2831	14.9885	11.49	1.016E-08	40.29	0.19	0.47	0.02	0.05	0.01	0.52	0.01	0.02	0.00	53.46	95.05
Durango_5	96	Dec 5 00:26 2020	39.2472	15.0045	11.49	1.016E-08	41.97	0.15	0.45	0.00	0.07	0.05	0.34	0.02	0.00	0.00	53.33	96.38
Durango_6	97	Dec 5 00:31 2020	39.2057	15.0046	11.49	1.016E-08	41.40	0.10	0.48	0.00	0.03	0.07	0.48	0.02	0.00	0.00	53.34	95.92

Durango_7	98	Dec 5 00:37 2020	39.1789	14.9525	11.49	1.016E-08	40.82	0.12	0.47	0.00	0.04	0.09	0.52	0.04	0.02	0.00	53.96	96.08
							40.97	**0.16**	**0.47**	**0.00**	**0.04**	**0.05**	**0.48**	**0.05**	**0.01**	**0.00**	**53.67**	**95.90**
							0.64	**0.04**	**0.02**	**0.01**	**0.02**	**0.03**	**0.07**	**0.04**	**0.01**	**0.00**	**0.39**	**0.45**
								0.15			**0.04**		**0.42**	**0.11**	**0.01**	**0.00**	**54.22**	
								0.02			**0.01**		**0.03**	**0.04**	**0.01**	**0.00**	**0.40**	

Label	Number	Date	X	Y	Z	Current	P2O5	Na2O	Cl	K2O	FeO	Al2O3	SiO2	SrO	MnO	MgO	CaO	Total
Bamble_2	2	Dec 8 13:40 2020	35.5507	19.141	11.4603	2.213E-08	39.05	0.29	6.54	0.01	0.07	0.06	0.03	0.01	0.02	0.00	52.68	98.74
Bamble_3	3	Dec 8 13:45 2020	35.5378	18.7965	11.4575	1.01E-08	39.28	0.28	6.41	0.01	0.10	0.04	0.01	0.01	0.00	0.00	52.02	98.15
							39.17	**0.28**	**6.48**	**0.01**	**0.08**	**0.05**	**0.02**	**0.01**	**0.01**	**0.00**	**52.35**	**98.45**
							0.16	**0.00**	**0.09**	**0.00**	**0.02**	**0.01**	**0.01**	**0.00**	**0.01**	**0.00**	**0.47**	**0.42**
Durango_1	4	Dec 8 13:50 2020	40.2122	18.542	11.4793	1.01E-08	38.15	0.17	0.39	0.00	0.03	0.07	0.49	0.06	0.01	0.00	53.36	92.73
Durango_2	5	Dec 8 13:56 2020	40.245	18.5239	11.4793	1.01E-08	38.03	0.19	0.38	0.00	0.04	0.03	0.52	0.07	0.01	0.00	53.56	92.83

Durango_3	6	Dec 8 14:01 2020	40.3282	18.4922	11.4793	1.01E-08	37.36	0.14	0.36	0.00	0.01	0.06	0.41	0.10	0.00	0.00	53.80	92.24
							Na2O	**P2O5**	**CaO**	**FeO**	**Al2O3**	**Cl**	**K2O**	**MnO**	**MgO**	**SiO2**	**SrO**	**Total**
Devee_no1	1	Dec 9 13:45 2020	70.0283	44.7306	11.29	1.001E-08	1.37	29.66	48.73	0.011	0	0.0788	0.0167	0.0018	0.5173	0.0086	0.1324	80.53
Devee_no1-2	2	Dec 9 13:51 2020	70.1411	44.6261	11.29	1.002E-08	1.48	28.08	48.71	0	0.0292	0.0866	0.0237	0	0.5322	0.0433	0.0755	79.06
Devee_no1-3	3	Dec 9 13:57 2020	70.3159	44.4949	11.287	1.002E-08	1.47	28.3	49.53	0.0016	0	0.0507	0.0181	0.0054	0.5315	0	0.1207	80.02
Devee_no1-4	4	Dec 9 14:03 2020	70.4315	44.5263	11.2843	1.002E-08	1.48	27.98	48.54	0.0107	0.0304	0.0846	0.0145	0.0138	0.5147	0.0059	0.0818	78.76
Devee_no2-1	5	Dec 9 14:09 2020	75.0548	45.1845	11.181	1.002E-08	1.51	28.44	48.17	0.003	0.0419	0.0828	0.025	0.0022	0.484	0	0.1454	78.91
Devee_no2-2	6	Dec 9 14:14	75.0857	45.1629	11.181	1.002E-08	1.56	28.31	48.44	0	0.0261	0.097	0.0139	0.0144	0.4633	0	0.1244	79.05

		2020																
Devee_no2-3	7	Dec 9 14:20 2020	75.0876	45.1177	11.181	1.002E-08	1.48	28.27	47.9	0.0122	0	0.0802	0.0175	0	0.4756	0	0.1072	78.35
Devee_no2-4	8	Dec 9 14:26 2020	75.0913	45.0813	11.181	1.002E-08	1.51	27.75	48.2	0.0093	0	0.094	0.0357	0.0103	0.4718	0.0058	0.0898	78.18
							1.4825	**28.34875**	**48.5275**	**0.005975**	**0.01595**	**0.0818375**	**0.0206375**	**0.005975**	**0.4988**	**0.00795**	**0.10965**	**79.1075**
							0.05391793	**0.57377042**	**0.49511182**	**0.00530195**	**0.01764086**	**0.01409417**	**0.00727165**	**0.00602766**	**0.02809789**	**0.01469538**	**0.0252902**	**0.79781398**

Label	Number	Date	X	Y	Z	Current	Na2O	P2O5	CaO	FeO	Al2O3	Cl	K2O	MnO	MgO	SiO2	SrO	Total
Bamble_1	1	Dec 10 18:54 2020	39.0712	8.1159	11.227	1.001E-08	0.2481	39.82	53.23	0.0951	0.0829	6.15	0.0097	0	0	0.0496	0.0098	99.69
Bamble_2	2	Dec 10 19:00 2020	39.0807	8.0766	11.227	1.004E-08	0.2694	39.65	53.3	0.1079	0.0205	6.15	0.0098	0	0.0029	0.0182	0.0281	99.56
Bamble_3	3	Dec 10 19:06 2020	38.9937	8.0797	11.227	1.007E-08	0.2384	39.39	53.3	0.0861	0.0485	6.13	0	0.0128	0	0.0069	0	99.22

Bamble_4	125	Dec 11 07:06 2020	38.9866	8.1162	11.223	1.061E-08	0.2655	40.26	53.72	0.0471	0.0283	6.11	0	0.0263	0	0	0.0729	100.53
Bamble_5	126	Dec 11 07:12 2020	38.9976	8.0856	11.223	1.061E-08	0.2733	40.81	53.38	0.0956	0.0312	6.11	0	0.0046	0.0338	0.0405	0.046	100.83
Bamble_6	127	Dec 11 07:18 2020	39.0236	8.0589	11.223	1.061E-08	0.222	40.75	53.64	0.0951	0.0475	6.01	0.0045	0	0	0.0387	0.0555	100.86
							0.25278333	**40.113 3333**	**53.428 3333**	**0.0878 1667**	**0.04315**	**6.11**	**0.004**	**0.00728333**	**0.00611667**	**0.02565**	**0.03538333**	**100.115**
							0.02017517	**0.58925942**	**0.20222924**	**0.02112254**	**0.02237836**	**0.05215362**	**0.00478289**	**0.01056795**	**0.01361153**	**0.02014654**	**0.02787267**	**0.71107665**
Durango_1	4	Dec 10 19:12 2020	40.631	7.9842	11.2115	1.01E-08	0.116	39.45	55.03	0.0221	0.0525	0.4472	0.0049	0.011	0	0.5292	0.0634	95.73
Durango_2	5	Dec 10 19:18 2020	40.6313	7.9044	11.2095	1.012E-08	0.124	39.15	55.09	0.0389	0.0862	0.4499	0.0003	0.0295	0	0.4654	0.0564	95.5
Durango_3	6	Dec 10 19:	40.5794	7.9105	11.2095	1.015E-08	0.1396	39.72	54.89	0.0309	0.0333	0.4356	0	0	0	0.5486	0.0478	95.84

		23 2020																
Durango_4	7	Dec 10 19:29 2020	40.5208	7.9247	11.2095	1.016E-08	0.2077	39.11	54.91	0.0544	0.0062	0.408	0.0042	0.0506	0	0.4286	0.0318	95.21
Wilberforce_1	8	Dec 10 19:35 2020	37.3079	8.4536	11.251	1.018E-08	0	0.0008	19.99	0.0091	11.89	0	0	0.0041	0	42.71	0.0054	74.6
Wilberforce_2	9	Dec 10 19:41 2020	37.2208	8.3972	11.2513	1.02E-08	0.0125	0.0538	20.25	0.0388	12.09	0.0086	0.0235	0.004	0	42.65	0.0522	75.18
Wilberforce_3	10	Dec 10 19:47 2020	37.1753	8.4118	11.2513	1.021E-08	0.0145	0.0125	20.17	0.0575	11.83	0.0004	0.0126	0.0318	0	43.62	0	75.75
Wilberforce_4	11	Dec 10 19:53 2020	37.1141	8.4414	11.252	1.022E-08	0.0092	0.0281	20.12	0.0347	11.77	0.0069	0.0261	0	0	43.19	0	75.18

Label	Number	Date	X	Y	Z	Current	Na2O	P2O5	CaO	FeO	Al2O3	Cl	K2O	MnO	MgO	SiO2	SrO	Total

Bamble_1	4	Dec 11 16:15 2020	38.5395	8.0291	11.2265	1.004E-08	0.2525	40.61	53.14	0.0461	0.0461	6.17	0	0.0056	0	0.0724	0.1161	100.45
Bamble_2	5	Dec 11 16:21 2020	38.4957	7.9648	11.2265	1.004E-08	0.2542	40.06	52.88	0.0789	0.0034	6.09	0.0101	0.0087	0.0082	0.0869	0.0618	99.53
Bamble_3	6	Dec 11 16:27 2020	38.4205	7.9648	11.2265	1.005E-08	0.2533	39.72	53.2	0.092	0.0968	6.07	0.0016	0.0018	0	0.0284	0.0509	99.52
Bamble_5	122	Dec 12 03:52 2020	38.8264	7.8349	11.2165	1.011E-08	0.2305	39.77	53.47	0.0866	0.0649	6.17	0.0005	0.018	0.0213	0.0287	0.018	99.88
Bamble_6	123	Dec 12 03:58 2020	38.8293	7.7783	11.2165	1.011E-08	0.2698	39.57	53.51	0.1053	0.1012	6.12	0	0.0131	0	0.0446	0	99.73
Bamble_7	124	Dec 12 04:04 2020	38.7316	7.7806	11.2165	1.012E-08	0.2814	40.19	53.07	0.0874	0.0605	6.16	0	0.0017	0	0.0354	0.0514	99.94

							0.25695	39.9866667	53.2116667	0.0827167	0.06215	6.13	0.0020333	0.00815	0.0049167	0.0494	0.0497	99.8416667
							0.0173906	0.3812964	0.2412813	0.0199426	0.0359025	0.0433589	0.0040033	0.0064846	0.0086705	0.0245917	0.0400866	0.3447559
Label	**Number**	**Date**	**X**	**Y**	**Z**	**Current**	**Na2O**	**P2O5**	**CaO**	**FeO**	**Al2O3**	**Cl**	**K2O**	**MnO**	**MgO**	**SiO2**	**SrO**	**Total**
Durango_2	1	Dec 11 15:58 2020	41.6388	8.2398	11.198	1.004E-08	0.1626	40.36	54.77	0.0346	0.0325	0.4082	0	0	0	0.3845	0.0438	96.2
Durango_3	2	Dec 11 16:03 2020	41.6745	8.2214	11.198	1.004E-08	0.194	39.21	54.8	0.0323	0.0667	0.4075	0	0.0057	0	0.489	0.0298	95.24
Durango_4	3	Dec 11 16:09 2020	41.7114	8.2049	11.198	1.004E-08	0.1917	38.36	55.04	0.04	0.0668	0.3957	0.0001	0.0304	0	0.4729	0.118	94.71
Wilberforce_1	7	Dec 11 16:33 2020	36.7837	8.8783	11.2615	1.005E-08	0	0.0403	20.04	0	12.18	0.005	0	0	0	43.26	0.021	75.54
Wilberforce_2	8	Dec 11 16:39 2020	36.7486	8.8343	11.2615	1.006E-08	0	0.0218	20.08	0.0078	12.15	0.0153	0.0126	0	0	42.76	0.0145	75.06

Wilberforce_3	9	Dec 11 16:44 2020	36.7011	8.8082	11.2615	1.006E-08	0	0.0846	20.1	0	12.08	0	0.0081	0.0015	0	42.5	0.0677	74.84

Comment	No.	Na2O	P2O5	Cl	K2O	FeO	Al2O3	SiO2	SrO	MnO	MgO	CaO	Total
Durango-1	1	0.19	41.34	0.43	0.00	0.04	0.00	0.44	0.07	0.01	0.00	53.26	95.77
Durango-2	2	0.20	41.71	0.44	0.00	0.05	0.05	0.44	0.07	0.01	0.00	53.95	96.92
Durango-3	3	0.19	40.61	0.43	0.00	0.01	0.01	0.39	0.08	0.00	0.00	53.92	95.64
Durango-4	4	0.17	40.48	0.43	0.00	0.01	0.00	0.45	0.09	0.00	0.00	53.29	94.92
Durango_5	137	0.16	41.55	0.44	0.00	0.04	0.01	0.48	0.08	0.00	0.00	54.68	97.44
Durango_6	138	0.17	40.66	0.44	0.00	0.04	0.04	0.49	0.07	0.01	0.00	54.62	96.54
		0.18	**41.06**	**0.43**	**0.00**	**0.03**	**0.02**	**0.45**	**0.08**	**0.00**	**0.00**	**53.95**	
		0.01	**0.54**	**0.01**	**0.00**	**0.02**	**0.02**	**0.04**	**0.01**	**0.00**	**0.00**	**0.62**	
		0.15	**40.96**	**0.45**		**0.04**		**0.42**	**0.11**	**0.01**	**0.00**	**54.22**	
Bamble_5	139	0.34	42.07	7.27	0.00	0.11	0.05	0.03	0.02	0.00	0.00	52.88	102.78
Bamble_6	140	0.32	41.44	7.25	0.00	0.09	0.04	0.02	0.02	0.02	0.00	52.92	102.12
Bamble_1	5	0.28	41.09	7.35	0.00	0.10	0.03	0.01	0.02	0.00	0.00	52.19	101.05
Bamble_2	6	0.30	42.28	7.40	0.01	0.10	0.03	0.00	0.06	0.01	0.00	52.61	102.78
Bamble_3	7	0.32	41.07	7.39	0.02	0.12	0.03	0.01	0.01	0.00	0.00	52.66	101.64
Bamble_4	8	0.34	40.31	7.12	0.00	0.09	0.00	0.01	0.03	0.01	0.00	52.43	100.33
		0.32	**41.38**	**7.30**	**0.01**	**0.10**	**0.03**	**0.01**	**0.02**	**0.01**	**0.00**	**52.62**	
		0.03	**0.72**	**0.11**	**0.01**	**0.01**	**0.02**	**0.01**	**0.02**	**0.01**	**0.00**	**0.28**	
		0.28	**41.47**	**7.09**		**0.10**		**0.07**	**0.15**	**0.01**	**0.11**	**52.35**	

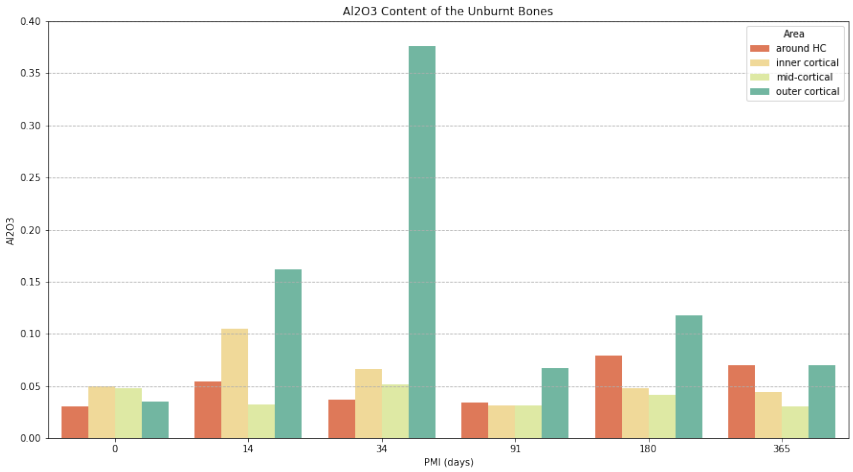
Appendix D.3.2: Bone Secondary Standard

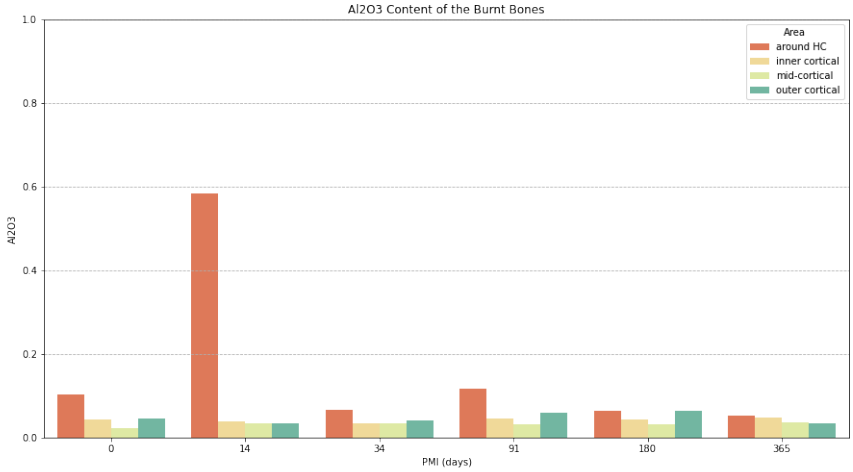
Label	Number	Date	X	Y	Z	Current	Na2O	P2O5	CaO	FeO	Al2O3	Cl	K2O	MnO	MgO	SiO2	SrO	Total
Devee_no1	1	Dec 9 13:45 2020	70.0283	44.7306	11.29	1.001E-08	1.37	29.66	48.73	0.011	0	0.0788	0.0167	0.0018	0.5173	0.0086	0.1324	80.53
Devee_no1-2	2	Dec 9 13:51 2020	70.1411	44.6261	11.29	1.002E-08	1.48	28.08	48.71	0	0.0292	0.0866	0.0237	0	0.5322	0.0433	0.0755	79.06
Devee_no1-3	3	Dec 9 13:57 2020	70.3159	44.4949	11.287	1.002E-08	1.47	28.3	49.53	0.0016	0	0.0507	0.0181	0.0054	0.5315	0	0.1207	80.02
Devee_no1-4	4	Dec 9 14:03 2020	70.4315	44.5263	11.2843	1.002E-08	1.48	27.98	48.54	0.0107	0.0304	0.0846	0.0145	0.0138	0.5147	0.0059	0.0818	78.76
Devee_no2-1	5	Dec 9 14:09 2020	75.0548	45.1845	11.181	1.002E-08	1.51	28.44	48.17	0.003	0.0419	0.0828	0.025	0.0022	0.484	0	0.1454	78.91
Devee_no2-2	6	Dec 9 14:14 2020	75.0857	45.1629	11.181	1.002E-08	1.56	28.31	48.44	0	0.0261	0.097	0.0139	0.0144	0.4633	0	0.1244	79.05
Devee_no2-3	7	Dec 9 14:20 2020	75.0876	45.1177	11.181	1.002E-08	1.48	28.27	47.9	0.0122	0	0.0802	0.0175	0	0.4756	0	0.1072	78.35

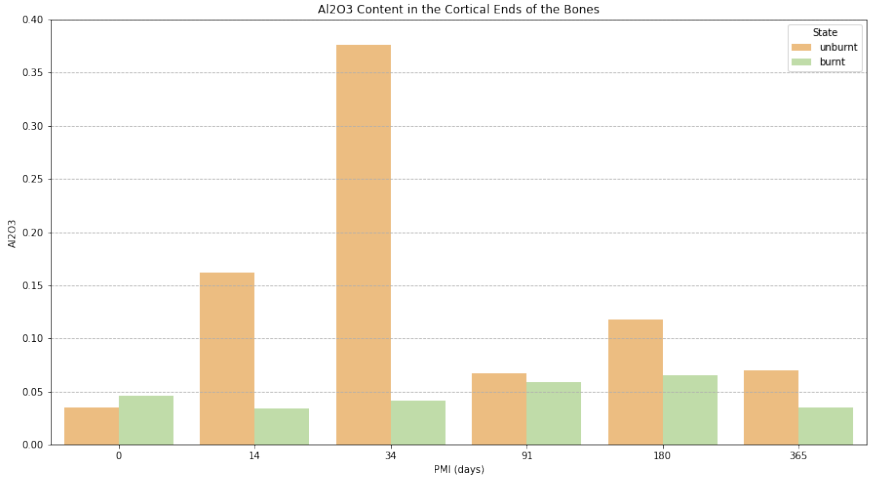
Devee_no2-4	8	Dec 9 14:26 2020	75.0913	45.0813	11.181	1.002E-08	1.51	27.75	48.2	0.0093	0	0.094	0.0357	0.0103	0.4718	0.0058	0.0898	78.18

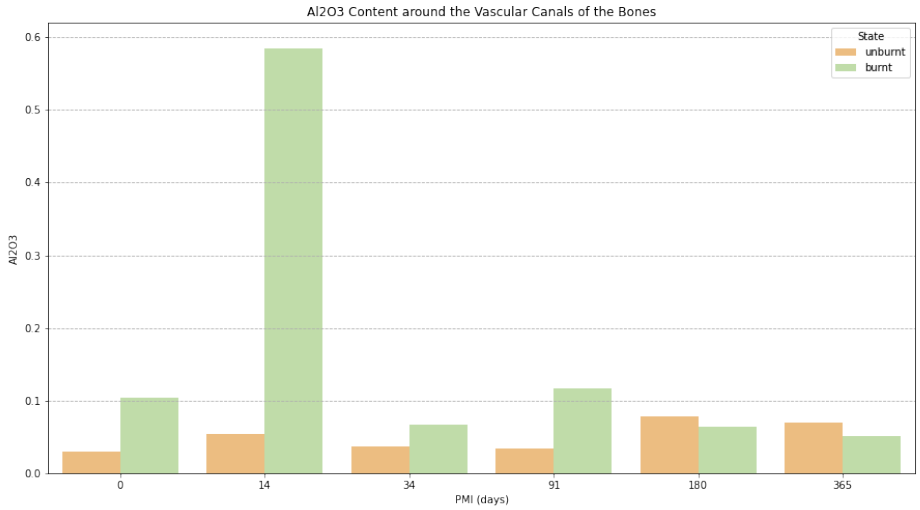
Appendix D.4: Graphs of Elemental Concentrations

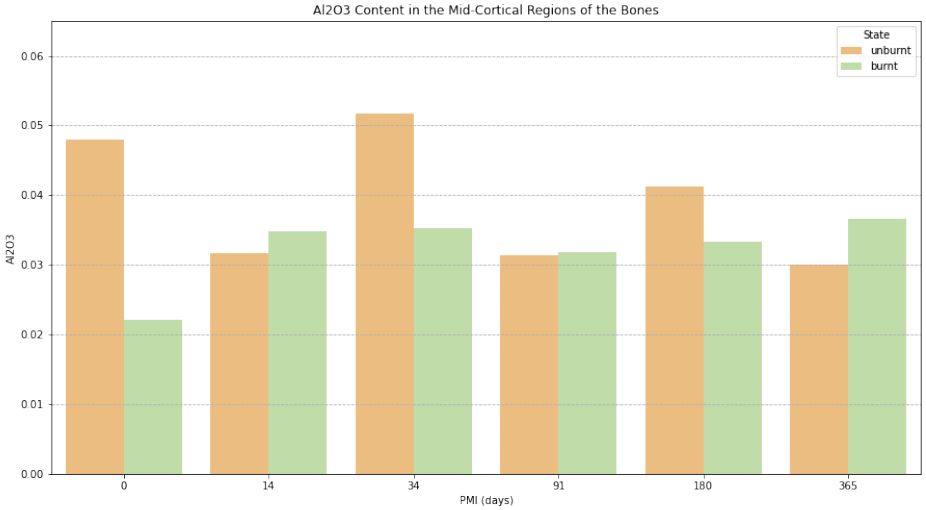
Appendix D.4.1: Aluminium

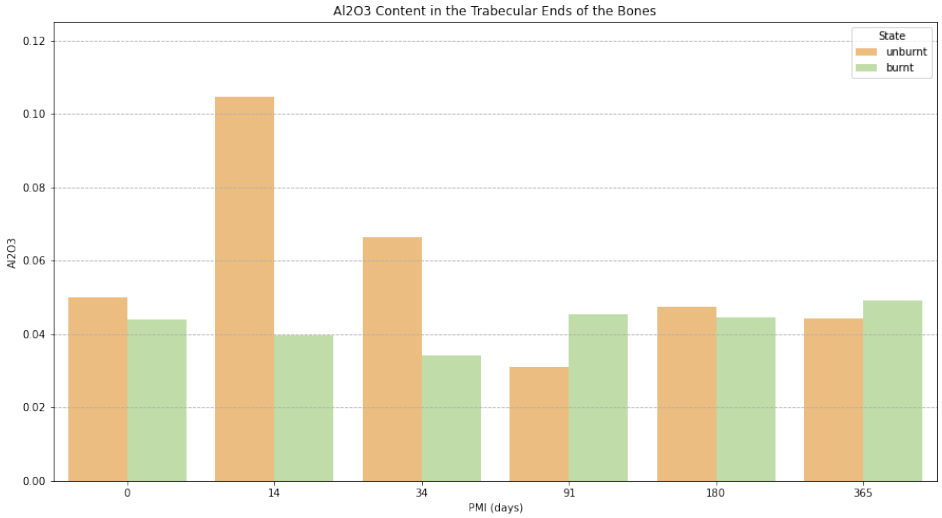




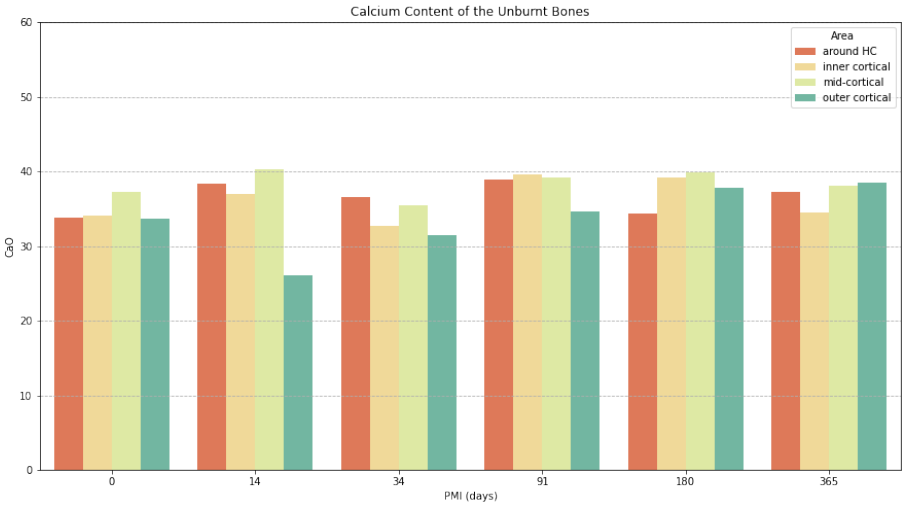


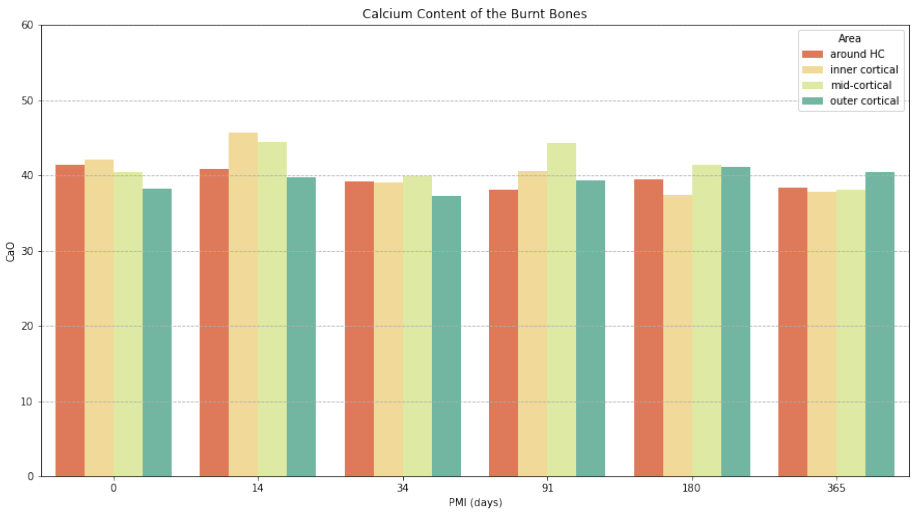

Al2O3 Content around the Vascular Canals of the Bones
State
unburnt
burnt
Al2O3
0.0
0.1
0.2
0.3
0.4
0.5
0.6
0
14
34
91
180
365
PMI (days)

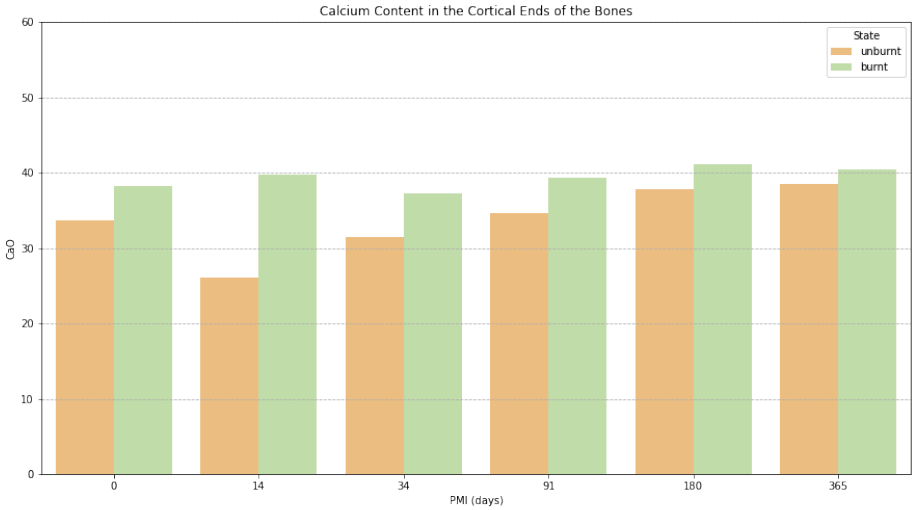

Al2O3 Content in the Mid-Cortical Regions of the Bones
State
unburnt
burnt
Al2O3
0.00
0.01
0.02
0.03
0.04
0.05
0.06
0
14
34
91
180
365
PMI (days)

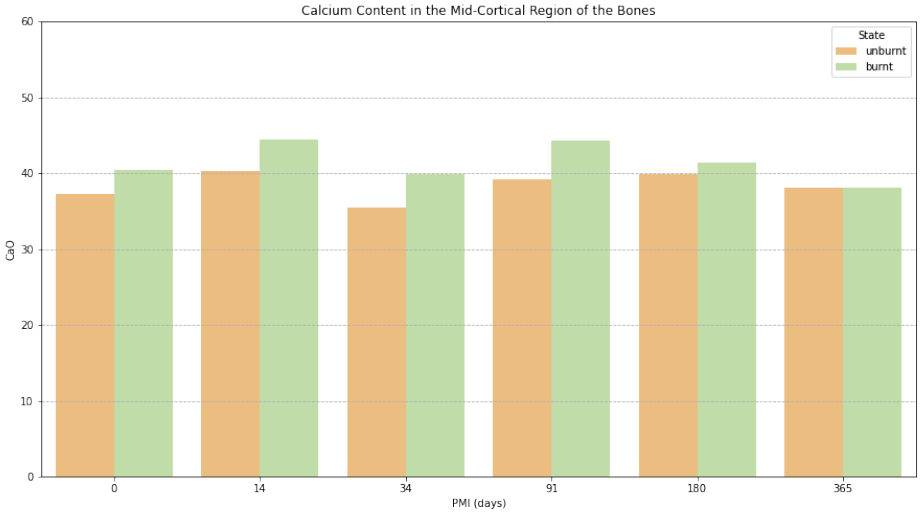

Al2O3 Content in the Trabecular Ends of the Bones
State
unburnt
burnt
Al2O3
0.00
0.02
0.04
0.06
0.08
0.10
0.12
0
14
34
91
180
365
PMI (days)

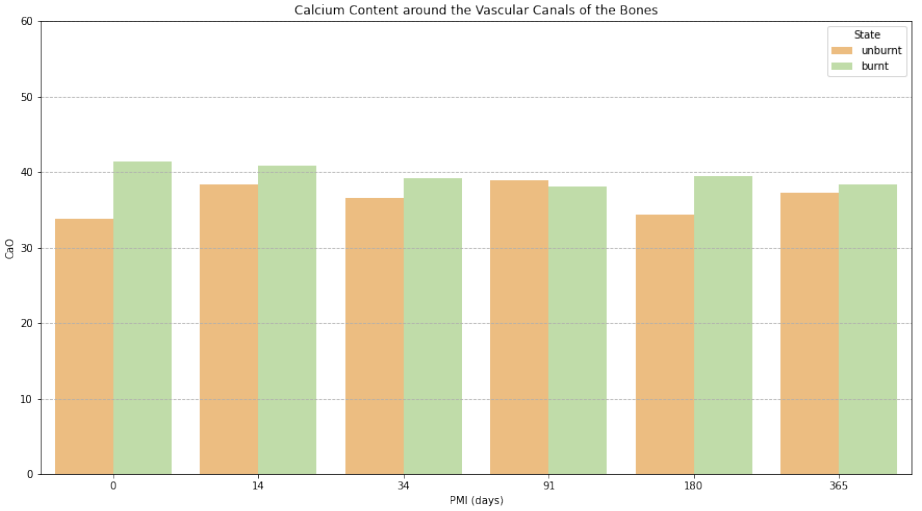
Appendix D.4.2: Calcium

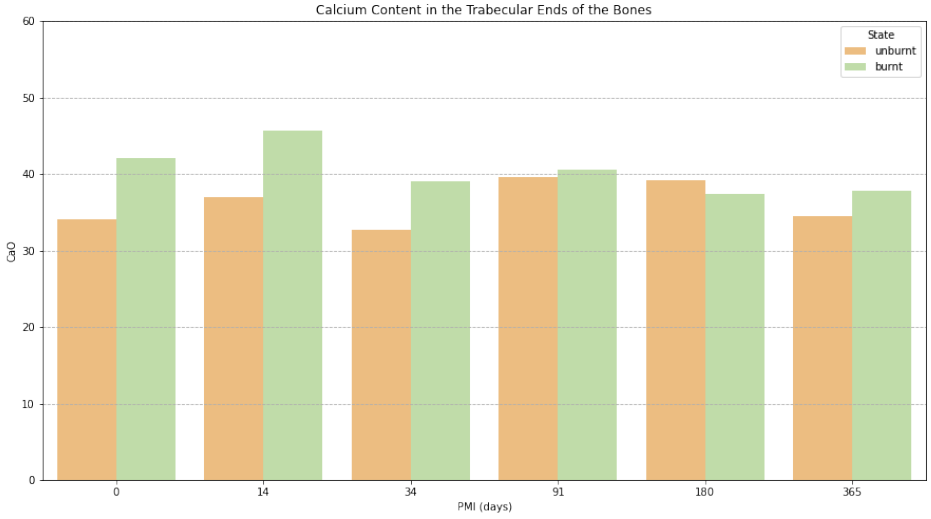




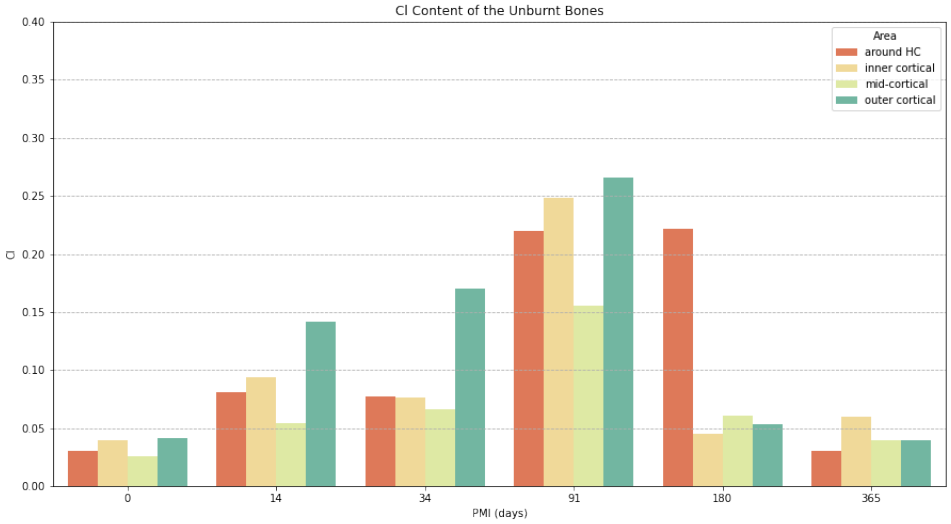


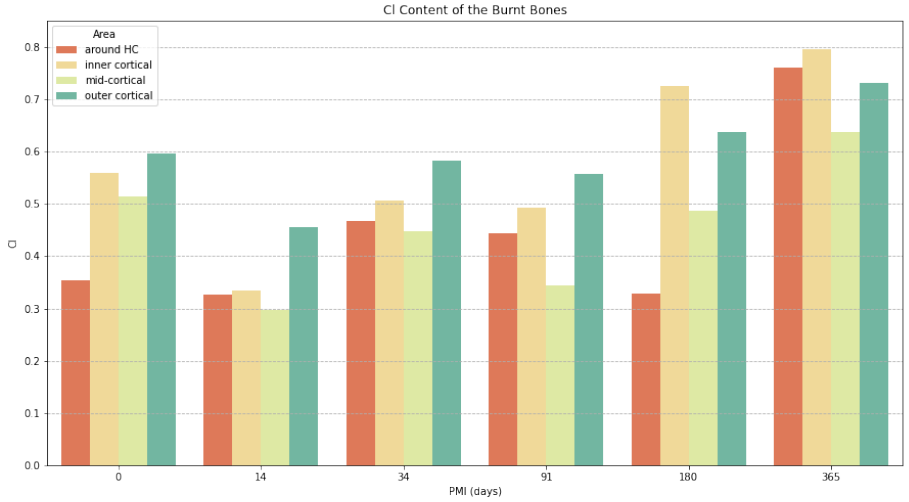

Calcium Content in the Mid-Cortical Region of the Bones
State
unburnt
burnt
CaO
0
10
20
30
40
50
60
0
14
34
91
180
365
PMI (days)

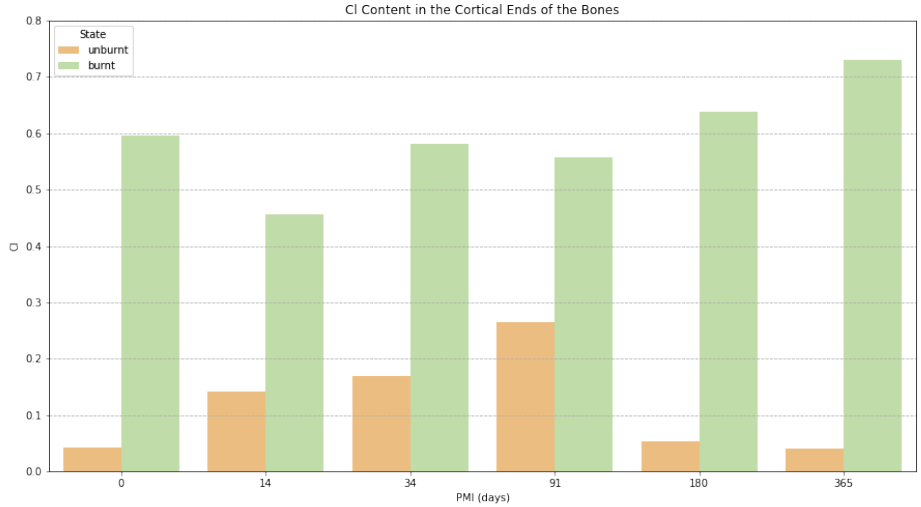

Calcium Content around the Vascular Canals of the Bones
State
unburnt
burnt
CaO
0
10
20
30
40
50
60
0
14
34
91
180
365
PMI (days)

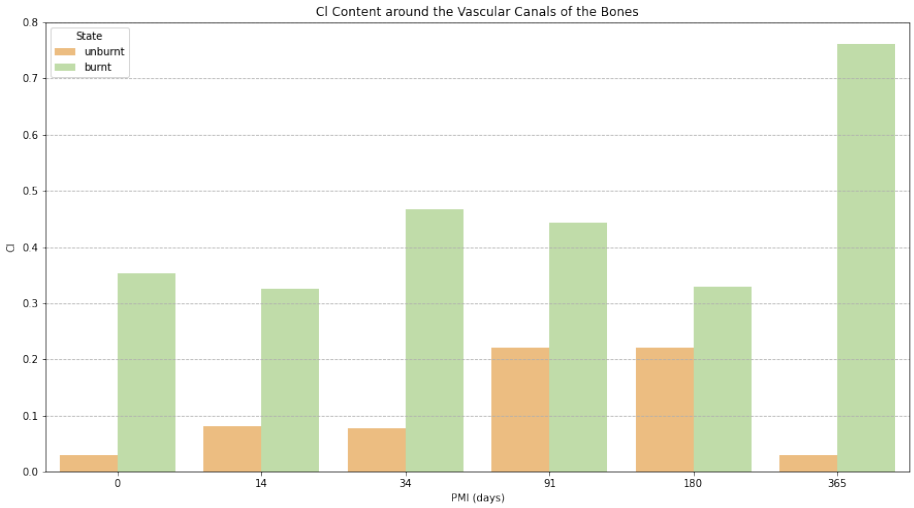

Calcium Content in the Trabecular Ends of the Bones
State
unburnt
burnt
CaO
0
10
20
30
40
50
60
0
14
34
91
180
365
PMI (days)

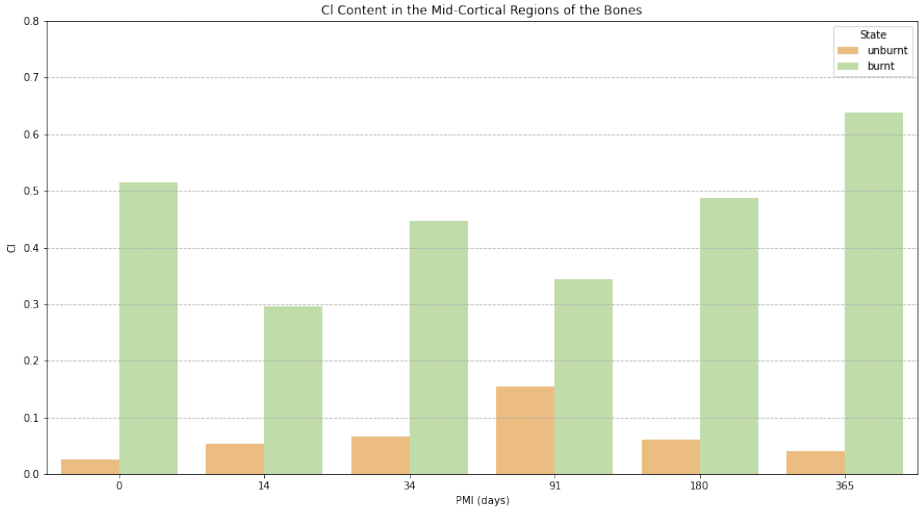
Appendix D.4.3: Chlorine

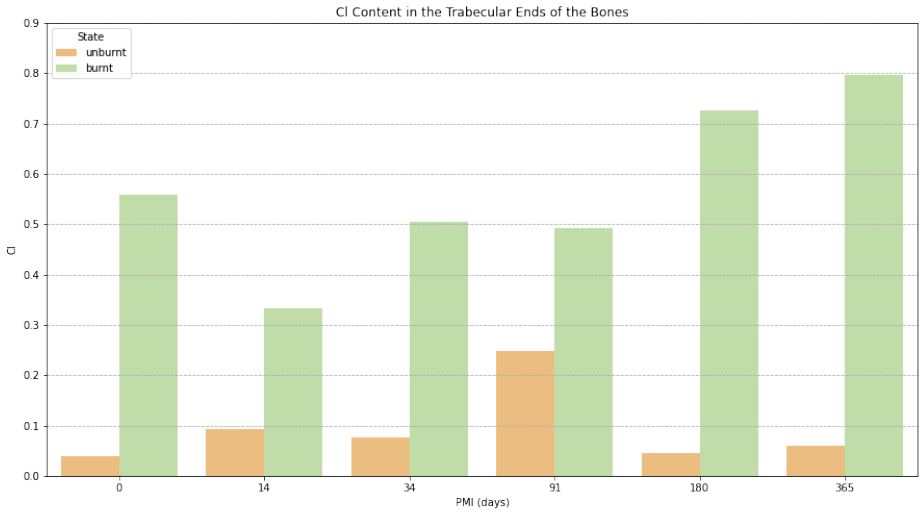




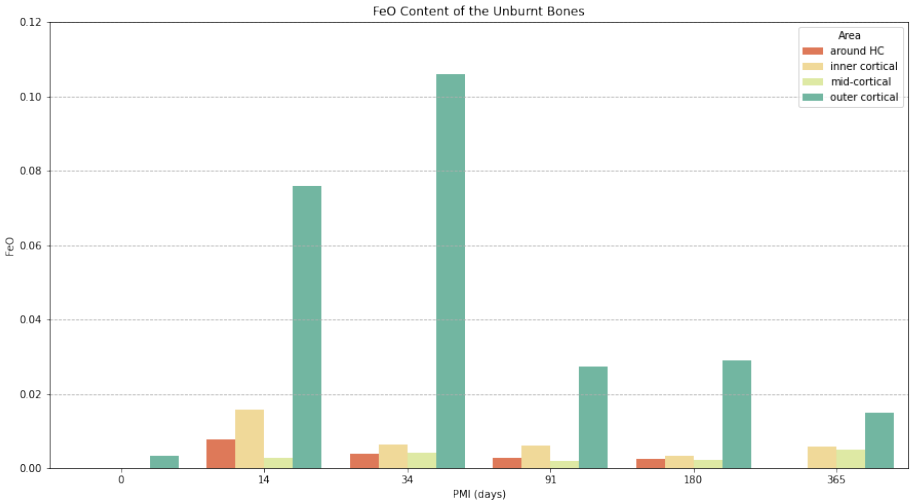


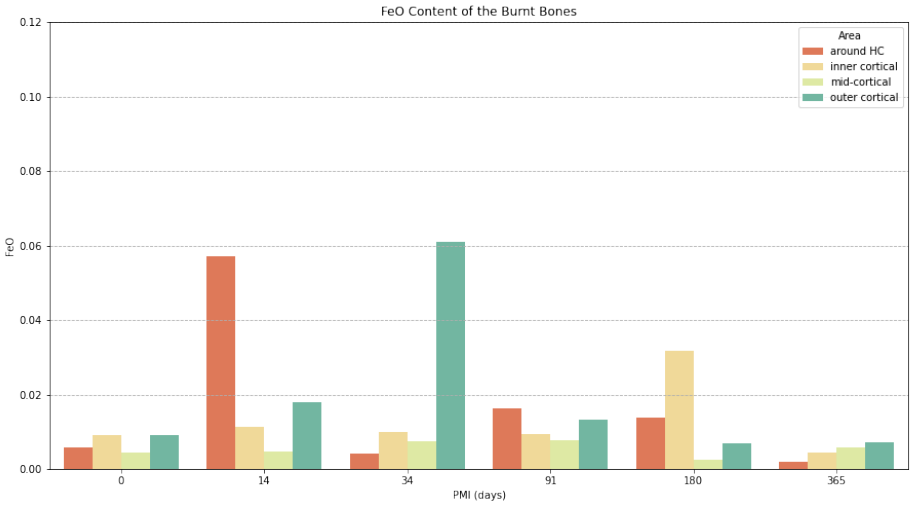

Cl Content around the Vascular Canals of the Bones
State
unburnt
burnt
Cl
PMI (days)
0
14
34
91
180
365

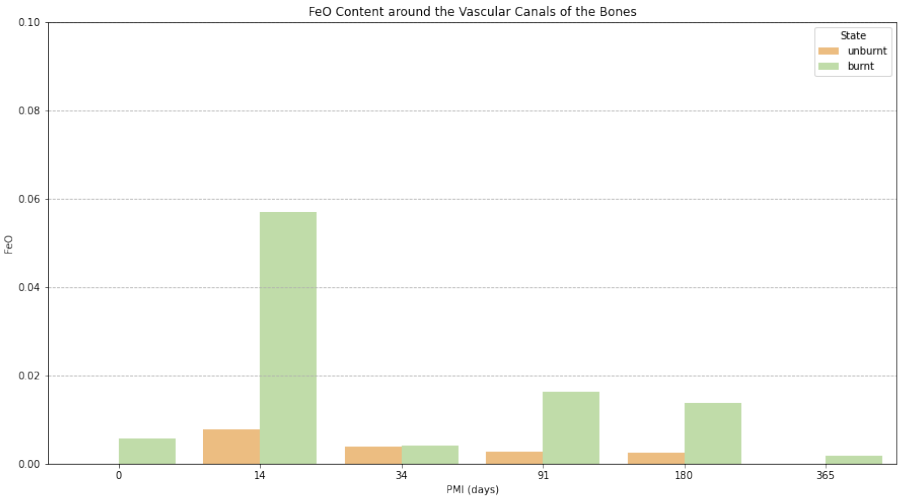

Cl Content in the Mid-Cortical Regions of the Bones
State
unburnt
burnt
Cl
PMI (days)
0
14
34
91
180
365

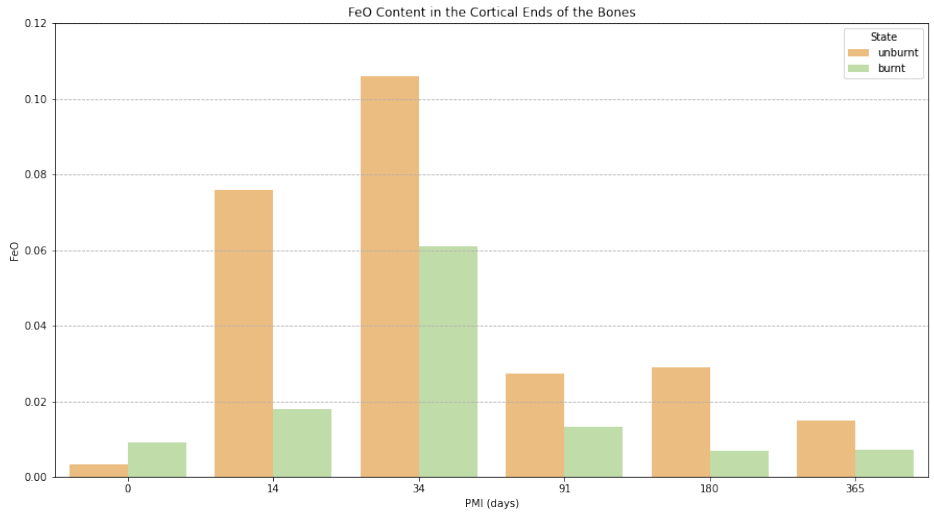

Cl Content in the Trabecular Ends of the Bones
State
unburnt
burnt
Cl
PMI (days)
0
14
34
91
180
365

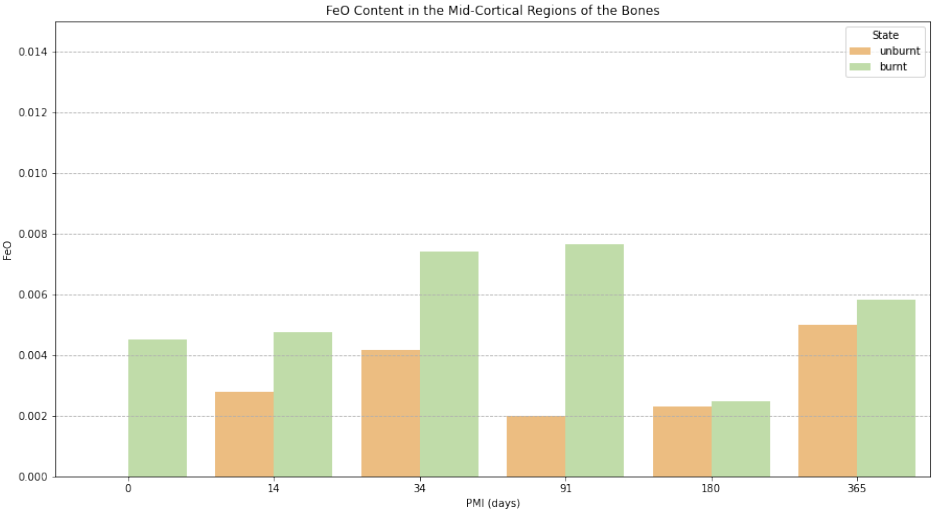
Appendix D.4.4. Iron

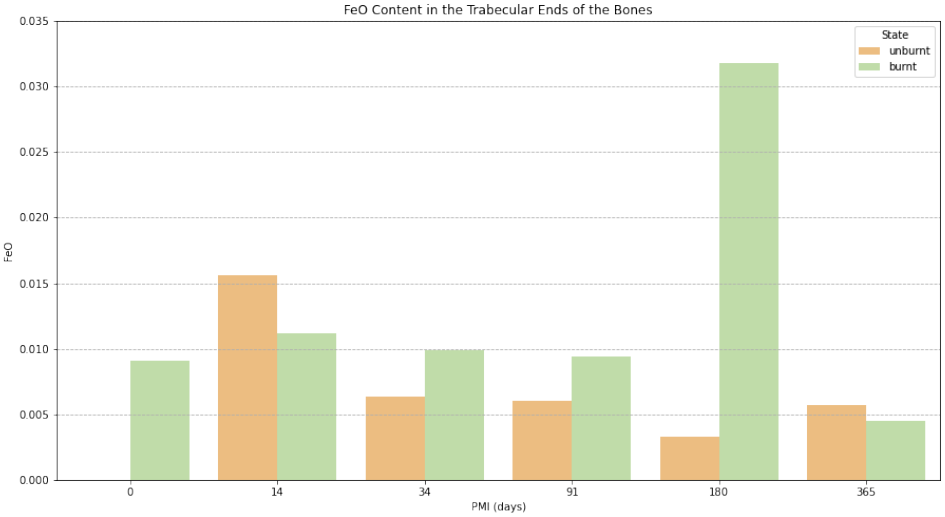




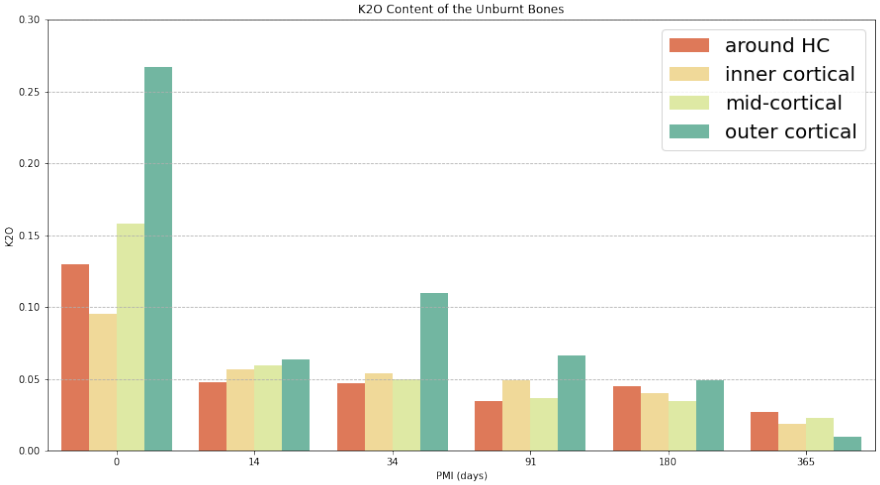


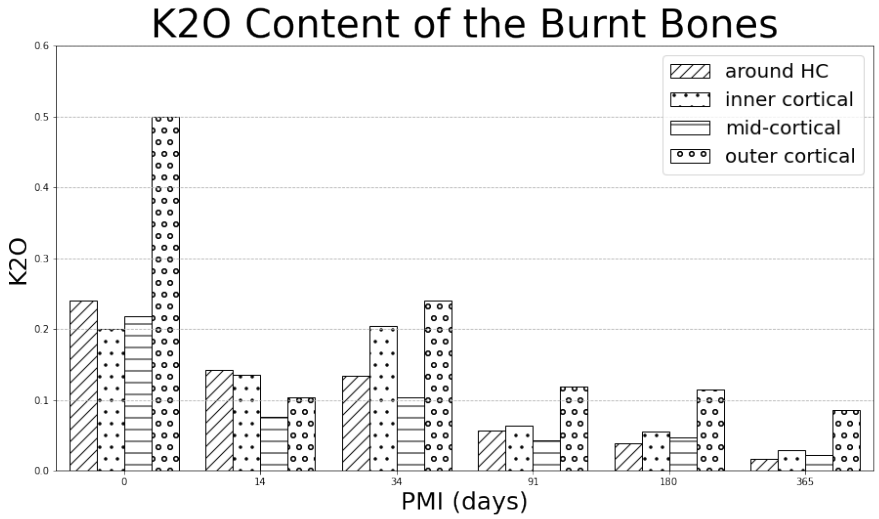

FeO Content in the Cortical Ends of the Bones
State
unburnt
burnt
FeO
0.12
0.10
0.08
0.06
0.04
0.02
0.00
0
14
34
91
180
365
PMI (days)

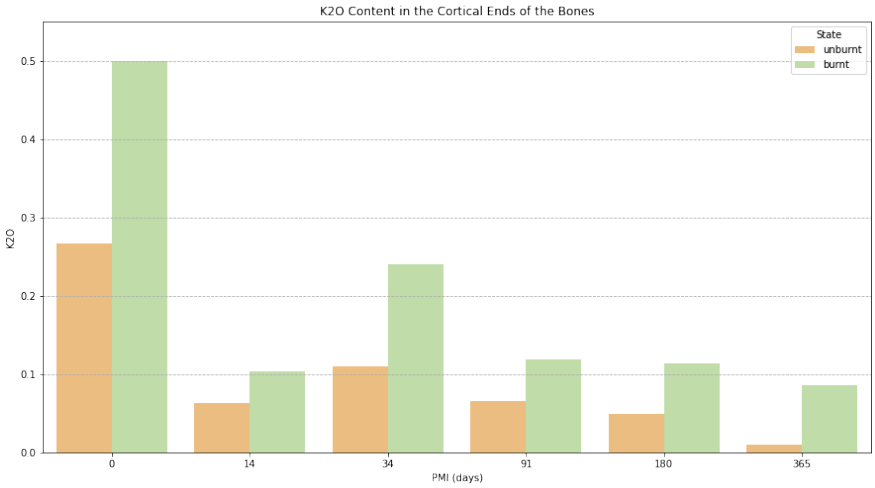

FeO Content in the Mid-Cortical Regions of the Bones
State
unburnt
burnt
FeO
0.014
0.012
0.010
0.008
0.006
0.004
0.002
0.000
0
14
34
91
180
365
PMI (days)

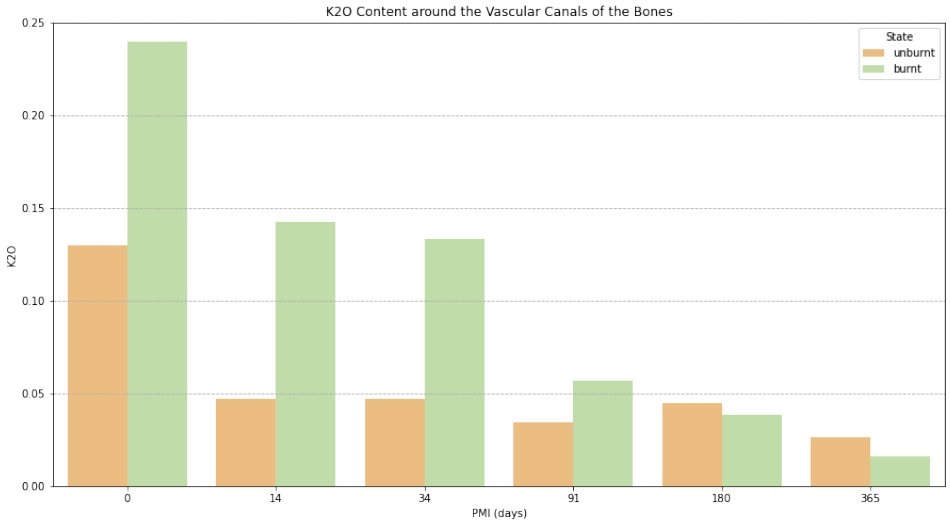

FeO Content in the Trabecular Ends of the Bones
State
unburnt
burnt
FeO
0.035
0.030
0.025
0.020
0.015
0.010
0.005
0.000
0
14
34
91
180
365
PMI (days)

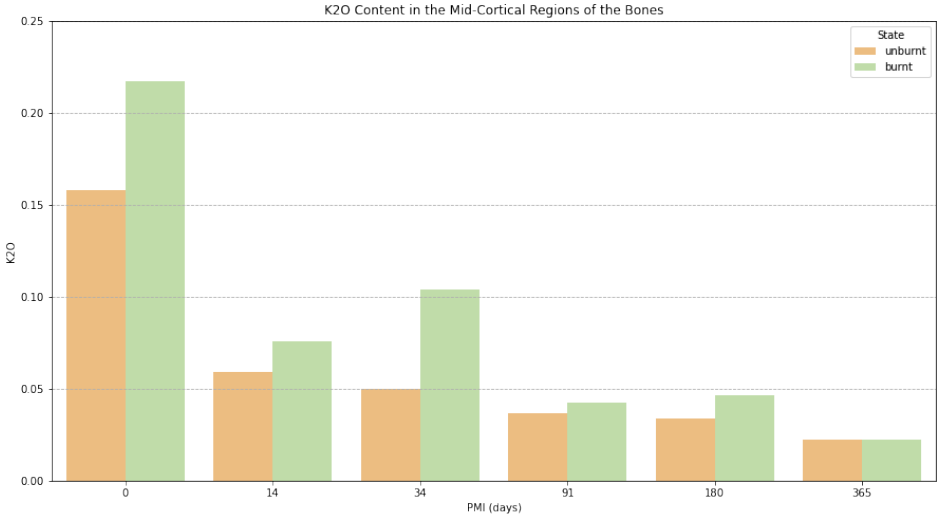
Appendix D.4.5: Potassium

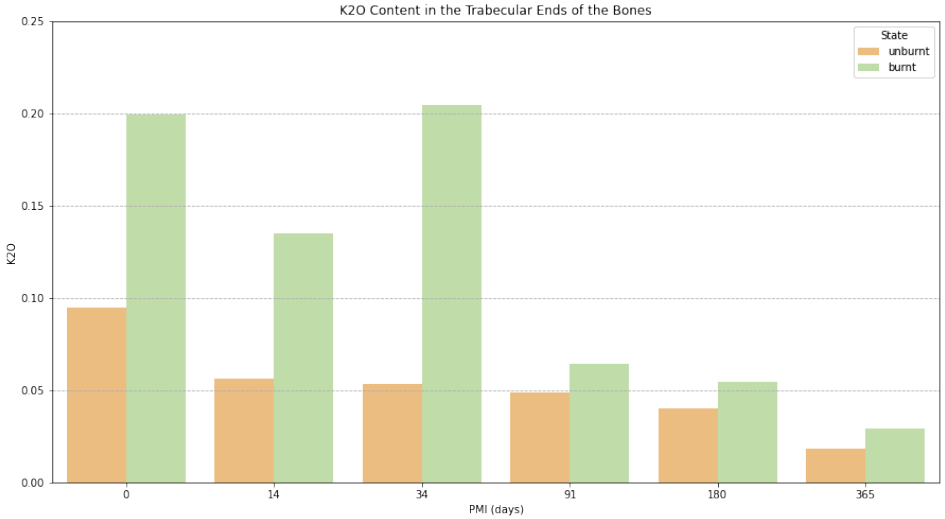




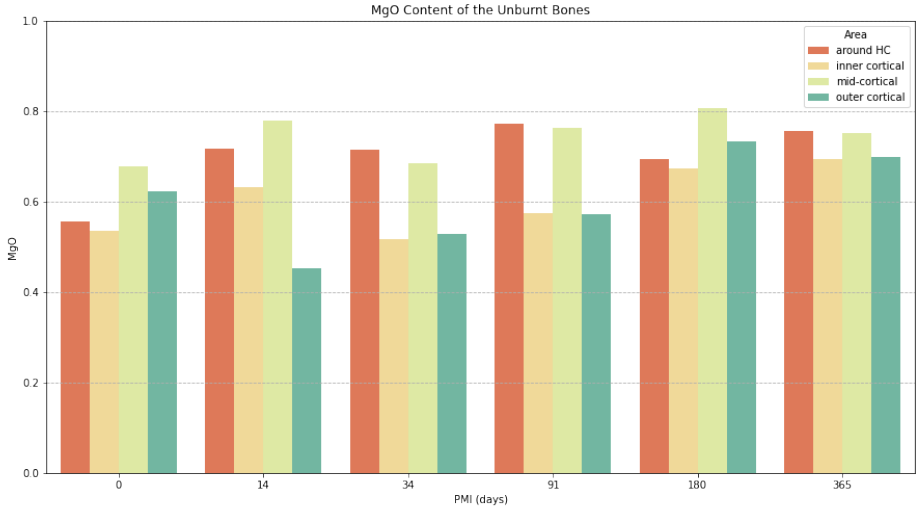


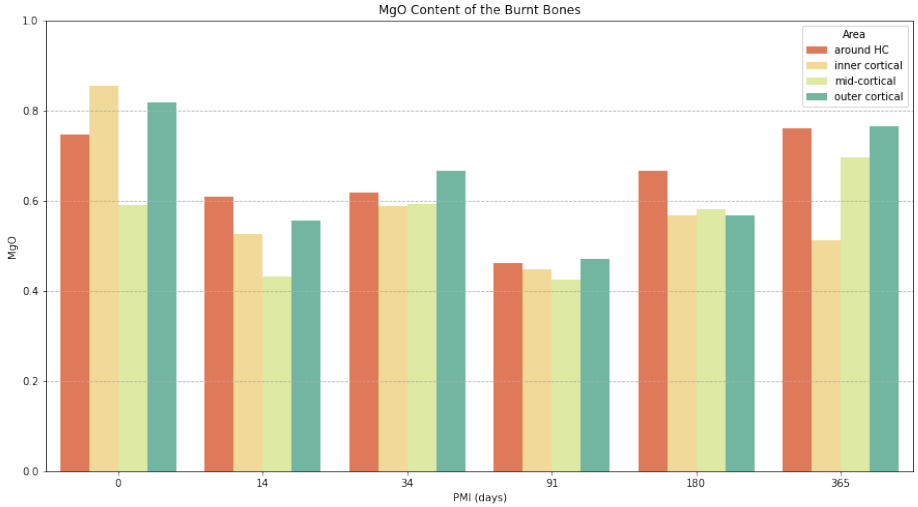

K2O Content around the Vascular Canals of the Bones
State
unburnt
burnt
K2O
0.25
0.20
0.15
0.10
0.05
0.00
0
14
34
91
180
365
PMI (days)

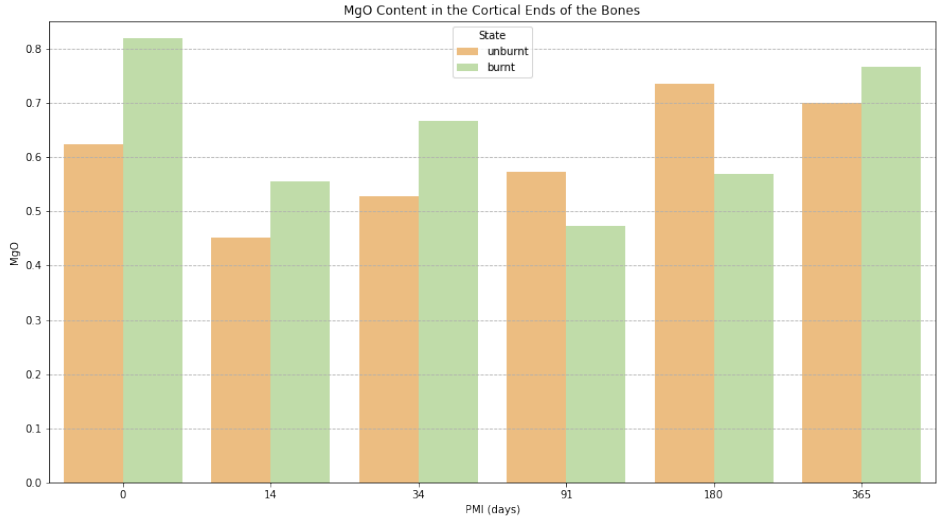

K2O Content in the Mid-Cortical Regions of the Bones
State
unburnt
burnt
K2O
0.25
0.20
0.15
0.10
0.05
0.00
0
14
34
91
180
365
PMI (days)

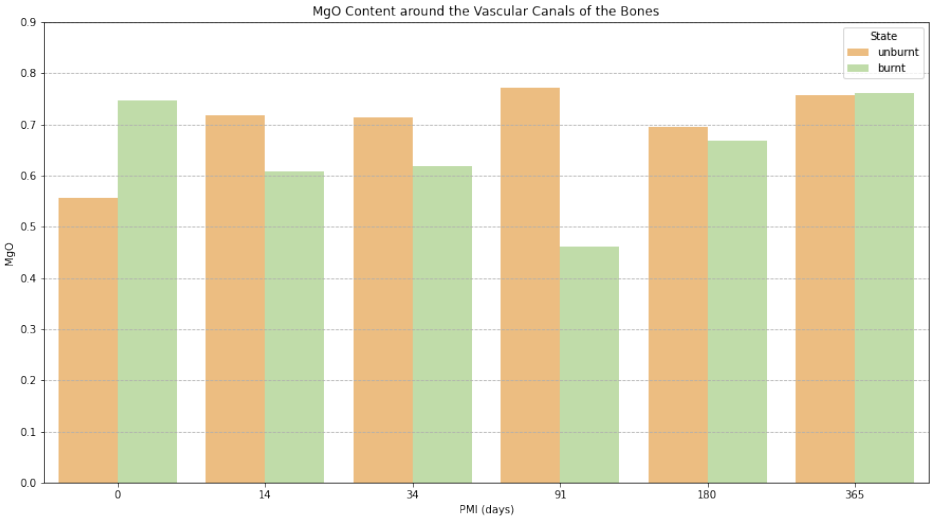

K2O Content in the Trabecular Ends of the Bones
State
unburnt
burnt
K2O
0.25
0.20
0.15
0.10
0.05
0.00
0
14
34
91
180
365
PMI (days)

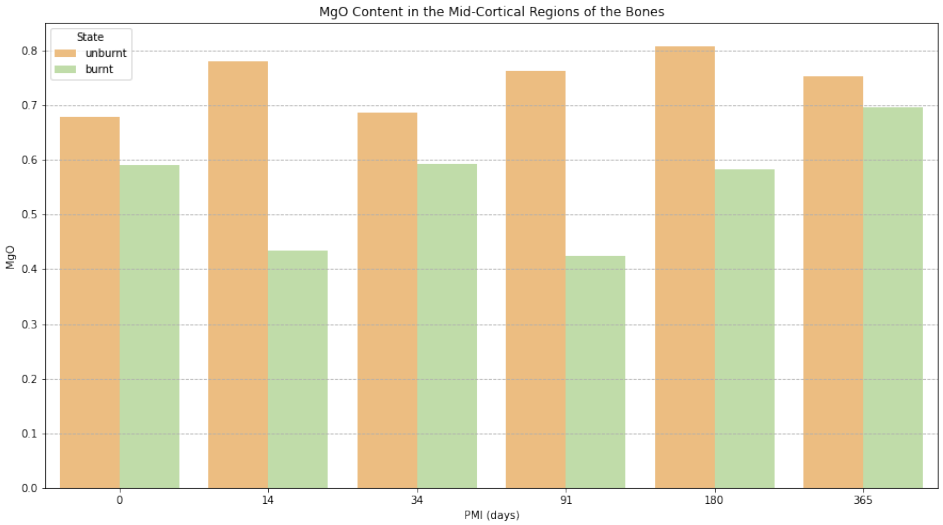
Appendix D.4.6: Magnesium

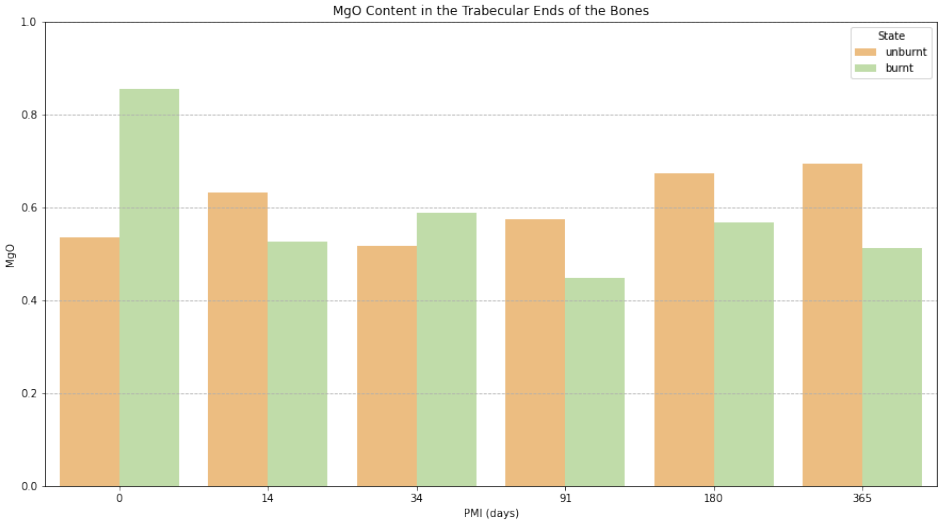




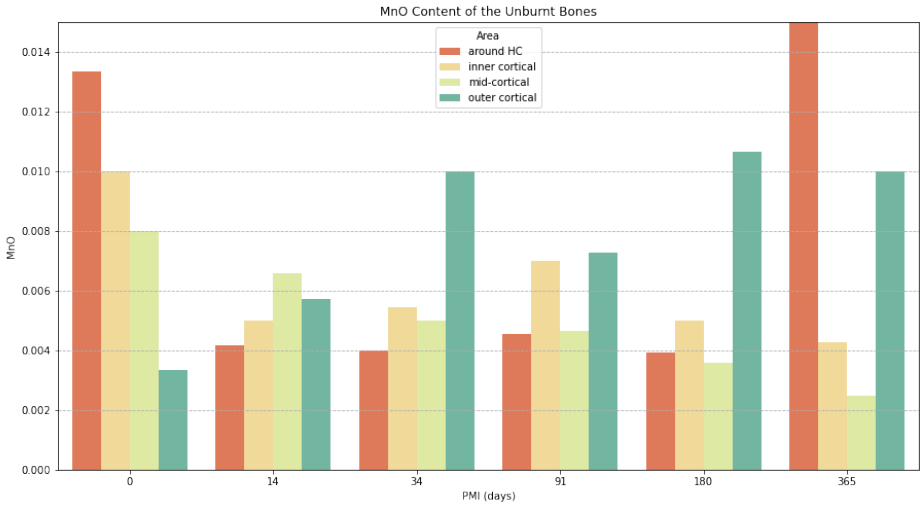


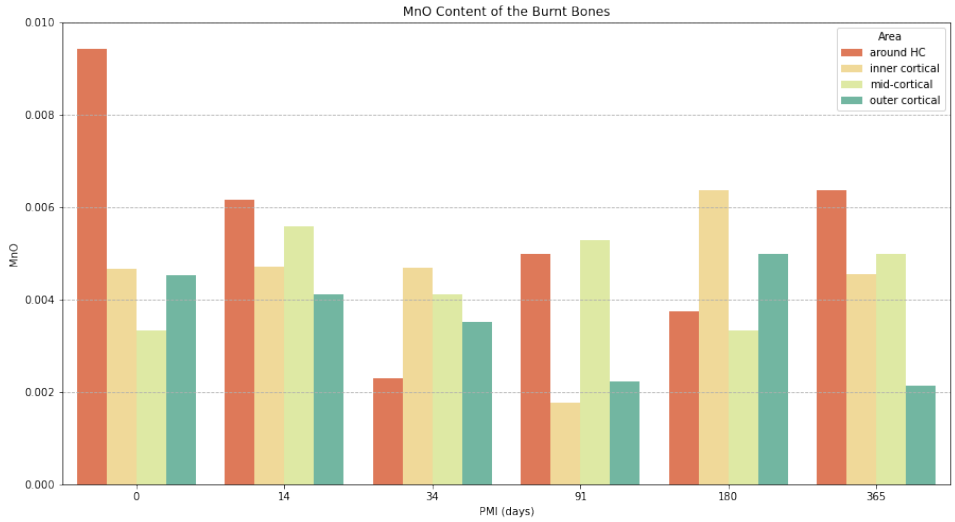

MgO Content around the Vascular Canals of the Bones
State
unburnt
burnt
MgO
PMI (days)
0
14
34
91
180
365

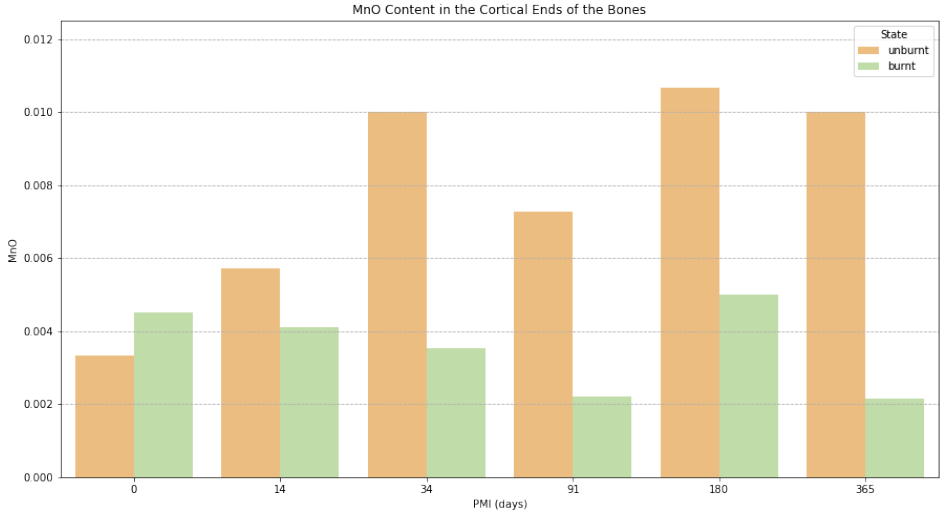

MgO Content in the Mid-Cortical Regions of the Bones
State
unburnt
burnt
MgO
PMI (days)
0
14
34
91
180
365

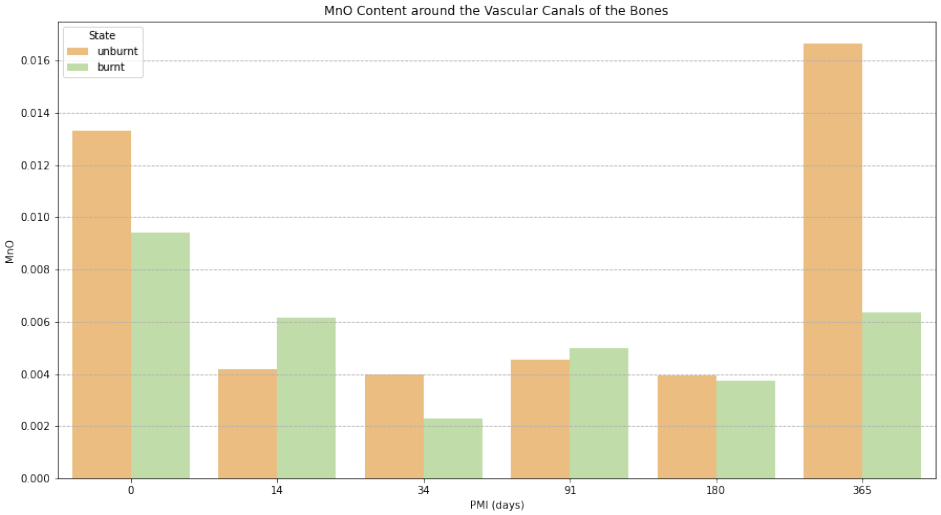

MgO Content in the Trabecular Ends of the Bones
State
unburnt
burnt
MgO
PMI (days)
0
14
34
91
180
365

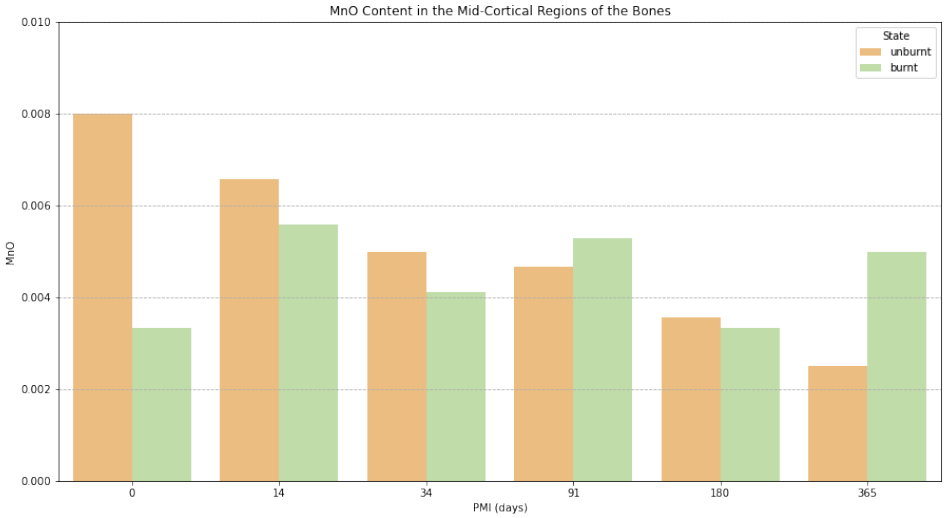
Appendix D.4.7: Manganese

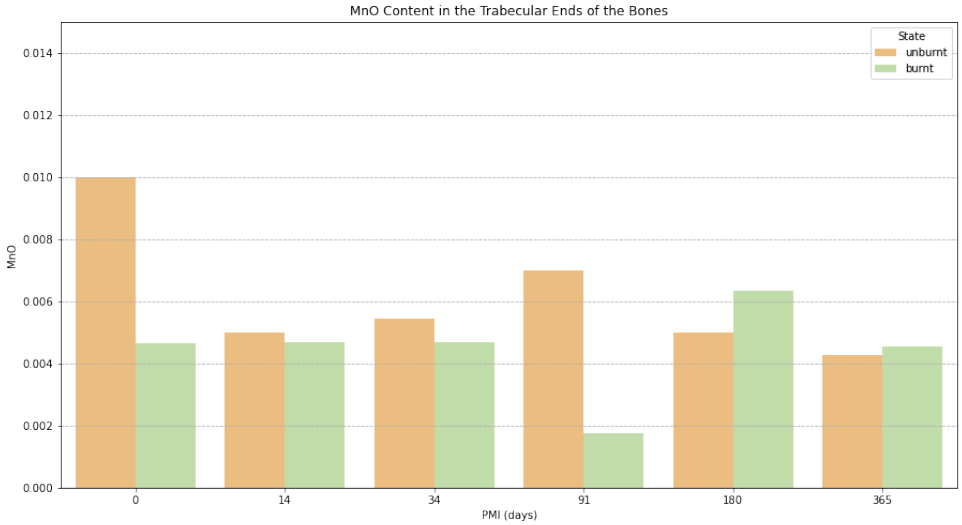




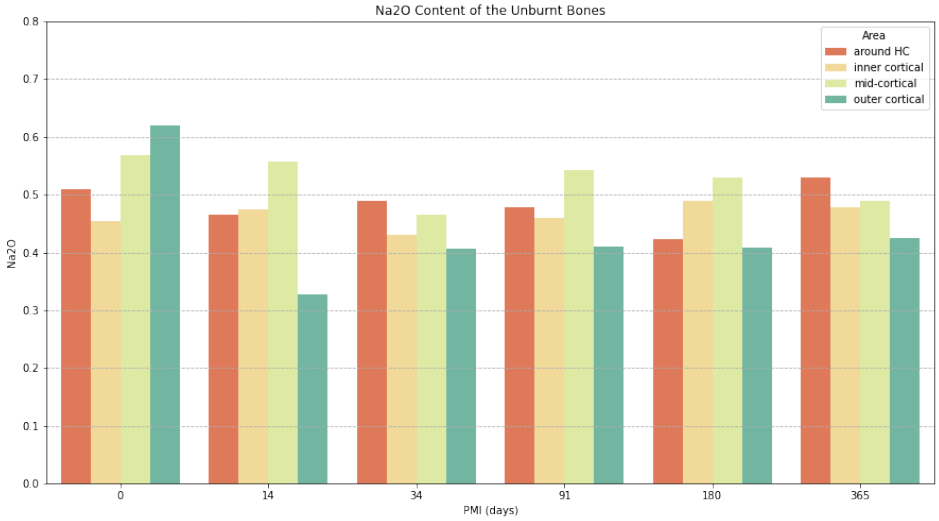


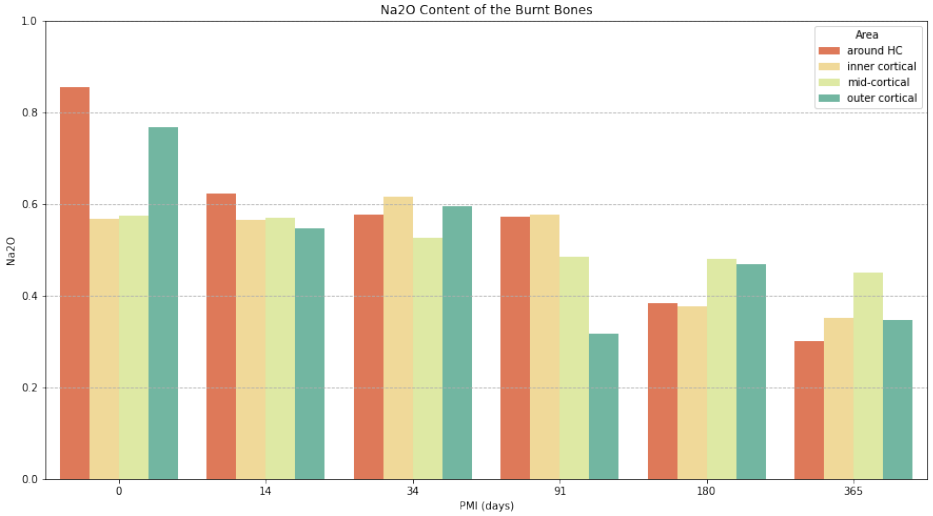

MnO Content around the Vascular Canals of the Bones
State
unburnt
burnt
MnO
0.016
0.014
0.012
0.010
0.008
0.006
0.004
0.002
0.000
0
14
34
91
180
365
PMI (days)

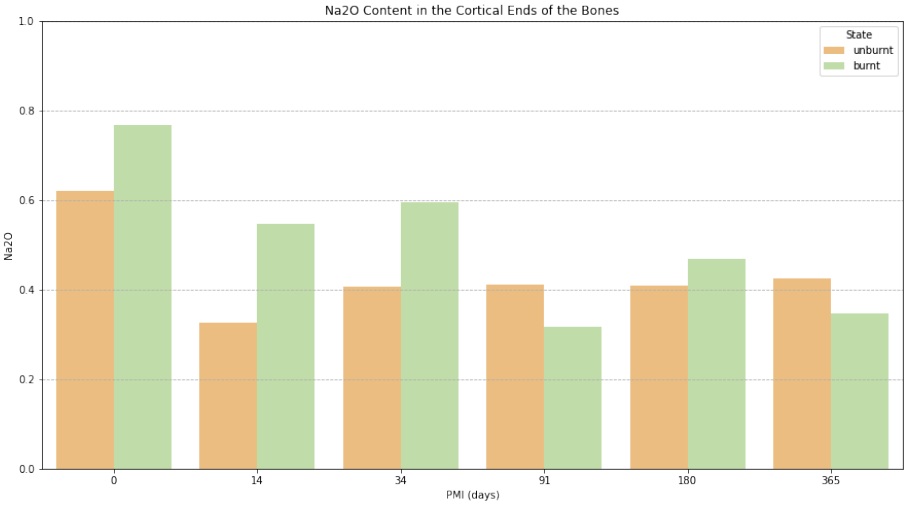

MnO Content in the Mid-Cortical Regions of the Bones
State
unburnt
burnt
MnO
0.010
0.008
0.006
0.004
0.002
0.000
0
14
34
91
180
365
PMI (days)

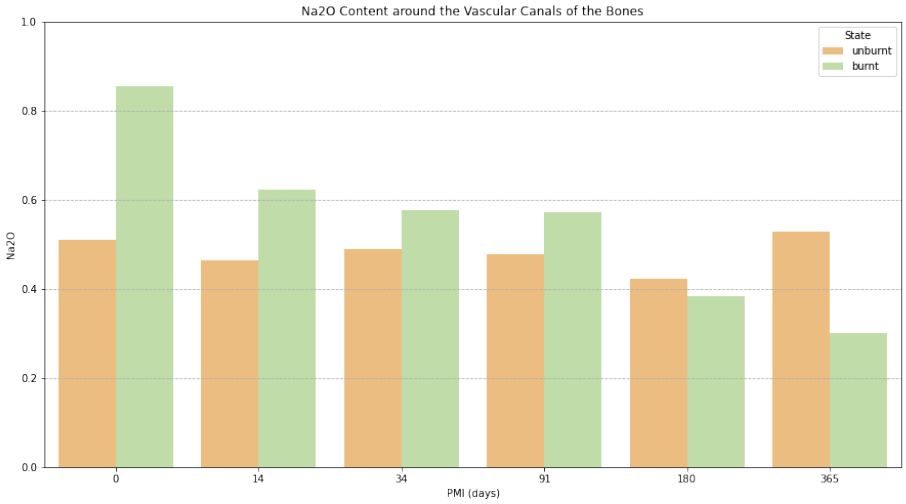

MnO Content in the Trabecular Ends of the Bones
State
unburnt
burnt
MnO
0.014
0.012
0.010
0.008
0.006
0.004
0.002
0.000
0
14
34
91
180
365
PMI (days)

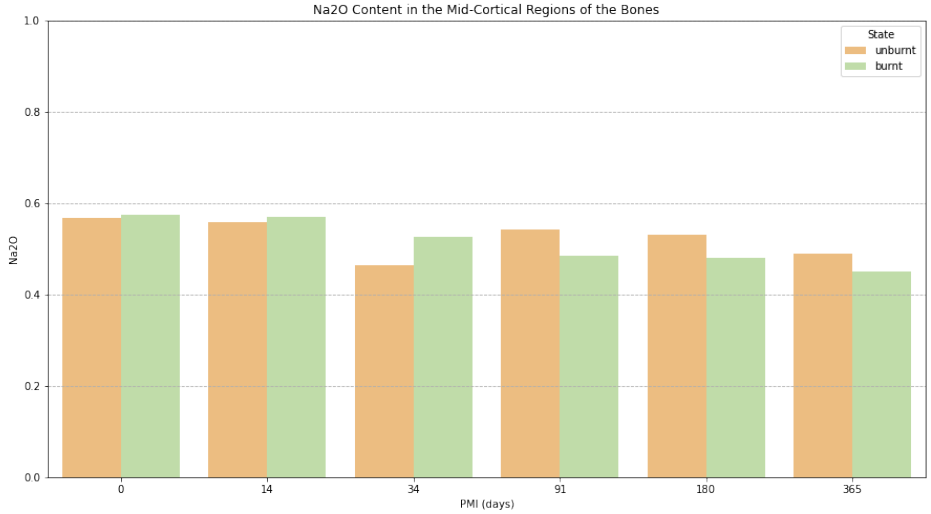
Appendix D.4.8: Sodium

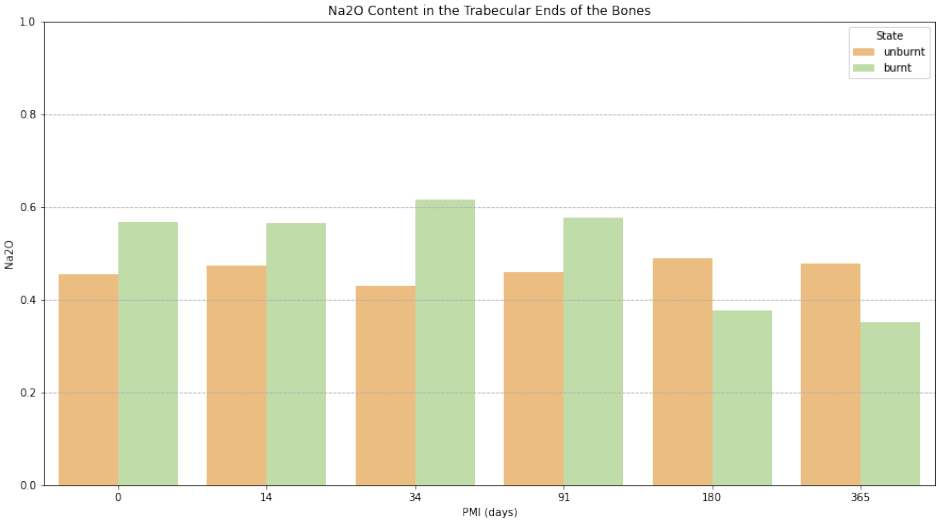




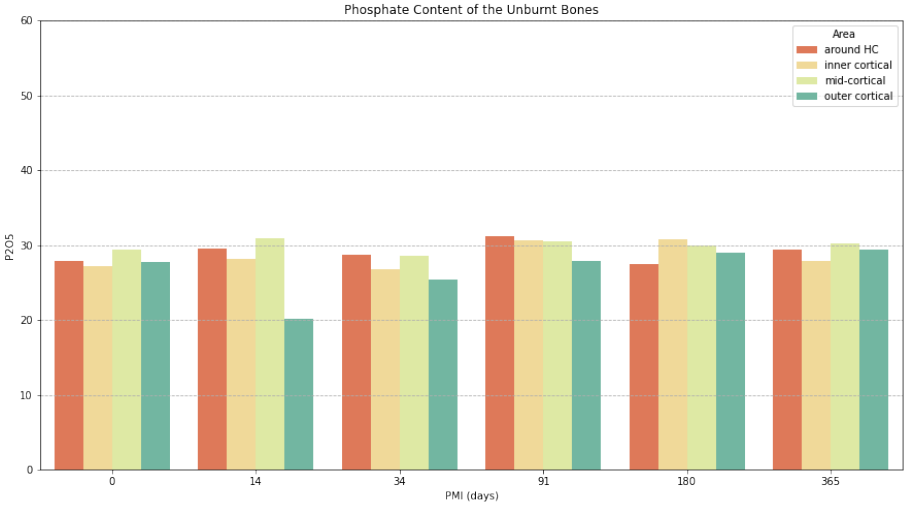


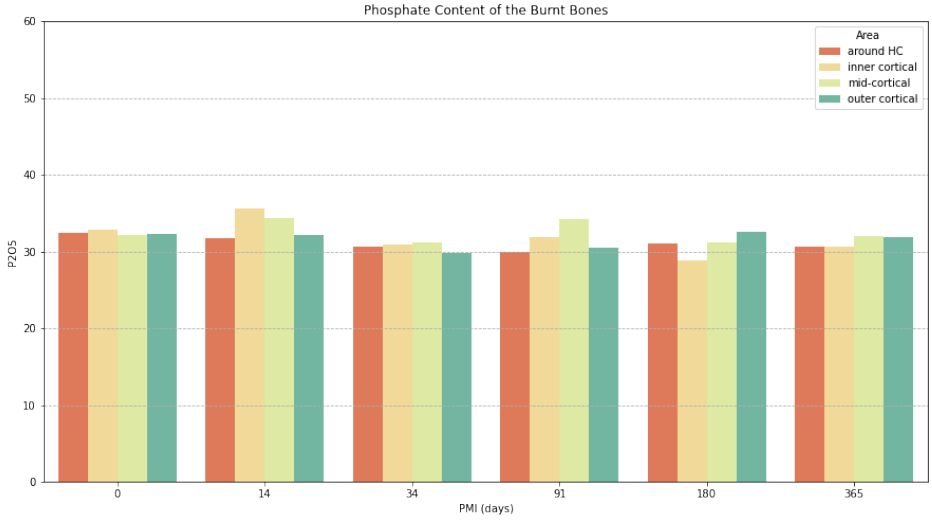

Na2O Content around the Vascular Canals of the Bones
State
unburnt
burnt
Na2O
1.0
0.8
0.6
0.4
0.2
0.0
0
14
34
91
180
365
PMI (days)

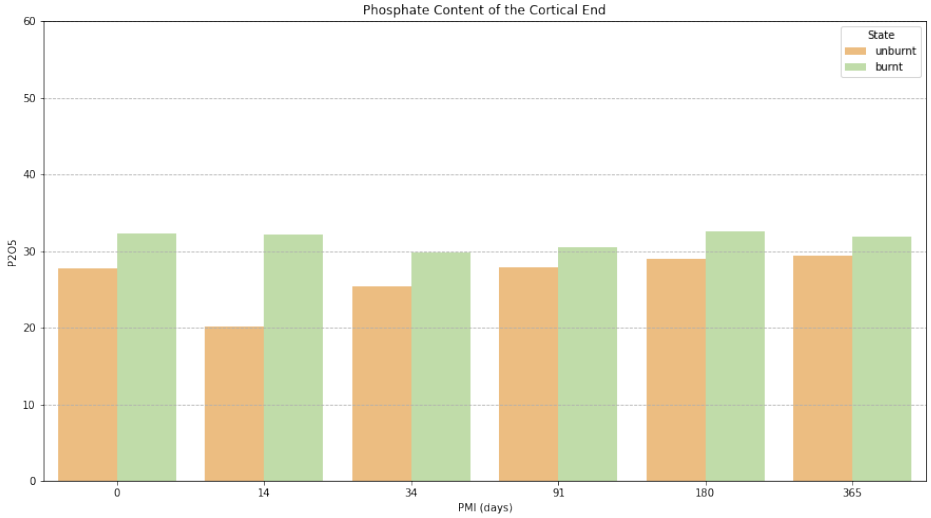

Na2O Content in the Mid-Cortical Regions of the Bones
State
unburnt
burnt
Na2O
1.0
0.8
0.6
0.4
0.2
0.0
0
14
34
91
180
365
PMI (days)

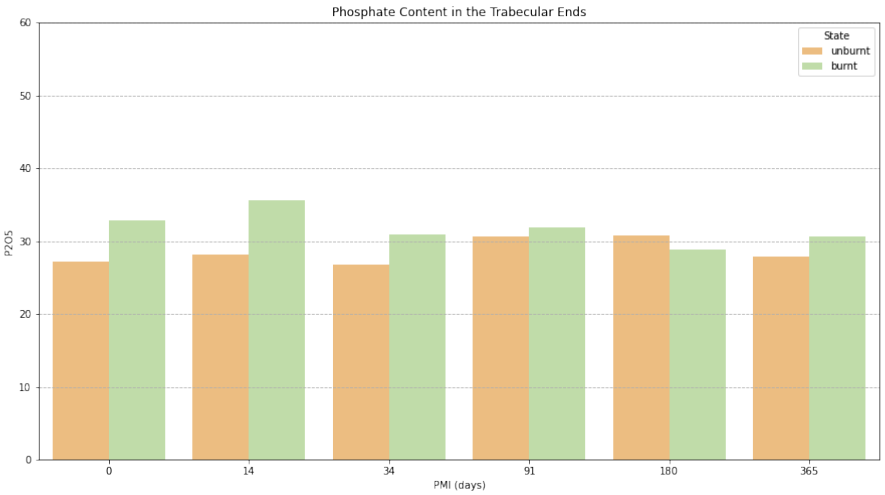

Na2O Content in the Trabecular Ends of the Bones
State
unburnt
burnt
Na2O
1.0
0.8
0.6
0.4
0.2
0.0
0
14
34
91
180
365
PMI (days)

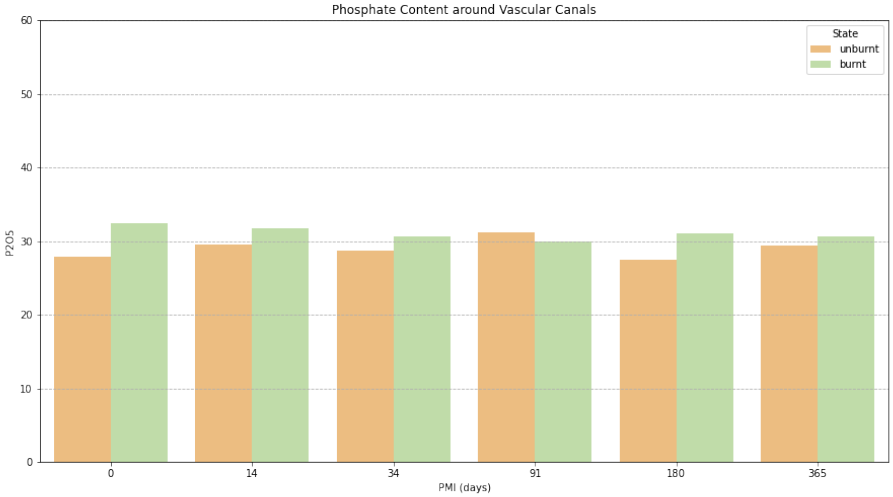
Appendix D.4.9: Phosphorus



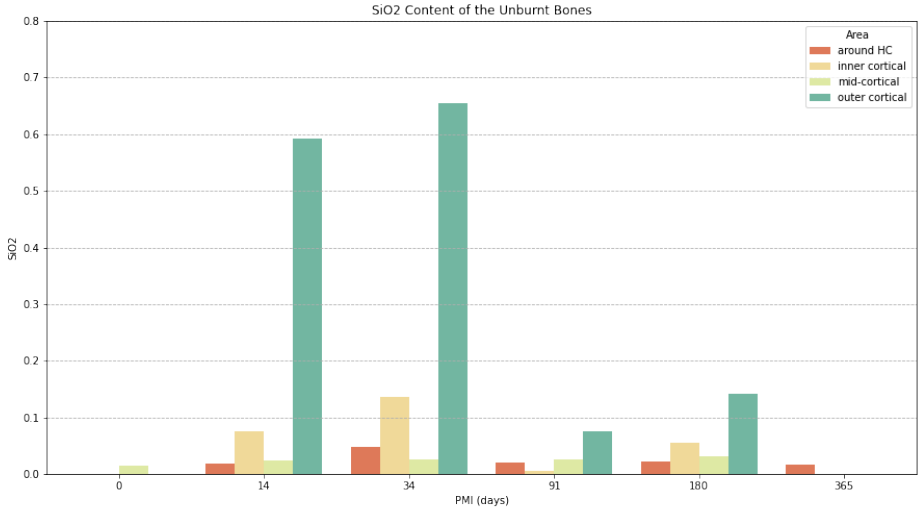


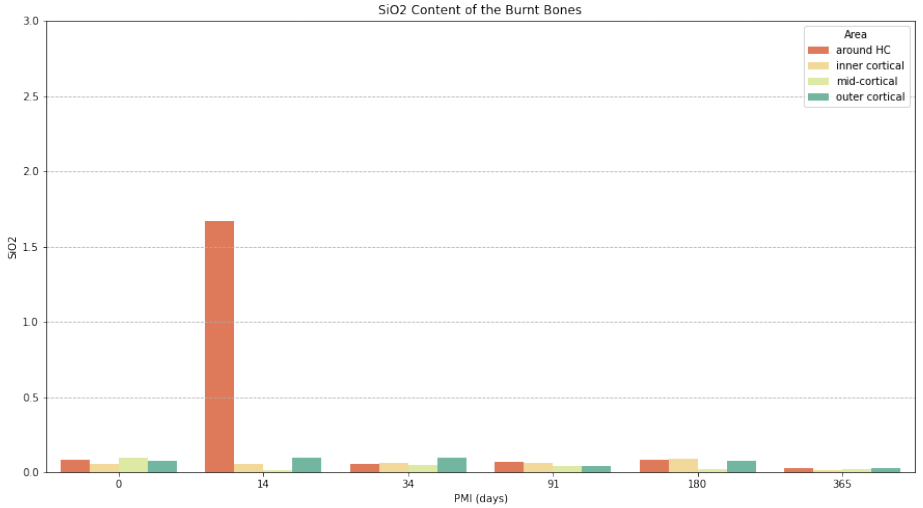


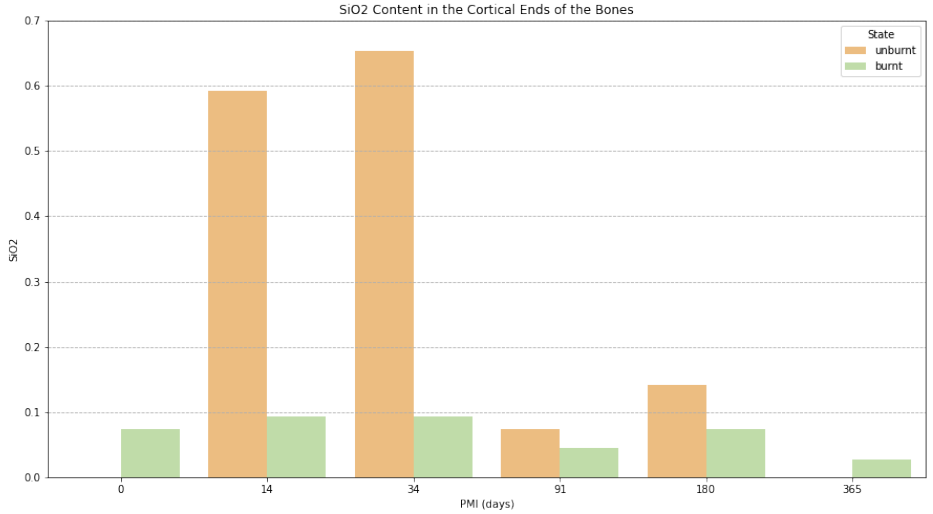

Phosphate Content in the Trabecular Ends
State
unburnt
burnt
P2O5
PMI (days)
0
14
34
91
180
365
0
10
20
30
40
50
60

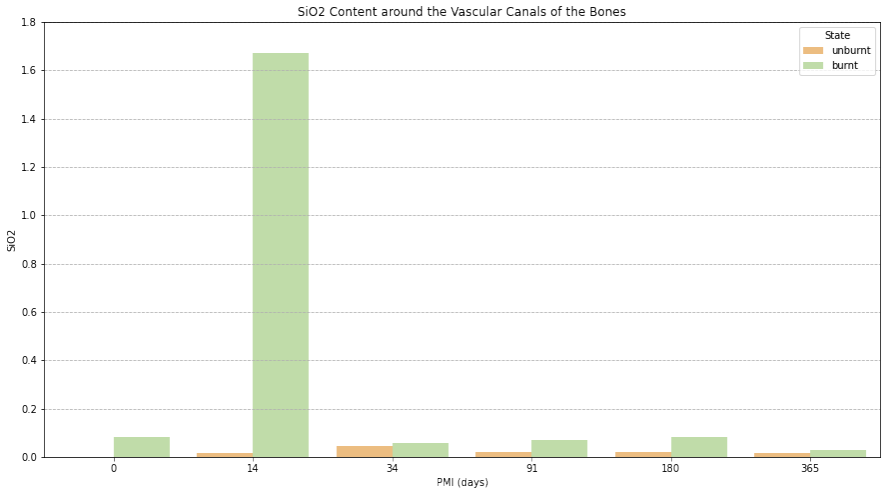

Phosphate Content around Vascular Canals
State
unburnt
burnt
P2O5
PMI (days)
0
14
34
91
180
365
0
10
20
30
40
50
60

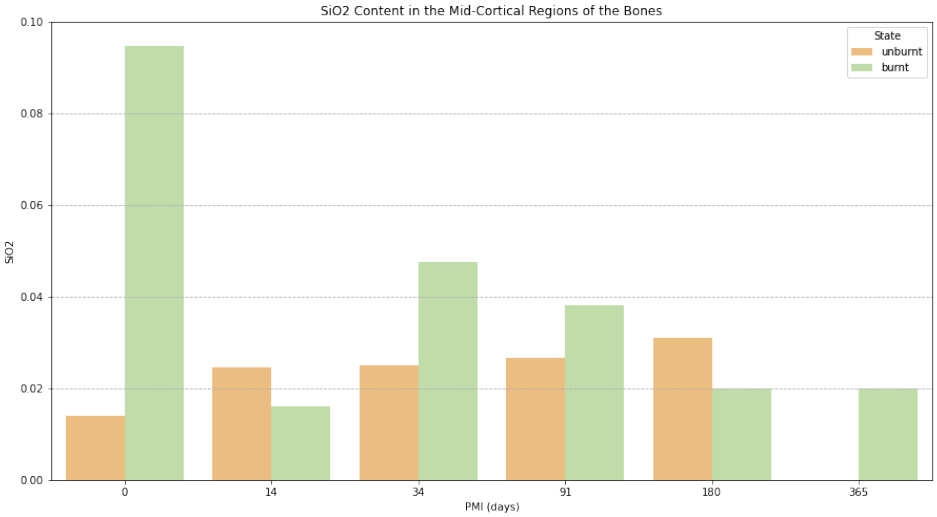
Appendix D.4.10: Silicon

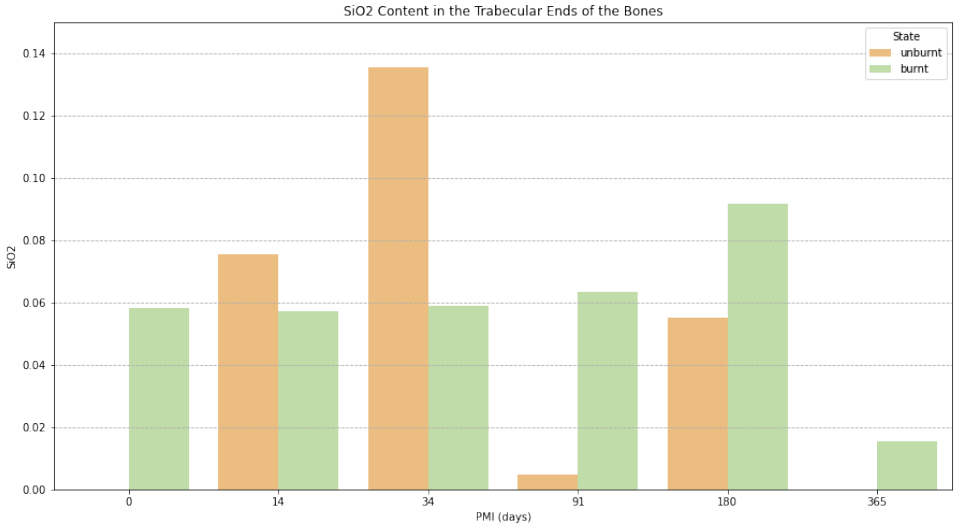




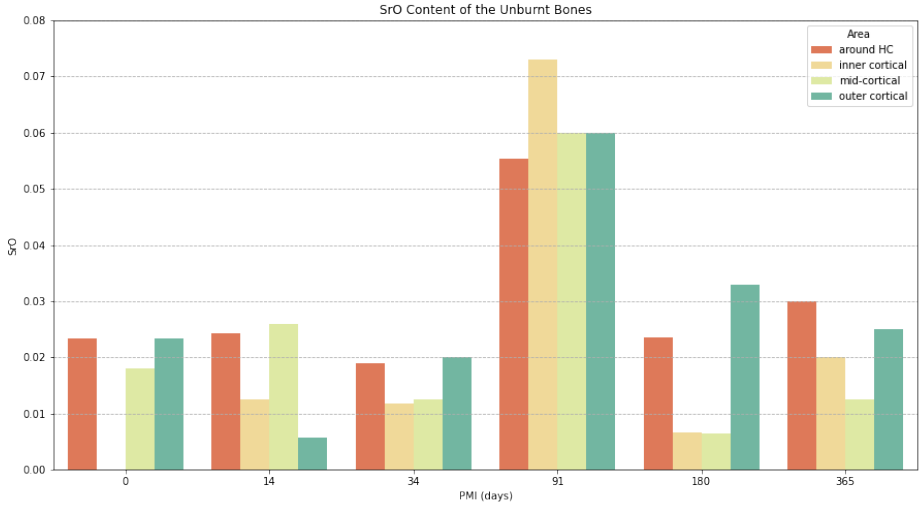


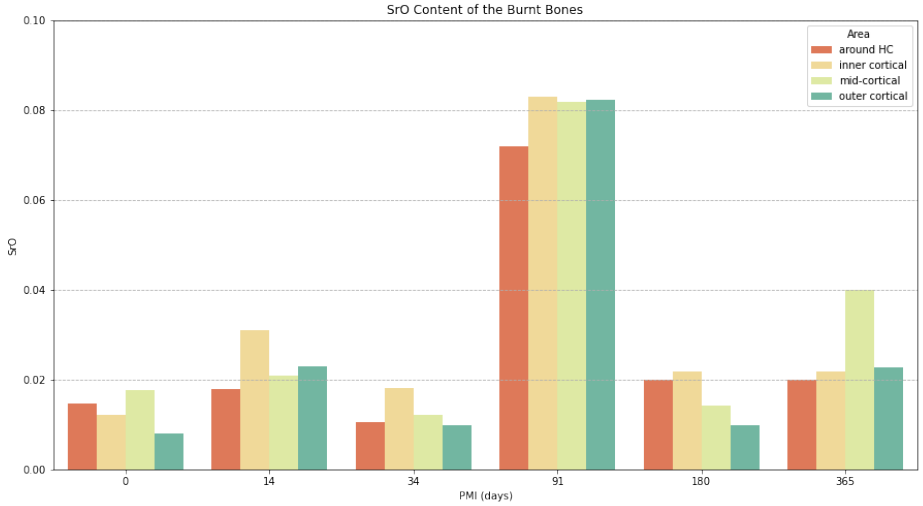

SiO2 Content around the Vascular Canals of the Bones
State
unburnt
burnt
SiO2
PMI (days)
0
14
34
91
180
365

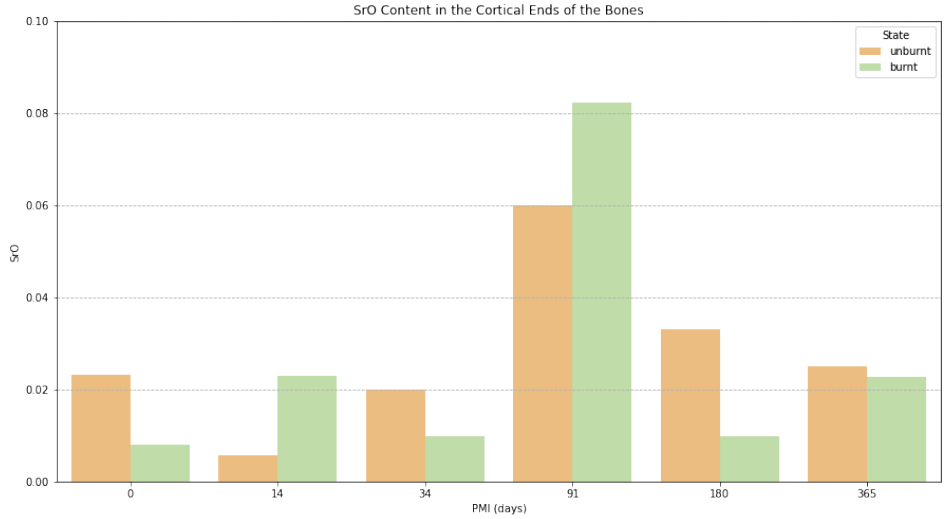

SiO2 Content in the Mid-Cortical Regions of the Bones
State
unburnt
burnt
SiO2
PMI (days)
0
14
34
91
180
365

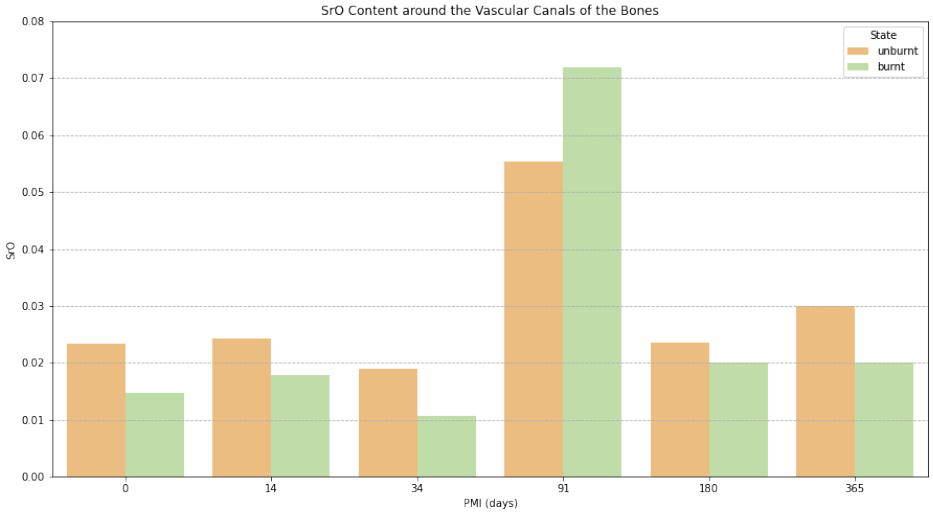

SiO2 Content in the Trabecular Ends of the Bones
State
unburnt
burnt
SiO2
PMI (days)
0
14
34
91
180
365

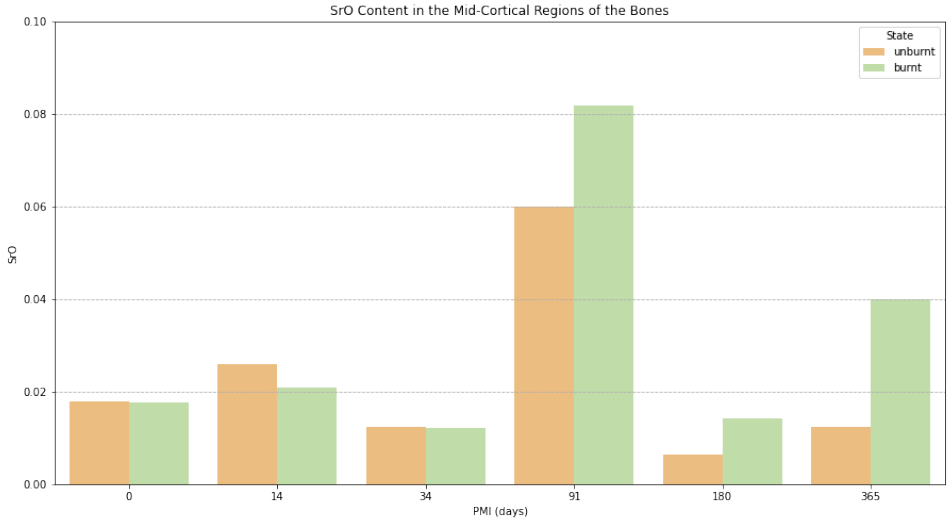
Appendix D.4.11: Strontium

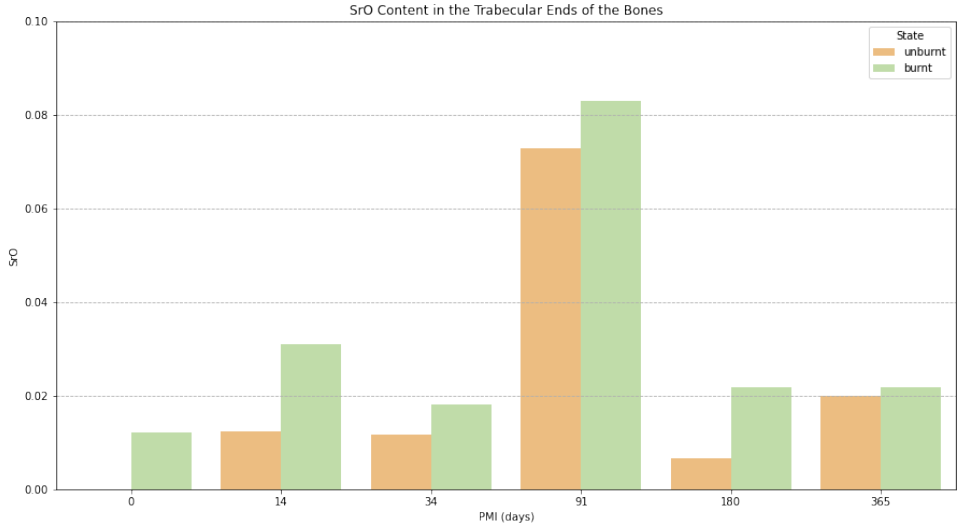






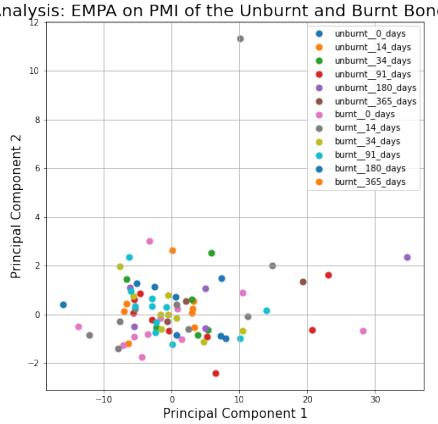

SrO Content around the Vascular Canals of the Bones
State
unburnt
burnt
SrO
0.08
0.07
0.06
0.05
0.04
0.03
0.02
0.01
0.00
0
14
34
91
180
365
PMI (days)


SrO Content in the Mid-Cortical Regions of the Bones
State
unburnt
burnt
SrO
0.10
0.08
0.06
0.04
0.02
0.00
0
14
34
91
180
365
PMI (days)

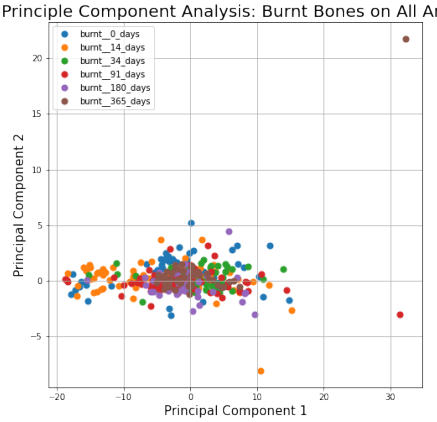

SrO Content in the Trabecular Ends of the Bones
State
unburnt
burnt
SrO
0.10
0.08
0.06
0.04
0.02
0.00
0
14
34
91
180
365
PMI (days)

Appendix D.5: PCA Scree Plots from EMPA Dataset

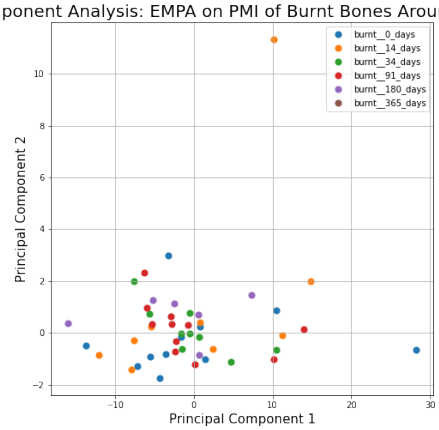
Analysis: EMPA on PMI of the Unburnt and Burnt Bones A



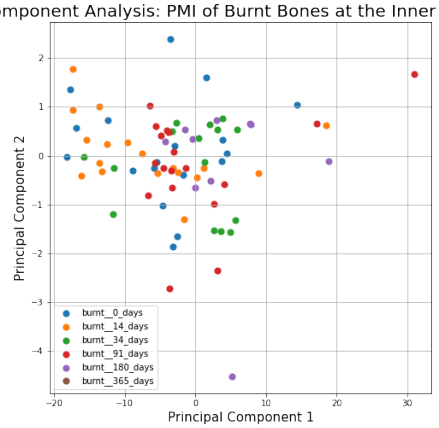
Principle Component Analysis: Burnt Bones on All Areas



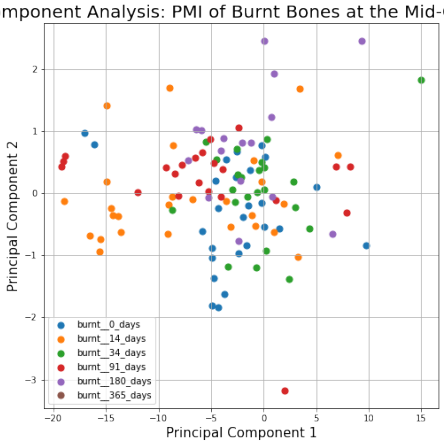
nponent Analysis: EMPA on PMI of Burnt Bones Around Va



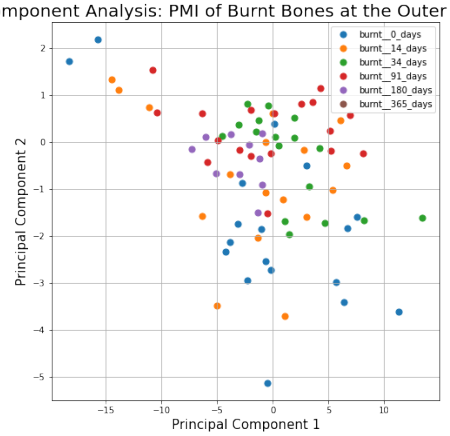
omponent Analysis: PMI of Burnt Bones at the Inner Corti



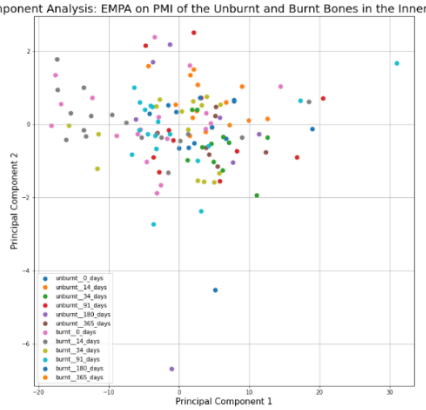
Component Analysis: PMI of Burnt Bones at the Mid-Cortic



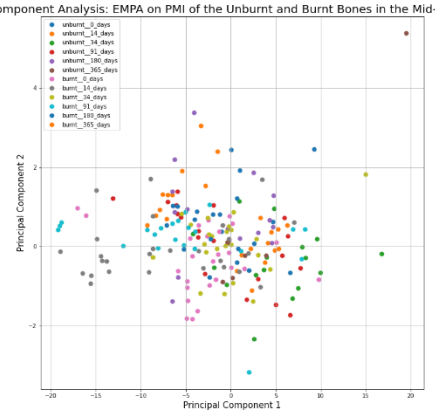
omponent Analysis: PMI of Burnt Bones at the Outer Cort



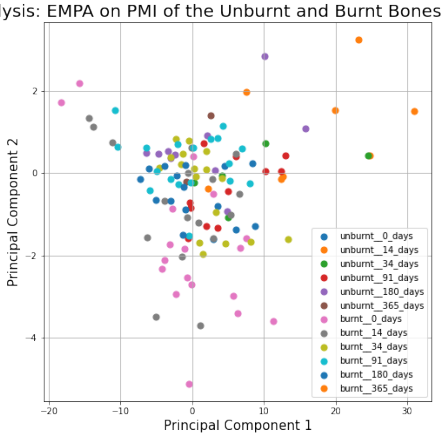
Component Analysis: EMPA on PMI of the Unburnt and Burnt Bones in the Inner Cortic



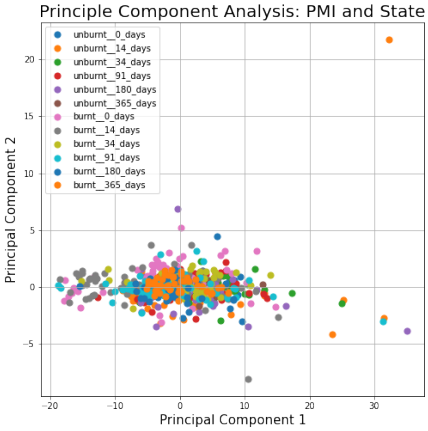
Component Analysis: EMPA on PMI of the Unburnt and Burnt Bones in the Mid-Cortica



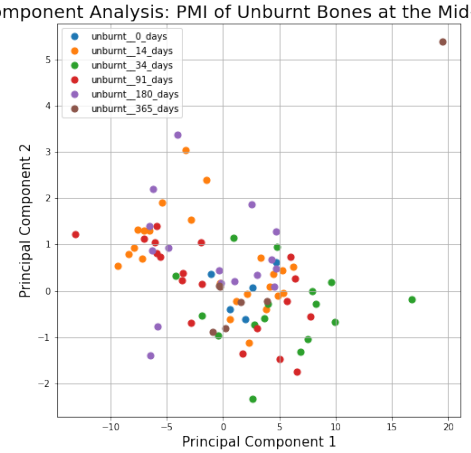
nalysis: EMPA on PMI of the Unburnt and Burnt Bones in th



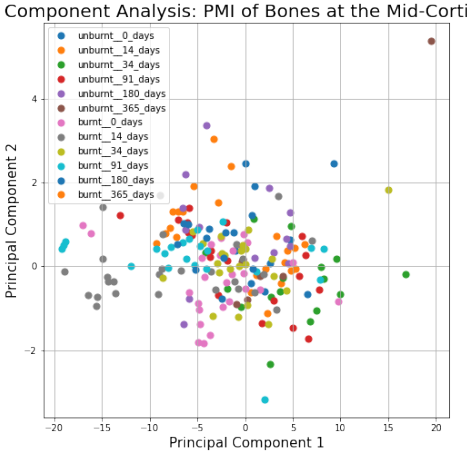
Principle Component Analysis: PMI and State



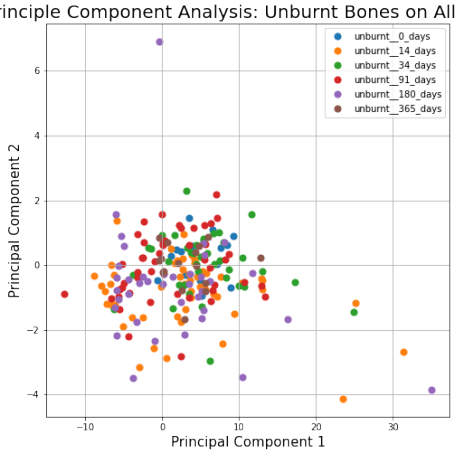
omponent Analysis: PMI of Unburnt Bones at the Mid-Cort



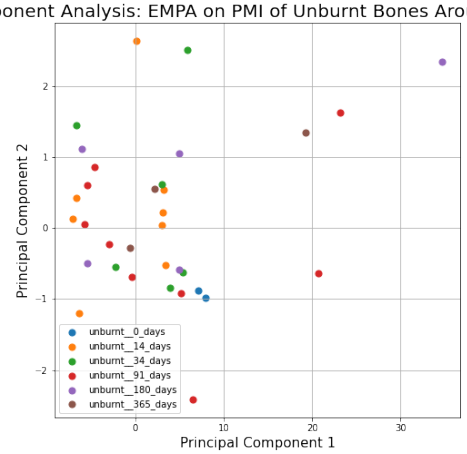
le Component Analysis: PMI of Bones at the Mid-Cortical



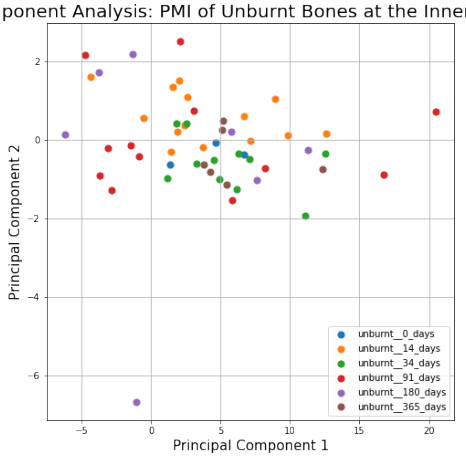
Principle Component Analysis: Unburnt Bones on All Area



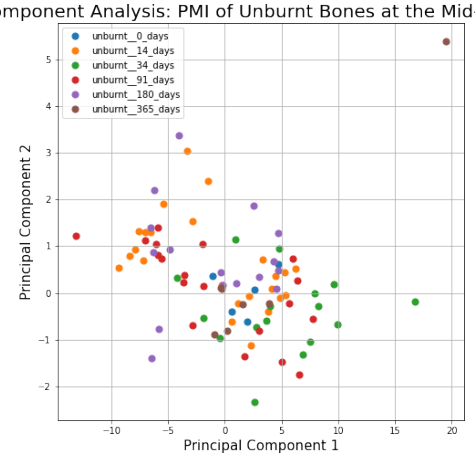
ponent Analysis: EMPA on PMI of Unburnt Bones Around \



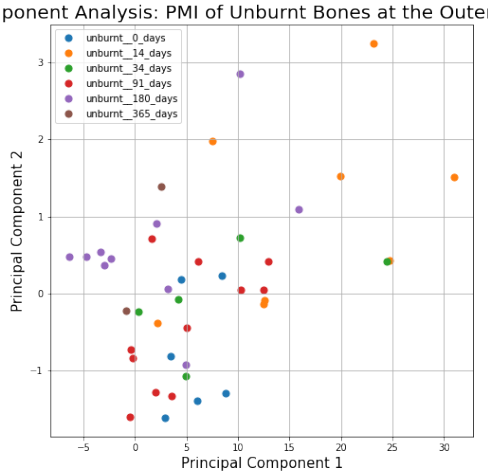
mponent Analysis: PMI of Unburnt Bones at the Inner Cor



omponent Analysis: PMI of Unburnt Bones at the Mid-Cort

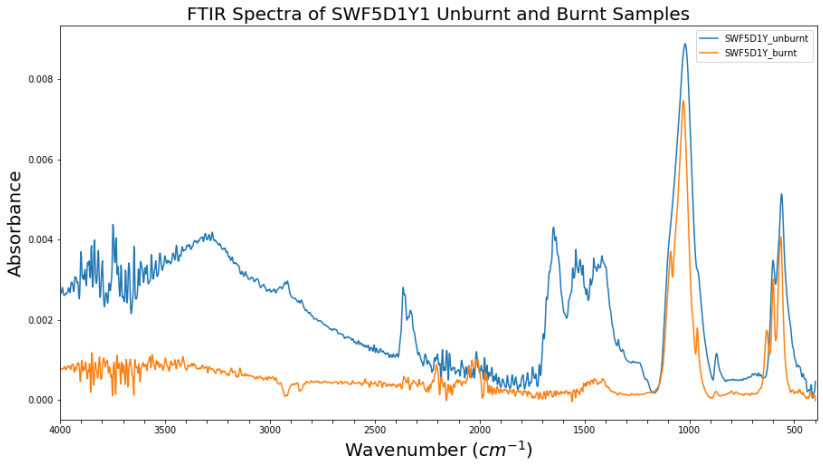


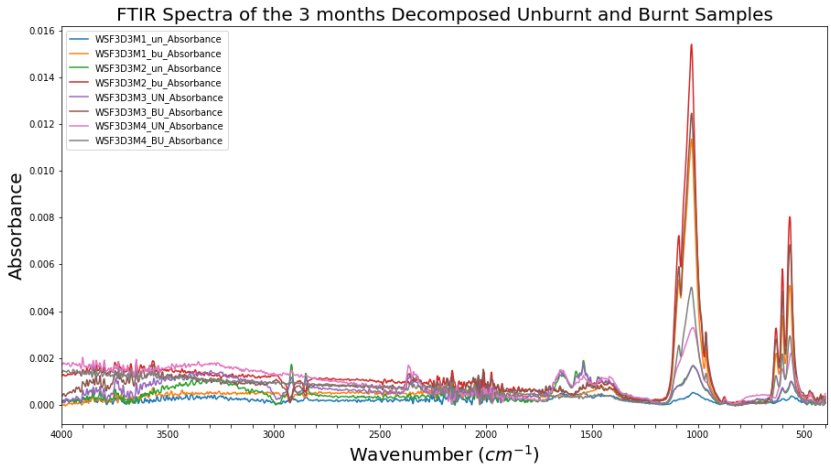
mponent Analysis: PMI of Unburnt Bones at the Outer Cor

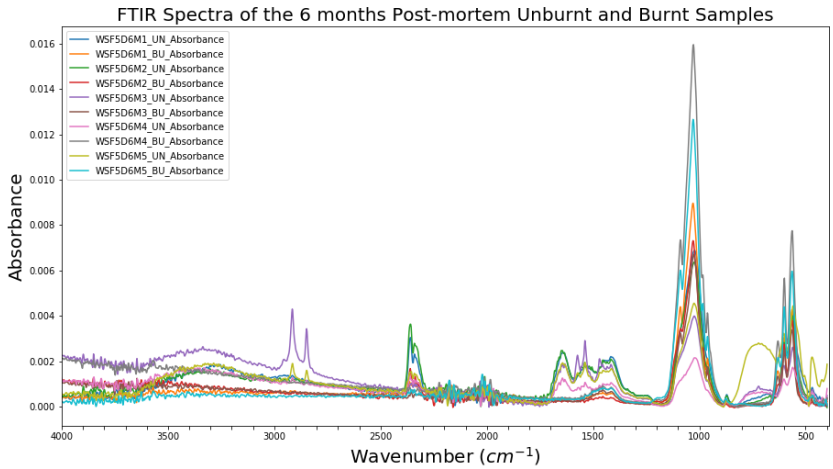


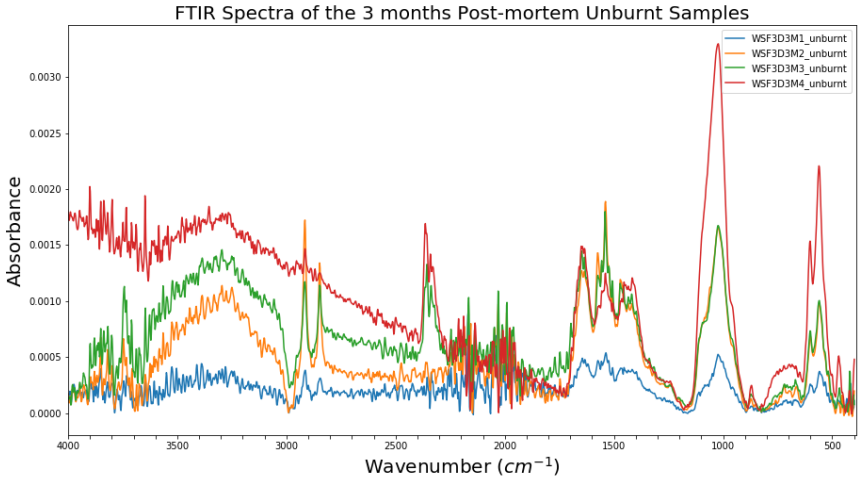
Appendix E: FTIR Data

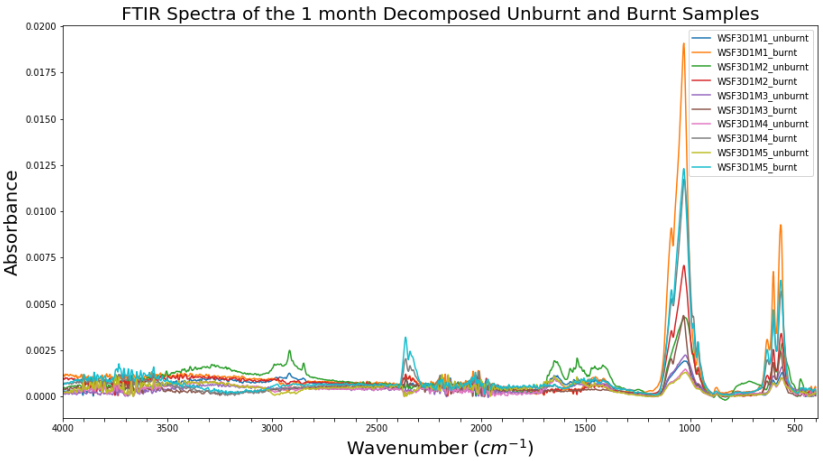
Appendix E.1: IR Spectra

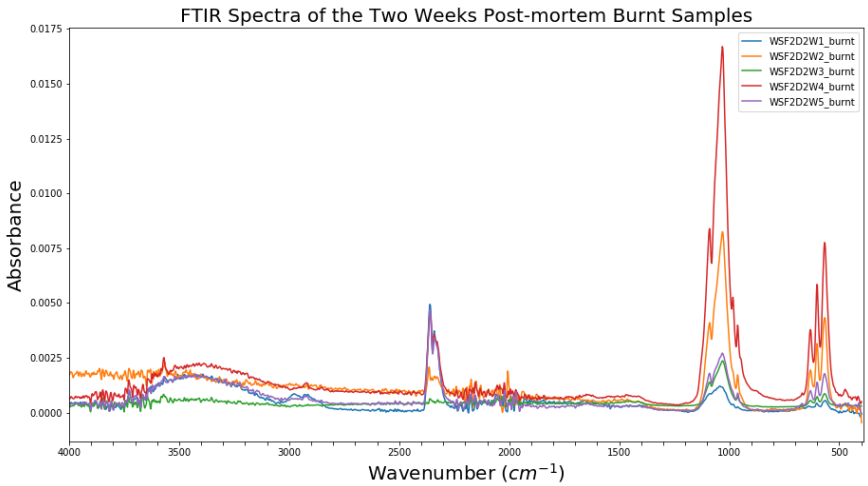


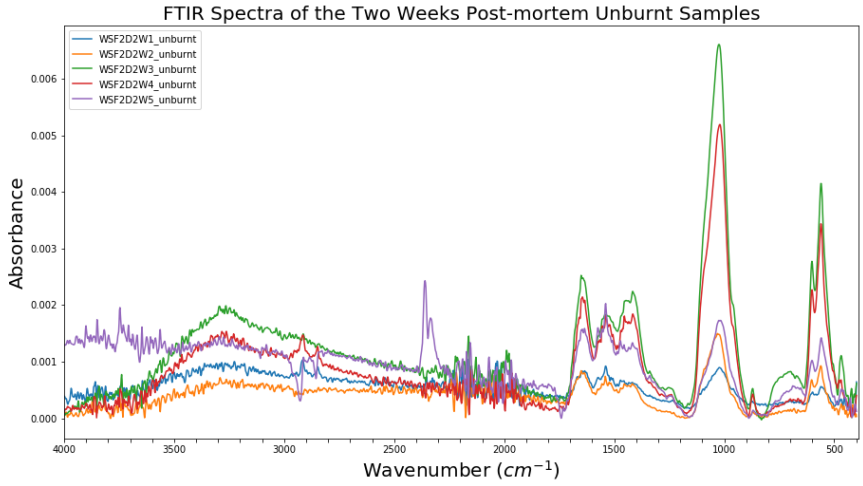


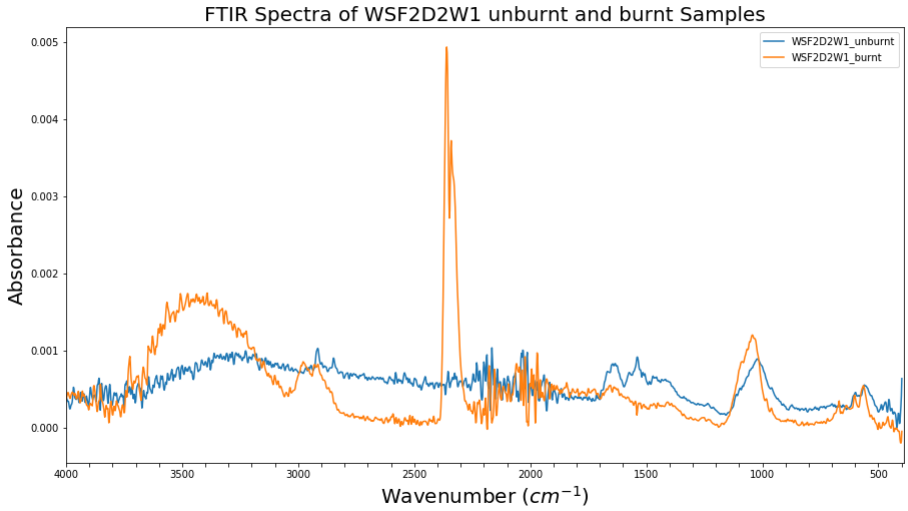


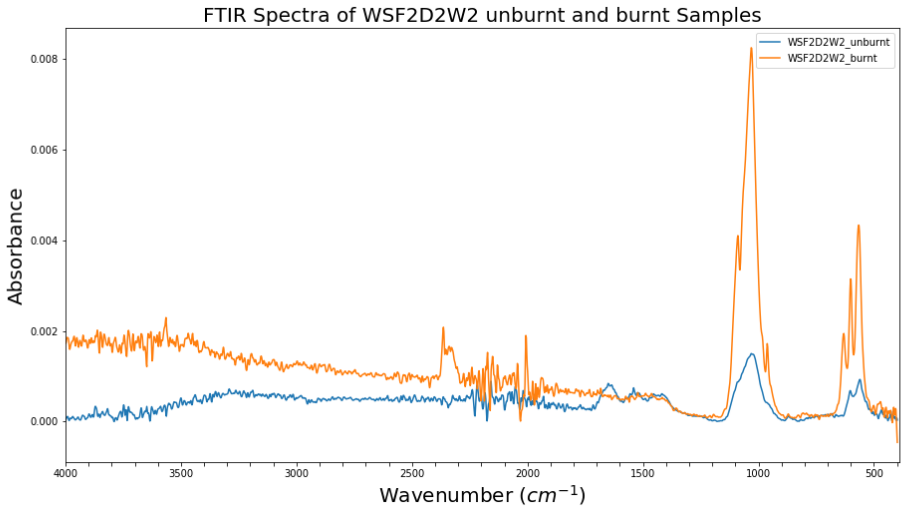

FTIR Spectra of the 3 months Post-mortem Unburnt Samples
WSF3D3M1_unburnt
WSF3D3M2_unburnt
WSF3D3M3_unburnt
WSF3D3M4_unburnt
Absorbance
Wavenumber (cm^{-1})

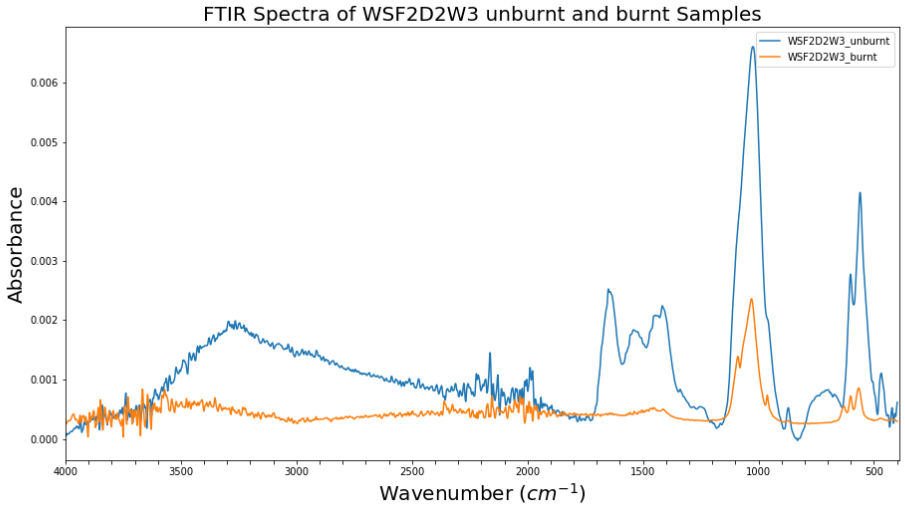

FTIR Spectra of the 1 month Decomposed Unburnt and Burnt Samples
WSF3D1M1_unburnt
WSF3D1M1_burnt
WSF3D1M2_unburnt
WSF3D1M2_burnt
WSF3D1M3_unburnt
WSF3D1M3_burnt
WSF3D1M4_unburnt
WSF3D1M4_burnt
WSF3D1M5_unburnt
WSF3D1M5_burnt
Absorbance
Wavenumber (cm^{-1})

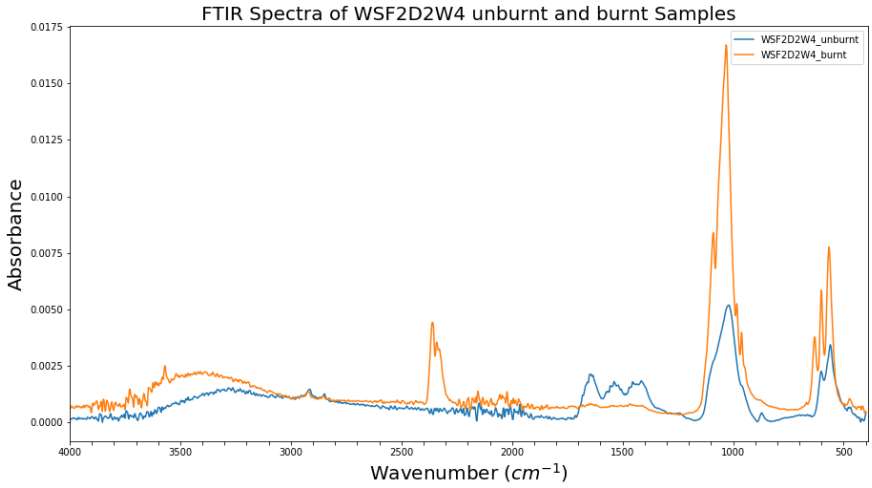

FTIR Spectra of the Two Weeks Post-mortem Burnt Samples
WSF2D2W1_burnt
WSF2D2W2_burnt
WSF2D2W3_burnt
WSF2D2W4_burnt
WSF2D2W5_burnt
Absorbance
Wavenumber (cm^{-1})

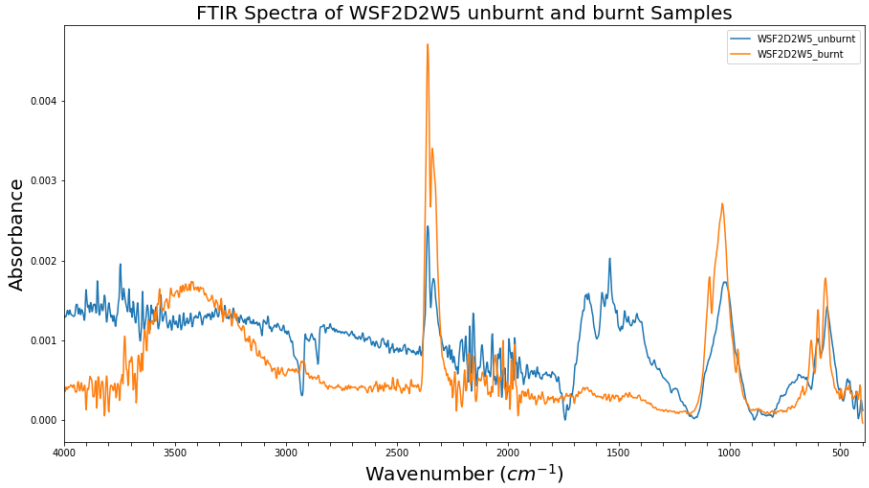

FTIR Spectra of the Two Weeks Post-mortem Unburnt Samples
WSF2D2W1_unburnt
WSF2D2W2_unburnt
WSF2D2W3_unburnt
WSF2D2W4_unburnt
WSF2D2W5_unburnt
Absorbance
Wavenumber (cm^{-1})

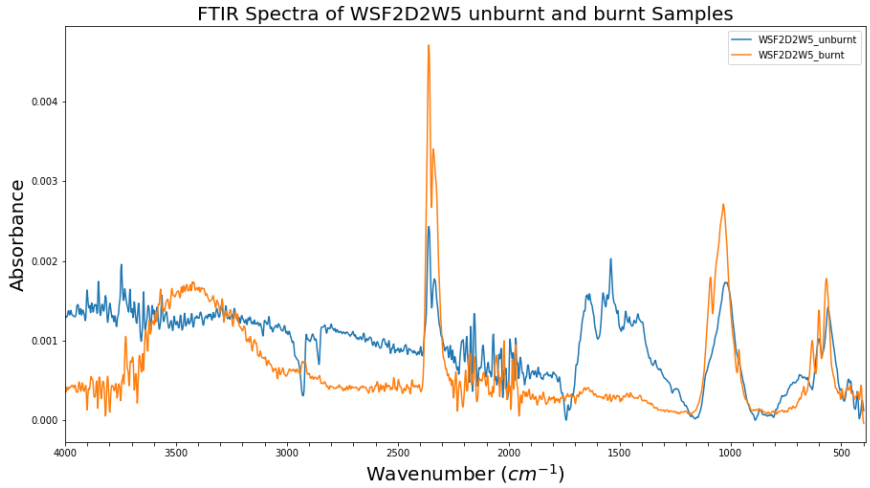

FTIR Spectra of WSF2D2W1 unburnt and burnt Samples
WSF2D2W1_unburnt
WSF2D2W1_burnt
Absorbance
Wavenumber (cm^{-1})

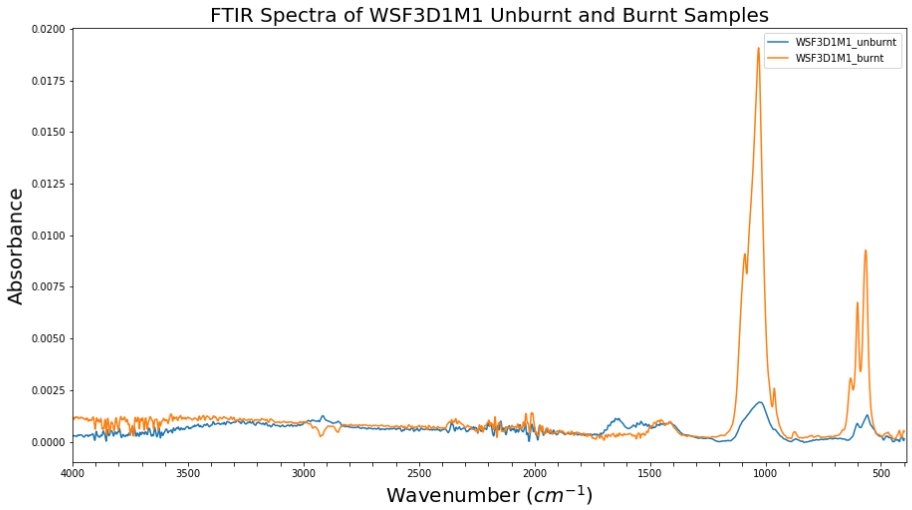

FTIR Spectra of WSF2D2W2 unburnt and burnt Samples
WSF2D2W2_unburnt
WSF2D2W2_burnt
Absorbance
Wavenumber (cm^{-1})

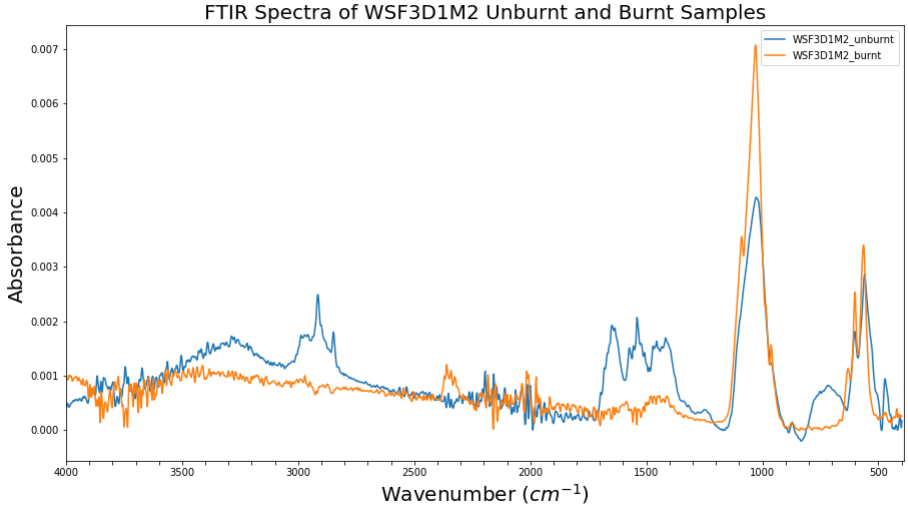

FTIR Spectra of WSF2D2W3 unburnt and burnt Samples
WSF2D2W3_unburnt
WSF2D2W3_burnt
Absorbance
Wavenumber (cm^{-1})

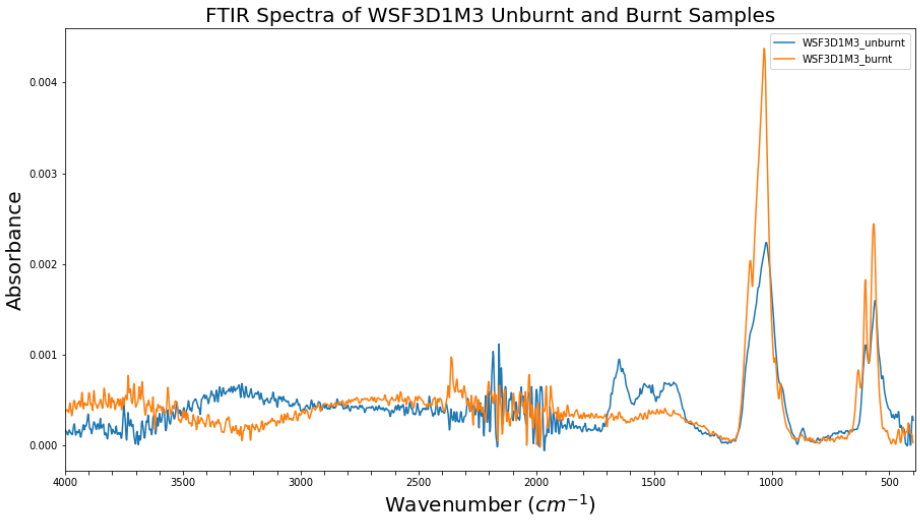

FTIR Spectra of WSF2D2W4 unburnt and burnt Samples
WSF2D2W4_unburnt
WSF2D2W4_burnt
Absorbance
Wavenumber (cm^{-1})

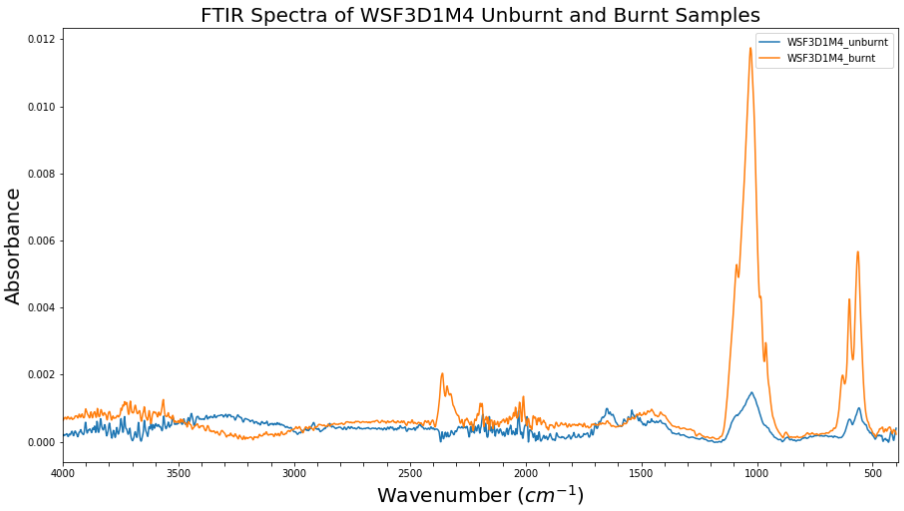

FTIR Spectra of WSF2D2W5 unburnt and burnt Samples
WSF2D2W5_unburnt
WSF2D2W5_burnt
Absorbance
Wavenumber (cm^{-1})

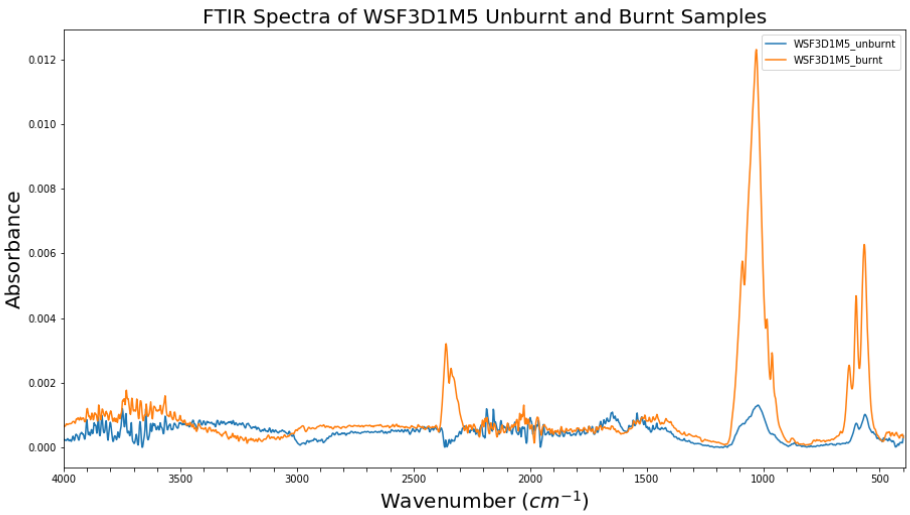

FTIR Spectra of WSF2D2W5 unburnt and burnt Samples
WSF2D2W5_unburnt
WSF2D2W5_burnt
Absorbance
Wavenumber (cm^{-1})

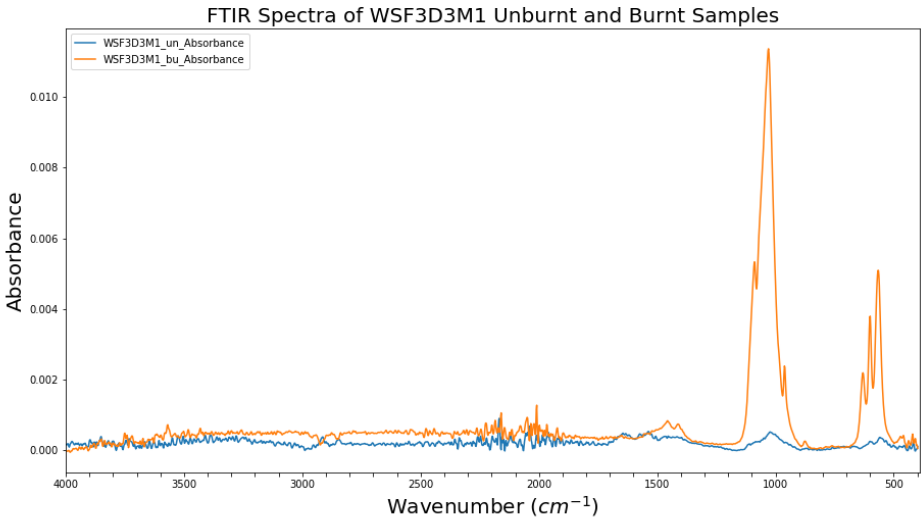

FTIR Spectra of WSF3D1M1 Unburnt and Burnt Samples
WSF3D1M1_unburnt
WSF3D1M1_burnt
Absorbance
Wavenumber (cm^{-1})

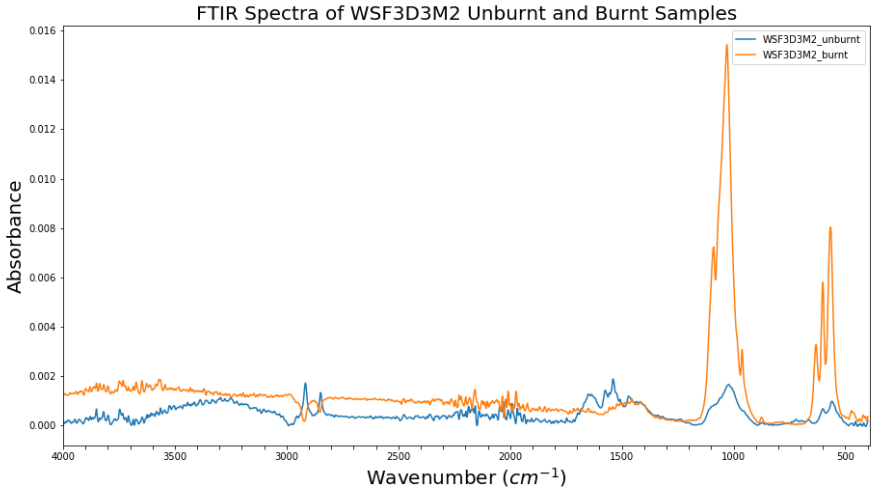

FTIR Spectra of WSF3D1M2 Unburnt and Burnt Samples
WSF3D1M2_unburnt
WSF3D1M2_burnt
Absorbance
Wavenumber (cm^{-1})

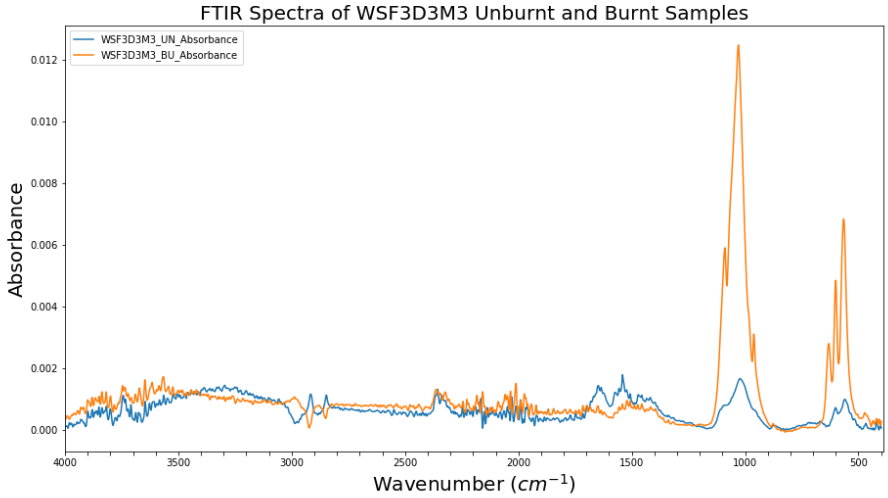

FTIR Spectra of WSF3D1M3 Unburnt and Burnt Samples
WSF3D1M3_unburnt
WSF3D1M3_burnt
Absorbance
0.000
0.001
0.002
0.003
0.004
4000
3500
3000
2500
2000
1500
1000
500
Wavenumber (cm^{-1})

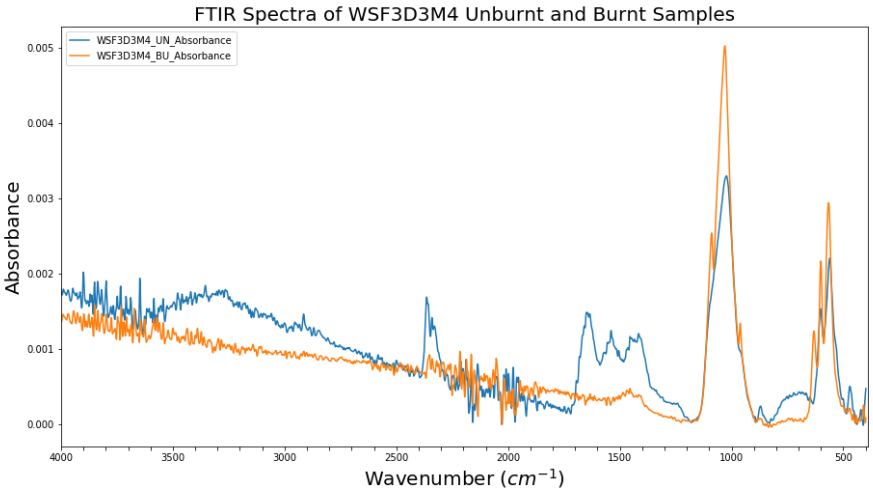

FTIR Spectra of WSF3D1M4 Unburnt and Burnt Samples
WSF3D1M4_unburnt
WSF3D1M4_burnt
Absorbance
0.000
0.002
0.004
0.006
0.008
0.010
0.012
4000
3500
3000
2500
2000
1500
1000
500
Wavenumber (cm^{-1})

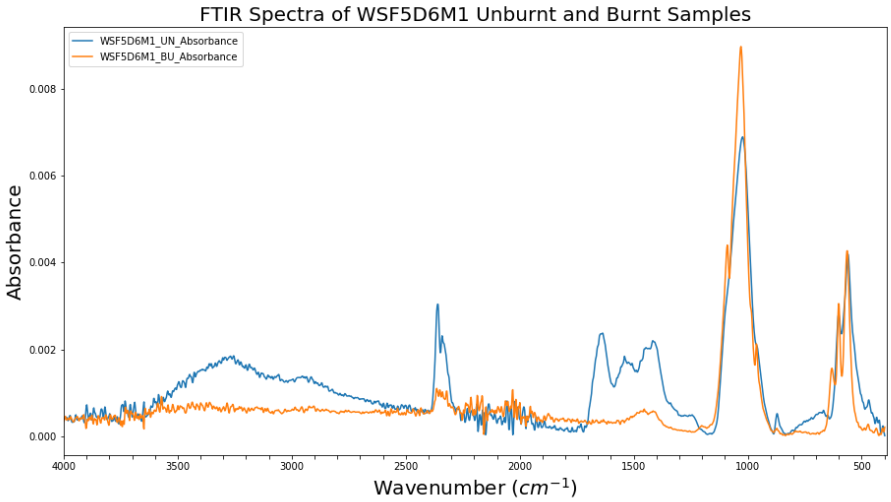

FTIR Spectra of WSF3D1M5 Unburnt and Burnt Samples
WSF3D1M5_unburnt
WSF3D1M5_burnt
Absorbance
0.000
0.002
0.004
0.006
0.008
0.010
0.012
4000
3500
3000
2500
2000
1500
1000
500
Wavenumber (cm^{-1})

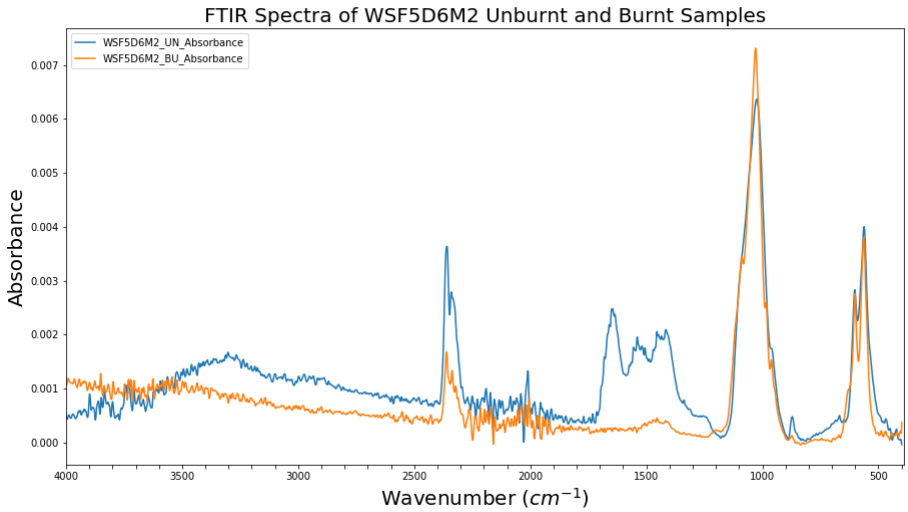

FTIR Spectra of WSF3D3M1 Unburnt and Burnt Samples
WSF3D3M1_un_Absorbance
WSF3D3M1_bu_Absorbance
Absorbance
Wavenumber (cm^{-1})

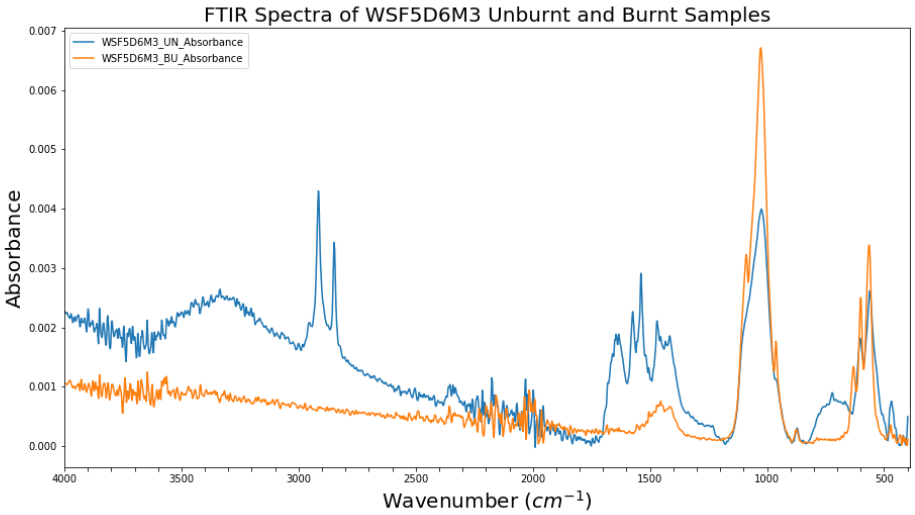

FTIR Spectra of WSF3D3M2 Unburnt and Burnt Samples
WSF3D3M2_unburnt
WSF3D3M2_burnt
Absorbance
Wavenumber (cm^{-1})

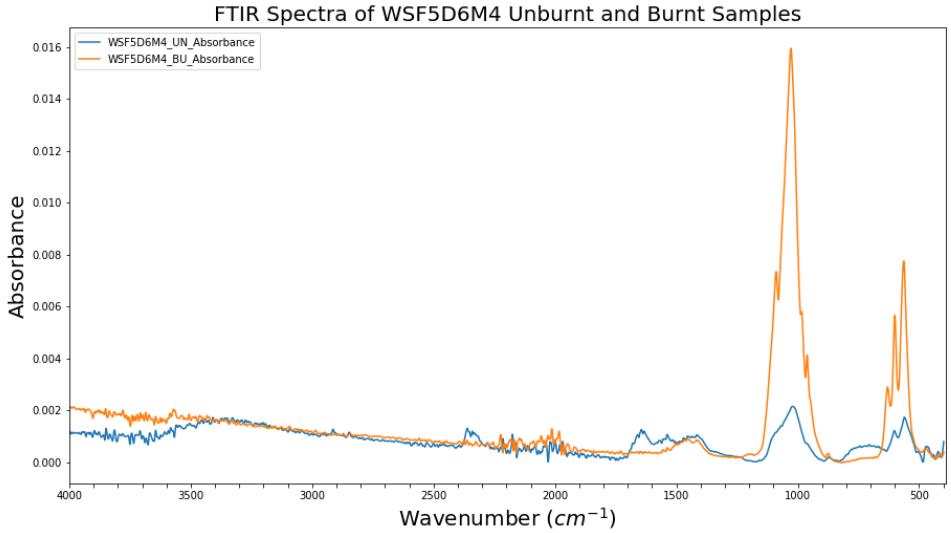

FTIR Spectra of WSF3D3M3 Unburnt and Burnt Samples
WSF3D3M3_UN_Absorbance
WSF3D3M3_BU_Absorbance
Absorbance
Wavenumber (cm^{-1})

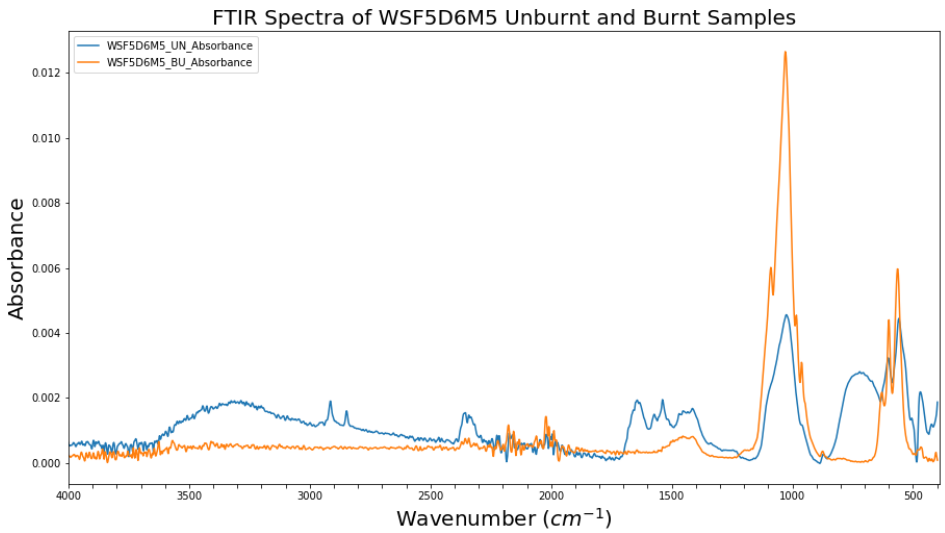

FTIR Spectra of WSF3D3M4 Unburnt and Burnt Samples
WSF3D3M4_UN_Absorbance
WSF3D3M4_BU_Absorbance
Absorbance
Wavenumber (cm^{-1})


FTIR Spectra of WSF5D6M1 Unburnt and Burnt Samples
WSF5D6M1_UN_Absorbance
WSF5D6M1_BU_Absorbance
Absorbance
Wavenumber (cm^{-1})


FTIR Spectra of WSF5D6M2 Unburnt and Burnt Samples
WSF5D6M2_UN_Absorbance
WSF5D6M2_BU_Absorbance
Absorbance
Wavenumber (cm^{-1})


FTIR Spectra of WSF5D6M3 Unburnt and Burnt Samples
WSF5D6M3_UN_Absorbance
WSF5D6M3_BU_Absorbance
Absorbance
Wavenumber (cm^{-1})


FTIR Spectra of WSF5D6M4 Unburnt and Burnt Samples
WSF5D6M4_UN_Absorbance
WSF5D6M4_BU_Absorbance
Absorbance
Wavenumber (cm^{-1})


FTIR Spectra of WSF5D6M5 Unburnt and Burnt Samples
WSF5D6M5_UN_Absorbance
WSF5D6M5_BU_Absorbance
Absorbance
Wavenumber (cm^{-1})

Part 1

Sample	605	Location (605)	565	Location (565)	min. v3PO4	Location (min.)	1020	Location (1020)	1030	Location (1030)	1415	Location (1415)	1035	Location (1035)
WSFresh_un	0.000385	601.575491	0.000522	564.941086	0.000251	590.006732	0.000799	1019.978957	0.000789	1029.61959	0.000441	1417.173032	0.000781	1033.475843
SWF2FR1_bu	0.008283	601.575491	0.011328	566.869213	0.0038	588.078605	0.023864	1029.61959	0.023864	1029.61959	0.000954	1415.244905	0.023864	1029.61959
SWF2FR3_un	0.000518	601.575491	0.000662	561.084833	0.000395	588.078605	0.000677	1021.907084	0.000591	1031.547717	0.00061	1419.101158	0.000591	1031.547717
SWFR2FR3_BU	0.013249	599.647364	0.018254	566.869213	0.006249	588.078605	0.036031	1029.61959	0.036031	1029.61959	0.001714	1411.388652	0.036031	1029.61959
SWF2FR4_BU	0.016162	601.575491	0.022268	566.869213	0.007801	586.150478	0.044749	1031.547717	0.044749	1031.547717	0.001236	1413.316778	0.044749	1031.547717
C4_bu	0.00055	601.575491	0.000754	566.869213	0.000249	588.078605	0.002018	1031.547717	0.002018	1031.547717	0.000668	1419.101158	0.002018	1031.547717
C5_bu	0.002619	601.575491	0.003466	566.869213	0.001277	588.078605	0.007189	1031.547717	0.007189	1031.547717	0.000879	1417.173032	0.007189	1031.547717
WSF2D2W1_un	0.000462	599.647364	0.000559	561.084833	0.00041	578.437972	0.000897	1021.907084	0.000897	1021.907084	0.000633	1417.173032	0.000897	1021.907084
WSF2D2W1_bu	0.000426	603.503618	0.000552	564.941086	0.000273	584.222352	N/A	N/A	0.001208	1043.116476	0.000337	1409.460525	0.001208	1043.116476
WSF2D2W2_Un	0.00068	603.503618	0.000928	561.084833	0.000553	588.078605	0.001482	1023.835211	0.001497	1031.547717	0.000611	1417.173032	0.001497	1031.547717
WSF2D2W2_bu	0.003146	601.575491	0.004334	566.869213	0.001471	588.078605	0.00825	1031.547717	0.00825	1031.547717	0.000529	1417.173032	0.00825	1031.547717
WSF2D2W3_un	0.002774	601.575491	0.00415	561.084833	0.002259	588.078605	0.006609	1023.835211	0.006609	1023.835211	0.002242	1417.173032	0.006609	1023.835211
WSF2D2W3_bu	0.000722	601.575491	0.000858	566.869213	0.000493	588.078605	0.00236	1029.61959	0.00236	1029.61959	0.000501	1413.316778	0.00236	1029.61959
WSF2D2W4_un	0.002271	601.575491	0.003351	563.012959	0.001867	590.006732	0.005194	1019.978957	0.005194	1019.978957	0.001844	1415.244905	0.005194	1019.978957
WSF2D2W4_bu	0.00585	601.575491	0.00776	566.869213	0.002984	586.150478	0.016701	1031.547717	0.016701	1031.547717	0.000751	1413.316778	0.016701	1031.547717
WSF2D2W5_un	0.001023	601.575491	0.001422	559.156706	0.00083	586.150478	0.00173	1016.122704	0.00173	1016.122704	0.001335	1417.173032	0.00173	1016.122704
WSF2D2W5_bu	0.001382	601.575491	0.001779	566.869213	0.000776	588.078605	0.002714	1031.547717	0.002714	1031.547717	0.000313	1407.532399	0.002714	1031.547717
WSF3D1M1_un	0.000882	603.503618	0.001298	559.156706	0.000685	588.078605	0.001902	1018.050831	0.001913	1025.763337	0.000951	1415.244905	0.001913	1025.763337
WSF3D1M1_bu	0.006748	601.575491	0.009278	566.869213	0.003401	588.078605	0.019087	1029.61959	0.019087	1029.61959	0.00098	1413.316778	0.019087	1029.61959
WSF3D1M2_un	0.001816	601.575491	0.002871	559.156706	0.001326	588.078605	0.004279	1025.763337	0.004279	1025.763337	0.001695	1417.173032	0.004279	1025.763337

WSF3D1M2_bu	0.002535	601.575491	0.0034	564.941086	0.001382	588.078605	0.007079	1029.61959	0.007079	1029.61959	0.000627	1411.388652	0.007079	1029.61959
WSF3D1M3_un	0.00111	601.575491	0.0016	561.084833	0.000908	588.078605	0.002238	1021.907084	0.002238	1021.907084	0.000698	1415.244905	0.002238	1021.907084
WSF3D1M3_bu	0.001828	601.575491	0.002444	566.869213	0.000913	588.078605	N/A	N/A	0.004376	1031.547717	0.00039	1417.173032	0.004376	1031.547717
WSF3D1M4_un	0.000673	599.647364	0.001012	559.156706	0.000509	588.078605	0.001474	1021.907084	0.001474	1021.907084	0.000639	1417.173032	0.001474	1021.907084
WSF3D1M4_bu	0.004254	601.575491	0.005668	563.012959	0.002444	586.150478	0.011747	1027.691464	0.011747	1027.691464	0.000886	1417.173032	0.011747	1027.691464
WSF3D1M5_un	0.000741	601.575491	0.001017	563.012959	0.00056	588.078605	0.001305	1021.907084	0.001305	1021.907084	0.000607	1419.101158	0.001305	1021.907084
WSF3D1M5_bu	0.004687	601.575491	0.006276	566.869213	0.002444	586.150478	0.012314	1029.61959	0.012314	1029.61959	0.000888	1417.173032	0.012314	1029.61959
WSF3D3M1_un	0.000257	599.647364	0.000372	559.156706	0.000181	584.222352	0.000524	1023.835211	0.000524	1023.835211	0.000389	1417.173032	0.000524	1023.835211
WSF3D3M1_bu	0.003799	599.647364	0.005094	564.941086	0.001763	588.078605	0.011365	1029.61959	0.011365	1029.61959	0.000747	1411.388652	0.011365	1029.61959
WSF3D3M2_un	0.000684	599.647364	0.000987	561.084833	0.000509	586.150478	0.001667	1021.907084	0.001667	1021.907084	0.000975	1417.173032	0.001667	1021.907084
WSF3D3M2_bu	0.005808	601.575491	0.008038	566.869213	0.002487	588.078605	0.015417	1029.61959	0.015417	1029.61959	0.000964	1417.173032	0.015417	1029.61959
WSF3D3M3_un	0.000734	601.575491	0.001005	559.156706	0.00054	590.006732	0.001675	1023.835211	0.001675	1023.835211	0.001063	1419.101158	0.001675	1023.835211
WSF3D3M3_bu	0.004855	599.647364	0.006844	564.941086	0.002161	588.078605	0.01247	1029.61959	0.01247	1029.61959	0.00076	1417.173032	0.01247	1029.61959
WSF3D3M4_un	0.001536	601.575491	0.002208	561.084833	0.001153	590.006732	0.003299	1021.907084	0.003299	1021.907084	0.001207	1417.173032	0.003299	1021.907084
WSF3D3M4_bu	0.002171	601.575491	0.002941	564.941086	0.001076	588.078605	0.005025	1029.61959	0.005025	1029.61959	0.000397	1415.244905	0.005025	1029.61959
WSF5D6M1_un	0.002817	601.575491	0.004195	561.084833	0.002365	588.078605	0.006889	1021.907084	0.006889	1021.907084	0.002204	1417.173032	0.006889	1021.907084
WSF5D6M1_bu	0.003057	601.575491	0.004272	563.012959	0.001393	586.150478	0.008965	1029.61959	0.008965	1029.61959	0.000591	1415.244905	0.008965	1029.61959
WSF5D6M2_un	0.002831	601.575491	0.004003	561.084833	0.002258	590.006732	0.006369	1023.835211	0.006369	1023.835211	0.002092	1415.244905	0.006369	1023.835211
WSF5D6M2_bu	0.002756	601.575491	0.003795	563.012959	0.001503	586.150478	0.007312	1029.61959	0.007312	1029.61959	0.000406	1417.173032	0.007312	1029.61959
WSF5D6M3_un	0.001819	603.503618	0.002617	561.084833	0.001404	588.078605	0.001675	1023.835211	0.001675	1023.835211	0.001858	1415.244905	0.001675	1023.835211
WSF5D6M3_bu	0.002503	599.647364	0.003387	564.941086	0.001294	588.078605	0.006712	1027.691464	0.006712	1027.691464	0.000667	1415.244905	0.006712	1027.691464
WSF5D6M4_un	0.001218	601.575491	0.001733	561.084833	0.000946	586.150478	0.002152	1021.907084	0.002152	1021.907084	0.001058	1415.244905	0.002152	1021.907084
WSF5D6M4_bu	0.005664	599.647364	0.007751	563.012959	0.002777	586.150478	0.01595	1027.691464	0.01595	1027.691464	0.00086	1415.244905	0.01595	1027.691464

WSF5D6M5_un	0.003223	603.503618	0.004442	559.156706	0.002471	586.150478	0.004556	1025.763337	0.004556	1025.763337	0.001674	1413.316778	0.004556	1025.763337
WSF5D6M5_bu	0.004398	599.647364	0.005966	564.941086	0.002138	586.150478	0.012654	1029.61959	0.012654	1029.61959	0.00081	1413.316778	0.012654	1029.61959
SWF5D1Y1_un	0.003482	601.575491	0.005134	561.084833	0.002889	588.078605	0.008881	1019.978957	0.008881	1019.978957	0.003595	1417.173032	0.008881	1019.978957
SWF5D1Y1_bu	0.003012	599.647364	0.004069	564.941086	0.001484	588.078605	0.007456	1029.61959	0.007456	1029.61959	0.000536	1415.244905	0.007456	1029.61959

Part 2

Sample	603	Location (603)	900	Location (900)	1450	Location (1450)	1540	Location (1540)	600	Location (600)	2010	Location (2010)	1650	Location (1650)	625	Location (625)	610	Location (610)	1660	Location (1660)
WSFresh_un	0.000385	601.575491	0.000024	896.578857	0.000475	1455.735563	0.000526	1540.573132	0.000385	601.575491	N/A	N/A	0.000065	1650.476347	N/A	N/A	0.000385	601.575491	0.000549	1667.829486
SWF2FR1_bu	0.008283	601.575491	N/A	N/A	0.000965	1453.807436	0.000417	1548.285639	0.008283	601.575491	0.001457	2007.179763	0.000337	1642.763841	0.004499	630.49739	0.008283	601.575491	0.000328	1665.90136
SWF2FR3_un	0.000518	601.575491	N/A	N/A	0.000809	1457.66369	0.001527	1540.573132	0.000518	601.575491	0.000485	2009.10789	0.001133	1648.54822	0.000254	640.138022	0.000518	601.575491	0.000895	1669.757613
SWFR2FR3_BU	0.013249	599.647364	0.000678	873.441338	0.001928	1455.735563	0.001019	1536.716879	0.013249	599.647364	0.001761	2005.251637	0.000675	1650.476347	0.008436	630.49739	0.013249	599.647364	0.000068	1665.90136
SWF2FR4_BU	0.016162	601.575491	N/A	N/A	0.001353	1455.735563	0.000857	1540.573132	0.016162	601.575491	0.002422	2007.179763	0.000731	1650.476347	0.009217	630.49739	0.016162	601.575491	0.000072	1660.11698
C4_bu	0.00055	601.575491	0.000054	900.43511	0.000997	1455.735563	0.001608	1540.573132	0.00055	601.575491	0.000069	2001.395383	0.001144	1648.54822	0.000256	630.49739	0.00055	601.575491	0.000669	1662.045106
C5_bu	0.002619	601.575491	N/A	N/A	0.001179	1455.735563	0.000681	1540.573132	0.002619	601.575491	0.000727	2005.251637	0.00045	1650.476347	0.00143	630.49739	0.002619	601.575491	0.000314	1662.045106
WSF2D2W1_un	0.000462	599.647364	0.000312	910.075743	0.00062	1446.09493	0.000923	1538.645006	0.000462	599.647364	0.000982	2012.964143	0.000834	1644.691967	0.000256	632.425516	0.000462	599.647364	0.000735	1667.829486
WSF2D2W1_bu	0.000426	603.503618	0.000099	902.363236	0.000327	1449.951183	0.000348	1546.357512	0.000426	603.503618	0.000926	2022.604776	0.000555	1654.3326	0.000295	638.209896	0.000426	603.503618	0.000509	1671.685739
WSF2D2W2_Un	0.00068	603.503618	0.000036	894.65073	0.000608	1453.807436	0.000742	1540.573132	0.00068	603.503618	0.000681	2018.748523	0.00084	1650.476347	N/A	N/A	0.00068	603.503618	0.000697	1669.757613
WSF2D2W2_bu	0.003146	601.575491	0.000146	894.65073	0.000551	1453.807436	0.000566	1548.285639	0.003146	601.575491	0.001898	2007.179763	0.000581	1650.476347	0.001941	630.49739	0.003146	601.575491	0.000578	1660.11698
WSF2D2W3_un	0.002774	601.575491	N/A	N/A	0.002083	1446.09493	0.001837	1542.501259	0.002774	601.575491	0.000972	2011.036016	0.002526	1650.476347	N/A	N/A	0.002774	601.575491	0.002526	1650.476347
WSF2D2W3_bu	0.000722	601.575491	N/A	N/A	0.000527	1453.807436	0.000463	1538.645006	0.000722	601.575491	0.000559	2003.32351	0.000435	1644.691967	0.000554	630.49739	0.000722	601.575491	0.000425	1660.11698
WSF2D2W4_un	0.002271	601.575491	N/A	N/A	0.001807	1453.807436	0.001813	1538.645006	0.002271	601.575491	0.000786	2009.10789	0.002145	1644.691967	N/A	N/A	0.002271	601.575491	0.001786	1658.188853

WSF2D2 W4_bu	0.005 85	601.57 5491	N/A	N/A	0.000 777	1451.87 931	0.000 747	1544.42 9385	0.005 85	601.57 5491	0.000 975	2003.32 351	0.000 833	1650.47 6347	0.003 783	630.49 739	0.005 85	601.57 5491	0.000 789	1660.11 698
WSF2D2 W5_un	0.001 023	601.57 5491	N/A	N/A	0.001 298	1455.73 5563	0.002 028	1538.64 5006	0.001 023	601.57 5491	0.000 653	2012.96 4143	N/A	N/A	N/A	N/A	N/A	N/A	N/A	N/A
WSF2D2 W5_bu	0.001 382	601.57 5491	0.000 135	892.72 2604	0.000 346	1449.95 1183	0.000 322	1542.50 1259	0.001 382	601.57 5491	0.000 403	2011.03 6016	0.000 402	1646.62 0094	0.001	630.49 739	0.001 382	601.57 5491	0.000 408	1658.18 8853
WSF3D1 M1_un	0.000 882	603.50 3618	N/A	N/A	0.000 861	1444.16 6804	0.000 985	1538.64 5006	0.000 882	603.50 3618	0.000 846	2011.03 6016	0.001 126	1650.47 6347	N/A	N/A	0.000 882	603.50 3618	0.000 997	1658.18 8853
WSF3D1 M1_bu	0.006 748	601.57 5491	0.000 191	896.57 8857	0.001 064	1451.87 931	0.000 372	1536.71 6879	0.006 748	601.57 5491	0.001 399	2012.96 4143	0.000 239	1646.62 0094	0.003 081	630.49 739	0.006 748	601.57 5491	0.000 401	1660.11 698
WSF3D1 M2_un	0.001 816	601.57 5491	0.000 045	896.57 8857	0.001 635	1455.73 5563	0.002 071	1540.57 3132	0.001 816	601.57 5491	0.000 838	2012.96 4143	0.001 925	1648.54 822	N/A	N/A	0.001 816	601.57 5491	0.001 816	601.575 491
WSF3D1 M2_bu	0.002 535	601.57 5491	0.000 068	898.50 6983	0.000 625	1451.87 931	0.000 393	1536.71 6879	0.002 535	601.57 5491	0.001 018	2007.17 9763	0.000 219	1650.47 6347	0.001 137	630.49 739	0.002 535	601.57 5491	0.000 394	1660.11 698
WSF3D1 M3_un	0.001 11	601.57 5491	N/A	N/A	0.000 695	1455.73 5563	0.000 684	1540.57 3132	0.001 11	601.57 5491	0.000 651	2018.74 8523	0.000 954	1646.62 0094	N/A	N/A	0.001 11	601.57 5491	N/A	N/A
WSF3D1 M3_bu	0.001 828	601.57 5491	0.000 082	894.65 073	0.000 411	1453.80 7436	0.000 362	1538.64 5006	0.001 828	601.57 5491	0.000 45	2016.82 0396	0.000 37	1646.62 0094	0.000 834	632.42 5516	0.001 828	601.57 5491	0.000 326	1660.11 698
WSF3D1 M4_un	0.000 673	599.64 7364	0.000 073	898.50 6983	0.000 684	1455.73 5563	0.000 947	1540.57 3132	0.000 673	599.64 7364	0.000 287	2016.82 0396	0.000 99	1646.62 0094	0.000 127	642.06 6149	0.000 673	599.64 7364	0.000 735	1667.82 9486
WSF3D1 M4_bu	0.004 254	601.57 5491	N/A	N/A	0.000 97	1455.73 5563	0.000 734	1538.64 5006	0.004 254	601.57 5491	0.001 355	2009.10 789	0.000 625	1646.62 0094	0.001 987	630.49 739	0.004 254	601.57 5491	0.000 562	1667.82 9486
WSF3D1 M5_un	0.000 741	601.57 5491	N/A	N/A	0.000 746	1455.73 5563	0.001 061	1540.57 3132	0.000 741	601.57 5491	0.000 822	2007.17 9763	0.001 087	1646.62 0094	0.000 151	642.06 6149	0.000 741	601.57 5491	0.000 904	1669.75 7613
WSF3D1 M5_bu	0.004 687	601.57 5491	N/A	N/A	0.001 016	1455.73 5563	0.000 839	1538.64 5006	0.004 687	601.57 5491	0.000 871	2007.17 9763	0.000 66	1650.47 6347	0.002 538	630.49 739	0.004 687	601.57 5491	0.000 585	1660.11 698
WSF3D3 M1_un	0.000 257	599.64 7364	N/A	N/A	0.000 406	1453.80 7436	0.000 538	1536.71 6879	0.000 257	599.64 7364	0.000 43	2011.03 6016	N/A	N/A	N/A	N/A	0.000 257	599.64 7364	0.000 49	1644.69 1967
WSF3D3 M1_bu	0.003 799	599.64 7364	N/A	N/A	0.000 839	1455.73 5563	0.000 491	1536.71 6879	0.003 799	599.64 7364	0.001 28	2009.10 789	N/A	N/A	0.002 197	630.49 739	0.003 799	599.64 7364	N/A	N/A
WSF3D3 M2_un	0.000 684	599.64 7364	N/A	N/A	0.001 07	1459.59 1816	0.001 89	1538.64 5006	0.000 684	599.64 7364	0.000 639	2009.10 789	0.001 271	1648.54 822	N/A	N/A	0.000 684	599.64 7364	0.001 271	1648.54 822
WSF3D3 M2_bu	0.005 808	601.57 5491	N/A	N/A	0.001 095	1455.73 5563	0.000 764	1540.57 3132	0.005 808	601.57 5491	0.001 395	2009.10 789	0.000 698	1650.47 6347	0.003 276	630.49 739	0.005 808	601.57 5491	N/A	N/A
WSF3D3 M3_un	0.000 734	601.57 5491	!!!!!!!	!!!!!	0.001 139	1455.73 5563	0.001 8	1540.57 3132	0.000 734	601.57 5491	0.000 789	2011.03 6016	0.001 448	1646.62 0094	N/A	N/A	0.000 734	601.57 5491	0.001 448	1646.62 0094
WSF3D3 M3_bu	0.004 855	599.64 7364	N/A	N/A	0.000 857	1455.73 5563	0.000 849	1540.57 3132	0.004 855	599.64 7364	0.001 518	2011.03 6016	0.000 792	1650.47 6347	0.002 811	630.49 739	0.004 855	599.64 7364	N/A	N/A
WSF3D3 M4_un	0.001 536	601.57 5491	N/A	N/A	0.001 17	1453.80 7436	0.001 249	1538.64 5006	0.001 536	601.57 5491	0.000 739	2009.10 789	0.001 489	1644.69 1967	N/A	N/A	0.001 536	601.57 5491	0.001 489	1644.69 1967

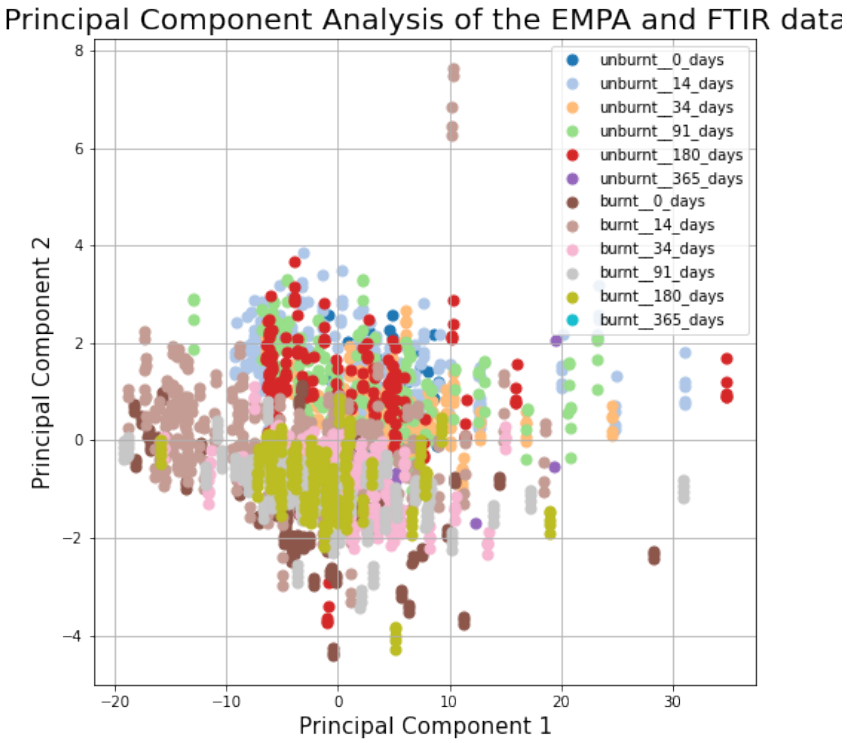
WSF3D3 M4_bu	0.002171	601.575491	N/A	N/A	0.000481	1453.807436	0.000357	1530.932499	0.002171	601.575491	0.000616	2016.820396	N/A	N/A	N/A	N/A	0.002171	601.575491	N/A	N/A
WSF5D6 M1_un	0.002817	601.575491	N/A	N/A	0.002046	1446.09493	0.001848	1540.573132	0.002817	601.575491	0.000811	2020.676649	N/A	N/A	N/A	N/A	0.002817	601.575491	0.002363	1640.835714
WSF5D6 M1_bu	0.003057	601.575491	N/A	N/A	0.000635	1453.807436	0.000407	1530.932499	0.003057	601.575491	0.000857	2016.820396	N/A	N/A	0.001574	630.49739	0.003057	601.575491	N/A	N/A
WSF5D6 M2_un	0.002831	601.575491	N/A	N/A	0.002057	1453.807436	0.001955	1538.645006	0.002831	601.575491	0.001326	2011.036016	0.000264	1644.691967	N/A	N/A	0.002831	601.575491	0.002478	1644.691967
WSF5D6 M2_bu	0.002756	601.575491	N/A	N/A	0.000452	1453.807436	0.000288	1548.285639	0.002756	601.575491	0.000808	2005.251637	N/A	N/A	N/A	N/A	0.002756	601.575491	N/A	N/A
WSF5D6 M3_un	0.001819	603.503618	N/A	N/A	0.001842	1453.807436	0.002912	1538.645006	0.001819	603.503618	0.000873	2022.604776	0.001887	1644.691967	N/A	N/A	0.001819	603.503618	0.001559	1658.188853
WSF5D6 M3_bu	0.002503	599.647364	!!	!!	0.000755	1453.807436	0.000372	1530.932499	0.002503	599.647364	0.000947	2014.892269	N/A	N/A	N/A	N/A	0.002503	599.647364	N/A	N/A
WSF5D6 M4_un	0.001218	601.575491	!!	!!	0.001013	1453.807436	0.001066	1538.645006	0.001218	601.575491	0.000796	2020.676649	0.001262	1644.691967	N/A	N/A	0.001218	601.575491	0.00106	1660.11698
WSF5D6 M4_bu	0.005664	599.647364	N/A	N/A	0.000926	1453.807436	0.000561	1538.645006	0.005664	599.647364	0.001291	2012.964143	N/A	N/A	0.002894	630.49739	0.005664	599.647364	N/A	N/A
WSF5D6 M5_un	0.00323	603.503618	N/A	N/A	0.001598	1453.807436	0.001945	1538.645006	0.00323	603.503618	0.000878	2020.676649	0.001931	1642.763841	N/A	N/A	0.00323	603.503618	0.001931	1642.763841
WSF5D6 M5_bu	0.004398	599.647364	N/A	N/A	0.000824	1453.807436	0.000492	1536.716879	0.004398	599.647364	0.001427	2020.676649	N/A	N/A	0.002169	628.569263	0.004398	599.647364	N/A	N/A
SWF5D1 Y1_un	0.003482	601.575491	N/A	N/A	0.003535	1455.735563	0.003753	1540.573132	0.003482	601.575491	0.000852	2005.251637	0.004307	1646.620094	N/A	N/A	0.003482	601.575491	0.003199	1667.829486
SWF5D1 Y1_bu	0.003012	599.647364	0.000072	896.578857	0.000542	1453.807436	0.000275	1536.716879	0.003012	599.647364	0.001011	2009.10789	0.000105	1650.476347	0.001737	630.49739	0.003012	599.647364	0.000224	1660.11698

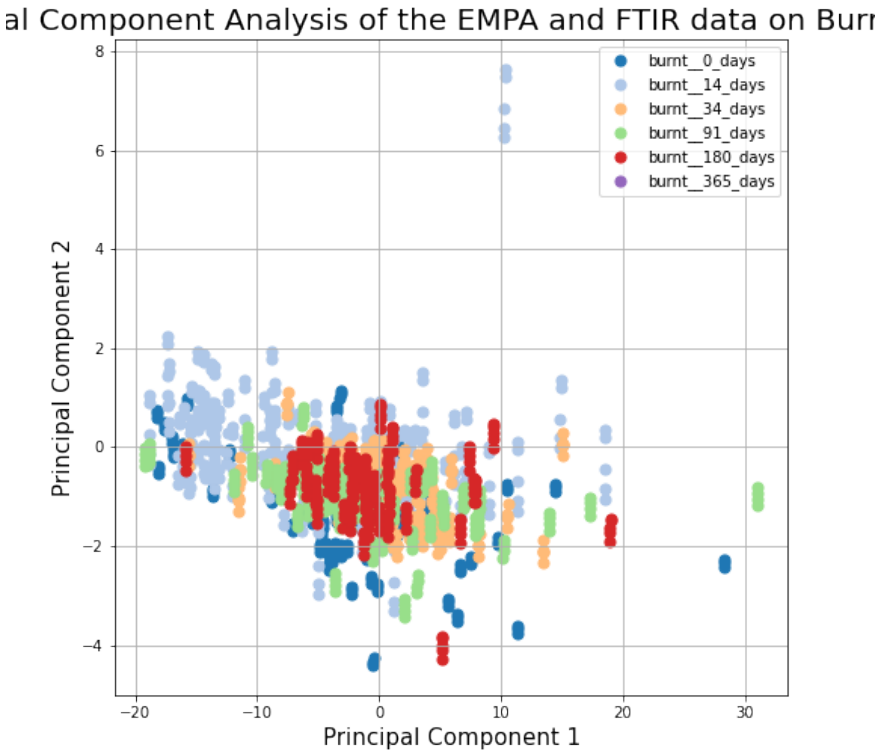
Appendix E.3: FTIR Measured Ratios

Sample	IRSF	Maturity (1020/1030)	C/P (1415/1035)	BPI (1415/603)	API (1540/603)	CO3/P (900/1035)	C/C (1450/1415)	CN/P (2010/1035)	CO/CO3 (1650/1415)	PHT (625/610)	N/P (1660/1035)
WSFresh_un	3.613545817	1.012674271	0.564660691	1.145454545	1.366233766	0.030729834	1.077097506	0.44431374	1.473922902	#NUM!	0.702944942
SWF2FR1_bu	5.160789474	1	0.039976534	0.115175661	0.050344078	#NUM!	1.011530398	0.061054308	0.353249476	0.543160691	0.013744552
SWF2FR3_un	2.987341772	1.145516074	1.0321489	1.177606178	2.947876448	#NUM!	1.326229508	0.820642978	1.857377049	0.49034749	1.514382403
SWFR2FR3_BU	5.041286606	1	0.047570148	0.129368254	0.076911465	0.01881713	1.124854142	0.04887458	0.393815636	0.6367273	0.018872637
SWF2FR4_BU	4.926291501	1	0.027620729	0.076475684	0.053025616	#NUM!	1.094660194	0.054124115	0.591423948	0.570288331	0.016089745
C4_bu	5.236947791	1	0.331020813	1.214545455	2.923636364	0.026759167	1.49251497	0.048034251	1.71257485	0.465454545	0.331516353
C5_bu	4.765074393	1	0.122270135	0.335624284	0.26002291	#NUM!	1.341296928	-0.03122165	0.511945392	0.546009927	0.043677841
WSF2D2W1_un	2.490243902	1	0.705685619	1.37012987	1.997835498	#NUM!	0.979462875	-0.11047754	1.317535545	0.554112554	0.819397993
WSF2D2W1_bu	3.582417582	#NUM!	0.27897351	0.791079812	0.816901408	0.081953642	0.970326409	0.766556291	1.646884273	0.692488263	0.421357616
WSF2D2W2_Un	2.907775769	0.98997996	0.408149633	0.898529412	1.091176471	0.024048096	0.995090016	0.45490982	1.374795417	#NUM!	0.465597862
WSF2D2W2_bu	5.084976207	1	0.064121212	0.168150032	0.179910998	0.01769697	1.041587902	0.230060606	1.098298677	0.616973935	0.070060606
WSF2D2W3_un	3.065073041	1	0.339234377	0.808219178	0.66222062	#NUM!	0.929081178	0.147072174	1.126672614	#NUM!	0.382206083
WSF2D2W3_bu	3.204868154	1	0.212288136	0.693905817	0.641274238	#NUM!	1.051896208	0.236864407	0.868263473	0.767313019	0.180084746
WSF2D2W4_un	3.011247991	1	0.355025029	0.811977103	0.798326728	#NUM!	0.979934924	0.151328456	1.163232104	#NUM!	0.343858298
WSF2D2W4_bu	4.560991957	1	0.044967367	0.128376068	0.127692308	#NUM!	1.034620506	0.058379738	1.10918775	0.646666667	0.04724268
WSF2D2W5_un	2.945783133	1	0.771676301	1.304985337	1.982404692	#NUM!	0.972284644	0.377456647	1.127467495	#NUM!	#VALUE!
WSF2D2W5_bu	4.073453608	1	0.115327929	0.226483357	0.232995658	0.049742078	1.10543131	0.148489315	1.284345048	0.723589001	0.150331614
WSF3D1M1_un	3.182481752	0.994249869	0.497124935	1.078231293	1.116780045	#NUM!	0.905362776	0.442237324	1.184016824	#NUM!	0.521170936

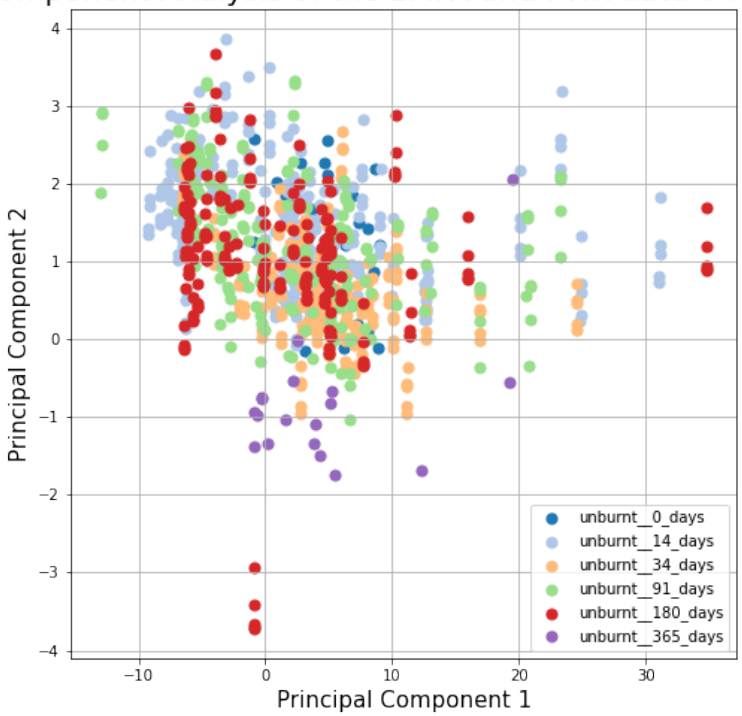
WSF3D1M1_bu	4.712143487	1	0.051343847	0.145228216	0.055127445	0.010006811	1.085714286	0.073295961	0.243877551	0.456579727	0.021009064
WSF3D1M2_un	3.534690799	1	0.396120589	0.933370044	1.140418502	0.010516476	0.96460177	0.19584015	1.135693215	#NUM!	0.424398224
WSF3D1M2_bu	4.294500724	1	0.088571832	0.247337278	0.155029586	0.088289306	0.996810207	0.143805622	0.349282297	0.44852071	0.055657579
WSF3D1M3_un	2.984581498	1	0.311885612	0.628828829	0.616216216	#NUM!	0.995702006	0.290884718	1.366762178	#NUM!	#VALUE!
WSF3D1M3_bu	4.679079956	#REF!	0.089122486	0.213347921	0.198030635	0.018738574	1.053846154	0.102833638	0.948717949	0.456236324	0.074497258
WSF3D1M4_un	3.310412574	1	0.433514247	0.949479941	1.407132244	0.049525102	1.070422535	0.194708277	1.549295775	0.188707281	0.498643148
WSF3D1M4_bu	4.059738134	1	0.075423512	0.208274565	0.172543488	#NUM!	1.094808126	0.1153486	0.705417607	0.467089798	0.047842002
WSF3D1M5_un	3.139285714	1	0.4651341	0.819163293	1.431848853	#NUM!	1.228995058	0.629885057	1.7907743	0.203778677	0.692720307
WSF3D1M5_bu	4.485679214	#REF!	0.072113042	0.189460209	0.179005761	#NUM!	1.144144144	0.0707325	0.743243243	0.54149776	0.047506903
WSF3D3M1_un	3.475138122	1	0.742366412	1.513618677	2.093385214	#NUM!	1.043701799	0.820610687	1.117637353	#NUM!	0.935114504
WSF3D3M1_bu	5.044242768	1	0.065728113	0.196630692	0.129244538	#NUM!	1.123159304	0.112626485	1.136550171	0.578310082	#VALUE!
WSF3D3M2_un	3.282907662	1	0.584883023	1.425438596	2.763157895	#NUM!	1.097435897	0.383323335	1.303589744	#NUM!	0.76244751
WSF3D3M2_bu	5.567350221	1	0.062528378	0.165977961	0.1315427	0.071025491	1.135892116	0.09048453	0.72406639	0.564049587	#VALUE!
WSF3D3M3_un	3.22037037	#REF!	0.634626866	1.448228883	2.452316076	#NUM!	1.071495767	0.471044776	1.362182502	#NUM!	0.864477612
WSF3D3M3_bu	5.413697362	1	0.060946271	0.15653965	0.174871267	0.06872494	1.127631579	0.121732157	1.042105263	0.578990731	#VALUE!
WSF3D3M4_un	3.247181266	1	0.365868445	0.785807292	0.813151042	#NUM!	0.969345485	0.224007275	1.233637117	#NUM!	0.451348894
WSF3D3M4_bu	4.750929368	1	0.079004975	0.182865039	0.16444035	0.095721393	1.211586902	0.122587065	1.084096242	#NUM!	#VALUE!
WSF5D6M1_un	2.964904863	1	0.319930324	0.782392616	0.656017039	#NUM!	0.92831216	0.117723908	1.01982355	#NUM!	0.343010597
WSF5D6M1_bu	5.261306533	1	0.065923034	0.193326791	0.133137062	0.070831009	2.071495767	0.095593977	0.955550857	0.514883873	#VALUE!
WSF5D6M2_un	3.026572188	1	0.328466007	0.738961498	0.690568704	#NUM!	0.983269598	0.208195949	0.126195029	#NUM!	0.389072068

WSF5D6M2_bu	4.358616101	1	0.055525164	0.147314949	0.104499274	0.061816193	2.071495767	0.110503282	-0.19310538	#NUM!	#VALUE!
WSF5D6M3_un	3.15954416	#REF!	1.109253731	1.021440352	1.600879604	#NUM!	0.99138859	0.52119403	-0.63991964	#NUM!	0.930746269
WSF5D6M3_bu	4.551777434	1	0.099374255	0.266480224	0.148621654	0.112485101	1.969345485	0.141090584	-1.0867339	#NUM!	#VALUE!
WSF5D6M4_un	3.119450317	1	0.491635688	0.86863711	0.875205255	#NUM!	0.957466919	0.369888476	-1.53354816	#NUM!	0.492565056
WSF5D6M4_bu	4.830752611	1	0.053918495	0.151836158	0.09904661	0.058056426	2.071495767	0.080940439	-1.98036242	0.510946328	#VALUE!
WSF5D6M5_un	3.104815864	1	0.367427568	0.518266254	0.602167183	#NUM!	0.954599761	0.192712906	-2.42717668	#NUM!	0.423836699
WSF5D6M5_bu	4.847521048	1	0.06401138	0.184174625	0.111869031	#NUM!	1.017283951	0.112770665	-2.87399094	0.493178718	#VALUE!
SWF5D1Y1_un	5.041286606	1	0.404796757	0.129368254	0.076911465	0.01881713	1.124854142	0.04887458	0.393815636	0.6367273	0.360207184
SWF5D1Y1_bu	4.771563342	1	0.071888412	0.177954847	0.091301461	0.009656652	1.01119403	0.135595494	0.195895522	0.576693227	0.030042918

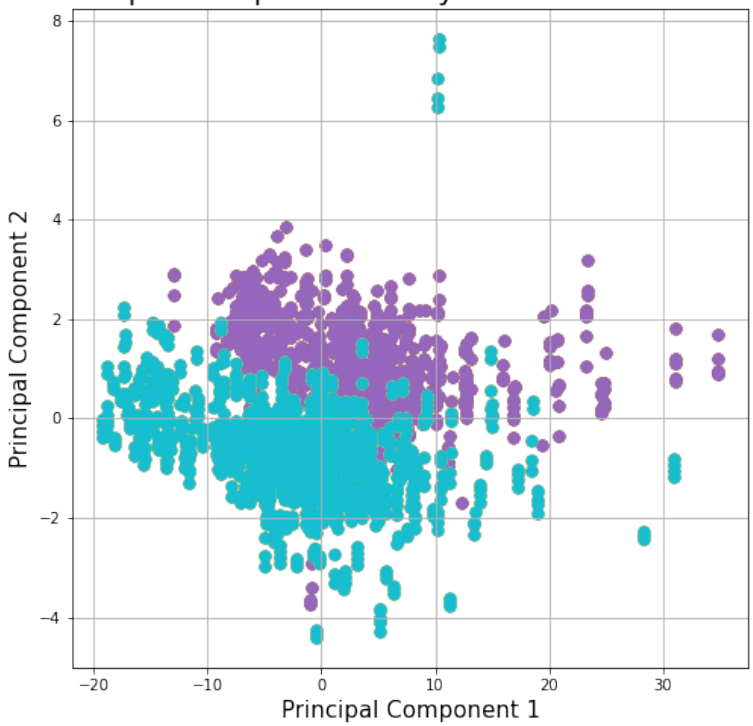

Principal Component Analysis of the EMPA and FTIR data
unburnt__0_days
unburnt__14_days
unburnt__34_days
unburnt__91_days
unburnt__180_days
unburnt__365_days
burnt__0_days
burnt__14_days
burnt__34_days
burnt__91_days
burnt__180_days
burnt__365_days
Principal Component 2
Principal Component 1

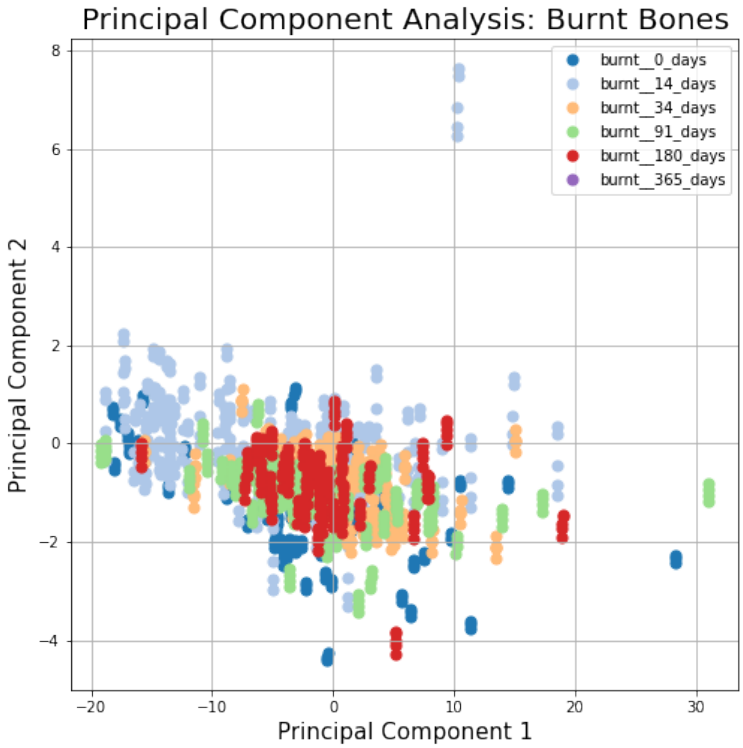

al Component Analysis of the EMPA and FTIR data on Burn
burnt__0_days
burnt__14_days
burnt__34_days
burnt__91_days
burnt__180_days
burnt__365_days
Principal Component 2
Principal Component 1

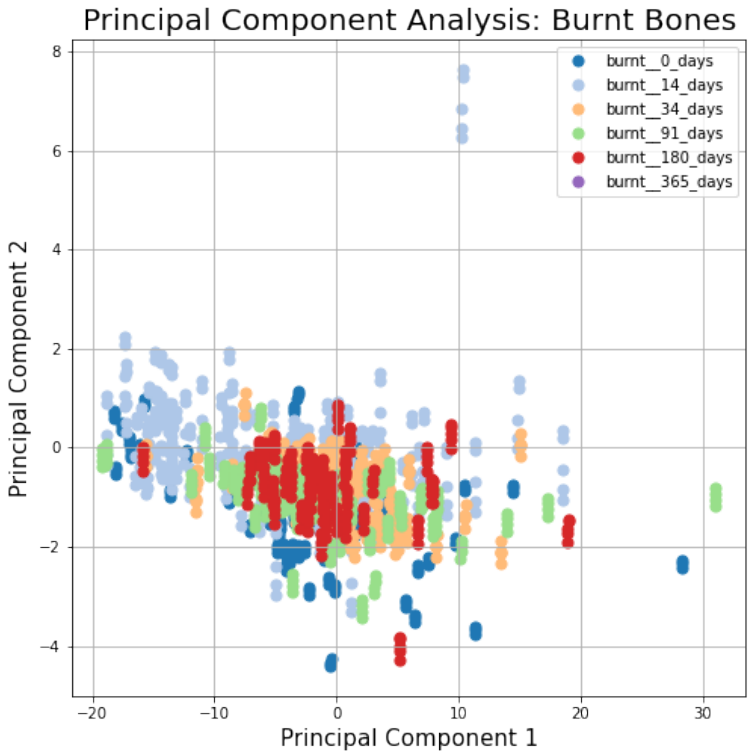
Component Analysis of the EMPA and FTIR data on Unbu

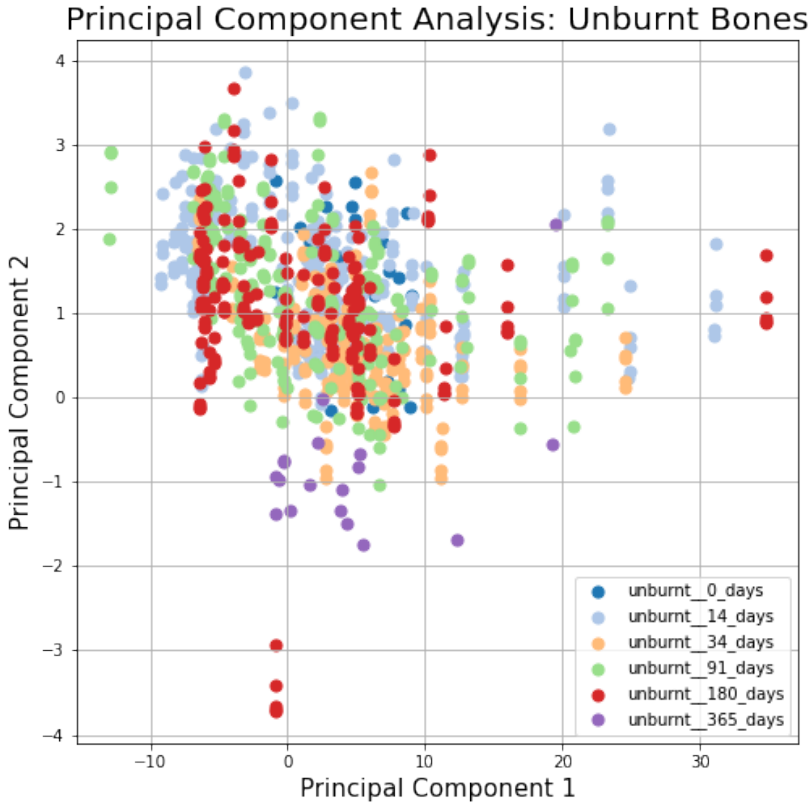


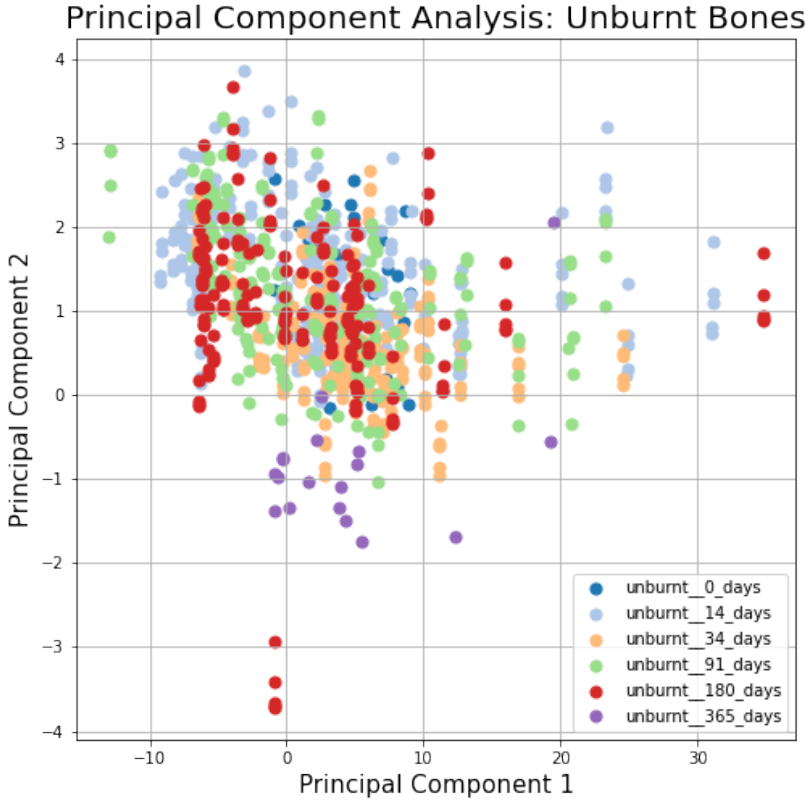
Principal Component Analysis: Unburnt vs Burnt




Principal Component Analysis: Burnt Bones
burnt__0_days
burnt__14_days
burnt__34_days
burnt__91_days
burnt__180_days
burnt__365_days
Principal Component 2
Principal Component 1
8
6
4
2
0
−2
−4
−20
−10
0
10
20
30


Principal Component Analysis: Burnt Bones
burnt__0_days
burnt__14_days
burnt__34_days
burnt__91_days
burnt__180_days
burnt__365_days
Principal Component 2
Principal Component 1
8
6
4
2
0
−2
−4
−20
−10
0
10
20
30


Principal Component Analysis: Unburnt Bones
Principal Component 2
Principal Component 1
unburnt_0_days
unburnt_14_days
unburnt_34_days
unburnt_91_days
unburnt_180_days
unburnt_365_days


Principal Component Analysis: Unburnt Bones
Principal Component 2
Principal Component 1
unburnt_0_days
unburnt_14_days
unburnt_34_days
unburnt_91_days
unburnt_180_days
unburnt_365_days

Spectroscopic Investigations on bone				
Assignment	**Wavenumber**	**Mode**	**Notes**	**Citations**
OH	630	OH libration	in synthetic HAP	(Elliott, 2002)
	3500	satellite	OH stretch perturbed by a neighbouring Cl^- ion on the c-axis	
	3700-2700	H_2O stretching	broad peak	
	1640	H_2O bending	weak	
CO_3^{2-}	1063	v1	Cannot be seen, overlaps with $_{v4}PO_4$ which is stronger	(Elliott, 2002)
	879	v2	2nd strongest, when two peaks present here, it means CO_3^{2-} is in two different environments	
	1415	v3	strongest, doubly degenerate, transition moment in plane	
	680	v4	weakest, not present in bioapatite	
PO_4^{3-}	938	v1	IR inactive, but visible as a weak signal next to v3 due to PO_4^{3-} distortion	(Elliott, 2002)
	420	v2	IR inactive	
	1017	v3	Very intense	
	567	v4	Split into two bands (used for crystallinity estimation)	
HPO_4^{2-}	870	P -- (OH) stretch	Next to $_{v2}CO_3$	(Elliott, 2002)
	1020	v3	Weak	(Rey *et al.*, 1991)
	1100			
	1145			
	1100	v3	In poorly crystallised, easily solubilised regions	(Elliott, 2002)
	1125			
	520-530	v4	Intensity falls with maturation	(Rey *et al.*, 1990)
	540-550			

Appendix F: MANOVA of EMPA and FTIR Dataset

MANOVA																					
	PMI													State				Area (EMP)				
	Unburnt				Burnt				Both states					EMP		FTIR		Unburnt		Burnt		Both states
	EMP		FTIR		EMP		FTIR		EMP		FTIR											
	F	PR > F	F	PR > F	F	PR > F	F	PR > F	F	PR > F	F	PR > F	F	PR > F	F	PR > F	F	PR > F	F	PR > F	F	PR > F
Wilks' lambda	7.3791	0	22	1.593	7.7405	0	0.6078	0.8634	9.4844	0	0.7571	0.7405	66.6194	0	29.7751	0	3.1648	0	3.5394	0	4.4197	0
Pillai's trace	5.9688	0	24	1.55	6.8887	0	0.5649	0.8972	8.469	0	0.765	0.7323	66.6194	0	29.7751	0	3.0818	0	3.4401	0	4.3141	0
Hotelling-Lawley trace	8.9684	0	14.94	1.67	8.674	0	0.6591	0.8106	10.5266	0	0.7541	0.7409	66.6194	0	29.7751	0	3.2467	0	3.6355	0	4.5224	0
Roy's greatest root	29.3986	0	12	3.04	24.8456	0	1.3916	0.2746	33.9707	0	1.1561	0.3514	66.6194	0	29.7751	0	6.3251	0	7.198	0	9.25	0

Appendix G: Images of Cutmarks

Please find the images of cutmarks in the electronic file attached with the thesis.

Appendix H: Permissions

Reprinted by permission from Springer Nature: Springer eBook: Reiner Bartl, Christoph Bartl: Structure and Architecture of Bone 2016, pp. 15, Fig. 2.1 [License Number: 5244221406277], license date: Feb 08, 2022.

Permission acquired to reuse Fig. 2 in this dissertation from Prof Joseph Wallace, BBML, Indiana University-Purdue University Indianapolis, from his website (https://bbml.sitehost.iu.edu/) on Feb 08, 2022.

Permission to reuse Fig 7. (Brönnimann et al., 2018, 46, Fig. 4) was requested 13 April 2020 from Elsevier. It has been reprinted in Végh *et al.* 2021.